Aero-dynam-ics

N. F. Krasnov

2

Methods of Aerodynamic Calculations

Mir Publishers

This textbook deals with the general laws of the flow of a liquid and with the application of aerodynamics in rocketry and modern aviation. The book is in two part, each forming a separate volume. The first concerns the fundamental concepts and definitions of aerodynamics and the theory of flow over an air-foil or a wing, The second part is devoted the aerodynamic design of craft and their individual parts, taking particular account of interference between them, Considerable space is devoted to matters associated with determination of aerodynamic coefficients and their derivatives (the stability derivative) in unsteady flow.

An important space is allocated to a treatment of the applied problems of modern high-speed aerodynamics. Particularly, supersonic flow over a cone is considered with a view to the influence of chemical transformations in the air (dissociation). The topics covered in the second part include the motion of a gas in the boundary layer, the calculation of friction and heat transfer, ablation, and also force and thermal action in conditions of the motion of bodies in a rarefied fluid. The two parts are designed for a two-semester course in aerodynamics, although the first part can be used independently by those interested in individual area theoretical aerodynamics

The book is the result of the author's experience of teaching aerodynamics at the N.E. Baumen Higher Engineering College in Moscow, USSR, Intended for college and junior-college students, it will also be a useful aid to engineers in research institutions, design departments, and industrial enterprises.

Nikolai F. Krasnov, D.Sc. (Engineering), is a professor and the head of the Department of Aerodynamics at the N.E. Bauman Higher Engineering College (Moscow, USSR). He graduated from the college in 1946 and completed a postgraduate course, receiving a Candidate's degree in 1950. Starting work at the college as a senior instructor, he was appointed an associate professor in 1952, and after receiving his Doctor's degree in 1960, became a full professor. In addition to teaching at the college, he worked for many years at a research institute.

Nikolai Krasnov is an outstanding scientist in the field of aerodynamics. His numerous monographs have gained deserved popularity and have become reference works for college instructors and engineers at aerodynamic laboratories, research institutions, and design offices. He has published important results on determining the velocity and pressure distribution in supersonic flows around axisymmetric bodies, a method for calculating the flow over bodies in a non-linear formulation based on the method of local conical flow, relations for calculating the base drag at subsonic and supersonic velocities, and the aerodynamic characteristics of elongated bodies of revolution at hypersonic velocities. He has also dealt with non-stationary supersonic flow over slender bodies, laminar-turbulent transition, and skin friction and heat transfer on blunt curved surfaces. His monographs include *Rocket Aerodynamics, Applied Aerodynamics, Fundamentals of Aerodynamic Calculations* (in Russian), and *Aerodynamics of Bodies of Revolution* (translated into English).

Dr. Krasnov has worked particularly on finding engineering methods of calculating aerodynamic parameters. He sas proposed approximating relations for finding a number of aerodynamic parameters of craft elements and also interference characteristics.

His latest interests include aerodynamic control. Some of his results in this field were published in *Control and Stability in Aerodynamics* (in Russian). Nikolai Krasnov received the awarded the USSR State Prize in 1982 for the textbook *Aerodynamics*.

Aero-
dynamics
2

Н. Ф. Краснов

Аэродинамика

Часть 2

Методы аэродинамического расчёта

Издательство
«Высшая школа»
Москва

First published 1985
Revised from the 1980 Russian edition

На английском языке

© Издательство «Высшая школа», 1980
© English translation, Mir Publishers, 1985

Aerodynamics

2

N. F. Krasnov

Methods of Aerodynamic Calculations

Translated from the Russian by G. Leib

Mir Publishers Moscow

Preface

The textbook *Aerodynamics* consists of two parts, each forming a separate volume: *Fundamentals of Theory, Aerodynamics of an Airfoil and a Wing*, and *Methods of Aerodynamic Calculations*. Before beginning the second part, readers should be familiar with the theoretical fundamentals of aerodynamics set out in the first part. Study of the material on applied aerodynamics, i.e. on the determination of aerodynamic characteristics, will help students master aerodynamic theory because according to didactic principles, scientific information is best assimilated when used actively to solve practical problems. Such an approach relies on the information stored in the researcher's memory and on a comprehensive understanding of the logical relations that exist between individual elements.

Mastery of the methods of aerodynamic calculations is important as an introduction to problems involving the relations between the theory and the practical solution of specific problems. Study of these methods will also acquaint the reader with new phenomena inherent in the processes of flow over bodies.

For the most complete and systematic presentation of applied problems of aerodynamics, academic courses should first treat the aerodynamics of airfoils and isolated wings [lifting, control, and stabilizing surfaces (Chaps. 6-9 of Part 1)]. The aerodynamics of bodies of revolution should be studied next and followed by a discussion of various combinations of wings, empennage, control surfaces, and bodies of revolution with account taken of the interference between them (Chaps. 10-12 of Part 2). Section 11.6 considers unsteady flow over bodies of revolution, which is one of the main elements in the design of modern high-speed craft. The section includes a solution to a problem of practical significance: the calculation of stability derivatives for conditions of slender body oscillations at low frequencies.

Special attention is given to the development of methods for calculating the aerodynamic characteristics of craft, particularly to the definition of the concepts of aerodynamic interference underlying these methods. An important section deals with the calculation of aerodynamic drag with account taken of interference. Considerable space in Part 2 is devoted to the determination of aerodynamic coefficients and their derivatives (stability derivatives) for unsteady flow. A special section deals with the non-stationary characteristics of craft that combine thin bodies of revolution (fuselages) and wings. The section presents a numerical method for determining stability derivatives at subsonic velocities. It also considers ways to approximate these derivatives using interference corrections and corresponding values of the derivatives for separate wings and bodies of revolution.

An important place in the book is allocated to applied modern high-speed aerodynamics. Supersonic flow over a cone, for example, is considered in rela-

tion to the influence of physicochemical transformations in the air (dissociation). Among the problems of this kind reflected in the second part of the book (Chaps. 13-15) are the flow of a gas in the boundary layer, the calculation of skin friction and heat transfer, ablation, and force and thermal action during the motion of bodies in a rarefied fluid. The important theoretical and practical questions of heat protection are too specific for detailed treatment here, and students may want to consult other sources for more information on these topics.

An appreciable part of the book is devoted to the stability of craft. A section deals specifically with the influence of the planform and Mach number on the aerodynamic characteristics of a swept wing and its static stability in rolling. Information is also given on the role of aerodynamic interference in producing a rolling moment.

Modern aerodynamics is characterized by two approaches to applied engineering problems. Firstly, general flow equations can be compiled and solved with the aid of computers. This approach is suitable when a model has been chosen in advance that includes multivariant initial conditions and provides for a large volume of calculations. The flow over bodies can also be studied analytically by posing theoretical problems, formulating their correct physical and mathematical statements, and creating new ways of solving the problems. Such analytical solutions, which are extremely useful to engineers if properly applied, are discussed in great detail in the textbook.

In performing aerodynamic calculations, it is important to find solutions in the dimensionless form. When conditions are similar aerodynamically, such solutions may then be extended from model to natural phenomena associated with the flow over craft and the flow of a gas in general. Dimensionless solutions are important even when conditions are dissimilar aerodynamically, however. By solving a definite problem, which may have no analogue, in the dimensionless form, we find the required parameters that determine the process and relate to the characteristic gasdynamic quantities known for such a process. For example, instead of calculating the absolute pressures, densities, or temperatures, we calculate their values related to the corresponding stagnation quantities. This aids in problem solving and reliable estimation of the values of the gasdynamic parameters being sought.

Naturally, the sections on applied aerodynamics in the second part of the textbook are not a complete treatment of the methodology of aerodynamic calculations. The material included, however, is a useful introduction to the principles of aerodynamic research. Part 2 should assist readers in developing the skills needed to formulate and solve aerodynamic problems that may arise in their future research.

Nikolai F. Krasnov

Contents

Preface

Chapter 10
A Cone in a Supersonic Flow

10.1. System of Equations for Axisymmetric Flow over a Sharp-Nosed Cone 12
10.2. Flow over a Cone at Constant Specific Heats 14
10.3. Influence of Equilibrium Dissociation and Ionization of a Gas on the Flow over a Cone 24
10.4. Blunt-Nosed Cone 30
Shape of Blunt Noses 30
Features of Supersonic Flow 32
Flow over a Cone with a Spherical Nose 35
Flow over a Flat Nose 57
Drag of a Slender Cone with Slight Blunting 58

Chapter 11
A Sharp-Nosed Body of Revolution in a Supersonic Flow

11.1 Use of the Method of Characteristics 61
11.2. Linearization of Equations for the Flow over Slender Bodies of Revolution 75
11.3. Calculation of Axisymmetric Flow 81
11.4. Non-Axisymmetric Flow 93
11.5. Calculation of Aerodynamic Coefficients 99
Axial Force Coefficient 99
Coefficients of Normal Force and Pitching Moment 100
Aerodynamic Coefficients in a Linearized Flow 102
Results of the Aerodynamic Theory of a Slender Body 107
Suction Force 110
11.6. Unsteady Flow over a Body of Revolution 111

General Relations 111
Boundary Conditions 116
Aerodynamic Characteristics in Conditions of Low-Frequency Oscillations 118
Analysis of the Change in the Aerodynamic Coefficients 123

Chapter 12
Aerodynamic Interference

12.1. Nature of Aerodynamic Interference 128
Wing-Body Interference 128
Wing-Empennage Interference 130
12.2. Normal Force of a Body-Flat Wing Combination 132
Interference Factors 132
Determination of the Velocity Potential 134
Velocity and Pressure on a Body in the Presence of a Wing 137
Velocity and Pressure on a Wing in the Presence of a Body 140
Determination of Interference Factors 143
Centre of Pressure 148
Change in the Interference Factors under Varying Influence 151
Normal Force of Body-Wing Combination 153
12.3. Influence of the Rolling Angle on Body-Flat Wing Interference 154
General Relation for the Pressure Coefficient 154
Pressure on a Body 157
Pressure on a Wing 159
Normal Force and Centre of Pressure 160
General Relations for the Forces and Moments of a Flat Combination in Rolling 164
12.4. Cruciform Combination 166
Pressure and Normal Force 166
Interference Factors and Centre-of-Pressure Coefficients 170
General Relations for the Forces and Moments 171
Influence of Compressibility on Aerodynamic Interference 173
Influence of Flow Stagnation 178
12.5. Influence of Wing Shape and Number M_∞ on the Flow Parameters in Roll 180
Normal Force 180
Moment 182
Wing-Body Interference 183
Influence of V-Shape 183
Asymmetric Vertical Wing (Empennage) 185

Influences of Vortices Forming on a Body 185
Total Rolling Moment 186
12.6. Wing-Empennage Interference 187
General 187
Subsonic Velocities 189
Supersonic Velocities 190
Interference Factor
Influence of the Angle of Attack and Shocks on the Empennage Effectiveness 204
Influence of Flow Stagnation 205
Aerodynamic Characteristics 206
Rolling Moment of a Tail Unit 207
12.7. Controls 208
Basic Kinds of Controls 208
Controllability 212
Aerodynamic Calculations of Control Surfaces 213
12.8. Aerodynamic Drag 224
Drag in the Absence of a Lift Force ($c_{y_a} = 0$) 224
Induced Drag 229
12.9. Non-Stationary Characteristics of a Craft 231
Numerical Method of Determining the Stability Derivatives at Subsonic Velocities 231
Pitch Damping 232
Yawing Moment 234
Roll Damping 235
Application of the Results of Calculating the Wing and Body Derivatives 239
Rotary Derivatives of a Craft 243

Chapter 13
Friction

13.1. Boundary Layer Equation 245
13.2. Generalized Boundary Layer Equation 251
Differential Form of the Equation 251
Integral Relation for a Boundary Layer 253
Conditional Thickness of the Boundary Layer 255
13.3. Laminar Boundary Layer on a Flat Plate 257
13.4. Turbulent Boundary Layer on a Flat Plate 265
Use of a Logarithmic Velocity Distribution Law 265
Power Law of Velocity Distribution 273
13.5. Temperature and Enthalpy in a Boundary Layer with Heat Transfer 277
Distribution of the Temperature and Enthalpy 277

Reference Temperature 282
13.6. Use of the Reference Parameters for Calculating the Boundary Layer on a Flat Plate at High Flow Velocities 285
Laminar Boundary Layer 285
Turbulent Boundary Layer 288
Skin Friction on a Cone in Supersonic Flow 290
13.7. Influence of Longitudinal Pressure Gradient on Friction 295
Boundary Layer on a Curved Surface 295
Calculation of Laminar Boundary Layer 297
Influence of Boundary Layer Separation on the Aerodynamic Characteristics 299
Boundary Layer Control (BLC) 304
13.8. Mixed Boundary Layer. Critical Reynolds Number 307

Chapter 14
Heat Transfer

14.1. Aerodynamic Heating 318
Heat Balance Equation 318
Heat Transfer from a Heated Gas 319
Solar and Terrestrial Radiations. Radiant Flux from a Wall Surface 328
14.2. Relation Between Skin Friction and Heat Transfer 331
14.3. Heat Transfer in a Laminar Boundary Layer on a Curved Surface 338
Arbitrary Surface Shape 338
Hemisphere 349
Blunt-Nosed Cone 351
Flat Nose 354
Calculation of Heat Transfer in a Turbulent Boundary Layer 355
14.4. Diffusion Heat Transfer 356
14.5. Determination of Wall Temperature 363
Equilibrium Emission Temperature 363
Equilibrium Temperature when Additional Heat Sources or Sinks are Present 367

Chapter 15
Aerodynamics of Rarefied Gases

15.1. Limits of Validity of the Continuum Flow Theory 369
Mean Free Path of Molecules 369
Conditions of Gas Flow 370
15.2. Pressure and Skin Friction in a Free-Molecule Flow 374
Molecule-Wall Interaction 374
Mass Transfer 375
Pressure 382
Shear Stress 385
Transfer of Kinetic Energy 387
15.3. Accommodation 388
Momentum Exchange 388

Energy Exchange 391
15.4. Aerodynamic Forces 392
General Expression for the Drag Force 392
Cone 395
Cylinder 399
Plate 401
15.5. Heat Transfer 404
Temperature of Reflected Molecules 404
Calculation of Heat Transfer and Wall Temperature 407

References 411

Supplementary Reading 412

Name Index 414
Subject Index 416

10

A Cone in a Supersonic Flow

10.1. System of Equations for Axisymmetric Flow over a Sharp-Nosed Cone

The problem of the flow over a sharp-nosed cone is one of the most important ones in aerodynamics. Its solution is of a major practical significance because it allows one to calculate the aerodynamic characteristics of craft or their elements having a conical shape, and, furthermore, to use the results of the solution for calculating a supersonic flow about sharp-nosed bodies of revolution. For example, this solution yields the initial point on the curve of flow parameter distribution for a sharp-nosed curved body. In addition, the model of axisymmetric flow over cones is used for an approximate calculation of the distribution of the parameters of a gas over the periphery surface of bodies of revolution (the method of "local cones"). The same results are used as comparative ones when investigating the aerodynamics of blunt-nosed cones.

A number of approximations for the simplified calculation of the flow over a cone have been developed in theoretical aerodynamics in addition to the exact solutions. Some of them relate to slender cones in a linearized flow or in a flow with very large numbers **M**. The exact solution may be applied to cones of any angle in flows of any velocity. The main condition that must be fulfilled here is associated with the retaining of a **conical flow** near the body. A conical flow is one whose parameters remain constant along straight lines issuing from the apex of a cone in an inviscid flow. The results obtained are also used, however, when studying viscous flow. The inviscid properties such as the pressure, velocity, and density, are treated as the parameters on the edge of the boundary layer formed on the cone, and are factors determining the skin friction and heat transfer from the gas to the wall.

Let us imagine a cone with a semi-apex angle β_c in an axisymmetric supersonic flow. Our task is to calculate the flow of a gas between this cone and a conical shock wave ahead of it. It is also necessary to determine the angle θ_s of the linear generatrix of the

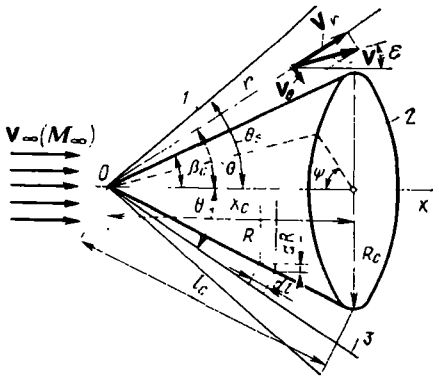

Fig. 10.1.1
Velocity components on an intermediate conical surface:
1—shock; *2*—cone inflow; *3*—intermediate conical surface

conical shock (Fig. 10.1.1). To do this, we shall consider a system of equations in spherical coordinates (θ, r, ψ) as applied to a case of flow when the gas behind the shock experiences physicochemical transformations under the influence of a high temperature. We shall assume further that **thermodynamic equilibrium** is established in the disturbed region.

The solution being sought for a cone must correspond to an axisymmetric conical field of a disturbed flow in which the gas parameters remain constant along straight lines that issue from the apex and are generatrices of the intermediate conical surfaces (including the conical surfaces with the semi-apex angles $\theta = \theta_s$ and $\theta = \beta_c$)

In view of the indicated property of the solution being sought, any partial derivative of the gas parameters with respect to the spherical coordinate r (Fig. 10.1.1) equals zero. Accordingly, continuity equation (2.4.37)*, in which we must take the partial derivatives with respect to r and ψ (two-dimensional flow) equal to zero, has the form

$$2\rho V_r + V_\theta \, d\rho/d\theta + \rho \, dV_\theta/d\theta + \rho V_\theta \cot\theta = 0 \qquad (10.1.1)$$

The equations of two-dimensional flow near a cone obtained from system (3.1.45) in which the terms characterizing the viscosity are taken equal to zero, as well as the partial derivatives with respect to t and r, can be written as

$$dV_r/d\theta = V_\theta \qquad (10.1.2)$$

$$\rho V_\theta \, dV_\theta/d\theta + \rho V_r V_\theta + dp/d\theta = 0 \qquad (10.1.3)$$

In accordance with the number of parameters being determined, we shall add the following equation to these relations:

$$\frac{p}{p_s} = \frac{m_s}{m} \frac{\rho}{\rho_s} \frac{T}{T_s} \qquad (10.1.4)$$

* Please do not forget that Chapters 1-9 are in Part 1 (Vol. 1) of the book.

It has been obtained from equation of state (1.5.8) for a gas at an arbitrary point of a flow and from the equation of state $p_s = \rho_s T_s R_0/m_0$ related to the conditions directly behind the shock (the subscript "s"). The system being considered must also include the energy equations (3.4.14)

$$i + V^2/2 = i_s + V_s^2/2 \tag{10.1.5}$$

and general relations of the type of (4.2.8)-(4.2.11) for calculating the enthalpy, entropy, mean molar mass, and the speed of sound:

$$i = f_1(p, T) \tag{10.1.6}$$

$$S = f_2(p, T) \tag{10.1.7}$$

$$m = f_3(p, T) \tag{10.1.8}$$

$$a = f_4(p, T) \tag{10.1.9}$$

The system can be used in this form for studying the flow of a dissociating gas over a cone. In the particular case of the absence of dissociation, this system is simplified. If we assume that in the disturbed region between the shock and the cone surface the specific heats and the mean molar mass of the gas remain the same as in the undisturbed flow, while the speed of sound and enthalpy depend only on the temperature, then instead of Eqs. (10.1.6)-(10.1.9) we must use relations (4.3.1)-(4.3.4) written in the following form:

$$i = c_p T = \frac{c_p p}{R\rho} = \frac{k}{k-1} \cdot \frac{p}{\rho} \tag{10.1.10}$$

$$S = c_v \ln \frac{T}{\rho^{k-1}} + C_1 = c_v \ln \frac{p}{\rho^k} + C_2 \tag{10.1.11}$$

$$m = \text{const} \tag{10.1.12}$$

$$a^2 = kRT = kp/\rho \tag{10.1.13}$$

Equations (10.1.1)-(10.1.3) remain unchanged.

10.2. Flow over a Cone at Constant Specific Heats

Results of an important practical significance have been obtained for a flow over a cone for constant specific heats. They can also be used for approximate estimates of several parameters (for example, pressure) when the flow is attended by considerable heating that produces physicochemical transformations and, consequently, a change in the specific heats.

To solve the problem, we shall use Eqs. (10.1.1)-(10.1.3) and (10.1.10)-(10.1.13). It is more convenient to use Eq. (10.1.3) if some transformations are performed. For this purpose, we shall use the

expression $a^2 = dp/d\rho$ for the speed of sound written in the form

$$dp/d\theta = a^2 \, d\rho/d\theta \qquad (10.2.1)$$

After introducing the values of $dp/d\theta$ from (10.2.1) into (10.1.3), we obtain

$$\rho V_\theta \, dV_\theta/d\theta + \rho V_r V_\theta + a^2 \, d\rho/d\theta = 0$$

Inserting here the value of the derivative $d\rho/d\theta$ evaluated by (10.1.1), we find the transformed equation

$$dV_\theta/d\theta = [-V_\theta \cot \theta + V_r \, (V_\theta^2/a^2 - 2)] \, (1 - V_\theta^2/a^2)^{-1} \qquad (10.2.2)$$

The square of the speed of sound in this equation by (3.6.21) is

$$a^2 = \frac{k+1}{2} a^{*2} - \frac{k-1}{2} (V_r^2 + V_\theta^2) \qquad (10.2.3)$$

We see from the system of equations (10.1.2) and (10.2.3) that the problem of the flow over a cone has been reduced to a kinematic problem associated with determination of the velocity field in the disturbed flow near the cone, i.e. with finding of the functions $V_r(\theta)$ and $V_\theta(\theta)$ for the velocity components, or the function $V(\theta) = \sqrt{V_r^2 + V_\theta^2}$ for the total velocity. Using the calculated total velocity and formulas (10.1.4), (10.1.5), (10.1.10), and (10.1.11), we can determine the pressure, density, temperature, enthalpy, and entropy of the gas. We can use relations (3.6.26), (3.6.31), and (3 6.33) instead of the indicated formulas to determine the pressure, density, and temperature, respectively.

The boundary conditions at which numerical integration of the differential equations (10.1.2) and (10.2.2) is performed are determined by the conditions of flow of the gas on the cone, and also by the conditions characterizing the gas parameters directly behind the shock.

The boundary condition of flow over the cone consists in that the velocity component normal to its surface is zero, i.e.

$$V_\theta = 0 \quad \text{when} \quad \theta = \beta_c \qquad (10.2.4)$$

We have two conditions for the shock. We obtain the first of them taking the tangential velocity components ahead of the shock equal to those behind it, i.e. $V_{r,\infty} = V_{s,r}$ (Fig. 10.2.1). Accordingly,

$$V_{s,r} = V_\infty \cos \theta_s \qquad (10.2.5)$$

Using this equation, we can obtain the second condition. To do this, let us compile an expression for the horizontal velocity component u_s of the gas on the shock (Fig. 10.2.1):

$$u_s = V_{s,r} \cos \theta_s - V_{s,\theta} \sin \theta_s$$

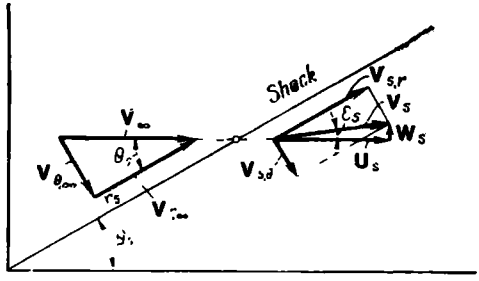

Fig. 10.2.1
Triangles of velocities ahead of a shock and directly behind it with supersonic flow over a cone

Multiplying both sides of this expression by $V_{s,r}$ and having in view (10.2.5), we obtain

$$u_s V_\infty = V_{s,r}\,(V_{s,r} - V_{s,\theta}\,\tan\theta_s) \qquad (10.2.6)$$

where $V_{s,r}$ and $V_{s,\theta}$ are the tangential and normal velocity components on the shock, respectively.

We shall now use Eq. (4.4.4) of a shock polar (hodograph) and write it in the form

$$\frac{w_s^2}{(V_\infty - u_s)^2} = \frac{(V_\infty u_s - a^{*2})\,(k+1)}{2V_\infty^2 + (k+1)\,(a^{*2} - V_\infty u_s)}$$

where w_s is the vertical component of the velocity of the shock.

Using (4.4.3), we have

$$-\tan^2\theta_s = \frac{2}{k+1}\cdot\frac{V_\infty^2}{a^{*2} - V_\infty u_s} + 1$$

Taking into account that $\tan^2\theta_s = \cos^{-2}\theta_s - 1$, while the value of $V_\infty u_s$ is determined from (10.2.6), we find

$$-\frac{1}{\cos^2\theta_s} = \frac{2}{k+1}\,\frac{V_\infty^2}{a^{*2} - V_{s,r}^2 + V_{s,\theta}V_{s,r}\tan\theta}$$

Having in view (10.2.5), we obtain the boundary condition on the shock:

$$\tan\theta_s = \frac{1}{V_{s,r}V_{s,\theta}}\left(\frac{k-1}{k+1}V_{s,r}^2 - a^{*2}\right) \qquad (10.2.7)$$

The system of equations (10.1.2), (10.2.2), and (10.2.3) is integrated by a numerical method. The magnitude of the shock angle θ_s and the free-stream velocity V_∞ are usually considered to be set. The solution of the equations is aimed at determining the velocity field and finding the corresponding semi-apex angle β_c of the cone and the velocity $V_r = V_c$ on it.

Let us consider how the problem is solved. We use the given values of θ_s and V_∞ to find the radial velocity component from (10.2.5):

$$V_{r,\infty} = V_{s,r} = V_\infty \cos\theta_s \qquad (10.2.8)$$

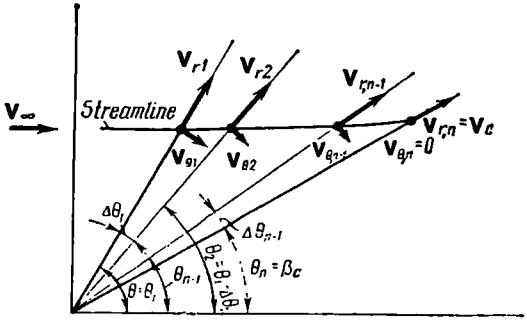

Fig. 10.2.2
To the calculation of the flow over a cone

We shall designate this velocity, which is identical for the conditions both ahead of the shock and directly behind it, by $V_{r1} = V_\infty \cos\theta_1$, where $\theta_1 = \theta_s$. Using this value of $V_{s,r} = V_{r1}$, by (10.2.7) we calculate the normal velocity component $V_{s,\theta} = V_{\theta 1}$ behind the shock:

$$V_{\theta 1} = \frac{1}{V_\infty \sin\theta_1}\left(\frac{k-1}{k+1}V_{r1}^2 - a^{*2}\right) \qquad (10.2.9)$$

Let us consider an intermediate conical surface near the shock with an inclination of its generatrix of $\theta_1 - \Delta\theta_1$, where $\Delta\theta_1$ is a small increment of the angle θ (Fig. 10.2.2).

The radial velocity component V_{r2} on this surface can be calculated by Eq. (10.1.2) written as a difference one:

$$V_r - V_{r1} = V_{\theta 1}\,\Delta\theta \qquad (10.2.10)$$

Assuming here that $V_r = V_{r2}$ and $\Delta\theta = \Delta\theta_1 = \theta_1 - \theta_2$, we obtain

$$V_{r2} = V_{r1} + V_{\theta 1}\,\Delta\theta_1 \qquad (10.2.10')$$

We determine the normal component $V_{\theta 2}$ from Eq. (10.2.2), also written as a difference one:

$$V_\theta - V_{\theta 1} = (dV_\theta/d\theta)_1\,\Delta\theta \qquad (10.2.11)$$

Assuming that $V_\theta = V_{\theta 2}$ and $\Delta\theta = \Delta\theta_1$, we find

$$V_{\theta 2} = V_{\theta 1} + (dV_\theta/d\theta)_1\,\Delta\theta_1 \qquad (10.2.11')$$

where the derivative $(dV_\theta/d\theta)_1$ is evaluated from (10.2.2) according to the parameters on the shock:

$$\left(\frac{dV_\theta}{d\theta}\right)_1 = \left[-V_{\theta 1}\cot\theta_1 + V_{r1}\left(\frac{V_{\theta 1}^2}{a_1^2} - 2\right)\right]\left(1 - \frac{V_{\theta 1}^2}{a_1^2}\right)^{-1} \qquad (10.2.12)$$

where by (10.2.3)

$$a_1^2 = a_s^2 = \frac{k+1}{2}a^{*2} - \frac{k-1}{2}(V_{r1}^2 + V_{\theta 1}^2) \qquad (10.2.13)$$

Taking as the initial quantities the obtained values of V_{r2}, $V_{\theta 2}$, and also the value of a_2^2 determined by (10.2.3) in the form

$$a_2 = \frac{k+1}{2} a^{*2} - \frac{k-1}{2} (V_{r2}^2 + V_{\theta 2}^2)$$

we can find in a similar way the parameters V_{r3}, $V_{\theta 3}$, and a_3 on the following intermediate surface with an angle of inclination of the generatrix of

$$\theta_3 = \theta_2 - \Delta\theta_2 = \theta_1 - \sum_1^{i=2} \Delta\theta_i$$

For an arbitrary conical surface with a generatrix angle of

$$\theta_m = \theta_1 - \sum_1^{i=m-1} \Delta\theta_i \qquad (10.2.14)$$

the velocity components are calculated by the formulas

$$V_{r,m} = V_{r,m-1} + V_{\theta,m-1}\, \Delta\theta_{m-1} \qquad (10.2.15)$$

$$V_{\theta,m} = V_{\theta,m-1} + (dV_\theta/d\theta)_{m-1}\, \Delta_{m-1} \qquad (10.2.16)$$

where the derivative $(dV_\theta/d\theta)_{m-1}$ is found from (10.2.2) according to the parameters $V_{\theta,m-1}$, $V_{r,m-1}$, a_{m-1}, and $\theta_{m-1} = \theta_{m-2} - \Delta\theta_{m-2}$. The calculations are terminated when a certain value of the angle of the intermediate cone (Fig. 10.2.2) is reached:

$$\theta_n = \theta_{n-1} - \Delta\theta_{n-1} = \theta_1 - \sum_1^{i=n-1} \Delta\theta_i \qquad (10.2.17)$$

and the normal velocity component becomes equal to zero, i.e.

$$V_{\theta,n} = V_{\theta,n-1} + (dV_\theta/d\theta)_{n-1}\, \Delta\theta_{n-1} = 0 \qquad (10.2.18)$$

Here the derivative $(dV_\theta/d\theta)_{n-1}$ is found from (10.2.2) according to the values of $V_{\theta,n-1}$, $V_{r,n-1}$, and a_{n-1} on the neighbouring intermediate conical surface with a generatrix angle of

$$\theta_{n-1} = \theta_1 - \sum_1^{i=n-2} \Delta\theta_i \qquad (10.2.19)$$

In the process of calculations, as a rule, we do not succeed in choosing such a small angle $\Delta\theta_{n-1}$ in the very first approximation so that the equality $V_{\theta,n} = 0$ will be satisfied. Usually a calculated value of $V_{\theta,n}$ that reverses its sign in comparison with that of $V_{\theta,n}$ on the neighbouring surface with a generatrix angle of θ_{n-1} corresponds to the chosen value of $\Delta\theta_{n-1}$. This indicates that an increment of the angle $\Delta\theta_{n-1}$ smaller than the chosen one corresponds to the value of $V_{\theta,n} = 0$. To determine this increment, we have to perform inter-

polation using the equation

$$\Delta\theta_{n-1} = -V_{\theta,n-1}\,(dV_\theta/d\theta)^{-1}_{n-1} \qquad (10.2.18')$$

We use the value of $\Delta\theta_{n-1}$ to evaluate the velocity on the cone:

$$V_{r,c} = V_c = V_{r,n-1} + V_{\theta,n-1}\,\Delta\theta_{n-1} \qquad (10.2.20)$$

and the angle

$$\theta_n = \beta_c = \theta_1 - \sum_{1}^{i=n-1} \Delta\theta_i \qquad (10.2.21)$$

Similar calculations can be performed in the reverse sequence, by setting the conditions on the cone. We also have to know the angle β_c and the velocity V_c on the cone. Numerical integration is completed when the boundary conditions (10.2.5) and (10.2.7) are satisfied. As a result, we find the parameters of the gas in the disturbed region, and also the shock angle ahead of the cone, as well as the free-stream velocity (Mach number).

Each operation of numerical integration, with the values of θ_s and V_∞ given (or β_c and V_c), allows one to determine the velocity field, i.e. the function $V = V(\theta)$, where $V = \sqrt{V_r^2 + V_\theta^2}$, and to establish the correspondence between a given semi-apex angle β_c and the velocity V_c on it, on the one hand, and between the shock angle θ_s and the velocity V_∞, on the other.

By repeating the calculations at various given angles θ_s and a fixed value of the velocity V_∞, we can find relations of the form $\beta_c = \beta_c(\theta_s)$, $V_c = V_c(\beta_c)$, or $V_c = V_c(\theta_s)$. The results obtained can be presented graphically in the plane of the hodograph w, u in the form of what we call an **apple curve** (Fig. 10.2.3*a*). This curve is the locus of the tips of the velocity vectors $\mathbf{V}_c$ of the disturbed flow directly on the cone. Point A on the apple curve and belonging to the tip of the velocity vector corresponds to a cone with a given semi-apex angle β_c; point B on the shock polar coincides with the tip of the velocity vector $\mathbf{V}_{s,r}$ on the corresponding shock with the angle θ_s.

Curve AB is a **hodograph**, i.e. the locus of the tips of the velocity vectors in the disturbed region of the flow between the cone and the shock. The following must be done when constructing the hodograph. We use the velocity triangle in Fig. 10.1.1 to determine the velocity components for an intermediate conical surface:

$$V_r = V\cos(\theta - \varepsilon); \quad V_\theta = -V\sin(\theta - \varepsilon) \qquad (10.2.22)$$

When integrating numerically, we use the found values of V_r and V_θ for the given angles θ to determine the relation

$$V_r/V_\theta = -\cot(\theta - \varepsilon) \qquad (10.2.23)$$

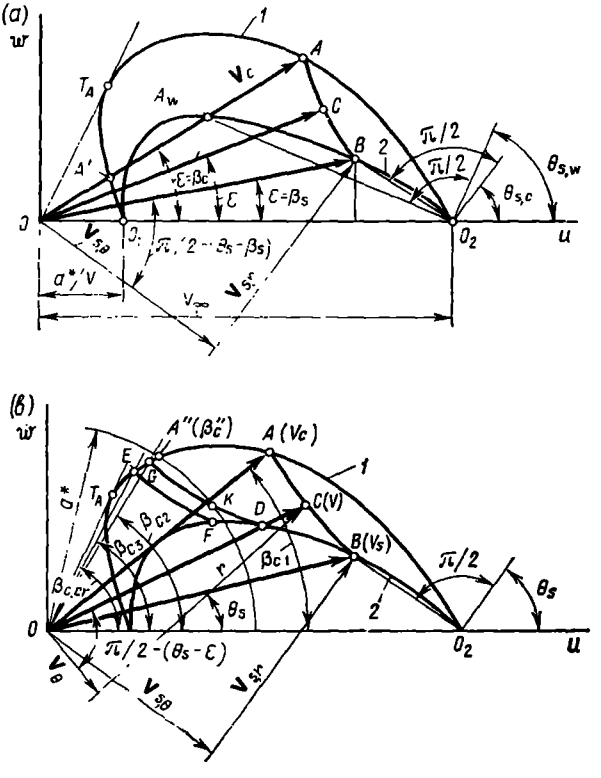

Fig. 10.2.3
Apple curve (1) and shock polar (2)

according to which we evaluate the angle ε of inclination of the velocity vector **V** to the cone axis. The polar coordinates V and ε determine the position of the points on the hodograph (see point C in Fig. 10.2.3*a*).

The described graphical method of solving the problem on the supersonic flow over a circular cone was proposed by A. Busemann.

With the aid of an apple curve and a family of hodographs, we can graphically explain the physical nature of a supersonic gas flow over a cone. Gradual isentropic compression of the gas occurs along the streamlines in the region between the shock and the cone. In Fig. 10.2.3*a*, displacement from point B on the shock polar along the hodograph to point A on the apple curve corresponds to this. The streamlines, as can be seen from Fig. 10.2.2, gradually curve and approach the surface of the cone, adopting the direction of the generatrix.

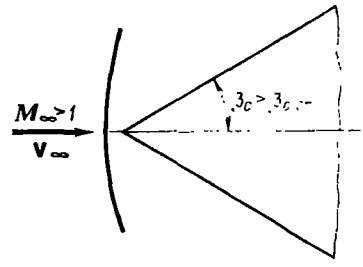

Fig. 10.2.4
Supercritical flow over a cone

Let us draw an arc of radius a^* with point O as its centre (Fig. 10.2.3*b*). If hodograph AB for the given angle β_{c1} of the cone is to the right of the arc, then isentropic compression behind the shock wave occurs at supersonic velocities. For a certain cone angle $\beta_{c2} > \beta_{c1}$, part GK of the hodograph may be to the left of the arc, and part KD to the right of it. Hence, the disturbed flow is **mixed.** In the region adjoining the shock, it is supersonic, and near the cone surface, it is subsonic. For a larger angle $\beta_{c3} > \beta_{c2}$, hodograph EF is to the left of arc a^*, and, consequently, the disturbed flow is **completely subsonic.**

An analysis of the apple curve reveals that two solutions (see points A and A' of intersection of straight line AO and the apple curve) correspond theoretically to each cone angle β_c. One solution yields a lower velocity and a larger shock angle, and the other, a higher velocity and a smaller shock angle. Experimental investigations show that the second solution corresponding to a stable flow behind the shock is suitable.

We can indicate point T_A at which a ray from the origin of coordinates is tangent to the apple curve. This point corresponds theoretically to a unique solution and determines the **critical cone angle** $\beta_{c,cr}$. If the actual cone angle is larger than the critical one, this curve cannot be used formally to study the flow over the cone. In real conditions, the shock detaches from the tip and becomes curved (Fig. 10.2.4). Such a flow is called **supercritical**. It is not difficult to note that the critical angle is a function of only the free-stream velocity (or, correspondingly, of the number $M_\infty = V_\infty/a_\infty$ or the speed ratio $\lambda_\infty = V_\infty/a^*$).

According to experimental data, the shock moves away from the tip at angles β_c somewhat larger than those determined by the exact theory of flow over a cone. For example, it has been found experimentally for the number $M_\infty = 2.45$ that the shock moves away at an angle of $\beta_c = 46°$, whereas the theoretically calculated value is $\beta_c = 45°46'$.

Experimental investigations show that a conical flow corresponding to a constant velocity on the cone is retained until the speed of sound

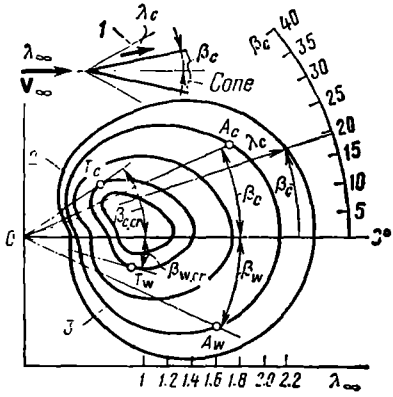

Fig. 10.2.5
Family of apple curves and shock polars:
1—shock; *2*—family of apple curves; *3*—family of shock polars

is reached on its surface. The corresponding cone angle β_c'' can be determined from point A'' of intersection of an arc of radius a^* and the apple curve (see Fig. 10.2.3*b*). Consequently, in practice, the apple curve may be used in calculating the flow over the entire conical surface for angles of $\beta_c \leqslant \beta_c''$. The velocity at the cone tip found with the aid of the conical theory (using the apple curve) agrees with experimental data for all values of the angles $\beta_c \leqslant \beta_{c.cr}$, i.e. for the conditions of flow in which the shock still remains attached.

The apple curve shows how the velocity V_c on the cone and the shock angle θ_s depend on the cone angle β_c at a given free-stream velocity V_∞ (at given values of M_∞ or λ_∞). To obtain such a relation for a different velocity V_∞ (M_∞ or λ_∞), it is necessary to perform numerical calculations of the flow over the cone and construct the relevant apple curve for the new conditions of flow. A family of such curves shows how the velocity on the cone and the shock angle depend on the cone angle β_c and the velocity V_∞ (M_∞ or λ_∞). Figure 10.2.5 shows a family of apple curves constructed for various values of the speed ratio $\lambda_\infty = V_\infty/a^*$. This figure also contains the corresponding shock polars, which allows us to compare the flow over a wedge with the same semi-apex angle β_c as the cone.

A close look at Fig. 10.2.5 reveals that the velocity on the cone is higher than on the wedge ($\overline{OA}_c > \overline{OA}_w$). For a wedge, the flow on an oblique shock turns through the wedge angle $\beta_s = \beta_w$, whereas for a cone, the flow on the shock occurs at a smaller angle $\beta_s < \beta_c$. Consequently, the angle $\theta_{s,w}$ of inclination of the leading shock wave ahead of a wedge is larger than the angle $\theta_{s.c}$ ahead of a cone.

The same result can be obtained from Fig. 10.2.3*a*. Let us connect points A_w and B to point O_2 and erect perpendiculars from point O_2 to the straight lines A_wO_2 and BO_2 obtained. The angles between

the perpendiculars and the horizontal axis u determine the slope of the shocks formed ahead of the wedge $\theta_{s,w}$ and the cone $\theta_{s,c}$. A glance at the figure reveals that $\theta_{s,w} > \theta_{s,c}$. In accordance with this result, the angle of inclination of a shock ahead of a cone (the same as ahead of a wedge) behind which the flow turns through the critical angle is reached at a larger semi-apex angle than for the wedge. Hence, the critical angle of a cone is larger than of a wedge with the same semi-apex angle (see also Fig. 10.2.5). The explanation is that unlike the plane flow near a wedge, the flow in the vicinity of a cone is spatial and ensures a smoother change in its direction.

Of importance in calculating the flow over a cone is the determination of the pressure density, and temperature from the found values of V_c and θ_s. Taking into account the isentropic nature behind a shock, we shall use the corresponding relations (3.6.26)-(3.6.33). Having in view that in formula (3.6.33) the temperature T_0 does not change behind a shock and is determined from (3.6.35), we shall find the following formula for the temperature on a cone:

$$\frac{T_c}{T_\infty} = (1 - \bar{V}_c^2)\left(1 + \frac{k-1}{2} M_\infty^2\right) \qquad (10.2.24)$$

where $\bar{V}_c = V_c/V_{max}$.

The stagnation pressure in formula (3.6.26) has to be calculated with a view to the losses in the shock. Designating the value of this pressure by p_0' and introducing the parameter $\nu_0 = p_0'/p_0$ evaluated from the stagnation pressure p_0 ahead of a shock by (3.6.29), we obtain for the pressure on a cone

$$\frac{p_c}{p_\infty} = \nu_0 \left[(1 - \bar{V}_c^2)\left(1 + \frac{k-1}{2} M_\infty^2\right)\right]^{k/(k-1)} \qquad (10.2.25)$$

The parameter $\nu_0 = p_0'/p_0$ is determined depending on the number M_∞ and the angle θ_s ahead of the cone with the aid of (4.3.21) and (4.3.22) as follows:

$$\nu_0 = [(1+\delta) M_\infty^2 \sin^2\theta_s - \delta]^{\frac{\delta-1}{2\delta}} \left[\frac{M_\infty^2 \sin^2\theta_s}{(1-\delta)\left(1 + \frac{\delta}{1-\delta} M_\infty^2 \sin^2\theta_s\right)}\right]^{\frac{1+\delta}{2\delta}} \qquad (10.2.26)$$

We use the equation of state to calculate the density ratio:

$$\rho_c/\rho_\infty = (p_c/p_\infty)\, T_\infty/T_c \qquad (10.2.27)$$

According to the absolute value of p_c, we determine the pressure coefficient on the cone:

$$\bar{p}_c = (p_c - p_\infty)/q_\infty = 2(p_c - p_\infty)/(k M_\infty^2 p_\infty) \qquad (10.2.28)$$

We determine the drag force due to the pressure (the wave drag) with the aid of relation (1.3.2). Assuming that $\bar{p} = \bar{p}_c$, $c_{f,x} = 0$,

$S_r = S_{mid} = \pi R_c^2$, $dS = 2\pi R\, dl$, and $\cos(\widehat{n, x}) = \sin\beta_c$ (see Fig. 10.1.1), we obtain

$$X_w = q_\infty S_{mid} \int_0^{l_c} \bar{p}_c \sin\beta_c \frac{2\pi R\, dl}{\pi R_c^2}$$

Having in view that $dl \sin\beta_c = dR$, we find the following expression for the wave drag coefficient:

$$c_{x,w} = X_w/(q_\infty S_{mid}) = 2\int_0^1 \bar{p}_c \bar{R}\, d\bar{R} \qquad (10.2.29)$$

where $\bar{R} = R/R_c$.

Since the pressure coefficient $\bar{p}_c$ on the cone in supersonic flow is constant, we find the following expression for the wave drag coefficient:

$$c_{x,w} = \bar{p}_c \qquad (10.2.30)$$

Hence, the wave drag coefficient of a cone at axisymmetric supersonic flow equals the pressure coefficient on its surface. As a result of processing the data of the exact theory, we can recommend the following approximate formula for calculating the wave drag coefficient (or the pressure coefficient) in such a flow (see [1]):

$$c_{x,w} = \bar{p}_c = 2 \cdot 10^{-3}(0.8 + M_\infty^{-2})\,\beta_c^{1.7} \qquad (10.2.31)$$

where β_c is the semi-apex angle of the cone, deg.

Calculations by this formula may be performed up to values of $\beta_c \leqslant 50°$ and $M_\infty = 7$-8. The lower limit of the number M_∞ corresponds to the critical value of the cone angle $\beta_{c,cr}$ at which a shock still remains attached. To calculate the shock angle ahead of a sharp-nosed cone, we can use the approximate relation (see [2])

$$M_\infty \sin\theta_s = 1 - \cos\beta_c + \left(1 + \frac{k+1}{2} M_\infty^2 \sin^2\beta_c\right)^{1/2} \qquad (10.2.32)$$

This relation yields satisfactory results at values of β_c and M_∞ such that may be used when calculating by formula (10.2.31). The error grows at high values of β_c and M_∞ when the influence of dissociation becomes significant ($M_\infty > 10$ and $\beta_c > 30$-40°).

10.3. Influence of Equilibrium Dissociation and Ionization of a Gas on the Flow over a Cone

To solve the problem of the flow over a cone with account taken of the influence of equilibrium dissociation and ionization, we shall use a system including differential equations (10.1.2), (10.2.2), equa-

tions of state (10.1.4) and energy (10.1.5), and also the general relations (10.1.6)-(10.1.9) for determining the enthalpy, entropy, mean molar mass, and the speed of sound in the dissociating and ionizing gas. The general scheme of numerical integration of the differential equations is the same as with constant specific heats.

We begin our calculations with determination of the gas parameters behind an oblique shock according to the given angle θ_s. We determine the radial velocity component $V_{s,r}$ by (10.2.8), and the normal component $V_{s,\theta}$ according to the shock theory taking into account dissociation and ionization (see Sec. 4.2). In a first approximation, we assume the value [see (4.2.12)]

$$\Delta\overline{V}_n^{(1)} = (V_{n1} - V_{n2})/V_{n1} = (V_{\theta,\infty} - V_{s,\theta})/V_{\theta,\infty} \qquad (10.3.1)$$

equal to unity, i.e. consider the condition of stagnation behind the shock at which $V_{s,\theta} \approx 0$. We find the pressure corresponding to these conditions by formula (4.2.15). Assuming that $\Delta\overline{V}_n = 1$ and having in view that $M_{n1} = M_\infty \sin\theta_s$, we obtain

$$p_s^{(1)} = (1 + k_1 M_\infty^2 \sin^2\theta_s)\, p_\infty \qquad (10.3.2)$$

By expression (4.2.16), in which we assume that $\Delta\overline{V}_n = 1$ and $V_{n1} = V_\infty \sin\theta_s$, we calculate the enthalpy:

$$i_s^{(1)} = i_\infty + V_\infty^2 \sin^2\theta_s/2 \qquad (10.3.3)$$

We can find the density $\rho_s^{(1)}$ from the values of $p_s^{(1)}$ and $i_s^{(1)}$ by using graphs of the thermodynamic functions of air [3, 4], and then in a second approximation determine the change in the relative velocity by (4.2.21):

$$\Delta\overline{V}_n^{(2)} = 1 - \rho_\infty/\rho_s^{(1)} \qquad (10.3.4)$$

We use this velocity increment to determine more precisely the pressure

$$p_s^{(2)} = p_\infty (1 + k_1 M_\infty^2 \sin^2\theta_s\, \Delta\overline{V}_n^{(2)}) \qquad (10.3.5)$$

and the enthalpy

$$i_s^{(2)} = i_\infty \left[1 + \frac{V_\infty^2 \sin^2\theta_s}{2} \cdot \frac{\Delta\overline{V}_n^2}{i_1} (2 - \Delta\overline{V}_n^{(2)})\right] \qquad (10.3.6)$$

Using graphs of the thermodynamic functions, we find the density $\rho_s^{(2)}$ and determine more precisely the quantity $\Delta\overline{V}_n^{(3)}$:

$$\Delta\overline{V}_n^{(3)} = 1 - \rho_\infty/\rho_s^{(2)} \qquad (10.3.7)$$

If the value of $\Delta\overline{V}_n^{(3)}$ differs only slightly from that of $\Delta\overline{V}_n^{(2)}$, the iteration is terminated and the normal velocity component behind the shock is determined:

$$V_{s,\theta} = V_{\theta 1} = V_{\theta,\infty}(1 - \Delta\overline{V}_n^{(3)}) = V_\infty \sin\theta_s (1 - \Delta\overline{V}_n^{(3)}) \qquad (10.3.8)$$

We can also use the tables contained in [5] for our calculations. From these tables according to the values of $p_s^{(1)}$ and $i_s^{(1)}$ (in these tables the enthalpy is designated by h, m^2/s^2), we can determine the temperature $T_s^{(1)}$ and the mean molar mass of the air $m_s^{(1)}$, and then calculate the density by (4.2.17):

$$\rho_s^{(1)} = \frac{p_s^{(1)}}{p_\infty} \frac{m_s^{(1)}}{m_\infty} \frac{T_\infty}{T_s^{(1)}} \rho_\infty \qquad (10.3.9)$$

where we may assume for undissociated air that $m_\infty = 29$ g/(g·mol).

Next by formulas (10.3.4)-(10.3.6), we evaluate $p_s^{(2)}$ and $i_s^{(2)}$, find $T_s^{(2)}$ and $m_s^{(2)}$ from the corresponding tables, and by expression (10.3.9) determine the quantity

$$\rho_s^{(2)} = \frac{p_s^{(2)}}{p_\infty} \cdot \frac{m_s^{(2)}}{m_\infty} \cdot \frac{T_\infty}{T_s^{(2)}} \rho_\infty \qquad (10.3.9')$$

Introduction of the value of $\rho_s^{(2)}$ into formula (10.3.7) yields $\Delta \overline{V}_n^{(3)}$, while expression (10.3.8) yields $V_{s,\theta} = V_{\theta 1}$.

For the given integration step $\Delta\theta_1$, we calculate V_{r2} and $V_{\theta 2}$ on the neighbouring conical surface by (10.2.10′) and (10.2.11′), respectively. In formula (10.2.11′), we determine the derivative $(dV_\theta/d\theta)_1$ by expression (10.2.12) in which we find the speed of sound a_1 from tables or graphs of thermodynamic functions according to the known values of $p_s^{(2)}$ and $i_s^{(2)}$ (or of $p_s^{(2)}$ and $T_s^{(2)}$).

On the chosen conical surface, we determine the enthalpy by Eq. (10.1.5):

$$i_2 = i_s^{(2)} + [V_{r1}^2 + V_{\theta 1}^2 - (V_{r2}^2 + V_{\theta 2}^2)]/2 \qquad (10.3.10)$$

For further calculations, one should use the value of the entropy of the gas assuming that the disturbed flow behind the shock is isentropic in the entire region, and, therefore, that the entropy is everywhere the same as in the gas flow behind the shock. We determine this entropy $S = S_s = \text{const}$ from tables of the thermodynamic functions according to the values of $p_s^{(2)}$ and $i_s^{(2)}$ (or $p_s^{(2)}$ and $T_s^{(2)}$).

Using the enthalpy i_2 and the entropy S, we can find the speed of sound a_2 from tables or graphs, and by formulas (10.2.10′) and (10.2.11′) calculate the velocity components V_{r3} and $V_{\theta 3}$, respectively, on a conical surface with the angle $\theta = \theta_s - \sum_{i=1}^{2} \Delta\theta_i$. In a similar way, we calculate the flow parameters for neighbouring intermediate conical surfaces. We terminate these calculations when on one of these surfaces the normal velocity component $V_{\theta,n}$ is zero. The corresponding angle (10.2.21) is the semi-apex angle of the cone in the flow, and the velocity is the velocity V_c (10.2.20) on this cone. The corresponding enthalpy is

$$i_c = i_s + (V_s^2 - V_c^2)/2$$

where

$$V_s^2 = V_{\theta 1}^2 + V_{r1}^2 \quad \text{and} \quad i_s = i_s^{(2)}$$

We can determine the temperature T_c, pressure p_c, and density ρ_c on the cone from the enthalpy i_c and entropy $S = S_s$ according to tables and graphs or the relevant formulas.

All the parameters on a cone in a flow with the preset Mach number M_∞ depend not only on the temperature T_∞, which is characteristic for varying specific heats, but also on the free-stream pressure p_∞, on which the degrees of dissociation and ionization depend. With given parameters β_c, M_∞, and T_∞, we can choose the flight altitude H instead of p_∞ as the function determining the change in the parameters of the gas on a conical surface. At given values of T_∞ and M_∞, the flow parameters on a cone are functions of the angle β_c and the altitude H.

Processing of the results of calculating the parameters of the flow over a cone by this method, and also of experimental data, allows us to obtain approximate relations for the pressure coefficient $\bar{p}_c$, the relative density $\bar{\rho} = \rho_\infty/\rho_c$, and the shock angle θ_s (see [6]):

$$\bar{p}_c = 2 \sin^2 \beta_c \left[(1 - 0.25\bar{\rho}) \cos^2 (\theta_s - \beta_c)\right]^{-1} \qquad (10.3.11)$$

$$\bar{\rho} = 2\left\{1 - (2 \tan \beta_c / \tan \theta_s)\left[1 + \sqrt{1 - 2\bar{\rho} \tan^2 \beta_c/(1 - 0.5\bar{\rho})^2}\right]^{-1}\right\} \qquad (10.3.12)$$

$$10^2 M_\infty \sin \theta_s = 44 - \log p_\infty + 0.5\,(201 + \log p_\infty)\, M_\infty \sin \beta_c \qquad (10.3.13)$$

where p_∞ is the atmospheric pressure, Pa.

The above relations yield satisfactory results for values of $\bar{\rho} \approx 0.1$ and less. Calculations with the aid of these relations do not require the use of tables of the thermodynamic functions. We use the known values of M_∞, β_c, and p_∞ (these values are given) and Eq. (10.3.13) to determine first θ_s, next $\bar{\rho}$ with the aid of (10.3.12), and then the pressure coefficient by (10.3.11).

To determine the temperature T_c, we must use equation of state (1.5.8). Relating this equation once to the flow of the gas on the cone and a second time to the conditions in the oncoming stream, we find

$$T_c = \underbrace{\left(\frac{kM_\infty^2}{2} \bar{p}_c + 1\right)}_{a} \frac{\bar{\rho} T_\infty}{m_\infty} m_c = a m_c \qquad (10.3.14)$$

By (10.3.14) and the found values of $\bar{p}_c$ and $\bar{\rho}$, we calculate $T_c = am_c$ or with the aid of a graph of the function $m_c = f_3(p_c, T_c)$ (see Fig. 1.5.7), we find the corresponding value of T_c by fitting.

Some results of calculating the parameters on a cone are presented

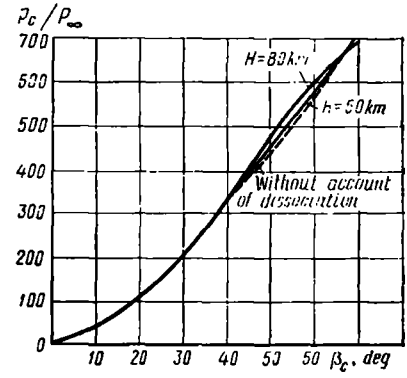

Fig. 10.3.1
Pressure on a cone with account taken of the dissociation of the gas
(T_∞=220 K, M_∞=23.5)

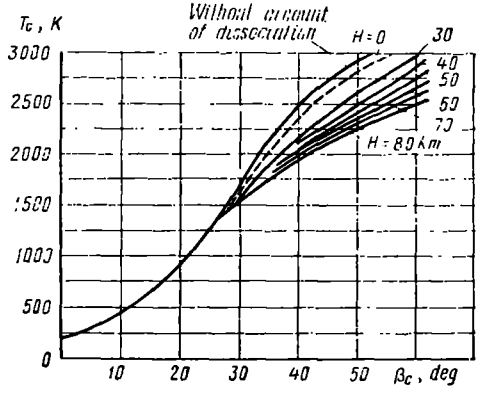

Fig. 10.3.2
Temperature on a cone with account taken of the dissociation of the gas
(T_∞=220 K, M_∞=10)

in Figs. 10.3.1-10.3.3. The nature of the change in the pressure p_c, temperature T_c, and the density ρ_c on a cone when dissociation and ionization occur is the same as directly behind a shock. The pressure here, like that behind a shock, depends only slightly on the dissociation and ionization. Its magnitude depends mainly on the free-stream conditions; the maximum excess pressure on a cone cannot exceed a certain limiting value $p_2 - p_1$ obtained from (4.2.14) provided that $V_{n2} = 0$, $V_{n1} = V_1 = V_\infty$ (a normal shock) and equal to $p_2 - p_1 = \rho_\infty V_\infty^2$. At the same time, the temperature and density change appreciably, this change being greater with an increasing cone thickness.

If the cone angles are not large, then even at appreciable flow velocities these parameters on a cone are under a slight influence of physicochemical transformations. Calculations reveal that at $M_\infty = 24$ the density does not virtually change with the altitude up to angles of $\beta_c = 15°$, and at $M_\infty = 10$ (Fig. 10.3.3)—up to angles

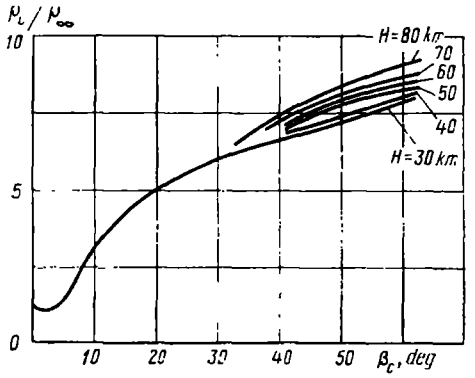

Fig. 10.3.3
Density on a cone in a dissociating air flow
(T_∞=220 K, M_∞=10)

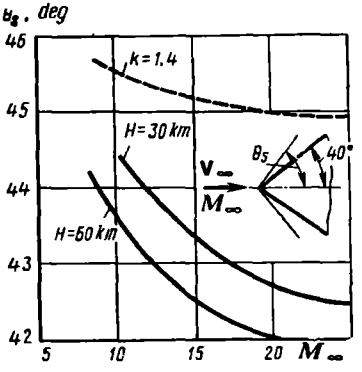

Fig. 10.3.4
Change in the shock angle ahead of a cone in a supersonic flow
(solid line—real gas, dashed line—perfect gas)

of $\beta_c = 35°$. Consequently, the interval of angles β_c which comparatively low temperatures and a negligibly small degree of dissociation correspond to expands with diminishing of the velocity. The same phenomenon is observed when the flight altitude decreases.

Larger angles of a cone cause more intense heating, and, as a result, dissociation and ionization, which can substantially affect the flow parameters. Figure 10.3.4 shows this influence on the change in the shock angle θ_s ahead of a cone with the semi-apex angle β_c = = 40°. The angle θ_s is smaller than what is observed for constant specific heats (k = 1.4). This causes a reduction in the strength of the shock and an increase in the velocity behind it, which leads to a growth in the velocity on the cone in the flow.

A growth in the flow velocity and a decrease in the sound speed lead to an increase in the number M_c on a conical surface in a dissociating gas.

An increase in the local Mach number causes the pressure to drop. At the same time, it grows because of the increase in the number

of gas particles upon dissociation and, consequently, on the larger number of their collisions. The overall effect manifests itself in a growth, although insignificant, in the pressure (see Fig. 10.3.1).

We have considered two cases of inviscid flow over a cone. One of them is associated with the flow of the gas at constant specific heats that is entirely non-equilibrium, and the other with equilibrium dissociation. The two cases can be considered as limiting ones corresponding to the boundaries of an interval inside of which non-equilibrium flows in the disturbed region are arranged. The parameters in such a region vary from their completely non-equilibrium values on a shock to equilibrium values at the end of the relaxation length (near the surface or on it).

10.4. Blunt-Nosed Cone

Shape of Blunt Noses

In many craft, the noses are blunted. Such nose shapes are employed first of all for very high airspeeds when the main requirement is for the noses to withstand the high temperatures of the gases flowing over them. But quite often, low-speed craft (or their separate elements) have a blunt-nosed shape, which may be due to the structural features, the designation of the craft, etc. It is virtually always necessary to consider a blunt body because it is impossible technologically to create an absolutely sharp nose.

Let us consider conical bodies with various shapes of their blunted noses as the most widespread ones. Figure 10.4.1 shows a cone-sphere (a conical body with a blunt spherical nose). The equation of the straight part of the generatrix of such a body tangent to the sphere has the form

$$r - r_n = (x - x_n) \tan \beta_c \qquad (10.4.1)$$

where r_n and x_n are the coordinates of the point of tangency of the spherical nose and the generatrix determined in terms of the nose radius R_n and the semi-apex angle β_c:

$$r_n = R_n \cos \beta_c; \quad x_n = R_n \cot \beta_c \cos \beta_c \qquad (10.4.2)$$

The equation of the generatrix of a spherical nose in a system of coordinates whose origin coincides with its apex is as follows in a dimensionless form:

$$\bar{r}^2 = 1 - (\bar{x} - 1)^2 \qquad (10.4.3)$$

where $\bar{r} = r/R_n$ and $\bar{x} = x/R_n$.

The slope of a tangent at a given point of the generatrix to the axis is

$$\tan \beta = dr/dx = (1 - \bar{x})/\bar{r} \qquad (10.4.4)$$

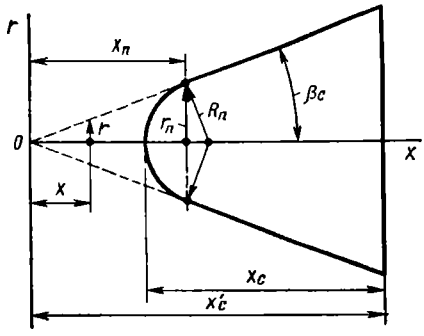

Fig. 10.4.1
Tangent cone-sphere

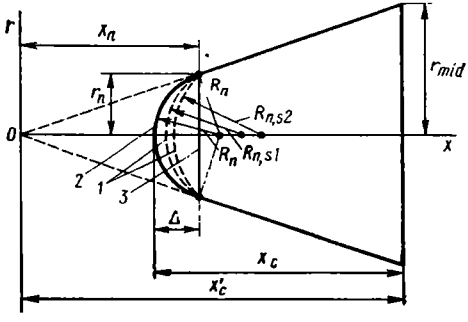

Fig. 10.4.2
Secant cone-sphere:
1—secant cone-sphere; *2*—tangent cone-sphere; *3*—flat-nosed cone

The nose of a cone can be designed so that the generatrix will be not a tangent, but a secant with respect to a spherical surface (Fig. 10.4.2). The radius of such a surface constructed for a point with the coordinates r_n and x_n will be $R_{n,s} > R_n$, where R_n is the radius of a tangential nose related to r_n and x_n by expressions (10.4.2).

Figure 10.4.2 shows a cone blunted in the form of a flat surface (a flat nose) that may be considered as a sphere with an infinitely large radius. A spherical nose and a flat one, in turn, may be considered as the "limiting" shapes of an elliptic surface. Figure 10.4.3 depicts a cone with a blunted nose in the form of such a surface.

A spherical tangential nose and a flat nose are the most characteristic shapes of blunting that can be considered as the extremes of an interval, as it were, containing other possible shapes. Both these characteristic shapes are of interest when studying the aerodynamics of blunted bodies with an intermediate nose shape because they allow us to estimate the extreme values of the aerodynamic parameters inherent in them.

The aerodynamic characteristics of blunt-nosed bodies depend substantially with a given type of nose on the **degree of blunting**, by which is meant the ratio of the radius of the nose base r_n to that

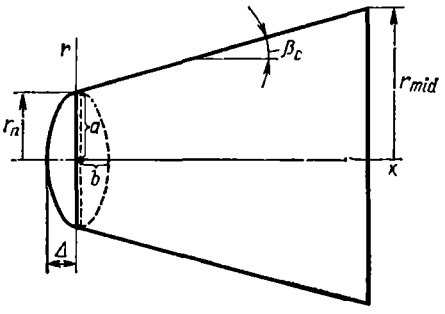

Fig. 10.4.3
Cone with elliptical blunting

of the mid-section (maximum cross section) of the body r_{mid} ($\bar{r}_n = r_n/r_{mid}$). A change in the degree of blunting of a cone with a spherical tangential nose or a flat nose corresponds to the interval $0 \leqslant \bar{r}_n \leqslant 1$. At $\bar{r}_n = 0$, we have a sharp-nosed cone, and at $\bar{r}_n = 1$, a cylinder. Blunting in the form of tangential and secant noses is characterized by the ratio $r_n/R_{n.s}$ that varies from $r_n/R_{n.s} = 0$ (a flat nose) to $(r_n/R_{n.s})_{sph}$ for a tangential sphere of radius $R_{n.s} = R_n$.

Features of Supersonic Flow

An aerodynamic property of blunt-nosed bodies that is important in practice consists in that upon motion in the atmosphere at very high speeds, *they are heated and destroyed less than sharp-nosed bodies.*

Let us consider the gas-dynamic phenomena that underlie this property of blunt-nosed bodies. Figure 10.4.4 shows a flow near a blunt-nosed conical body. A detached shock wave with a varying strength at different points of its surface forms ahead of the body. Far away from the nose, the shock wave transforms into an ordinary disturbance wave with an infinitely small strength and an angle of $\theta_s = \mu_\infty = \sin^{-1}(1/M_\infty)$. The strength will be maximum at the crest of the wave (point B in Fig. 10.4.4) where $\theta_s = \pi/2$. Since in the vicinity of the nose the angle θ_s differs only slightly from $\pi/2$, then the corresponding part of the wave has a sufficiently high strength close to that of a normal shock.

The transition of the gas particles through such a strong shock is attended by appreciable losses of the total head and by an increase in the entropy. As a result, a layer of some thickness forms at the surface of the body in which the gas has a high entropy. It is assumed that such a **high-entropy layer** is confined by a part of the shock wave and the surface obtained by the rotation of a "sonic" streamline, i.e. a streamline passing through a "sonic" point on the wave (point S with the coordinate $r_{s.n}$ in Fig. 10.4.4).

In the high-entropy layer, owing to the different stagnation at various points of the shock wave, the flow is characterized (Fig. 10.4.4)

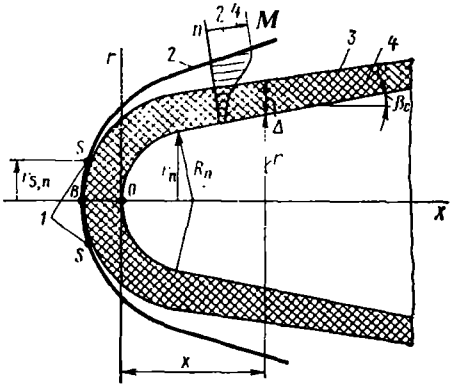

Fig. 10.4.4
Supersonic flow over a blunted cone:
1—"sonic points", *2*—shock wave; *3*—"sonic" streamline; *4*—high-entropy layer

by a velocity gradient in the direction of the normal n and, therefore, by a varying value of the local number M over the thickness Δ. If the boundary layer has a considerably smaller thickness than the high-entropy one, the velocity gradient in it may be disregarded in comparison with that in the high-entropy layer. This simplifies investigation. It is assumed that in the high-entropy layer, the velocity at various points of the section is the same. It can be assumed to approximate the mean velocity between the values on the sonic streamline, and also on the zero one passing through the wave crest. This velocity is obviously lower than that on a sharp-nosed cone. Near the surface, the region of the flow occupied by the high-entropy layer and characterized by *low velocities* (and, consequently, by *low Mach and Reynolds numbers*) has a decisive influence on the formation of the processes in the boundary layer.

A significant feature of the flow consists in that under the influence of blunting, the flow conditions in the boundary layer change. Owing to the decrease in the local Reynolds numbers based on the velocity in the high-entropy layer, the laminar boundary layer transforms into a turbulent one much farther downstream, and, consequently, *the length of the laminar boundary layer grows.* This facilitates a diminishing of the skin friction and a reduction of the heat fluxes to the wall.

The reduction of the heat fluxes due to the increase in the entropy of the gas during a transition through a shock is called the **entropy effect.** It should be had in view here that the entropy effect consists not only in a decrease in the velocity on the boundary layer edge, but also in a drop in the density of the gas, i.e. in lowering of the Reynolds numbers. At the same time, the increase in the entropy also leads to elevation (in comparison with a sharp-nosed body) of the temperature on the boundary layer edge. This is the opposite effect of the high-entropy layer resulting in a certain increase in the heat

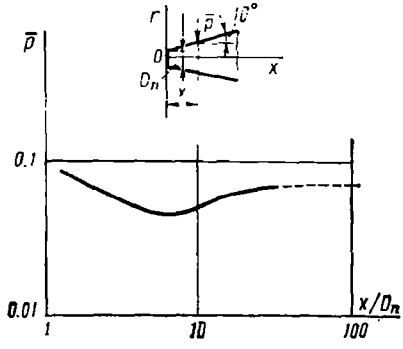

Fig. 10.4.5
Pressure coefficient on the surface of a flat-nosed cone at $M_\infty = 6.85$:
solid line—experimental data; dashed line—data calculated according to the cone theory for a sharp-nosed body

flux from the boundary layer to the wall. But calculations and experimental investigations show that the overall entropy effect upon an appropriate choice of the wall and the shape of the blunting is associated with diminishing of the heat fluxes.

The wave drag of a blunt-nosed body in comparison with a sharp-nosed one, as a rule, grows, although slender conical bodies with small blunting are characterized by lowering of the drag. The explanation is that notwithstanding the increase in the pressure at the nose, a reduced pressure in comparison with that for a sharp-nosed cone appears on a considerable part of the surface in the flow. Such a decrease in the pressure behind the nose is shown in Fig. 10.4.5. The latter depicts experimental results obtained in a wind tunnel for a slender flat-nosed cone in a supersonic flow at $M_\infty = 6.85$. The minimum pressure is reached at a distance from the nose of about 10 blunting diameters ($x \approx 10D_n$). At $x \approx 100D_n$, the pressure regains its value on a sharp-nosed cone. If such a cone has a small length and, consequently, a small surface with a reduced pressure, the decrease in the drag for this part is not sufficient to compensate its growth because of the increase in the drag of the face. For a sufficiently long cone, the decrease in the drag of the peripheral part may be more substantial and will lead to a decrease in the total drag of the blunt-nosed conical surface in comparison with the sharp-nosed one.

The main effect due to blunting consists not in the change in the drag, which at a low degree of blunting is comparatively small, but *in a substantial decrease in heat transfer*. Investigations show that this advantage of blunting manifests itself mainly in the region of **hypersonic velocities**.

We may also indicate other cases of the use of blunt-nosed surfaces associated not so much with the need to diminish heat transfer as with *the increase of the drag*. **Landing spacecraft modules** are designed with surfaces of this shape. They are characterized by high values of

c_{x_a} ensuring their more intensive retardation in the atmosphere.

Measures must be taken to protect such modules or craft from destruction because of aerodynamic heating.

Flow over a Cone with a Spherical Nose

Equations of Flow and Their Solution. Investigation of the aerodynamics of an entire blunt-nosed body is associated with the studying of the flow over its blunted nose. The results of these investigations are the basis for calculating the flow parameters on the remaining part of the body. In addition, these results are of an independent significance because they allow one to determine the aerodynamic characteristics of a blunted nose. The overall aerodynamic characteristics of a body can be determined by summating the components for the nose and for the remaining part. We must indicate here that if the flow over the peripheral part of a body depends on the blunting, the conditions of flow over the nose itself are determined only by the shape of the part of the nose up to the sonic point on its surface. If such a sonic point is on the peripheral surface (downstream of the line where the nose joins the body), the disturbances on this surface of the body propagate upstream in the direction of the nose, and the flow over it may not be treated without regard to the flow over this region.

Let us consider the problem of the flow over the spherical nose of a conical body assuming that the flow over the nose is not affected by its peripheral surface of the body. Although we shall study inviscid flow, the solution being sought is of a major practical significance: it allows us to determine the basic conditions of the flow outside the boundary layer needed for studying the skin friction and heat transfer in the boundary layer.

We shall first consider *the flow in the vicinity of the stagnation point*, which is one of the most characteristic points of a spherical surface. It is interesting to investigate this flow first of all because it is associated with such a practical problem as the determination of the heat fluxes, which may reach their highest value here. The solution of the problem on the flow near the stagnation point also allows us to determine the distance from the shock wave to the nose, as well as the distribution of the gas-dynamic parameters in this small region; the solution can be obtained in the general case *with account taken of the physicochemical transformations of the gas.*

To solve the stated problem, we shall use the equation of motion, which according to (3.1.21) for an "inviscid" ($\nu = 0$) and a "weightless" gas ($\bar{G} = 0$) is as follows in the vector form:

$$d\mathbf{V}/dt = -(1/\rho)\,\mathrm{grad}\,p \qquad (10.4.5)$$

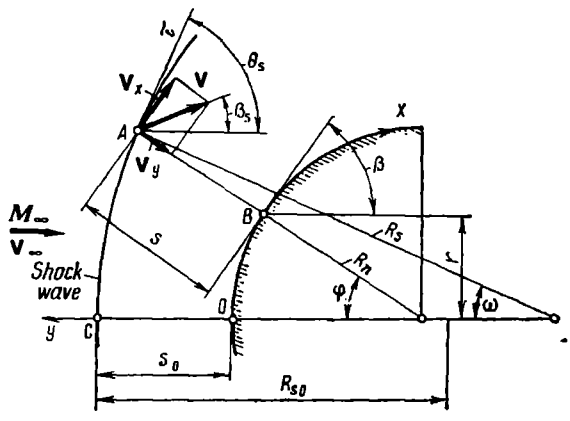

Fig. 10.4.6
Supersonic flow over a spherical surface

Let us write Eq. (10.4.5) in a system of curvilinear orthogonal coordinates. We make the origin of coordinates of this system coincide with stagnation point O on the spherical surface, measure the coordinate x along the surface, and y along a normal to it (Fig. 10.4.6). Using (3.1.22) and taking into account that we are studying a steady flow ($\partial \mathbf{V}/\partial t = 0$), we transform Eq. (10.4.5) as follows:

$$\text{grad}\,(V^2/2) + \text{curl}\,\mathbf{V} \times \mathbf{V} = -(1/\rho)\,\text{grad}\,p \qquad (10.4.6)$$

Considering the projections of the vectors onto the directions of the coordinate lines q_1 and q_2 of the curvilinear system [see (2.4.11)], we obtain equations of motion:

$$\left.\begin{aligned}[\text{grad}\,(V^2/2)]_1 + (\text{curl}\,\mathbf{V} \times \mathbf{V})_1 &= -(1/\rho)\,(\text{grad}\,p)_1 \\ [\text{grad}\,(V^2/2)]_2 + (\text{curl}\,\mathbf{V} \times \mathbf{V})_2 &= -(1/\rho)\,(\text{grad}\,p)_2\end{aligned}\right\} \qquad (10.4.7)$$

The values of $[\text{grad}\,(V^2/2)]_1$ and $[\text{grad}\,(V^2/2)]_2$ can be determined by (3.1.24). Substituting $V^2/2$ for p, we obtain

$$\text{grad}\,\frac{V^2}{2} = \frac{1}{h_1}\cdot\frac{\partial\,(V^2/2)}{\partial q_1}\,\mathbf{i}_1 + \frac{1}{h_2}\cdot\frac{\partial\,(V^2/2)}{\partial q_2}\,\mathbf{i}_2 + \frac{1}{h_3}\cdot\frac{\partial\,(V^2/2)}{\partial q_3}\,\mathbf{i}_3 \qquad (10.4.8)$$

where by (2.4.40), $q_1 = x$, $q_2 = y$, and $q_3 = \gamma$.

Since we are dealing with axisymmetric flow, we have

$$\partial\,(V^2/2)/\partial q_3 = \partial\,(V^2/2)/\partial\gamma = 0$$

Using the values given by (2.4.42) for Lamé's coefficients h_1 and h_2, we shall write formula (10.4.8) as

$$\left(\text{grad}\,\frac{V^2}{2}\right)_1 \mathbf{i}_1 + \left(\text{grad}\,\frac{V^2}{2}\right)_2 \mathbf{i}_2 = \left(1 + \frac{y}{R_n}\right)^{-1}\cdot\frac{\partial\,(V^2/2)}{\partial x}\,\mathbf{i}_1 + \frac{\partial\,(V^2/2)}{\partial y}\,\mathbf{i}_2$$

whence

$$\left(\operatorname{grad}\frac{V^2}{2}\right)_1=\left(1+\frac{y}{R_n}\right)^{-1}\frac{\partial(V^2/2)}{\partial x};\quad \left(\operatorname{grad}\frac{V^2}{2}\right)_2=\frac{\partial(V^2/2)}{\partial y} \tag{10.4.9}$$

Let us consider the cross (vector) product

$$\operatorname{curl}\mathbf{V}\times\mathbf{V}=[(\operatorname{curl}\mathbf{V})_1\mathbf{i}_1+(\operatorname{curl}\mathbf{V})_2\mathbf{i}_2+(\operatorname{curl}\mathbf{V})_3\mathbf{i}_3]\times(V_1\mathbf{i}_1+V_2\mathbf{i}_2+V_3\mathbf{i}_3)$$

Hence we find the projections:

$$(\operatorname{curl}\mathbf{V}\times\mathbf{V})_1=(\operatorname{curl}\mathbf{V})_2V_3-(\operatorname{curl}\mathbf{V})_3V_2$$
$$(\operatorname{curl}\mathbf{V}\times\mathbf{V})_2=-(\operatorname{curl}\mathbf{V})_1V_3+(\operatorname{curl}\mathbf{V})_3V_1$$

Since we are considering axisymmetric flow, in these expressions $V_3=0$. The projection of the vector $(\operatorname{curl}\mathbf{V})_3$ in accordance with (3.1.28) is

$$(\operatorname{curl}\mathbf{V})_3=\frac{1}{h_1h_2}\left[\frac{\partial(h_2V_2)}{\partial q_1}-\frac{\partial(h_1V_1)}{\partial q_2}\right]$$

or with a view to (2.4.40) and (2.4.42),

$$(\operatorname{curl}\mathbf{V})_3=\left(1+\frac{y}{R_n}\right)^{-1}\left\{\frac{\partial V_y}{\partial x}-\frac{\partial[(1+y/R_n)V_x]}{\partial y}\right\} \tag{10.4.10}$$

Therefore,

$$\left.\begin{aligned}(\operatorname{curl}\mathbf{V}\times\mathbf{V})_1&=-(\operatorname{curl}\mathbf{V})_3V_2\\&=-\left(1+\frac{y}{R_n}\right)^{-1}V_y\left\{\frac{\partial V_y}{\partial x}-\frac{\partial[(1+y/R_n)V_x]}{\partial y}\right\}\\(\operatorname{curl}\mathbf{V}\times\mathbf{V})_2&=(\operatorname{curl}\mathbf{V})_3V_1\\&=\left(1+\frac{y}{R_n}\right)^{-1}V_x\left\{\frac{\partial V_y}{\partial x}-\frac{\partial[(1+y/R_n)V_x]}{\partial y}\right\}\end{aligned}\right\} \tag{10.4.11}$$

It follows from (3.1.24) that

$$(\operatorname{grad}p)_1=\frac{1}{h_1}\cdot\frac{\partial p}{\partial q_1},\quad (\operatorname{grad}p)_2=\frac{1}{h_2}\cdot\frac{\partial p}{\partial q_2}$$

or with a view to (2.4.40) and (2.4.42),

$$(\operatorname{grad}p)_1=\left(1+\frac{y}{R_n}\right)^{-1}\frac{\partial p}{\partial x},\quad (\operatorname{grad}p)_2=\frac{\partial p}{\partial y} \tag{10.4.12}$$

Introducing (10.4.9), (10.4.11), and (10.4.12) into (10.4.7), after transformations we obtain the following equations of motion:

$$\frac{V_x}{1+y/R_n}\cdot\frac{\partial V_x}{\partial x}+V_y\frac{\partial V_x}{\partial y}+\frac{V_xV_y}{y+R_n}=-\frac{1}{\rho(1+y/R_n)}\cdot\frac{\partial p}{\partial x} \tag{10.4.13}$$

$$\frac{V_x}{1+y/R_n}\cdot\frac{\partial V_y}{\partial x}+V_y\frac{\partial V_y}{\partial y}-\frac{V_x^2}{y+R_n}=-\frac{1}{\rho}\cdot\frac{\partial p}{\partial y} \tag{10.4.14}$$

The equations of motion have to be supplemented with an equation of continuity, which by (2.4.46) for steady flow ($\partial\rho/\partial t = 0$) can be written as

$$\partial(\rho r V_x)/\partial x + \partial[\rho r(1 + y/R_n)V_y]/\partial y = 0 \qquad (10.4.15)$$

If we assume that we are investigating a region in the vicinity of a critical point and the oncoming flow has a very high supersonic velocity, the initial equations (10.4.13)-(10.4.15) can be simplified. Actually in these conditions, the flow behind a shock wave is virtually incompressible because the number M_2 differs only slightly from its value $[(k-1)/2k]^{1/2}$ corresponding to a limiting case of flow (at $M_\infty \to \infty$ and $k = \text{const}$) behind a normal shock. Consequently, in the vicinity being considered, we can assume that the density is constant and equals ρ_{s0}—the density behind the shock at the stagnation point. Hence, we may substitute the constant quantity ρ_{s0} for the variable density ρ in the equations of motion and continuity.

Since we are dealing with high velocities, in this case a shock wave comes close to the surface of the body. The region of disturbed flow occupies a layer of thickness s very small in comparison with the radius of curvature R_n of the nose surface.

Therefore, if we assume that $s/R_n \ll 1$, then evidently $y/R_n \ll 1$ because $0 \ll y \ll s$. Consequently, we may disregard the quantity y/R_n in the equations of motion (10.4.13) and (10.4.14) and of continuity (10.4.15). With a view to the above simplifications and to the fact that for the conditions near the stagnation point we may assume that $r \approx x$ in (10.4.15), Eqs. (10.4.13)-(10.4.15) can be written as follows:

$$V_x\frac{\partial V_x}{\partial x} + V_y\frac{\partial V_x}{\partial y} + \frac{V_x V_y}{R_n} = -\frac{\bar{\rho}}{\rho_\infty}\cdot\frac{\partial p}{\partial x} \qquad (10.4.16)$$

$$V_x\frac{\partial V_y}{\partial x} + V_y\frac{\partial V_y}{\partial y} - \frac{V_x^2}{R_n} = -\frac{\bar{\rho}}{\rho_\infty}\cdot\frac{\partial p}{\partial y} \qquad (10.4.17)$$

$$\frac{\partial(xV_x)}{\partial x} + \frac{\partial(xV_y)}{\partial y} = 0 \qquad (10.4.18)$$

In Eqs. (10.4.16) and (10.4.17), we have introduced the dimensionless density $\bar{\rho} = \rho_\infty/\rho \approx \rho_\infty/\rho_{s0} = \text{const}$. We shall show that Eqs. (10.4.16) and (10.4.17) can be simplified still further. To do this, let us consider the order of magnitude of the terms in these equations. According to its physical meaning, the order of the quantity V_y will be $V_y \sim V_{s0}$, where V_{s0} is the velocity behind the normal part of the shock wave. The order of x and y for a small vicinity is determined respectively by the values of $x \sim s_0$ and $y \sim s_0$ (s_0 is the distance from the normal part of the wave to the surface of the nose).

It follows from Eq. (10.4.18) that the order of the quantity xV_x is

$$xV_x \sim \int_0^{s_0} \frac{\partial (xV_y)}{dy}\, dx \quad \text{or} \quad s_0 V_x \sim \int_0^{s_0} \frac{s_0 V_{s0}}{s_0}\, dx$$

whence we find $V_x \sim V_{s0}$. Hence, the order of magnitude of the component V_x is the same as of V_y. It is not difficult to see that the order of the third terms on the left-hand side of the equations is V_{s0}^2/R_n, and of the other ones is V_{s0}^2/s_0. Since $s_0 \ll R_n$, the order of the third terms is smaller, and they may be disregarded.

Hence, instead of (10.4.16) and (10.4.17), we have

$$V_x \frac{\partial V_x}{\partial x} + V_y \frac{\partial V_x}{\partial y} = -\frac{\bar{\rho}}{\rho_\infty} \cdot \frac{\partial p}{\partial x} \qquad (10.4.16')$$

$$V_x \frac{\partial V_y}{\partial x} + V_y \frac{\partial V_y}{\partial y} = -\frac{\bar{\rho}}{\rho_\infty} \cdot \frac{\partial p}{\partial y} \qquad (10.4.17')$$

The solution of the simultaneous equations (10.4.16'), (10.4.17'), and (10.4.18) must satisfy the boundary conditions on the surface of the body at an arbitrary point where at $y = 0$ the normal velocity component $V_y = 0$, and then at the stagnation point where at $y = x = 0$ the velocity components $V_x = V_y = 0$. In addition, the solution must satisfy the boundary conditions behind the shock wave. These conditions for the components of the velocity at point A at a distance of s from the nose surface have the form (see Fig. 10.4.6):

$$V_x = V_s \cos(\beta - \beta_s) \qquad (10.4.19)$$

$$V_y = -V_s \sin(\beta - \beta_s) \qquad (10.4.20)$$

where β is the angle made by a tangent to the surface at point B that is on the same normal as point A.

The total velocity V_s behind the shock is determined by formula (4.3.18). Assuming that $V_2 = V_s$, $V_1 = V_\infty$, and $\rho_1/\rho_2 \approx \rho_\infty/\rho_{s0} = \bar{\rho}$, we find

$$V_s/V_\infty = (\cos^2 \theta_s + \bar{\rho}^2 \sin^2 \theta_s)^{1/2} \qquad (10.4.21)$$

The solution of the problem on the flow in the vicinity of the stagnation point can be reduced to finding of the velocity field. Hence, the problem being considered is a purely *kinematic* one. For this purpose, we must exclude the density and pressure from the equations of motion and differentiate (10.4.16') with respect to y, and (10.4.17') with respect to x:

$$\frac{\partial V_x}{\partial y} \cdot \frac{\partial V_x}{\partial x} + V_x \frac{\partial^2 V_x}{\partial x\, \partial y} + \frac{\partial V_y}{\partial y} \cdot \frac{\partial V_x}{\partial y} + V_y \frac{\partial^2 V_x}{\partial y^2} = -\frac{\bar{\rho}}{\rho_\infty} \cdot \frac{\partial^2 p}{\partial x\, \partial y} \qquad (10.4.22)$$

$$\frac{\partial V_x}{\partial x} \cdot \frac{\partial V_y}{\partial x} + V_x \frac{\partial^2 V_y}{\partial x^2} + \frac{\partial V_y}{\partial x} \cdot \frac{\partial V_y}{\partial y} + V_y \frac{\partial^2 V_y}{\partial y\, \partial x} = -\frac{\bar{\rho}}{\rho_\infty} \cdot \frac{\partial^2 p}{\partial y\, \partial x} \qquad (10.4.23)$$

Let us introduce a function determining the **double vortex component** [the component of the velocity curl (curl $\mathbf{V})_z = 2\omega_z$; see (2.2.3)]:

$$-2\omega_z = \Omega_z = \partial V_x/\partial y - \partial V_y/\partial x \qquad (10.4.24)$$

Using the function (10.4.24), and also continuity equation (10.4.18), we can transform equations (10.4.22) and (10.4.23). Since the right-hand sides of these equations are the same, we have

$$\frac{\partial V_x}{\partial y}\cdot\frac{\partial V_x}{\partial x} + V_x\frac{\partial^2 V_x}{\partial x\,\partial y} + \frac{\partial V_y}{\partial y}\cdot\frac{\partial V_x}{\partial y} + V_y\frac{\partial^2 V_x}{\partial y^2}$$
$$-\frac{\partial V_x}{\partial x}\cdot\frac{\partial V_y}{\partial x} - V_x\frac{\partial^2 V_y}{\partial x^2} - \frac{\partial V_y}{\partial x}\cdot\frac{\partial V_y}{\partial y} - V_y\frac{\partial^2 V_y}{\partial y\,\partial x} = 0$$

or

$$\left(\frac{\partial V_x}{\partial y} - \frac{\partial V_y}{\partial x}\right)\left(\frac{\partial V_x}{\partial x} + \frac{\partial V_y}{\partial y}\right) + V_x\left(\frac{\partial^2 V_x}{\partial x\,\partial y} - \frac{\partial^2 V_y}{\partial x^2}\right)$$
$$+ V_y\left(\frac{\partial^2 V_x}{\partial y^2} - \frac{\partial^2 V_x}{\partial y\,\partial x}\right) = 0 \qquad (10.4.25)$$

It follows from (10.4.24) that

$$\frac{\partial^2 V_x}{\partial x\,\partial y} - \frac{\partial^2 V_y}{\partial x^2} = \frac{\partial \Omega_z}{\partial x}, \qquad \frac{\partial^2 V_x}{\partial y^2} - \frac{\partial^2 V_y}{\partial y\,\partial x} = \frac{\partial \Omega_z}{\partial y}$$

From continuity equation (10.4.18), we find

$$\partial V_x/\partial x + \partial V_y/\partial y = -V_x/x$$

Therefore, Eq. (10.4.25), in which $\partial V_x/\partial y - \partial V_y/\partial x = \Omega_z$, can be written in the form

$$\Omega_z V_x/x = V_x\,\partial\Omega_z/\partial x + V_y\,\partial\Omega_z/\partial y \qquad (10.4.25')$$

Hence, our task consists in finding the solutions of Eqs. (10.4.18) and (10.4.25') satisfying the indicated boundary conditions.

We shall find the solution for V_x in the vicinity of the stagnation point (whose coordinates are $x = 0$ and $y = 0$) in the form of the series

$$V_x = a_0(y) + a_1(y)\,x + a_2(y)\,x^2 + a_3(y)\,x^3 + \ldots \qquad (10.4.26)$$

where x is a small parameter, and a_n are coefficients that are functions of the coordinate y.

The structure of series (10.4.26) can be simplified. Indeed, owing to symmetry of the flow, the function $V_x(x)$ is odd, i.e. velocity components V_x equal in magnitude, but opposite in sign correspond to values of x that are identical in magnitude, but opposite in sign. Consequently, only terms with odd exponents are retained in expansion (10.4.26), i.e.

$$V_x = a_1(y)\,x + a_3(y)\,x^3 + \ldots \qquad (10.4.27)$$

Having in view that we are considering a small neighbourhood near the stagnation point, the terms containing x to the third and higher powers may be ignored. Hence,

$$V_x = a_1(y)\, x \tag{10.4.28}$$

Let us introduce the function

$$F(y) = \int_0^y a_1(y)\, dy \tag{10.4.29}$$

satisfying the condition $F(0) = 0$. Therefore,

$$V_x = x\, dF/dy = xF'(y) \tag{10.4.30}$$

Let us insert the expression (10.4.30) for V_x into (10.4.18):

$$xF'(y) + xF''(y) + x\frac{\partial V_y}{\partial y} = 0$$

From this equation, we find an expression for the second velocity component:

$$V_y = -2\int F'(y)\, dy + f(x) = -2F(y) + f(x) \tag{10.4.31}$$

where $f(x)$ is an arbitrary function of x.

According to the condition of flow without separation, $V_y(x, 0) = 0$. Consequently, $f(x) = -2F(0)$. But the function $F(0) = 0$, therefore $f(x) = 0$ and

$$V_y = -2F(y) \tag{10.4.32}$$

To determine the form of the function $F(y)$, we shall introduce (10.4.30) and (10.4.32) into (10.4.25'):

$$[xF'''(y)/x]\, V_x = V_x F''(y) - 2F(y)\, F'''(y)$$

From (10.4.32), the function $F(y) \neq 0$, hence

$$F'''(y) = 0 \tag{10.4.33}$$

The general solution of this equation has the form

$$F(y) = -V_y/2 = c_0 + c_1 y + c_2 y^2 \tag{10.4.34}$$

Since $V_y = 0$ when $y = 0$, then $c_0 = 0$. We can determine the other two coefficients if we use the conditions on a shock wave near the critical point at $x \to 0$. Particularly, it follows from condition (10.4.21) that directly behind the normal part of the shock wave ($\theta_s = \pi/2$) the velocity at point C (see Fig. 10.4.6) $V_y = V_s = -\rho V_\infty$. Since the coordinate of the point $y = s_0$, we have $V_y = V_s = -2(c_1 s_0 + c_2 s_0^2)$. Therefore, we can compile the first

equation for finding the coefficients c_1 and c_2:

$$\bar{\rho} V_\infty = 2 (c_1 s_0 + c_2 s_0^2) \tag{10.4.35}$$

To find the second equation, we shall differentiate (10.4.34) with respect to y:

$$F'(y) = c_1 + 2c_2 y$$

In accordance with this result and by (10.4.31), the velocity component is

$$V_x = x (c_1 + 2c_2 y) \tag{10.4.36}$$

Let us consider point A on the shock wave at a distance of $y = s$ from the surface of the nose. Equating the velocity V_x found from (10.4.36), i.e.

$$V_{x,A} = x (c_1 + 2c_2 s)$$

to its value (10.4.19) on the shock wave:

$$V_{x,A} = V_s \cos (\beta - \beta_s)$$

we obtain

$$x (c_1 + 2c_2 s) = V_s \cos (\beta - \beta_s)$$

Going over to the limit at $x \to 0$ and assuming that $s = s_0$ and $V_s = \bar{\rho} V_\infty$, we find an expression relating to point C on the normal part of the shock wave

$$\lim_{x \to 0} \frac{\cos (\beta - \beta_s)}{x} = \frac{c_1 + 2c_2 s_0}{\bar{\rho} V_\infty} \tag{10.4.37}$$

We can calculate the limit on the left-hand side as follows. Inspection of Fig. 10.4.6 reveals that at point A on the shock wave the angle $\beta - \beta_s = \pi/2 - (\varphi + \beta_s)$. Consequently, we have $\cos (\beta - \beta_s) = \sin (\varphi + \beta_s)$. Near the stagnation point, the angles φ and β_s are small, and we may assume that $\cos (\beta - \beta_s) \approx \varphi + \beta_s$. Accordingly,

$$\lim_{x \to 0} \frac{\cos (\beta - \beta_s)}{x} = \lim_{x \to 0} \frac{\varphi}{x} + \lim_{x \to 0} \frac{\beta_s}{x}$$

It is evident that $\lim\limits_{x \to 0} (\varphi/x) = 1/R_n$, while the second limit can be written as

$$\lim_{x \to 0} \frac{\beta_s}{x} = \lim_{x \to 0} \left(\frac{\beta_s}{\omega} \cdot \frac{\omega}{x} \right) = \left(\frac{\beta_s}{\omega} \right)_{x=0} \cdot \frac{1}{R_{s0}} \tag{10.4.38}$$

where $\lim\limits_{x \to 0} \frac{\beta_s}{\omega} = \left(\frac{\beta_s}{\omega} \right)_{x=0}$; $\lim\limits_{x \to 0} \frac{\omega}{x} = \frac{1}{R_{s0}}$; R_{s0} is the radius of curvature of the shock wave at its crest (if R_s is the running value of the radius of curvature of the wave, we have $R_{s0} = \lim\limits_{x \to 0} R_s$). The angle ω (see Fig. 10.4.6) is related to the shock wave angle θ_s by

the formula

$$\omega = \pi/2 - \theta_s \tag{10.4.39}$$

To determine $(\beta_s/\omega)_{x=0}$, we shall use formula (4.2.19), which we obtain with the aid of (4.2.21) and (10.4.39) as follows:

$$\rho_\infty/\rho_s = [\tan(\theta_s - \beta_s)]/\tan\theta_s = \tan\omega/\tan(\omega + \beta_s)$$

For small values of ω and β_s, the ratio $\rho_\infty/\rho_s = \omega/(\omega + \beta_s)$. Consequently,

$$\lim_{x\to 0}\frac{\beta_s}{\omega} = \lim_{x\to 0}\left(\frac{\rho_s}{\rho_\infty} - 1\right) \quad \text{or} \quad \left(\frac{\beta_s}{\omega}\right)_{x=0} = \frac{\rho_{s0}}{\rho_\infty} - 1 = \frac{1}{\bar{\rho}} - 1$$

Hence,

$$\lim_{x\to 0}\frac{\cos(\beta - \beta_s)}{x} = \frac{1}{R_n} + \left(\frac{1}{\bar{\rho}} - 1\right)\frac{1}{R_{s0}}$$

Let us introduce this expression into (10.4.37):

$$\frac{1}{R_n} + \left(\frac{1}{\bar{\rho}} - 1\right)\frac{1}{R_{s0}} = \frac{c_1 + 2c_2 s_0}{\bar{\rho} V_\infty} \quad \text{or} \quad \frac{R_{s0}}{R_n} + \frac{1}{\bar{\rho}} - 1 = \frac{R_{s0}(c_1 + 2c_2 s_0)}{\bar{\rho} V_\infty}$$

At high flow velocities, we may assume that $R_{s0}/R_n \approx 1$, therefore

$$c_1 + 2c_2 s_0 = V_\infty/R_{s0} \tag{10.4.40}$$

Equations (10.4.35) and (10.4.40), in addition to c_1, c_2, contain a third unknown—the distance s_0 from the shock wave to the nose. Therefore, we must add another independent equation to the system (10.4.35) and (10.4.40) that follows from the expression for a vortex:

$$\Omega_z = \frac{\partial V_x}{\partial y} - \frac{\partial V_y}{\partial x} = \frac{\partial}{\partial y}[x(c_1 + 2c_2 y)] - \frac{\partial}{\partial x}[-2(c_1 y + c_2 y^2)] = 2c_2 \tag{10.4.41}$$

Expression (10.4.41) is suitable for determining a vortex on the surface of the nose and directly behind the shock wave on the part of the flow near the stagnation point. A vortex in the flow behind the shock wave can also be found from Eq. (10.4.6), which in accordance with the relation $i + V^2/2 = \text{const}$ transforms to the expression

$$\text{curl } \mathbf{V} \times \mathbf{V} = \text{grad } i - (1/\rho)\,\text{grad } p \tag{10.4.42}$$

Let us take advantage of the relation for the entropy known from thermodynamics:

$$T\,dS = di - dp/\rho \tag{10.4.43}$$

according to which we can obtain the vector relation

$$T\,\text{grad } S = \text{grad } i - (1/\rho)\,\text{grad } p \tag{10.4.44}$$

Hence, we can write (10.4.42) as

$$\text{curl } \mathbf{V} \times \mathbf{V} = T\,\text{grad } S \tag{10.4.45}$$

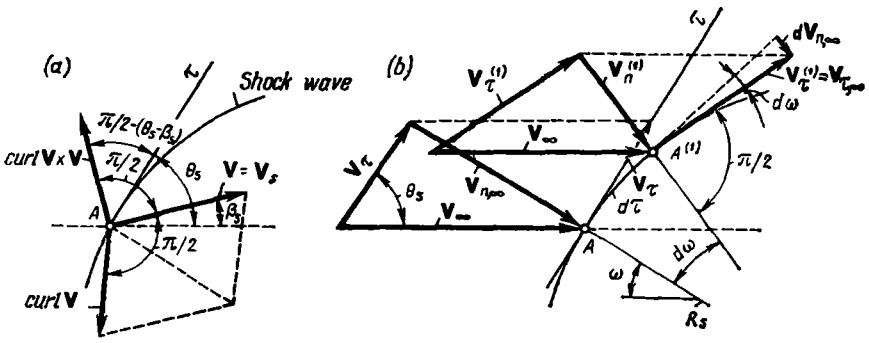

Fig. 10.4.7
To the determination of the strength of a vortex behind a shock wave

This equation can be related to the conditions on the shock wave. Let us consider arbitrary point A on the wave (see Fig. 10.4.6). By projecting the vectors in (10.4.5) onto the direction of the tangent τ, we obtain the expression

$$(\text{curl } \mathbf{V} \times \mathbf{V})_\tau = T_2 \, dS_2/d\tau \qquad (10.4.46)$$

where T_2 is the temperature at point A behind the shock.

The component $(\text{curl } \mathbf{V} \times \mathbf{V})_\tau$ of the cross product is determined as follows. At point A, the vector curl V, whose magnitude is Ω_z, is oriented along a normal to the vertical plane of symmetry (Fig. 10.4.7*a*). The quantity V is the velocity vector behind the shock wave, $\mathbf{V} = \mathbf{V}_s$, in this plane of symmetry. Since the vectors curl V and V are perpendicular to each other, the magnitude of their cross product is

$$|\,\text{curl } \mathbf{V} \times \mathbf{V}\,| = |\,\text{curl } \mathbf{V}\,|\,|\,\mathbf{V}\,| \sin(\pi/2) = \Omega_z V_s$$

The vector equal to the cross product curl V × V is perpendicular to the plane containing the vectors curl V, V, and belongs evidently, like the vector $\mathbf{V} = \mathbf{V}_s$, to the plane of symmetry (Fig. 10.4.7*a*). The projection of the cross product curl V × V onto the direction of a tangent, as can be seen from Fig. 10.4.7, is

$$(\text{curl } \mathbf{V} \times \mathbf{V})_\tau = \Omega_z V_s \sin(\theta_s - \beta_s) \qquad (10.4.47)$$

To compute the right-hand side of (10.4.46), we shall use Eq. (10.4.43), relating it to the conditions at the same point A behind the shock wave:

$$T_2 \, dS_2 = di_2 - dp_2/\rho_2 \qquad (10.4.43')$$

We shall take the equations for the enthalpy i_2 and the pressure p_2 in the form of (4.2.6) and (4.2.4), respectively. Since we are considering high velocities at which $i_1 \ll i_2$ and $p_1 \ll p_2$, we can write

these equations in the form

$$i_2 = V_{n1}^2/2 - V_{n2}^2/2 \tag{10.4.48}$$

$$p_2 = \rho_1 V_{n1}^2 - \rho_2 V_{n2}^2 \tag{10.4.49}$$

or with a view to (4.2.3)

$$i_2 = [V_{n,\infty}^2 (1 - \bar{\rho}^2)]/2 \tag{10.4.48'}$$

$$p_2 = \rho_1 V_{n,\infty}^2 (1 - \bar{\rho}) \tag{10.4.49'}$$

where $V_{n1} = V_{n,\infty}$, and $\bar{\rho} = \rho_1/\rho_2 = \rho_\infty/\rho$.

Differentiation yields

$$di_2 = (1-\bar{\rho}^2)\, V_{n,\infty}\, dV_{n,\infty} - V_{n,\infty}^2\, \bar{\rho}\, d\bar{\rho};$$

$$dp_2 = 2(1-\bar{\rho})\, \rho_1 V_{n,\infty}\, dV_{n,\infty} - [\rho_1 V_{n,\infty}^2\, d\bar{\rho}$$

Inserting these expressions into (10.4.43'), we find

$$T_2\, dS_2 = (1 - \bar{\rho})^2\, V_{n,\infty}\, dV_{n,\infty} \tag{10.4.50}$$

It follows from Fig. 10.4.7*b* that the increment of the normal component $dV_{n,\infty} = V_\tau^{(1)}\, d\omega$. Here, since the velocity $V_\tau^{(1)}$ at point $A^{(1)}$ at a small distance from the given point A differs from the velocity V_τ at point A by an infinitesimal, the differential

$$dV_{n,\infty} = V_\tau\, d\omega = V_\tau\, d\tau/R_s \tag{10.4.51}$$

where $R_s = d\tau/d\omega$ is the radius of curvature of the wave at point A (Fig. 10.4.7*b*).

In accordance with (10.4.51), we shall write Eq. (10.4.50) in the form

$$T_2\, dS_2 = (1 - \bar{\rho})^2\, V_{n,\infty} V_\tau\, d\tau/R_s \tag{10.4.52}$$

Introducing (10.4.47) and (10.4.52) into (10.4.46), we find

$$\Omega_z V_s \sin(\theta_s - \beta_s) = (1 - \bar{\rho})^2\, V_{n,\infty} V_\tau/R_s$$

Using formula (10.4.21) for V_s, and also the expressions

$$V_{n,\infty} = V_\infty \sin\theta_s; \quad V_\tau = V_\infty \cos\theta_s \tag{10.4.53}$$

that are obtained from the triangle of velocities in Fig. 10.4.7*b*, we find the following expression for a vortex:

$$\Omega_z = V_\infty (1 - \bar{\rho})^2 \sin\theta_s \cos\theta_s/[(\bar{\rho}^2 \sin^2\theta_s + \cos^2\theta_s)^{1/2} R_s] \tag{10.4.54}$$

Substituting $\pi/2 - \omega$ for θ_s here, we have

$$\Omega_z = V_\infty (1 - \bar{\rho})^2 \cos\omega \sin\omega/[(\bar{\rho}^2 \cos^2\omega + \sin^2\omega)^{1/2} R_s] \tag{10.4.54'}$$

In the vicinity of the stagnation point, where the quantities ω are small and $R_s \to R_{s0}$, we obtain

$$\Omega_z = V_\infty (1 - \bar{\rho})^2\, \omega/(\bar{\rho} R_{s0}) \tag{10.4.54''}$$

Equating the right-hand sides of (10.4.41) and (10.4.54″) and taking into account that $\omega/x = 1/R_{s0}$, we find the coefficient

$$c_2 = V_\infty (1 - \bar{\rho})^2/(2\bar{\rho}R_{s0}^2) \qquad (10.4.55)$$

Introducing this value of c_2 into Eqs. (10.4.35) and (10.4.40) and solving them simultaneously, we obtain a relation for the coefficient c_1:

$$c_1 = (\pm V_\infty/R_{s0})\sqrt{2\bar{\rho} - \bar{\rho}^2} \qquad (10.4.56)$$

We determine the velocity on the surface of the nose from (10.4.36) provided that $y = 0$:

$$V_x = xc_1 = \pm (xV_\infty/R_{s0})\sqrt{2\bar{\rho} - \bar{\rho}^2} \qquad (10.4.57)$$

It follows from the property of oddness of the function V_x that when $x > 0$ or $x < 0$, we have, respectively, $V_x > 0$ or $V_x < 0$. This signifies that the plus sign has been taken for c_1 in formula (10.4.57) and, consequently, in Eq. (10.4.56).

Detachment and Shape of a Leading Shock Wave. In addition to the coefficient c_1, the solution of the system (10.4.35) and (10.4.40) yields a relation for the shock wave detachment (standoff) distance s_0 from the nose:

$$s_0 = \left(\frac{V_\infty}{R_{s0}} - c_1\right)\frac{1}{2c_2}$$

Let us introduce into this equation the values of c_2 from (10.4.55) and c_1 from (10.4.56) with the plus sign:

$$s_0 = \frac{\bar{\rho}R_{s0}}{(1-\bar{\rho})^2}\left[1 - (2\bar{\rho} - \bar{\rho}^2)^{1/2}\right] \qquad (10.4.58)$$

The right-hand side of this formula includes the radius of curvature R_{s0} of the wave on the axis, which in the preset free-stream boundary conditions should be considered as a function of the spherical nose radius R_n. If we proceed from the assumption that on the axis the wave is concentric to a sphere, then $R_{s0} = R_n + s_0$. Introducing the new notation $\bar{R}_{s0} = R_{s0}/R_n$ and $\tilde{s}_0 = s_0/R_{s0}$, we obtain

$$\bar{R}_{s0} = 1/(1 - \tilde{s}_0) \qquad (10.4.59)$$

In actual conditions, concentricity is not observed. The deviation from relation (10.4.59) increases with a decreasing number M_∞. To take account of the deviation from the concentric shape of a shock wave, we can use the expression obtained from experimental data:

$$\bar{R}_{s0} = R_{s0}/R_n = 1/(1 - \tilde{s}_0)^{2.5} \qquad (10.4.60)$$

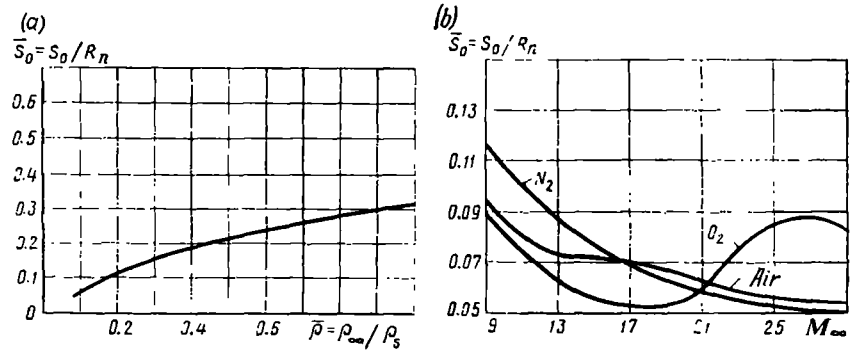

Fig. 10.4.8
Relative shock wave detachment distance ahead of a spherical nose in a supersonic flow:

a—for air (against $\bar{\rho}$); *b*—for oxygen, nitrogen, and air (against M_∞), $p_\infty = 103$ Pa, $T_\infty = 290$ K

As a result, the shock detachment distance related to the radius of a spherical nose is

$$\bar{s}_0 = \frac{s_0}{R_n} = \frac{s_0}{R_{s0}} \cdot \frac{R_{s0}}{R_n} = \tilde{s}_0 (1 - \tilde{s}_0)^{-2.5} \qquad (10.4.61)$$

where we take $\tilde{s}_0$ in accordance with (10.4.58) in the form

$$\tilde{s}_0 = \frac{\bar{\rho}}{(1-\bar{\rho})^2} [1 - (2\bar{\rho} - \bar{\rho}^2)^{1/2}] \qquad (10.4.62)$$

The quantity $\bar{s}_0$ calculated by (10.4.61) and (10.4.62) is plotted against $\bar{\rho} = \rho_\infty/\rho_s$ in Fig. 10.4.8*a*. On the section up to the value of $\bar{\rho} < 0.4$, the curve shown in Fig. 10.4.8*a* and characterizing the change in the detachment distance for a shock wave near a spherical nose is approximated by the simple relation (see [7])

$$\bar{s}_0 = 0.52 [\bar{\rho}/(1 - \bar{\rho})]^{0.86} \qquad (10.4.63)$$

In the obtained relations, the dimensionless density $\rho = \rho_\infty/\rho_s$ is a similarity criterion for the relative (dimensionless) detachment distance $\bar{s}_0 = s_0/R_n$ and is determined from the conditions of equilibrium dissociation directly behind the straight part of the shock wave.

Formula (10.4.63) reflects a real phenomenon consisting in that the temperature lowers in conditions of dissociation and this leads to an increase in the density. Consequently, additional compression of the gas takes place and, therefore, the shock wave approaches the surface of the body.

Of interest are the results of calculating the relative shock detachment distance obtained in [7]. These results are shown graphically in Fig. 10.4.8*b* and depict the change in the quantity $\bar{s}_0 = s_0/R_n$ depending on M_∞ for the flow of air, oxygen, and nitrogen over a sphere. A glance at the figure reveals that at values of $M_\infty = 9\text{-}13$, when the change in the specific heat of the air is mainly due to the dissociation of oxygen, the curve of $\bar{s}_0$ against M_∞ for air is closer to the corresponding curve for oxygen. With an increase in M_∞, the dissociation of nitrogen begins to have a greater and greater significance, and the curve characterizing the change in the relative shock detachment distance for air comes closer to the curve for nitrogen because this component predominates in the air.

How dissociation and ionization affect the detachment distance can be established clearly for pure gases such as oxygen and nitrogen. At $M_\infty = 18$, oxygen dissociates appreciably; as calculations show, its density reaches a maximum value, and the distance $\bar{s}_0$ (Fig. 10.4.8*b*) is minimum. With an increase in M_∞, the oxygen becomes completely dissociated, the compression diminishes, and the distance of detachment of a shock wave grows accordingly. With a further increase in M_∞, primary ionization of the gas occurs, its specific heat grows and, consequently, its compression, which leads to a decrease in the value of $\bar{s}_0$. For nitrogen, the effect of the variability in the specific heat is observed at considerably higher values of M_∞ than for oxygen. In addition, since dissociation and ionization in nitrogen proceed not consecutively, as in oxygen, but virtually simultaneously, the non-monotonic nature of the change in the values of $\bar{s}_0$ for nitrogen is less pronounced than for oxygen.

For air, which is a volume mixture (containing about 26% of oxygen and 74% of nitrogen), the $\bar{s}_0$ curve is more monotonic than for pure oxygen, which can be seen from Fig. 10.4.8*b*.

The shape of the generatrix of the leading shock wave can be determined by calculations based on the solution of a system of the corresponding gas-dynamic equations of the supersonic flow over blunt-nosed bodies, and also experimentally. Interesting results of determining the parameters of such flow and, particularly, the shape of a shock wave are given in [7].

Calculations and experimental investigations of the supersonic flow over cones with a spherical nose (cone spheres) show that the generatrix of a shock wave can be approximated by the hyperbola

$$(x + a)^2/a^2 - r^2/b^2 = 1 \qquad (10.4.64)$$

shown in Fig. 10.4.9. In Eq. (10.4.64), a and b are the semiaxes of the hyperbola. They can be determined as follows. It is known from

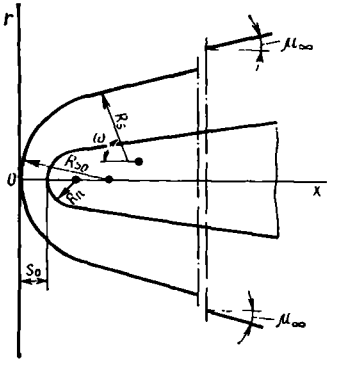

Fig. 10.4.9
Shock wave ahead of a cone-sphere in a supersonic flow

analytical geometry that the radius of curvature at a point of a curve given by the equation $r = r(x)$ is

$$R = -(1 + r'^2)^{3/2}/r'' \qquad (10.4.65)$$

where $r' = dr/dx$ and $r'' = d^2r/dx^2$.

In accordance with (10.4.64), we have

$$r' = (1 + r^2/b^2)^{1/2}\, b^2/(ra); \quad r'' = -b^4/(r^3a^2)$$

Let us introduce the values of these derivatives into (10.4.65):

$$R = \frac{b^2}{a}\left[1 + \frac{r^2}{b^2}\left(1 + \frac{a^2}{b^2}\right)\right]^{3/2} \qquad (10.4.66)$$

Assuming that $r = 0$, we find the radius of curvature R_{s0} on the axis

$$R_{s0} = b^2/a \qquad (10.4.67)$$

Accordingly, (10.4.66) can be written in the form

$$R = R_{s0}\left[1 + \frac{r^2}{b^2}\left(1 + \frac{a^2}{b^2}\right)\right]^{3/2} \qquad (10.4.66')$$

A shock a long way downstream from a body in a flow transforms into a weak disturbance wave whose inclination to the direction of the free-stream velocity is determined by the angle

$$\theta_s = \mu_\infty = \sin^{-1}(1/M_\infty) = \tan^{-1}\left(1/\sqrt{M_\infty^2 - 1}\right)$$

Inspection of hyperbola equation (10.4.64) reveals that the slope of the shock wave generatrix at an arbitrary point is

$$\tan\theta_s = r' = (1 + r^2/b^2)^{1/2}\, b^2/(ra)$$

Going over to the limit at $r \to \infty$, we obtain

$$\lim_{r\to\infty} \tan\theta_s = \tan\mu_\infty = b/a = 1/\sqrt{M_\infty^2 - 1} \qquad (10.4.68)$$

By solving (10.4.67) and (10.4.68) simultaneously and determining

$$b = R_{s0}\sqrt{M_\infty^2 - 1}, \quad a = R_{s0}(M_\infty^2 - 1) \tag{10.4.69}$$

we thereby obtain the possibility of calculating the radius of curvature of the shock wave by (10.4.66').

Initial Gradient and Velocity Distribution. By (10.4.57), the velocity gradient at the stagnation point (the initial gradient) is

$$\left(\frac{\partial V_x}{\partial x}\right)_{\substack{x=0\\y=0}} = \tilde{\lambda} = \frac{V_\infty}{R_{s0}}\sqrt{2\bar{\rho} - \bar{\rho}^2} \tag{10.4.70}$$

Experimental verification shows that if in (10.4.70) we assume

$$R_{s0} = R_n(1 - \bar{s}_0)^{-1/2} \tag{10.4.71}$$

i.e. proceed from an expression assuming a smaller deviation from a concentric shape of a shock wave near the spherical surface of the nose than follows from (10.4.60), the results obtained for the initial velocity gradient are suitable for both very high and low supersonic velocities. The working relation has the form

$$\tilde{\lambda} = (V_\infty/R_n)\sqrt{(2\bar{\rho} - \bar{\rho}^2)(1 - \tilde{s}_0)} \tag{10.4.72}$$

We can express the quantity $\tilde{s}_0$ in terms of the relative detachment distance $\bar{s}_0$ if we use the expression

$$\bar{s}_0 = \frac{s_0}{R_n} = \frac{s_0}{R_{s0}} \cdot \frac{R_{s0}}{R_n} = \frac{\tilde{s}_0}{\sqrt{1 - \tilde{s}_0}}$$

according to which

$$\tilde{s}_0 = -\frac{\bar{s}_0^2}{2}\left(1 - \sqrt{1 + \frac{4}{\bar{s}_0^2}}\right) \tag{10.4.73}$$

The relative detachment distance $\tilde{s}_0$ in this formula can be determined from (10.4.63). Relation (10.4.72) is suitable provided that expression (10.4.73) is used for values of $\bar{\rho} \leqslant 0.4$.

The velocity distribution on the spherical surface of the nose in the vicinity of the stagnation point can be expressed in accordance with (10.4.70) in terms of the initial velocity gradient $\tilde{\lambda}$:

$$V_x = \tilde{\lambda}x \tag{10.4.74}$$

Here x is the length of a circular arc calculated from the known central angle φ as $x = \varphi R_n$.

Hence,

$$V_x = \tilde{\lambda}R_n\varphi \tag{10.4.74'}$$

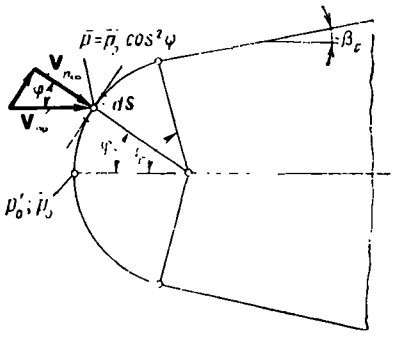

Fig. 10.4.10
To the determination of the pressure by Newton's method for a supersonic flow over a blunt-nosed surface

Experimental investigations show that Eq. (10.4.74') corresponding to the conditions of flow over a small section of the sphere near the stagnation point at a very high free-stream velocity can be used for calculating the velocity on a considerably greater section of the curved surface, and also with comparatively small Mach numbers M_∞. The results of experiments in wind tunnels at $M_\infty = 1.2\text{-}4.9$ confirm the linearity of dependence (10.4.74') of the velocity on the angle φ from $\varphi = 0$ to $\varphi = 50°$ and show that there is a small deviation from this relation within the interval of $50° < \varphi < 90°$. Formula (10.4.74') may be used in practical calculations for all values of φ from 0 to 90° with a good approximation.

The Use of Newton's Method for Calculating the Flow over a Blunt-Nosed Conical Body. This method is based on Newton's corpuscular theory according to which gas particles are disturbed only when they collide with a solid wall and completely lose the momentum component normal to the wall. If $V_{n,\infty}$ is the normal component of the free-stream velocity vector and dS is an elementary area of the surface in the flow (Fig. 10.4.10), then for a point being considered the loss in the momentum in unit time is

$$\rho_\infty V_{n,\infty}(V_{n,\infty} - 0)\, dS = \rho_\infty V_{n,\infty}^2\, dS$$

The value of the impulse of the force produced by the excess pressure $(p - p_\infty)\, dS$ during the same time, by the theorem on the impulse of a force, is determined by the loss in the momentum. Consequently, the excess pressure at the given point is $p - p_\infty = \rho_\infty V_{n,\infty}^2$. We can see from Fig. 10.4.10 that $V_{n,\infty} = V_\infty \cos\varphi$, hence

$$p - p_\infty = \rho_\infty V_\infty^2 \cos^2\varphi$$

Dividing both sides of this equation by the velocity head $\rho_\infty V_\infty^2/2$, we obtain **Newton's formula** for the pressure coefficient

$$\bar{p} = 2(p - p_\infty)/(\rho_\infty V_\infty^2) = 2\cos^2\varphi \qquad (10.4.75)$$

This formula corresponds to the flow model described above, i.e. **Newton's model**, *when gas particles rebound elastically upon interacting with a surface*. A drawback of this model is that it does not give a fundamentally correct reply to the question of how the gas particles behave after the collision. Actually, their velocities after a collision do not equal the components of the free-stream velocity vector tangent to the surface, while the velocities of these particles behind the place of collision are not determined in general by this model. Hence, in practice Newton's model does not consider the process itself of a flow over a body.

This shortcoming is absent in **Euler's model** *providing for the investigation of the flow of a fluid near a surface*, i.e. for the determination of the velocity and other parameters at each point and, as a result, for the calculation of the interaction of the fluid with the body in the flow.

But with a view to the simplicity and convenience of calculations according to Newton's theory, the necessity arises of improving it to obtain better results when calculating the aerodynamic variables. Let us consider one such improvement. Examination of formula (10.4.75) shows that at the stagnation point for which the central angle $\varphi = 0$, the pressure coefficient $\bar{p}_0 = 2$. Consequently, we shall write (10.4.75) in the form

$$\bar{p} = \bar{p}_0 \cos^2 \varphi \qquad (10.4.75')$$

Experimental investigations show that if instead of the value $\bar{p}_0 = 2$, which does not exist for real flows, we use in formula (10.4.75') a value of $\bar{p}_0$ obtained either experimentally or by exact theoretical calculations, this formula will yield results very close to actual ones on a considerable section of a spherical surface. Formula (10.4.75'), unlike (10.4.75), is called **Newton's modified or improved formula**, according to which the excess pressure is

$$p - p_\infty = (p_0' - p_\infty) \cos^2 \varphi$$

whence the ratio of the pressure p at a certain point to the pressure p_0' at the stagnation point is

$$p/p_0' = \cos^2 \varphi + (p_\infty/p_0') \sin^2 \varphi \qquad (10.4.76)$$

Near the stagnation point, the flow can be considered in a first approximation as incompressible, and it can be calculated with the aid of the Bernoulli equation

$$V_\infty^2/2 + p/\rho = p_0'/\rho \qquad (10.4.77)$$

where ρ is the density, assumed to be constant within a small vicinity of the stagnation point and equal to the density ρ_0' at this point.

After inserting (10.4.77) into (10.4.76), provided that $\rho = \rho_0'$, we get

$$\frac{V_x^2}{2} = \frac{p_0'}{\rho_0'} - \frac{p}{\rho_0'} = \frac{p_0'}{\rho_0'}\left[1 - \left(\cos^2\varphi + \frac{p_\infty}{p_0'}\sin^2\varphi\right)\right]$$

Let us calculate the derivative with respect to x:

$$V_x \frac{dV_x}{dx} = 2\cos\varphi \sin\varphi \frac{d\varphi}{dx} \cdot \frac{p_0'}{\rho_0'}\left(1 - \frac{p_\infty}{p_0'}\right)$$

Going over to the limit at $\varphi \to 0$, $x \to 0$ and taking into account that $(\cos\varphi)_{x\to 0} = 1$, $(\sin\varphi)_{x\to 0} = \varphi = x/R_n$, $(V_x/x)_{x\to 0} = (dV_x/dx)_{x\to 0} = \tilde{\lambda}$, and $(d\varphi/dx)_{x\to 0} = 1/R_n$, we find a relation for the initial velocity gradient:

$$\left(\frac{dV_x}{dx}\right)_{x\to 0} = \tilde{\lambda} = \frac{1}{R_n}\sqrt{\frac{2(p_0' - p_\infty)}{\rho_0'}} \qquad (10.4.78)$$

When using (10.4.78) to determine the initial velocity gradient, we must know the pressure p_0' and density ρ_0' at the stagnation point. In accordance with the linear law expressed by relation (10.4.74'), the velocity distribution can be represented by the relation

$$V_x = \varphi\sqrt{2(p_0' - p_\infty)/\rho_0'} \qquad (10.4.78')$$

In addition to this formula, the relation obtained from Eq. (3.6.26) for the pressure in an isentropic flow can be used to calculate the velocity. We shall assume in this equation that $p_0 = p_0'$, $V = V_x$, and that the quantity k equals the value of $\bar{k}$ calculated for the stagnation point with account taken of the influence of the temperature T_0' and the pressure p_0' at this point. Solving the equation relative to the velocity V_x, we find

$$V_x = V_{max}\left[1 - (p/p_0')^{(\bar{k}-1)/\bar{k}}\right]^{1/2}$$

Equation (3.6.22) yields the following expression for the maximum velocity:

$$V_{max}^2 = \frac{2}{k_\infty - 1}a_\infty^2 + V_\infty^2$$

where the variables with the subscript "∞" correspond to the undisturbed flow ahead of the shock wave. Dividing both sides of the last equation by V_∞^2 and having in view that $M_\infty^2 = V_\infty^2/a_\infty^2$, we find the relation

$$\frac{V_{max}^2}{V_\infty^2} = \frac{2}{k_\infty - 1}\cdot\frac{1}{M_\infty^2} + 1$$

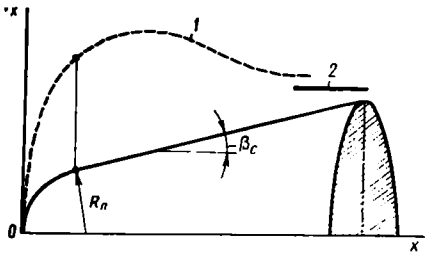

Fig. 10.4.11
Velocity distribution on a blunt cone in a supersonic flow:
1—experimental curve; *2*—velocity on a sharp-nosed cone (theory)

In accordance with this relation, the working expression for the velocity has the form

$$\frac{V_x}{V_\infty} = \left(\frac{2}{k_\infty - 1} \cdot \frac{1}{M_\infty^2} + 1\right)^{1/2} \left[1 - \left(\frac{p}{p_0'}\right)^{(\bar{k}-1)/\bar{k}}\right]^{1/2} \quad (10.4.79)$$

where p/p_0' is determined with the aid of Newton's formula (10.4.76).

We can simplify the calculations of the velocity and other parameters of a gas to a still greater extent with the aid of tables of the thermodynamic functions. Knowing the law of the change in the function $\pi(\lambda) = p/p_0'$ [see (10.4.76)], we can determine the values of the gas-dynamic functions $\lambda = V_x/a^*$, $\varepsilon = \rho/\rho_0'$, and $\tau = T/T_0'$ from tables [8].

Assuming here that the critical speed of sound a^* and the stagnation parameters ρ_0', p_0', T_0' are known, we can calculate the following quantities for the point on a blunt-nosed surface being considered:

$$V_x = \lambda a^*, \quad \rho = \varepsilon \rho_0', \quad p = \pi p_0', \quad T = \tau T_0'$$

The parameters of the gas on the peripheral conical surface joining the spherical nose can as a first approximation be taken the same as on the line of joining, i.e. at the end of the nose. Particularly, the velocity on the cone can be found by (10.4.78') assuming that $\varphi = \pi/2 - \beta_c$:

$$V_x = V_c = (\pi/2 - \beta_c) \sqrt{2(p_0' - p_\infty)/\rho_0'} \quad (10.4.80)$$

We obtain a different relation for the velocity on the cone from (10.4.79) if we assume in accordance with (10.4.76) that

$$\frac{p}{p_0'} = \frac{p_c}{p_0'} = \sin^2 \beta_c + \frac{p_\infty}{p_0'} \cos^2 \beta_c \quad (10.4.81)$$

where $\beta_c = \pi/2 - \varphi_c$ is the cone angle [φ_c is the central angle for a half-sphere (see Fig. 10.4.10)].

The velocity obtained in this way is considered as a constant quantity over the entire surface of the cone. Experimental investigations show that the real velocity differs from this value and that the velocity distribution has the form shown in Fig. 10.4.11. It

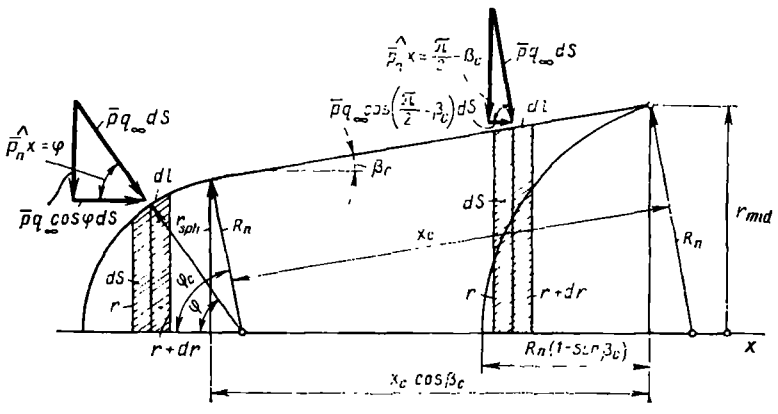

Fig. 10.4.12
To the calculation of the aerodynamic drag for a blunt cone

grows with an increasing distance from the stagnation point and reaches its maximum value at a certain distance from the point where the nose joins the cone. Farther downstream, the velocity decreases, and on remote peripheral sections reaches a value corresponding to the velocity on a sharp-nosed cone.

The pressure (wave) drag of a blunt cone can be found from the pressure distribution by calculating this drag as the sum of the drags of a spherical nose (the subscript "sph") and the conical part of the surface (the subscript "c"):

$$X_a = X_{\text{sph}} + X_{\text{c}}$$

Assuming in (1.3.2) that the drag coefficient $c_{f,x} = 0$ and taking the area of the base cross section (mid-section) of the cone as the characteristic area S, i.e. $S = S_{\text{mid}} = \pi r_{\text{mid}}^2$, we obtain for the nose

$$X_{\text{sph}} = q_\infty S_{\text{mid}} \int\limits_{S_{\text{sph}}} \bar{p} \cos \widehat{(n, x)} \frac{dS}{S_{\text{mid}}}$$

whence the wave drag coefficient is

$$(c_{x,\,w})_{\text{sph}} = \frac{X_{\text{sph}}}{q_\infty S_{\text{mid}}} = \int\limits_{S_{\text{sph}}} \bar{p} \cos \widehat{(n, x)} \frac{dS}{S_{\text{mid}}}$$

A close look at Fig. 10.4.12 reveals that $\cos \widehat{(n, x)} = \cos \varphi$ and $dS = 2\pi r\, dl = 2\pi r\, dr/\cos \varphi$. But since $r = R_{\text{n}} \sin \varphi$ and $dr = R_{\text{n}} \cos \varphi\, d\varphi$, we have

$$dS = 2\pi R_{\text{n}}^2 \sin \varphi\, d\varphi$$

With a view to the above expressions and to formula (10.4.75'), we obtain

$$(c_{x,\,w})_{sph} = \int_0^{\varphi_c=\pi/2-\beta_c} \bar{p}_0 \cos^2\varphi \cos\varphi \frac{2\pi R_n^2 \sin\varphi}{\pi r_{mid}^2} d\varphi$$

$$= \frac{\bar{p}_0 R_n^2}{r_{mid}^2} \cos^2\beta_c \left(1 - \frac{\cos^2\beta_c}{2}\right) \qquad (10.4.82)$$

If we assume in this formula that $r_{mid} = r_{sph}$, we obtain the wave drag coefficient for a blunted nose related to the base area $S = \pi r_{sph}^2$. Taking into account that $r_{sph} = R_n \sin\varphi_c$, we find

$$(c_{x,\,w})_{sph} = \bar{p}_0 (1 - \sin^2\varphi_c/2) \qquad (10.4.83)$$

The drag of a conical part with the side surface area S_{side} is

$$X_c = q_\infty S_{mid} \int_{S_{side}} \bar{p} \cos\widehat{(n,\,x)}\, dS/S_{mid}$$

Examination of Fig. 10.4.12 shows that

$$\cos\widehat{(n,\,x)} = \cos(\pi/2 - \beta_c) = \sin\beta_c; \quad dS = 2\pi r\, dl = 2\pi r\, dr/\sin\beta_c$$

Also taking into account that

$$\bar{p} = \bar{p}_0 \cos^2\varphi_c = \bar{p}_0 \cos^2(\pi/2 - \beta_c) = \bar{p}_0 \sin^2\beta_c; \quad S_{mid} = \pi r_{mid}^2$$

we obtain for the drag coefficient of the conical part

$$(c_{x,\,w})_c = \frac{X_c}{q_\infty S_{mid}} = \int_{r_{sph}}^{r_{mid}} \bar{p}_0 \sin^2\beta_c \sin\beta_c \frac{2\pi r\, dr}{\pi r_{mid}^2 \sin\beta_c}$$

$$= \frac{\bar{p}_0 \sin^2\beta_c}{r_{mid}^2}(r_{mid}^2 - r_{sph}^2) = \bar{p}_0 \sin^3\beta_c \frac{x_c}{r_{mid}^2}(2r_{mid} - x_c \sin\beta_c) \qquad (10.4.84)$$

By summing (10.4.82) and (10.4.84), we find the total drag coefficient related to the area $S_{mid} = \pi r_{mid}^2$:

$$c_{x_a} = \frac{X_a}{q_\infty S_{mid}} = (c_{x,\,w})_{sph} + (c_{x,\,w})_c$$

$$= \bar{p}_0 \left[\frac{R_n^2}{r_{mid}^2} \cos^2\beta_c \left(1 - \frac{\cos^2\beta_c}{2}\right)\right.$$

$$\left. + \frac{x_c}{r_{mid}^2} \sin^3\beta_c (2r_{mid} - x_c \sin\beta_c)\right] \qquad (10.4.85)$$

In the particular case when $R_n = 0$, we obtain the drag coefficient for a sharp-nosed cone. We find the value of this coefficient from the condition that $\bar{p}_0 = 2$ and $x_c \sin \beta_c = r_{mid}$:

$$c_{x_a} = (c_{x,w})_c = 2 \sin^2 \beta_c \qquad (10.4.86)$$

If $x_c = 0$, the surface in the flow becomes a spherical segment of height $R_n (1 - \sin \beta_c)$ (Fig. 10.4.12). Assuming in (10.4.85) that $x_c = 0$, we obtain formula (10.4.83) for the wave drag coefficient of such a spherical surface. In this formula, $\varphi_c = \pi/2 - \beta_c$.

Flow over a Flat Nose

The results of theoretical and experimental investigation of the pressure distribution over a flat nose are depicted graphically in Fig. 10.4.13. An analysis of these results allows us to establish a general law for the change in the pressure coefficient in the form of $\bar{p} = \bar{p}_0 f(\bar{r})$, where $\bar{p}_0$ is the pressure coefficient for the nose centre coinciding with the stagnation point, $\bar{r} = r/R_n$ is a dimensionless quantity (Fig. 10.4.13), and $f(\bar{r})$ is a "universal" function depending on $\bar{r}$.

Accordingly, the wave drag coefficient for a flat nose is

$$(c_{x,w})_{fl} = \bar{p}_0 \int_0^1 f(\bar{r})\, d\bar{r}^2$$

Assuming that the universal function $f(\bar{r})$ is suitable for any supersonic velocities, we can calculate the integral in the above formula and obtain

$$(c_{x,w})_{fl} = 0.915\bar{p}_0 \qquad (10.4.87)$$

This value is about double the drag coefficient for a hemisphere whose value by (10.4.83) is determined by the expression $(c_{x,w})_{sph} = 0.5\bar{p}_0$ (when $\varphi_c = \pi/2$).

The magnitude of the shock detachment distance from a flat nose is greater than from a sphere. An estimate leads to the conclusion that if for a spherical nose the quantity $\bar{s}_0 = s_0/R_n$ is of the order of the density ratio $\bar{\rho} = \rho_\infty/\rho_0'$, then for a flat nose we have $\bar{s}_0 \sim \sqrt{\bar{\rho}}$. In accordance with experimental data, the relative detachment distance is

$$\bar{s}_0 = s_0/R_n = 1.03 \sqrt{\bar{\rho}/(1-\bar{\rho})} \qquad (10.4.88)$$

The radius of curvature of the wave on the axis that determines the shape of the wave near the nose, like the detachment distance,

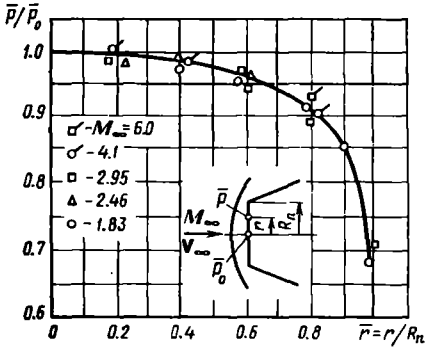

Fig. 10.4.13
Pressure distribution over a flat nose

is proportional to the radius of flat blunting. Experimental investigations show that

$$\bar{R}_{s0} = R_{s0}/R_n = 0.52\,(3-\bar{\rho})\,[\bar{\rho}\,(1-\bar{\rho})]^{-1/2} \qquad (10.4.89)$$

In accordance with (10.4.89), when $\bar{\rho} \to 0$, the quantity $R_{s0} \to \infty$ because at the limit the wave contacts the flat surface of the nose.

Let us consider the velocity gradient at the centre of the nose coinciding with the stagnation point. As shown by investigations, its value at this point does not equal zero. We can assume that a flat nose affects the flow in the vicinity of the stagnation point similar to a spherical surface having a radius of R_n^{eq}. Consequently, we can choose such an equivalent sphere radius R_n^{eq} at which the curvature of the wave on the axis will approximately equal its value ahead of the nose. Therefore, $(\bar{R}_{s0})_{fl}\, R_n = (\bar{R}_{s0})_{sph}\, R_n^{eq}$, where R_n is the radius of the nose. By (10.4.78), the velocity gradient at the centre of the flat nose is

$$\tilde{\lambda} = \frac{1}{R_n^{eq}} \sqrt{\frac{2\,(p_0' - p_\infty)}{\rho_0'}} \qquad (10.4.90)$$

where $R_n^{eq} = R_n\,(\bar{R}_{s0})_{fl}/(\bar{R}_{s0})_{sph}$; here $(\bar{R}_{s0})_{fl} = (R_{s0}/R_n)_{fl}$ is found by (10.4.89), and $(\bar{R}_{s0})_{sph} = (R_{s0}/\bar{R}_n)_{sph}$, by (10.4.71). Experimental investigations show that for high velocities formula (10.4.90) yields quite satisfactory results.

Drag of a Slender Cone with Slight Blunting

Relation (10.4.85) corresponds to the assumption of such a flow over a blunted body when the velocity and pressure on the conical surface are the same as at the tip of a spherical nose. This phenomenon

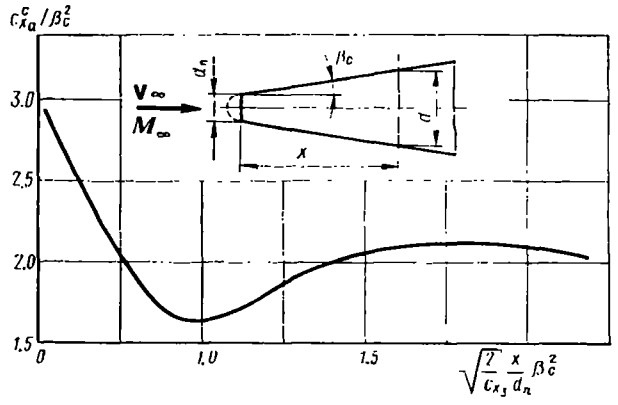

Fig. 10.4.14
Drag coefficient of a slender blunt cone

is not observed in real conditions, but as a first approximation such an assumption can be justified for a sufficiently thick cone. The phenomenon corresponds to the experimentally observed rapid recovery of the pressure coefficient to the value on a sharp-nosed conical surface $\bar{p}_c$ (at a high velocity, $\bar{p}_c = 2\sin^2\beta_c$). For example, for a cone sphere of 40° at $M_\infty = 6$, such a recovery occurs at a distance from the nose that is somewhat larger than its diameter. This phenomenon is most pronounced at moderate numbers M_∞. The influence of the part of the surface near the nose on the total drag is not great because of the small magnitude of this part, and therefore the pressure on it may be taken the same as on the remaining conical surface.

Investigations reveal, however, that for slightly blunted slender bodies the pressure on the conical part is appreciably lower than that on a sharp-nosed cone, and with an increasing distance from the nose it recovers fairly slowly to the pressure on a sharp-nosed cone (see Fig. 10.4.5). With an increase in the supersonic velocities, the influence of blunting on the pressure distribution grows. A blunted nose affects the flow in a disturbed region having a length of scores and hundreds of blunting diameters; the more slender the body, the longer is this region and, consequently, the more effective is the action of blunting. In addition, the blunting effect depends on the shape of the nose, for example, it is substantially greater for a flat nose than for a sphere. Aerodynamic investigations of slender blunted conical bodies were performed by acad. G. Cherny [9]. Figure 10.4.14 presents a graph plotted according to the data of these investigations that allows us to calculate the drag coefficient of a cone with bluntness of an arbitrary configuration [$c^c_{x_a} = 4X^c_a/(q_\infty \pi d_n^2)$].

Examination of this graph reveals that at a certain length of the cone its drag becomes minimum. A minimum drag coefficient is achieved in accordance with the graph depicted in Fig. 10.4.14 at a relative cone length of $x/d_n = (0.68/\beta_c^2)\, c_{x,b}^{1/2}$ (where $c_{x,b}$ is the drag coefficient of the blunted part related to the area $\pi d_n^2/4$). In comparison with the relevant value for a sharp-nosed cone, the minimum value of the drag coefficient is lower by about 10%.

11

A Sharp-Nosed Body of Revolution in a Supersonic Flow

11.1. Use of the Method of Characteristics

A craft (for example, a rocket or a missile) or certain of its structural elements may have the shape of a sharp-nosed body of revolution. Let us consider the calculation of the supersonic flow over a sharp-nosed body of revolution at a zero angle of attack. The configuration of the body of revolution (Fig. 11.1.1) is given by the equation of its generatrix $r = f(x)$. The free-stream parameters are also known (M_∞, p_∞, ρ_∞, T_∞). If the thickness of the body of revolution is such that it disturbs the flow significantly, the latter can be calculated by the method of characteristics.

The calculations are usually commenced with determination of the conical flow near the tip, which in the close vicinity of the nose may be replaced with a cone (in Fig. 11.1.1 point K corresponds to its boundary). As a result, the velocities are found on the generatrices OD, OA, and other intermediate conical surfaces (including the generatrices of the cone OK and of the shock OS), as well as the angles ω, μ, and β. The semi-apex angles θ of the intermediate cones are chosen arbitrarily, but so that the intervals $\Delta\theta$ are sufficiently small and ensure the preset accuracy of the parameters being calculated.

It is good practice to accompany the calculations by a graphical construction of a network of characteristic curves as shown in Fig. 11.1.1. Initially, we plot element KD of the first family characteristic by drawing through point K a straight line at the angle $\mu_K + \beta_K$ (where $\beta_K = \beta_0$) to the cone axis up to its intersection point D with the adjacent generatrix of the intermediate conical surface whose semi-apex angle is θ_D. As a result, we determine the coordinates x_D and r_D of point D graphically.

We obtain a higher accuracy when determining these coordinates analytically. To do this, let us write an equation for an element of a first family characteristic, i.e.

$$r_K - r_D = (x_K - x_D) \tan (\mu_K + \beta_K) \qquad (11.1.1)$$

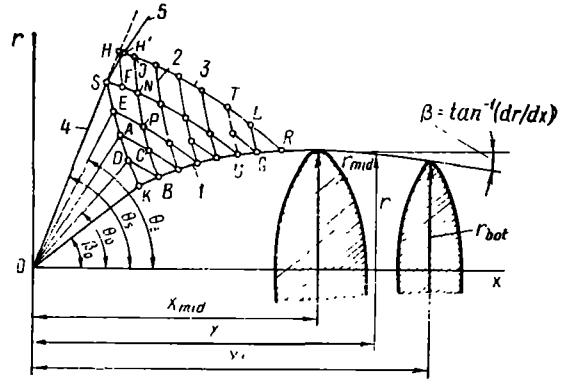

Fig. 11.1.1
To the calculation of a supersonic flow over a body of revolution according to the method of characteristics:
1—generatrix of the body of revolution: 2—first family characteristic; 3—second family characteristic; 4—normal shock; 5—curved part of shock

and an equation for the generatrix, i.e.

$$r_D = x_D \tan \theta_D \tag{11.1.2}$$

Upon solving these equations, we find the unknowns x_D and r_D. In a similar way, we calculate the coordinates of the remaining points of first family characteristic KS having the form of a broken line that is the boundary of the conical flow. Here we find the coordinates x_S and r_S of point S at the intersection of element ES of the first family characteristic with generatrix OS of the conical shock by solving the simultaneous equations

$$r_E - r_S = (x_E - x_S) \tan (\mu_E + \beta_E) \tag{11.1.3}$$

$$r_S = x_S \tan \theta_S \tag{11.1.4}$$

The coordinates of points of characteristic KS obtained in this way correspond to the angles μ and β assumed to be constant along each of the considered elements of the characteristic and equal to the values of these angles at the beginning of the element.

To obtain more accurate data, we can calculate the coordinates from the mean values of the angles μ and β between the extreme points of a characteristic element. Therefore, particularly, instead of 11.1.1) we shall write

$$r_K - r_D = (x_K - x_D) \tan [(\mu_K + \mu_D + \beta_K + \beta_D)/2] \tag{11.1.1'}$$

and instead of (11.1.3)

$$r_E - r_S = (x_E - x_S) \tan [(\mu_E + \mu_S + \beta_E + \beta_S)/2] \tag{11.1.3'}$$

In these equations, x_D, r_D, and x_S, r_S are the refined coordinates of points D and S.

After we have determined the form of curve of characteristic KS, the velocities, the numbers M, and the angles μ and β at points on this characteristic, we can reduce the solution of the problem to finding of the velocity field (the numbers M) in the region between the characteristic and a generatrix of the body in the flow. For this purpose, we shall use the relevant relations for the characteristics in a physical plane (the plane of the flow) and in the hodograph plane.

When choosing relations for characteristics in a hodograph plane, we must take into account that the flow is *vortex-free* (*isentropic*) in the region of the flow confined by (1) normal shock generatrix OS, (2) second family characteristic SU (which is gradually constructed in the course of solving the problem), and (3) body generatrix OU. In the adjacent region confined by the same characteristic SU, sections SH of the curved shock and UR of the body generatrix, the flow is *vortex* (*non-isentropic*).

To find the velocity field for the isentropic section of the flow, let us draw through each point of characteristic KS elements of a second family characteristic. One of them, passing through point D, will intersect the wall at point B, and it is just at this point that we have to find the velocity. We determine the coordinates of this point by simultaneously solving an equation of an element of a second family characteristic

$$r_D - r_B = (x_D - x_B) \tan (\beta_D - \mu_D) \qquad (11.1.5)$$

and an equation of a generatrix of the body

$$r_B = f(x_B) \qquad (11.1.6)$$

By solving Eqs. (11.1.5) and (11.1.6), we find the coordinates of point B (x_B, r_B). We determine the angle β_B of inclination of a tangent to the generatrix at point B that coincides (because of flow without separation) with the angle of inclination of the velocity vector at this point from the equation

$$(dr/dx)_B = \tan \beta_B = [df(x)/dx]_{x=x_B} \qquad (11.1.7)$$

To find the velocity at point B, we shall use Eq. (5.4.9). This equation, written in the difference form at $y = r$ and $\varepsilon = 1$ (axisymmetric flow), becomes

$$\Delta\omega_D + \Delta\beta_D - \frac{x_B - x_D}{r_D} m_D = 0 \qquad (11.1.8)$$

In this equation, the increment $\Delta\beta_D = \beta_B - \beta_D$ is the difference between the angles of inclination of the velocity vectors at points B and D. By (11.1.7), we have

$$\beta_B = \tan^{-1} [(dr/dx)_B] \qquad (11.1.7')$$

Taking into account that $\Delta\omega_D = \omega_B - \omega_D$, from (11.1.8) we find the angle

$$\omega_B = \omega_D - (\beta_B - \beta_D) + \frac{x_B - x_D}{r_D} m_D \qquad (11.1.9)$$

where by (5.4.6)

$$m_D = \sin \beta_D \sin \mu_D / \cos (\beta_D - \mu_D) \qquad (11.1.10)$$

We find the angle ω_D in (11.1.9) from Table 5.3.1 according to the value of the number M_D at point D. Having evaluated ω_B by (11.1.9), we use the same Table 5.3.1 to determine the values of the number M_B and the angle $\mu_B = \sin^{-1}(1/M_B)$ at point B corresponding to the value of ω_B. Next, we can calculate the pressure from the found numbers M.

Let us first find the pressure p_K at point K which the number M_K corresponds to:

$$p_K = p_0' \left(1 + \frac{k-1}{2} M_K^2\right)^{-k/(k-1)} = p_0' \pi (M_K) \qquad (11.1.11)$$

where the stagnation pressure behind a conical shock

$$p_0' = p_0 \nu_0 \qquad (11.1.12)$$

is determined according to the stagnation pressure p_0 (3.6.29) ahead of the shock and the value of the function ν_0 calculated from (10.2.26) according to the shock angle θ_S and the number M_∞.

The pressure at point B is

$$p_B = p_0' \left(1 + \frac{k-1}{2} M_B^2\right)^{-k/(k-1)} = p_0' \pi (M_B) \qquad (11.1.13)$$

We find the functions $\pi(M_K)$ and $\pi(M_B)$ in (11.1.11) and (11.1.13) using the values of the numbers M_K and M_B from tables contained in [8].

The pressure coefficients are

$$\bar{p}_K = 2 (p_K - p_\infty)/(k M_\infty^2 p_\infty) \text{ and}$$
$$\bar{p}_B = 2 (p_B - p_\infty)/(k M_\infty^2 p_\infty) \qquad (11.1.14)$$

We determine the velocity, temperature, and density from the following expressions, respectively,

$$V_{K(B)}/V_{max} = \{1 - [p_{K(B)}/p_0']^{(k-1)/k}\}^{1/2} \qquad (11.1.15)$$

$$T_{K(B)}/T_0 = \{1 + [(k-1)/2] M_{K(B)}^2\}^{-1} \qquad (11.1.16)$$

$$\rho_{K(B)}/\rho_0 = [T_{K(B)}/T_0]^{1/(k-1)} \nu_0 \qquad (11.1.17)$$

where we find ρ_0 and T_0 from the free-stream parameters by formulas (3.6.34) and (3.6.35), respectively, and the maximum velocity

from (3.6.22):

$$V_{max} = \left(V_\infty^2 + \frac{1}{k-1} a_\infty^2 \right)^{1/2} \qquad (11.1.18)$$

Having calculated the parameters at point B, we draw through it an element of a first family characteristic up to its intersection point C with the straight section of the second family characteristic issuing from point A (see Fig. 11.1.1). We determine the coordinates of point C from the solution of the equations for elements AC and BC of the characteristics. The equation of element AC of a characteristic has the form

$$r_A - r_C = (x_A - x_C) \tan (\beta_A - \mu_A) \qquad (11.1.19)$$

and the equation of element BC

$$r_B - r_C = (x_B - x_C) \tan (\beta_B + \mu_B) \qquad (11.1.20)$$

By solving these equations simultaneously, we find the coordinates of point C (x_C, r_C). To find the angles β_C and ω_C at this point, we must use Eqs. (5.4.8) and (5.4.9) for the characteristics. Writing these equations as difference ones and assuming that $\varepsilon = 1$, we obtain

$$\Delta\omega_B - \Delta\beta_B - \frac{x_C - x_B}{r_B} l_B = 0 \qquad (11.1.21)$$

$$\Delta\omega_A + \Delta\beta_A - \frac{x_C - x_A}{r_A} m_A = 0 \qquad (11.1.22)$$

where by (5.4.5) and (5.4.6), we have

$$\left.\begin{aligned} l_B &= \sin\beta_B \sin\mu_B / \cos(\beta_B + \mu_B) \\ m_A &= \sin\beta_A \sin\mu_A / \cos(\beta_B - \mu_A) \end{aligned}\right\} \qquad (11.1.23)$$

Instead of the four unknowns $\Delta\omega_B$, $\Delta\omega_A$, $\Delta\beta_B$, and $\Delta\beta_A$ in Eqs. (11.1.21) and (11.1.22), expressions (5.4.20) allow us to consider only two unknown quantities, namely, $\Delta\omega_B$ and $\Delta\beta_B$ (or $\Delta\omega_A$ and $\Delta\beta_A$).

With a view to expressions (5.4.20), Eq. (11.1.20) can be transformed as follows:

$$\Delta\omega_B + \omega_B - \omega_A + \Delta\beta_B + \beta_B - \beta_A - \frac{x_C - x_A}{r_A} m_A = 0 \qquad (11.1.24)$$

Solving this equation simultaneously with (11.1.21) for the variable $\Delta\beta_B$, we obtain

$$\Delta\beta_B = \frac{1}{2}\left[\frac{x_C - x_A}{r_A} m_A - \frac{x_C - x_B}{r_B} l_B - (\omega_B - \omega_A) - (\beta_B - \beta_A) \right] \qquad (11.1.25)$$

We use the found value of $\Delta\beta_B$ and (11.1.21) to find the angular increment

$$\Delta\omega_B = \Delta\beta_B + \frac{x_C - x_B}{r_B} l_B \qquad (11.1.21')$$

The absolute values of the angles at point C are as follows:

$$\beta_C = \Delta\beta_B + \beta_B, \quad \omega_C = \Delta\omega_B + \omega_B \tag{11.1.26}$$

We use the value of ω_C and Table 5.3.1 to find the number M_C and the disturbance angle $\mu_C = \sin^{-1}(1/M_C)$. When required, the number M_C allows us to find the other parameters, namely, the pressure, density, temperature, and velocity.

The parameters calculated in this way are a first approximation, because along the elements of the characteristics the coefficients l and m, and also the radial coordinates are assumed to be constant and equal to the corresponding values at points A and B. These parameters can be refined if instead of l_B, m_A, r_B, and r_A we introduce into Eqs. (11.1.21) and (11.1.22) the values calculated as the mean ones between those given at points A and B and those obtained at point C as a first approximation. For these mean values, we have the relations

$$l'_B = \sin\beta'_B \sin\mu'_B/\cos(\beta'_B + \mu'_B), \quad m'_A = \sin\beta'_A \sin\mu'_A/\cos(\beta'_A - \mu'_A) \tag{11.1.23'}$$

$$r'_B = (r_B + r_C)/2, \quad r'_A = (r_A + r_C)/2 \tag{11.1.27}$$

where

$$\left.\begin{aligned} \beta'_B &= (\beta_B + \beta_C)/2; \quad \mu'_B = (\mu_B + \mu_C)/2 \\ \beta'_A &= (\beta_A + \beta_C)/2; \quad \mu'_A = (\mu_A + \mu_C)/2 \end{aligned}\right\} \tag{11.1.28}$$

By continuing similar calculations, we can determine the parameters at all the points of the second row including point N at the intersection of elements PN of the first family characteristic and SN of the second family characteristic drawn from the end of a straight conical shock.

The further calculations consist in finding the parameters at the intersection point of an element of a first family characteristic drawn through point N with the extension of the shock beyond point S. In practice, to obtain a better approximation, we draw the characteristic not through point N, but through point F between N and S (see Fig. 11.1.1). We choose the coordinates x_F and r_F of point F so that element FH of the characteristic closest to the shock would be sufficiently small and could be considered as a straight section. We calculate the parameters at point F (ω, M, μ, β) according to their known values at points S and N by linear interpolation. For example,

$$\omega_F = \omega_S + (\omega_N - \omega_S)(x_F - x_S)/(x_N - x_S) \tag{11.1.29}$$

The equation of element FH of a first family characteristic has the form

$$r_F - r_H = (x_F - x_H)\tan(\beta_F + \mu_F) \tag{11.1.30}$$

By solving this equation simultaneously with the equation of a straight shock generatrix $r_H = x_H \tan \theta_s$, we determine the coordinates x_H and r_H and thus find as a first approximation the position of point H on the shock. These coordinates must be refined because the real shock behind point S becomes curved. Indeed, the first family characteristics (ES, FH, etc.) are expanding waves in their nature. When encountering a compression shock, these waves reduce its strength and, consequently, inclination, as a result of which the shock becomes curved.

The flow behind such a compression shock is vortex (non-isentropic), consequently to determine the velocity at point H we use Eq. (5.4.41) for element FH of a first family characreristic taking into consideration the change in the entropy behind a curved shock. Assuming in this equation that $y_F = r_F$ and $\varepsilon = 1$ (axisymmetric flow) and solving it for $\Delta\beta_F$ simultaneously with (5.4.38), we obtain relation (5.4.46) in which $\varepsilon = 1$ and $y_F = r_F$:

$$\Delta\beta_F = \left[\left(\frac{d\omega}{d\beta}\right)_S - 1\right]^{-1}\left(\omega_F - \omega_S + \frac{x_H - x_F}{r_F} l_F - \frac{x_H - x_F}{kR} \cdot \frac{\Delta S}{\Delta n} c_F\right) \tag{11.1.31}$$

where the derivative $(d\omega/d\beta)_S$ is found by (5.4.39), while the coefficients l_F and c_F are calculated by the relevant formulas (5.4.42).

Formula (11.1.31) includes the quantity ΔS determining the change in the entropy when passing from point H to point F. In first approximation calculations, we assume that point H is on the extension of the straight generatrix of the shock. We could therefore assume that the change in the entropy equals zero, i.e. $\Delta S = 0$. But this assumption lowers the accuracy of our calculations because point H is actually on the curved section of the shock (H'). Better results are obtained if we assume that the entropy (or stagnation pressure) at point H does not equal its value at point F.

The stagnation pressure $p'_{0,H}$ at point H is calculated in a first approximation as follows. Let us assume that the deflection angle β'_H of the flow through the shock at point H equals the angle of inclination of the velocity vector at point F. We can determine the corresponding shock angle $\theta'_{s,H}$ from the value of the angle $\beta'_H = \beta_F$. For this purpose, we shall use formula (4.3.25) in the form

$$\frac{\tan \theta'_{s,H}}{\tan(\theta'_{s,H} - \beta'_H)} = \frac{M_\infty^2 \sin^2 \theta'_{s,H}}{1 - \delta + \delta M_\infty^2 \sin^2 \theta'_{s,H}}. \tag{11.1.32}$$

At given values of β'_H, M_∞, and $\delta = (k-1)/(k+1)$, this transcendental equation is solved for $\theta'_{s,H}$ by successive approximations. We can use the value of $\theta'_{s,H}$ and formula (11.1.12) to determine the stagnation pressure at point H. Assuming that at point F the stagnation pressure $p'_{0,F}$ equals the stagnation pressure $p'_{0,S}$ at point S

calculated from the shock angle $\theta_{s.S}$ by formula (4.3.22), we can find the relation

$$(p'_{0,H} - p'_{0,F})/p'_{0,F} = (p'_{0,H} - p'_{0,S})/p'_{0,S}$$

Inserting this relation into (5.4.45), we determine the entropy gradient $\Delta S/\Delta n$ contained in formula (11.1.31). We now use the latter formula to find the value of $\Delta\beta_F$; next we calculate the angle increment $\Delta\omega_F$ from (5.4.41) at $y_F = r_F$ and $\varepsilon = 1$:

$$\Delta\omega_F = \Delta\beta_F + \frac{x_H - x_F}{r_F} l_F - \frac{x_H - x_F}{kR} \cdot \frac{\Delta S}{\Delta n} c_F \qquad (11.1.33)$$

The values of $\Delta\beta_F$ and $\Delta\omega_F$ give us the angles for point H:

$$\beta_H = \beta_{H'} = \Delta\beta_F + \beta_F, \quad \omega_H = \omega_{H'} = \Delta\omega_F + \omega_F \qquad (11.1.34)$$

Knowing the angle $\omega_{H'}$, we find $M_{H'}$ and $\mu_{H'}$ from Table 5.3.1. The found value of $\beta_{H'}$ allows us to refine the shock angle at point H by formula (11.1.32) and find the coordinates $x_{H'}$ and $r_{H'}$ of the new point H' in a second approximation. For this purpose, we shall compile an equation for the section of the shock behind point S:

$$r_S - r_{H'} = (x_S - x_{H'}) \tan \theta_{s,H'} \qquad (11.1.35)$$

and an equation of an element of a first family characteristic:

$$r_F - r_{H'} = (x_F - x_{H'}) \tan (\beta'_F + \mu'_F) \qquad (11.1.36)$$

where

$$\beta'_F = (\beta_F + \beta_{H'})/2, \quad \mu'_F = (\mu_F + \mu_{H'})/2$$

Solving (11.1.35) and (11.1.36) simultaneously, we find the refined coordinates $x_{H'}$ and $r_{H'}$. If required, one can calculate the parameters at point H ($\omega_{H'}$, $M_{H'}$ and $\beta_{H'}$) in a third approximation.

The data obtained on the parameters at points H' and N allow us to evaluate the parameters at point J (see Fig. 11.1.1). These calculations are similar to the solution of the first problem (see Sec. 5.4 in Part I) associated with the determination of the velocity at the intersection point of characteristics of different families issuing from two closely arranged points.

We find the coordinates x_J and r_J of point J by solving Eqs. (5.4.10) and (5.4.12) given respectively for elements NJ and $H'J$ of characteristics of the first and second families:

$$r_N - r_J = (x_N - r_J) \tan (\beta_N + \mu_N) \qquad (11.1.37)$$

$$r_{H'} - r_J = (x_{H'} - x_J) \tan (\beta_{H'} - \mu_{H'}) \qquad (11.1.38)$$

To calculate the parameters at point J in the vortex region of the flow, we use the relations for the characteristics in the plane of the hodograph taking into account the changes in the entropy. These difference equations have the form of (5.4.11) and (5.4.13). Equa-

tion (5.4.11) given for $\varepsilon = 1$ and $y = r$ with a view to the notation adopted for element NJ of a first family characteristic has the following form:

$$\Delta\omega_N - \Delta\beta_N - \frac{x_J - x_N}{r_N} l_N + \frac{x_J - x_N}{kR} \cdot \frac{\Delta S}{\Delta n} c_N = 0 \qquad (11.1.39)$$

For element $H'J$ of a second family characteristic, we use Eq. (5.4.13):

$$\Delta\omega_{H'} + \Delta\beta_{H'} - \frac{x_J - x_{H'}}{r_{H'}} m_{H'} - \frac{x_J - x_{H'}}{kR} \frac{\Delta S}{\Delta n} t_{H'} = 0 \qquad (11.1.40)$$

where

$$\left.\begin{aligned} \Delta\omega_N &= \omega_J - \omega_N, \quad & \Delta\beta_N &= \beta_J - \beta_N \\ \Delta\omega_{H'} &= \omega_J - \omega_{H'}, \quad & \Delta\beta_{H'} &= \beta_J - \beta_{H'} \end{aligned}\right\} \qquad (11.1.41)$$

To determine the coefficients l_N, c_N, $m_{N'}$, and $t_{H'}$, we must use formulas (5.4.15) in which we replace the parameters bearing the subscripts "B " and "A" with parameters bearing the subscripts "N" and "H'", respectively. We calculate the entropy gradient $\Delta S/\Delta n$ using relations (5.4.16) or (5.4.18) in which the subscripts "N" and "H'" should be substituted for "B" and "A", respectively. Here we determine the stagnation pressures $p'_{0,H}$ for point H' and $p'_{0,N}$ for point N by formula (4.3.22) from the shock angles $\theta_{s,H'}$ and $\theta_{s,S}$, respectively ($\theta_{s,H'} < \theta_{s,S}$).

The system of equations (11.1.39) and (11.1.40) includes four unknown quantities: $\Delta\omega_N$, $\Delta\beta_N$, $\Delta\omega_{H'}$, and $\Delta\beta_{H'}$. The number of unknowns can be halved if we take account of relation (5.4.20) by analogy with which

$$\Delta\omega_{H'} = \Delta\omega_N + \omega_N - \omega_{H'}; \quad \Delta\beta_{H'} = \Delta\beta_N + \beta_N - \beta_{H'} \qquad (11.1.42)$$

Let us perform the corresponding substitution in (11.1.40):

$$\Delta\omega_N + \omega_N - \omega_{H'} + \Delta\beta_N + \beta_N - \beta_{H'} - \frac{x_J - x_H}{r_{H'}} m_{H'} - \frac{x_J - x_{H'}}{kR} \cdot \frac{\Delta S}{\Delta n} t_{H'} = 0 \qquad (11.1.40')$$

Solving this equation simultaneously with (11.1.39) for $\Delta\beta_N$, we find

$$\Delta\beta_N = \frac{1}{2}\left\{\frac{1}{kR} \cdot \frac{\Delta S}{\Delta n} [(x_J - x_{H'}) t_{H'} + (x_J - x_N) c_N] + \frac{x_J - x_{H'}}{r_{H'}} m_{H'} - \frac{x_J - x_N}{r_N} l_N - (\omega_N - \omega_{H'}) - (\beta_N - \beta_{H'})\right\} \qquad (11.1.43)$$

According to the found value of $\Delta\beta_N$, we calculate the angular increment from (11.1.39):

$$\Delta\omega_N = \Delta\beta_N + \frac{x_J - x_N}{r_N} l_N - \frac{x_J - x_N}{kR} \cdot \frac{\Delta S}{\Delta n} c_N \qquad (11.1.44)$$

We use $\Delta\omega_N$ and $\Delta\beta_N$ to determine the absolute values of the angles at point J:

$$\omega_J = \Delta\omega_N + \omega_N; \quad \beta_J = \Delta\beta_N + \beta_N$$

Table 5.3.1 gives us the number M_J and the disturbance angle μ_J for the found value of ω_J. We find the stagnation pressure $p'_{0,J}$ (the entropy S_J) at point J by interpolation using the values of $p'_{0,H'}$ and $p'_{0,N}$ at points H' and N.

We can refine the found parameters if instead of l_N, $m_{H'}$, c_N, and $t_{H'}$ we introduce into Eqs. (11.1.39) and (11.1.40) the values calculated from the arithmetic means of the angles β and μ in accordance with formulas (5.4.25).

In this way, we consecutively, step by step, determine the coordinates of points H', J, . . ., L of the second family characteristic, and also the gas-dynamic parameters at these points. Using the variables found for point L, we can determine the velocity and other parameters at point R on the surface of the body in the flow. We find the coordinates of point R by solving the following equation for element LR of a second family characteristic:

$$r_L - r_R = (x_L - x_R) \tan(\beta_L - \mu_L) \qquad (11.1.45)$$

and the equation of the body's generatrix $r_R = f(x_R)$. Solution of these equations yields the values of x_R and r_R.

Point R is in the vortex region of the flow where element LR of a second family characteristic intersects the body's generatrix. Consequently, Eq. (5.4.27) has to be used to calculate the velocity. Assuming that $\varepsilon = 1$, and substituting r for y and the subscript "L" for "D", we can write the equation

$$\Delta\omega_L = -\Delta\beta_L + \frac{x_R - x_L}{r_L} m_L - \frac{x_R - x_L}{kR} \cdot \frac{\Delta S}{\Delta n} t_L \qquad (11.1.46)$$

where

$$\Delta\omega_L = \omega_R - \omega_L; \quad \Delta\beta_L = \beta_R - \beta_L \qquad (11.1.47)$$

We find the coefficients m_L and t_L by formulas (5.4.28) in which we replace the subscript "D" with "L". We find the entropy gradient $\Delta S/\Delta n$ by one of the formulas (5.4.29) provided that the subscripts "D" and "B" are replaced with "L" and "R", respectively. The stagnation pressure $p'_{0,R}$ at point R is known, and equals the pressure at points A, B, . . ., U, G belonging to the same streamline closest to the surface of the body. We calculate the value of $p'_{0,R}$ by formula (4.3.22) and the value of the shock angle $\theta_{s,S}$. We determine the stagnation pressure $p'_{0,L}$ at point L by interpolation of the values $p'_{0,T}$ and $p'_{0,G} = p'_{0,R}$ for points T and G, respectively.

The angle of inclination of a tangent to the surface of the body at point R is known from the equation of the generatrix $r = f(x)$ and

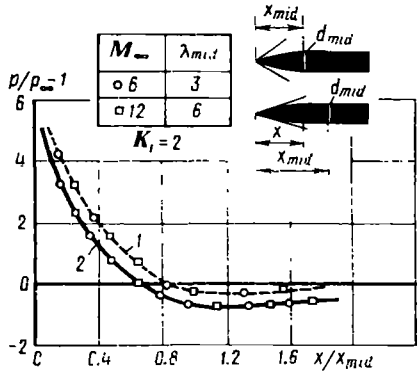

Fig. 11.1.2
Distribution of the pressure near bodies of revolution with a parabolic nose:
1—with account taken of the vortex flow behind the shock; *2*—for a potential flow behind the shock

is $\beta_R = \tan^{-1}[(dr/dx)_R]$. We therefore know the difference $\Delta\beta_L = \beta_R - \beta_L$, and by Eq. (11.1.46) we can directly calculate the angular increment $\Delta\omega_L$. We use this increment to calculate the angle $\omega_R = \Delta\omega_L + \omega_L$ and to determine the number M_R, the pressure and the other parameters at point R with account taken of the vortex nature of the flow.

Calculations and experimental investigations show that a substantial influence of the vortex nature of the flow behind a curved shock is observed only at high flow velocities. For example, for a parabolic nose with a fineness ratio of $\lambda_{mid} = x_{mid}/(2r_{mid}) = 5$ (the length of the nose is five times larger than the diameter of the mid-section, i.e. the maximum cross section $2r_{mid}$) at a value of the parameter $K_1 = M_\infty/\lambda_{mid} = 1$, which the number $M_\infty = 5$ corresponds to, the calculated wave drag increases at the expense of the vortex by 5% in comparison with its value in a potential flow. At the same time, when $K_1 = 4$ ($M_\infty = 20$), it grows by over 25%. The effect of the growth in the drag is explained from a physical viewpoint by the fact that an additional part of the kinetic energy of the flow has to be spent on the formation of vortices.

Figure 11.1.2 shows the pressure distribution found by the method of characteristics for two bodies with a parabolic nose, the equation of whose generatrix is

$$\bar{r} = \bar{x}(2 - \bar{x}) \qquad (11.1.48)$$

where $\bar{r} = r/r_{mid}$ and $\bar{x} = x/x_{mid}$ (x_{mid} is the distance from the nose to the location of the mid-section of the body whose radius is r_{mid}).

For a body of revolution with such a generatrix (Fig. 11.1.3), the tangent slope at an arbitrary point is

$$\tan\beta = \frac{dr}{dx} = \frac{2r_{mid}}{x_{mid}}(1 - \bar{x}) = \frac{1}{\lambda_{mid}}(1 - \bar{x}) \qquad (11.1.49)$$

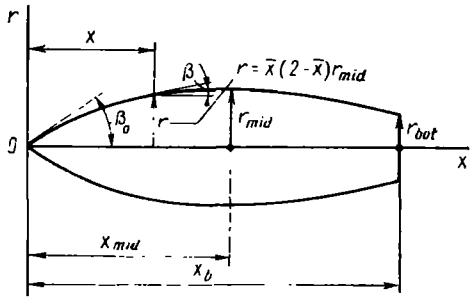

Fig. 11.1.3
Body of revolution with a parabolic generatrix

while at the tip, for which $\bar{x} = 0$, we have

$$\tan \beta_0 = 1/\lambda_{mid} \qquad (11.1.50)$$

where $\lambda_{mid} = x_{mid}/(2r_{mid})$ is the fineness ratio of the nose.

The graph in Fig. 11.1.2 shows the pressure distribution for a value of the parameter $K_1 = M_\infty \tan \beta_0 = M_\infty/\lambda_{mid} = 2$. It can be seen that the pressure for vortex flow is higher than that for potential flow. This increase should be taken into consideration in practical cases beginning from values of the parameter K_1 of about 1.2 to 1.5. At lower values of K_1, the vortex influence may be disregarded. The graph confirms the similarity for the parameter K_1 at high velocities not only for cones, but also for affine-similar bodies of revolution with a curved generatrix such as parabolic bodies (for affine similarity in greater detail see Sec. 11.3). This similarity also extends to cylindrical parts of bodies. The flow over two bodies differing in their dimensions can be seen to be characterized by a single curve for the pressure function $p/p_\infty - 1$ because in each case the parameter K_1 is the same.

The law of similarity in the parameter K_1 is of a great practical significance. Indeed, instead of experimenting with different models, we can test a single model in a wind tunnel, obtaining data on the pressure distribution for a number of values of the parameter K_1. Next, in accordance with the similarity law, these data may be extended to the entire set of affine-transformed bodies with specific geometric dimensions. For example, if the results in Fig. 11.1.2 were obtained at $M_\infty = 6$ for a body with a nose fineness ratio of $\lambda_{mid} = 3$ so that $K_1 = 2$, then evidently the found curve also holds (as can be seen from the graphs) for another body with a fineness ratio of $\lambda_{mid} = 6$, but when $M_\infty = 12$, i.e. provided that the same value of $K_1 = 2$ is retained. Using the similarity law, we can relate the results obtained, for example, to a body with $\lambda_{mid} = 5$ and $M_\infty = 10$, etc. Hence, in the given case, the validity of the similarity law is restricted to the single value of the parameter $K_1 = 2$. To extend these limits, experiments or calculations are performed for different values of K_1.

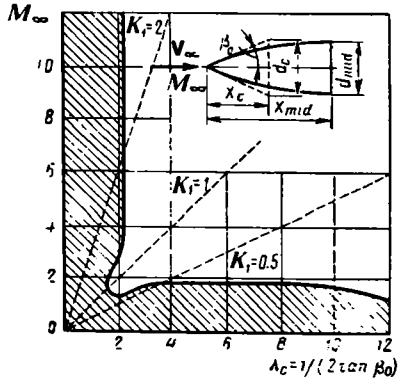

Fig. 11.1.4
Region of possible application of the similarity law in the parameter K_1
[$\lambda_c=x_c/d_c=1/(2\tan\beta_0)$; $\lambda_{mid}=x_{mid}/d_{mid}=1/\tan\beta_0$; $K_1=M_\infty\tan\beta_0$]

We shall note another important conclusion of the similarity law. It consists in that when it is impossible to obtain a high-velocity flow, the required results can be produced for smaller numbers M_∞. For this purpose, an experiment has to be run using a lower fineness ratio of an affine-similar model with retaining of the given parameter K_1. Here the field of application of the similarity law for a sharp-nosed body of revolution can be established by analysing the possibility of using this law for a cone tip. Such an analysis is performed by comparing the results of approximate aerodynamic calculations with the exact theory or an experiment and finding the deviation from the tolerated error. This method was employed to construct the hatched area in Fig. 11.1.4 for a cone (the zone of doubtful similarity) outside of which the application of the similarity law yields an error of under 5-6%.

When using the graph in Fig. 11.1.4 to determine the field of application of the similarity law for a parabolic nose with a fineness ratio of λ_{mid}, this graph should be reconstructed so that the fineness ratios of the nose calculated from the condition $\lambda_{mid}=1/\tan\beta_0$ are laid off along the horizontal axis.

When investigating the effect of a vortex flow, it was shown that an increase in the airspeed makes it necessary to take into consideration (when calculating an inviscid flow) the influence of factors that may be ignored at low velocities.

Experiments and theory show that at large numbers M_∞, factors such as the boundary layer and various effects observed in it (dissociation, ionization, heat transfer between the wall and the gas) influence the flow to some extent. Vibrational excitation, dissociation, and ionization of the air that may appear at very high flow velocities because of the substantial elevation of the temperature in the inviscid region of the flow between the shock wave and the body surface also affect the flow. It should be noted that the

influence of high gas temperatures on the change in the pressure distribution is considerably lower than on the distribution of the velocity, temperature, and density.

The parameters of inviscid flow, provided that the gas experiences physicochemical transformations owing to the high temperatures, can be calculated by a number of methods, including the method of characteristics (see [10-12]).

Knowing the distribution of the pressure coefficient $\bar{p} = (p - p_\infty)/q_\infty$, where $q_\infty = kM_\infty^2 p_\infty/2$, we can calculate the wave drag force and coefficient for a body of revolution in a supersonic flow at a zero angle of attack. To calculate the wave drag coefficient, we shall use formula (1.3.2), as we did when deriving formula (10.2.29). We shall take into account here that

$$S_r = S_{mid} = \pi r_{mid}^2; \quad dS = 2\pi r\, dl; \quad dl = dx/\cos\beta$$

$$\cos(\widehat{n, x}) = \sin\beta; \quad \sin\beta/\cos\beta = dr/dx$$

As a result,

$$c_{x,w} = \frac{X_w}{q_\infty S_{mid}} = \frac{2}{r_{mid}} \int_0^{x_b} \bar{p}\bar{r} \left(\frac{dr}{dx}\right) dx \qquad (11.1.51)$$

or

$$c_{x,w} = 4\lambda_{mid} \int_0^{\bar{x}_b} \bar{p}\bar{r} \tan\beta\, d\bar{x} \qquad (11.1.51')$$

where x_b is the length of the body of revolution;

$$\bar{x} = x/x_{mid}; \quad \bar{x}_b = x_b/x_{mid}$$

$$\bar{r} = r/r_{mid}; \quad \tan\beta = dr/dx; \quad \lambda_{mid} = x_{mid}/(2r_{mid})$$

Figure 11.1.5 gives an idea of the changes in the wave drag coefficient. It has been constructed from the results of calculating this coefficient by the method of characteristics for a parabolic body of revolution. It can be seen that an increase in the number M_∞ and the fineness ratio λ_{mid} is attended by diminishing of the drag coefficient. An increase in the fineness ratio corresponds to greater sharpening of the body, which, naturally, causes the drag to lower. As regards the influence of the number M_∞, the change in the coefficient $c_{x,w}$ indicated above points not to a decrease in the drag [with an increase in M_∞ it grows in accordance with the relation $X_w = c_{x,w}(kp_\infty M_\infty^2/2) S_{mid}$], but to a certain deviation of this change from a quadratic law (relative to M_∞). For large Mach numbers ($M_\infty > 5$-6), it is exactly such a law of the change in the drag that is realized in practice because the coefficients $c_{x,w}$ change insignificantly.

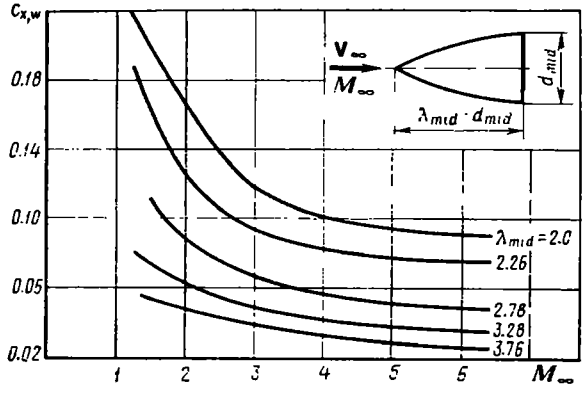

Fig. 11.1.5
Wave drag coefficients for a parabolic nose

To estimate the wave drag coefficient for parabolic noses or bodies of revolution close to them in shape, we can use the relation (see [1])

$$c_{x,w} = 0.08\,(15.5 + M_\infty)\,(3 + M_\infty)^{-1}\bar{p}_c \qquad (11.1.52)$$

where $\bar{p}_c$ is the pressure coefficient on the conical nose of the body of revolution in a flow.

Formula (11.1.52) yields satisfactory results for fineness ratios of $\lambda_{mid} \geqslant 2.5$ and the interval of $1.5 \leqslant M_\infty \leqslant 6$.

11.2. Linearization of Equations for the Flow over Slender Bodies of Revolution

Some craft are designed as slender sharp-nosed bodies of revolution (some kinds of rockets, missiles, etc.) or one of their structural elements is a body of such a shape. This gives rise to the expediency of investigating the aerodynamic characteristics of slender sharp-nosed bodies of revolution.

Let us consider the problem of a steady flow over slender bodies at small angles of attack. A disturbed flow near such bodies differs only slightly from an undisturbed one. Such a flow, called linearized above, can be studied with the aid of the relevant **linearized equations of aerodynamics**. Let us consider these linearized equations. They are obtained from the general equations of motion (3.1.35) and (3.1.35′) in cylindrical coordinates convenient for studying the flow over bodies of revolution and having the following form for

a steady inviscid flow ($\partial \bar{V}/\partial t = 0$, $\nu = 0$):

$$\left.\begin{aligned} V_x \frac{\partial V_x}{\partial x} + V_r \frac{\partial V_x}{\partial r} + \frac{V_\gamma}{r} \cdot \frac{\partial V_x}{\partial \gamma} &= -\frac{1}{\rho} \cdot \frac{\partial p}{\partial x} \\ V_x \frac{\partial V_r}{\partial x} + V_r \frac{\partial V_r}{\partial r} + \frac{V_\gamma}{r} \cdot \frac{\partial V_r}{\partial \gamma} - \frac{V_\gamma^2}{r} &= -\frac{1}{\rho} \cdot \frac{\partial p}{\partial r} \\ V_x \frac{\partial V_\gamma}{\partial x} + V_r \frac{\partial V_\gamma}{\partial r} + \frac{V_\gamma}{r} \cdot \frac{\partial V_\gamma}{\partial \gamma} + \frac{V_r V_\gamma}{r} &= -\frac{1}{\rho r} \cdot \frac{\partial p}{\partial \gamma} \end{aligned}\right\} \quad (11.2.1)$$

and also from continuity equation (2.4.31) in the same coordinates. Differentiation of this equation yields

$$r\left(\frac{\partial \rho}{\partial x} V_x + \frac{\partial \rho}{\partial r} V_r + \frac{1}{r} \cdot \frac{\partial \rho}{\partial \gamma} V_\gamma\right) + \rho r\left(\frac{\partial V_x}{\partial x} + \frac{\partial V_r}{\partial r} + \frac{1}{r} \cdot \frac{\partial V_\gamma}{\partial \gamma}\right) + \rho V_r = 0 \quad (11.2.2)$$

Taking into account that the partial derivative $\frac{\partial \rho}{\partial x} = \frac{d\rho}{dp} \cdot \frac{\partial p}{\partial x} = \frac{1}{a^2} \cdot \frac{\partial p}{\partial x}$, and replacing $\partial p/\partial x$ in accordance with the first of Eqs. (11.2.1), we find

$$\frac{\partial \rho}{\partial x} = -\frac{\rho}{a^2}\left(V_x \frac{\partial V_x}{\partial x} + V_r \frac{\partial V_x}{\partial r} + \frac{V_\gamma}{r} \cdot \frac{\partial V_x}{\partial \gamma}\right) \quad (11.2.3)$$

Similarly, from the second and third of Eqs. (11.2.1), we obtain

$$\frac{\partial \rho}{\partial r} = -\frac{\rho}{a^2}\left(V_x \frac{\partial V_r}{\partial x} + V_r \frac{\partial V_r}{\partial r} + \frac{V_\gamma}{r} \cdot \frac{\partial V_r}{\partial \gamma} - \frac{V_\gamma^2}{r}\right) \quad (11.2.4)$$

$$\frac{1}{r} \cdot \frac{\partial \rho}{\partial \gamma} = -\frac{\rho}{a^2}\left(V_x \frac{\partial V_\gamma}{\partial x} + V_r \frac{\partial V_\gamma}{\partial r} + \frac{V_\gamma}{r} \cdot \frac{\partial V_\gamma}{\partial \gamma} + \frac{V_r V_\gamma}{r}\right) \quad (11.2.5)$$

Let us introduce the values of the partial derivatives from (11.2.3)-(11.2.5) into continuity equation (11.2.2):

$$(V_x^2 - a^2)\frac{\partial V_x}{\partial x} + (V_r^2 - a^2)\frac{\partial V_r}{\partial r} + \frac{1}{r}(V_\gamma^2 - a^2)\frac{\partial V_\gamma}{\partial \gamma} + V_x V_r\left(\frac{\partial V_x}{\partial r} + \frac{\partial V_r}{\partial x}\right) + V_x V_\gamma\left(\frac{1}{r} \cdot \frac{\partial V_x}{\partial \gamma} + \frac{\partial V_\gamma}{\partial x}\right) + V_r V_\gamma\left(\frac{1}{r} \cdot \frac{\partial V_r}{\partial \gamma} + \frac{\partial V_\gamma}{\partial r}\right) - \frac{V_r a^2}{r} = 0 \quad (11.2.6)$$

Having in view relations (2.4.25′) and taking into account that

$$\frac{\partial V_\gamma}{\partial r} = \frac{\partial}{\partial r}\left(\frac{1}{r} \cdot \frac{\partial \varphi}{\partial \gamma}\right) = \frac{1}{r} \cdot \frac{\partial^2 \varphi}{\partial r\, \partial \gamma} - \frac{1}{r^2} \cdot \frac{\partial \varphi}{\partial \gamma}$$

we obtain from (11.2.6) an equation for the potential function:

$$(V_x^2 - a^2)\frac{\partial^2 \varphi}{\partial x^2} + (V_r^2 - a^2)\frac{\partial^2 \varphi}{\partial r^2} + \frac{1}{r^2}(V_\gamma^2 - a^2)\frac{\partial^2 \varphi}{\partial \gamma^2} + 2V_x V_r \frac{\partial^2 \varphi}{\partial x\, \partial r} + \frac{2}{r} V_x V_\gamma \frac{\partial^2 \varphi}{\partial x\, \partial \gamma} + \frac{2}{r} V_r V_\gamma \frac{\partial^2 \varphi}{\partial r\, \partial \gamma} - \frac{V_r(a^2 + V_\gamma^2)}{r} = 0 \quad (11.2.7)$$

Customarily, we use the single equation (11.2.7) for the velocity potential instead of the system of equations of motion (11.2.1) and continuity equation (11.2.2). In accordance with the properties of a linearized disturbed flow,

$$V_x = V_\infty + V'_x, \quad V_r = V'_r, \quad V_\gamma = V'_\gamma \tag{11.2.8}$$

where the additional disturbed velocity components

$$V'_x \ll V_\infty, \quad V'_r \ll V_\infty, \quad V'_\gamma = V_\infty$$

Consequently, for the speed of sound, we may use relation (7.1.2′) in which $u = V'_x$. Introducing this relation, and also the values (11.2.8) and the quantities

$$V_x^2 = V_\infty + 2V_\infty V'_x, \quad V_r^2 = V_r'^2, \quad V_\gamma^2 = V_\gamma'^2, \quad \varphi = \varphi_\infty + \varphi'$$

into Eq. (11.2.7), we obtain

$$[V_\infty^2 - a_\infty^2 + (k-1)\,V_\infty V'_x]\frac{\partial^2\varphi'}{\partial x^2} + [V_r'^2 - a_\infty^2 + (k-1)\,V_\infty V'_x]\frac{\partial^2\varphi'}{\partial r^2}$$
$$+ \frac{1}{r^2}[V_\gamma'^2 - a_\infty^2 + (k-1)\,V_\infty V'_x]\frac{\partial^2\varphi'}{\partial\gamma^2} + 2\,(V_\infty + V'_x)\,V'_r\frac{\partial^2\varphi'}{\partial x\,\partial r}$$
$$+ \frac{2}{r}\,(V_\infty + V'_x)\,V'_\gamma\frac{\partial^2\varphi'}{\partial x\,\partial\gamma} + \frac{2}{r}\,V'_r V'_\gamma\frac{\partial^2\varphi'}{\partial r\,\partial\gamma}$$
$$- \frac{V'_r}{r}[a_\infty^2 - (k-1)\,V_\infty V'_x + V_\gamma'^2] = 0 \tag{11.2.9}$$

Taking into account that the second derivatives of φ' are small quantities of the first order, in Eq. (11.2.9) we may disregard the terms containing products of these derivatives and the disturbed velocity components V'_x, V'_r, or V'_γ. As a result, we find a linearized differential equation for the additional value of the potential function φ':

$$(V_\infty^2 - a_\infty^2)\frac{\partial^2\varphi'}{\partial x^2} - a_\infty^2\frac{\partial^2\varphi'}{\partial r^2} - \frac{a_\infty^2}{r^2}\cdot\frac{\partial^2\varphi'}{\partial\gamma^2} - \frac{a_\infty^2}{r}\cdot\frac{\partial\varphi'}{\partial r} = 0 \tag{11.2.10}$$

Let us divide all the terms of this equation by $-a_\infty^2$:

$$(1 - M_\infty^2)\frac{\partial^2\varphi'}{\partial x^2} + \frac{\partial^2\varphi'}{\partial r^2} + \frac{1}{r^2}\cdot\frac{\partial^2\varphi'}{\partial\gamma^2} + \frac{1}{r}\cdot\frac{\partial\varphi'}{\partial r} = 0 \tag{11.2.10′}$$

Equation (11.2.10′) is used to investigate the flow near slender bodies of revolution at a small angle of attack, i.e. a **non-axisymmetric nearly uniform flow.**

For **axisymmetric flow** (the angle of attack is zero), the equation is simplified because the velocity component $V'_\gamma = (1/r)\,\partial\varphi'/\partial\gamma = 0$ and, consequently,

$$(1 - M_\infty^2)\frac{\partial^2\varphi'}{\partial x^2} + \frac{\partial^2\varphi'}{\partial r^2} + \frac{1}{r}\cdot\frac{\partial\varphi'}{\partial r} = 0 \tag{11.2.11}$$

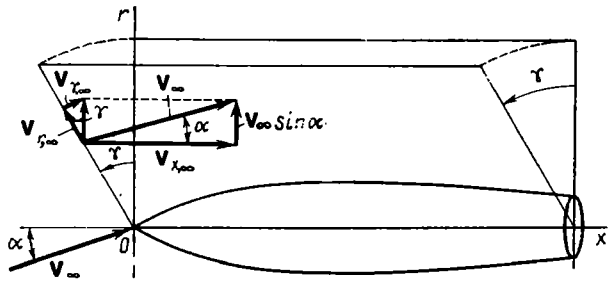

Fig. 11.2.1
Free-stream velocity components in cylindrical coordinates

Equations (11.2.10′) and (11.2.11) are the *theoretical basis of the aerodynamics of stationary linearized flows near slender bodies of revolution*. Solution of these equations yields the disturbance potential φ'. We solve the equation for the potential φ' for the following boundary conditions. At the boundary of the disturbed region, the potential $\varphi' = 0$. In the given case, this boundary is formed by the surface of a weak shock wave appearing ahead of a slender sharp-nosed body. This wave is actually a weak disturbance line (a simple compression wave) or a Mach line with the angle of inclination of the generatrix to the direction of the velocity vector $\mathbf{V}_\infty$ equal to $\mu_\infty = \sin^{-1}(1/M_\infty)$. On the surface of the body in the flow, the potential φ' must satisfy the condition of flow without separation (3.3.19) in which the function describing the surface of revolution in the flow can be written as $F = f(x) - r$. Hence,

$$\varphi_r/\varphi_x = dr/dx \tag{11.2.12}$$

where

$$\left.\begin{aligned} \varphi_r &= \frac{\partial\varphi}{\partial r} = \frac{\partial(\varphi_\infty+\varphi')}{\partial r} = \frac{\partial\varphi_\infty}{\partial r} + \frac{\partial\varphi'}{\partial r} = \varphi_{\infty,r} + \varphi'_r \\ \varphi_x &= \frac{\partial\varphi}{\partial x} = \frac{\partial(\varphi_\infty+\varphi')}{\partial x} = \frac{\partial\varphi_\infty}{\partial x} + \frac{\partial\varphi'}{\partial x} = \varphi_{\infty,x} + \varphi'_x \end{aligned}\right\} \tag{11.2.13}$$

The components of the free-stream velocity in cylindrical coordinates can be determined using the diagram in Fig. 11.2.1:

$$\left.\begin{aligned} V_{x,\infty} &= \partial\varphi_\infty/\partial x = \varphi_{x,\infty} = V_\infty\cos\alpha \\ V_{r,\infty} &= \partial\varphi_\infty/\partial r = \varphi_{r,\infty} = V_\infty\sin\alpha\cos\gamma \end{aligned}\right\} \tag{11.2.14}$$

The same diagram allows us to find the third component:

$$V_{\gamma,\infty} = \frac{1}{r}\cdot\frac{\partial\varphi_\infty}{\partial\gamma} = \frac{1}{r}\varphi_{\gamma,\infty} = -V_\infty\sin\alpha\sin\gamma \tag{11.2.15}$$

In accordance with relations (11.2.14) and (11.2.15), the velocity potential of an undisturbed flow is

$$\varphi_\infty = xV_\infty\cos\alpha + rV_\infty\sin\alpha\cos\gamma \tag{11.2.16}$$

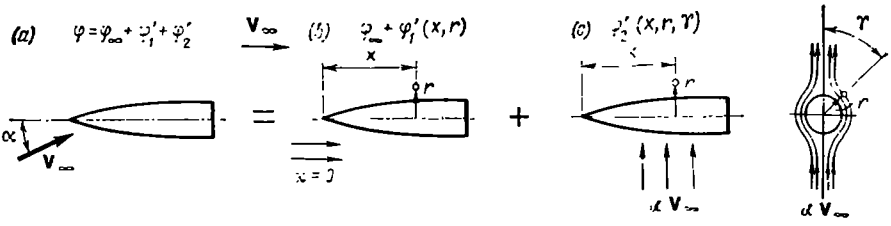

Fig. 11.2.2
A slender body of revolution in a linearized flow at a small angle of attack: *a*—non-axisymmetric flow; *b*—axisymmetric flow; c—additional crossflow

We shall assume for a nearly uniform flow that $\cos \alpha \approx 1 - \alpha^2/2$ and $\sin \alpha \approx \alpha$, therefore

$$\varphi_\infty = xV_\infty (1 - \alpha^2/2) + rV_\infty \alpha \cos \gamma \qquad (11.2.16')$$

Consequently, the summary potential is

$$\varphi = \varphi_\infty + \varphi' (x, r, \gamma) = xV_\infty (1 - \alpha^2/2) + rV_\infty \alpha \cos \gamma + \varphi' (x, r, \gamma) \qquad (11.2.17)$$

By calculating the derivatives of φ_r and φ_x, introducing them into (11.2.12), and disregarding the quantity $0.5\alpha^2$, we obtain

$$(V_\infty \alpha \cos \gamma + \varphi'_r)/(V_\infty + \varphi'_x) = dr/dx \qquad (11.2.18)$$

If the flow is axisymmetric, the condition of flow without separation (11.2.18) is simplified:

$$\varphi'_r/(V_\infty + \varphi'_x) = dr/dx \qquad (11.2.19)$$

The velocity potential φ of a linearized flow over a body of revolution at a small angle of attack (Fig. 11.2.2) can be written as the sum of three components: the potential φ_∞ of the undisturbed flow, the additional potential $\varphi'_1 (x, r)$ of the longitudinal disturbed (axisymmetric) flow, and the second additional potential $\varphi'_2 (x, r, \gamma)$ produced by the crossflow:

$$\varphi = \varphi_\infty + \varphi'_1 (x, r) + \varphi'_2 (x, r, \gamma) \qquad (11.2.20)$$

In the theory of linearized flows, φ'_1 and φ'_2 are considered as functions that, being solutions of equations of motion, determine flows independent of each other. Therefore, the boundary conditions may be superposed separately onto each such function. Particularly, the solution for φ'_1 obtained from Eq. (11.2.11), namely

$$(1 - M_\infty^2)\ \varphi'_{1xx} + \varphi'_{1rr} + \varphi'_1/r = 0 \qquad (11.2.11')$$

(where $\varphi'_{1xx} = \partial^2\varphi'_1/\partial x^2$, $\varphi'_{1rr} = \partial^2\varphi'_1/\partial r^2$, $\varphi'_{1r} = \partial\varphi'_1/\partial r$), must satisfy condition (11.2.19) of axisymmetric flow

$$\varphi'_{1r}/(V_\infty + \varphi'_{1x}) = dr/dx \qquad (11.2.19')$$

The boundary condition for the function φ'_2 satisfying (11.2.10')

$$(1 - M_\infty^2)\,\varphi'_{2xx} + \varphi'_{2rr} + \varphi'_{2\gamma\gamma}/r^2 + \varphi'_{2r}/r = 0 \qquad (11.2.10'')$$

is obtained from expression (11.2.18) written in the form

$$\alpha V_\infty \cos\gamma + \varphi'_{1r} + \varphi'_{2r} = \frac{dr}{dx}(V_\infty + \varphi'_{1x} + \varphi'_{2x}) \qquad (11.2.21)$$

In these expressions, $\varphi'_{1x} = \partial\varphi'_1/\partial x$, $\varphi'_{2x} = \partial\varphi'_2/\partial x$, etc.

Having in view Eq. (11.2.19') and discarding in (11.2.21) the term $(dr/dx)\,\varphi'_{2x}$, of the smaller order, we obtain the boundary condition for crossflow:

$$\varphi'_{2r} = -\alpha V_\infty \cos\gamma \qquad (11.2.22)$$

In accordance with condition (11.2.22), the additional potential due to the crossflow must be such that the radial component $V_{r,\infty} = \alpha V_\infty \cos\gamma$ of the free-stream velocity will vanish at the surface of the body. This velocity component may be either supersonic or subsonic. That $V_{r,\infty} < a_\infty$ (i.e. the radial component is subsonic) is of no significance for solving the problem because the additional crossflow being considered is a part of the total flow and is only a result of our mathematic representation of the model of such a flow.

Having determined the total velocity potential (11.2.20) with account taken of the boundary conditions, we can evaluate the velocity, and then the pressure, using the Bernoulli equation

$$\frac{k}{k-1}\cdot\frac{p}{\rho} + \frac{V^2}{2} = \frac{k}{k-1}\cdot\frac{p_\infty}{\rho_\infty} + \frac{V_\infty^2}{2}$$

Introducing into it the value of $\rho = \rho_\infty (p/p_\infty)^{1/k}$ (since the flow can be considered isentropic) we find

$$\frac{k}{k-1}\left(\frac{p}{p_\infty}\right)^{(k-1)/k}\frac{p_\infty}{\rho_\infty} + \frac{V^2}{2} = \frac{k}{k-1}\cdot\frac{p_\infty}{\rho_\infty} + \frac{V_\infty^2}{2}$$

Having in view that $kp_\infty/\rho_\infty = a_\infty^2$ and $M_\infty^2 = V_\infty^2/a_\infty^2$, we obtain

$$\frac{p}{p_\infty} = \left[1 + \frac{k-1}{2}M_\infty^2\left(1 - \frac{V^2}{V_\infty^2}\right)\right]^{k/(k-1)}$$

Since the square of the total velocity $V^2 = (V_\infty\cos\alpha + V'_x)^2 + V'^2_r + V'^2_\gamma$, we have

$$\frac{p}{p_\infty} = \left[1 - (k-1)M_\infty^2\left(\frac{V'_x}{V_\infty}\cos\alpha + \frac{V'^2_r}{2V_\infty^2} + \frac{V'^2_\gamma}{2V_\infty^2} + \frac{V'^2_x}{2V_\infty^2} - \frac{\sin^2\alpha}{2}\right)\right]^{k/(k-1)} \qquad (11.2.23)$$

Here the second term in the brackets is less than unity, and, therefore, the entire expression can be expanded into a binomial series. Retaining only the first two terms in the expansion, taking into consideration the smallness of the quantity $V_x'^2/(2V_\infty^2)$ in comparison with the first term in parentheses, and assuming for small angles of attack that $\cos\alpha \approx 1$ and $\sin^2\alpha \approx \alpha^2$, we obtain

$$\frac{p}{p_\infty} = 1 - kM_\infty^2\left(\frac{V_x'}{V_\infty} + \frac{V_r'^2}{2V_\infty^2} + \frac{V_\gamma'^2}{2V_\infty^2} - \frac{\alpha^2}{2}\right) \qquad (11.2.24)$$

whence the pressure coefficient is

$$\bar{p} = \frac{2(p-p_\infty)}{kM_\infty^2 p_\infty} = -2\left(\frac{V_x'}{V_\infty} + \frac{V_r'^2}{2V_\infty^2} + \frac{V_\gamma'^2}{2V_\infty^2} - \frac{\alpha^2}{2}\right) \qquad (11.2.25)$$

In accordance with condition (11.2.12), in which we may assume that $\varphi_x \approx \varphi_{x,\infty} = V_\infty$, we shall replace the component V_r' with the quantity

$$V_r' = \varphi_r' = V_\infty\, dr/dx \qquad (11.2.19'')$$

and V_x' and V_γ' with their expressions in terms of the additional potentials:

$$V_x' = \varphi_x'; \quad V_\gamma' = \varphi_{\gamma,\infty}'/r + \varphi_{2\gamma}'/r$$

where by (11.2.15), the quantity

$$\varphi_{\gamma,\infty}'/r = \alpha V_\infty \sin\gamma$$

Hence,

$$\bar{p} = \frac{-2}{V_\infty^2}\left[V_\infty\varphi_x + \frac{V_\infty^2}{2}\left(\frac{dr}{dx}\right)^2 + \frac{1}{2}\left(\frac{\varphi_{2\gamma}'}{r} - \alpha V_\infty \sin\gamma\right)^2 - \frac{\alpha^2 V_\infty^2}{2}\right] \qquad (11.2.26)$$

We can write this value of the pressure coefficient as the sum of two components, i.e. $\bar{p} = \bar{p}_1 + \bar{p}_2$. The first of them, $\bar{p}_1$, is determined by the conditions of axisymmetric flow:

$$\bar{p}_1 = \frac{-2}{V_\infty^2}\left[V_\infty\varphi_{1x}' + \frac{V_\infty^2}{2}\left(\frac{dr}{dx}\right)^2\right] \qquad (11.2.27)$$

and the second, $\bar{p}_2$, by the crossflow, which depends on the angle of attack:

$$\bar{p}_2 = \frac{-2}{V_\infty^2}\left[V_\infty\varphi_{2x}' + \frac{1}{2}\left(\frac{\varphi_{2\gamma}'}{r} - \alpha V_\infty \sin\gamma\right)^2 - \frac{\alpha^2 V_\infty^2}{2}\right] \qquad (11.2.28)$$

11.3. Calculation of Axisymmetric Flow

The problem of the linearized axisymmetric flow over a slender body of revolution will be solved if we find the additional velocity potential φ_1' satisfying linearized equation (11.2.11). We can see by

substitution that the potential

$$\varphi_1' = \int_0^{x-\alpha' r} f(\varepsilon)\, d\varepsilon / \sqrt{(x-\varepsilon)^2 - \alpha'^2 r^2} \qquad (11.3.1)$$

where $\alpha' = \sqrt{M_\infty^2 - 1}$, does indeed satisfy Eq. (11.2.11).

The meaning of solution (11.3.1) can be understood if we introduce a variable determined by the equality $\alpha' r \sqrt{-1} = p$. Now we can formally make Eq. (11.2.11) coincide with the equation for the velocity potential of an incompressible flow, namely,

$$\varphi_{1xx}' + \varphi_{1pp}' + \varphi_{1p}'/p = 0 \qquad (11.3.2)$$

where the subscripts x and p stand for the corresponding partial derivatives of φ_1' with respect to x and p.

Let us imagine that at a point $x = \varepsilon$ on the axis of a body there is a source of a fluid with a rate of flow (strength) q. The velocity potential induced by the source at a point with the coordinates x and p on a spherical surface of radius $\rho = \sqrt{(x-\varepsilon)^2 + p^2}$ is determined by formula (2.9.14) as $\varphi_1' = -q/[4\pi\sqrt{(x-\varepsilon)^2 + p^2}]$. If we imagine that along the axis of the body on the section from $\varepsilon = 0$ to $\varepsilon = x - \alpha' r$ there is a system of sources with the varying strength $q = -4\pi f(\varepsilon)$ related to a unit length, then the total potential at the point (x, r) being considered resulting from the action of all the sources is expressed by the formula

$$\varphi_1' = \int_0^{x-\alpha' r} f(\varepsilon)\, d\varepsilon / \sqrt{(x-\varepsilon)^2 + p^2} \qquad (11.3.3)$$

Substitution shows that integral (11.3.3) satisfies differential equation (11.3.2). Consequently, solution (11.3.3) is the potential function due to sources distributed continuously along the axis of the body. By comparing (11.3.3) and (11.3.1), we see that at $p = \alpha' r \sqrt{-1}$ these two expressions are identical. We have thereby shown by formal analogy that as for an incompressible fluid, the meaning of solution (11.3.1) consists in that the function φ_1' is the potential of sources distributed continuously along the axis of a body. The found solution (11.3.1) reflects the content of the **method of sources**, according to which *a body in a flow is replaced by a system of both sources and sinks continuously distributed along its axis.*

The law of distribution of the sources (sinks), i.e. the function $f(\varepsilon)$ must be such that superposition of the undisturbed flow onto the flow due to the sources will make one of the flow streamlines coincide with the generatrix of the body of revolution. In other words, the potential function φ_1' must satisfy condition (11.2.19') of flow without separation.

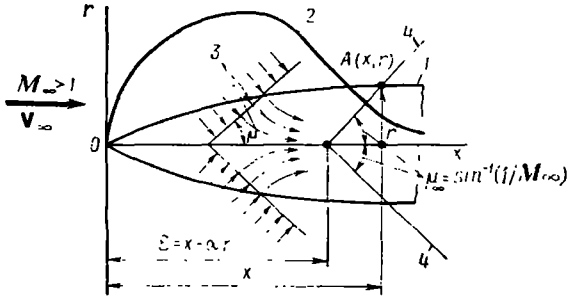

Fig. 11.3.1
Distribution of sources along the axis of a body of revolution and their influence at supersonic flow velocities:
1—generatrix of body of revolution; *2*—curve $f(x)$ characterizing the source distribution; *3*—streamlines due to sources; *4*—disturbance (Mach) cone

The formal analogy between an incompressible (or compressible subsonic) and a compressible supersonic flows due to sources or sinks must be supplemented with features characteristic of a supersonic flow. If a source in a subsonic flow affects *all points of space*, upstream and downstream, then in supersonic flow the disturbances produced by the sources propagate only *inside Mach cones* issuing from the sources. Hence, if we imagine a system of sources continuously distributed along the axis of a body (Fig. 11.3.1), the velocity and pressure at any point $A(x, r)$ will be determined by the disturbances emerging from upstream sources, beginning from the point $\varepsilon = x - \alpha' r$ and ending at the point $\varepsilon = x = 0$ coinciding with the tip of the body. At the point $\varepsilon = x = 0$, the strength of the source is zero because we assume that at $\varepsilon \leqslant 0$ the disturbances are absent. This determines the limits of the integral in formula (11.3.1).

The shape of the curve $f(\varepsilon)$ [or $f(x)$], which represents the distribution of the sources (sinks) for a slender body with an arbitrary generatrix, is shown in Fig. 11.3.1. This curve determines the continuous nature of the weak disturbances induced by sources (sinks) and corresponding to linearized flow. When finite disturbances appear, for example, in the flow over blunt-nosed bodies or over sharp-nosed bodies with large angles of their generatrices to the direction of the free-stream velocity, the linear theory may not be applied.

To find general relations for the velocity and pressure, let us transform (10.3.1), introducing a new integration variable:

$$z = \cosh^{-1}[(x - \varepsilon)/(\alpha' r)] \qquad (11.3.4)$$

Having in view that by (11.3.4) $\cosh z = (x - \varepsilon)/(\alpha' r)$, $\varepsilon = x - \alpha' r \cosh z$, $d\varepsilon = -\alpha' r \sinh z\, dz$, expression (11.3.1) can be trans-

formed as follows:

$$\varphi_1' = \int_0^{\cosh^{-1}(x/\alpha' r)} f(x - \alpha' r \cosh z)\, dz \qquad (11.3.5)$$

In formula (11.3.5), the upper limit $z = \cosh^{-1}(x/\alpha' r)$ of the integral corresponds to the lower limit $\varepsilon = 0$ of integral (11.3.1), whereas the lower limit $z = 0$ corresponds to the upper limit $\varepsilon = x - \alpha' r$ in (11.3.1).

Differentiating φ_1' with respect to x, let us find the axial additional component of the velocity:

$$V_{x1}' = \varphi_{1x}' = \frac{\partial}{\partial x} \int_0^{\cosh^{-1}(x/\alpha' r)} f(x - \alpha' r \cosh z)\, dz$$

$$= \int_0^{\cosh^{-1}(x/\alpha' r)} \dot{f}(x - \alpha' r \cosh z)\, dz$$

$$+ f(x - \alpha' r \cosh z)\,|_{z=\cosh^{-1}(x/\alpha' r)} \frac{\partial}{\partial x}\left(\cosh^{-1}\frac{x}{\alpha' r}\right) \qquad (11.3.6)$$

where $\dot{f}$ is the total derivative of the function f with respect to the argument $x - \alpha' r \cosh r$.

Since the strength of the source at the tip of the body is $f(\varepsilon) = f(0) = 0$, we have

$$V_{x1}' = \varphi_{1x}' = \int_0^{\cosh^{-1}(x/\alpha' r)} \dot{f}(x - \alpha' r \cosh z)\, dz \qquad (11.3.7)$$

Similar to (11.3.6), we find for the radial velocity component

$$V_{r1}' = \varphi_{1r}' = -\alpha' \int_0^{\cosh^{-1}(x/\alpha' r)} \dot{f}(x - \alpha' r \cosh z) \cosh z\, dz \qquad (11.3.8)$$

Let us rewrite expression (11.3.8) with the aid of the variable ε determined from (11.3.4), i.e. $\varepsilon = x - \alpha' r \cosh z$. Since

$$dz = \frac{-d\varepsilon}{\sqrt{[(x-\varepsilon)/(\alpha' r)]^2 - 1}} \cdot \frac{1}{\alpha' r} = \frac{-d\varepsilon}{\sqrt{(x-\varepsilon)^2 - \alpha'^2 r^2}}; \quad \cosh z = \frac{x-\varepsilon}{\alpha' r}$$

the integrand

$$\dot{f}(x - \alpha' r \cosh z) \cosh z\, dz = \dot{f}(\varepsilon)(x - \varepsilon)\, d\varepsilon / (\alpha' r \sqrt{(x-\varepsilon)^2 - \alpha'^2 r^2})$$

The lower limit $z = 0$ corresponds to the value of $1 = (x - \varepsilon)/(\alpha' r)$, whence the new limit $\varepsilon = x - \alpha' r$. The limit ε obtained from the condition $\cosh[\cosh^{-1}(x/\alpha' r)] = (x - \varepsilon)/(\alpha' r)$, in accordance with which $\varepsilon = 0$, corresponds to the upper limit $z = \cosh^{-1}(x/\alpha' r)$.

Consequently,

$$V'_{r1} = \frac{1}{r} \int\limits_{x-\alpha' r}^{0} \frac{\dot{f}(\varepsilon)(x-\varepsilon)\,d\varepsilon}{\sqrt{(x-\varepsilon)^2 - \alpha'^2 r^2}} \tag{11.3.9}$$

or

$$V'_{r1} = \frac{1}{r} \int\limits_{x-\alpha' r}^{0} \dot{f}(\varepsilon) \left[1 - \left(\frac{\alpha' r}{x-\varepsilon}\right)^2\right]^{-1/2} d\varepsilon \tag{11.3.9'}$$

Since $\alpha' r < (x - \varepsilon)$, the expression $[1 - (\alpha' r)^2/(x - \varepsilon)^2]^{-1/2}$ can be expanded into the series

$$V'_{r1} = \frac{1}{r} \int\limits_{x-\alpha' r}^{0} \dot{f}(\varepsilon) \left[1 + \frac{1}{2}\left(\frac{\alpha' r}{x-\varepsilon}\right)^2 - \ldots\right] d\varepsilon$$

When $r \to 0$, the term in brackets tends to unity, and the lower limit to the value $\varepsilon = x$. Accordingly, the limiting value for the radial velocity component at $r \to 0$ is

$$V'_{r1} = \frac{1}{r} \int\limits_{x}^{0} \dot{f}(\varepsilon)\,d\varepsilon$$

which after integration allows us to obtain the expression

$$V'_{r1} = [f(0) - f(x)]/r$$

But at the tip of the body $f(0) = 0$, hence

$$V'_{r1} = -f(x)/r \tag{11.3.10}$$

Taking advantage of condition (11.2.19) for a flow without separation in which the second term φ'_{1x} in the denominator may be disregarded for a very slender body, we obtain an equation for determining the function $f(x)$:

$$f(x) = -r\,(dr/dx)\,V_\infty \tag{11.3.11}$$

This equation can be written in the form

$$f(x) = -\frac{1}{2\pi} \cdot \frac{dS(x)}{dx} V_\infty = -\frac{V_\infty}{2\pi} S'(x) \tag{11.3.12}$$

where $S(x) = \pi r^2$ is the running value of the cross-sectional area of the slender body.

Expression (11.3.12) for the function $f(x)$, which determines the law of source distribution along the axis in the limiting case when $r \to 0$, can be used to evaluate the velocity component (11.3.7) needed for calculating the pressure by formula (11.2.27) on the surface of slender real bodies of revolution. For this purpose, we substitute $\varepsilon = x - \alpha' r \cosh z$ for x in (11.3.12) and introduce into

(11.3.7) the derivative

$$\dot{f}(\varepsilon)=\frac{df}{d\varepsilon}=-\frac{V_\infty}{2\pi}\cdot\frac{d^2S(\varepsilon)}{d\varepsilon^2}=-\frac{V_\infty}{2\pi}S''(x-\alpha' r\cosh z) \quad (11.3.13)$$

The result is

$$V'_{x1}=\varphi'_{1x}=\frac{-V_\infty}{2\pi}\int_0^{\cosh^{-1}(x/\alpha' r)}S''(x-\alpha' r\cosh z)\,dz \quad (11.3.14)$$

Hence, to calculate the velocity by formula (11.3.14), one must know the shape of the body of revolution and the distribution of its area along the axis, i.e. the form of the function $S(x)$.

Assume that we have a body of revolution with a parabolic generatrix (see Fig. 11.1.3) whose equation is given in the form of (11.1.48). By this equation, the cross-sectional area is

$$S(x)=\pi r^2=\frac{\pi x^2}{4\lambda^2_{\text{mid}}}\left(2-\frac{x}{x_{\text{mid}}}\right)^2 \quad (11.3.15)$$

whence we find the second derivative:

$$S''(x)=\frac{d^2S(x)}{dx^2}=\frac{\pi}{\lambda^2_{\text{mid}}}\left(2-\frac{6x}{x_{\text{mid}}}+\frac{3x^2}{x^2_{\text{mid}}}\right) \quad (11.3.16)$$

Substituting $\varepsilon=x-\alpha' r\cosh z$ for x, we have

$$S''(x-\alpha' r\cosh z)=\frac{\pi}{\lambda^2_{\text{mid}}}\left[2-\frac{6}{x_{\min}}(x-\alpha' r\cosh z)+\frac{3}{x^2_{\text{mid}}}(x-\alpha' r\cosh z)^2\right] \quad (11.3.16')$$

Introduction of (11.3.16') into (11.3.14) yields

$$V'_{x1}=\frac{-V_\infty}{2\lambda^2_{\text{mid}}}\int_0^{\cosh^{-1}u}\left[2-\frac{6\bar{x}}{u}(u-\cosh z)+\frac{3\bar{x}^2}{u^2}(u-\cosh z)^2\right]dz \quad (11.3.17)$$

where $\bar{x}=x/x_{\text{mid}}$;

$$u=x/(\alpha' r) \quad (11.3.18)$$

Let us introduce the notation

$$i^0_x=I^0;\quad i^1_x=uI_0-I_1;\quad i^2_x=u^2I_0-2uI_1+I_2 \quad (11.3.19)$$

where we determine the quantities I_n in the form of the integrals

$$I_n=\int_0^{\cosh^{-1}u}(\cosh z)^n\,dz\quad(n=0,\,1,\,2) \quad (11.3.20)$$

In accordance with the notation (11.3.19), we have

$$V'_{x1} = \frac{-V_\infty}{2\lambda^2_{\text{mid}}}\left(2i_x^0 - \frac{6\bar{x}i_{\bar{x}}^1}{u} + \frac{3\bar{x}^2 i_{\bar{x}}^2}{u^2}\right) \tag{11.3.21}$$

In a more general case, when the function $S''(x)$ is given as the polynomial

$$S''(x) = \sum_{n=0}^{k} a_n x^n \tag{11.3.22}$$

an expression similar to (11.3.21) can be written in the form

$$V'_{x1} = -\sum_{n=0}^{k} b_n i_x^n \tag{11.3.23}$$

The coefficients a_n depend on the shape of the generatrix of the body of revolution, while the coefficients b_n depend additionally on the velocity V_∞. The values of the function i_x^n for $n = 0$, 1, and 2, presented in the form of (11.3.19), correspond to a body having a parabolic generatrix.

For a body of revolution whose generatrix has an equation of a higher degree, it is necessary to calculate the values of i_x^n for $n = 3$, 4, etc. Particularly, if the equation of the generatrix is such that the derivative $S''(x)$ from (11.3.22) is determined by the equation

$$S''(x) = \sum_{n=0}^{3} a_n x^n \tag{11.3.22'}$$

then by (11.3.23), the velocity component is

$$V_{x1} = -\sum_{n=0}^{3} b_n i_x^n \tag{11.3.23'}$$

where i_x^n is calculated for values of $n = 0$, 1, and 2 by formulas (11.3.19), and for $n = 3$ by the expression

$$i_x^3 = u^3 I_0 - 3u^2 I_1 + 3uI_2 - I_3 \tag{11.3.24}$$

The functions i_x^n calculated for values of the parameter u from 1 to 8.8 are given in Table 11.3.1.

As a particular case, we can obtain an expression for the velocity component on a slender cone from relation (11.3.21). To do this, we must substitute $\beta_0 = \beta_c$ (the semiapex angle of a parabolic body of revolution) for $1/\lambda_{\text{mid}}$ and assume that $x = 0$:

$$V'_{x1,\,c} = -V_\infty (i_x^0)_c \beta_c^2 \tag{11.3.25}$$

Having in view that by (11.3.19) and (11.3.20) for a cone

$$i_{x,c}^0 = I_{0.c} = \cosh^{-1} u_c$$

Table 11.3.1

u	i_x^0	i_x^1	i_x^2	i_x^3	i_r^0	i_r^1	i_r^2	i_r^3
1.0	0	0	0	0	0	0	0	0
1.1	0.4435	0.0298	0.0019	0.0001	0.4582	0.0303	0.0026	0.0004
1.2	0.6223	0.0838	0.0149	0.0071	0.6633	0.0856	0.0109	0.0015
1.3	0.7567	0.1527	0.0392	0.0095	0.8312	0.1256	0.0383	0.0096
1.4	0.8673	0.2342	0.0753	0.0254	0.9804	0.2526	0.0794	0.0281
1.6	1.047	0.4265	0.2068	0.2412	1.249	0.4756	0.2230	0.1124
1.8	1.177	0.6691	0.4875	0.4631	1.450	0.7166	0.4137	0.2949
2.0	1.317	0.9024	0.7314	0.6332	1.732	1.073	0.8296	0.6950
2.4	1.522	1.472	1.675	2.030	2.182	1.857	1.990	2.326
2.8	1.690	2.116	3.107	4.854	2.615	2.816	3.846	5.946
3.2	1.831	2.820	5.076	9.701	3.040	3.948	6.543	11.90
3.6	1.954	3.578	7.634	17.28	3.458	5.247	10.21	21.84
4.0	2.064	4.382	10.81	28.28	3.873	6.714	14.98	36.84
4.4	2.162	5.227	14.65	43.46	4.286	8.348	21.00	58.34
4.8	2.251	6.111	19.19	63.76	4.694	10.14	28.37	87.74
5.2	2.333	7.028	24.44	89.85	5.103	12.10	37.26	127.0
5.6	2.408	7.976	30.44	122.7	5.510	14.22	47.78	177.9
6.0	2.478	8.953	37.21	163.2	5.916	16.51	60.07	242.4
6.4	2.544	9.958	44.77	212.3	6.322	18.96	74.25	322.8
6.8	2.605	10.99	53.17	271.1	6.726	21.56	90.44	421.4
7.2	2.663	12.04	62.37	340.2	7.130	24.34	108.8	540.7
7.6	2.717	13.12	72.43	421.0	7.534	27.27	129.4	683.4
8.0	2.769	14.22	83.37	514.5	7.937	30.36	152.5	852.2
8.4	2.818	15.33	95.18	621.4	8.341	33.62	178.1	1050.4
8.8	2.865	16.47	107.9	743.3	8.743	37.04	206.3	1280.6

where $u_c = (x/\alpha' r)_c = 1/(\alpha' \beta_c)$, we obtain for the velocity component

$$V'_{x1,\,c} = -V_\infty \beta_c^2 \cosh^{-1} u_c = -V_\infty \beta_c^2 \ln\left(u_c + \sqrt{u_c^2 - 1}\right) \quad (11.3.25')$$

We can use the found values of $V'_{x1,\,c}$ and (11.2.27) to determine the pressure coefficient on the surface of a body of revolution at the corresponding point. On a conical surface, where the additional velocity component is determined from (11.3.25'), the pressure coefficient is

$$\bar{p}_{1c} = \beta_c^2 \left[2 \ln\left(u_c + \sqrt{u_c^2 - 1}\right) - 1\right] \quad (11.3.26)$$

In accordance with (10.2.30), relation (11.3.26) determines the wave drag coefficient of a slender cone, i.e.

$$c_{x,\,w,\,c} = \bar{p}_{1c} = \beta_c^2 \left[2 \ln\left(u_c + \sqrt{u_c^2 - 1}\right) - 1\right] \quad (11.3.26')$$

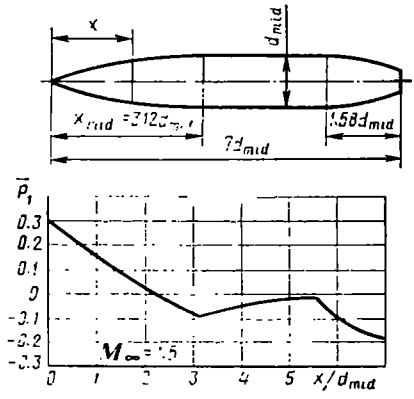

Fig. 11.3.2
Distribution of pressure coefficient over the surface of a body with a parabolic nose and parabolic boattail

The wave drag coefficient for a slender body of revolution of an arbitrary shape should be calculated by formula (11.1.51) in which the pressure coefficient from (11.3.14) and (11.2.27) is

$$\bar{p}_1 = \frac{1}{\pi} \int_0^{\cosh^{-1} u} S''(x - \alpha' r \cosh z)\, dz - \left(\frac{dr}{dx}\right)^2 \qquad (11.3.27)$$

Figure 11.3.2 shows the distribution of the pressure coefficient found according to the linearized theory at $M_\infty = 1.5$ for all three parts of a slender body of revolution—the nose, cylindrical, and tail ones. Examination of the figure reveals that the pressure along the cylinder, beginning from the end of the nose part, increases downstream and gradually recovers its free-stream value ($\bar{p}_1 \to 0$). The flow over the narrowing part (the boattail) is attended by an increase in the rarefaction.

Assuming that $dr/dx = \tan \beta \approx \beta$, we find a formula for the wave drag coefficient:

$$c_{x,w} = 2 \int_0^{\tilde{x}_c} \left[\frac{1}{\pi} \int_0^{\cosh^{-1} u} S''(x - \alpha' r \cosh z)\, dz - \beta^2\right] \bar{r}\beta\, d\tilde{x} \qquad (11.3.28)$$

where $\tilde{x} = x/r_{mid}$.

For a parabolic generatrix with the equation $r = (r_{mid}/x_{mid})\,(2 - x/x_{mid})$, the derivative is

$$\frac{dr}{dx} = \frac{2r_{mid}}{x_{mid}}(1 - \bar{x}) = \frac{1}{\lambda_{mid}}(1 - \bar{x}) = \beta_0(1 - \bar{x}) \qquad (11.3.29)$$

where $\bar{x} = x/x_{mid}$.

The coefficient (11.3.28) can be considered as the sum of two components: $c_{x,w} = c^n_{x,w} + c^{bt}_{x,w}$, where $c^n_{x,w}$ and $c^{bt}_{x,w}$ are the wave drag coefficients of the nose and boattail parts, respectively.

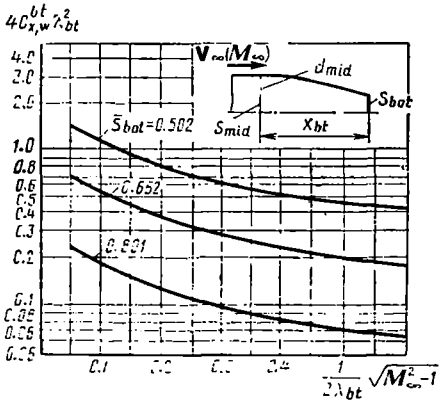

Fig. 11.3.3
Drag coefficient of a parabolic boattail

Having in view that in practice the pressure on the cylinder returns to atmospheric and, consequently, the flow ahead of the boattail part is considered to be undisturbed, the pressure distribution over this part and the corresponding value of $c^{bt}_{x,w}$ may be treated independently of the nose part.

The change in the quantity $c^{bt}_{x,w}$ is characterized by the graphs depicted in Fig. 11.3.3, a glance at which shows that it depends on the boattail fineness ratio $\lambda_{bt} = x_{bt}/d_{mid}$ (where x_{bt} is the length of the boattail part), on the number M_∞, and on the base taper ratio $\bar{S}_{base} = S_{base}/S_{mid}$. When $\bar{S}_{base}$ grows, the magnitude of the projection of the boattail surface onto a plane perpendicular to the longitudinal axis of the body increases, which leads to a lower base drag. The value of $c^{n}_{x,w}$ for the nose part can be calculated by (11.1.52) or with the aid of a relation obtained in accordance with the linearized theory (see [1]),

$$M^2_\infty c^{n}_{x,w} = K^2_1 \left(\frac{2}{3}\ln\frac{2}{K_1} + \frac{1}{18}\right) \qquad (11.3.28')$$

where $K_1 = M_\infty\beta_0$.

The integral in (11.3.27) can be expressed in accordance with (11.3.16') in the form

$$\int_0^{\cosh^{-1}u} S''(x-\alpha' r\cosh z)\,dz = \beta_0^2 N_1(u,\ \bar{x}) \qquad (11.3.30)$$

Here N_1 is a function of the dimensionless coordinate $\bar{x}$ and the parameter u; the latter is determined from the condition

$$u = \frac{x}{\alpha' r} = \frac{x_{mid}}{\alpha' r_{mid}}\cdot\frac{1}{2-x/x_{mid}} = \frac{u_0}{2-\bar{x}} \qquad (11.3.31)$$

where $u_0 = 1/(\alpha'\beta_0)$.

By using (11.3.29)-(11.3.31), we can write relation (11.3.27) in the general form

$$\bar{p}_1 = \beta_0^2 N(u_0, \bar{x}) \tag{11.3.32}$$

where N is a function of the parameter u_0 and the dimensionless coordinate $\bar{x}$.

With a view to (11.3.32), we can write the wave drag coefficient (11.3.28) in the general form

$$c_{x,w} = \beta_0^2 D(u_0) \tag{11.3.33}$$

where D is a function of the parameter u_0.

The general formulas (11.3.32) and (11.3.33) allow us to arrive at the following conclusion on the aerodynamic similarity of the flows near parabolic bodies of revolution.

If supersonic flows are characterized by the same value of the parameter u_0, the ratios $\bar{p}_1/\beta_0^2$ are the same at points with identical dimensionless coordinates $\bar{x}$. In aerodynamically similar flows, bodies of revolution experience axial forces such that the ratios $c_{x,w}/\beta_0^2$ for them are the same. Hence, the following parameter is the similarity criterion in the given case:

$$u_0 = 1/(\alpha'\beta_0) = 1/(\beta_0\sqrt{M_\infty^2 - 1}) = \lambda_{mid}/\sqrt{M_\infty^2 - 1} \tag{11.3.34}$$

For numbers $M_\infty \gg 1$, the parameter u_0 can be written as

$$u_0 = 1/K_1 \tag{11.3.34'}$$

where $K_1 = \beta_0 M_\infty = M_\infty/\lambda_{mid}$.

Multiplying both sides of (11.3.32) by M_∞^2 and taking into consideration relation (11.3.34'), we find

$$p_1/p_\infty - 1 = N_2(K_1, \bar{x}) \tag{11.3.35}$$

where N_2 is a function of the arguments K_1 and x.

Expression (11.3.35) shows that at a given point $\bar{x}$ the function of the pressure $(p_1/p_\infty - 1)$ depends only on the parameter K_1. The law of similarity according to this parameter is also confirmed by the results of calculations based on the method of characteristics.

Investigations show that when we use linearized methods of flow calculation, a satisfactory agreement of the results for the pressure function is obtained for values of the similarity criterion K_1 less than unity. The law of similarity in this criterion cannot be applied at certain combinations of the numbers M_∞ and the fineness ratios λ_{mid}, which follows directly from an analysis of the limits of application of the linearized theory. These limits can be established, for example, from formula (11.3.26) for the coefficient of the pressure on a cone. This formula is evidently not valid at $u_c = u_0 < 1$ because the quantity $\sqrt{u_0^2 - 1}$ is imaginary. On the other hand,

when u_0, while remaining larger than unity, approaches it, formula (11.3.26) yields an unreal (negative) value of the coefficient of the pressure on a slender cone. Consequently, calculations using the linearized theory yield satisfactory results only for conditions when $u_0 \gg 1$. It follows that the law of similarity evidently loses its validity when u_0 differs only slightly from unity.

Physically, deviation of the actual flow from a linearized one corresponds to such values of u_0. In practice, if the fineness ratio diminishes, i.e. a body becomes thicker (blunter), or if the number M_∞ grows at a constant fineness ratio, the flow differs increasingly from a linearized one. To retain a linearized flow, at large values of M_∞ the fineness ratio has to be increased, i.e. the body nose must be made sharper. Here the inequality $\lambda_{mid} > M_\infty$ must be satisfied. Accordingly, the similarity criterion $K_1 = M_\infty/\lambda_{mid}$ must be less than unity.

It follows from the expression $u_0 = (\alpha'\beta_0)^{-1}$ that if a body of revolution is slender, i.e. its fineness ratio is large, then to obey the inequality $u_0 > 1$ the condition $M_\infty > 1$ must be fulfilled. If the number $M_\infty \to 1$, it can be seen from formula (11.3.25′) that the magnitude of the disturbed velocity approaches infinity, which is impossible physically. Hence, the theory of linearized flows and the laws of their similarity are suitable upon the simultaneous fulfilment of two inequalities:

$$\lambda_{mid} > (M_\infty^2 - 1)^{1/2} \text{ and } M_\infty > 1 \qquad (11.3.36)$$

A comparison with experimental data shows that calculations according to the linearized theory and the use of similarity criteria are possible for a fineness ratio of $\lambda_{mid} \geqslant 2$ and Mach numbers $M_\infty \geqslant 1.4$ (i.e. $K_1 = M_\infty/\lambda_{mid} < 0.7$).

Similarity in the criterion $K_1 = M_\infty\beta_0$ for the pressure also determines similarity for the wave drag function; the application of this similarity law must be associated with the requirement of the conservation of a linearized flow. The possible limits of this application can be determined from a graph (see Fig. 11.1.4).

By multiplying both sides of formula (11.3.33) by M_∞^2, we obtain a general expression for the drag function:

$$M_\infty^2 c_{x,w} = \beta_0^2 H(K_1) \qquad (11.3.37)$$

where $H(K_1)$ is a function depending on the parameter K_1.

This expression indicates that *if the flow over two or more bodies of revolution with a different fineness ratio is characterized by the same parameter* K_1, *then for each of these bodies the value of the function* $M_\infty^2 c_{x,w}$ *is the same.*

The considered similarity criteria were obtained using parabolic bodies as an example. Parabolic bodies have a property following from Eq. (11.1.48) and consisting in the same distribution of the

relative thicknesses with respect to their length:

$\bar{x}=x/x_{\max}$	0	0.2	0.4	0.6	0.8	1.0	1.2	1.4	1.6	1.8	2.0
$\bar{r}=r/r_{\max}$	0	0.36	0.64	0.84	0.96	1.0	0.96	0.84	0.64	0.36	0

This set may contain geometrically similar bodies (all their linear dimensions differ by the same factor) which obviously will have the same fineness ratio, and they can be made to coincide with one another by homogeneous, i.e. identical for all directions, deformation. For aerodynamic similarity, it is necessary to ensure for a geometrically similar model being considered the same number M_∞ as for the full-scale body of revolution.

But parabolic bodies also include shapes that can be made to coincide only by inhomogeneous deformation. Let us imagine two bodies with different fineness ratios. If we introduce a linear scale identical for the radial and axial coordinates, deformation of the body in a longitudinal and axial directions does not produce complete coincidence. Such coincidence, called **affine**, can be achieved by affine transformation if the scales for the radial and the axial coordinates are different. Accordingly, parabolic bodies are called **affine-similar**. This class of **affine-similar bodies** includes conical ones whose generatrices are set by the equation $\bar{r} = \bar{x}$ in the dimensionless form. Consequently, conical bodies are characterized by an identical distribution of their relative thicknesses that do not depend on the fineness ratio of the bodies.

Unlike parabolic and conical bodies, in ogive noses (with a generatrix in the form of the arc of a circle), a change in $\lambda_{\max}$ is attended by a change in the distribution of the relative thicknesses $\bar{r}$ along the length. As a result, one ogive nose cannot be affine-mapped into another. When linearized flow over slender bodies is being investigated, however, the similarity criteria considered above may be used because at large fineness ratios ($\lambda_{\max} > 3$) an ogive nose differs only slightly from a parabolic one.

11.4. Non-Axisymmetric Flow

The problem of a non-axisymmetric flow consists in determining the additional potential φ_2' due to the crossflow of a gas around a slender body of revolution and satisfying Eq. (11.2.10′). We shall show that a solution for φ_2' can be obtained with the aid of the solution for φ_1' for an axisymmetric flow, i.e. we shall show that there is a mutual relation between φ_2' and φ_1'. For this purpose, we shall differentiate Eq. (11.2.11′) for an axisymmetric disturbed flow with respect to r:

$$(1-M_\infty^2)\frac{\partial^2}{\partial x^2}\left(\frac{\partial \varphi_1'}{\partial r}\right)+\frac{\partial^2}{\partial r^2}\left(\frac{\partial \varphi_1'}{\partial r}\right)-\frac{1}{r^2}\frac{\partial \varphi_1'}{\partial r}+\frac{1}{r}\cdot\frac{\partial^2 \varphi_1'}{\partial r^2}=0 \quad (11.4.1)$$

If we assume that

$$\varphi_2' = -(\partial\varphi_1'/\partial r)\cos\gamma, \qquad (11.4.2)$$

then after inserting it into the initial equation (11.2.10″) we obtain (11.4.1). Consequently, Eq. (11.4.2) is valid, and the total disturbance potential for non-axisymmetric flow can be considered in the form

$$\varphi' = \varphi_1' + \varphi_2' = \varphi_1' - (\partial\varphi_1'/\partial r)\cos\gamma \qquad (11.4.3)$$

To establish the physical meaning of the integral φ_2', let us use the method of analogy that was employed when dealing with axisymmetric flow and consists in that a body in both a compressible and incompressible flows is replaced with a system of sources and sinks.

In the case being considered of non-axisymmetric flow over a body, the method of analogy consists in the following. If φ_1' is considered as a potential function of sources (sinks) of an incompressible fluid continuously distributed along the axis of a body, then in accordance with expression (2.9.21′) the derivative $\partial\varphi_1'/\partial r$ should be considered as a function determining the flow due to doublets arranged along the same axis. Accordingly, *when studying a non-axisymmetric incompressible flow over a body, the latter may be replaced with a system of doublets continuously distributed along its axis.* Extending the analogy indicated above (axisymmetric flow) to the flow over a body with violation of axial symmetry, we assume that *a body in a supersonic linearized flow may be replaced with a system of doublets distributed along the axis*, and that φ_2' is the potential due to these doublets.

In accordance with (11.3.5), we have

$$\varphi_2' = -\cos\gamma\frac{\partial}{\partial r}\int_0^{\cosh^{-1}(x/\alpha' r)} f(x-\alpha' r\cosh z)\cosh z\,dz$$

$$= \alpha'\cos\gamma\int_0^{\cosh^{-1}(x/\alpha' r)} \dot{f}(x-\alpha' r\cosh z)\cosh z\,dz \qquad (11.4.4)$$

Substituting here $m(\varepsilon)$ for the function $\dot{f}(\varepsilon)$ and introducing the symbol $x/(\alpha' r) = u$, we obtain

$$\varphi_2' = \alpha'\cos\gamma\int_0^{\cosh^{-1}u} m(x-\alpha' r\cosh z)\cosh z\,dz \qquad (11.4.4')$$

The function $m(\varepsilon)$ in expression (11.4.4′) describes the distribution of the doublets, i.e. the change in their moments along the axis of the body of revolution. When replacing a body with doublets distributed along its axis, one should take into consideration the feature of propagation of a disturbance in a supersonic flow, consisting in that the disturbances due to the doublets, like those due to

sources, propagate only downstream within the confines of the Mach cone.

When using the above method of analogy in investigating non-axisymmetric, or "oblique" flow over a body of revolution, we replace the latter with a system of doublets. The meaning of this replacement consists in that the additional disturbance caused by the body in an oblique flow is equivalent to the disturbance produced by doublets arranged on its axis in a definite way depending on the shape and the conditions of the oncoming flow.

We shall find the solution of the problem of an oblique flow, which consists in calculating the parameters of a flow across the body's axis, if we choose the function $m(\varepsilon)$ so that the potential φ_2' satisfies an additional boundary condition on the surface of the body in non-axisymmetric flow. This condition on the basis of (11.2.22) and (11.4.4′) can be written as follows:

$$\alpha' \cos\gamma \frac{\partial}{\partial r} \int_0^{\cosh^{-1} u} m\,(x-\alpha' r \cosh z) \cosh z\, dz = -\alpha V_\infty \cos\gamma$$

Differentiation of this expression yields

$$\alpha'^2 \int_0^{\cosh^{-1} u} \dot{m}\,(x-\alpha' r \cosh z) \cosh^2 z\, dz = \alpha V_\infty \qquad (11.4.5)$$

where m is a derivative of the function m with respect to the argument $x - \alpha' r \cosh z$.

By solving integral equation (11.4.5) for a given body configuration and free-stream velocity, we can determine the doublet distribution function m. Solution of this equation can be simplified if we consider a very slender body of revolution. To do this, we shall transform (11.4.5) with the aid of the variable $\varepsilon = x - \alpha' r \cosh z$:

$$\frac{1}{r^2} \int_0^{x-\alpha' r} \frac{\dot{m}\,(\varepsilon)\,(x-\varepsilon)^2\, d\varepsilon}{\sqrt{(x-\varepsilon)^2 - \alpha'^2 r^2}} = \alpha V_\infty \qquad (11.4.6)$$

For a very slender body with a small r, the integral in (11.4.6) in a first approximation can be taken equal to its value at $r \to 0$. Hence,

$$\alpha V_\infty r^2 = \int_0^x \dot{m}\,(\varepsilon)\,(x-\varepsilon)\, d\varepsilon$$

or

$$\alpha V_\infty r^2 = \int_0^x (x-\varepsilon)\, dm$$

Integrating by parts and assuming $\bar{u} = x - \varepsilon$ and $d\bar{v} = dm$, we obtain

$$\alpha V_\infty r^2 = (x-\varepsilon)\, m(\varepsilon)\Big|_0^x + \int_0^x m(\varepsilon)\, d\varepsilon$$

At the tip $m(\varepsilon) = m(0) = 0$, while $\varepsilon \approx x$ because $r \ll x$. Therefore, we have

$$\alpha V_\infty r^2 = \int_0^x m(x)\, dx$$

Differentiation with respect to x yields

$$m(x) = 2\alpha V_\infty r\, dr/dx \qquad (11.4.7)$$

Expression (11.4.7) for the function $m(x)$ determining the doublet distribution for the limiting case when $r \to 0$ may be used to calculate non-axisymmetric flow over a body differing from a very slender one, by analogy with what we did in Sec. 11.3 when using the function f [see (11.3.11)] of source distribution for investigating axisymmetric flow. To do this, we have to go over from the variable x to the variable $\varepsilon = x - \alpha' r \cosh z$:

$$m(x - \alpha' r \cosh z) = \alpha V_\infty \frac{dr^2}{d\varepsilon} = \frac{\alpha V_\infty}{\pi} S'(x - \alpha' r \cosh z) \qquad (11.4.8)$$

whence the derivative

$$\dot{m}(x - \alpha' r \cosh z) = \frac{\alpha V_\infty}{\pi} S''(x - \alpha' r \cosh z) \qquad (11.4.9)$$

By calculating the derivative φ'_{2x} of the additional potential (11.4.4'), we obtain a relation for the axial velocity component:

$$V'_{x2} = \varphi'_{2x} = \alpha' \cos\gamma \int_0^{\cosh^{-1} u} \dot{m}(x - \alpha' r \cosh z) \cosh z\, dz \qquad (11.4.10)$$

Substituting for $\dot{m}$ in (11.4.10) its value from (11.4.9), we find

$$V'_{x2} = \frac{\alpha' \alpha V_\infty \cos\gamma}{\pi} \int_0^{\cosh^{-1} u} S''(x - \alpha' r \cosh z) \cosh z\, dz \qquad (11.4.11)$$

For the particular case of a parabolic generatrix with equation (11.1.48), the second derivative of the function $S(x)$ is determined

by formula (11.3.16), consequently,

$$V'_{x2}=\frac{\alpha'\alpha V_\infty\cos\gamma}{\lambda^2_{\text{mid}}}\int_0^{\cosh^{-1}u}\left[2-\frac{6\bar{x}}{u}(u-\cosh z)+\frac{3\bar{x}^2}{u^2}(u-\cosh z)^2\right]\cosh z\,dz \qquad (11.4.12)$$

where $\bar{x}=x/x_{\text{mid}}$ and $u=x/(\alpha' r)$.

Let us introduce the notation

$$i_r^0=I_1;\quad i_r^1=uI_1-I_2;\quad i_r^2=u^2I_1-2uI_2+I_3 \qquad (11.4.13)$$

where the quantities I_n ($n=1, 2, 3$) are determined in the form of integrals (11.3.20).

In accordance with this notation, we have

$$V'_{x2}=\frac{\alpha'\alpha V_\infty\cos\gamma}{\lambda^2_{\text{mid}}}\left(2i_r^0-\frac{6\bar{x}}{u}i_r^1+\frac{3\bar{x}^2}{u^2}i_r^2\right) \qquad (11.4.14)$$

For the more general case of the function $S''(x)$ given in (11.3.22), an expression similar to (11.4.12) can be written as

$$V'_{x2}=\sum_{n=0}^{l}g_n i_r^n \qquad (11.4.15)$$

The coefficients g_n depend on the shape of the generatrix of the body of revolution and the free-stream conditions (the angle of attack α and the velocity V_∞). We calculate the values of the function i_r^n for $n=0, 1, 2$ by (11.4.13), and for $n=3$ from the expression

$$i_r^3=u^3I_1-3u^2I_2+3uI_3-I_4 \qquad (11.4.16)$$

The function i_r^n calculated for values of the parameter u from 1 to 8.8 are given in Table 11.3.1 (p. 88).

For a slender cone in a flow at a small angle of attack, assuming $\bar{x}=0$ and $\lambda^2_{\text{mid}}=1/\beta_c^2$, we obtain from (11.4.14)

$$V'_{x2,c}=2\alpha'\alpha V_\infty i^0_{r,c}\beta_c^2\cos\gamma \qquad (11.4.17)$$

By (11.3.20), we have

$$i^0_{r,c}=\int_0^{\cosh^{-1}u_c}\cosh z\,dz=\sqrt{u_c^2-1} \qquad (11.4.18)$$

Having also in view that $u_c=1/(\alpha'\beta_c)$, we find

$$V'_{x2c}=2\alpha\beta_c V_\infty\cos\gamma\sqrt{1-(\alpha'\beta_c)^2} \qquad (11.4.19)$$

Using formula (11.2.28), we can evaluate the pressure coefficient for the point being considered on the surface of a body of revolution.

The derivative $\varphi'_{2\gamma}$ in this formula, with a view to (11.4.4') and (11.4.8) is

$$\varphi'_{2\gamma} = \frac{\partial \varphi'_2}{\partial \gamma} = \alpha' \sin \gamma \int_0^{\cosh^{-1} u} m\,(x - \alpha' r \cosh z) \cosh z\, dz$$

$$= \frac{\alpha' \alpha V_\infty \cos \gamma}{\pi} \int_0^{\cosh^{-1} u} S'\,(x - \alpha' r \cosh z) \cosh z\, dz \qquad (11.4.20)$$

Instead of (11.4.20), we can use a simplified relation for $\varphi'_{2\gamma}$ that is obtained from the potential φ'_2, written on the basis of (11.3.10) and (11.4.2) as

$$\varphi'_2 = -\,(\partial \varphi'_1/\partial r) \cos \gamma = [f(x)/r] \cos \gamma \qquad (11.4.21)$$

Differentiation with respect to γ yields

$$\partial \varphi'_2/\partial \gamma = \gamma'_{2\gamma} = -\,[f(x)/r] \sin \gamma \qquad (11.4.22)$$

By calculating the derivative with respect to r, we determine the additional radial velocity component for the conditions $r \to 0$:

$$V'_{2r} = \varphi'_{2r} = \partial \varphi'_2/\partial r = -\,[f(x)/r^2) \cos \gamma \qquad (11.4.23)$$

From condition (11.2.22) of flow without separation, this velocity component is

$$V'_{2r} = -\,[f(x)/r^2] \cos \gamma = -\,\alpha V_\infty \cos \gamma$$

whence

$$f(x) = \alpha V_\infty r^2 \qquad (11.4.24)$$

Consequently,

$$\varphi'_{2\gamma} = -\,\alpha V_\infty r \sin \gamma \qquad (11.4.25)$$

Introducing this expression into (11.2.28), we obtain

$$\bar{p}_2 = \frac{-2}{V_\infty^2}\left[V_\infty \varphi'_{2x} + \frac{\alpha^2 V_\infty^2}{2}(4 \sin^2 \gamma - 1)\right] \qquad (11.4.26)$$

where φ'_{2x} is calculated with the aid of (11.4.14) or (11.4.15), and for the particular case of flow over a cone, by formula (11.4.19).

With account taken of (11.2.27), the total pressure coefficient is

$$\bar{p} = \bar{p}_1 + \bar{p}_2 = \frac{-2}{V_\infty^2}\left[V_\infty \varphi'_{1x} + \frac{V_\infty^2}{2}\left(\frac{dr}{dx}\right)^2 + V_\infty \varphi'_{2x} + \frac{\alpha^2 V_\infty^2}{2}(4 \sin^2 \gamma - 1)\right] \qquad (11.4.27)$$

11.5. Calculation of Aerodynamic Coefficients

We can use the found distribution of the pressure near a body of revolution in a flow at an angle of attack, i.e. with the violation of axial symmetry, to determine the aerodynamic forces, moments, and their aerodynamic coefficients. Diagrams showing the action of the forces and moment are given in Figs. 7.5.4 and 7.5.5.

We shall obtain general expressions for calculating the forces, moments, and coefficients provided that the shape of the body in the flow is known and that the pressure distribution over the side surface of the body has been found for the given free-stream angle of attack α, pressure p_∞, and number M_∞.

Axial Force Coefficient

To calculate the axial force X and the coefficient of this force $c_x = X/(q_\infty S_{\text{mid}})$, let us consider a body of revolution (Fig. 11.5.1) with an arbitrary generatrix determined by the equation $r = f(x)$. Let us separate an element of the surface of width dx at a distance of x from the nose. This element with an area of $dS = r\,d\gamma\,dl$ experiences a force of the excess pressure equal to $(p - p_\infty)\,dS$.

With account taken of these data and by formula (1.3.1), in which we assume that $\tau = 0$, the magnitude of the elementary longitudinal force acting on the separated area is

$$(p - p_\infty)\cos\widehat{(n, x)}\,dS = (p - p_\infty)\,r\,d\gamma\,dl\sin\beta \qquad (11.5.1)$$

Going over to the pressure coefficient $\bar{p} = (p - p_\infty)/q_\infty$ here and having in view that $dl = dx/\cos\beta$, we find

$$\bar{p}q_\infty\cos\widehat{(n, x)}\,dS = \bar{p}q_\infty r\tan\beta\,d\gamma\,dx$$

Introducing this expression into formula (1.3.2) in which we assume that $X_a = X_p$, $c_{f,x} = 0$, and taking into consideration the symmetry of pressure distribution about the vertical plane of symmetry coinciding with the plane of the angle of attack containing the velocity vector $\mathbf{V}_\infty$ (this plane is also known as the zero meridian plane), we obtain for the axial force ($X_p = X$, we drop the subscript p)

$$X = 2q_\infty\int_0^{x_b} r\tan\beta\,dx\int_0^{\pi}\bar{p}\,d\gamma \qquad (11.5.2)$$

where x_b is the distance from the tip to the bottom.

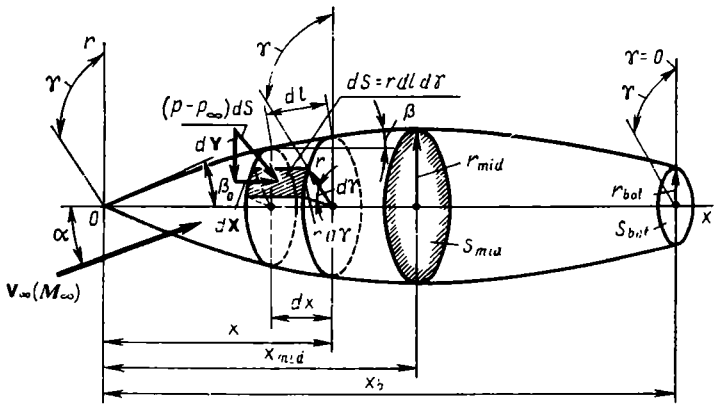

Fig. 11.5.1
To the determination of the aerodynamic coefficients from the known pressure distribution on the surface of a body of revolution

This force can be expressed in terms of the coefficient c_x by

$$X = c_x q_\infty S_{\text{mid}}$$

With account taken of (11.5.2), the axial force coefficient is

$$c_x = \frac{X}{q_\infty S_{\text{mid}}} = \frac{4\lambda_{\text{mid}}}{\pi} \int_0^{\bar{x}_b} \bar{r} \tan\beta \, d\bar{x} \int_0^{\pi} \bar{p} \, d\gamma \qquad (11.5.3)$$

where $\bar{r} = r/r_{\text{mid}}$, $\bar{x} = x/x_{\text{mid}}$, $\bar{x}_b = x_b/x_{\text{mid}}$; $\bar{p} = (p - p_\infty)/q_\infty$ is the pressure coefficient whose distribution is considered to be a known function of $r(x)$ and γ.

Coefficients of Normal Force and Pitching Moment

Inspection of Fig. 11.5.1 reveals that the magnitude of the elementary normal force is

$$dY = -(p - p_\infty)\, r \, d\gamma \, dl \cos\gamma \cos\beta \qquad (11.5.4)$$

Introducing the pressure coefficient $\bar{p}$ and taking into account that $dl \cos\beta = dx$, we obtain the following expression for the total normal force:

$$Y = -2q_\infty \int_0^{x_b} r \, dx \int_0^{\pi} \bar{p} \cos\gamma \, d\gamma \qquad (11.5.5)$$

We can use this value to calculate the normal force coefficient:

$$c_y = \frac{Y}{q_\infty S_{\text{mid}}} = \frac{-4\lambda_{\text{mid}}}{\pi} \int_0^{\bar{x}_b} \bar{r}\, d\bar{x} \int_0^{\pi} \bar{p} \cos\gamma\, d\gamma \qquad (11.5.6)$$

In axisymmetric flow, $c_y = 0$ because the pressure in this case is distributed in accordance with circular symmetry and, consequently, does not depend on the angle γ.

The magnitude of the elementary moment produced by the pressure force (the pitching moment) calculated about the nose of the body equals, as follows from Fig. 11.5.1,

$$dM_z = -x\, dY + r \cos\gamma\, dX$$

The elementary moment is positive, therefore the first term has a minus sign with a view to the negative sign of dY in (11.5.4). Using this formula, and also expression (11.5.1), we obtain

$$dM_z = x(p - p_\infty)\, r\, d\gamma\, dl \cos\gamma \cos\beta + r \cos\gamma\, (p - p_\infty)\, r\, d\gamma\, dl \sin\beta \qquad (11.5.7)$$

Taking into consideration the symmetric distribution of the pressure, we find for the total moment

$$M_z = 2 \int_0^{x_b} xr\, dx \int_0^{\pi} (p - p_\infty) \cos\gamma\, d\gamma + 2 \int_0^{x_b} r^2 \tan\beta\, dx \int_0^{\pi} (p - p_\infty) \cos\gamma\, d\gamma \qquad (11.5.8)$$

whence the moment coefficient is

$$m_z = \frac{M_z}{q_\infty S_{\text{mid}} x_b} = \frac{4\lambda_{\text{mid}}}{\pi \bar{x}_b} \int_0^{\bar{x}_b} \bar{x}\bar{r}\, d\bar{x} \int_0^{\pi} \bar{p} \cos\gamma\, d\gamma + \frac{2}{\pi \bar{x}_b} \int_0^{\bar{x}_b} \bar{r}^2 \tan\beta\, d\bar{x} \int_0^{\pi} \bar{p} \cos\gamma\, d\gamma \qquad (11.5.9)$$

In accordance with the diagram showing how the moment reducing the angle of attack acts (see Fig. 7.5.5), the coefficient of this moment obtained from (11.5.9) has a minus sign. If a body of revolution is slender ($r \ll x_b$), the second term in this expression may be disregarded.

In axisymmetric flow, the pressure distribution does not depend on the angle γ, hence

$$\int_0^{\pi} \bar{p} \cos\gamma \, d\gamma = \bar{p} \int_0^{\pi} \cos\gamma \, d\gamma = 0$$

and, consequently, $m_z = 0$.

Aerodynamic Coefficients in a Linearized Flow

Let us find the values of the aerodynamic coefficients for slender bodies of revolution in a linearized flow at an angle of attack. For this purpose, we shall use relation (11.4.27) for the pressure coefficient in which we shall write φ'_{sx} according to (11.4.2) in the form

$$\varphi'_{sx} = -(\partial^2 \varphi'_1 / \partial r \, \partial x) \cos\gamma = -\varphi'_{1r,x} \cos\gamma \qquad (11.5.10)$$

Let us separate from (11.4.27) the terms not depending on γ and the terms that determine the asymmetric nature of pressure distribution and are functions of the angle γ:

$$\bar{p} = P_0(x, r) + P_\gamma(x, r, \gamma) \qquad (11.5.11)$$

where

$$P_0(x, r) = \frac{-2}{V_\infty^2}\left[V_\infty \varphi'_{1x} + \frac{V_\infty^2}{2}\left(\frac{dr}{dx}\right)^2 - \frac{\alpha^2 V_\infty^2}{2}\right] \qquad (11.5.12)$$

$$P_\gamma(x, r, \gamma) = \frac{-2}{V_\infty^2}(-V_\infty \varphi'_{1r,x} \cos\gamma + 2\alpha^2 V_\infty^2 \sin^2\gamma) \qquad (11.5.13)$$

To determine the axial force coefficient by (11.5.3), we have to calculate the integral

$$\int_0^{\pi} \bar{p} \, d\gamma = \int_0^{\pi} [P_0(x, r) + P_\gamma(x, r, \gamma)] \, d\gamma = \frac{-2}{V_\infty^2} \int_0^{\pi} \left[V_\infty \varphi'_{1x} + \frac{V_\infty^2}{2}\left(\frac{dr}{dx}\right)^2 - \frac{\alpha^2 V_\infty^2}{2}\right] d\gamma - \frac{2}{V_\infty^2} \int_0^{\pi} (-V_\infty \varphi'_{1r,x} \cos\gamma + 2\alpha^2 V_\infty^2 \sin^2\gamma) \, d\gamma$$

Having in view that the terms in brackets, and also the quantity $\varphi'_{1r,x}$ do not depend on γ, integration yields

$$\int_0^{\pi} \bar{p} \, d\gamma = \frac{-2\pi}{V_\infty^2}\left[V_\infty \varphi'_{1x} + \frac{V_\infty^2}{2}\left(\frac{dr}{dx}\right)^2 - \frac{\alpha^2 V_\infty^2}{2}\right] - 2\alpha^2\pi$$

$$= \frac{-2\pi}{V_\infty^2}\left[V_\infty \varphi'_{1x} + \frac{V_\infty^2}{2}\left(\frac{dr}{dx}\right)^2 + \frac{\alpha^2 V_\infty^2}{2}\right]$$

Introducing this expression into (11.5.3) and taking into account that for slender bodies $dr/dx \approx \beta$, while φ'_{1x} is determined from (11.3.14), we have

$$c_x = \frac{4\lambda_{mid}}{\pi} \int_0^{\bar{x}_b} \bar{r}\beta \, d\bar{x} \int_0^{\cosh^{-1} u} S''(x - \alpha' r \cosh z)\, dz$$

$$- 4\lambda_{mid} \int_0^{\bar{x}_b} \bar{r}\beta^3 \, d\bar{x} - 4\lambda_{mid}\alpha^2 \int_0^{\bar{x}_b} \bar{r}\beta \, d\bar{x} \qquad (11.5.14)$$

Comparing the value of c_x from (11.5.14) with the value of the axial force coefficient at a zero angle of attack (the wave drag coefficient) determined from (11.3.28), we see that the influence of the violation of flow symmetry on the coefficient c_x is taken into account by the third term in (11.5.14) depending on the square of the angle of attack.

We obtain the corresponding expression for a cone if we insert into (11.5.14) the values

$$\left.\begin{aligned} &\beta = \beta_c, \quad S'' = d^2(\pi r^2)/dx^2 = 2\pi\beta_c^2 \\ &\bar{x} = \bar{r}, \quad \bar{x}_b = 1, \quad \lambda_{mid} = 1/(2\beta_c) = \alpha' u_c/2 \end{aligned}\right\} \qquad (11.5.15)$$

and then integrate it:

$$c_x = \beta_c^2 [2 \ln (u_c + \sqrt{u_c^2 - 1}) - 1] - \alpha^2 \qquad (11.5.16)$$

For very small angles of attack, the term α^2 in (11.5.14) and (11.5.16) may be disregarded, hence the expressions obtained for the axial force coefficients will coincide with the corresponding relations (11.3.28) and (11.3.26') for axisymmetric flow.

To determine the normal force coefficient, we have to calculate the following integral in (11.5.6):

$$\int_0^{\pi} \bar{p} \cos\gamma \, d\gamma = \int_0^{\pi} [P_0(x, r) + P_\gamma(x, r, \gamma)] \cos\gamma \, d\gamma$$

$$= \frac{-2}{V_\infty^2} \int_0^{\pi} \left[V_\infty \varphi'_{1x} + \frac{V_\infty^2}{2} \left(\frac{dr}{dx}\right)^2 - \frac{\alpha^2 V_\infty^2}{2} \right] \cos\gamma \, d\gamma$$

$$- \frac{2}{V_\infty^2} \int_0^{\pi} (-V_\infty \varphi'_{1r,x} \cos\gamma + 2\alpha^2 V_\infty^2 \sin^2\gamma) \cos\gamma \, d\gamma$$

The first term on the right-hand side of this expression is zero because the quantities in brackets do not depend on the angle γ,

while the integral $\int_0^{\pi} \cos\gamma\, d\gamma = 0$. Also having in view that the integral $\int_0^{\pi} \sin^2\gamma \cos\gamma\, d\gamma$ in the second term is zero, while the integral $\int_0^{\pi} \cos^2\gamma\, d\gamma = \pi/2$, we obtain

$$\int_0^{\pi} \bar{p} \cos\gamma\, d\gamma = \frac{\pi}{V_\infty} \varphi'_{1r,x} \tag{11.5.17}$$

Introducing this expression into (11.5.6), we have

$$c_y = \frac{-4\lambda_{\text{mid}}}{V_\infty} \int_0^{\bar{x}_b} \varphi'_{1r,\bar{x}}\, \bar{r}\, d\bar{x} \tag{11.5.18}$$

From (11.5.10) and (11.4.11)]

$$\varphi'_{1r,x} = -\frac{\varphi'_{2x}}{\cos\gamma} = -\frac{\alpha'\alpha V_\infty}{\pi} \times \int_0^{\cosh^{-1} u} S''(x - \alpha' r \cosh z) \cosh z\, dz \tag{11.5.19}$$

Consequently,

$$c_y = \frac{4\lambda_{\text{mid}}\alpha'\alpha}{\pi} \int_0^{\bar{x}_b} \bar{r}\, d\bar{x} \int_0^{\cosh^{-1} u} S''(x - \alpha' r \cosh z) \cosh z\, dz \tag{11.5.20}$$

For a slender cone by (11.5.15) and with a view to the value of the integral $\int_0^{\cosh^{-1} u_c} \cosh z\, dz = \sqrt{u_c^2 - 1}$, we find

$$c_y = 2\alpha'\alpha\beta_c \sqrt{u_c^2 - 1} \tag{11.5.21}$$

For the moment coefficient (11.5.9), using (11.5.17) and (11.5.19) and the expression $\tan\beta \approx \beta$, we obtain

$$m_z = \frac{-4\lambda_{\text{mid}}\alpha'\alpha}{\pi\bar{x}_b} \int_0^{\bar{x}_b} \bar{x}\bar{r}\, d\bar{x} \int_0^{\cosh^{-1} u} S''(x - \alpha' r \cosh z) \cosh z\, dz - \frac{2\alpha'\alpha}{\pi\bar{x}_b} \int_0^{\bar{x}_b} \bar{r}^2\beta\, d\bar{x} \int_0^{\cosh^{-1} u} S''(x - \alpha' r \cosh z) \cosh z\, dz \tag{11.5.22}$$

For a slender cone

$$m_z = -(4/3)\,\alpha'\alpha\beta_c\,(1+\beta_c^2)\sqrt{u_c^2-1} \qquad (11.5.23)$$

For very slender conical bodies, the quantity β_c^2 may be ignored in comparison with unity. Evidently, for all very slender bodies of revolution with an arbitrary generatrix, the second addends in (11.5.9) and correspondingly in (11.5.22) may be omitted.

The coordinate of the centre of pressure (see Fig. 7.5.5) measured from the nose is

$$x_p = -M_z/Y \qquad (11.5.24)$$

while the coefficient of the centre of pressure is

$$\bar{c}_p = x_p/x_b = -m_z/c_y \qquad (11.5.25)$$

Introducing into (11.5.25) the values of m_z and c_y from (11.5.22) and (11.5.21), respectively, we can calculate the centre-of-pressure coefficient for a slender body of revolution with an arbitrary generatrix in a linearized flow. We can obtain the value of this coefficient for a cone without imposing conditions of a linearized flow. The flow over inclined cones in it has the property of conicity according to which the pressure coefficient $\bar{p}$ does not depend on the coordinates x and r, but is a **function of the meridional angle**. Therefore, (11.5.24) with a view to (11.5.6) and (11.5.9) can be written as

$$c_p = \left(2\lambda_{mid}\int_0^{\bar{x}_b}\bar{x}\bar{r}\,d\bar{x} + \int_0^{\bar{x}_b}\bar{r}^2\tan\beta_c\,d\bar{x}\right)\Big/\left(2\lambda_{mid}\,\bar{x}_b\int_0^{\bar{x}_b}\bar{r}\,d\bar{x}\right) \qquad (11.5.26)$$

Taking into account that for a cone we have $\bar{x} = \bar{r}$, $\bar{x}_b = 1$, and $\lambda_{mid} = 1/(2\tan\beta_c)$, after integration we obtain

$$c_p = 2\,(1+\tan^2\beta_c)/3 \qquad (11.5.27)$$

For slender cones, we may assume in (11.5.27) that $\tan^2\beta_c \approx \beta_c^2$. We thereby obtain the relation $c_p = 2\,(1+\beta_c^2)/3$ that can be seen to be determined from the formulas (11.5.23) and (11.5.21) for the moment and normal force coefficients, respectively. By (11.5.27), an increase in the thickness of a cone (in the angle β_c) is attended by shifting of the centre of pressure toward the tail portion because the forces produced by the pressure acting on this portion grow, and the stabilizing moment of these forces, facilitating such a shift of the centre of pressure, becomes appreciable.

The coefficients of the normal c_y and axial c_x forces related to a body-axis system can be used to obtain the coefficients of the aerodynamic forces in a wind coordinate system. The relevant calculations are performed with the aid of formulas (7.5.25') by which

the wave drag and lift force coefficients are

$$c_{x_a} = \beta_c^2 [2 \ln (u_c + \sqrt{u_c^2 - 1}) - 1] + \alpha^2 (2\alpha' \beta_c \sqrt{u_c^2 - 1} - 1) \quad (11.5.28)$$

$$c_{y_a} = 2\alpha' \alpha \beta_c \sqrt{u_c^2 - 1} \quad (11.5.29)$$

Similarity Law. To derive a similarity law for a body of revolution in a linearized flow, let us use expression (11.4.26) for the pressure coefficient $\bar{p}_2$ which we shall write as

$$\bar{p}_2 = (-2/V_\infty) V'_{x2} - \alpha^2 (4 \sin^2 \gamma - 1) \quad (11.5.30)$$

For a parabolic body, the additional velocity component V'_{x2} for a given point on the surface is determined from (11.4.14) as a function of the parameter u calculated, in turn, depending on the quantity $u_0 = 1/(\alpha' \beta_0)$ by (11.3.31). Also keeping in mind the equation $\lambda_{mid} = 1/\beta_0$, we can write relation (11.5.30) in the general form

$$\bar{p}_2 = -2\alpha \beta_0 G (u_0, \bar{x}) \cos \gamma - \alpha^2 (4 \sin^2 \gamma - 1) \quad (11.5.31)$$

where G is a function depending on the quantity u_0 for a given point on the surface.

Let us consider the case when the number M_∞ of a flow over a body of revolution is large, and we can assume that $\alpha' \approx M_\infty$. Hence, multiplying both sides of Eq. (11.5.31) by M_∞^2, we find

$$p_2/p_1 - 1 = -k (\alpha/\beta_0) K_1^2 G_1 (K_1, \bar{x}) - (k/2) (\alpha/\beta_0)^2 \times K_1^2 (4 \sin^2 \gamma - 1) \quad (11.5.32)$$

where G_1 is a function determined for a given point by the parameter $K_1 = M_\infty \beta_0 = M_\infty/\lambda_{mid}$.

Let us introduce the similarity criterion

$$K_2 = \alpha/\beta_0 = \alpha \lambda_{mid} \quad (11.5.33)$$

and write (11.5.32) in a more general form:

$$p_2/p_1 - 1 = B (K_1, K_2, \bar{x}, \gamma) \quad (11.5.34)$$

where B is a function.

Equation (11.5.34) expresses the law of similarity in a flow over slender affine-similar bodies. It follows from it that the function of the pressure at a given point of a surface with the coordinates $\bar{x}$, γ is the same if the quantities K_1 and K_2 for the bodies in the flow are the same. The quantities K_1 and K_2 are called the **similarity criteria** of flows over slender bodies of revolution at an angle of attack. In accordance with (11.5.20) and (11.5.22), the functions determining the relations for the normal force and moment coefficients depend

on these criteria, namely,

$$M_\infty^2 c_y = E(K_1, K_2); \quad M_\infty^2 m_z = F(K_1, K_2) \qquad (11.5.35)$$

where E and F are functions of the similarity criteria K_1 and K_2.

Here the law of similarity consists in that when two affine-similar bodies of revolution having different fineness ratios are in flows with different numbers M_∞ and angles of attack α, the quantities $M_\infty^2 c_y$ (or $M_\infty^2 m_z$) are the same if the similarity criteria K_1 and K_2 are the same.

Results of the Aerodynamic Theory of a Slender Body

By this theory, the normal force and longitudinal moment coefficients are determined for small lateral dimensions of bodies of revolution provided that $r \to 0$. Experimental investigations reveal that the theoretical results obtained for c_y, m_z, and $\bar{c}_p = -m_z/c_y$ are suitable in a first approximation for estimating the aerodynamic properties of real bodies of revolution (with sufficiently small finite values of r) at small angles of attack.

Let us consider relation (11.5.20) and replace the quantity S'' in it according to (11.4.9):

$$c_y = \frac{4\lambda_{mid}\alpha'}{V_\infty} \int_0^{\bar{x}_b} \bar{r}\, d\bar{x} \int_0^{\cosh^{-1} u} \dot{m}(x - \alpha' r \cosh z) \cosh z\, dz$$

We shall transform this expression with the aid of the variable $\varepsilon = x - \alpha' r \cosh z$:

$$c_y = \frac{4\lambda_{mid}}{V_\infty} \int_0^{\bar{x}_b} \bar{r}\, d\bar{x} \int_0^{x-\alpha' r} \frac{\dot{m}(\varepsilon)(x-\varepsilon)\, d\varepsilon}{r\sqrt{(x-\varepsilon)^2 - \alpha'^2 r^2}}$$

Going over to the limit at $r \to 0$ and taking into account that $\bar{x} = x/x_{mid}$, we find

$$c_y = \frac{2}{V_\infty r_{mid}^2} \int_0^{x_b} m(x)\, dx$$

Inserting into this equation the value of $m(x)$ from (11.4.7), we obtain

$$c_y = \frac{4\alpha}{r_{mid}^2} \int_0^{r_{bot}} r\, dr$$

Here the quantity $r\, dr/r_{mid}^2$ can be written as $0.5 d\bar{S}$, where $\bar{S}$ is the relative area of a cross section at the distance x from the nose.

Hence,

$$c_y = 2\alpha \bar{S}_{bot} \tag{11.5.36}$$

where $\bar{S}_{bot} = S_{bot}/S_{mid}$ is the base taper ratio.

Inspection of (11.5.36) reveals that the normal force coefficient for a long slender body of revolution does not depend on the dimensions or shape of the nose part. Formula (11.5.36) reflects the experimentally observed decrease in c_y due to taper of the base ($\bar{S}_{bot} < 1$), or, conversely, the increase in this coefficient with a flaring base part (afterbody) ($\bar{S}_{bot} > 1$).

To obtain the moment coefficient, we shall use relation (11.5.22) in which we shall delete the second term on the right-hand side (owing to the small thickness of the body of revolution). Going over to the variable $\varepsilon = x - \alpha' r \cos z$, as we did when finding the coefficient c_y, we obtain

$$m_z = \frac{-2}{V_\infty r_{mid}^2 x_b} \int_0^{x_b} m(x)\, x\, dx$$

After replacing $m(x)$ here in accordance with (11.4.7), we have

$$m_z = \frac{-4\alpha}{r_{mid}^2 x_b} \int_0^{r_{bot}} xr\, dr$$

Integration by parts yields the moment coefficient:

$$m_z = -2\alpha (\bar{S}_{bot} - W_b/W_{cyl}) \tag{11.5.37}$$

where $W_b = \pi \int_0^{x_b} r^2\, dx$ is the volume of the body of revolution, and $W_{cyl} = \pi r_{mid}^2 x_b = S_{mid} x_b$ is the volume of a cylinder whose bottom area equals the area of the mid-section (maximum cross section) and whose altitude equals the length of the body.

By (11.5.36) and (11.5.37), the centre-of-pressure coefficient is

$$c_p = x_p/x_b = -m_z/c_y = 1 - W_b/(\bar{S}_{bot} W_{cyl}) \tag{11.5.38}$$

The above estimation of the aerodynamic coefficients takes no account of the influence of flow separation for long bodies in a lateral flow at a velocity of $V_\infty \alpha$. Experimental investigations show that the beginning of separation almost coincides with the place where the nose part joins the cylinder. The appearance of a separation zone with a relative length of $\lambda_{cyl} + \lambda_{bt}$ (where $\lambda_{cyl} = x_{cyl}/d_{mid}$, $\lambda_{bt} = x_{bt}/d_{mid}$, x_{cyl} and x_{bt} are the lengths of the cylinder and the boattail or afterbody, respectively) causes the initiation of an additional normal force and longitudinal moment, so that the total

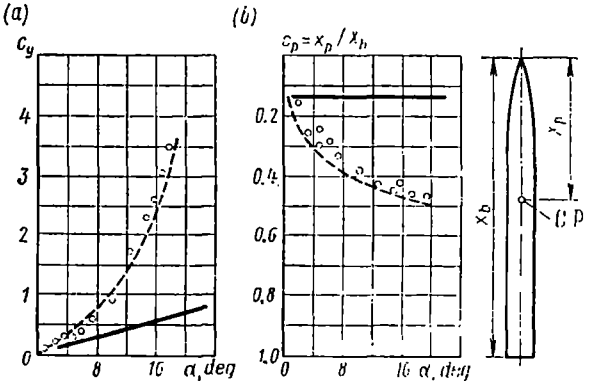

Fig. 11.5.2
Coefficients of normal force (*a*) and centre of pressure (*b*) for a sharp-nosed body of revolution

The overall fineness ratio of the body is 21, that of nose $\lambda_{mid} = 4.75$; the solid line corresponds to the aerodynamic slender-body theory; the dashed line – to the same with account of flow separation; the circles are the results of experiments at $M_\infty = 2$

values of the corresponding aerodynamic coefficients (see [1]) are

$$c_y = 2\alpha \bar{S}_{bot} + \Delta c_y \qquad (11.5.39)$$

$$m_z = -2\alpha (\bar{S}_{bot} - W_b/W_{cyl}) + \Delta m_z \qquad (11.5.40)$$

where

$$\Delta c_y = \frac{4c\alpha^2}{\pi} (\lambda_{cyl} + \lambda_{bt}); \qquad \Delta m_z = \frac{-2c\alpha^2}{\pi} (\lambda_{cyl} + \lambda_{bt}) \qquad (11.5.41)$$

The coefficient c in Eqs. (11.5.41) depends on whether the boundary layer is laminar or turbulent. For a laminar flow, $c \approx 1.2$, and for a turbulent one, $c \approx 0.3$-0.4.

With a view to the new values of c_y and m_z [see (11.5.39) and (11.5.40)], the centre-of-pressure coefficient is

$$c_p = [2\alpha (\bar{S}_{bot} - W_b/W_{cyl}) - \Delta m_z]/(2\alpha \bar{S}_{bot} + \Delta c_y) \qquad (11.5.42)$$

This coefficient is larger than the value that is determined without account taken of separation.

Figure 11.5.2 shows experimental data that are compared with the results of calculations by the theory of a slender body [see (11.5.36), (11.5.38)], and also by (11.5.39) and (11.5.42).

The normal force determined by the slender-body theory acts only on the expanding part of the body before the region of separation. The magnitude of this force is proportional to α, while the normal force in the separation zone changes depending on α^2. Examination of Fig. 11.5.2 reveals that formulas (11.5.39) and (11.5.42) yield satisfactory results.

Suction Force

Let us consider relation (7.5.25) for the drag coefficient. For small angles of attack, when $c_{y_a} \approx c_y$, we shall write this relation in the form $c_{x_a} = c_x + c_{y_a}\alpha$. The axial force coefficient c_x in this formula depends on the angle of attack, and it can be determined as the sum $c_x = c_{x0} + c_{x,s}$, in which c_{x0} is the axial force coefficient in axisymmetric flow, and $c_{x,s}$ is the supplementary axial force coefficient depending on α. Consequently, in non-axisymmetric flow, the main part of the induced drag of the body $c_{y_a}\alpha$ is supplemented by the longitudinal force $c_{x,s}$ due to the angle of attack. Particularly, from formula (11.5.16) for a cone, we can see that by the linearized theory the longitudinal force coefficient $c_{x,s} = -\alpha^2$. The occurrence of this force is associated with the specific conditions of flow. At subsonic velocities, such flow is characterized not so much by compression of the gas on the bottom (windward) side as by rarefaction on the upper (lee) side of the body. At supersonic velocities, the generation of an aerodynamic force is mainly due to the increase in the pressure on the bottom side, while the rarefaction on the upper side is of a smaller significance. Accordingly, at subsonic velocities, a buoyant (suction) force arises, and at supersonic ones, a drag force.

One must have in view that formula (11.5.16) for c_x includes the term $-\alpha^2$ determining the suction force of a body in a supersonic flow with the number $M_\infty > 1$ ($V_\infty > a_\infty$). The occurrence of this force is associated with the fact that non-axisymmetric flow over the body is determined by a supplementary crossflow at the velocity $V_\infty\alpha$ that is treated as subsonic in the linearized theory.

According to experimental data, both for subsonic and supersonic flow, the coefficient of the supplementary longitudinal force can be calculated with the aid of the relation

$$c_{x,s} = \xi\alpha^2 \tag{11.5.43}$$

in which ξ is a coefficient determined for a given shape of the nose (see [13]).

Particularly, for a conical nose with the fineness ratio λ_{mld}, we have

$$\xi \approx 0.08\left(\frac{\pm 2}{\lambda_{mld}}\sqrt{|M_\infty^2 - 1|} - 1\right) \tag{11.5.44}$$

where we take the plus sign for a supersonic velocity ($M_\infty > 1$) and the minus sign for a subsonic one ($M_\infty < 1$). Formula (11.5.43) is suitable for Mach number values of $0.8 \leqslant M_\infty \leqslant 2.8$. A glance at this formula reveals that a suction force or drag is absent for $M_\infty > 1$ if $\xi = 0$, i.e. provided that $\gamma = \sqrt{M_\infty^2 - 1}/\lambda_{mld} = 0.5$. A drag ($\xi > 0$) is always present at $M_\infty > 1$ and $\gamma > 0.5$.

A suction force ($\xi < 0$) is present at subsonic velocities or with supersonic flow ($M_\infty > 1$) if $\gamma < 0.5$. The generation of a suction force when $M_\infty > 1$ is due to the fact that a detached curved leading wave originates ahead of the conical nose, and the flow over the surface is subsonic.

11.6. Unsteady Flow over a Body of Revolution

General Relations

When moving along their trajectories, craft having the shape of bodies of revolution oscillate in various ways. In inverted motion, this is equivalent to the unsteady flow of the air stream over these bodies. The investigation of such a flow allows us to determine the aerodynamic derivatives used in appraising the flight stability of bodies of revolution.

The problem of determining the stability derivatives is solved, as for steady flow, by using the method of sources. The only difference here is that the slender body in a flow is replaced with a system of unsteady sources (sinks) and doublets.

Let us assume that a slender body of revolution in a linearized supersonic flow with the number M_∞ is subjected to an additional crossflow at the velocity $w(x, t)$ depending on the time t and coordinate x of an arbitrary section of the body (Fig. 11.6.1). Hence, this additional flow is unsteady. Following the method of sources, we can consider the velocity potential of such a flow as the potential produced by unsteady sources and doublets, whose power and moment change with time.

The velocity potential due to the unsteady sources (or sinks) and doublets along the axis of the slender body is determined by a linearized equation in cylindrical coordinates:

$$\alpha'^2\varphi_{xx} - \varphi_{rr} - \frac{1}{r^2}\varphi_{\gamma\gamma} - \frac{1}{r}\varphi_r + \frac{2M_\infty}{a_\infty}\varphi_{xt} + \frac{\varphi_{tt}}{a_\infty^2} = 0 \quad (11.6.1)$$

This equation can be obtained by transforming Eq. (3.8.29) with the use of the corresponding relations between cylindrical and Cartesian coordinates (2.4.9).

When solving Eq. (11.6.1), φ is found as the sum of two potentials: φ_1—the potential of axisymmetric flow that produces no disturbances leading to the origination of a normal force, and φ_2—the additional potential produced by violation of symmetry and causing a normal force. As for steady flow, the solution for the additional potential φ_2 can be written in the form of (11.4.2), i.e.

$$\varphi_2 = -\frac{\partial\varphi_1}{\partial r}\cos\gamma \quad (11.6.2)$$

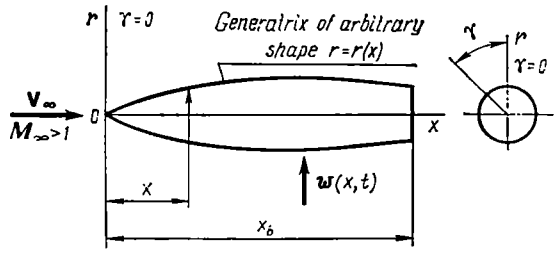

Fig. 11.6.1
Unsteady flow over a body of revolution with an additional crossflow (perpendicular to the axis of the body) at a velocity of w (x, t)

where φ_1 is the velocity potential of an axisymmetric unsteady flow determined by solving the equation

$$\alpha'^2\varphi_{xx} - \varphi_{rr} - \frac{1}{r}\varphi_r + \frac{2M_\infty}{a_\infty}\varphi_{xt} + \frac{\varphi_{tt}}{a_\infty^2} = 0 \qquad (11.6.3)$$

Let us find the solution of Eq. (11.6.3), i.e. the potential of an unsteady source (sink) in the form of the harmonic function

$$\varphi_1 = \eta\,(x,\ r)\ \exp\ \{ip\,[t - M_\infty x/(a_\infty \alpha'^2)]\} \qquad (11.6.4)$$

where p is the angular frequency of the body, and $\eta\ (x, r)$ is a variable depending on x and r. Consequently, Eq. (11.6.3) for the variable η acquires the form

$$\eta_{rr} + \frac{1}{r}\eta_r - \alpha'^2\eta_{xx} - p^2\eta/(a_\infty^2\alpha'^4) = 0 \qquad (11.6.5)$$

where the subscripts x, r, xx, and rr stand for the corresponding first and second partial derivatives of the function η.

Differential equation (11.6.5) can be solved by the operational method based on the Laplace transformation. This method as applied to the given case consists in that what is studied is not the function $\eta\ (x, r)$ itself, called the original one, but its modification, or Laplace transform.

The function $\eta\ (x, r)$ is transformed with respect to the variable x as follows. It is multiplied by $\exp\ (-sx)$, and then the following integral is calculated:

$$\bar{\eta}\,(s,\ r) = \int_0^\infty \exp\,(-sx)\,\eta\,(x,\ r)\,dx \qquad (11.6.6)$$

where $\bar{\eta}\ (s, r)$ is the Laplace transform of the original function $\eta\ (x, r)$, and s is a complex variable.

Laplace's transformation is described in greater detail in special literature. We shall give some results of the transformation of Eq. (11.6.5) and its solution based on the application of the Laplace transformation. Let us apply transformation (11.6.6) to Eq. (11.6.5), designating the operation in the general case by L. For example, the function $\bar{\eta}(s, r)$ in Eq. (11.6.6) will have the form of $L[\eta(x, r)]$, which signifies the transformation operation applied to the function $\eta(x, r)$ with respect to the variable x. We shall write the transformation operation L applied to Eq. (11.6.5), provided that α'^2 and $p^2/(a_\infty^2\alpha'^4)$ are constants for the given conditions of flow over a body of revolution, as follows:

$$L\left(\frac{\partial^2\eta}{\partial r^2}\right)+L\left(\frac{1}{r}\cdot\frac{\partial\eta}{\partial r}\right)-\alpha'^2L\left(\frac{\partial^2\eta}{\partial x^2}\right)-\frac{p^2}{a_\infty^2\alpha'^4}L(\eta)=0$$

Hence we can see that to perform a transformation, it is necessary to find the Laplace transform of the derivatives both with respect to the coordinate x (relative to which transformation (11.6.6) has been applied) and to the coordinate r.

When calculating the Laplace transforms of derivatives with respect to x, one must use the following basic theorem: the Laplace transform of a first derivative equals the product of s and the Laplace transform of the function minus the value of the original function at $x = 0$. Consequently, when applying the Laplace transformation, we replace the differentiation of the original function with an algebraic operation on the Laplace transform. To apply a transformation to a second derivative, we have to represent the latter as a derivative of the first one.

Consequently, the transformation L applied to the derivative $\partial^2\eta/\partial x^2$ acquires the form

$$L\left[\frac{\partial}{\partial x}\left(\frac{\partial\eta}{\partial x}\right)\right]=sL\left[\frac{\partial\eta}{\partial x}\right]-\frac{\partial\eta(0, r)}{\partial x}$$

$$=s\{L[\eta(x, r)]s-\eta(0, r)\}-\frac{\partial\eta(0, r)}{\partial x}$$

Since for the shape of the body of revolution being considered (sharp-nosed) $\eta(0, r) = \partial\eta(0, r)/\partial x = 0$, which indicates the absence of disturbances at the tip, then for the Laplace transform of the second derivative provided that $L[\eta(x, r)] = \bar{\eta}(s, r)$, we obtain

$$L[\partial^2\eta/\partial x^2] = s^2\bar{\eta}$$

When considering the application of the Laplace transformation to derivatives with respect to r, we should have the following in view. Since the transformation L is introduced with respect to the variable x, then the Laplace transform L to the derivative with

respect to the coordinate r equals the derivatives of the Laplace transform with respect to r. This follows from the fact that in the given case the coordinate r in transformation may be assumed to be a constant parameter, and according to the linearity of the transformation we obtain

$$L\left[\frac{\partial^2\eta}{\partial r^2}\right]=\frac{d^2}{dr^2}L[\eta(x,\ r)]=\frac{d^2\bar{\eta}}{dr^2}$$

$$L\left[\frac{1}{r}\ \frac{\partial\eta}{\partial r}\right]=\frac{1}{r}\ \frac{d}{dr}L[\eta(x,\ r)]=\frac{1}{r}\ \frac{d\bar{\eta}}{dr}$$

where, as previously, we have adopted the following notation for the Laplace transform:

$$L[\eta(x,\ r)]=\bar{\eta}(s,\ r)$$

With a view to the above operations of transformation, we obtain the following equation for the Laplace transform of a function:

$$\frac{d^2\bar{\eta}}{dr^2}+\frac{1}{r}\ \frac{d\bar{\eta}}{dr}-\alpha'^2\left(s^2+\frac{p^2}{a_\infty^2\alpha'^4}\right)\bar{\eta}=0 \qquad (11.6.7)$$

Examination of Eq. (11.6.7) reveals that after applying the Laplace transformation, the number of variables decreases by one, and we can go over from partial differential equation (11.6.5) to ordinary differential equation (11.6.7). This is the Bessel equation, and its solution is

$$\bar{\eta}=K_0\left\{\alpha' r\left(s^2+\frac{p^2}{a_\infty^2\alpha'^4}\right)^{1/2}\right\} \qquad (11.6.8)$$

where K_0 is **MacDonald's function.**

Having found the Laplace transform $\bar{\eta}$, we must find the original function η. To do this, we must use the Laplace inverse transformation. Using special literature describing how to find an original function according to its Laplace transform, we obtain a final expression for the required function η:

$$\eta(x,\ r)=(x^2-\alpha'^2r^2)^{-1/2}\cos\left[\left(\frac{p}{a_\infty\alpha'^2}\right)(x^2-\alpha'^2r^2)^{1/2}\right] \qquad (11.6.9)$$

On the basis of expressions (11.6.4) and (11.6.9), we obtain a relation for the potential of an unsteady point source:

$$\varphi_1=-\frac{\exp\left[ip\left(t-\frac{M_\infty x}{a_\infty\alpha'^2}\right)\right]\cos\left[\left(\frac{p}{a_\infty\alpha'^2}\right)(x^2-\alpha'^2r^2)^{1/2}\right]}{(x^2-\alpha'^2r^2)^{1/2}} \qquad (11.6.10)$$

If sources with a varying strength $f(\varepsilon)$ are arranged along the x-axis at points ε, Eq. (11.6.10) acquires the form

$$\varphi_1 = \exp(ipt)$$

$$\times \int_0^{x-\alpha' r} \frac{f(\varepsilon) \exp\left[-\frac{ipM_\infty}{a_\infty \alpha'^2}(x-\varepsilon)\right] \cos\left\{\frac{p}{a_\infty \alpha'^2}[(x-\varepsilon)^2-\alpha'^2 r^2]^{1/2}\right\} d\varepsilon}{[(x-\varepsilon)^2-\alpha'^2 r^2]^{1/2}} \tag{11.6.11}$$

where the minus sign in Eq. (11.6.10) is included in the function $f(\varepsilon)$.

The angular frequency p is a characteristic parameter in Eq. (11.6.11) indicating that the flow is unsteady. If $p = 0$, we have a flow from a steady source. In this case, the potential function (11.6.11) coincides with its value determined by expression (11.3.1). By applying relation (11.6.3), we can differentiate Eq. (11.6.11) with respect to r and find the additional potential of an unsteady doublet.

Prior to differentiation, let us transform Eq. (11.6.11) to the variable $z = \cosh^{-1}[(x-\varepsilon)/(\alpha' r)]$. Next differentiating with respect to r and again going over to the variable $\varepsilon = x - \alpha' r \cosh z$, we find the following expression for the potential of continuously distributed unsteady doublets:

$$\varphi_2 = \exp(ipt)\cos\gamma \left\{\frac{p}{r a_\infty \alpha'^2} \int_0^{x-\alpha' r} f(\varepsilon) \exp\left[-\frac{ipM_\infty}{a_\infty \alpha'^2}(x-\varepsilon)\right] \times \sin\left\{\frac{p}{a_\infty \alpha'^2}[(x-\varepsilon)^2-\alpha'^2]^{1/2}\right\} d\varepsilon \right.$$

$$+ \int_0^{x-\alpha' r} \frac{\dot{f}(\varepsilon)(x-\varepsilon) \exp\left[-\frac{ipM_\infty}{a_\infty \alpha'^2}(x-\varepsilon)\right] \cos\left\{\frac{p}{a_\infty \alpha'^2}[(x-\varepsilon)^2-\alpha'^2 r^2]^{1/2}\right\} d\varepsilon}{r[(x-\varepsilon)^2-\alpha'^2 r^2]^{1/2}}$$

$$+ \frac{ipM_\infty}{a_\infty \alpha'^2}$$

$$\left. \times \int_0^{x-\alpha' r} \frac{f(\varepsilon)(x-\varepsilon) \exp\left[-\frac{ipM_\infty}{a_\infty \alpha'^2}(x-\varepsilon)\right] \cos\left\{\frac{p}{a_\infty \alpha'^2}[(x-\varepsilon)^2-\alpha'^2 r^2]^{1/2}\right\} d\varepsilon}{[(x-\varepsilon)^2-\alpha'^2 r^2]^{1/2}} \right\} \tag{11.6.12}$$

If we assume in this expression that $p = 0$ and introduce the notation $\dot{f}(\varepsilon) = m(\varepsilon)$, we obtain relation (11.4.4') for the potential of a steady doublet (by going over in this expression from the variable z to the variable $\varepsilon = x - \alpha' r \cosh z$).

Boundary Conditions

In each specific case of unsteady flow, the boundary conditions needed to determine the function $f(\varepsilon)$ in (11.6.12) are the conditions of flow without separation, according to which the velocity components normal to the surface must equal zero. This signifies that the disturbed potential due to an unsteady doublet must be such that on the surface of the body (or on the x-axis if the thickness of the body is very small) the normal velocity component of the undisturbed flow will vanish, i.e. a condition similar to (11.2.22) will be fulfilled:

$$\partial\varphi_2/\partial r = -w\,(x,\ t)\ \cos\gamma \qquad (11.6.13)$$

This condition takes on various forms for each case of motion determining the corresponding solution of Eq. (11.6.13).

Let us consider two possible cases of motion:

1. *Harmonic oscillations of a body about a lateral axis passing through its centre of mass* (Fig. 11.6.2*a*). In this case, the motion is determined by the equation

$$\alpha = \alpha_0\ \exp\,(ipt) \qquad (11.6.14)$$

where α_0 is the initial angle of attack corresponding to the instant $t = 0$ (the amplitude of oscillation).

From Eq. (11.6.14), we determine the normal component of the velocity of the undisturbed flow:

$$w\,(x,\ t) = V_\infty\alpha_0 \exp\,(ipt) + \frac{d\alpha}{dt}\,(x - x_{CM})$$

$$= [V_\infty + ip\,(x - x_{CM})]\,\alpha_0 \exp\,(ipt) \qquad (11.6.15)$$

Boundary condition (11.6.13) accordingly becomes

$$\frac{\partial\varphi_2}{\partial r} = -[V_\infty + ip\,(x - x_{CM})]\,\alpha_0 \exp\,(ipt)\cos\gamma \qquad (11.6.16)$$

2. *Steady rotation of a body about a lateral axis passing through its centre of mass* (Fig. 11.6.2*b*). The velocity component at a point on the surface of the body at a constant angle of attack α_0 is

$$w\,(x) = \alpha_0 V_\infty + \Omega_z\,(x - x_{CM}) \qquad (11.6.17)$$

where Ω_z is the angular velocity.

Hence, we can write boundary condition (11.6.13) in the form

$$\partial\varphi_2/\partial r = -[\alpha_0 V_\infty + \Omega_z\,(x - x_{CM})]\cos\gamma \qquad (11.6.18)$$

The above boundary conditions are used to determine the function $f(\varepsilon)$ in each case of motion of a body of revolution. If we consider a very slender body, we shall find the form of this function as follows. We shall first transform expression (11.6.12) to the integration variable $z = \cosh^{-1}\,[(x - \varepsilon)/(\alpha' r)]$ and calculate the partial deriva-

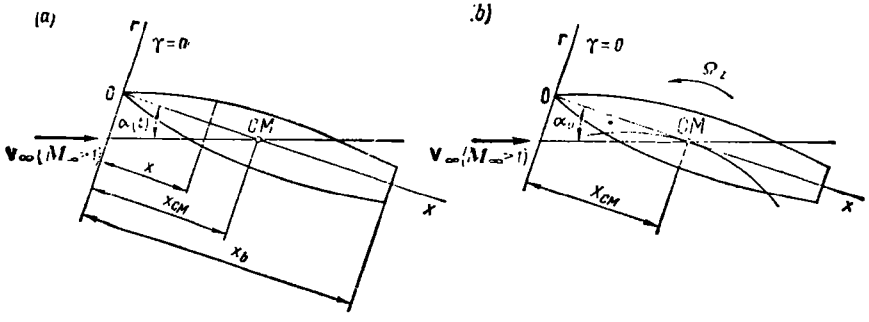

Fig. 11.6.2
Particular cases of body motion:
a–harmonic oscillations about a lateral axis passing through the centre of mass of the body; *b*–steady rotation about a lateral axis passing through the centre of mass

tive φ_{2r}. Next, having again transformed the expression obtained for the derivative φ_{2r} to the variable $\varepsilon = x - \alpha' r \cosh z$, we go over to the limit at $r \to 0$. We combine the above boundary conditions (11.6.16) and (11.6.18) with the found limit relation. Now the limiting value of the partial derivative φ_{2r} at $r \to 0$, which is treated in the aerodynamics of a slender body for unsteady flow, acquires the form

$$\frac{\partial \varphi_2}{\partial r} = -\frac{\pi f(x)}{S(x)} \exp(ipt) \cos\gamma \qquad (11.6.19)$$

where $S(x) = \pi r^2$ is the area of the cross section at a distance x from the tip.

Calculation of the function $f(\varepsilon)$ with the aid of the above boundary conditions allows us to determine the velocity potential φ_2 by (11.6.12) and then find the additional pressure coefficient using (9.6.20):

$$\bar{p}_2 = -2(\varphi_{2x}/V_\infty + \varphi_{2t}/V_\infty^2) \qquad (11.6.20)$$

For the normal force coefficient, having in view that by (11.4.21) the pressure coefficient $\bar{p}_2 = -(2/V_\infty)\varphi_{2x}$ is proportional to $\cos\gamma$, we obtain the expression

$$c_y = -\frac{\pi}{S_{\text{mid}}} \int_0^{x_b} \frac{\bar{p}_2}{\cos\gamma} r\, dx \qquad (11.6.21)$$

Let us consider the relation determining the coefficient of the moment about an axis passing through the centre of mass of a body

of revolution. For this purpose, we shall write formula (11.5.9) as follows:

$$m_z = -\frac{2}{S_{\text{mid}} x_b} \int_0^{x_b} \int_0^{\pi} \bar{p}_2 (x_{CM} - x) \cos\gamma \, d\gamma \, dr$$

whence, taking into account that the coefficient $\bar{p}_2$ is proportional to $\cos\gamma$, we have

$$m_z = c_y \frac{x_{CM}}{x_b} + \frac{\pi}{S_{\text{mid}} x_b} \int_0^{x_b} \frac{\bar{p}_2}{\cos\gamma} r x \, dx \qquad (11.6.22)$$

Aerodynamic Characteristics in Conditions of Low-Frequency Oscillations

The solution of the problem of determining the non-stationary aerodynamic characteristics is simplified if a body of revolution performs oscillations at a low frequency, which is typical of real flight conditions. If we develop (11.6.10) as a series in powers of a parameter $p^* = M_\infty pr/(\alpha' V_\infty)$ equal to the Strouhal number, we can see that for frequencies of the order of $p = a_\infty \alpha'/x_b$ the potential of an unsteady flow is expressed to a sufficient accuracy in the form of a linear dependence on p^*. Going over in the expansion obtained to the variable $z = \cosh^{-1}[(x - \varepsilon)/(\alpha' r)]$, we have

$$\varphi_2 = \cos\gamma \exp(ipt) \left[\int_0^{\cosh^{-1} u} \dot{f}(x - \alpha' r \cosh z) \cosh z \, dz \right.$$
$$\left. - iM_\infty \alpha' p^* \int_0^{\cosh^{-1} u} \dot{f}(x - \alpha' r \cosh z) \, dz \right] \qquad (11.6.23)$$

If we assume in this expression that $p^* = 0$ and designate $\dot{f}(x - \alpha' r \cosh z)$ by $m(x - \alpha' r \cosh z)$, we obtain formula (11.4.4') for the velocity potential of an unsteady flow.

Let us now calculate the derivatives with respect to x and t needed to determine the pressure coefficient.

Assuming as previously that $f = m$, we obtain

$$\varphi_{2x} = \alpha' \cos\gamma \exp(ipt) \left[\int_0^{\cosh^{-1} u} \dot{m}(x - \alpha' r \cosh z) \cosh z \, dz \right.$$
$$\left. - iM_\infty p^* \int_0^{\cosh^{-1} u} \dot{m}(x - \alpha' r \cosh z) \, dz \right] \qquad (11.6.24)$$

$$\varphi_{2t} = \alpha' ip \cos\gamma \exp(ipt)\left[\int_0^{\cosh^{-1} u} m(x-\alpha' r\cosh z)\cosh z\, dz\right.$$

$$\left. - iM_\infty p^* \int_0^{\cosh^{-1} u} m(x-\alpha' r\cosh z)\, dz\right] \qquad (11.6.25)$$

We determine the form of the functions m and $\dot{m}$ with the aid of the boundary conditions, and also from formula (11.6.20). Let us consider these functions, and also the values of the aerodynamic characteristics corresponding to them for particular cases of motion.

1. *Harmonic oscillation of a body about a lateral axis passing through its centre of mass.* In this case, we determine the form of the function $f(\varepsilon)$ from (11.6.16) and (11.6.19) as follows:

$$f(\varepsilon) = \frac{S(\varepsilon)\alpha_0}{\pi}[V_\infty + ip(\varepsilon - x_{CM})] \qquad (11.6.26)$$

Upon calculating the first and second derivatives, we find, respectively:

$$m(\varepsilon) = \frac{S'(\varepsilon)\alpha_0}{\pi}[V_\infty + ip(\varepsilon - x_{CM})] + \frac{S(\varepsilon)}{\pi} ip\alpha_0 \qquad (11.6.27)$$

$$\dot{m}(\varepsilon) = \frac{S''(\varepsilon)\alpha_0}{\pi}[V_\infty + ip(\varepsilon - x_{CM})] + \frac{2S'(\varepsilon)}{\pi} ip\alpha_0 \qquad (11.6.28)$$

where $S'(\varepsilon) = dS/d\varepsilon$ and $S''(\varepsilon) = d^2S/d\varepsilon^2$ are the first and second derivatives of the cross-sectional area S with respect to the coordinate ε.

Let us introduce expressions (11.6.27) and (11.6.28) into Eqs. (11.6.24) and (11.6.25), after first going over in these equations to the variable $z = \cosh^{-1}[(x-\varepsilon)/(\alpha' r)]$. By calculating the integrals obtained and using formula (11.6.20), we find

$$\bar{p}_2 = -\frac{2\alpha'\cos\gamma}{\pi}\left[\Omega_3\left(\alpha_0 - \frac{\dot{\alpha} x_{CM}}{V_\infty}\right)\right.$$

$$\left. + \frac{\dot{\alpha} x_b}{V_\infty}(\Omega_4 - 3\Omega_1) - \frac{\dot{\alpha} M_\infty^2 r}{V_\infty \alpha'}\Omega_2\right] \qquad (11.6.29)$$

where

$$\dot{\alpha} = d\alpha/dt$$

$$\Omega_1 = \frac{1}{x_b}\int_0^{\cosh^{-1} u} S'(x-\alpha' r\cosh z)\cosh z\, dz \qquad (11.6.30)$$

$$\Omega_2 = \int_0^{\cosh^{-1} u} S''(x-\alpha' r\cosh z)\, dz \qquad (11.6.31)$$

$$\Omega_3 = \int_0^{\cosh^{-1} u} S''(x-\alpha' r\cosh z)\cosh z\,dz \qquad (11.6.32)$$

$$\Omega_4 = \frac{1}{x_b}\int_0^{\cosh^{-1} u} [S''(x-\alpha' r\cosh z)](x-\alpha' r\cosh z)\cosh z\,dz \qquad (11.6.33)$$

To obtain a relation for the normal force coefficient, let us introduce expression (11.6.29) into (11.6.21):

$$c_y = \frac{2\alpha'}{S_{mid}}\int_0^{x_b}\left[\Omega_3\left(\alpha_0 - \frac{\dot{\alpha}x_{CM}}{V_\infty}\right) + \frac{\dot{\alpha}x_b}{V_\infty}(\Omega_4 + 3\Omega_1) - \frac{\dot{\alpha}M_\infty^2 r}{V_\infty\alpha'}\Omega_2\right] r\,dx \qquad (11.6.34)$$

We find the pitching moment coefficient in a similar way from expression (11.6.22) by substituting for the coefficient $\bar{p}_2$ its value from (11.6.29):

$$m_z = c_y\frac{x_{CM}}{x_b} - \frac{2\alpha'}{S_{mid}x_b}\int_0^{x_b}\left[\Omega_2\left(\alpha_0 - \frac{\dot{\alpha}x_{CM}}{V_\infty}\right) + \frac{\dot{\alpha}x_b}{V_\infty}(\Omega_4 + 3\Omega_1) - \frac{\dot{\alpha}M_\infty^2 r}{V_\infty\alpha'}\Omega_2\right] rx\,dx \qquad (11.6.35)$$

We can obtain the coefficients c_y and m_z for very slender bodies from the above expressions if we replace the functions Ω_n with their corresponding values from the aerodynamics of slender bodies. To obtain these values, in expressions (11.6.30)-(11.6.33) we must go over to the variable $\varepsilon = x - \alpha' r\cosh z$ and after this perform a limiting process at $r \to 0$. Introducing the found values of the functions Ω_n into expressions (11.6.34) and (11.6.35), we obtain

$$c_y = 2\alpha_0\bar{S}_{bot} + 2\bar{S}_{bot}\dot{\bar{\alpha}}[1 - x_{CM}/x_b + W_b/(x_b S_{bot})] \qquad (11.6.36)$$

$$m_z = 2\alpha_0\bar{S}_{bot}[x_{CM}/x_b + W_b/(x_b S_{bot}) - 1] - 2\bar{S}_{bot}\dot{\bar{\alpha}}(1 - x_{CM}/x_b)^2 \qquad (11.6.37)$$

where $\bar{S}_{bot} = S_{bot}/S_{mid}$; $\dot{\bar{\alpha}} = (d\alpha/dt)x_b/V_\infty$; and W_b is the volume of the body of revolution.

Let us introduce the following notation for the stability derivatives:

$$c_y^\alpha = \frac{\partial c_y}{\partial\alpha},\quad c_y^{\dot{\bar{\alpha}}} = \frac{V_\infty}{x_b}\frac{\partial c_y}{\partial\dot{\alpha}},\quad m_z^\alpha = \frac{\partial m_z}{\partial\alpha},\quad m_z^{\dot{\bar{\alpha}}} = \frac{V_\infty}{x_b}\frac{\partial m_z}{\partial\dot{\alpha}} \qquad (11.6.38)$$

From formulas (11.6.36) and (11.6.37), we obtain

$$c_y^{\alpha} = \frac{2\alpha'}{S_{\text{mid}}} \int_0^{x_b} \Omega_3 r \, dx \tag{11.6.39}$$

$$\dot{c}_y^{\alpha} = \frac{2\alpha'}{S_{\text{mid}}} \int_0^{x_b} \left(-\Omega_3 \bar{x}_{\text{CM}} + \Omega_4 + 3\Omega_1 - \frac{M_\infty^2 r}{\alpha' x_{\text{CM}}} \Omega_2 \right) r \, dx \tag{11.6.40}$$

$$m_z^{\alpha} = c_y^{\alpha} \bar{x}_{\text{CM}} - \frac{2\alpha'}{S_{\text{mid}} x_b} \int_0^{x_b} \Omega_2 r x \, dx \tag{11.6.41}$$

$$\dot{m}_z^{\alpha} = \dot{c}_y^{\alpha} \bar{x}_{\text{CM}} - \frac{2\alpha'}{S_{\text{mid}} x_b} \times \int_0^{x_b} \left[-\Omega_3 \bar{x}_{\text{CM}} + \Omega_4 + 3\Omega_1 - \frac{M_\infty^2 r}{\alpha' x_b} \Omega_2 \right] r x \, dx \tag{11.6.42}$$

In these relations, $\bar{x}_{\text{CM}} = x_{\text{CM}}/x_b$ is the dimensionless coordinate of the centre of mass.

The corresponding expressions obtained in the aerodynamic theory of a slender body have the following form:

$$c_y^{\alpha} = 2\bar{S}_{\text{bot}} \tag{11.6.43}$$

$$\dot{c}_y^{\alpha} = 2\bar{S}_{\text{bot}} [1 - \bar{x}_{\text{CM}} + W_b/(x_b S_{\text{bot}})] \tag{11.6.44}$$

$$m_z^{\alpha} = 2\bar{S}_{\text{bot}} [\bar{x}_{\text{CM}} + W_b/(x_b S_{\text{bot}}) - 1] \tag{11.6.45}$$

$$\dot{m}_z^{\alpha} = -2\bar{S}_{\text{bot}} (1 - \bar{x}_{\text{CM}})^2 \tag{11.6.46}$$

2. *Steady rotation of a body about a lateral axis passing through its centre of mass.* In this particular case of motion, the law of distribution of the function $f(\varepsilon)$ determined from expressions (11.6.18) and (11.6.19) has the form

$$f(\varepsilon) = \frac{S(\varepsilon)}{\pi} [\alpha_0 V_\infty + \Omega_z (\varepsilon - x_{\text{CM}})]$$

Double differentiation of this function yields

$$\ddot{f}(\varepsilon) = \dot{m}(\varepsilon) = \frac{S''(\varepsilon)}{\pi} [\alpha_0 V_\infty + \Omega_z (\varepsilon - x_{\text{CM}})] + \frac{2S'(\varepsilon)}{\pi} \Omega_z \tag{11.6.47}$$

Now let us determine the coefficient $\bar{p}_2$ from (11.6.20). To do this, we first obtain from expression (11.6.17), after going over to the variable $z = \cosh^{-1}[(x - \varepsilon)/\alpha' r]$, a relation determining the derivative $\dot{m}(x - \alpha' r \cosh z)$. Next we introduce this derivative into for-

mula (11.6.24), which for steady flow acquires the form

$$\varphi_{2x} = \alpha' \cos\gamma \int_0^{\cosh^{-1} u} \dot{m}\,(x - \alpha' r \cosh z) \cosh z\, dz$$

To determine the coefficient $\bar{p}_2$, we introduce this quantity into formula (11.6.20), in which the function φ_{2t} should be taken equal to zero when $\Omega_z = \text{const}$. As a result of simple transformations, we have the following expression for the pressure coefficient:

$$\bar{p}_2 = -\frac{2\alpha' \cos\gamma}{\pi} (\alpha_0\Omega_3 + \omega_z\Omega_4 - \omega_z\bar{x}_{CM}\Omega_3 + 2\omega_z\Omega_1) \qquad (11.6.48)$$

where the dimensionless kinematic parameter $\omega_z = \Omega_z x_b / V_\infty$.

After introducing the obtained expression for $\bar{p}_2$ into (11.6.21) and (11.6.22), we find

$$c_y = \frac{2\alpha'}{S_{mid}} \int_0^{x_b} (\alpha_0\Omega_3 + \omega_z\Omega_4 - \omega_z\bar{x}_{CM}\Omega_3 + 2\omega_z\Omega_1)\, r\, dx \qquad (11.6.49)$$

$$m_z = c_y\bar{x}_{CM} - \frac{2\alpha'}{S_{mid}x_b} \int_0^{x_b} (\alpha_0\Omega_3 + \omega_z\Omega_4 - \omega_z\bar{x}_{CM}\Omega_3 + 2\omega_z\Omega_1)\, rx\, dx \qquad (11.6.50)$$

The static stability derivatives c_y^α and m_z^α are evidently the same as in (11.6.39) and (11.6.41). We determine the derivatives with respect to the angular velocity in the form

$$c_y^{\omega_z} = \frac{V_\infty}{x_b}\frac{\partial c_y}{\partial\Omega_z}; \quad m_z^{\omega_z} = \frac{V_\infty}{x_b}\frac{\partial m_z}{\partial\Omega_z} \qquad (11.6.51)$$

Differentiating (11.6.49) and (11.6.50) with respect to ω_z, we find:

$$c_y^{\omega_z} = \frac{2\alpha'}{S_{mid}} \int_0^{x_b} (\Omega_4 - \bar{x}_{CM}\Omega_3 + 2\Omega_1)\, r\, dx \qquad (11.6.52)$$

$$m_z^{\omega_z} = c_y^{\omega_z}\bar{x}_{CM} = \frac{2\alpha'}{S_{mid}x_b} \int_0^{x_b} (\Omega_4 - \bar{x}_{CM}\Omega_3 + 2\Omega_1)\, rx\, dx \qquad (11.6.53)$$

The formulas from the aerodynamic theory of a slender body corresponding to expressions (11.6.52) and (11.6.53) are as follows:

$$c_y^{\omega_z} = 2\bar{S}_{bot}(1 - \bar{x}_{CM}) \qquad (11.6.54)$$

$$m_z^{\omega_z} = -2\bar{S}_{bot}\left[(1 - \bar{x}_{CM})^2 + \frac{\bar{x}_{CM}W_b}{S_{bot}x_b} - \frac{\int_0^{x_b} S(x)\, x\, dx}{x_b^2 S_{bot}}\right] \qquad (11.6.55)$$

A body when moving along a trajectory is in complicated motion consisting of translational motion at a constant angle of attack, longitudinal harmonic oscillations, and rotation at a constant angular velocity Ω_z. The aerodynamic coefficients for such motion are determined by intricate relations that include static and dynamic stability derivatives. For the motion of a body of revolution being considered, its normal force and longitudinal moment coefficients are written as a sum:

$$\left.\begin{aligned} c_y &= c_y^{\alpha}\alpha_0 + c_y^{\dot{\alpha}}\dot{\alpha} + c_y^{\omega_z}\omega_z \\ m_z &= m_z^{\alpha}\alpha_0 + m_z^{\dot{\alpha}}\dot{\alpha} + m_z^{\omega_z}\omega_z \end{aligned}\right\} \qquad (11.6.56)$$

Inspection of the above relations reveals that they allow us to estimate only the dotted derivatives $c_y^{\dot{\alpha}}$ and $m_z^{\dot{\alpha}}$. Theoretical investigations have resulted in the finding of approximate methods for determining other similar derivatives. Particularly, it is established in the aerodynamics of slender bodies that the derivative $c_y^{\dot{\omega}_z}$ calculated with account taken of rotation relative to the centre of mass is zero, while the derivative

$$m_z^{\dot{\omega}_z} = -2J/(x_b^3 S_{bot}) \qquad (11.6.55')$$

where J is the moment of inertia of the body about the lateral axis Oz.

Analysis of the Change in the Aerodynamic Coefficients

The aerodynamic properties of bodies of revolution in unsteady flow can be treated using the example of calculating the stability derivatives of slender bodies with a parabolic generatrix. For this purpose, we shall determine the function Ω_n by formulas (11.6.30)-(11.6.33) using the equation of a parabola

$$r = \frac{x}{2\lambda_{mid}}\left(2 - \frac{x}{x_{mid}}\right) \qquad (11.6.57)$$

and the expression for the cross-sectional area

$$S(\varepsilon) = \frac{\pi}{4\lambda_{mid}^2}\left(4\varepsilon^2 - \frac{4\varepsilon^3}{x_{mid}} + \frac{\varepsilon^4}{x_{mid}^2}\right) \qquad (11.6.58)$$

After calculating the first and second derivatives of $S(\varepsilon)$ with respect to ε, we introduce them into formulas (11.6.30)-(11.6.33), replacing ε with the expression $x - \alpha' r \cosh z$. Integration and trans-

formation of the obtained expressions yield:

$$\left.\begin{aligned}
\Omega_1 &= \frac{\pi}{\lambda_{\text{mid}}^2 \bar{x}_\text{b}}\left(\frac{2\bar{x}}{u} i_r^1 - \frac{3\bar{x}^2}{u^2} i_r^2 + \frac{\bar{x}^3}{u^3} i_r^3\right)\\
\Omega_2 &= \frac{\pi}{\lambda_{\text{mid}}^2}\left(2i_x^0 - \frac{6\bar{x}}{u} i_x^1 + \frac{3\bar{x}^2}{u^2} i_x^2\right)\\
\Omega_3 &= \frac{\pi}{\lambda_{\text{mid}}^2}\left(2i_r^0 - \frac{6\bar{x}}{u} i_r' + \frac{3\bar{x}^2}{u^2} i_r^2\right)\\
\Omega_4 &= \frac{\pi}{\lambda_{\text{mid}}^2 \bar{x}_\text{b}}\left(\frac{2\bar{x}}{u} i_r^1 - \frac{6\bar{x}^2}{u^2} i_r^2 + \frac{3\bar{x}^3}{u^3} i_r^3\right)
\end{aligned}\right\} \qquad (11.6.59)$$

In formulas (11.6.59), $\lambda_{\text{mid}} = x_{\text{mid}}/(2r_{\text{mid}})$ is the fineness ratio of the nose of the parabolic body, $\bar{x} = x/x_{\text{mid}}$ is the dimensionless coordinate of the section, and $\bar{x}_\text{b} = x_\text{b}/x_{\text{mid}}$ is the relative length of the body. The functions i_r^n and i_x^n are given by formulas (11.4.13) and (11.3.19) depending on the parameter $u = x/(\alpha' r)$ (their values are also given in Table 11.3.1, see p. 88).

Formulas (11.6.59) and Table 11.3.1 allow us to comparatively simply calculate the distribution of the coefficient $\bar{p}_2$ by using relations (11.6.29) or (11.6.48). The found values of $\bar{p}_2$ allow us to calculate the coefficients of the normal force, pitching moment, and their derivatives from relations (11.6.34), (11.6.35), (11.6.49), and (11.6.50).

To determine these coefficients and stability derivatives by the aerodynamic theory of a slender body, we must find the volume of a body with a parabolic generatrix:

$$W_\text{b} = \frac{\pi x_\text{b}}{4\lambda_{\text{mid}}^2}\left[\frac{4}{3} - \frac{x_\text{b}}{x_{\text{mid}}}\left(1 - \frac{x_\text{b}}{5x_{\text{mid}}}\right)\right] \qquad (11.6.60)$$

We shall cite as an illustration the stability derivatives for a slender body with a total fineness ratio of $\lambda_\text{b} = x_\text{b}/(2r_{\text{mid}}) = 8$ and a bottom taper ratio of $S_{\text{bot}} = S_{\text{bot}}/S_{\text{mid}} = 0.41$; the length of the body is $x_\text{b} = 8$ m, and the coordinate of the centre of mass measured from the nose is $x_{\text{CM}} = 5$ m.

The results obtained are presented as graphs in Figs. 11.6.3-11.6.5, which show how the stability derivatives change depending on the number M_∞. An increase in M_∞ is attended by a growth in the absolute value of the derivative $m_z^{\dot{\alpha}}$ and a decrease in the derivative $m_z^{\omega_z}$.

Hence, the nature of damping with an increase in the velocity varies. It grows with harmonic oscillations and lowers with rotation at the angular velocity Ω_z. The derivative m_z^α characterizing longitudinal static stability grows with increasing M_∞. Here the coefficient c_y^α appreciably increases. It thereby follows that the static

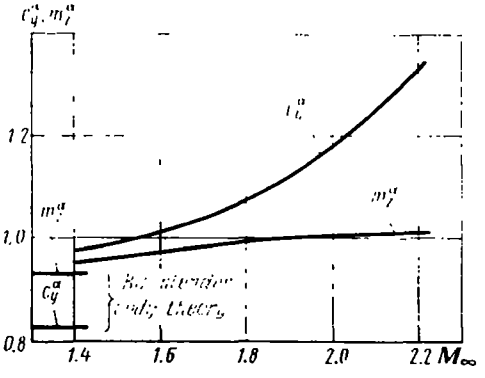

Fig. 11.6.3
Change in the static stability derivatives of a body of revolution depending on the number M_∞

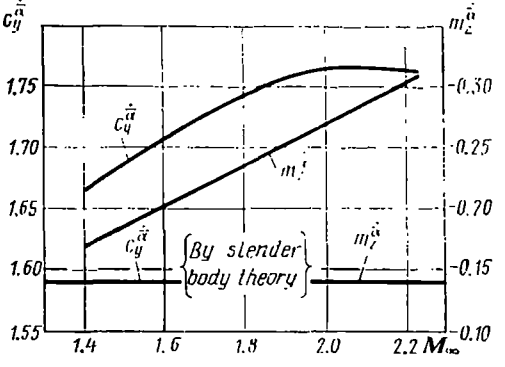

Fig. 11.6.4
Dynamic stability derivatives of a body of revolution moving harmonically versus the number M_∞

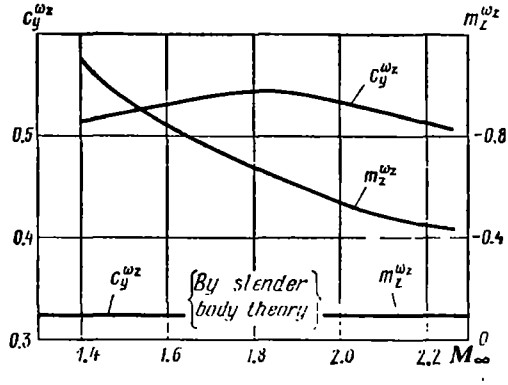

Fig. 11.6.5
Influence of the number M_∞ on the dynamic stability derivatives for a body of revolution rotating about a lateral axis

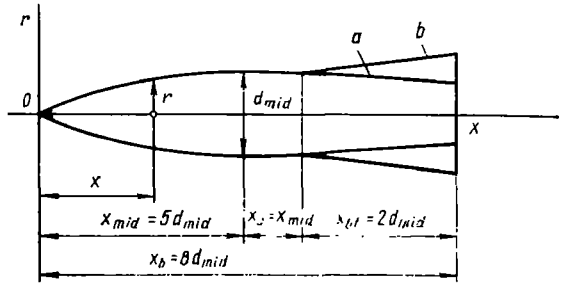

Fig. 11.6.6
Shape of bodies of revolution with a boattail (*a*) and with a flaring afterbody (*b*)

stability becomes greater because the centre of pressure (determined by the centre-of-pressure coefficient $c_p = m_z^\alpha / c_y^\alpha$) is closer to the centre of mass.

The origination of a damping moment upon harmonic oscillations or rotation causes additional displacement of the centre of pressure toward the centre of mass, the oscillations producing a larger displacement than the rotation. This is favourable from the viewpoint of the static stability of a body. But owing to the reduction of damping and the increase in the longitudinal moment, the parameters of dynamic stability upon oscillations are inferior to those upon rotation. This leads to greater "swing" of the body and slower attenuation of the oscillations.

The actual damping of a body is more considerable than according to the aerodynamic theory of a slender body; the normal forces are also larger. This indicates that the stability derivatives found by the aerodynamic theory of a slender body may be used only for an estimate of the order of their magnitude.

In analysing the results of determining the aerodynamic characteristics for bodies of revolution of various shapes, we can conclude that the taper ratio $\bar{S}_{bot}$ substantially affects the stability derivatives. To see that this is true, let us compare the values of the corresponding stability derivatives for two bodies whose shapes and dimensions are shown in Fig. 11.6.6. Body *a* has over its entire length a parabolic generatrix given by the equation $\tilde{r} = 0.2\tilde{x}\,(1 - 0.1\tilde{x})$ (where $\tilde{x} = x/d_{mid}$ and $\tilde{r} = r/d_{mid}$); body *b* has a parabolic nose with the same generatrix equation, a short cylindrical part with the relative length $\lambda_c = x_c/d_{mid} = 1$, and a flaring afterbody (boattail) with a length of $\lambda_{bt} = x_{bt}/d_{mid} = 2$. The fineness ratio of the nose part of both bodies is $\lambda_{mid} = x_{mid}/d_{mid} = 5$, and the total fineness ratio is $\lambda_b = x_b/d_{mid} = 8$. The bottom taper ratio of body *a*

is $\overline{S}_{bot} = S_{bot}/S_{mid} = 0.41$, and of body b, 1.82. The values of their stability derivatives calculated by formulas from the aerodynamic theory of slender bodies are given in Table 11.6.1.

Table 11.6.1

Body	Aerodynamic parameters					
	c_y^{α}	m_z^{α}	$c_y^{\dot{\alpha}}$	$m_z^{\dot{\alpha}}$	$c_y^{\omega_z}$	$m_z^{\omega_z}$
a	0.82	0.93	1.58	—0.13	0.33	—0.13
b	3.63	0.15	3.08	—0.59	1.47	—0.48

A glance at Table 11.6.1 reveals that body b with a flaring afterbody has a better static stability because its centre of pressure is closer to its centre of mass. Both bodies experience damping upon harmonic oscillations and rotation, the damping of body b being larger than that of body a.

The above data indicate the possibility of altering the aerodynamic characteristics of a body by selecting the appropriate shape of its afterbody.

12

Aerodynamic Interference

12.1. Nature of Aerodynamic Interference

Wing-Body Interference

A body of revolution, which is usually employed as a design element of a craft, may have wings, empennage (a fin assembly), and controls. An aircraft, for example, is a combination of design elements such as a fuselage, which is either a body of revolution or close to one, wings, a tail unit, rudders, and elevators. An unguided rocket consists of a body (of revolution) and a fin assembly (stabilizers). A guided rocket is close in its design to an aircraft because it has lifting surfaces, a tail unit, and controls.

When considering the aerodynamics of craft as combinations of bodies of revolution, wings, empennage, and controls, we have to do with the *problem of taking into account the aerodynamic interference*, i.e. interaction between individual elements of these combinations; this problem is quite involved and meanwhile has not been solved adequately. As a result of such interference, the sum of the aerodynamic forces and moments of a wing and a body (fuselage); a tail unit and a body; a body, wing, and tail unit; or a body, wing, tail unit, and controls taken separately (isolated) does not equal the total force or moment of a combination consisting of the corresponding elements and forming a single entity (Fig. 12.1.1). Hence, individual elements such as a body, wings, empennage, controls, when combined into a single design of a craft, lose their individual aerodynamic characteristics, as it were, and acquire new ones because of interference.

Calculations and experimental investigations show that for the same angle of attack, the normal and consequently the lift force of a wing in the presence of a body increase in comparison with an isolated wing. The same phenomenon is observed for the lift of a body attached to a wing in comparison with an isolated one.

Let us consider the physical essence of the mutual influence of a body of revolution and a wing causing their lift (normal) force to grow. We shall assume that the wing is on the cylindrical part of the

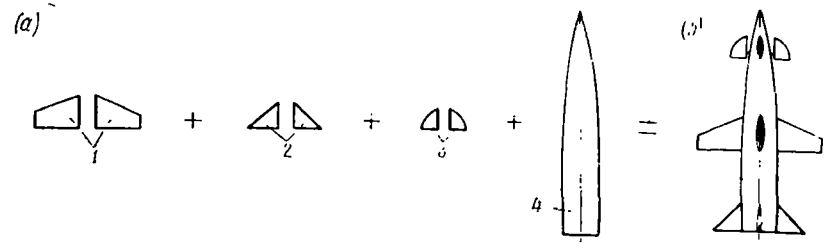

Fig. 12.1.1
Illustration of the concept of interaction (interference) of a body of revolution and a wing, empennage, and controls installed on it:
a–separate elements; *b*–elements joined into a single entity (combination) of a craft: *1*–wings; *2*–empennage; *3*–controls; *4*–body of revolution; *5*–craft

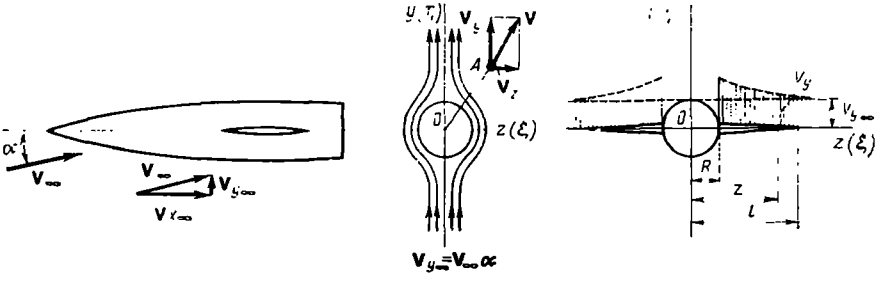

Fig. 12.1.2
Change in the normal velocity component along the span of a wing due to the influence of a body of revolution

body remote from the nose as in a midwing monoplane. Let us also assume that the body and wing are slender and the flow is at a small angle of attack (Fig. 12.1.2).

It was shown in Sec. 11.2 that a disturbed flow near a slender body of revolution may be obtained by superposition of the velocity field produced by the longitudinal axisymmetric undisturbed flow over the body at a velocity of $V_{x\infty} = V_\infty \cos\alpha \approx V_\infty$ and the velocity field of the additional disturbed flow produced in crossflow over this body at the velocity $V_{y\infty} = V_\infty \sin\alpha \approx V_\infty\alpha$.

At low angles of attack, the crossflow is usually subsonic, and for approximate calculations of the velocity field, we can take advantage of the theory of the potential incompressible flow over a circular cylinder. The complex potential of such a flow is determined by expression (6.2.4). Assuming that $V = \alpha V_\infty$, substituting σ for ζ, and calculating the derivative $dW/d\sigma$, we can write the expression for the complex velocity as

$$dW/d\sigma = V_z - V_y i = -\alpha V_\infty i\,(1 + R^2/\sigma^2) \qquad (12.1.1)$$

where $\sigma = z + iy$.

On the line $z - z$ ($y = 0$), we have

$$V_z - V_y i = -\alpha V_\infty i\,(1 + R^2/z^2) \qquad (12.1.2)$$

whence it follows that $V_\infty = 0$ and

$$V_y = \alpha V_\infty\,(1 + R^2/z^2) \qquad (12.1.3)$$

By this formula in the plane $y = 0$, the velocity V_y of the cross-flow changes from $V_y = 2\alpha V_\infty$ on the surface of the cylinder ($z = R$) to $V_y = V_{y\infty} = \alpha V_\infty$ remote from it at $z \to \infty$ (Fig. 12.1.2). If a wing is mounted on the cylindrical body, then at a given angle of attack α it is in a composite flow that can be obtained by superposition of the additional flow induced by the body onto the undisturbed flow. Owing to this influence of the body, the lateral component of the velocity on the surface of a wing is

$$\alpha V_\infty + \alpha V_\infty R^2/z^2$$

i.e. an additional lateral component is produced, namely,

$$V_y' = V_y - \alpha V_\infty = \alpha V_\infty R^2/z^2 \qquad (12.1.4)$$

The generation of this additional velocity component is affected by the wash produced by the body. The angle of this wash is

$$\varepsilon_{1,b} = V_y'/V_\infty = \alpha R^2/z^2 \qquad (12.1.5)$$

Wash leads to an increase in the local angles of attack in the sections of the wing panels. These local (effective) angles of attack are

$$\alpha_e = \alpha + \varepsilon_{1,b} = \alpha\,(1 + R^2/z^2) \qquad (12.1.6)$$

It can be seen from (12.1.6) that the effective angle of attack reaches its maximum value in the boundary section of the panels when $z = R$, where $\alpha_e = 2\alpha$, and gradually diminishes with an increasing distance of them from the body. In the tip section of the wing, where $z = l$, the effective angle of attack is

$$\alpha_{e,t} = \alpha\,(1 + R^2/l^2) \qquad (12.1.6')$$

As a result of the increase in the local angles of attack, the lift of the wing panels in the presence of a body is greater than for an isolated wing. The wing, in turn, affects the flow over the body because the increased pressure on the bottom surface of the wing and the rarefaction on its upper surface extend to the body. Redistribution of the pressure therefore occurs, and an additional lift force of the body is produced that is due to the influence of the wing.

Wing-Empennage Interference

For craft that are a combination of a body of revolution, a wing, and empennage (a tail unit, fins, and the like), account must be taken of the interaction not only between the body and the wing, but

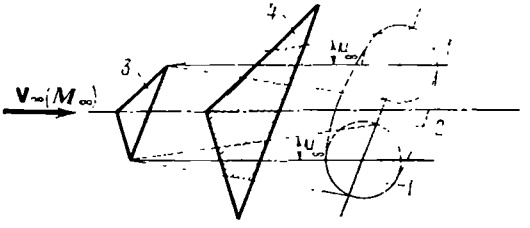

Fig. 12.1.3
Zone of influence of a wing on a tail unit in a supersonic linearized flow (hatched region):
1—Mach cone; *2*—wave surface constructed for the wing (the envelope of the Mach cones); *3*—wing; *4*—tail unit

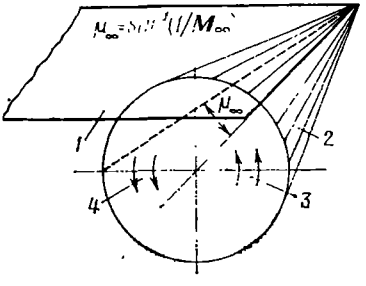

Fig. 12.1.4
Wash behind a rectangular wing:
1—wing; *2*—disturbance (Mach) cone; *3*—upwash; *4*—downwash

also between the body and the empennage, which is similar in its physical nature to the body-wing interference treated above. In addition, account must be taken of the wash behind the wing on the empennage (with front arrangement of the wing on the body), or of the influence of the flow behind the empennage on the wing (with front arrangement of the empennage in what is called a "canard").

In a supersonic flow, a wing affects a tail unit if the latter is inside the Mach cone (wave surface) for the wing, i.e. if it gets into the zone of the wing wash (Fig. 12.1.3). This wash depends on the wing planform and the position of the point at which the flow parameters including the wash angle are being determined.

Let us consider a rectangular wing (Fig. 12.1.4). The region of the disturbed flow in which the influence of the tip on the flow over the wing manifests itself is confined by the Mach cone issuing from the front point of the tip. Inside the Mach cone, the air flows over from the region of increased pressure under the wing into that of reduced pressure on its upper side. As a result, the flow is twisted into a vortex causing a wash behind the wing. There is a downwash in the inner region of the Mach cone including the wing and an upwash in the wave zone outside the wing. Accordingly, the wash on the tip is zero (Fig. 12.1.4).

If a wing is joined to a body of revolution, the wash behind the

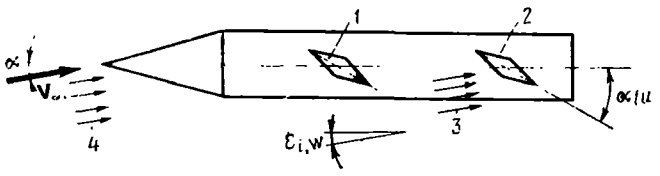

Fig. 12.1.5
Interaction of a wing and a tail unit:
1—wing; *2*—tail unit; *3*—wash; *4*—oncoming flow

wing differs from that for an isolated wing. In this case, the difference between the pressures under the wing and above it grows, the flow of air from the region of increased pressure into that of reduced pressure becomes more intensive, and, consequently, both the upwash in the outer region and the downwash in the inner one grow.

If the span of the tail unit is smaller than that of the wing ahead of it, the tail unit is in the region of downwash, and the effective angle of attack of the unit diminishes. If for a given wing panel section the wash angle is $\varepsilon_{i,w}$, while the setting angle of the tail unit (the angle between a chord of the unit and the body axis) is α_{tu}, then the effective angle of attack of the tail unit panel (Fig. 12.1.5) is

$$\alpha_{e.tu} = \alpha + \alpha_{tu} - \varepsilon_{i,w} \qquad (12.1.7)$$

Diminishing of the effective angle of attack leads to a *reduction of the lift force* and, consequently, to diminishing of the stabilizing moment of the tail unit.

In the vicinity of the tail unit, stagnation of the flow occurs under the action of the wing and, as a result, the velocity head diminishes in comparison with the undisturbed flow. This must also be taken into consideration when determining the aerodynamic characteristics of flow. If the tail unit has a larger span than the wing, a part of the panel surface gets into the region of the upwash and this may compensate the negative effect due to the downwash that consists in reduction of the lift force.

12.2. Normal Force of a Body-Flat Wing Combination

Interference Factors

The total normal force of a craft at a small angle of attack with a zero rolling angle consisting of a combination of a slender body of revolution and a two-panel wing made of thin plates (a flat combination, Fig. 12.2.1) can be determined as the sum of the normal forces for the body and wing taken separately, and additional forces

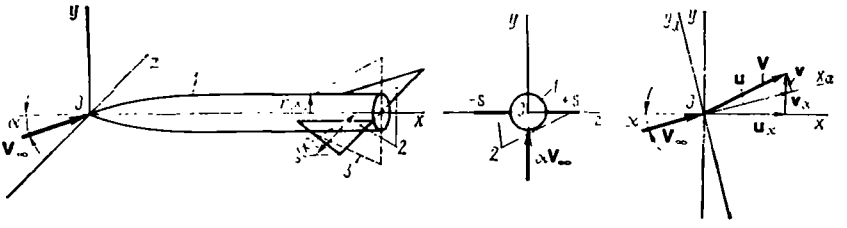

Fig. 12.2.1
Body-flat wing combination (flat combination) at a small angle of attack and in zero rolling:
1—body (body of revolution); *2*—flat wing panels; *3*—panels of four-panel combination

called **interference corrections**. One of these corrections is due to the influence of the body on the flow over the wing, and the other to the effect of the wing on the flow over the body. The total normal force is thus

$$Y_{b,w} = Y_b + Y_w + \Delta Y_{b(w)} + \delta Y_{w(b)} \qquad (12.2.1)$$

where Y_b is the normal force of the isolated body of revolution, Y_w is the normal force of the isolated wing, $\Delta Y_{b(w)}$ is the additional normal force of the body due to the influence of the wing, and $\delta Y_{w(b)}$ is the additional normal force of the wing due to the influence of the body. Expression (12.2.1) can also be written as

$$Y_{b,w} = Y_b + \Delta Y_{b(w)} + \Delta Y_{w(b)} \qquad (12.2.2)$$

where

$$\Delta Y_{w(b)} = Y_w + \delta Y_{w(b)} \qquad (12.2.3)$$

is the normal force of the wing in the presence of the body.

Relation (12.2.2) for the total normal force, apart from a flat (two-panel) combination, can also be applied to an aircraft with a plus-shaped (crossed) wing (a four-panel combination, Fig. 12.2.1). The flow over this craft without sideslipping is the same as with a flat combination because the upper panels in the shape of very thin plates do not change the nature of this flow.

The last two components in (12.2.2) can be written in a form that is more convenient for calculations, namely,

$$\Delta Y_{b(w)} = K_b Y_w \qquad (12.2.4)$$

$$\Delta Y_{w(b)} = K_w Y_w \qquad (12.2.5)$$

where K_b and K_w are **interference factors.**

By (12.2.4) and (12.2.5), the additional normal force of the body produced by the presence of the wing and the normal force of the wing with account taken of interaction with the body are presented as the product of the appropriate interference factors and the normal force of the wing.

By an isolated or separate wing is meant a wing consisting of two panels joined together. According to (12.2.4) and (12.2.5), the normal force of the flat combination "body-wing" is

$$Y_{b,w} = Y_b + (K_b + K_w) Y_w \tag{12.2.6}$$

If we write the normal force of the body in the form

$$Y_b = K_{b,1} Y_w \tag{12.2.7}$$

where $K_{b,1}$ is a factor relating the normal forces of the separate body and wing, we have

$$Y_{b,w} = (K_{b,1} + K_b + K_w) Y_w \tag{12.2.8}$$

The corresponding total normal force coefficient of the combination is

$$c_{y,b,w} = Y_{b,w}/(q_\infty S_w) = (K_{b,1} + K_b + K_w) c_{y,w} \tag{12.2.9}$$

where $q_\infty = \rho_\infty V_\infty^2/2$ is the free-stream velocity head, and S_w is the area of the separate wing panels.

In linearized flow, there is a linear dependence of the normal force on the angle of attack, i.e. $c_y = \alpha c_y^\alpha$ (where $c_y^\alpha = \partial c_y/\partial\alpha$). Consequently,

$$c_{y,b,w}^\alpha = (K_{b,1} + K_b + K_w) c_{y,w}^\alpha \tag{12.2.10}$$

The factors $K_{b,1}$, K_b, and K_w in (12.2.9) and (12.2.10) can be considered in the form of ratios of the corresponding normal force coefficients:

$$K_{b,1} = c_{y,b}/c_{y,w}; \quad K_b = \Delta c_{y,b(w)}/c_{y,w}; \quad K_w = \Delta c_{y,w(b)}/c_{y,w} \tag{12.2.11}$$

or of ratios of the derivatives of the corresponding normal force coefficients with respect to the angle of attack:

$$K_{b,1} = c_{y,b}^\alpha/c_{y,w}^\alpha; \quad K_b = \Delta c_{y,b(w)}^\alpha/c_{y,w}^\alpha; \quad K_w = \Delta c_{y,w(b)}^\alpha/c_{y,w}^\alpha \tag{12.2.12}$$

Determination of the Velocity Potential

Let us consider aerodynamic interference as applied to craft formed of various combinations of slender elements (body, wing, empennage) that cause *weak disturbances* in the flow. In modern aerodynamics, such problems have been solved the most completely, and their application to the above-mentioned craft yields results that are satisfactory enough for practical purposes.

The potential φ' of the disturbance velocities in a linearized flow over slender bodies satisfies an equation of the type of (7.1.4') for

a three-dimensional flow. Let us introduce the dimensionless coordinates

$$\bar{x} = x/L, \quad \bar{y} = y/l, \quad \bar{z} = z/l \tag{12.2.13}$$

where L and l are characteristic lengths in the direction of the x and y axes (for example, L is the length of the entire combination, and l is the span of a wing panel). Equation (7.1.4′) transformed to the variables (12.2.13) has the form

$$(M_\infty^2 - 1)\frac{l^2}{L^2}\cdot\frac{\partial^2\varphi'}{\partial\bar{x}^2} - \frac{\partial^2\varphi'}{\partial\bar{y}^2} - \frac{\partial^2\varphi'}{\partial\bar{z}^2} = 0 \tag{12.2.14}$$

Let us consider the combination of a slender body and wing panels with a small span. For such combinations extended in the direction of the x-axis, the ratio $l^2/L^2 \ll 1$, therefore the first term in Eq. (12.2.14) may be disregarded. As a result, we obtain a differential equation for determining the potential of the disturbance velocities upon interaction between the body and the flat wing:

$$\partial^2\varphi'/\partial\bar{y}^2 + \partial^2\varphi'/\partial\bar{z}^2 = 0$$

or after introducing the values of $\bar{y}$ and $\bar{z}$ from (12.2.13), we have

$$\partial^2\varphi'/\partial y^2 + \partial^2\varphi'/\partial z^2 = 0 \tag{12.2.15}$$

This equation is known to correspond to a disturbed flow of an incompressible fluid in plane yOz. Hence, to find the velocity field of the flow produced by interference, we must solve differential equation (12.2.15) for the function φ', which is the potential of the disturbance velocities of a two-dimensional incompressible cross-flow at the velocity αV_∞ over a wing-body combination (Fig. 12.2.1). The velocity field of the incompressible flow near the body and the wing attached to it in plane yOz can be determined with the aid of a method based on the theory of conformal transformation.

The plane in which the flow is determined is the **physical plane** of the complex variable $\sigma = z + iy$, while the plane for which the flow is known as the flow near a transformed circle is the **transformed plane** of the variable $\zeta = \xi + i\eta$ (Fig. 12.2.2).

Let us write an equation relating the variables σ and ζ:

$$\sigma + r^2/\sigma = \zeta + r_0^2/\zeta \tag{12.2.16}$$

where

$$r_0 = 0.5\,(s + r^2/s) \tag{12.2.16′}$$

s is the running value of the wing semispan (panel span).

Equation (12.2.16) is the relation used for the conformal transformation of a circle of radius r_0 in the plane $\zeta = \xi + i\eta$ into the contour obtained by the intersection of the slender wing-body combination by plane yOz. This contour on the plane $\sigma = z + iy$ is obvious-

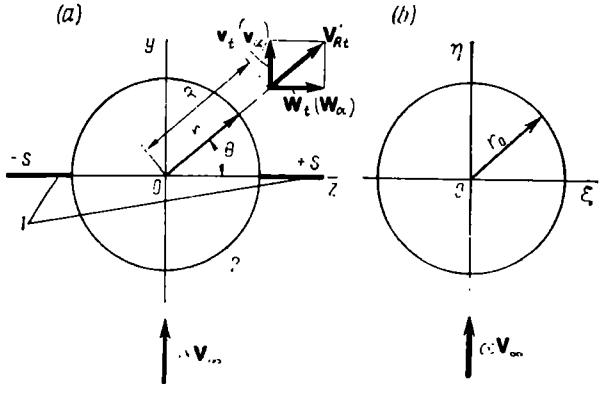

Fig. 12.2.2
Conformal transformation for a body-flat wing combination:
a — physical plane σ (*1*–wing; *2* — body); *b* — transform plane ζ

ly a circle of radius r and a pair of straight line segments each having a length of $s - r_0$ on the z-axis (Fig. 12.2.2). To see that we have correctly chosen formula (12.2.16) for this conformal mapping, we should use this formula for transformations similar to those described in Sec. 6.2 for the conformal mapping of a circle into a plane [see (6.2.1)].

Solving quadratic equation (11.2.16) for ζ, we obtain

$$\zeta = 0.5\ \{(\sigma + r^2/\sigma) + [(\sigma + r^2/\sigma)^2 - 4r_0^2]^{1/2}\} \qquad (12.2.17)$$

The plus sign in front of the bracket indicates a relation between the complex variables ζ and σ for the upper half-plane. When performing a transformation for the bottom half-plane, one must take the minus sign.

The complex potential for a flow over a circular cylinder of radius r_0 in the plane ζ (Fig 12.2.2b) can be determined by formula (6.2.4), substituting r_0 for R:

$$W = -i\alpha V_\infty (\zeta - r_0^2/\zeta) \qquad (12.2.18)$$

This complex potential can be transformed into the potential of the crossflow near the flat body-wing combination in the plane $\sigma = z + iy$ by substituting for the complex variable $\zeta = \xi + i\eta$ in (12.2.18) its value from transformation equation (12.2.17):

$$W = -i\alpha V_\infty [(\sigma + r^2/\sigma)^2 - 4r_0^2]^{1/2} \qquad (12.2.19)$$

To find the total value of the complex potential W_α, we have to add to (12.2.19) the potential function of a flow that is parallel to the y-axis and equals $i\alpha V_\infty \sigma$. As a result, we have

$$W_\alpha = -i\alpha V_\infty \{[(\sigma + r^2/\sigma)^2 - 4r_0^2]^{1/2} - \sigma\}$$

or, taking into account the value of r_0 from (12.2.16'),

$$W_\alpha = -i\alpha V_\infty \{[(\sigma + r^2/\sigma)^2 - (s + r^2/s)^2]^{1/2} - \sigma\} \quad (12.2.20)$$

The complex potential W_α can be expressed in terms of the velocity potential φ_α and the stream function ψ_α in the form $W_\alpha = \varphi_\alpha + i\psi_\alpha$. Considering this and having in view that $\sigma = z + iy$, we can write (12.2.20) as

$$\varphi_\alpha + i\psi_\alpha = -i\alpha V_\infty \left\{\left[\left(z + iy + \frac{r^2}{r + iy}\right)^2 - (s + r^2/s)^2\right]^{1/2} - (z + iy)\right\} \quad (12.2.20')$$

Velocity and Pressure on a Body in the Presence of a Wing

Let us evaluate the partial derivatives with respect to x of the left-hand and right-hand sides of (12.2.20'):

$$\frac{\partial \varphi_\alpha}{\partial x} + i\frac{\partial \psi_\alpha}{\partial x} = -i\alpha V_\infty \times \frac{2\left(z + iy + \frac{r^2}{z + iy}\right)\left(\frac{dr}{dx} \cdot \frac{r}{z + iy} - \left(s + \frac{r^2}{s}\right)\left(\frac{ds}{dx} + \frac{2r\frac{dr}{dx}s - r^2\frac{ds}{dx}}{s^2}\right)\right)}{\left[\left(z + iy + \frac{r^2}{z + iy}\right)^2 - \left(s + \frac{r^2}{s}\right)^2\right]^{1/2}} \quad (12.2.21)$$

Considering the surface of a body for which $\sigma = z + iy = re^{i\theta}$ and having in view that $e^{-i\theta} = \cos\theta - i\sin\theta$ and $e^{i\theta} + e^{-i\theta} = 2\cos\theta$, we obtain

$$\frac{\partial \varphi_\alpha}{\partial x} + i\frac{\partial \psi_\alpha}{\partial x} = -i\alpha V_\infty \times \frac{4\cos\theta(\cos\theta - i\sin\theta)\, r\frac{dr}{dx} - \left(s + \frac{r^2}{s}\right)\left[2\frac{r}{s} \cdot \frac{dr}{dx} + \frac{ds}{dx}\left(1 - \frac{r^2}{s^2}\right)\right]}{\left[4r^2\cos^2\theta - \left(s + \frac{r^2}{s}\right)^2\right]^{1/2}}$$

Separating the real part from the complex right-hand side, we obtain an expression for the additional axial component of the disturbance velocity:

$$\frac{\partial \varphi_\alpha}{\partial x} = u_\alpha = \alpha V_\infty \times \frac{4r\frac{dr}{dx}\cos^2\theta - \left(s + \frac{r^2}{s}\right)\left[2\frac{r}{s} \cdot \frac{dr}{dx} + \frac{ds}{dx}\left(1 - \frac{r^2}{s^2}\right)\right]}{\left[\left(s + \frac{r^2}{s}\right)^2 - 4r^2\cos^2\theta\right]^{1/2}} \quad (12.2.22)$$

To obtain the vertical v_α and lateral w_α components of the disturbance velocity (Fig. 12.2.2*a*), we calculate the derivative of the complex potential (12.2.20) with respect to σ:

$$\frac{dW_\alpha}{d\sigma} = w_\alpha - v_\alpha i = -i\alpha V_\infty \left\{ \frac{(\sigma + r^2/\sigma)(1 - r^2/\sigma^2)}{[(\sigma + r^2/\sigma)^2 - (s + r^2/s)^2]^{1/2}} - 1 \right\} \quad (12.2.23)$$

For the surface of the body provided that $\sigma = re^{i\theta}$, we have

$$w_\alpha - v_\alpha i = -i\alpha V_\infty \left\{ \frac{2r\cos\theta\,(1 + i\sin 2\theta - \cos 2\theta)}{[4r^2\cos^2\theta - (s + r^2/s)^2]^{1/2}} - 1 \right\}$$

Separating the right-hand side of this equation into real and imaginary quantities, we find:

$$w_\alpha = \frac{4\alpha r V_\infty \cos\theta \sin^2\theta}{[(s + r^2/s)^2 - 4r^2\cos^2\theta]^{1/2}} \quad (12.2.24)$$

$$v_\alpha = -\alpha V_\infty \left\{ \frac{2r\cos\theta\sin 2\theta}{[(s + r^2/s)^2 - 4r^2\cos^2\theta]^{1/2}} + 1 \right\} \quad (12.2.25)$$

It follows from physical considerations that formulas (12.2.22), (12.2.24), and (12.2.25) give the values of the velocity components on the lower (bottom) surface of the body, i.e.

$$u_{\alpha,\mathrm{L}} = u_\alpha, \quad w_{\alpha,\mathrm{L}} = w_\alpha, \quad v_{\alpha,\mathrm{L}} = v_\alpha^* \quad (12.2.26)$$

The following relations for the velocity components on the upper surface of the body are obtained from symmetry:

$$u_{\alpha,\mathrm{u}} = -u_{\alpha,\mathrm{L}}, \quad w_{\alpha,\mathrm{u}} = -w_{\alpha,\mathrm{L}}, \quad v_{\alpha,\mathrm{u}} = v_{,\alpha\mathrm{L}} \quad (12.2.27)$$

Let us see how the pressure coefficient can be determined. In Sec.6.1, we obtained formula (6.1.5) for this coefficient when dealing with a plane nearly uniform flow. Investigations show that this formula needs refining if we are considering a *three-dimensional linearized flow*. For such a flow, the square of the total velocity at a point of space is

$$V^2 = V_x^2 + V_y^2 + V_z^2 = (V_\infty + u)^2 + v^2 + w^2$$
$$= V_\infty^2 + 2uV_\infty + u^2 + v^2 + w^2$$

Accordingly, formula (7.1.4″) for the pressure ratio p/p_∞ can be written as follows:

$$\frac{p}{p_\infty} = \left\{ 1 - \frac{k-1}{k} \cdot \frac{\rho_\infty}{p_\infty} \left[uV_\infty + \frac{1}{2}(u^2 + v^2 + w^2) \right] \right\}^{k/(k-1)}$$

Owing to the smallness of the additional velocity components in comparison with V_∞, the ratio p/p_∞ differs only slightly from unity

* To avoid confusion with the subscript "b" designating "body" in this chapter, the subscript "L" and the term "lower" have been resorted to instead of "b" and "bottom" used in Part I and elsewhere in this part—*Translator's note.*

and, consequently, the expression for p/p_∞ can be expanded into a binomial series. Retaining the quadratic term, we obtain

$$\frac{p}{p_\infty} = 1 - \frac{\rho_\infty}{p_\infty}\left[uV_\infty + \frac{1}{2}(u^2+v^2+w^2)\right] + \left(\frac{k-1}{k}\right)^2 \frac{k}{k-1}\left(\frac{k}{k-1}-1\right)\frac{\rho_\infty^2}{2p_\infty^2}\left[uV_\infty + \frac{1}{2}(u^2+v^2+w^2)\right]^2$$

The corresponding relation for the pressure coefficient is

$$\bar{p} = \frac{2(p-p_\infty)}{\rho_\infty V_\infty^2} = -\frac{2u}{V_\infty} - \frac{u^2+v^2+w^2}{V_\infty^2} + \frac{\rho_\infty V_\infty^2}{kp_\infty}\left[\frac{u}{V_\infty} + \frac{1}{2V_\infty^2}(u^2+v^2+w^2)\right]^2$$

Retaining terms of the second order of smallness in comparison with u/V_∞ and taking into consideration that $kp_\infty/\rho_\infty = a_\infty^2$ and $V_\infty^2/a_\infty^2 = M_\infty^2$, we find

$$\bar{p} = -2u/V_\infty + [u^2(M_\infty^2 - 1) - v^2 - w^2]/V_\infty^2$$

Disregarding the term $u^2(M_\infty^2 - 1)$, we finally obtain

$$\bar{p} = -2u/V_\infty - (v^2 + w^2)/V_\infty^2 \qquad (12.2.28)$$

Here, although the flow is nearly uniform, the quadratic terms have been retained, which is of significance for the flow over slender bodies of revolution.

We shall express the velocity components u, v, and w given in formula (12.2.28) for the wind coordinate system in terms of the components u_α, v_α, and w_α in a body-axis system. Since the body has no roll, and the body axes of coordinates are turned through the angle of attack α relative to the lateral axis Oz of the wind system, it is evident that the component $w = w_\alpha$. A glance at Fig. 12.2.1 reveals that the relations $u = u_\alpha + \alpha v_\alpha$ and $v = v_\alpha - \alpha u_\alpha$ hold for the other components. Introducing the expressions obtained for u, v, and w into (12.2.28) and discarding the terms $\alpha v_\alpha u_\alpha/V_\infty^2$ and $\alpha^2 u_\alpha/V_\infty^2$ as terms of a higher order of smallness, we obtain

$$\bar{p} = -(2V_\infty)(u_\alpha + \alpha v_\alpha) - (v_\alpha^2 + w_\alpha^2)/V_\infty^2 \qquad (12.2.28')$$

For the lower surface of the body

$$\bar{p}_{b(w)L} = -2[(u_{\alpha,L} + \alpha v_{\alpha,L})/V_\infty + w_{\alpha,L}^2/(2V_\infty^2) + v_{\alpha,L}^2/(2V_\infty^2)] \qquad (12.2.29)$$

With a view to the symmetry expressed by (12.2.27), the coefficient of pressure on the upper surface is

$$\bar{p}_{b(w)u} = -2[(-u_{\alpha,L} + \alpha v_{\alpha,L})/V_\infty + w_{\alpha,L}^2/(2V_\infty^2) + v_{\alpha,L}^2/(2V_\infty^2)] \qquad (12.2.30)$$

In practice when determining the aerodynamic coefficients, we have to use the pressure-drop coefficients, which we calculate from the corresponding pressure coefficients for the lower and upper surfaces in the form $\Delta\bar{p} = \bar{p}_L - \bar{p}_u$. For the body, this coefficient is

$$\bar{\Delta}p_{b(w)} = \bar{p}_{b(w)L} - \bar{p}_{b(w)u} = -4u_{\alpha,u}/V_\infty \quad (12.2.31)$$

The pressure-drop coefficient can be seen to depend only on the longitudinal velocity component. With a view to (12.2.22), we have

$$\Delta\bar{p}_{b(w)} = \frac{-4\alpha\left\{4r\frac{dr}{dx}\cos^2\theta - (s+r^2/s)\left[2\frac{r}{s}\cdot\frac{dr}{dx}+\frac{ds}{dx}(1-r^2/s^2)\right]\right\}}{[(s+r^2/s)^2-4r^2\cos^2\theta]^{1/2}} \quad (12.2.32)$$

Since for points on the body the coordinate $z = r\cos\theta$ (Fig. 12.2.2), we have

$$\Delta\bar{p}_{b(w)} = \frac{4\alpha\left[(1-r^4/s^4)\frac{ds}{dx}+2\frac{r}{s}\cdot\frac{dr}{dx}(1+r^2/s^2-2z^2/r^2)\right]}{[(1+r^2/s^2)^2-4z^2/s^2]^{1/2}} \quad (12.2.33)$$

Velocity and Pressure on a Wing in the Presence of a Body

Assuming in formula (12.2.21) that $y = 0$ and taking into account that the right hand side of this formula is a real quantity, we find the following expression for the axial component of the velocity:

$$\frac{\partial\varphi_\alpha}{\partial x} = u_\alpha = \alpha V_\infty \times \frac{2\frac{r}{z}\cdot\frac{dr}{dx}(z+r^2/z) - (s+r^2/s)\left[\frac{ds}{dx}(1-r^2/s^2)+2\frac{r}{s}\cdot\frac{dr}{dx}\right]}{[(s+r^2/s)^2-(z+r^2/z)^2]^{1/2}} \quad (12.2.34)$$

Assuming in (12.2.23) that $\sigma = z$ and separating the right-hand side into a real and imaginary quantities, we obtain relations for the lateral w_α and vertical v_α velocity components

$$w_\alpha = \frac{\alpha V_\infty (z+r^2/z)(1-r^2/z^2)}{[(s+r^2/s)^2-(z+r^2/z)^2]^{1/2}} \quad (12.2.35)$$

$$v_\alpha = -\alpha V_\infty \quad (12.2.36)$$

By formulas (12.2.34)-(12.2.36), we obtain the values of the velocity components for the lower surface of the panels, the way of writing these values being the same as (12.2.26). It follows from symmetry that the velocity components for the upper surface of the wing are determined by expressions similar to (12.2.27).

The velocity, and therefore the pressure on the body do not change with axial flow (the angle of attack is zero) in the presence of zero

thickness panels. With such a flow, however, the panels are under the influence of the field of velocities and pressures formed near the body. The resultant flow at the panels consists of the velocity field induced by the body in axial flow and the velocity field in crossflow due to the presence of an angle of attack.

Let us consider the velocity field near the body in a flow at a zero angle of attack, using the conclusions of the aerodynamic theory of a slender body (see Sec. 11.3). By this theory, the additional radial component of the velocity in axial flow (we shall designate it by $V'_{R,t} = V'_{r1}$, see Fig. 12.2.2) according to formula (11.3.10), in which we shall substitute the running radial coordinate of point R for r, is

$$V'_{R,t} = -f(x)/R \tag{12.2.37}$$

From condition (11.2.19) of flow without separation, which owing to the smallness of φ'_x in comparison with V_∞ can be written as

$$\varphi'_r = V'_{R,t} = V_\infty \, dr/dx \tag{12.2.38}$$

we obtain an expression for the function

$$f(x) = -V_\infty r \, dr/dx \tag{12.2.39}$$

Consequently, (12.2.37) can be expressed as

$$V'_{R,t} = \frac{V_\infty r}{R} \cdot \frac{dr}{dx} \tag{12.2.40}$$

Examination of Fig. 12.2.2 reveals that the lateral w_t and vertical v_t components of the velocity of the disturbed flow produced by axial flow over the body are

$$w_t = V'_{R,t} \cos\theta = \frac{V_\infty r}{R} \cdot \frac{dr}{dx} \cos\theta \tag{12.2.41}$$

$$v_t = V'_{R,t} \sin\theta = \frac{V_\infty r}{R} \cdot \frac{dr}{dx} \sin\theta \tag{12.2.42}$$

For the conditions on the surface of a panel, $\theta = 0$, $R = z$, and, consequently,

$$w_t = \frac{V_\infty r}{z} \cdot \frac{dr}{dx} \tag{12.2.43}$$

$$v_t = 0 \tag{12.2.44}$$

If expression (12.2.43) for w_t determines the value of the velocity for the lower surface ($w_{t.l.} = w_t$), it follows from symmetry that on the upper surface

$$w_{t,u} = w_{t,L} \tag{12.2.45}$$

For the axial additional velocity component u_t, which we do not give here in the explicit form, the equation $u_{t.u} = u_{t.L}$ holds; it also follows from symmetry.

We obtain the values of the disturbance velocity components on a panel by summation of the relevant velocity components for axial and lateral flow, i.e.

$$u = u_\alpha + u_t, \quad w = w_\alpha + w_t, \quad v = v_\alpha + v_t = v_\alpha \qquad (12.2.46)$$

Introducing these values into the formula for the pressure coefficient written by analogy with (12.2.28) in the form

$$\bar{p} = -2\left[(u + \alpha v)/V_\infty + v^2/(2V_\infty^2) + w^2/(2V_\infty^2)\right] \qquad (12.2.47)$$

we obtain

$$\bar{p}_{w(b)} = -2\left[(u_\alpha + u_t + \alpha v)/V_\infty + v_\alpha^2/(2V_\infty^2) + (w_\alpha + w_t)^2/(2V_\infty^2)\right] \qquad (12.2.48)$$

For the lower surface of a panel, we have

$$\bar{p}_{w(b)L} = -2\left[(u_{\alpha,L} + u_{t,L} + \alpha v_{\alpha,L})/V_\infty + v_{\alpha,L}^2/(2V_\infty^2) + (w_{\alpha,L}^2 + w_{t,L}^2)/(2V_\infty^2) + w_{\alpha,L}\, w_{t,L}/V_\infty^2\right]$$

For the upper surface with account taken of the property of symmetry [see (12.2.27) and (12.2.45); $u_{t,u} = u_{t,L}$], we have

$$\bar{p}_{w(b)u} = -2\left[(-u_{\alpha,L} + u_{t,L} + \alpha v_{\alpha,L})/V_\infty + v_{\alpha,L}^2/(2V_\infty^2) + (w_{\alpha,L}^2 + w_{t,L}^2)/(2V_\infty^2) - w_{\alpha,L} w_{t,L}/V_\infty^2\right]$$

The pressure-drop coefficient is

$$\Delta\bar{p}_{w(b)} = \bar{p}_{w(b)L} - \bar{p}_{w(b)u} = -4u_{\alpha,L}/V_\infty - 4w_{\alpha,L} w_{t,L}/V_\infty^2 \qquad (12.2.49)$$

Formula (12.2.49) for the pressure-drop coefficient on a panel, unlike the corresponding formula (12.2.31) for a body, has a quadratic form. Introducing into (12.2.49) instead of $u_{\alpha,L}$, $w_{\alpha,L}$, and $w_{t,L}$ their values from (12.2.34), (12.2.35), and (12.2.43), respectively, we find the coefficient of the pressure drop on the wing panels in the presence of the body:

$$\Delta\bar{p}_{w(b)} = 4\alpha\left[\left(s + \frac{r^2}{s}\right)^2 - \left(z + \frac{r^2}{z}\right)^2\right]^{-1/2}\left\{s\frac{ds}{dx}\left(1 - \frac{r^4}{s^4}\right) + r\frac{dr}{dx}\left[2\left(\frac{r^2}{s^2} - 1\right) + \left(1 - \frac{r^2}{z^2}\right)^2\right]\right\} \qquad (12.2.50)$$

If the body is a circular cylinder, then $dr/dx = 0$, and relations (12.2.33) and (12.2.50) acquire the following form, respectively:

$$\Delta\bar{p}_{b(w)} = 4\alpha\frac{ds}{dx}\left(1 - \frac{r^4}{s^4}\right)\left[\left(1 + \frac{r^2}{s^2}\right)^2 - 4\frac{z^2}{s^2}\right]^{-1/2} \qquad (12.2.51)$$

$$\Delta\bar{p}_{w(b)} = 4\alpha\frac{ds}{dx}\left(1 - \frac{r^4}{s^4}\right)\left[\left(1 + \frac{r^4}{s^4}\right) - \frac{z^2}{s^2}\left(1 + \frac{r^4}{z^4}\right)\right]^{-1/2} \qquad (12.2.52)$$

$$(r \leqslant z \leqslant s)$$

Expressions (12.2.51) and (12.2.52) are suitable for an approximate calculation of the pressure distribution over a surface in a flow when the body at the point where it joins the wing flares, and $dr/dx \neq 0$. This is confirmed by calculations showing that the influence of broadening of the body on the nature of pressure distribution is not great. Equations (12.2.51) and (12.2.52) yield quite satisfactory results when the wing is arranged on the body in the zone of undisturbed flow. Investigations show that this condition can be satisfied in practice if the distance from the beginning of the cylindrical part of a slender sharp-nosed body to the wing root chord exceeds two or three body diameters.

Determination of Interference Factors

Let us consider the relations for the normal force of a wing and body with a view to their mutual influence and determine the corresponding interference factors. We shall assume that the wing panels on the cylindrical body ($dr/dx = 0$) are of a triangular configuration for which $ds/dx = \tan \varepsilon$ (Fig. 12.2.3). It should be remembered that the results obtained for the interference factors may be related to any other configuration. In other words, the theoretical values of these factors found below do not depend on the planform of the panels.

It is general knowledge that a slender separate cylindrical body upon deflection does not produce a normal force. Hence, the quantity $\Delta Y_{b(w)}$ (12.2.4) may be considered as the normal force $Y_{b(w)}$ on the body in the presence of a wing. We can find the elementary value of this force with the aid of formula (11.5.4). Assuming that $\cos \beta \approx 1$ and $\cos \gamma = \sin \theta$, we obtain the following expression for the normal force acting on the area $dS = r\, d\theta\, dx$ (Fig. 12.2.3):

$$d\,(\Delta Y_{b(w)}) = dY_{b(w)} = -\,(p - p_\infty)_{b(w)}\, r \sin \theta\, d\theta\, dx$$

The normal force for the part of the body under the wing is

$$\Delta Y_{b(w)} = -\int_{r/\tan \varepsilon}^{s_m/\tan \varepsilon} \int_0^{2\pi} (p - p_\infty)_{b(w)}\, r \sin \theta\, d\theta\, dx$$

The corresponding normal force coefficient related to the cross-sectional area of the body $S = \pi r^2$ is

$$\Delta c'_{y,\,b(w)} = \frac{\Delta Y_{b(w)}}{q_\infty \pi r^2} = -\frac{1}{\pi r} \int_{r/\tan \varepsilon}^{s_m/\tan \varepsilon} dx \int_0^{2\pi} \bar{p}_{b(w)} \sin \theta\, d\theta$$

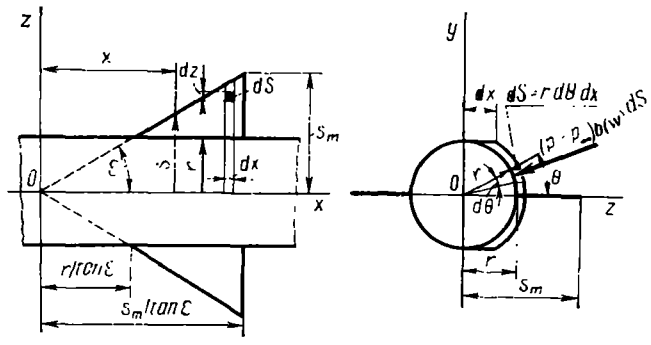

Fig. 12.2.3
Combination of a cylindrical body and a triangular wing

Taking account of the symmetry of pressure distribution at both sides of the zero meridian plane, and also of the conditions in which the pressure coefficients at points of the surface determined by the angular coordinates θ (upper surface) and —θ (lower surface) are $\bar{p}$ and $-\bar{p}$, respectively, we obtain the relation

$$\Delta c'_{y,\mathrm{b(w)}} = -\frac{2}{\pi r}\int_{r/\tan\varepsilon}^{s_m/\tan\varepsilon} dx \int_0^{\pi/2} \Delta\bar{p}_{\mathrm{b(w)}} \sin\theta\, d\theta$$

Substituting for $\Delta\bar{p}_{\mathrm{b(w)}}$ its expression from (12.2.51) and having in view the equality $z = r\cos\theta$, we find (the magnitude)

$$\Delta c'_{y,\mathrm{b(w)}} = \frac{8\alpha\tan\varepsilon}{\pi r^2}\int_{r/\tan\varepsilon}^{s_m/\tan\varepsilon} dx \int_0^{r} \left(1-\frac{r^4}{s^4}\right)\left[\left(1+\frac{r^2}{s^2}\right)^2 - 4\frac{z^2}{s^2}\right]^{-1/2} dz$$

Single integration, provided that $x = s/\tan\varepsilon$ and $dx = ds/\tan\varepsilon$, yields

$$\Delta c'_{y,\mathrm{b(w)}} = \frac{4\alpha}{\pi}\int_1^{\bar{s}_m} \frac{\bar{s}^4-1}{\bar{s}^3}\sin^{-1}\frac{2\bar{s}}{\bar{s}^2+1}\, d\bar{s} \qquad (12.2.53)$$

where $\bar{s} = s/r$ and $\bar{s}_m = s_m/r$.

Introducing the variables $\bar{u} = \sin^{-1}\dfrac{2\bar{s}}{\bar{s}^2+1}$ and $\bar{v} = \dfrac{1}{2}\left(\bar{s}^2+\dfrac{1}{\bar{s}^2}\right)$, we find, integrating by parts,

$$\Delta\bar{c}'_{y,\mathrm{b(w)}} = \frac{4\alpha}{\pi}\left[\frac{1}{2}\left(\bar{s}_m^2+\frac{1}{\bar{s}_m^2}\right)\sin^{-1}\frac{2\bar{s}_m}{\bar{s}_m^2+1} + \frac{\bar{s}_m^2-1}{\bar{s}_m} - 2\tan^{-1}\bar{s}_m\right] \qquad (12.2.53')$$

The corresponding normal force coefficient $\Delta c_{y,\mathrm{b(w)}}$ calculated for the area of the separate panels

$$S_{\mathrm{w}} = (s_m - r)^2/\tan\varepsilon \qquad (12.2.54)$$

is

$$\Delta c_{y,\mathrm{b(w)}} = \Delta c'_{y,\mathrm{b(w)}} \frac{\pi r^2}{S_{\mathrm{w}}} = \frac{\pi r^2 \tan\varepsilon}{(s_m - r)^2} \Delta c'_{y,\mathrm{b(w)}} \qquad (12.2.55)$$

With account taken of expression (8.8.47) for the normal force coefficient $c_{y,\mathrm{w}}$ of a separate wing in which it should be assumed that $\cot\varkappa = \tan\varepsilon$, the interference factor is

$$K_{\mathrm{b}} = \Delta c_{y,\mathrm{b(w)}}/c_{y,\mathrm{w}} = \Delta c'_{y,\mathrm{b(w)}}/[2(\bar{s}_m - 1)^2\alpha] \qquad (12.2.56)$$

After introducing (12.2.53') and performing simple transformations, we have

$$K_{\mathrm{b}} = \frac{2}{\pi(\bar{s}_m - 1)^2}$$

$$\times \left[\frac{\bar{s}_m^2 - 1}{\bar{s}_m} + \frac{\pi}{2}\left(\bar{s}_m^2 + \frac{1}{\bar{s}_m^2}\right) - \frac{(\bar{s}_m^2 + 1)^2}{\bar{s}_m^2}\tan^{-1}\bar{s}_m\right] \qquad (12.2.57)$$

Let us find a relation for the wing-body interference factor. The value of the elementary normal force acting on an elementary area of the wing $dS_{\mathrm{w}} = dx\,dz$ is

$$d(\Delta Y_{\mathrm{w(b)}}) = \Delta\bar{p}_{\mathrm{w(b)}}\,dx\,dzq_\infty$$

The force of two panels with expression (12.2.52) taken into consideration is

$$\Delta Y_{\mathrm{w(b)}} = 8\alpha\tan\varepsilon q_\infty \int_{r/\tan\varepsilon}^{s_m/\tan\varepsilon} \left(1 - \frac{r^4}{s^4}\right) dx$$

$$\times \int_r^s \left[\left(1 + \frac{r^4}{s^4}\right) - \frac{z^2}{s^2}\left(1 + \frac{r^4}{x^4}\right)\right]^{-1/2} dz \qquad (12.2.52')$$

The corresponding normal force coefficient is

$$\Delta c_{y,\mathrm{w(b)}} = \frac{\Delta Y_{\mathrm{w(b)}}}{q_\infty S_{\mathrm{w}}} = \frac{8\alpha\tan^2\varepsilon}{(s_m - r)^2}$$

$$\times \int_{r/\tan\varepsilon}^{s_m/\tan\varepsilon} \left(1 - \frac{r^4}{s^4}\right) dx \int_r^s \left[\left(1 + \frac{r^4}{s^4}\right) - \frac{z^2}{s^2}\left(1 + \frac{r^4}{x^4}\right)\right]^{-1/2} dz$$

Single integration of this expression yields (for $x = s/\tan\varepsilon$ and $dx = ds/\tan\varepsilon$)

$$\Delta c_{y(\mathrm{w})\mathrm{b}} = \frac{4\alpha\tan\varepsilon}{(\bar{s}_m - 1)^2} \int_1^{\bar{s}_m} \frac{\bar{s}^4 - 1}{\bar{s}^3}\left(\frac{\pi}{2} + \sin^{-1}\frac{\bar{s}^2 - 1}{\bar{s}^2 + 1}\right) d\bar{s}$$

Upon partial integration

$$\Delta c_{y,\mathrm{w(b)}} = \frac{4\alpha \tan \varepsilon}{(\bar{s}_m - 1)^2}\left[\frac{\pi}{4}\frac{(\bar{s}_m^2-1)^2}{\bar{s}_m^2} + \int_1^{\bar{s}_m} \frac{\bar{s}^4-1}{\bar{s}^3}\sin^{-1}\frac{\bar{s}^2-1}{\bar{s}^2+1}\,d\bar{s}\right]$$

Introducing the variables

$$\bar{u} = \sin^{-1}[(\bar{s}^2-1)/(\bar{s}^2+1)], \qquad \bar{v} = 0.5\,(\bar{s}^2 + 1/\bar{s}^2) \qquad (12.2.58)$$

and performing integration by parts, we find

$$\Delta c_{y,\mathrm{w(b)}} = \frac{4\alpha \tan \varepsilon}{(\bar{s}_m - 1)^2}\left[\frac{\pi}{4}\cdot\frac{(\bar{s}_m^2-1)^2}{\bar{s}_m^2} - \frac{\bar{s}_m^2-1}{\bar{s}_m} + \frac{(\bar{s}_m^2+1)^2}{2\bar{s}_m^2}\cdot\sin^{-1}\frac{\bar{s}_m^2-1}{\bar{s}_m^2+1}\right] \qquad (12.2.59)$$

The interference factor with account taken of (8.8.47) for $c_{y,\mathrm{w}}$ is

$$K_{\mathrm{w}} = \frac{\Delta c_{y(\mathrm{w})\mathrm{b}}}{c_{y,\mathrm{w}}} = \frac{2}{\pi(\bar{s}_m-1)^2}\left[\frac{\pi}{4}\cdot\frac{(\bar{s}_m^2-1)^2}{\bar{s}_m^2} - \frac{\bar{s}_m^2-1}{\bar{s}_m} + \frac{(\bar{s}_m^2+1)^2}{2\bar{s}_m^2}\sin^{-1}\frac{\bar{s}_m^2-1}{\bar{s}_m^2+1}\right] \qquad (12.2.60)$$

Taking into account that

$$\tan^{-1}\bar{s}_m = \frac{1}{2}\left(\sin^{-1}\frac{\bar{s}_m^2-1}{\bar{s}_m^2+1} + \frac{\pi}{2}\right)$$

we shall transform formula (12.2.57) for the interference factor K_{b} into the expression

$$K_{\mathrm{b}} = \frac{2}{\pi(\bar{s}_m-1)^2}\left[\frac{\pi}{4}\frac{(\bar{s}_m^2-1)^2}{\bar{s}_m^2} + \frac{\bar{s}_m^2-1}{\bar{s}_m} - \frac{(\bar{s}_m^2+1)^2}{2\bar{s}_m^2}\sin^{-1}\frac{\bar{s}_m^2-1}{\bar{s}_m^2+1}\right] \qquad (12.2.57')$$

Summation of (12.2.60) and (12.2.57) yields

$$K_{\mathrm{w}} + K_{\mathrm{b}} = (\bar{s}_m + 1)^2/\bar{s}_m^2 \text{ or } K_{\mathrm{w}} + K_{\mathrm{b}} = (1 + r_m)^2 \qquad (12.2.61)$$

where $r_m = r/s_m$.

A glance at expressions (12.2.60) and (12.2.57′) reveals that the interference factors are *functions of only the ratio* r/s_m. Hence, this parameter (or its reciprocal s_m/r) is the *main criterion* in assessing the mutual influence of a body and a wing on the normal force. Values of K_{w} and K_{b} are given in Fig. 12.2.4 and Table 12.2.1 depending on the value of $1/\bar{s}_m = r_m$.

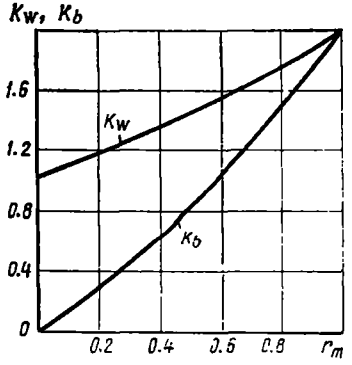

Fig. 12.2.4
Interference factors for a flat body-wing combination in the absence of rolling

If the ratio $r_m = r/s_m = 0$ (a body is absent), we obviously have $K_w = 1$ and $K_b = 0$. Let us assume that the radius of the body grows and the lifting panels become small, i.e. the parameter r_m differing from zero increases. It follows from (12.1.6′) that the ef-

Table 12.2.1

r_m	K_w	K_b	$(c_p)_{\alpha,w(b)}$	$(c_p)_{\alpha,b(w)}$	$(\bar{z}_p)_{\alpha,w(b)}$
0.0	1.000	1.000	0.667	0.500	0.424
0.1	1.077	0.133	0.657	0.521	0.421
0.2	1.162	0.278	0.650	0.542	0.419
0.3	1.253	0.437	0.647	0.563	0.418
0.4	1.349	0.611	0.646	0.581	0.417
0.5	1.450	0.800	0.647	0.598	0.417
0.6	1.555	1.005	0.650	0.613	0.416
0.7	1.663	1.227	0.654	0.628	0.418
0.8	1.774	1.467	0.658	0.641	0.420
0.9	1.887	1.725	0.662	0.654	0.422
1.0	2.000	2.000	0.667	0.667	0.424

fective angle of attack of the panels grows. When $R/l \to 1$ ($r_m \to 1$), the body induces the local angle of attack $\alpha_{e,t} \to 2\alpha$ along its side surface. Consequently, the panels in the presence of a body develop a normal force double that developed by an isolated wing, and, therefore, $K_w = 2$.

The smaller the size of a panel, the greater is the part of the normal force of the wing transferred to the body. When the value of $r_m \to 1$, the maximum normal force is induced on the body, and $K_w = 2$.

Centre of Pressure

The coordinate of the centre of pressure of the normal force induced by a body on a wing is

$$(x_p)_{\alpha,w(b)} = -\Delta M_{z,w(b)}/\Delta Y_{w(b)} \qquad (12.2.62)$$

where $\Delta M_{z,w(b)}$ is the pitching moment about the nose of the root (boundary) section of a panel produced by the forces due to the influence of the body on the wing:

$$\Delta M_{z,w(b)} = -\int_0^{(s_m-r)/\tan\varepsilon} \int_r^{r} \Delta\bar{p}_{w(b)} q_\infty x\, dx\, dz \qquad (12.2.63)$$

We measure the coordinates x and $(x_p)_{\alpha,w(b)}$ from the nose of the root section of the panel (Fig. 12.2.5). Taking into consideration the value of $\Delta Y_{w(b)}$, the coordinate is

$$(x_p)_{\alpha,\,w(b)} = \int_0^{(s_m-r)/\tan\varepsilon} \int_r^{s} \Delta\bar{p}_{w(b)} q_\infty x\, dx\, dz \Big/ \int_0^{(s_m-r)/\tan\varepsilon} \int_r^{s} \Delta\bar{p}_{w(b)} q_\infty\, dx\, dz \qquad (12.2.62')$$

The coordinate of the centre of pressure of the normal force induced by a wing on a body is

$$(x_p)_{\alpha,b(w)} = -\Delta M_{z,b(w)}/\Delta Y_{b(w)} \qquad (12.2.64)$$

where $\Delta M_{z,b(w)}$ is the pitching moment about the nose of the boundary section of a panel due to the influence of the wing (Fig. 12.2.5):

$$\Delta M_{z,\,b(w)} = -\int_0^{(s_m-r)/\tan\varepsilon} \int_0^{r} \Delta\bar{p}_{b(w)} q_\infty x\, dx\, dz \qquad (12.2.65)$$

and $\Delta Y_{b(w)}$ is the normal force of the part of the body under the panels due to the influence of the wing.

With a view to the value of $\Delta Y_{b(w)}$, the coordinate

$$(x_p)_{\alpha,\,b(w)} = \int_0^{(s_m-r)/\tan\varepsilon} \int_0^{r} \Delta\bar{p}_{b(w)} q_\infty x\, dx\, dz \Big/ \int_0^{(s_m-r)/\tan\varepsilon} \int_0^{r} \Delta\bar{p}_{b(w)} q_\infty\, dx\, dz \qquad (12.2.64')$$

From (12.2.62') and (12.2.64'), we can determine the corresponding coefficients of the centres of pressure:

$$(c_p)_{\alpha,w(b)} = (x_p)_{\alpha,w(b)}/b_0;\quad (c_p)_{\alpha,b(w)} = (x_p)_{\alpha,b(w)}/b_0 \qquad (12.2.66)$$

where b_0 is the length of the root chord of a panel (Fig. 12.2.5).

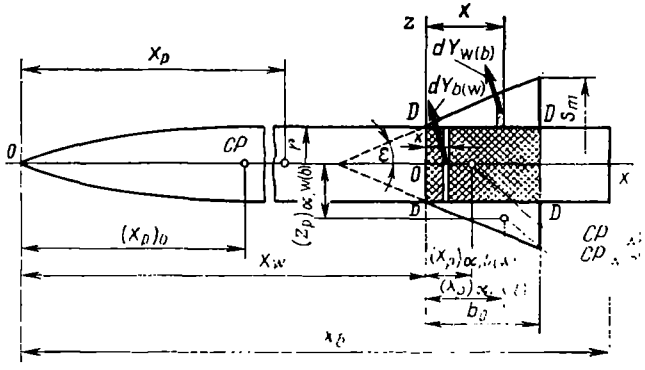

Fig. 12.2.5
To the determination of the centre-of-pressure for a body and a wing with account taken of interference

Using these values, we can find the coefficient of the pitching moment for a body of revolution-wing combination about the nose:

$$m_{z,b,w} = M_{z,b,w}/(q_\infty S_w x_b) = -c_{y,b,w} c_p$$
$$= -[c_{y,b} + c_{y,w}(K_b + K_w)]\, c_p = -[(c_p)_b c_{y,b}$$
$$+ (c'_p)_{\alpha,b(w)} \Delta c_{y,b(w)} + (c'_p)_{\alpha,w(b)} \Delta c_{y,w(b)}] \qquad (12.2.67)$$

where

$$\left.\begin{aligned}(c'_p)_{\alpha,b(w)} &= x_w/x_b + (c_p)_{\alpha,b(w)}\, b_0/x_b \\ (c'_p)_{\alpha,w(b)} &= x_w/x_b + (c_p)_{\alpha,w(b)}\, b_0/x_b\end{aligned}\right\} \qquad (12.2.68)$$

Here $c_p = x_p/x_b$ is the centre-of-pressure coefficient for the entire combination, $(c_p)_b = (x_p)_b/x_b$ and $c_{y,b}$ are the centre-of-pressure and normal force coefficients for the separate body, respectively. All the geometric dimensions are shown in Fig. 12.2.5, where the area onto which the normal force from the panels is transferred is cross-hatched.

The lateral coordinate of the centre of pressure of the normal force $\Delta Y_{w(b)}$ for the wing panels due to the influence of the body (Fig. 12.2.5), is

$$(z_p)_{\alpha,w(b)} = -\Delta M_{x,w(b)}/\Delta Y_{w(b)} \qquad (12.2.69)$$

where $\Delta M_{x,w(b)}$ is the rolling moment due to the normal force $\Delta Y_{w(b)}$ and determined about the longitudinal axis x:

$$\Delta M_{x,w(b)} = -\int_0^{(s_m - r)/\tan\varepsilon} \int_r^s \Delta \bar{p}_{w(b)} q_\infty z\, dx\, dz \qquad (12.2.70)$$

With a view to the value of $\Delta Y_{w(b)}$, the coordinate of the centre of pressure is

$$(z_p)_{\alpha,w(b)} = \int_0^{(s_m-r)/\tan\varepsilon} \int_r^s \Delta\bar{p}_{w(b)} q_\infty z \, dx \, dz \Big/ \int_0^{(s_m-r)/\tan\varepsilon} \int_r^s \Delta\bar{p}_{w(b)} q_\infty \, dx \, dz \tag{12.2.71}$$

From (12.2.71) we can find the coordinate of the centre of pressure measured along the span of a panel from the root chord on the body and related to the panel width $s_m - r$, i.e. the quantity

$$(\bar{z}_p)_{\alpha,w(b)} = [(z_p)_{\alpha,w(b)} - r]/(s_m - r)$$

This quantity, and also the values of the centre-of-pressure coefficients (12.2.66) calculated for triangular panels [in (12.2.51) and (12.2.52) for $\Delta\bar{p}_{b(w)}$ and $\Delta\bar{p}_{w(b)}$, respectively, the derivative ds/dx is taken equal to $\tan\varepsilon$] are given in Table 12.2.1 depending on the parameter $r/s_m = 1/\bar{s}_m$. Examination of the table reveals that the centre-of-pressure coefficient $(c_p)_{\alpha,w(b)}$ differs only slightly from the value 2/3 corresponding to a separate triangular wing. The ratio $(\bar{z}_p)_{\alpha,w(b)}$ is close to the value $4/(3\pi)$ upon the elliptic distribution of the normal force over the span of a separate wing.

Both these results show that the wing-body interference does not affect noticeably the position of the centre of pressure of the lifting panels both along the span and along the chord. Consequently, in practical cases, when the aerodynamic calculations are based on the application of the aerodynamic theory of a slender body, the influence of the interference on the position of the centre of pressure of wings may be ignored. Here one should have in view that according to the aerodynamic theory of a slender body, the value of $(\bar{z}_p)_{\alpha,w(b)}$ does not depend on the wing planform, whereas the position of the centre of pressure of the panels in a longitudinal direction does depend on the planform. Particularly, calculations by the aerodynamic theory of a slender body show that the centre of pressure of rectangular wings is on their leading edge.

Table 12.2.1 shows that the influence of interference on the position of the centre of pressure of the body is substantial. When $r_m = r/s_m = 0$, which signifies that the body is absent (more exactly, the body transforms into an infinitely slender cylinder coinciding with the root chord of a panel), we obtain the obvious result $(c_p)_{\alpha,b(w)} = 1/2$. When the dimensions of the panels are very small in comparison with the radius of the body, i.e. at values of $r_m \to 1$, virtually the entire normal force of the wing acts on the body (the interference factor $K_b \to 2$), and, accordingly, the centre-of-pressure coefficient is close to the value for a separate wing, i.e. $(c_p)_{\alpha,b(w)} \to 2/3$.

Change in the Interference Factors under Varying Influence

Experimental investigations have established (see [13]) that theoretical formulas (12.2.60) and (12.2.57′) allow one to obtain good results for the interference factors K_w and K_b for a wing with rectangular panels for which the *taper ratio* $\eta_w = b_0/b_t = 1$ (b_0 and b_t are the root and tip chords of the wing, respectively). It is obvious from physical considerations that the use of panels with an increased taper ratio ($\eta_w > 1$) leads to larger interference factors. Indeed, in such panels, the major part of their area adjoins the body, therefore they experience increased interference and, in turn, affect the flow over the body more appreciably. This increase in the interference factors can be taken into account by the correction factors

$$\nu_{b,\eta} = K_b/(K_b)_{th}; \quad \nu_{w,\eta} = K_w/(K_w)_{th} \qquad (12.2.72)$$

where the subscript "th" designates the theoretical parameters (12.2.57′) and (12.2.60). Experiments show that these factors are virtually the same and can be assumed equal:

$$\nu_{b,\eta} = \nu_{w,\eta} = \nu_\eta = 1 + \frac{r_m(1-r_m)}{(1+r_m)^2}\left(1 - \frac{1}{\eta_w}\right) \qquad (12.2.73)$$

For rectangular panels when $\eta_w = 1$, the value of $\nu_\eta = 1$, and the interference factors coincide with their corresponding theoretical values.

It follows from experimental data that the interference factors are affected by the **boundary layer of the body**. This influence manifests itself in a change in the effective radius of the body where the panels are located by the value of the displacement thickness of the boundary layer δ^* (see Chapter 13). Using this value of the radius $r' = r + \delta^*$ and the parameter $r'_m = r'/s_m$, we determine the refined interference factor (Fig. 12.2.6). Its value allows us to calculate the correction factors:

$$\nu'_{b,bl} = K_b/(K_b)_{th}; \quad \nu'_{w,bl} = K_w/(K_w)_{th} \qquad (12.2.74)$$

where the subscript "bl" stands for "boundary layer".

Since the interference factors in the numerator are found from the increased parameter $r'_m > r_m$, then the correction factors are greater than unity. The corresponding physical effect manifests itself in an additional normal force due to greater interference to the body because of the increase in its thickness. But the boundary layer also has a negative action, causing the normal force to decrease because of the reduction in the area of the panels in the external flow (S'_w, Fig. 12.2.6).

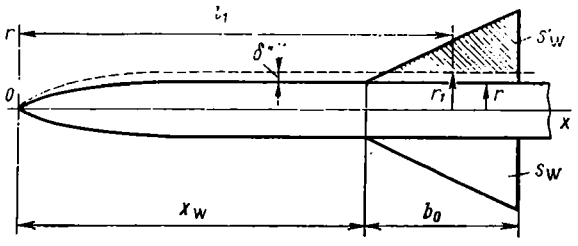

Fig. 12.2.6
Influence of the boundary layer on the interaction of the body and the wing (empennage) panels

Assuming the values (12.2.74) to be identical, i.e. $\nu'_{b,bl} = \nu'_{w,bl} = \nu'_{bl}$, the corresponding total change in the normal force can be taken into consideration with the aid of the coefficient

$$\nu_{bl} = \nu'_{bl} S'_w / S_w \qquad (12.2.75)$$

Investigations reveal that

$$\nu_{bl} \approx 1 - r_m (1 + r_m^2) [r_m + \eta_w (1 + 3r_m) - 1] \bar{\delta}^* / (\eta_w + 1) \qquad (12.2.76)$$

where $\bar{\delta}^* = \delta^*/r$.

It can be seen that the value given by (12.2.76) is always less than unity. This points to the more considerable effect of the reduction in the normal force because of the decrease in the wing area than of its growth because of the increase in the body thickness.

The relative displacement thickness $\bar{\delta}^* = \delta^*/r$ in (12.2.76) can be determined with the aid of (13.4.65) and (13.4.58) for a boundary layer beginning from the nose of the body. For calculations, we adopt the thickness δ^* at a point with the coordinate $l_1 = x_w + 0.5b_0$, i.e. in the middle part of the root chord of the wing. Accordingly, in (13.4.58) we should adopt $x = l_1$ and $Re_x = V_\infty l_1/\nu_\infty$.

For interference factors (12.2.57') and (12.2.60), the theoretical relations have been obtained by assuming that a wing located on a slender cylindrical body is sufficiently remote from the nose, and therefore the latter (together with the cylindrical part) does not virtually affect the flow over the wing. In other words, the wing is in a region of the flow whose velocity corresponds to that of the free stream. When a wing is not far from the nose, the influence of the part of the body ahead of it may be appreciable. Investigations show that the interference factors here decrease in accordance with the relation

$$\nu_l = K_b/(K_b)_{th} = K_w/(K_w)_{th} = [0.6 + (1 + 0.2\bar{l}_1)^2]/[1 + (1 + 0.2\bar{l}_1)^2] \qquad (12.2.77)$$

where $\bar{l}_1 = l_1/r$ (Fig. 12.2.6).

For a wing at a large distance from the nose part of the combination [$\bar{l}_1 > (15\text{-}20)$], the coefficient $\nu_l \approx 1$, i.e. the interference factors do not practically change. For a canard aircraft, however, such a change may be substantial because the distances l_1 are relatively small.

The results obtained show that it is expedient to evaluate the interference factors with the aid of the following relations:

$$K_w = (K_w)_{th}\nu_\eta\nu_{bl}\nu_l; \quad K_b = (K_b)_{th}\nu_\eta\nu_{bl}\nu_l \qquad (12.2.78)$$

Normal Force of Body-Wing Combination

We shall use formula (12.2.6) to determine the total normal force $Y_{b,w}$. We determine the normal force Y_b of a separate slender body in this formula as follows. Let us consider a slender body in the form of a cone with a very small semiapex angle β_c. For a slender cone and small angles of attack, as follows from (11.5.29), the normal force coefficient can be taken equal to $c_y = 2\alpha$. Applying this formula to a slender body of revolution of an arbitrary shape, we obtain

$$Y_b = 2\alpha\pi r^2 q_\infty \qquad (12.2.79)$$

where r is the radius of the body mid-section.

By this formula, the normal force of a slender body of revolution is determined for a given angle of attack only by the diameter of the mid-section (maximum cross section).

The normal force for a separate wing is

$$Y_w = c_{y,w}S_w q_\infty$$

where by formula (8.8.47), in which we assumed that $\cot\varkappa = \tan\varepsilon$, the coefficient $c_{y,w} = 2\alpha\pi\tan\varepsilon$. Since S_w is found from (12.2.54), we have

$$Y_w = 2\alpha\pi\,(s_m - r)^2\, q \qquad (12.2.80)$$

Having in view that the sum of the theoretical interference factors $K_b + K_w$ is determined by formula (12.2.61), and also considering the obtained values of Y_b and Y_w, we find the following expression for the total normal force:

$$Y_{b,w} = 2\alpha\pi s_m^2\,(1 - r_m^2 + r_m^4)\, q_\infty \qquad (12.2.81)$$

Introducing into the formula for the normal force coefficient $c_{y,b,w} = Y_{b,w}/(q_\infty S_w)$ the value of S_w from (12.2.54), we find

$$c_{y,b(w)} = \frac{c_{y,w}}{(1-r_m)^2}(1 - r_m^2 + r_m^4) \qquad (12.2.82)$$

The total normal force does not depend on the configuration of the panels and the part of the body ahead of the section with the

maximum semispan s_m. It also follows from formula (12.2.81) that even if there is a certain wing area behind this section, it does not affect the lifting properties of the body-wing combination.

Normal force coefficient (12.2.82) can be refined by calculating the interference factors with account taken of the wing taper ratio, the boundary layer, and the location of the panels. By (12.2.78), the sum of the coefficients is

$$K_b + K_w = (K_b + K_w)_{th} \nu_\eta \nu_{bl} \nu_l$$

or with a view to (12.2.61)

$$K_b + K_w = (1 + r_m)^2 \nu_\eta \nu_{bl} \nu_l \qquad (12.2.83)$$

By (12.2.83), the normal force is

$$Y_{b,w} = Y_b + (K_b + K_w) Y_w$$
$$= 2\alpha\pi s_m^2 [r_m^2 + (1 - r_m^2)^2 \nu_\eta \nu_{bl} \nu_l] q_\infty \qquad (12.2.84)$$

and the coefficient of this force is

$$c_{y,b,w} = \frac{Y_{b,w}}{q_\infty S_w} = \frac{c_{y,w}}{(1-r_m)^2} [r_m^2 + (1-r_m^2)^2 \nu_\eta \nu_{bl} \nu_l] \qquad (12.2.85)$$

The total normal force diminishes at values of the multipliers on the right-hand side less than unity, i.e. with the influence of the taper ratio, boundary layer, and location of the wing taken into consideration.

12.3. Influence of the Rolling Angle on Body-Flat Wing Interference

General Relation for the Pressure Coefficient

A body-flat wing combination turned through the rolling angle φ is shown in Fig. 12.3.1. In addition to the angle φ, the flow over this combination and, consequently, the interaction of the body and the wing panels also depend on the angle α_v between the longitudinal axis and the direction of the free-stream velocity. This angle (Fig. 12.3.1) is determined in plane $x'Oy'$ formed by body axes Ox' and Oy' constructed for a combination with no roll. The flow being considered is equivalent to the one produced upon the presence of an angle of attack α and a sideslip angle β. The angle of attack α is measured in vertical plane yOx in body axes Oy and Ox for a banked body and is determined as the angle between the projection V'_∞ of the vector V_∞ onto this plane and axis Ox.

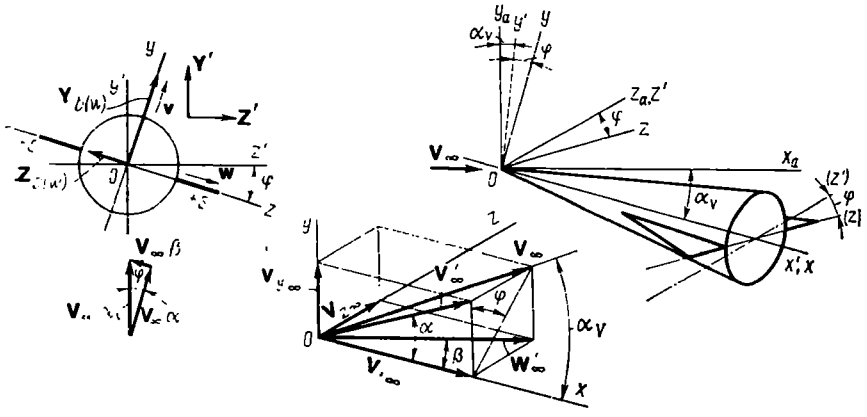

Fig. 12.3.1
Body-flat wing combination in rolling

In accordance with Fig. 12.3.1, the small angle α equals the ratio of the vertical $V_{y\infty}$ and horizontal $V_{x\infty}$ components of the free-stream velocity, i.e.

$$\alpha = V_{y\infty}/V_{x\infty} \tag{12.3.1}$$

The sideslip angle β is found in lateral plane zOx of the same body-axis coordinate system as the angle between the projection $\mathbf{W}'_\infty$ of the vector $\mathbf{V}_\infty$ onto this plane and longitudinal axis Ox. Examination of Fig. 12.3.1 reveals that

$$\beta = V_{z\infty}/V_{x\infty} \tag{12.3.2}$$

where $V_{z\infty}$ is the lateral component of the free-stream velocity.

It can be seen from Fig. 12.3.1 that

$$V_{x\infty} = V_\infty \cos\alpha_v;\ V_{y\infty} = V_\infty \sin\alpha_v \cos\varphi,\ V_{z\infty} = V_\infty \sin\alpha_v \sin\varphi \tag{12.3.3}$$

For small values of α_v

$$V_{x\infty} = V_\infty;\ V_{y\infty} = \alpha_v V_\infty \cos\varphi;\ V_{z\infty} = \alpha_v V_\infty \sin\varphi \tag{12.3.3'}$$

Accordingly,

$$\alpha = \alpha_v \cos\varphi \tag{12.3.1'}$$

$$\beta = \alpha_v \sin\varphi \tag{12.3.2'}$$

Having in view the linearized nature of the flow, we can determine the total potential function in the form of the sum

$$\varphi'_\Sigma = \varphi'_f + \varphi'_\alpha + \varphi'_\beta \tag{12.3.4}$$

where φ_t' is the potential of axisymmetric flow at the velocity $V_{x\infty} = V_\infty$, φ_α' and φ_β' are, respectively, the additional potentials of flow in the direction of α at the velocity $V_{y\infty} = \alpha V_\infty = \alpha_v V_\infty \cos\varphi$ and in the direction of β at the velocity $V_{z\infty} = \beta V_\infty = \alpha_v V_\infty \sin\varphi$.

By (12.3.4), the velocity components are

$$u = u_t + u_\alpha + u_\beta;\ v = v_t + v_\alpha + v_\beta;\ w = w_t + w_\alpha + w_\beta \quad (12.3.5)$$

We obtain a general expression for the pressure coefficient on a body determined with account taken of interference with the aid of formula (12.2.28'), in which we replace the components of the disturbance velocity in the wind coordinates x_a, y_a and z_a with the corresponding values of u, v and w in the body-axis coordinates x, y and z. When performing this substitution, we proceed from the fact that in accordance with Fig. 12.3.1 the body axes are obtained by turning the wind axes first through the angle α_v relative to axis Oz, and then through the angle φ clockwise relative to the new position of longitudinal axis Ox. The direction cosines of the angles between the axes x_a, y_a, z_a and x, y, z are given in Table 12.3.1.

Table 12.3.1

Coordinates	x_a	y_a	z_a
x_1	$\cos\alpha_v$	$-\sin\alpha_v$	0
y_1	$\sin\alpha_v\cos\varphi$	$\cos\alpha_v\cos\varphi$	$\sin\varphi$
z_1	$-\sin\alpha_v\sin\varphi$	$-\cos\alpha_v\sin\varphi$	$\cos\varphi$

Using the data of Table 12.3.1 and with a view to the smallness of the angle α_v we can write the following expressions for the disturbed velocity components in wind coordinates:

$$\left.\begin{aligned} u_a &= u + v\alpha_v\cos\varphi - w\alpha_v\sin\varphi \\ v_a &= -u\alpha_v + v\cos\varphi - w\sin\varphi \\ w_a &= v\sin\varphi + w\cos\varphi \end{aligned}\right\} \quad (12.3.6)$$

Introducing the found expressions for the velocity components in (12.3.28') and discarding the small quantities $u^2\alpha_v^2$, $uv\alpha_v\sin\varphi$, and $uv\alpha_v\cos\varphi$, we find

$$\bar{p} = -(2/V_\infty)(u + v\alpha - w\beta) - (v^2 + w^2)/V_\infty^2 \quad (12.3.7)$$

Pressure on a Body

The coefficient of the pressure on the lower side of a body with (12.3.5) taken into consideration is

$$\bar{p}_{b(w)L} = -(2/V_\infty)[u_{t,L} + u_{\alpha,L} + u_{\beta,L} + \alpha(v_{t,L} + v_{\alpha,L} + v_{\beta,L}) - \beta(w_{t,L} + w_{\alpha,L} + w_{\beta,L})] - (1/V_\infty^2)[(v_{t,L} + v_{\alpha,L} + v_{\beta,L})^2 + (w_{t,L} + w_{\alpha,L} + w_{\beta,L})^2] \quad (12.3.8)$$

The expression for the upper surface is similar. This expression can be written somewhat differently if we have in view the symmetry of the velocity components on a body. Relations (12.2.27) are derived from the property of symmetry of flow over the body in the direction of α. Similar expressions can be written corresponding to the property of symmetry in the direction of β, namely,

$$u_{\beta,u} = u_{\beta L}, \quad v_{\beta,u} = -v_{\beta,L}, \quad w_{\beta,u,} = w_{\beta,L} \quad (12.3.9)$$

Taking into account the symmetry expressed by relations (12.2.27) and (12.3.9), and also the relations

$$u_{t,L} = u_{t,u}, \quad v_{t,L} = -v_{t,u}, \quad w_{t,L} = w_{t,u} \quad (12.3.9')$$

the coefficient of the pressure on the upper surface of a body is

$$\bar{p}_{b(w)u} = -(2/V_\infty)[u_{t,L} - u_{\alpha,L} + u_{\beta,L} + \alpha(-v_{t,L} + v_{\alpha,L} - v_{\beta,L}) - \beta(w_{t,L} - w_{\alpha,L} + w_{\beta,L})] - (1/V_\infty^2)[(-v_{t,L} + v_{\alpha,L} - v_{\beta,L})^2 + (w_{t,L} - w_{\alpha,L} + w_{\beta,L})^2] \quad (12.3.10)$$

The pressure-drop coefficient is obtained as the difference between the values (12.3.8) and (12.3.10), i.e.

$$\Delta\bar{p}_{b(w)} = \bar{p}_{b(w)L} - \bar{p}_{b(w)u} = -(4/V_\infty)u_{\alpha,L} - (4\alpha/V_\infty)(v_{t,b} + v_{\beta,L}) + (4\beta/V_\infty)w_{\alpha,L} - (4/V_\infty^2)(v_{t,L}v_{\alpha,L} + v_{\alpha,L}v_{\beta,L}) - (4/V_\infty^2)(w_{t,L}w_{\alpha,L} + w_{\alpha,L}w_{\beta,L}) \quad (12.3.11)$$

Let us consider an arbitrary point on the lower surface of a body. For this point, the vector of the disturbance velocity in a lateral plane due to longitudinal flow over a body of finite length is $\mathbf{V}_{t,L} = w_{t,L}\mathbf{i} + v_{t,L}\mathbf{j}$. For the same point, the vector of the disturbance velocity due to the presence of an angle of attack is

$$\mathbf{V}_{\alpha,L} = w_{\alpha,L}\mathbf{i} + (v_{\alpha,L} + \alpha V_\infty)\mathbf{j}$$

It can be seen from (12.2.42) that the vector $\mathbf{V}_{t,L}$ coincides with a radial direction and is in a meridional plane. The second vector $\mathbf{V}_{\alpha,L}$ in accordance with the condition of flow without separation coincides with the direction of a tangent to the contour at the point being considered. Consequently, the vectors $\mathbf{V}_{t,L}$ and $\mathbf{V}_{\alpha,L}$ are

perpendicular, and their dot product equals zero, i.e.

$$(w_{t,L}\mathbf{i} + v_{t,L}\mathbf{j})\cdot[w_{\alpha,L}\mathbf{i} + (v_{\alpha,L} + \alpha V_\infty)\,\mathbf{j}]$$
$$= w_{t,L}w_{\alpha,L} + v_{t,L}(v_{\alpha,L} + \alpha V_\infty) = 0 \qquad (12.3.12)$$

With a view to this value, expression (12.3.11) becomes

$$\Delta\bar{p}_{b(w)} = -(4/V_\infty)\,u_{\alpha,L} - (4/V_\infty)\,(v_{\beta,L}\,\alpha - w_{\alpha,L}\beta)$$
$$- (4/V_\infty^2)\,(v_{\alpha,L}v_{\beta,L} + w_{\alpha,L}w_{\beta,L}) \qquad (12.3.13)$$

In comparison with (12.2.31), expression (12.3.13) contains the terms $v_{\beta,L}\alpha$, $w_{\alpha,L}\beta$, $v_{\alpha,L}\,v_{\beta,L}$, and $w_{\alpha,L}w_{\beta,L}$ characterizing the influence of the rolling angle and known as **interaction terms.** The velocity components $u_{\alpha,L}$, $w_{\alpha,L}$, and $v_{\alpha,L}$ are given by expressions (12.2.22), (12.2.24), and (12.2.25), respectively. The components $w_{\beta,L}$ and $v_{\beta,L}$ can be obtained with the aid of a formula for the complex potential of crossflow over the body in the direction of the negative axis Oz at the free-stream velocity βV_∞. By analogy with (12.2.18), this potential is

$$W = -\beta V_\infty(\sigma + r^2/\sigma) \qquad (12.3.14)$$

We obtain the field of disturbance velocities if onto the flow with the potential (12.3.14) we impose a parallel flow in the direction of the positive axis Oz at the velocity βV_∞ and with the corresponding potential $\beta V_\infty\sigma$. As a result, the complex potential of the disturbance velocities is

$$W_\beta = -\beta V_\infty r^2/\sigma \qquad (12.3.15)$$

Hence, the complex velocity of the disturbances is

$$dW_\beta/d\sigma = w_\beta - v_\beta i = \beta V_\infty r^2/\sigma^2 \qquad (12.3.16)$$

For the surface of a body, provided that $\sigma = re^{i\theta}$, we obtain

$$w_\beta - v_\beta i = \beta V_\infty e^{-2i\theta} = \beta V_\infty(\cos 2\theta - i\sin 2\theta) \qquad (12.3.17)$$

Relating this expression to the lower surface, we obtain the following equations for the velocity components:

$$w_{\beta,L} = \beta V_\infty \cos 2\theta;\quad v_{\beta,L} = \beta V_\infty \sin 2\theta \qquad (12.3.18)$$

Inserting (12.2.22), (12.2.24), (12.2.25), and (12.3.18) into (12.3.13) we find a relation for the pressure-drop coefficient on the body:

$$\Delta\bar{p}_{b(w)} = \frac{4\alpha\left[\left(1-\frac{r^4}{s^4}\right)\frac{ds}{dx} + 2\frac{r}{s}\cdot\frac{dr}{dx}\left(1+\frac{r^2}{s^2}-2\frac{z^2}{r^2}\right)\right]}{\left[\left(1+\frac{r^2}{s^2}\right)^2 - 4\frac{z^2}{s^2}\right]^{1/2}}$$
$$+ \frac{32\alpha\beta\,(r/s)\cos\theta\sin^2\theta}{\left[\left(1+\frac{r^2}{s^2}\right)^2 - 4\frac{z^2}{s^2}\right]^{1/2}} \qquad (12.3.19)$$

In the absence of rolling, the second term with the factor $\alpha\beta$ characterizing wing-body interaction due to the presence of a sideslip angle vanishes, i.e. we have relation (12.2.33) for a body-flat wing combination in a flow without sideslip.

The first term in (12.3.19) contains the derivatives ds/dx and dr/dx, which indicates that the interference depends (if rolling is absent) on the change in a panel span and the body diameter. At the same time, such derivatives are absent in the second term and, consequently, do not affect body-wing interaction in sideslip.

Pressure on a Wing

Using (12.3.8) and (12.3.5), let us derive a relation for the coefficient of the pressure on the lower surface of a wing with account taken of interference:

$$\bar{p}_{w(b)L} = -(2/V_\infty)[u_{t,L} + u_{\alpha,L} + u_{\beta,L} + \alpha(v_{t,L} + v_{\alpha,L} + v_{\beta,L}) - \beta(w_{t,L} + w_{\alpha,L} + w_{\beta,L})] - (1/V_\infty^2)[(v_{t,L} + v_{\alpha,L} + v_{\beta,L})^2 + (w_{t,L} + w_{\alpha,L} + w_{\beta,L})^2] \quad (12.3.20)$$

The pressure coefficient for the upper surface can be represented by formula (12.3.20) by substituting the subscript "u" for "L". The resulting expression can be transformed with the aid of symmetry formulas that relate the velocity components on the upper surface to those on the lower one.

For the conditions on the lower and upper surfaces of the starboard panel, these relations are as follows:

$$\left.\begin{aligned} u_{t,L} &= u_{t,u},\ w_{t,L} = w_{t,u},\ v_{t,L} = -v_{t,u} \\ u_{\alpha,L} &= -u_{\alpha,u},\ w_{\alpha,L} = -w_{\alpha,u},\ v_{\alpha,L} = v_{\alpha,u} \\ u_{\beta,L} &= u_{\beta,u},\ w_{\beta,L} = w_{\beta,u},\ v_{\beta,L} = -v_{\beta,u} \end{aligned}\right\} \quad (12.3.21)$$

Writing (12.3.20) for the conditions on the upper surface and replacing terms with the subscript "u" by the corresponding quantities given by (12.3.21), we find

$$\bar{p}_{w(b)u} = -(2/V_\infty)[u_{t,L} - u_{\alpha,L} + u_{\beta,L} - \alpha(-v_{t,L} + v_{\alpha,L} - v_{\beta,L}) - \beta(w_{t,L} - w_{\alpha,L} + w_{\beta,L})] - (1/V_\infty^2)[(-v_{t,L} + v_{\alpha,L} - v_{\beta,L})^2 + (w_{t,L} - w_{\alpha,L} + w_{\beta,L})^2] \quad (12.3.22)$$

The pressure-drop coefficient is

$$\Delta\bar{p}_{w(b)} = \bar{p}_{w(b)L} - \bar{p}_{w(b)u} = -(4/V_\infty)u_{\alpha,L} - (4/V_\infty) \times [(v_{t,L} + v_{\beta,L})\alpha - w_{\alpha,L}\beta] - (4/V_\infty^2)(v_{t,L}v_{\beta,L} + v_{\alpha,L}v_{\beta,L} + w_{t,L}w_{\alpha,L} + w_{\alpha,L}w_{\beta,L})$$

With a view to (12.2.44), i.e. $v_t = 0$, and to the condition of crossflow over the wing without separation, i.e. $v_\beta = 0$, we obtain

$$\Delta\bar{p}_{w(b)} = -(4/V_\infty)\, u_{\alpha,L} + (4/V_\infty)\, w_{\alpha,L}\beta - (4/V_\infty^2)\,(w_{t,L}\, w_{\alpha,L} + w_{\alpha,L}\, w_{\beta,L}) \qquad (12.3.23)$$

The velocity components $u_{\alpha,L}$, $w_{\alpha,L}$, and $w_{t,L}$ have been determined by expressions (12.2.34), (12.2.35), and (12.2.43). We find the component w_β from Eq. (12.3.16), assuming that $\sigma = z$:

$$w_{\beta,L} = \beta V_\infty r^2/z^2 \qquad (12.3.24)$$

After the corresponding substitutions in (12.3.23), we have

$$\Delta\bar{p}_{w(b)} = \frac{4\alpha\left\{\frac{r}{s}\cdot\frac{dr}{dx}\left[\left(1-\frac{r^2}{z^2}\right)^2+2\left(\frac{r^2}{s^2}-1\right)\right]+\frac{ds}{dx}\left(1-\frac{r^4}{s^4}\right)\right\}}{\left[\left(1+\frac{r^2}{s^2}\right)^2-\frac{z^2}{s^2}\left(1+\frac{r^2}{z^2}\right)^2\right]^{1/2}} + \frac{4\alpha\beta\,\frac{z}{s}\left(1+\frac{r^2}{z^2}\right)\left(1-\frac{r^2}{z^2}\right)^2}{\left[\left(1+\frac{r^2}{s^2}\right)^2-\frac{z^2}{s^2}\left(1+\frac{r^2}{z^2}\right)^2\right]^{1/2}} \qquad (12.3.25)$$

In (12.3.25), the term with the factor $\alpha\beta$ characterizes the wing-body interaction due to sideslip. This term is asymmetric for the port and starboard panels because the angle β is negative for the port panel and positive for the starboard one.

Normal Force and Centre of Pressure

The interaction between a wing and a body with sideslip results in an increase in the normal force on the starboard panel with an increase in the rolling angle φ and a decrease in this force on the port panel by the same amount. Therefore, the total normal force for the combination does not change, and its value remains the same as in the absence of sideslip.

The normal force in the direction of the y-axis (see Fig. 12.3.1) by (12.2.81) is

$$Y_{b,w} = 2\alpha_v \cos\varphi \pi s_m^2 (1 - r_m^2 + r_m^4)\, q_\infty \qquad (12.3.26)$$

The lateral force in the direction of the z-axis is produced only by the body as a result of crossflow over it at the velocity $-\beta V_\infty$ and does not depend on the presence of a zero-thickness wing, which does not affect this flow. By (12.2.79)

$$Z_{b,w} = Z_b = -2\beta\pi r^2 q_\infty = -2\alpha_v \pi r^2 \sin\varphi\, q_\infty \qquad (12.3.27)$$

The normal force in the direction of the axis Oy' (see Fig. 12.3.1) is

$$Y' = Y_{b,w} \cos \varphi - Z \sin \varphi = 2\alpha_v \pi s_m^2 [(1 - r_m^2)^2 \cos^2 \varphi + r_m^2] q_\infty \tag{12.3.28}$$

The lateral force in the direction of the axis Oz' is

$$Z' = Y_{b,w} \sin \varphi + Z \cos \varphi = 2\alpha_v \pi s_m^2 \sin \varphi \cos \varphi (1 - r_m^2) q_\infty \tag{12.3.29}$$

Let us consider the normal force and centre of pressure of a lifting panel due to rolling. For a starboard triangular panel, the magnitude of this force determined by the second term in (12.3.25), which we shall designate by $[\Delta \bar{p}_{w(b)}]_\varphi$, is

$$\Delta Y_{w(b)} = q_\infty \int\limits_{(S_w)} \int [\Delta \bar{p}_{w(b)}]_\varphi \, dS_w \tag{12.3.30}$$

A glance at Fig. 12.2.3 reveals that the elementary area of a panel is

$$dS_w = dz\, dx = dz\, ds/\tan \varepsilon$$

In accordance with this value and with a view to (12.3.25) for the second term, we have

$$\Delta Y_{w(b)} = \frac{q_\infty}{\tan \varepsilon} \int\limits_r^{s_m} dz \int\limits_z^{s_m} [\Delta \bar{p}_{w(b)}]_\varphi \, ds = \frac{4\alpha\beta q_\infty}{\tan \varepsilon} \int\limits_r^{s_m} z \left(1 + \frac{r^2}{z^2}\right) \left(1 - \frac{r^2}{z^2}\right)^2$$

$$\times dz \int\limits_z^{s_m} ds \Big/ \left\{ s \left[\left(1 + \frac{r^2}{s^2}\right)^2 - \frac{z^2}{s^2} \left(1 + \frac{r^2}{z^2}\right)^2 \right]^{1/2} \right\}$$

After evaluating the second integral, we obtain

$$\Delta Y_{w(b)} = \frac{2\alpha\beta q_\infty}{\tan \varepsilon} \int\limits_r^{s_m} z \left(1 + \frac{r^2}{z^2}\right) \left(1 - \frac{r^2}{z^2}\right)^2 \cosh^{-1} \frac{2s_m^2 - (z^2 + r^4/z^2)}{z^2 - r^4/z^2} \, dz \tag{12.3.30'}$$

We integrate further by the numerical method. We shall introduce an interference factor calculated as

$$K_\varphi = \Delta Y_{w(b)} \tan \varepsilon / (Y_w \beta) \tag{12.3.31}$$

where Y_w is the normal force for one triangular separate wing panel. By (12.2.80), we have

$$Y_w = \alpha\pi (s_m - r)^2 q_\infty$$

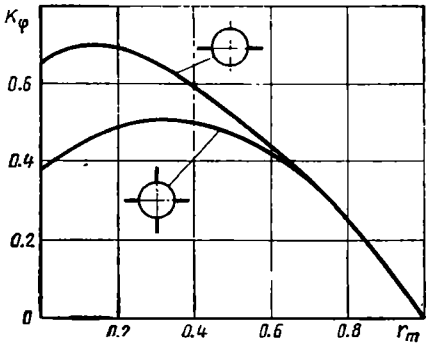

Fig. 12.3.2
Interference factors for a flat and cruciform combinations in rolling

Taking the above expressions into account, we obtain the following equation for the factor:

$$K_\varphi = \frac{2}{\pi (s_m - r)^2} \int_r^{s_m} z \left(1 + \frac{r^2}{z^2}\right) \left(1 - \frac{r^2}{z^2}\right)^2 \cosh^{-1} \frac{2s_m^2 - (z^2 + r^4/z^2)}{z^2 - r^4/z^2}\, dz \tag{12.3.32}$$

Calculations show that the factor K_φ can be taken the same for panels of various configurations and be considered as a function of only the ratio $r_m = r/s_m$. These values, obtained by numerical integration, are presented in Table 12.3.2 and in Fig. 12.3.2 as a function of the ratio r_m. Examination of (12.3.23) reveals that the force characterized by the factor K_φ depends on the total action

Table 12.3.2

$\frac{r}{s_m}$	Flat combination			Cruciform combination		
	K_φ	$(c_p)_{\varphi,\,w\,(b)}$	$(\bar{z}_p)_{\varphi,w\,(b)}$	K_φ	$(c_p)_{\varphi,w\,(b)}$	$(\bar{z}_p)_{\varphi,w\,(b)}$
0	0.637	0.667	0.524	0.382	0.667	0.556
0.1	0.687	0.667	0.518	0.447	0.654	0.532
0.2	0.681	0.677	0.531	0.490	0.660	0.530
0.3	0.649	0.688	0.546	0.508	0.673	0.540
0.4	0.597	0.699	0.560	0.502	0.687	0.554
0.5	0.529	0.709	0.575	0.471	0.700	0.569
0.6	0.447	0.719	0.588	0.417	0.714	0.585
0.7	0.352	0.729	0.601	0.342	0.725	0.598
0.8	0.249	0.736	0.614	0.244	0.734	0.612
0.9	0.128	0.744	0.616	0.127	0.743	0.625
1.0	0	0.750	0.637	0	0.750	0.637

of the field of the velocities w_α and w_β due to the angles of attack and sideslip. By (12.3.31), the magnitude of this force is

$$\Delta Y_{w(b)} = K_\varphi Y_w \beta/\tan \varepsilon \qquad (12.3.33)$$

while the corresponding coefficient is

$$\Delta c_{y,w(b)} = \Delta Y_{w(b)}/(q_\infty S_w) = K_\varphi c^\alpha_{y,w} \alpha\beta/\tan \varepsilon \qquad (12.3.33')$$

The longitudinal coordinate of the centre of pressure of a panel measured from the nose of the root chord is determined from the condition

$$(x_p)_{\varphi,w(b)} = -\Delta M_{z,w(b)}/\Delta Y_{w(b)} \qquad (12.3.34)$$

where the additional pitching moment due to rolling is

$$\Delta M_{z,w(b)} = \frac{-q_\infty}{\tan^2 \varepsilon} \int_r^{s_m} dz \int_z^{s_m} [\Delta \bar{p}_{w(b)}]_\varphi \, s \, ds \qquad (12.3.35)$$

The distance from the axis of symmetry of the body to the centre of pressure in a lateral direction is calculated from the expression

$$(z_p)_{\varphi,w(b)} = -\Delta M_{x,w(b)}/\Delta Y_{w(b)} \qquad (12.3.36)$$

where the additional value of the rolling moment in sideslip is

$$\Delta M_{x,w(b)} = \frac{-q_\infty}{\tan \varepsilon} \int_r^{s_m} z \, dz \int_z^{s_m} [\Delta \bar{p}_{w(b)}]_\varphi \, ds \qquad (12.3.37)$$

We use the values of both coordinates of the centre of pressure found by numerical integration to calculate the coefficients of the centre of pressure:

$$\left.\begin{aligned} (\bar{c}_p)_{\varphi,w(b)} &= [(x_p)_{\varphi,w(b)}]/b_0 \\ (\bar{z}_p)_{\varphi,w(b)} &= [(z_p)_{\varphi,w(b)} - r]/(s_m - r) \end{aligned}\right\} \qquad (12.3.38)$$

These coefficients are given in Table 12.3.2. They can be used to determine the rolling moment and bending moment in the root section of a panel depending on the rolling angle. Here we do not consider the loads acting on the body upon rolling. These loads, which, as for a wing, are of an asymmetric nature, do not virtually affect the normal force, moment, and, consequently, the position of the centre of pressure of the combination.

General Relations for the Forces and Moments of a Flat Combination in Rolling

The longitudinal moment coefficient (or the hinge moment coefficient) determined about the lateral axis passing through the vertex of a panel (point D in Fig. 12.2.5) is

$$m_{\text{h, pan}} = -0.5 c^{\alpha}_{y,\text{w}} \alpha \bar{b}_0 \left[(c_{\text{p}})_{\alpha,\text{w(b)}} + \frac{K_{\varphi}\beta}{\tan \varepsilon} (c_{\text{p}})_{\varphi,\text{w(b)}} \right] \quad (12.3.39)$$

where

$$\alpha = \alpha_{\text{w}} \cos \varphi, \ \bar{b}_0 = b_0/x_{\text{b}}$$

Since in rolling an additional normal force is not produced from both panels, the summary coefficient of this force (in the direction of the axis Oy, Fig. 12.3.3) is

$$c_{y,\text{b,w}} = Y_{\text{b,w}}/(q_{\infty} S_{\text{w}}) = c_{y,\text{b}} + c^{\alpha}_{y,\text{w}} (K_{\text{b}} + K_{\text{w}}) \alpha \quad (12.3.40)$$

With a view to this value, the pitching moment coefficient calculated about the nose of the body is

$$m_{z,\text{b,w}} = m_{z,\text{b}} - \{K_{\text{b}} [(c_{\text{p}})_{\alpha,\text{b(w)}} \bar{b}_0 + \bar{x}_{\text{w}}] + K_{\text{w}} [(c_{\text{p}})_{\alpha,\text{w(b)}} \bar{b}_0 + \bar{x}_{\text{w}}]\} c^{\alpha}_{y,\text{w}} \alpha \quad (12.3.41)$$

where $m_{z,\text{b}}$ is the pitching moment coefficient of the body computed in the plane of the angle of attack α from the area of the wing panels S_{w} and the length x_{b}, $\bar{b}_0 = b_0/x_{\text{b}}$, $\bar{x}_{\text{w}} = x_{\text{w}}/x_{\text{b}}$ (see Fig. 12.2.5).

By (12.3.40) and (12.3.41), we shall calculate the coefficient of the centre of pressure that is the point of application of the total normal force $Y_{\text{b,w}}$:

$$(c_{\text{p}})_{\alpha} = (x_{\text{p}})_{\alpha}/x_{\text{b}} = -m_{z,\text{b,w}}/c_{y,\text{b,w}} \quad (12.3.42)$$

The coefficient of the lateral force (in the direction of the z-axis) is found provided that this force is produced only by the body in a flow having the velocity $-V_{\infty}\beta$ and does not depend on the presence of a zero-thickness wing that has no influence on this flow. Accordingly,

$$c_{z,\text{b,w}} = c_{z,\text{b}} \quad (12.3.43)$$

Like the lateral force, a yawing moment in the plane of the side slip angle is produced only by the body. The coefficient of this moment is

$$m^{\beta}_{y,\text{b,w}} = m^{\beta}_{z,\text{b}} \beta \quad (12.3.44)$$

where the derivative $m^{\beta}_{y,\text{b}} = -m^{\alpha}_{z,\text{b}}$.

Evidently, for the combination being considered, the coefficient of the centre of pressure of the lateral force is the same as for an isolated body, i.e.

$$(c_{\text{p}})_{\beta} = (x_{\text{p}})_{\beta}/x_{\text{b}} = -m_{y,\text{b}}/c_{z,\text{b}} \quad (12.3.45)$$

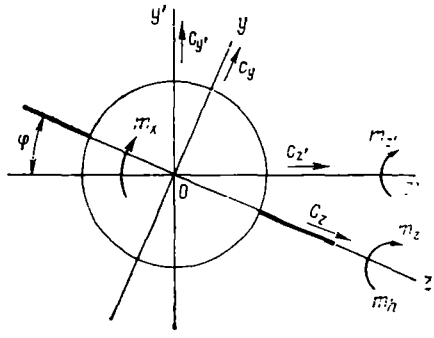

Fig. 12.3.3
Coefficients of the forces and moments acting on a flat combination in rolling

An increase in the normal force on the starboard panel and a decrease in it by the same amount on the port panel (or vice versa) in sideslip produce a rolling moment whose coefficient is

$$m_{x,b,w} = -\frac{K_\varphi}{\tan\varepsilon} c^{\alpha}_{y,w} \alpha\beta \left[(\bar{z}_p)_{\varphi,w(b)} + \frac{1}{\bar{s}_m - 1} \right] \frac{s_m - r}{x_b} \qquad (12.3.46)$$

Knowing the aerodynamic characteristics relative to the axes y and z, we can determine their values relative to the axes y' and z'. According to Fig. 12.3.3, the coefficient of the normal force acting in the direction of the y' axis is

$$c_{y',\,b,w} = c_{y,b,w} \cos\varphi - c_{z,b} \sin\varphi \qquad (12.3.47)$$

In this expression, with a view to (12.3.40), we can assume that

$$c_{y,b,w} = c^{\alpha}_{y,b}\alpha_v \cos\varphi + c^{\alpha}_{y,w} (K_b + K_w)\,\alpha \cos\varphi \qquad (12.3.48)$$

Assuming also that

$$c_{z,b} = -c^{\alpha}_{y,b}\beta = -c^{\alpha}_{y,b}\alpha_v \sin\varphi \qquad (12.3.49)$$

from (12.3.47) we obtain

$$c_{y',b,w} = c^{\alpha}_{y,b}\alpha_v + c^{\alpha}_{y,w} (K_b + K_w)\,\alpha_v \cos^2\varphi \qquad (12.3.47')$$

The coefficient of the lateral force in the direction of the z'-axis is

$$c_{z',b,w} = c_{y,b,w} \sin\varphi + c_{z,b} \cos\varphi \qquad (12.3.50)$$

Inserting into (12.3.50) the values of $c_{y,b(w)}$ and $c_{z,b}$ from (12.3.48) and (12.3.49), we find

$$c_{z\ b\ w} = c^{\alpha}_{y,w} (K_b + K_w)\,\alpha_v \sin\varphi \cos\varphi \qquad (12.3.50')$$

Knowing the coefficients of the normal and lateral forces (12.3.47') and (12.3.50'), and also the arrangement of the relevant centres of pressure for the panels and body, we can find the coefficients of the

longitudinal and yawing moments about the lateral axes y' and z' passing through the nose.

The coefficients of the forces $c_{y,b}$ and $c_{z,b}$, and also of the moment $m_{z,b}$ produced by the nose part of the body are calculated by the linearized theory for an isolated body.

12.4. Cruciform Combination

Pressure and Normal Force

Let us consider the aerodynamic coefficients of a cruciform combination consisting of a circular cylinder and flat panels of zero thickness in a nearly uniform (linearized) supersonic flow (Fig. 12.4.1). We shall assume that the vertical wing panels have the same planform and semispan as the horizontal ones. We shall also assume that the vertical panels do not affect the nature of flow over the combination in longitudinal plane xOy at the angle of attack $\alpha = \alpha_v \cos \varphi$ and that the horizontal panels do not affect the flow pattern obtained when the angle $\beta = \alpha_v \sin \varphi$ changes.

Hence, the problem being considered consists in solving two independent problems, one of which is associated with finding of the velocity field for the flat combination "body-vertical wing" installed at the angle α, and the second, with finding of the velocity field of the flat combination "body-horizontal wing" at the angle β. Summation of the fields yields the total flow near the cruciform combination turned through the pitching angle α_v and the rolling angle φ.

Accordingly, the total values of the disturbance velocities are determined by formulas (12.3.5), and the pressure coefficient, by relation (12.3.7). We compute the pressure-drop coefficient for the body from expression (12.3.13) in which we find the components $u_{\alpha,L}$, $w_{\alpha,L}$, and $v_{\alpha,L}$ by formulas (12.2.22), (12.2.24), and (12.2.25), respectively, obtained for a flat combination provided that $\alpha = \alpha_v \cos \varphi$ in these formulas.

To determine the components w_β and v_β, we shall use an expression for the complex potential of a flat combination in a crossflow with the velocity βV_∞. We find this expression as follows. By analogy with (12.2.18), we obtain a formula for the complex potential for flow over a circular cylinder of radius r_0 in the plane $\zeta = \xi + i\eta$:

$$W = -\beta V_\infty (\zeta + r_0^2/\zeta) \qquad (12.4.1)$$

Next, by analogy with (12.2.16), we obtain the equation

$$\sigma - r^2/\sigma = \zeta - r_0^2/\zeta \qquad (12.4.2)$$

in which $r_0 = 0.5\,(s + r^2/s)$.

We can see that this equation allows us to perform a conformal transformation of a circle of radius r_0 into a contour consisting of

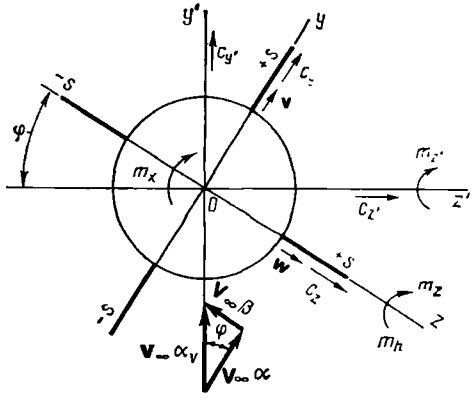

Fig. 12.4.1
Cruciform combination

a circle of radius r and a pair of vertical panels with a span of $\pm s$. This contour is obtained as a result of intersection of the body-wing combination with plane yOz.

Solving quadratic equation (12.4.2) for ζ, we have

$$\zeta = 0.5\,[\sigma - r^2/\sigma + \sqrt{(\sigma - r^2/\sigma)^2 + 4r_0^2}] \qquad (12.4.3)$$

Substitution of this quantity into (12.4.1) yields the complex potential

$$W = -\beta V_\infty\,[(\sigma - r^2/\sigma)^2 + 4r_0^2]^{1/2} \qquad (12.4.4)$$

To find the total value of the complex potential, we have to add to (12.4.4) the potential function of a flow parallel to the z-axis. This function equals $\beta V_\infty \sigma$. Thereby, the total complex potential is

$$W_\beta = -\beta V_\infty\,\{[(\sigma - r^2/\sigma)^2 + 4r_0^2]^{1/2} - \sigma\} \qquad (12.4.5)$$

Let us differentiate this expression with respect to σ:

$$\frac{dW_\beta}{d\sigma} = w_\beta - iv_\beta = -\beta V_\infty \left\{\frac{(\sigma - r^2/\sigma)(1 + r^2/\sigma^2)}{[(\sigma - r^2/\sigma)^2 + 4r_0^2]^{1/2}} - 1\right\} \qquad (12.4.6)$$

For the surface of the body, provided that $\sigma = re^{i\theta}$, we have

$$w_\beta - iv_\beta = -\beta V_\infty \left[\frac{2r\sin\theta\,(1 + \cos 2\theta - i\sin 2\theta)\,i}{(4r_0^2 - 4r^2\sin^2\theta)^{1/2}} - 1\right] \qquad (12.4.7)$$

Hence

$$w_\beta = -\beta V_\infty \left\{\frac{2r\sin\theta\sin 2\theta}{[(s + r^2/s)^2 - 4r^2\sin^2\theta]^{1/2}} - 1\right\} \qquad (12.4.8)$$

$$v_\beta = \frac{2\beta r V_\infty \sin\theta\,(1 + \cos 2\theta)}{[(s + r^2/s)^2 - 4r^2\sin^2\theta]^{1/2}} \qquad (12.4.9)$$

Let us insert (12.4.8), (12.4.9), (12.2.22), (12.2.24), and (12.2.25) into formula (12.3.13). Having in view that $r\cos\theta = z$, we find

$$\bar{\Delta p}_{b(w)} = -4\alpha \frac{4\frac{z^2}{r^2}\frac{dr}{dx}\frac{r}{s} - \left(1+\frac{r^2}{s^2}\right)\left[2\frac{r}{s}\frac{dr}{dx} + \frac{ds}{dx}\left(1-\frac{r^2}{s^2}\right)\right]}{\left[\left(1+\frac{r^2}{s^2}\right)^2 - 4\left(\frac{z^2}{s^2}\right)\right]^{1/2}} + \frac{64\alpha\beta\frac{z^2}{s^2}\left(1-\frac{z^2}{r^2}\right)}{\left[\left(1+\frac{r^2}{s^2}\right)^2 - 4\frac{z^2}{s^2}\right]^{1/2}\left[\left(1-\frac{r^2}{s^2}\right)^2 + 4\frac{z^2}{s^2}\right]^{1/2}} \quad (12.4.10)$$

The first summand of this equation contains terms proportional to the derivatives dr/dx and ds/dx that characterize the influence of a change in the radius of the body and in the semispan of the panels, respectively. But both these derivatives do not affect the second summand due to sideslip and pitching. This interaction term proportional to the product $\alpha\beta$ determines the growth of the pressure-drop coefficient for the right half of the body. This coefficient decreases by the same amount on the left half of the body. This follows from formula (12.3.13) in which the component $v_{\beta,L}$ has to be taken with the opposite sign for the left half; this leads to the appearance of a negative sign in front of the second summand in (12.4.10).

To determine the pressure-drop coefficient for the starboard horizontal panel, we shall use formula (12.3.23), in which we find the velocity components $u_{\alpha,L}$, $w_{\alpha,L}$, and $w_{t,L}$ from expressions (12.2.34), (12.2.35), and (12.2.43), respectively. We find the component $w_{\beta,L}$ from (12.4.6), assuming that $\sigma = z$:

$$w_\beta = -\beta V_\infty \left\{\frac{z(1-r^4/z^4)}{[(z-r^2/z)^2+(s+r^2/s)^2]^{1/2}} - 1\right\} \quad (12.4.11)$$

The corresponding substitutions yield

$$\bar{\Delta p}_{w(b)} = 4\alpha \frac{\frac{r}{s}\frac{dr}{dx}\left[\left(1-\frac{r^2}{z^2}\right)^2 + 2\left(\frac{r^2}{s^2}-1\right)\right] + \frac{ds}{dx}\left(1-\frac{r^4}{s^4}\right)}{\left[1+\frac{r^4}{s^4} - \frac{z^2}{s^2}\left(1+\frac{r^4}{z^4}\right)\right]^{1/2}} + \frac{4\alpha\beta\frac{z^2}{s^2}\left(1-\frac{r^4}{z^4}\right)^2}{\left[\left(1+\frac{r^4}{s^4}\right)^2 - \frac{z^4}{s^4}\left(1+\frac{r^4}{z^4}\right)^2\right]^{1/2}} \quad (12.4.12)$$

This formula shows that the excess pressure on the starboard panel grows when it moves downward, and diminishes by the same amount on the port panel.

The pressure-drop coefficient for the upper and lower panels can be determined with a view to symmetry using relation (12.4.12)

in which y should be substituted for z, and interchanging the angles α and β. Hence, we obtain for the lower panel

$$\Delta\bar{p}_{w(b)} = 4\beta \frac{\frac{r}{s}\frac{dr}{dx}\left[\left(1-\frac{r^2}{y^2}\right)^2+2\left(\frac{r^2}{s^2}-1\right)\right]+\frac{ds}{dx}\left(1-\frac{r^4}{s^4}\right)}{\left[1+\frac{r^4}{s^4}-\frac{y^2}{s^2}\left(1+\frac{r^4}{s^4}\right)\right]^{1/2}} + \frac{4\alpha\beta\,\frac{y^2}{s^2}\left(1-\frac{r^4}{y^4}\right)^2}{\left[\left(1+\frac{r^4}{s^4}\right)^2-\frac{y^4}{s^4}\left(1+\frac{r^4}{y^4}\right)^2\right]^{1/2}} \qquad (12.4.13)$$

We shall assume the angles α and β to be positive. The pressure on the upper panel is determined by the same formula (12.4.13) provided that we consider the angle β to be positive and α negative. The second term with $\alpha\beta$ (the interaction term) is asymmetric for the lower and upper panels. The asymmetric term in (12.4.12) and (12.4.13) leads to the fact that although a normal force does arise on the panels, no additional normal force is created because of the asymmetry of the load.

Having in view that the total normal forces on the panels do not depend on the interaction terms, we can find the total normal force acting on the body-cruciform wing combination in sideslip by summing the forces acting on the two flat body-wing combinations in the flow at the corresponding angles

$$\alpha = \alpha_v \cos\varphi \text{ and } \beta = \alpha_v \sin\varphi$$

By analogy with (12.3.26), the normal force in the direction of axis Oy acting on the body-horizontal panel combination is

$$Y_{b,w} = 2\alpha\pi s_m^2 (1 - r_m^2 + r_m^4)\, q_\infty \qquad (12.4.14)$$

The normal (lateral) force acting on the body-vertical panel combination in a direction opposite to the positive sense of the axis Oz is

$$Z_{b,w} = -2\beta\pi s_m^2 (1 - r_m^2 + r_m^4)\, q_\infty \qquad (12.4.15)$$

The normal (lateral) force in the direction of the axis Oy' (see Fig. 12.3.1) is

$$Y' = Y_{b,w}\cos\varphi - Z_{b,w}\sin\varphi = 2\alpha_v\pi s_m^2 q_\infty (1-r_m^2+r_m^4)\cos^2\varphi + 2\alpha_v\pi s_m^2 q_\infty (1-r_m^2+r_m^4)\sin^2\varphi = 2\alpha_v\pi s_m^2 (1-r_m^2+r_m^4)\, q_\infty \qquad (12.4.16)$$

The normal (lateral) force in the direction of the axis Oz' equals zero. Indeed,

$$Z' = Y_{b,w}\sin\varphi + Z_{b,w}\cos\varphi = [2\alpha_v\pi s_m^2 q_\infty (1-r_m^2+r_m^4) - 2\alpha_v\pi s_m^2 q_\infty (1-r_m^2+r_m^4)]\sin\varphi\cos\varphi = 0 \qquad (12.4.17)$$

The results obtained point to an important property of a cruciform combination: *during the rotation of a craft, i.e. with sideslip, the normal force in a vertical plane parallel to the oncoming stream and passing through the longitudinal axis of the craft does not change.*

Interference Factors and Centre-of-Pressure Coefficients

Let us calculate the normal force and centre of pressure for a panel due to rolling. By expression (12.3.30), in which $[\Delta\bar{p}_{w(b)}]\,\varphi$ is determined by the second term in (12.4.12), we obtain

$$\Delta Y_{w(b)} = \frac{q_\infty}{\tan\varepsilon}\int_r^{s_m} dz \int_z^{s_m} [\Delta\bar{p}_{w(b)}]_\varphi\, ds = \frac{4\alpha_v^2 \sin\varphi\cos\varphi q_\infty}{\tan\varepsilon}$$

$$\times \int_r^{s_m} z^2\left(1-\frac{r^4}{z^4}\right)^2 dz \int_z^{s_m} \frac{ds}{s^2\left[\left(1+\frac{r^4}{s^4}\right)^2 - \frac{z^4}{s^4}\left(1+\frac{r^4}{z^4}\right)^2\right]^{1/2}}$$

Let us introduce the notation

$$\bar{s} = s^2/r^2, \quad \bar{z} = z^2/r^2 \tag{12.4.18}$$

in accordance with which

$$\Delta Y_{w(b)} = \frac{\alpha_v^2 r^2 q_\infty \sin\varphi\cos\varphi}{\tan\varepsilon}\int_1^{\bar{z}_m} \frac{(\bar{z}^2-1)^2\,d\bar{z}}{\bar{z}^{5/2}} \int_{\bar{s}}^{\bar{s}_m} \frac{\bar{s}^{1/2}\,d\bar{s}}{\sqrt{(\bar{s}^2-\bar{z}^2)(\bar{z}^2\bar{s}^2-1)}} \tag{12.4.19}$$

where $\bar{z}_m = \bar{s}_m = s_m^2/r^2$. Integration of (12.4.19) with respect to $\bar{s}$ yields

$$\int_{\bar{s}}^{\bar{s}_m} \frac{\bar{s}^{1/2}\,d\bar{s}}{\sqrt{(\bar{s}^2-\bar{z}^2)(\bar{z}^2\bar{s}^2-1)}} = \frac{1}{\sqrt{2\bar{z}(\bar{z}^2-1)}}\left[F_1(\psi_1,\ k_1)+F_2(\psi_2,\ k_2)\right] \tag{12.4.20}$$

where F_1 and F_2 are elliptic integrals of the second kind:

$$F(\psi,\ k) = \int_0^{\psi} \frac{d\varphi}{\sqrt{1-k^2\sin\varphi^2}}$$

which are evaluated provided that

$$\left.\begin{aligned} \sin\psi_1 &= \sqrt{1-\frac{\bar{s}_m^2(\bar{z}-1)^2}{(\bar{s}_m^2-1)^2\bar{z}}}, \quad k_1 = \frac{\bar{z}+1}{\sqrt{2(\bar{z}^2+1)}} \\ \sin\psi_2 &= \sqrt{1-\frac{\bar{s}_m^2(\bar{z}+1)^2}{(\bar{s}_m^2+1)^2\bar{z}}}, \quad k_2 = \frac{\bar{z}-1}{\sqrt{2(\bar{z}^2+1)}} \end{aligned}\right\} \tag{12.4.21}$$

In accordance with the result obtained, we have

$$\Delta Y_{w(b)} = \frac{\alpha_v^2 r^3 q_\infty \sin\varphi\cos\varphi}{\sqrt{2}\tan\varepsilon}\int_1^{\bar{s}_m}\frac{(\bar{z}^2-1)^{3/2}}{\bar{z}^3}$$

$$\times [F_1(\psi_1, k_1) + F_2(\psi_2, k_2)]\,\overline{dz} \qquad (12.4.22)$$

Numerical integration is needed to determine the normal force by (12.4.22). The found value of the normal force can be used to compute the interference factor by means of relation (12.3.31):

$$K_\varphi = \frac{\Delta Y_{w(b)}\tan\varepsilon}{Y_w\beta} = \frac{1}{\pi\sqrt{2}(\bar{s}_m-1)^2}\int_1^{\bar{s}_m}\frac{(\bar{z}^2-1)^{3/2}}{\bar{z}^3}$$

$$\times [F_1(\psi_1 k_1) + F_2(\psi_2, k_2)]\,\overline{dz} \qquad (12.4.23)$$

The results of calculating the value of K_φ are given in Table 12.3.2 and in the graph in Fig. 12.3.2. We can use the table or graph to find the difference between the values of K_φ for a flat and cruciform combinations that characterize the mutual interference of the lifting panels. The vertical panels in a cruciform combination *lower the interference* in comparison with a flat combination and decrease the factor K_φ.

Formulas (12.3.34)-(12.3.38) allow us to determine the position of the centre of pressure on the panels of a cruciform combination. The results are given in Table 12.3.2. A comparison of the data for a flat and cruciform combinations reveals that actually the centres of pressure in both cases coincide.

A comparison of the data with the results obtained for the absence of rolling (see Table 12.2.1) shows that for the forces produced by rolling a greater displacement of the centre of pressure is observed than for the interference forces arising at $\alpha \neq 0$ and $\beta = 0$ ($\varphi = 0$).

General Relations for the Forces and Moments

The relations obtained for the interference factors and centre-of-pressure coefficients allow us to calculate the coefficients of the forces and moments acting on a cruciform combination (see Fig. 12.4.1).

When investigating the influence of rolling on body-wing interference, it was established that the rolling angle produces additional asymmetric loads on the right and left half-bodies, and also on opposite panels and does not produce, therefore, an additional normal (lateral) force. This is why the flow over a body may be considered as the result of the addition of flows obtained at the

angles $\alpha = \alpha_v \cos \varphi$ and $\beta = \alpha_v \sin \varphi$. The forces produced here are also summed.

Accordingly, the normal force coefficient $c_{y,b,w}$ (in the plane of the angle α) is determined by formula (12.3.40), and the lateral force coefficient (in the plane of the angle β), by a similar expression

$$c_{z,b,w} = Z_{b,w}/(q_\infty S_w) = c_{z,b} + c^{\beta}_{z,w} (K_b + K_w) \beta \quad (12.4.24)$$

where $c_{z,b} = -c^{\alpha}_{y,b}\beta$ and $c^{\beta}_{z,w} = -c^{\alpha}_{y,w}$.

The coefficient of the pitching moment in the plane of the angle α is found by formula (12.3.41), and the coefficient of the yawing moment (in the plane of the angle β), by a similar relation

$$m_{y,b,w} = m_{y,b} - \{K_b [(c_p)_{\beta,b(w)} \bar{b}_0 + \bar{x}_w] + K_w [(c_p)_{\beta,w(b)} \bar{b}_0 + \bar{x}_w]\} c^{\beta}_{z,w}\beta \quad (12.4.25)$$

in which $m_{y,b} = -m^{\alpha}_{z,b}\beta$; $(c_p)_{\beta,b(w)} = (c_p)_{\alpha,b(w)}$; $(c_p)_{\beta,w(b)} = (c_p)_{\alpha,w(b)}$; and $c^{\beta}_{z,w} = -c^{\alpha}_{y,w}$.

Having determined the moments and normal forces, we can calculate the corresponding centre-of-pressure coefficients for the conditions of flow in the planes of α and β. For the aerodynamically symmetric cruciform combination being considered, these coefficients are identical and will be the same as for a flat combination.

Inspection of the data for a flat and cruciform combinations reveals that the centres of pressure of the additional forces produced by rolling coincide in both cases. A comparison with the results obtained in the absence of rolling shows that a larger displacement of the centre of pressure occurs in sideslip.

Let us consider the coefficient of the normal force in the plane of the angle α_v. On the basis of formulas (12.3.47)-(12.3.49), and (12.4.24), and using the value of $c^{\beta}_{z,w} = -c^{\alpha}_{y,w}$, we have

$$c_{y',b,w} = c^{\alpha}_{y,w} (K_b + K_w) \alpha_v \quad (12.4.26)$$

By (12.4.17), the lateral force coefficient $c_{z',b,w} = 0$. The total rolling moment of a cruciform combination is also zero because the vertical panels produce a rolling moment of the same magnitude as the horizontal ones, but in the opposite direction.

We remind our reader that the problems being considered in this chapter are being solved within the scope of the linearized theory for slender bodies whose aerodynamic properties do not depend on the number M_∞ and, in addition, no account is taken of the effect due to viscosity. If "non-slender" bodies are being investigated even within the scope of the above-mentioned theory, or if account is taken of the viscosity leading to flow separation, a lateral (normal) force and a rolling moment appear that are due to the redistribution of the pressure.

Wings or an empennage may be arranged on a body so that a tail portion of the body of some length is behind them. In this connection, we must note that for thin combinations, the length of the body after a wing does not affect the normal force and the position of the centre of pressure of the body. The explanation is that according to the aerodynamic theory of a slender body, the load induced by the wing extends onto the body in the direction of the diameter *DD* (see Fig. 12.2.5), and, consequently, the area onto which the normal force acts is directly under the panels (in Fig. 12.2.5—the hatched region).

Influence of Compressibility on Aerodynamic Interference

The results of calculating the interference factors for combinations including slender bodies and panels may be used as the basis of a method for determining the normal force of craft consisting of non-slender elements. This method consists in calculating an aerodynamic coefficient for such configurations according to the interference factor found from the slender body theory (see Tables 12.2.1 and 12.3.2) and to the aerodynamic coefficient of an isolated wing taken from the linearized theory. By this method, the additional coefficients of the normal force due to interference are

$$\Delta c_{y,\,w(b)} = K_w c_{y,\,w}; \quad \Delta c_{y,\,b(w)} = K_b c_{y,\,w} \qquad (12.4.27)$$

Here $c_{y,\,w}$ is determined with a view to the number M_∞ by the linearized theory of flow over a wing.

The interference factors may be calculated up to values of $M_\infty \approx$ $\approx$ 1-1.5 using the relations given above without account of compressibility, taking into consideration their change only depending on the taper ratio of the wing panels, the thickness of the boundary layer, and on the location along the length of the body.

When the flow velocities grow, the interference becomes more and more dependent on compressibility. This relation can be expressed, particularly, in terms of the change in the relative boundary layer displacement thickness $\bar{\delta}^* = \delta^*/r$ in (12.2.76) depending on the number M_∞ in accordance with (13.6.23′).

The interference factor is also directly affected by the compressibility, which can be taken into consideration by means of the correction factor

$$\nu_f = K_w/(K_w)_{th} = K_b/(K_b)_{th} = \exp\,[0.05\,(1 - M_\infty)] \qquad (12.4.28)$$

suitable for $M_\infty \leqslant 5$. Equation (12.4.28) is used to refine the values of the interference factors given by (12.2.78):

$$K_w = (K_w)_{th}\nu_\eta\nu_{bl}\nu_l\nu_f; \quad K_b = (K_b)_{th}\nu_\eta\nu_{bl}\nu_l\nu_f \qquad (12.4.29)$$

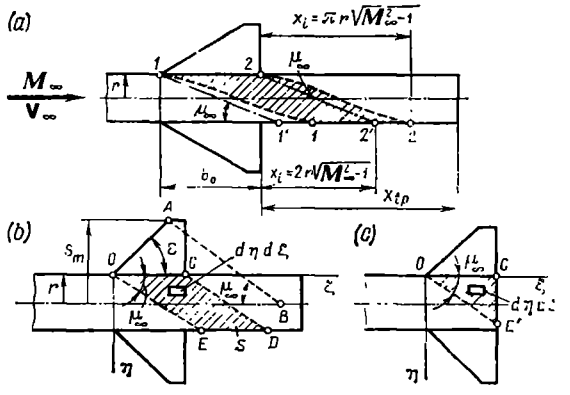

Fig. 12.4.2
Region of influence of a wing on a body for a non-slender configuration in a supersonic linearized flow:
a, b—plane models of configuration with the tail part having curved (helical) and straight Mach lines, respectively; *c*—model without a tail part with straight Mach lines

It has been noted that for slender combinations, the length of the body after the wing does not affect the normal force and the position of the centre of pressure. For non-slender combinations, however, this influence may be appreciable.

Unlike a slender configuration for which the load induced by the wing extends to the portion of the body directly under it, for a non-slender body the disturbance waves from the wing extend to a region of the body after the wing. For each panel, this region is between the helical lines *1-1* and *2-2* issuing from the beginning and end of the root chord and intersecting the body generatrices at the Mach angle $\mu_\infty = \cot^{-1}\sqrt{M_\infty^2 - 1}$ (Fig. 12.4.2). In a simplified way, such a region can be considered as a portion of a plane surface confined on the body by straight Mach lines issuing from points on the leading and trailing edges of the wing (lines *1-1'* and *2-2'* in Fig. 12.4.2*a*). If the length of the tail part of the body x_{tp} after the wing is long enough ($x_{tp} > x_i = 2r\sqrt{M_\infty^2 - 1}$), the interference effect is maximum and, consequently, the normal force induced by the wing is transferred to the body completely. With a short tail section ($x_{tp} < x_i$), a fraction of this force is not realized because the dimensions of the region of normal force transfer to the body are reduced. As a result, the interference factor K_b decreases. It can be evaluated by the formula

$$K_b = (K_b)_{th} \nu_\eta \nu_{bl} \nu_l \nu_f F \qquad (12.4.30)$$

where

$$F = 1 - d\,[\Phi_1(z_1) - \Phi_2(z_2)] \qquad (12.4.31)$$

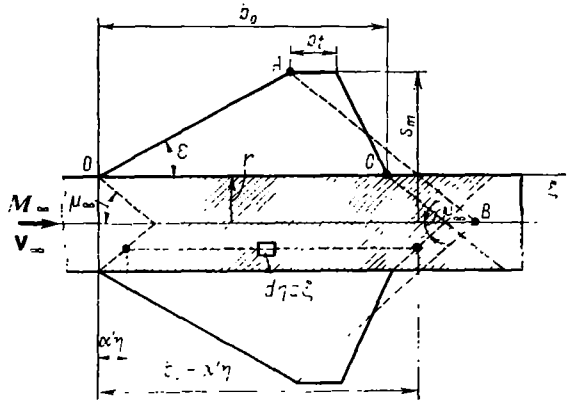

Fig. 12.4.3
Plane model for calculating the normal force with a view to wing-body interference

while $\Phi_1(z_1)$ and $\Phi_2(z_2)$ are Laplace-Gauss functions determined from the relevant tables according to the following arguments:

$$z_1 = \frac{b_0 + x_{tp}}{x_1}\left[2\left(4 + 1/\eta_w\right)\left(1 + 8r_m^2\right)\right]^{1/2}; \quad z_2 = z_1 \frac{x_{tp}}{b_0 + x_{tp}} \tag{12.4.32}$$

The parameter d in (12.4.31) is

$$d = 0.866\left[\left(b_0/x_1\right)^2\left(4 + 1/\eta_w\right)\left(1 + 8r_m^2\right)\right]^{-1/2} \tag{12.4.32'}$$

In the above relations, the value of x_1 may be taken equal to $x_1 = 2r\sqrt{M_\infty^2 - 1}$ or (for a somewhat greater accuracy of the calculations) to $x_1 = \pi r\sqrt{M_\infty^2 - 1}$ (assuming a helical Mach line).

The interference factor K_b, the coordinate of the centre of pressure on the body with a view to compressibility, the length of the tail part of the body, and the taper ratio of the panel can be determined directly if the region of normal force transfer is considered in the form of a portion of a plane surface (Fig. 12.4.2).

Here the flow is calculated like that near an isolated triangular semi-infinite wing. By (8.3.31), the coefficient of the pressure drop induced by a wing with a supersonic leading edge on the portion between the Mach lines issuing from the beginning and end of the root chord (Fig. 12.4.3, the hatched region) is

$$\Delta\bar{p} = \bar{p}_L - \bar{p}_u = \frac{4\alpha_w \tan\varepsilon}{\pi\sqrt{\alpha'^2\tan^2\varepsilon - 1}} \cos^{-1}\frac{1 + \alpha'^2\left(\eta/\xi\right)\tan\varepsilon}{\alpha'\left(\tan\varepsilon + \eta/\xi\right)} \tag{12.4.33}$$

where α_w is the angle of attack of the wing, and η, ξ are the coordinates shown in Figs. 12.4.2 and 12.4.3.

The coefficient of the pressure drop induced by a wing with a subsonic leading edge is (see [14])

$$\Delta\bar{p} = \bar{p}_{\mathrm{L}} - \bar{p}_{\mathrm{u}} = \frac{8\alpha_{\mathrm{w}}(\alpha' \tan\varepsilon)^{3/2}}{\pi\alpha'(\alpha' \tan\varepsilon + 1)} \cdot \sqrt{\frac{1-\alpha'\eta/\xi}{\alpha'(\tan\varepsilon + \eta/\xi)}} \qquad (12.4.34)$$

Formulas (12.4.33) and (12.4.34) may be applied for conditions when the Mach line issuing from point A on the wing tip passes behind point C of the trailing edge on the body, i.e. the tip does not affect the region of transfer of the normal force. These conditions are fulfilled (Fig. 12.4.3) if

$$\frac{\alpha'(s_m - r)}{b_0}\left(1 + \frac{1}{\alpha' \tan\varepsilon}\right) \geqslant 1 \qquad (12.4.35)$$

For a combination with a tail part, the elementary normal force acting on the portion of the body under the wing is

$$dY = \Delta\bar{p} q_\infty \, d\eta \, d\xi \qquad (12.4.36)$$

where $d\eta \, d\xi$ is an elementary area of this portion of the body (Fig. 12.4.3).

The coefficient of the normal force related to the area of the two separate panels is:

for a supersonic sweptback edge

$$\Delta c_{y,\mathrm{b(w)}} = \frac{Y}{q_\infty S_{\mathrm{w}}} = \frac{2\iint_{(S)} \Delta\bar{p} \, d\eta \, d\xi}{(s_m - r)(b_0 + b_{\mathrm{t}})}$$

$$= \frac{8\alpha_{\mathrm{w}} \tan\varepsilon}{\pi\sqrt{\alpha'^2 \tan^2\varepsilon - 1}\,(s_m - 1)(1 + b_{\mathrm{t}}/b_0) r b_0} \times \int_0^r d\eta \int_{\alpha'\eta}^{b_0 + \alpha'\eta} \cos^{-1}\frac{1 + (\eta/\xi)\alpha'^2 \tan\varepsilon}{\alpha'(\tan\varepsilon + \eta/\xi)} \, d\xi \qquad (12.4.37)$$

for a subsonic sweptback edge

$$\Delta c_{y,\mathrm{b(w)}} = \frac{16(\alpha' \tan\varepsilon)^{3/2}\alpha_{\mathrm{w}}}{(s_m - 1)(1 + b_{\mathrm{t}}/b_0)(\alpha' \tan\varepsilon + 1)\pi\alpha' r b_0} \times \int_0^r d\eta \int_{\alpha'\eta}^{b_0 + \alpha'\eta} \sqrt{\frac{1-\alpha'\eta/\xi}{\alpha'(\tan\varepsilon + \eta/\xi)}} \, d\xi \qquad (12.4.38)$$

For a configuration without a tail part of the body after the wing, the normal force should be computed with the aid of the same formulas (12.4.37) and (12.4.38), but with the value b_0 taken instead of $b_0 + \alpha'\eta$ as the upper limit of the second integral.

The interference factor K_{b} for the plane model being considered is calculated by formula (12.2.11) in which $c_{y,\mathrm{w}}$ is determined according to the linearized theory for a separate wing (see Sec. 8.1).

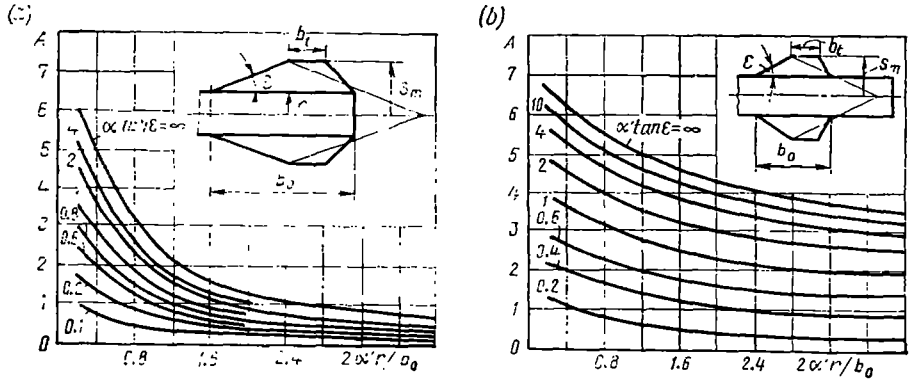

Fig. 12.4.4
Curves characterizing the interference factor K_b for a flat body-wing configuration:
a—body without a tail part; *b*—body with a tail part

By analogy with the determination of the normal force, we can compute the longitudinal moment of the forces induced by the wing on the body about an axis passing through the vertex of a panel and then find the corresponding coordinate of the centre of pressure:

$$(x_p)_{\alpha,b(w)} = \frac{\Delta M_{z,b(w)}}{\Delta Y_{b(w)}}$$

$$= \int_0^r d\eta \int_{\alpha'\eta}^{b_0+\alpha'\eta} \xi \Delta\bar{p}\, d\xi \Big/ \int_0^r d\eta \int_{\alpha'\eta}^{b_0+\alpha'\eta} \Delta\bar{p}\, d\xi \qquad (12.4.39)$$

We use this coordinate to find the centre-of-pressure coefficient:

$$(c_p)_{\alpha,b(w)} = (x_p)_{\alpha,b(w)}/b_0$$

The corresponding calculations have been performed for craft with and without a tail part of the body after the wing (see Fig. 12.4.2). The results of these calculations plotted in Fig. 12.4.4 indicate an increase in the interference factors K_b for a craft with a tail part after the wing. The presence of this part (Fig. 12.4.5) also leads to displacement of the centre of pressure backward, this position depending only slightly on the sweep angle of the panel.

The data in Figs. 12.4.4*a* and 12.4.5*a* relate to a body-wing combination without a tail part ($x_{tp} = 0$), and in Figs. 12.4.4*b* and 12.4.5*b*, to a combination with a body tail part whose length is at least x_1 (i.e. $x_{tp} \geqslant x_1 = 2r\sqrt{M_\infty^2 - 1}$). For a shorter tail part

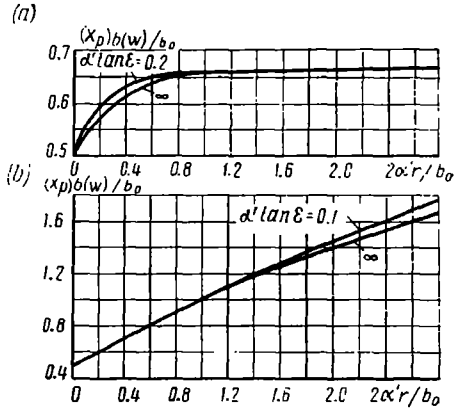

Fig. 12.4.5
Coordinates of the centre of pressure for a flat body-wing configuration:
a–body without a tail part;
b–body with a tail part

($x_{tp} < x_t$), the interference factors and centre-of-pressure coefficients can be determined by linear interpolation:

$$K_b = K_{b0} + (K_{b1} - K_{b0})\, x_{tp}/x_t \qquad (12.4.40)$$

$$(c_p)_{\alpha, b(w)} = (c_p)_{\alpha, b(w)0} + [(c_p)_{\alpha, b(w)1} - (c_p)_{\alpha, b(w)0}]\, x_{tp}/x_t \qquad (12.4.41)$$

where the parameters with the subscripts "0" and "1" correspond to lengths of the tail part of the body equal to $x_{tp} = 0$ and $x_{tp} = x_t = 2r\sqrt{M_\infty^2 - 1}$, respectively. We determine the interference factors from the general expression

$$K = A\,[\alpha' c_{y,w}^{\alpha}\,(1 + 1/\eta_w)\,(\bar{s}_m - 1)]^{-1} \qquad (12.4.42)$$

where we find A from graphs (Figs. 12.4.4 and 12.4.5). According to these graphs, an increase in $\alpha' \tan \varepsilon$ is attended by a growth in the interference factors. The opposite effect is observed when the quantity $2\alpha' r/b_0$ increases.

The influence of the tail part increases as M_∞ grows because as a result of the greater Mach cone angles, there is a larger transfer area within the Mach cones whose apexes coincide with the intersection points of the wing panel trailing edge and the body generatrix.

Influence of Flow Stagnation

The aerodynamic calculations of a body-wing combination considered above were performed while assuming that the wing is in a flow that does not practically differ from an undisturbed one. The corresponding velocity head was evaluated from the parameters of this flow, i.e. $q = q_\infty = kp_\infty M_\infty^2/2$. All the aerodynamic coefficients correspond to this value of the velocity head.

An actual flow is characterized by stagnation of the flow ahead of a wing that must be taken into consideration when determining the aerodynamic parameters. The degree of this stagnation can be characterized by the **mean stagnation coefficient** $k_1 = q/q_\infty$, for which the velocity head $q = kpM_1^2/2$ is found from an averaged value of the number M_1 of the disturbed flow ahead of the wing. Assuming the pressures in the disturbed and undisturbed flows to be the same ($p = p_\infty$), the mean stagnation coefficient can be expressed as $k_1 = M_1^2/M_\infty^2$. The change in this coefficient is negligibly small at subsonic velocities, but is appreciable for a flow at large numbers M_∞. The value of k_1 depends on the nature and strength of the shocks occurring ahead of the nose.

If the wing is at a distance of $x_w > (1.5\text{-}2)\, x_{mid}$ from the tip of the nose having the form of a cone with a semi-apex angle $\beta_c < \beta_{c,cr}$ (where $\beta_{c,cr}$ is the critical value of this angle), then k_1 can be determined from the condition that the pressure ahead of the wing is $p = p_\infty$. The following value of the square of the Mach number corresponds to this pressure:

$$M_1^2 = \frac{2}{k-1}\left[\left(\frac{p_0'}{p_\infty}\right)^{(k-1)/k} - 1\right] \qquad (12.4.43)$$

where p_0' is the stagnation pressure behind an oblique shock. The ratio p_0'/p_∞ can be taken equal to $(p_0'/p_0)\, p_0/p_\infty$, expressing it in terms of the pressure of isentropic stagnation. Introducing the symbol $\nu_0 = p_0'/p_0$, we obtain

$$\frac{p_0'}{p_\infty} = \nu_0\left(1 + \frac{k-1}{2} M_\infty^2\right)^{k/(k-1)}$$

Accordingly,

$$k_1 = \frac{M_1^2}{M_\infty^2} = \frac{2}{M_\infty^2 (k-1)} \cdot \left[\nu_0^{(k-1)/k}\left(1 + \frac{k-1}{2} M_\infty^2\right) - 1\right] \qquad (12.4.44)$$

The ratio of the stagnation pressures is found with the aid of formula (10.2.26) or of the approximate relation (see [13])

$$\nu_0 = \left(\frac{k+1}{2}\right)^{(k+1)/(k-1)} \left(\frac{x^2}{1 + [(k-1)/2]\, x^2}\right)^{k/(k-1)} \times \left(kx^2 - \frac{k-1}{2}\right)^{-k/(k-1)} \qquad (12.4.45)$$

in which

$$x = 1 - \cos\beta_c + \left(1 + \frac{k-1}{2} M_\infty^2 \sin^2\beta_c\right)^{1/2} \qquad (12.4.46)$$

If the nose part differs from a conical one, the stagnation coefficient can be calculated as follows. First we find the wave drag coefficient $c_{x,w}$ for the given nose from the relevant aerodynamic relations, next we use approximating formula (10.2.31) to evaluate

the corresponding semi-apex angle β_c of a conditional conical surface with which we replace the given nose. After this, we calculate the quantity $M_\infty \sin \beta_c$ and then the parameters x, ν_0 and the coefficient k_1. This coefficient allows us to refine the aerodynamic characteristics computed with account of interference. For example, the normal force coefficient for a body-wing combination is determined as

$$c_{y,b.w} = c_{y,b} + (K_b + K_w)\, c_{y,w} k_1 \qquad (12.4.47)$$

where it is good to calculate $c_{y,w}$ according to the linearized theory. Such calculation may be performed using the refined value of $M_1 < M_\infty$ instead of M_∞.

12.5. Influence of Wing Shape and Number M_∞ on the Flow Parameters in Roll

Normal Force

The derivative of $c_{y,w}$ in formula (12.3.33′) can be calculated by the linearized theory. This allows us to take into consideration the influence of the number M_∞ and also of the shape of the wing (empennage) on the normal force in roll to a certain extent. But as we have already pointed out, the interference factor K_φ does not depend on these parameters, and, consequently, formula (12.3.33′) does not reflect completely all the features of flow over a wing in roll. Particularly, by this formula, the sign of the additional normal force does not change, although more accurate calculations show that such a change does occur. For example, at some sweep angles, the normal force acts in the opposite direction. This drawback of the linear theory can be compensated by using the relation (Fig. 12.5.1)

$$\Delta c_{y,w(b)} = c_{y\chi} = \Delta c_{y\ w} K_w k_1 \qquad (12.5.1)$$

in which the coefficient of the normal force for an isolated (separate) wing panel is

$$\Delta c_{y,w} = \Delta Y_w / (q_\infty S_{w(b)}/2)$$
$$= 2\alpha\beta \tan \chi_{1/2} c^{\alpha}_{y,w} [1 - B_1 + 0.5 B_2 (1/\tan^2 \chi_{1/2} - 1)] \qquad (12.5.2)$$

Here B_1 and B_2 are coefficients that are functions of the parameters $\lambda_w \sqrt{M^2_\infty - 1}$ and $\lambda_w \tan \chi_{1/2}$ (Fig. 12.5.2). A glance at expression (12.5.2) reveals that at small sweep angles ($\tan \chi_{1/2} \ll 1$) and sufficiently large numbers M_∞ (at which $B_1 = 1$ and $B_2 < 0$), the sign of the normal force may change to the opposite one.

The area $S_{w(b)}$ in (12.5.2) is evaluated for isolated panels with account taken of their part under the body; the quantity $\tan \chi_{1/2}$ is the tangent of the sweep angle based on one half of the chord (see Fig. 12.5.1).

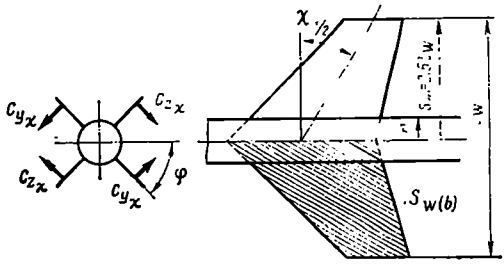

Fig. 12.5.1
Forces acting in rolling

A

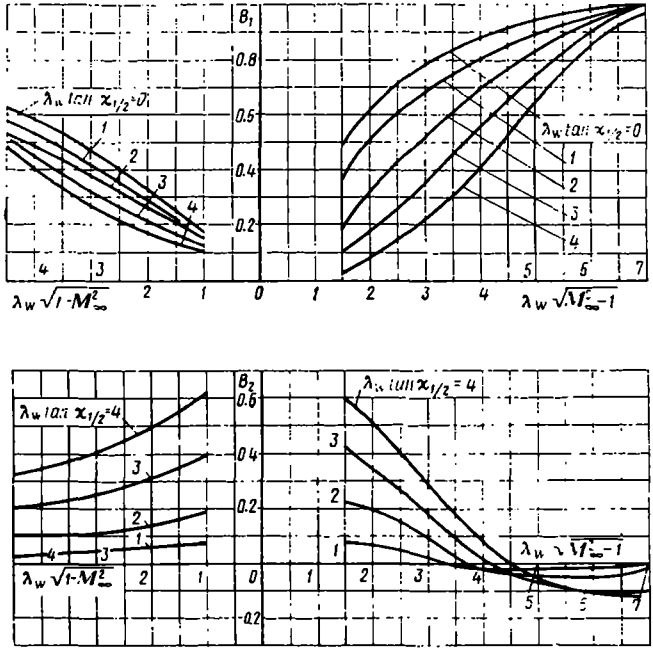

Fig. 12.5.2
Graphs for determiuing the coefficients B_1 and B_2

The expressions obtained for the normal forces produced in roll by the horizontal panels of the empennage may be related both to cruciform stabilizers and to a body-wing combination. With a cruciform empennage, the symmetric vertical panels produce lateral forces similar to the normal forces of the horizontal lifting surfaces. Since the sideslip angle for the vertical panels is α, and the angle of attack is $-\beta$, for any combination of these angles we have $c_{z,\chi}=$

$= -c_{y,\chi}$. Accordingly, the normal and lateral forces acting on the lower and upper panels are directed toward one another (see Fig. 12.5.1).

Moment

Relation (12.3.46) obtained on the basis of the aerodynamic theory of a slender body may be applied for triangular panels in a flow with small Mach numbers ($M_\infty \approx 1$). A noticeable shortcoming of this relation is that it does not reflect the possibility of a change in the sign of the rolling moment when the number M_∞ and the shape of a panel change. Using the value of the normal force coefficient (12.5.1), we can obtain a formula that allows us to establish the corresponding change in the sign of this moment:

$$m_{x,\chi} = M_{x,\chi} / (q_\infty S_{w(b)} l_w)$$
$$= -0.5\, \Delta c_{y,w} K_w [r_m + (1 - r_m)(\bar{z}_p)_{\Phi,w(b)}] \qquad (12.5.3)$$

where $l_w = 2S_m$ is the wing span, and $\Delta c_{y,w}$ is the normal force coefficient determined by (12.5.2).

Examination of (12.5.2) and (12.5.3) reveals that at small sweep angles ($\tan \chi_{1/2} \ll 1$) and sufficiently large numbers M_∞ ($B_1 \approx 1$ and $B_2 < 0$) the sign of the moment may become positive. This indicates that a destabilizing moment is produced in rolling.

When a straight wing tip is present, an additional rolling moment appears, which facilitates the increase of lateral static stability. The reason is that such a tip upon sideslip of the craft is, as it were, a portion of the leading edge. It has been established experimentally that with a known approximation the coefficient of the additional moment is

$$m_{x,t} = -\frac{0.04\alpha\beta}{(\eta_w + 1)^3} \cdot \frac{c_{y,w}}{\lambda_w} \qquad (12.5.4)$$

This formula may be applied for subsonic and small supersonic velocities. The total rolling moment coefficient is

$$m_x = m_{x,\chi} + m_{x,t}$$

and the corresponding mixed derivative with respect to $\alpha\beta$ is

$$m_x^{\alpha\beta} = (m_{x,\chi}] + m_{x,t})/(\alpha\beta) \qquad (12.5.5)$$

Panels with rounded tips do not produce an additional rolling moment in sideslip, i.e. the total derivative is $m_x^{\alpha\beta} = m_{x,\chi}^{\alpha\beta}$.

In a cruciform (plus-shaped) combination, the panels produce the lateral forces $c_{z,\chi} = -c_{y,\chi}$ whose moment is equal in magnitude, but opposite in sign to the moment of the horizontal panels. Hence, the total rolling moment of such a combination is zero.

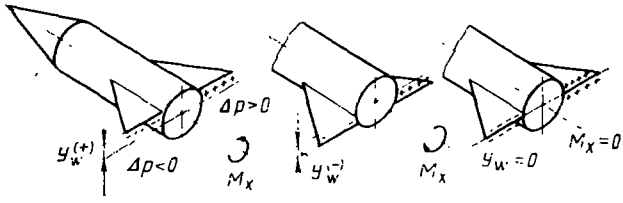

Fig. 12.5.3
Body-empennage interference

Wing-Body Interference

In definite conditions, such interference may cause an additional rolling moment of a lifting surface. This occurs, for example, with an upper or lower arrangement of a wing or empennage (Fig. 12.5.3). In the first case, the moment is due to the additional overpressure of the air on the lower side of the starboard panel ($\Delta p = p - p_\infty > 0$) and lowering of the pressure in the zone where the body joins the port panel ($\Delta p < 0$). This moment tilts the craft to the left. In the second case, the direction of the moment is reversed because an increased pressure arises over the starboard panel and a reduced one over the port panel. It is obvious that upon central arrangement of the lifting surface ($y_w = 0$), no additional rolling moment appears.

Investigations show that the produced rolling moment due to the off-centre arrangement of the wing (empennage) can be calculated approximately as follows:

$$m_{x_1} = -0.22 r_m^{3/2} c^{\alpha}_{y,w} \beta \sin(\pi y_w/2) \qquad (12.5.6)$$

where $y_w = y_w/r$.

It follows from (12.5.6) that upon upper arrangement of the panels ($y_w > 0$), a stabilizing rolling moment is produced, and upon lower arrangement ($y_w < 0$), a destabilizing one.

Influence of V-Shape

When a lifting V-shaped surface is installed at an angle ψ (the angle between the plane of the panel and the axis Oz) in sideslip ($\beta \neq 0$, $\alpha = 0$), the starboard panel is at the local angle of attack $\Delta\alpha_{st} = \beta\psi$, and the port one, at an angle of the same magnitude, but with the opposite sign, i.e. $\Delta\alpha_{pt} = -\beta\psi$ (Fig. 12.5.4). The additional normal force due to this angle of attack is

$$Y_\psi = c^{\alpha}_{y,w} \beta\psi K_\psi \, (S_{w(b)}/2) \, q$$

and the corresponding force coefficient is

$$c_{y,\psi} = Y_\psi/(q_\infty S_{w(b)}/2) = \pm c^{\alpha}_{y,w} \beta\psi K_\psi k_1 \qquad (12.5.7)$$

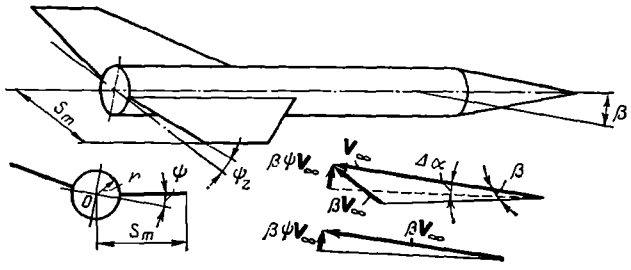

Fig. 12.5.4
Influence of a lateral V-shape on the rolling moment

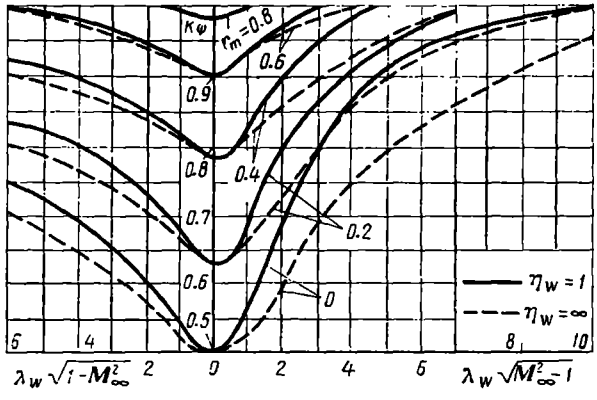

Fig. 12.5.5
Graphs for determining the factor K_ψ

where the plus sign related to the starboard panel, and the minus, to the port one; K_ψ is the **interference factor** characterizing the mutual influence of the panels.

The values of the factor K_ψ as a function of the relative radius $r_m = r/s_m$ and the parameter $\lambda_w\sqrt{M_\infty^2 - 1}$ (or $\lambda_w\sqrt{M_\infty^2 k_1 - 1}$) for a rectangular and triangular panels ($\eta_w = 1$ and ∞) are given in Fig. 12.5.5.

The coefficient of the rolling moment related to the wing (empennage span $l_w = 2S_m$ is found from the expression

$$m_{x,\psi} = M_{x,\psi}/(q_\infty S_{w(b)} l_w)$$
$$= -0.5 c^{\alpha}_{y,w}\beta\psi K_\psi k_1 [r_m + (1 - r_m)(\bar{z}_p)_{\psi,w(b)}] \qquad (12.5.8)$$

This formula shows that a V-shaped lifting surface with a positive angle ψ always has lateral static stability (the sign of the moment is negative). A reduction of this angle lowers the stability, while

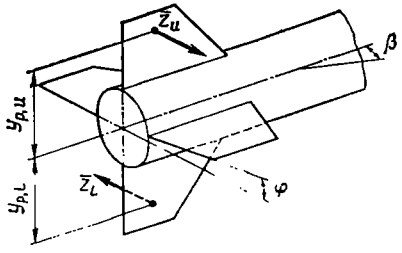

Fig. 12.5.6
Diagram showing how a rolling moment is produced with an asymmetric vertical wing (empennage)

an inverted V-shape may also lead to static instability. Stability is restored by employing lifting surfaces with a sufficiently large sweep.

Asymmetric Vertical Wing (Empennage)

Some kinds of craft may have a vertical wing (empennage) of an asymmetric shape (Fig. 12.5.6). In this case, it produces an additional rolling moment so that unlike a symmetric cruciform (plus-shaped) combination, its total magnitude does not equal zero. The additional rolling moment, opposite in sign to the moment produced by the horizontal wing (empennage), is

$$M_{x,u,L} = \Delta M_{x\,u} + \Delta M_{x,L} = Z_u y_{p,u} + Z_L y_{p,L}$$

where the lateral forces calculated from the relative area of the upper and lower panels with account taken of the part under the body $[S_{w(b,u)}, S_{w(b,L)}]$ are found from the relations

$$Z_u = \Delta c_{z\,w(u)} K_{w(u)}\, qS_{w(b,u)}, \qquad Z_L = \Delta c_{z,w(L)} K_{w(L)} qS_{w(b,L)}$$

Here we take the lateral force coefficients the same as the coefficients $\Delta c_{y,w}$ calculated by (12.5.2) in accordance with the values of the areas of the upper and lower panels $[S_w = S_{w(u)}, S_{w(L)}]$; we determine the coordinates $y_{p,u}$ and $y_{p,L}$ of the centres of pressure like the distances $(z_p)_{\varphi,w(b)}$ to the centre of pressure of a horizontal wing (empennage); we find the interference factors $K_{w(u)}$ and $K_{w(L)}$ from the values of $r/s_{m,u}$ and $r/s_{m,L}$ as for a horizontal wing.

The coefficient of the additional rolling moment calculated for a characteristic area S and length x_b is

$$m_{x,u,L} = M_{x,u,L}/(q_\infty S x_b) = [\Delta c_{z\,w(u)} K_w S_{w(b,u)} y_{p,u} + \Delta c_{z\,w(L)} K_{w(L)} S_{w(b,L)} y_{p,L}]\, k_1/(Sx_b) \qquad (12.5.9)$$

Influence of Vortices Forming on a Body

Separation of the boundary layer developing on the upper (lee) side of a body belonging to a cruciform configuration of a craft at a small angle of attack and with a small sideslip is insignificant.

For this reason, it does not virtually affect the rolling moment whose magnitude may be taken equal to zero. Separation has the same negligibly small influence on the rolling moment of a flat combination consisting of a body and wing (empennage).

Upon strong deviation of the craft, however, separation of the boundary layer becomes significant and determines the free-stream force action. The separated boundary layer produces a non-uniform wash of the flow in the zone of the wing (empennage). As a result, the carrying capacity of the wing (empennage) panels changes. In a flat combination, this leads to a change in the rolling moment in comparison with that in the absence of separation, while in a cruciform one this produces an additional moment other than zero. The coefficient of this moment can be written as the approximating relation

$$m_{x,v} = A\,(\beta^2 - \alpha^2)\,\alpha\beta k_1 \qquad (12.5.10)$$

where A is a function of the geometric parameters of the wing (empennage) and the number $M_1 = M_\infty \sqrt{k_1}$.

The function A can be determined experimentally for a flat or cruciform combination at fixed values of α and β and with changing geometric parameters and number M_1. The angle of attack and the sideslip angle must be large ($\alpha, \beta > 15°$) because when they are small the effect of vortex influence on the body vanishes.

Total Rolling Moment

In accordance with the relations obtained for the rolling moment components, its total value for a flat craft combination can be written as

$$m_x = m_{x\,1} + m_{x\,\psi} + m_{x,u,L} + m_{x\,\chi} + m_{x\,t} + m_{x\,v} \qquad (12.5.11)$$

By calculating the derivatives with respect to β of the corresponding moment coefficients and taking into account the quantity $m_x^\beta \alpha = m_x^\gamma$ determining the degree of static lateral stability (see Sec. 1.4), we obtain

$$m_x^\gamma = (m_{x,1}^\beta + m_{x,\psi}^\beta + m_{x,u,L}^\beta)\,\alpha + (m_{x,\chi}^\beta + m_{x,t}^\beta)\alpha + A\,(3\beta^2 - \alpha^2)\,k_1\alpha^2 \qquad (12.5.12)$$

When analysing lateral stability by this formula, one should have in view that all the partial derivatives and also the quantity Ak_1 are functions of the geometric parameters of the wing (empennage) and M_∞. The degree of this stability is not the same for different angles of attack; at small values of the angles, it is not large, while at large values it becomes quite significant. This is especially noticeable for lifting surfaces with a large sweep. To diminish the

excessive lateral stability, such surfaces are given a zero or even a negative (inverted) V-shape. For wings (empennage) without sweep, conversely, a decrease in the stability is observed. To increase it, lifting V-shaped surfaces are used with a positive angle ψ of inclination of the panels.

Separation of the boundary layer may affect lateral stability differently. Considering the second term in (12.5.10), we can see that at positive values of α and A and at sideslip angles $\beta < \alpha$ an additional restoring rolling moment appears; at large values of the sideslip angle ($\beta > \alpha$), the sign of the moment reverses. All these features of vortex action on rolling motion can be studied in detail experimentally.

12.6 Wing-Empennage Interference

General

If there are no other lifting or control surfaces ahead of the empennage on a body, the body-empennage interaction is calculated in the same way as for a wing-body combination. If there is a wing ahead of the empennage on a body, the additional influence of the wing must be taken into consideration when determining the aerodynamic properties of the empennage and the body. This also relates to a canard craft in which the empennage is ahead of the wing.

Let us consider the physical nature of the interaction between an empennage and a wing ahead of it. The vortex sheet cast off the wing and passing near the empennage causes a wash, as a result of which the angle of attack decreases, and, consequently, the lift force of the empennage panels lowers.

The wash at any point of space behind a wing is determined by the angle $\varepsilon = -w/V_\infty$ computed according to the vertical component of the velocity w induced by the vortex sheet cast off the wing (Fig. 12.6.1). As we already know, for an isolated wing the angle ε at a point of space in question depends on its geometric and aerodynamic properties. For a wing-body combination, the influence of interference must also be taken into account when determining this angle. Owing to its action, a wing attached to a body produces a greater wash. Such a wing owing to interaction with the body has a greater normal force than an isolated wing. Upon a growth in its value, the vortex sheet cast off the wing will be stronger, inducing higher velocities and a greater wash behind it.

Let us assume that the part of the body behind the wing has a constant diameter, therefore the vortex sheet is in the plane of the wing. Experimental investigations show that this assumption can be made as a first approximation for a very thin body-wing combination. In these conditions, the flow behind the wing is paral-

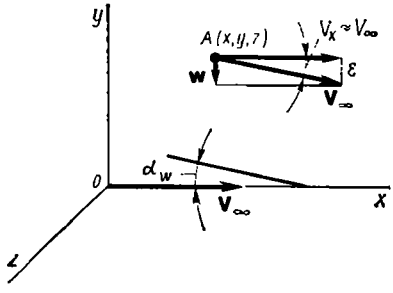

Fig. 12.6.1
Formation of a wash behind a wing

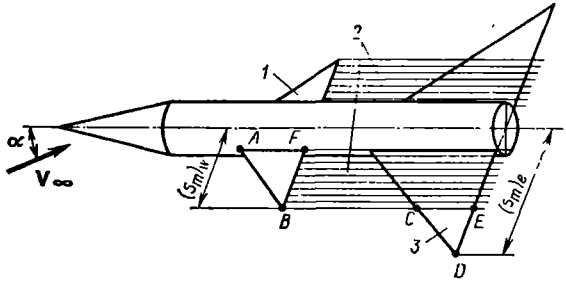

Fig. 12.6.2
Wing-empennage interference for a thin combination:
1 – wing; 2 – vortex sheet; 3 – empennage

el to an empennage chord if the wing and empennage are arranged on the body along the same generatrix and at the same setting angles (Fig. 12.6.2).

Hence, the parts of the empennage with a span equal to that of the wing have no normal force. The remaining part of the empennage panel with a span of $(s_m)_e - (s_m)_w$ [here $(s_m)_w$ is the span of a wing panel and $(s_m)_e$ is that of the empennage] should be considered together with the wing panel as a single lifting surface with a span of $(s_m)_e$ (surfaces *ABF* and *CDE* in Fig. 12.6.2).

Accordingly, and with a view to (12.4.14), the normal force of the combination body-wing-empennage, including that of the nose of the body, can be expressed as

$$Y_{b,w,e} = 2\alpha\pi\,(s_m^2)_e q_\infty\,[1 - (r_m^4)_e + (r^4)_e] \qquad (12.6\,1)$$

where $(r_m)_e = r/(s_m)_e$, and $(s_m)_e > (s_m)_w$ is the empennage semi-span.

To appraise the influence of interference on the normal force of the empennage, let us introduce the **empennage effectiveness** η_e determined as the ratio of the increment of the normal force when a tail empennage is installed on a wing-body combination to the increment of the normal force when a tail empennage is installed

on an isolated body:

$$\eta_e = (Y_{b\,w\,e} - Y_{b\,w})/(Y_{b,e} - Y_b) \qquad (12.6.2)$$

where by (12.4.14) we have

$$Y_{b\,w} = 2\alpha\pi\,(\bar{s}_m^3)_w q_\infty\,[1 - (\bar{r}_m^2)_w + (\bar{r}_m^4)_w] \qquad (12.6.3)$$

Having in view that the normal force for a body-empennage combination $Y_{b,e}$ in (12.6.2) is determined, like $Y_{b,w,e}$, by formula (12.6.1), while the value of $Y_b = 2\pi r^2 \alpha q_\infty$, the empennage effectiveness is

$$\eta_e = \frac{(\bar{r}_m^{-2})_e\,[1+(\bar{r}_m^4)_e] - (\bar{r}_m^{-2})_w\,[1+(\bar{r}_m^4)_w]}{(\bar{r}_m^{-2})_e\,[1-(\bar{r}_m^2)_e]^2} \qquad (12.6.4)$$

According to our hypothesis, when the span of the empennage is smaller than or equal to that of the wing, the normal force of the empennage as a result of interference vanishes, and the empennage effectiveness equals zero.

The found effectiveness can be considered as the limiting value corresponding to the most unfavourable case of flow when the vortex sheet cast off the trailing edge of the wing is flat and coincides with the plane of the panels, while their normal force is therefore minimum. In practice, however, such an unfavourable effect of the interference is smaller because, first, the vortex sheet is not flat, but curls up into vortex cores when it approaches the empennage, and, second, the direction of the vortices is closer to that of the free-stream velocity than to the direction of the plane of the empennage chords; therefore the vortices, as a rule, are not in this plane, but depending on the sign of the angle of attack are higher or lower than the empennage.

Subsonic Velocities

When calculating wing-empennage interference, the wash angle with a known approximation is assumed to be constant over the span and equal to its mean value determined by (6.4.23).

The wash behind a wing having the same setting angle as the empennage results in a decrease in the effective angle of attack of the empennage, which we can compute by the expression

$$\alpha_{\text{eff.h.}}^{\,e} = \alpha - \varepsilon \qquad (12.6.5)$$

Accordingly, the normal force coefficient of the empennage is

$$c_{y\,h,e} = c_{y\,h\,e}^{\alpha}\,(\alpha - \varepsilon) \qquad (12.6.6)$$

where $c_{y,h,e} = (\partial c_y/\partial\alpha)_{h,e}$ is the derivative with respect to the angle of attack α of the coefficient $c_{y,h,e}$ for an isolated horizontal empennage.

When designing the installation of wings and empennage on a body, one must take account of the change in their normal force due to interference. The normal force coefficient c_y for a wing in (6.4.23) should be determined with a view to the change in the effective angle of attack of the sections under the influence of interaction with the body according to (12.1.6). To simplify calculations, one can use the concept of the span-averaged effective angle of attack, which is determined using the rule of averaging by the formula

$$\bar{\alpha}_{\text{eff, w}} = \frac{\alpha}{l_w/2 - r} \int_r^{l_w/2} (1 + r^2/z^2)\, dz = \alpha\,(1 + 2r/l_w) \qquad (12.6.7)$$

For the empennage, accordingly, we have

$$\bar{\alpha}_{\text{eff, e}} = \alpha\,(1 + 2r/l_e) \qquad (12.6.7')$$

Hence, the normal force coefficient of the empennage on the basis of (12.6.7′) is

$$c_{y,\text{h,e}} = c^{\alpha}_{y,\text{h,e}}\,(\bar{\alpha}_{\text{eff, e}} - \varepsilon) \qquad (12.6.6')$$

here $\varepsilon = \varepsilon_{av}$ is determined from expression (6.4.23) in which $c_y = c_{y,w} = c^{\alpha}_{y,w}\bar{\alpha}_{\text{eff, w}}$ where $c^{\alpha}_{y,w} = (\partial c_y/\partial\alpha)_w$ is the derivative of the normal force coefficient for an isolated wing with respect to the angle of attack.

Supersonic Velocities

When studying the interaction of an empennage with a wing, we can proceed from a simplified vortex model of a body-wing combination (Fig. 12.6.3). According to this model, each panel is replaced with an attached (bound) vortex of strength Γ_0 and with a free vortex of the same strength cast off the trailing edge of the panel. Since the body has a lifting capacity, it must also be replaced with a section of the attached vortex and with a vortex cast off downstream. These vortices of strength Γ_0 are called **conjugate**. The arrangement of the conjugate free vortices corresponds to the **rule of conjugate radii** (see [15]) according to which

$$r_c = r^2/r_0 \qquad (12.6.8)$$

where c is he subscript of a conjugate vortex (c = 1, 2).

A right conjugate vortex has the same value of the strength Γ_0 as a right free (external) vortex, but rotates in the opposite direction. The same relates to left vortices. Consequently, the vortex model of the body-wing combination being considered includes two pairs of horseshoe vortices of strength Γ_0.

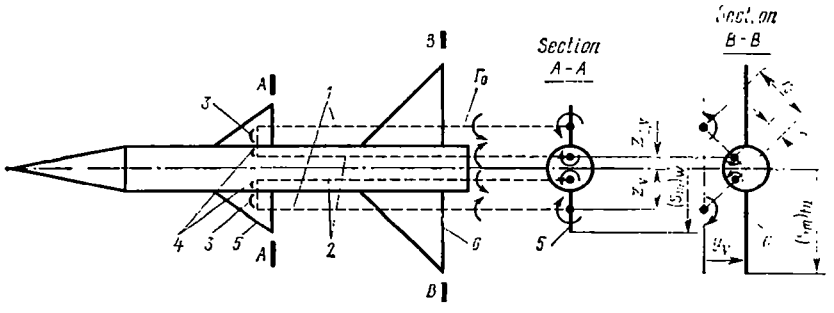

Fig. 12.6.3
Vortex model of a body-wing combination:
1—cast off (free) vortices for a panel; *2*—cast off (conjugate) vortices for the body; *3*—attached vortices for a panel; *4*—attached (conjugate) vortices for the body; *5*—wing; *6*—tail unit (empennage)

By Zhukovsky's formula (6.3.22), the normal force of the panels in the presence of a body is

$$\Delta Y_{w(b)} = 2\rho_\infty V_\infty \Gamma_0 (z_v - r) \tag{12.6.9}$$

while the normal force of the body in the presence of a wing is

$$Y_b + \Delta Y_{b(w)} = 2\rho_\infty V_\infty \Gamma_0 (r - z_{cv}) \tag{12.6.10}$$

where z_v is the lateral coordinate of a free (rolled-up) vortex coinciding with the centre of mass of the vortex sheet, z_{cv} is the coordinate of the conjugate vortex; by (12.6.8), we have

$$z_{cv} = r^2/z_v \tag{12.6.11}$$

$z_v - r$ is the length of an attached vortex (a lifting vortex line) on a panel, and $r - z_{cv}$ is the length of the conjugate attached vortex inside the body.

The normal force of the body-wing combination (without the normal force of the body nose) is

$$Y_{b\,w} - Y_b = \Delta Y_{b(w)} + \Delta Y_{w(b)} = 2\rho_\infty V_\infty \Gamma_0 (z_v - r^2/z_v) \tag{12.6.12}$$

This normal force is also determined by (12.6.3) without account taken of the normal force of the body $2\pi\alpha r^2 q_\infty$. Consequently,

$$2\rho_\infty V_\infty \Gamma_0 (z_v - r^2/z_v) = 2\pi\alpha (s_m^2)_w q_\infty [1 - (r_m^2)_w + (r_m^4)_w]$$

$$- 2\pi\alpha r^2 q_\infty = 2\pi\sigma (s_m^2)_w [1 - (r_m^2)_w]^2 q_\infty \tag{12.6.13}$$

Let us consider expression (12.6.2). The values of the normal force can be written as

$$Y_{b,w,e} = Y_b + \Delta Y_{b(w)} + \Delta Y_{w(b)} + \Delta Y_{b(e)} + \Delta Y_{e(b)} + \Delta Y_{b(e)v} + \Delta Y_{e(b)v}$$

(the last two components with the subscript "v" are due to the influence of the vortices). This expression can be written differently, having in view that

$$Y_{b,w} = Y_b + \Delta Y_{b(w)} + \Delta Y_{w(b)};$$
$$Y_{b,e} = Y_b + \Delta Y_{b(\cdot)} + \Delta Y_{e(b)}$$

Consequently,

$$\eta_e = 1 + (\Delta Y_{b(e)v} + \Delta Y_{e(b)v})/(\Delta Y_{b(e)} + \Delta Y_{e(b)}) \qquad (12.6.14)$$

whence

$$\Delta Y_{b(e)v} + \Delta Y_{e(b)v} = \Delta Y_{(b,e)v} = [\Delta Y_{b(e)} + \Delta Y_{e(b)}](\eta_e - 1)$$

or

$$\Delta Y_{b(e)v} = Y_e (K_w + K_b)(\eta_e - 1) \qquad (12.6.15)$$

We obtain the difference $\eta_e - 1$ from (12.6.4) in the following form:

$$\eta_e - 1 = -\frac{(\bar{s}_m^2)_w}{(\bar{s}_m^2)_e} \frac{[1-(r_m^2)_w]^2}{[1-(r_m^2)_e]^2} \qquad (12.6.16)$$

Taking (12.6.13) into account, we have

$$\eta_e - 1 = -\frac{2\Gamma_0 (z_v/r - r/z_v)}{\pi\alpha r V_\infty (\bar{s}_m^2)_e [1-(r_m^2)_e]^2} \qquad (12.6.17)$$

After introducing (12.6.17) into (12.6.15) and substituting $[(\bar{s}_m)_e + 1]^2/(\bar{s}_m^2)_e$ for $K_w + K_b$ [see (12.2.61)], we obtain

$$\Delta Y_{(b,e)v} = -\frac{2\Gamma_0 (r_v - r^2/z_v) Y_e}{\pi\alpha V_\infty [(s_m)_e - r]^2} \qquad (12\ 6\ 18)$$

The radii r in the numerator and denominator of this formula should be taken equal to their values for the wing and empennage, i.e. $r = r_w$ and $r = r_e$. Formula (12.6.18) has been obtained proceeding from the assumption that the vortex sheet cast off the wings and the corresponding free vortices are in the plane of the empennage. Hence, the part of the empennage covered by the cast off vortex sheet completely loses its lifting properties, i.e. the normal force on this part is zero. Actually, this assumption as we already indicated, is not completely correct, and, consequently, formula (12.6.18) has to be considered as a relation determining only the order of magnitude of $\Delta Y_{(b,e)v}$. To refine relation (12.6.18), we shall introduce the correction factor $\varphi(y_v)$, which takes into account how the vertical

coordinate y_v of a free vortex (Fig. 12.6.3) affects the normal force $\Delta Y_{(b,e)v}$. This yields

$$\Delta Y_{(b,e)v} = -\frac{4\varphi(y_v)(z_v - r^2/z_v)}{(s_m)_e - r} \cdot \frac{\Gamma_0}{2\pi V_\infty [(s_m)_e - r]} \cdot \frac{Y_e}{\alpha}$$

The second multiplier here determines the dimensionless vortex strength, and the third one, the normal force of a separate empennage per degree of the angle of attack. The first multiplier including the factor $\varphi(y_v)$ depends on the position of a vortex and does not depend on its strength. This multiplier is called the **interference factor**, and is designated by i_e.

Introducing this factor and going over from r to the radius of the body at the empennage r_e, we have

$$\Delta Y_{(b,e)v} = i_e \frac{\Gamma_0}{2\pi V_\infty [(s_m)_e - r_e]} \cdot \frac{Y_e}{\alpha} \qquad (12.6.19)$$

By (12.6.9), the circulation is

$$\Gamma_0 = \Delta Y_{w(b)}/[2\rho_\infty V_\infty (z_v - r_w)] \qquad (12.6.20)$$

Substituting for $\Delta Y_{w(b)}$ from (12.2.5) yields

$$\Gamma_0 = K_w Y_w/[2\rho_\infty V_\infty (z_v - r_w)]$$

Since

$$Y_w = (\partial c_y/\partial\alpha)_w \alpha (\rho_\infty V_\infty^2/2) S_w$$

we have

$$\Gamma_0 = K_w (\partial c_y/\partial\alpha)_w \alpha S_w V_\infty/[4(z_v - r_w)] \qquad (12.6.21)$$

Let us assume in (12.6.19) that

$$\Delta Y_{(b,e)v} = (\Delta c_y)_{(b,e)v} q_\infty S, \quad Y_e = (\partial c_y/\partial\alpha)_e \alpha q_\infty S_e \qquad (12.6.22)$$

where S is a characteristic area, and S_e is the plan view area of the separate empennage, which is related to the aspect ratio λ_e by the formula

$$\lambda_e = 4[(s_m)_e - r_e]^2/S_e \qquad (12.6.23)$$

With a view to (12.6.21)-(12.6.23), relation (12.6.19) can be transformed into an expression determining the normal force coefficient for the tail part:

$$(\Delta c_y)_{(b,e)v} = i_e \frac{K_w \alpha (\partial c_y/\partial\alpha)_w (\partial c_y/\partial\alpha)_e [(s_m)_e - r_e] S_w/S}{2\pi\lambda_e (z_v - r_w)} \qquad (12.6.24)$$

To use formula (12.6.24), one has to know the horizontal coordinate z_v of a free vortex and the interference factor i_e that depends on z_v and, additionally, on the vertical coordinate y_v of the vortex (Fig. 12.6.4).

To determine the coordinate z_v of a rolled-up (free) vortex, let us use a vortex model of a body-wing combination. We shall consider the vortex sheet cast off the wing panels and evaluate the cir-

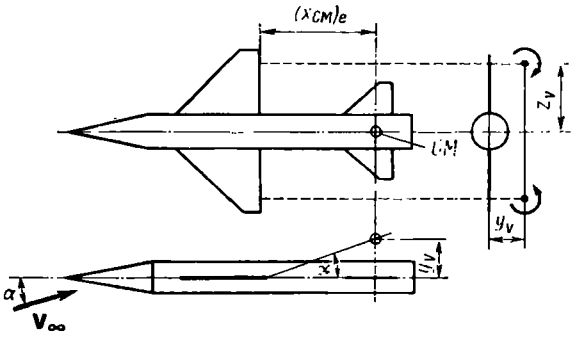

Fig. 12.6.4
To the determination of the arrangement of a cast off free vortex

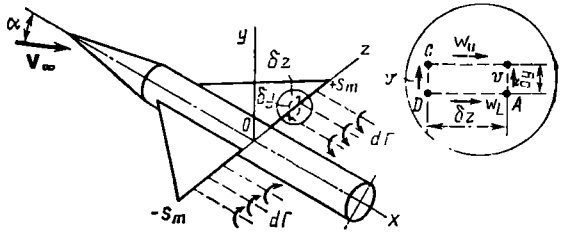

Fig. 12.6.5
Formation of a vortex sheet cast off a wing panel

culation around an elementary rectangular contour *ABCD* of sides δy and δz in the vicinity of the trailing edge of the wing. Examination of Fig. 12.6.5 reveals that

$$\delta\Gamma_{ABCD} = \delta\Gamma_{AB} + \delta\Gamma_{BC} + \delta\Gamma_{CD} + \delta\Gamma_{DA}$$
$$= v\delta y - w_u\delta z - v\delta y + w_L\delta z = (-w_u + w_L)\ \delta z$$

The circulation has been taken positive for a vortex with counterclockwise rotation. Let the potential on the upper side be φ_u and on the lower one φ_L. Hence

$$\delta\Gamma_{ABCD} = (\partial\varphi_L/\partial z - \partial\varphi_u/\partial z)\ \delta z$$

Since the potentials φ_L and φ_u at the trailing edge are determined for the conditions $y = 0$ and, consequently, depend only on z, we may go over to total derivatives and obtain

$$d\Gamma/dz = d(\varphi_L - \varphi_u)/dz \qquad (12.6.25)$$

whence the distribution of the circulation is

$$\Gamma = \varphi_L - \varphi_u \qquad (12.6.26)$$

The subscript "ABCD" has been discarded here. Knowing the velocity potential along the trailing edge of the panels, we can calculate the strength of vorticity per unit of span, i.e. the derivative $d\Gamma/dz$, and also the distribution of the circulation. This potential can be determined from (12.2.20'), assuming that $y = 0$:

$$\varphi_\alpha = \varphi_{u,L} = \pm V_\infty \alpha [(s_m + r^2/s_m)^2 - (z + r^2/z)^2]^{1/2} \qquad (12.6.27)$$

where the plus and minus signs correspond to the potentials φ_u and φ_L on the upper and lower surfaces, respectively.

By (12.6.26), we have

$$\Gamma = 2\alpha V_\infty [(s_m + r^2/s_m)^2 - (z + r^2/z)^2]^{1/2} \qquad (12.6.28)$$

We obtain the circulation in the root (central) section at $z = r$:

$$\Gamma_0 = 2\alpha V_\infty [(s_m + r^2/s_m)^2 - 4r^2]^{1/2} \qquad (12.6.29)$$

The ratio of the circulations is

$$\Gamma/\Gamma_0 = [(s_m^2 z^2 - r^4)(s_m^2 - z^2)]^{1/2}/[z(s_m^2 - r^2)] \qquad (12.6.30)$$

If we assume that the vortex sheet has been replaced with a vortex of a strength equal to the circulation Γ_0 in the root section, we have

$$\int_r^{s_m} \Gamma\, dz = \Gamma_0 (z_v - r) \qquad (12.6.31)$$

where the integral is the area confined by the circulation curve for the panels, and $\Gamma_0 (z_v - r)$ is a quantity equal to this area.

Introducing into (12.6.31) the value of Γ from (12.6.30), we obtain

$$\int_r^{s_m} [(s_m^2 z^2 - r^4)(s_m^2 - z^2)]^{1/2}\, dz/[z(s_m^2 - r^2)] = z_v - r \qquad (12.6.32)$$

Let us introduce the dimensionless parameter

$$(z_v - r)/(s_m - r) = \int_{r_0}^{1} [(\bar{z}^2 - r_0^4)(1 - \bar{z}^2)]^{1/2} \bar{z}^{-1}\, d\bar{z}/[(1 - r_0)^2 (1 + r_0)] \qquad (12.6.33)$$

where $\bar{z} = z/s_m$ and $r_m = r/s_m$.

The integral is computed by numerical methods. The following results are obtained:

$r_m = r/s_m$	0	0.1	0.2	0.3	0.4	0.5	0.6	0.7	0.8	0.9	1.0
$(z_v - r)/(s_m - r)$	0.786	0.769	0.760	0.757	0.757	0.759	0.763	0.768	0.774	0.780	0.786

We use these data to find the parameter $(z_v - r)/(s_m - r)$ as a function of $r_m = r/s_m$. The span of a panel and the radius of the body are taken equal to $s_m = (s_m)_w$ and $r = r_w$, respectively.

The obtained coordinates z_v determine the lateral position of a vortex on the wing. Investigations show that the analogical coordinate of an empennage vortex differs from the found value of z_v for a wing vortex. This difference is not large, however, because the vortices are very insignificantly displaced spanwise. Therefore the value of z_v for the empennage can be taken with a reasonable accuracy the same as for the wing in interference calculations. This allows us to take into account more accurately the influence on the coordinate z_v of the number M_∞, the taper ratio $\eta_w = b_0/b_t$, the aspect ratio $\lambda_w = 2\,(s_m - r)_w/[0.5\,(b_0 + b_t)]$, and the sweep angle (it is customary practice to take the sweep angle $\varkappa_{1/2}$ for the rectilinear edge joining the middles of the chords). Calculations reveal that the results obtained correspond best of all to the data of the aerodynamic theory of a slender body for a panel for which $\eta_w = 2$ and $\lambda_w \tan \varkappa_{1/2} = 0$ and 2/3.

When determining the span coordinate y_v of the cast off vortices at the empennage, we assume that these vortices coincide with the direction of the flow. If we also assume that the coordinate is over the centre of mass of the empennage area computed with a view to the part of the area occupied by the body, then in accordance with Fig. 12.6.4 we have

$$y_v = a(x_{CM})_e \tag{12.6.34}$$

where $(x_{CM})_e$ is the distance from the trailing edge of the wing to the centre of mass of the empennage area.

Interference Factor

Let us see how the interference factor is determined. It follows from (12.6.19) that

$$i_e = \frac{\Delta Y_{(b,e)v}}{Y_e} \frac{2\pi\alpha V_\infty [(s_m)_e - r_e]}{\Gamma_0} \tag{12.6.35}$$

This expression shows that the interference factor can be considered as the ratio of two dimensionless quantities, one of which is the ratio of the normal forces $\Delta Y_{(b,e)v}/Y_e$, and the other is the dimensionless circulation characterizing the strength of a cast off vortex. That the factor i_e depends on the ratio of the normal forces allows us to use very simple methods for determining i_e even if they do not yield exact values of the magnitudes of $\Delta Y_{(b,e)v}$ or Y_e, but allow us to find their exact ratio. Here we have a certain analogy between the interference factors K_w and K_b, on the one hand, and the factor i_e on the other. We have already indicated that the factors K_w and K_b, which are the ratios of the relevant normal forces, are determined adequately according to the aerodynamic theory of a slender body; this allows us to evaluate the magnitudes of the

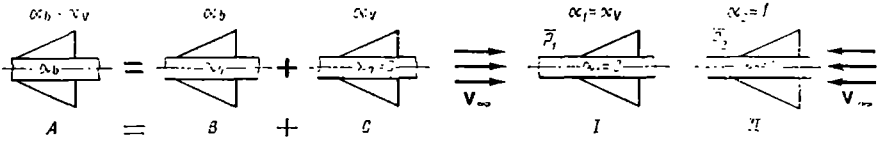

Fig. 12.6.6
To the calculation of the effectiveness of an empennage by the reverse-flow method for a body-empennage combination:
I—combination in a forward flow; *II*—combination in an inverse flow

normal force with account taken of the interaction of some combinations.

Having this in view, let us use the deductions of the aerodynamic theory of flow over slender bodies to determine the ratio $\Delta Y_{(b,e)v}/Y_e$ and the corresponding coefficient i_e. Our aim is to use the data obtained to calculate the interference of the tail part of a non-slender combination.

To find the normal force $\Delta Y_{(b,e)v}$, we shall use the reverse-flow **method** which we considered when investigating the flow over a slender wing in forward and inverse flows. In the given case with the aid of the basic relation of this method found in Sec. 8.13, we establish the relation between the aerodynamic characteristics of a body-wing-empennage combination in oppositely directed flows.

Assume that the empennage is installed relative to the body axis at a zero angle of attack, while the combination is in a flow at the angle of attack α_b. The vortices cast off the wing cause upwash at the empennage with the angle $-\varepsilon = \alpha_v$, therefore the effective angle of attack of the empennage panels will be $\alpha_b + \alpha_v$. The flow past combination A consisting of a body and an empennage (Fig. 12.6.6) can be represented as a complex flow formed as a result of the superposition of flows near similar combinations B and C according to the formula $A = B + C$. In combination B, the body and empennage have an identical angle of attack α_b; in combination C, the body is not deflected ($\alpha_b = 0$), while the empennage is in a flow at the angle of attack α_v produced by the vortices.

We shall find the normal force for combination C by the reverse-flow method. Let us adopt for the forward flow (Fig. 12.6.6) with a view to the notation used in formula (8.13.8′) the conditions:

$$\left.\begin{aligned} \alpha_1 = \alpha_b = 0 \quad &\text{on the area } S_b \text{ occupied by the part} \\ &\text{of the body under the empennage} \\ \alpha_1 = \alpha_v \quad &\text{on the area } S_e \text{ of the panels} \end{aligned}\right\} \quad (12.6.36)$$

We shall assume for the inverse flow (Fig. 12.6.6) that the body and the empennage are at a unit angle of attack, i.e.

$$\alpha_2 = 1 \text{ on area } S_b; \quad \alpha_2 = 1 \text{ on area } S_e \quad (12.6.37)$$

Using formula (8.13.8'), we obtain

$$\int\limits_{(S_b+S_e)}\int \Delta\bar{p}_1 \cdot 1\, dS = \int\limits_{S_e}\int \Delta\bar{p}_2 \alpha_v\, dS$$

The integral on the left-hand side determines the total normal force of the body-empennage combination due to the vortex,

$$\Delta Y_{(b,\,e)v} = Y_{b(e)v} + \Delta Y_{e(b)v} = q_\infty \int\limits_{(S_b+S_e)}\int \Delta\bar{p}_1\, dS$$

consequently,

$$\Delta Y_{(b,\,e)v} = q_\infty \int\limits_{(S_e)}\int \Delta\bar{p}_2 \alpha_v\, dS \tag{12.6.38}$$

Let us assume that the angle of attack α_v depends only on the span coordinate of a point z and remains constant along the empennage chord. Having in view that $dS = dx\, dz$, after integration with respect to x, we obtain

$$\Delta Y_{(b,\,e)v} = 2q_\infty \int\limits_{r}^{(s_m)_e} \alpha_v\, (bc_y')\, dz \tag{12.6.39}$$

The quantity

$$bc_y' = \int\limits_{x_{ld}}^{x_{tr}=x_{ld}+b} \Delta\bar{p}_2\, dx \tag{12.6.40}$$

is the **loading in a section along the wing span** determined for a unit angle of deflection of the body and panel. In expression (12.6.40), x_{ld} and x_{tr} are the coordinates of points on the leading and trailing edges, respectively, b is the chord of the section, and c_y' is the lift coefficient of the section.

To compute the loading (12.6.40), let us consider formula (12.2.52') for $\Delta Y_{w(b)}$. Introducing the notation $\alpha = \alpha_b$, $\Delta Y_{w(b)} = \Delta Y_{e(b)}$, $s_m = (s_m)_e$ and integrating with respect to x, we obtain

$$\Delta Y_{(e)b} = 8\alpha_b q_\infty \int\limits_{r}^{(s_m)_e} \{[(s_m)_e + r^2/(s_m)_e]^2 - (z + r^2/z)^2\}^{1/2}\, dz \tag{12.6.41}$$

By comparing (12.6.41) and (12.6.39), we can see that the loading along the span of the empennage for a unit deflection of a panel and the body ($\alpha_b = \alpha_v = 1$) is determined by the quantity

$$(bc_y')_{e(b)} = 4\, \{[(s_m)_e + r^2/(s_m)_e]^2 - (z + r^2/z)^2\}^{1/2} \tag{12.6.42}$$

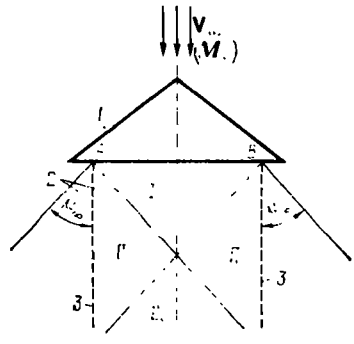

Fig. 12.6.7
Zones of vortex influence in a supersonic flow:
1 – wing; *2* – Mach cone; *3* – attached vortex

Although we have performed integration for a triangular panel in a forward flow, a glance at (12.6.42) reveals that for slender configurations the distribution of the loading along the span does not depend on the planform of the panels. Its value at a given point with the coordinate z of the surface of a panel mounted on a body of radius r is determined only by the semispan $(s_m)_e$. This is why formula (12.6.42) may be used to evaluate the loading of a triangular wing in an inverse flow. Accordingly, the loading in (12.6.39) equals the loading in (12.6.42), i.e. $bc_y' = (bc_y')_{e(b)}$. Hence

$$\Delta Y_{(b,\,e)v} = 8q_\infty \int_r^{(s_m)_e} \alpha_v \{[(s_m)_e + r^2/(s_m)_e]^2 - (z + r^2/z)^2\}^{1/2}\, dz \tag{12.6.43}$$

In this expression, it is necessary to find the angle of attack $\alpha_v = -\varepsilon$ equal in magnitude to the vertical downwash angle at the empennage.

In a supersonic flow, the downwash angles are determined with a view to the limitedness of the zone of vortex influence. The zone of influence for the left attached vortex is limited by the Mach cone issuing from point A, and for the right vortex, by the Mach cone issuing from point B (Fig. 12.6.7). In region I outside these cones, there is no vortex influence, and the downwash equals zero. In region II confined by the Mach cone issuing from the beginning of the attached vortex, the downwash is determined by the influence of the vortex confined in this cone. In zone III coinciding with the region of intersection of the two Mach cones, the downwash is determined by the influence of both attached vortices.

Let us consider an empennage in region III where the velocities induced by the right and left vortices are summed up. At a certain distance from the trailing edge of the wing, the vertical downwashes of the linearized supersonic flow caused by the attached vortex are

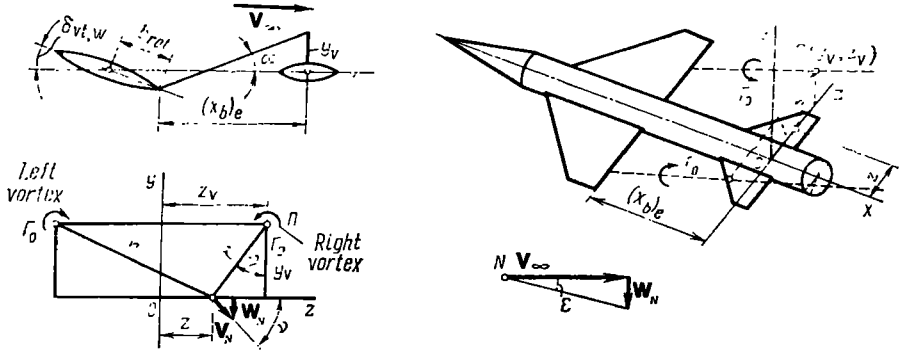

Fig. 12.6.8
To the calculation of the flow downwash at an empennage (tail unit) behind the wing

the same as the downwashes produced by infinite vortex lines in an incompressible fluid. Particularly, for a wing with $\alpha'\lambda_w = 2.5$, this distance equals two chords, and for $\alpha'\lambda_w = 1$, about three-fourths of a chord length. Assuming that the empennage is at a sufficiently large distance from the wing, we determine the downwash of the flow with the aid of the expression $\varepsilon = -w_N/V_\infty$ in which the induced velocity is evaluated by (2.7.12). Assuming in this formula that $w = w_N$, $\Gamma = \Gamma_0$, and $h = r$, for point N ($y = 0$) on the empennage (Fig. 12.6.8), we have

$$w_N = \Gamma_0/(2\pi r)$$

The vertical component of the velocity induced by the right vortex is

$$w_{N_r} = -\frac{\Gamma_0}{2\pi r}\sin\nu = -\frac{\Gamma_0}{2\pi r}\cdot\frac{z_v - z}{r} = -\frac{\Gamma_0 (z_v - z)}{2\pi\,[y_v^2 + (z_v - z)^2]} \qquad (12.6.44)$$

and that induced by the left vortex is

$$w_{N_l} = -\frac{\Gamma_0 (z_v + z)}{2\pi\,[y_v^2 + (z_v + z)^2]} \qquad (12.6.45)$$

The total velocity of the vertical downwash is

$$w_N = w_{N_r} + w_{N_l} = -\frac{\Gamma_0}{2\pi}\left[\frac{z_v - z}{y_v^2 + (z_v - z)^2} + \frac{z_v + z}{y_v^2 + (z_v + z)^2}\right] \qquad (12.6.46)$$

The corresponding downwash angle is

$$\varepsilon = -\frac{w_N}{V_\infty} = \frac{\Gamma_0}{2\pi V_\infty}\left[\frac{z_v - z}{y_v^2 + (z_v - z)^2} + \frac{z_v + z}{y_v^2 + (z_v + z)^2}\right] \qquad (12.6.47)$$

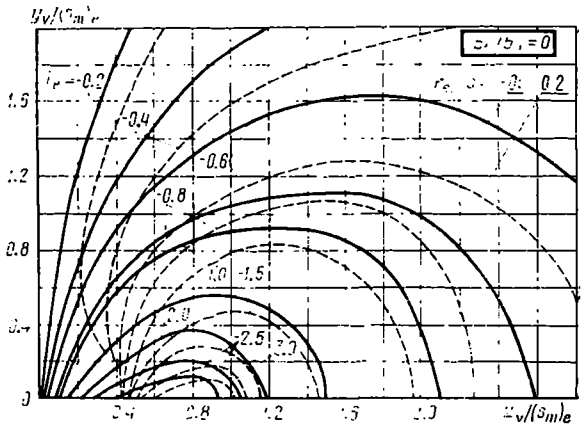

Fig. 12.6.9
Interference factors for a triangular empennage

Introducing the value of $\alpha_v = -\varepsilon$ into (12.6.43), we obtain

$$\Delta Y_{(b,\,e)v} = \frac{-4q_\infty \Gamma_0}{\pi V_\infty} \int_r^{(s_m)_e} \left[\frac{z_v - z}{y_v^2 + (z_v - z)^2} + \frac{z_v + z}{y_v^2 + (z_v + z)^2} \right] \times \{[(s_m)_e + r^2/(s_m)_e]^2 - (z + r^2/z)^2\}^{1/2}\, dz \qquad (12.6.48)$$

Inserting (12.6.48) into (12.6.35), in which in accordance with (8.8.46) we assume that

$$Y_e = (c_y)_e\, q_\infty S_e = 2\alpha\pi \cot \varkappa q_\infty S_e = 2\alpha\pi q_\infty [(s_m)_e - r_e]^2$$

we find that

$$i_e = \frac{-4}{[(s_m)_e - r]\,\pi} \int_r^{(s_m)_e} \left[\frac{z_v - z}{y_v^2 + (z_v - z)^2} + \frac{z_v + z}{y_v^2 + (z_v + z)^2} \right] \times \{[(s_m)_e + r_e^2/(s_m)_e]^2 - (z + r_e^2/z)^2\}^{1/2}\, dz \qquad (12.6.49)$$

Numerical integration yields the values of i_e which by (12.6.49) are functions of the dimensionless variables $y_v/(s_m)_e$, $z_v/(s_m)_e$, and $r_e/(s_m)_e$ and do not depend on the planform of the empennage.

Calculations by another method based on the strip theory (see [16]) show that i_e also depends on the shape determined by the reciprocal taper ratio of the empennage b_t/b_0. Figure 12.6.9 shows a typical diagram plotted according to the results of these calculations for a triangular empennage ($1/\eta_e = b_t/b_0 = 0$). Here i_e is actually a slightly varying function of b_t/b_0 and $r_e/(s_m)_e$ for small values of $r_e/(s_m)_e$.

Using such diagrams, we usually find the factors i_e by interpolation over the parameters $(r_m)_e = r_e/(s_m)_e$ and η_e (or $1/\eta_e$) at $z_v/(s_m)_e$. If a vortex is near the axis of the body, it is good to perform this interpolation for conditions of constancy of another parameter, for example $(z_v/s_m - r_m)_e/(1 - r_m)_e$.

Let us consider an approximate method of determining i_e with the use of (12.6.49) based on the assumption that the downwash of the flow along the span is constant and equal to its value at the aerodynamic centre (centre of pressure) of the empennage. Assuming that point N (see Fig. 12.6.8) coincides with the aerodynamic centre, which is at the origin of coordinates ($y = z = 0$), we find the downwash angle from (12.6.47):

$$\varepsilon = \frac{\Gamma_0}{\pi V_\infty} \cdot \frac{z_v}{y_v^2 + z_v^2} \tag{12.6.50}$$

Hence, (12.6.48) acquires the form

$$\Delta Y_{(b,e)v} = \frac{-8q_\infty \Gamma_0}{\pi V_\infty} \cdot \frac{z_v}{y_v^2 + z_v^2} \times \int_r^{(s_m)_e} \{[(s_m)_e + r_e^2/(s_m)_e]^2 - (z + r_e^2/z)^2\}^{1/2}\, dx \tag{12.6.51}$$

Integrating and using (8.8.47'), we obtain the relation

$$\frac{\Delta Y_{(b,e)v}}{Y_e} = \frac{-2\Gamma_0 z_v}{\pi \alpha V_\infty (y_v^2 + z_v^2)} \left\{ \frac{\pi}{2} \left[\frac{(\bar{s}_m^2)_e - 1}{(\bar{s}_m)_e} \right]^2 + \left[\frac{(\bar{s}_m^2)_e + 1}{(\bar{s}_m)_e} \right]^2 \sin^{-1} \left[\frac{(\bar{s}_m^2)_e - 1}{(\bar{s}_m^2)_e + 1} \right] - \frac{2[(\bar{s}_m^2)_e - 1]}{(\bar{s}_m)_e} \right\} \times \frac{1}{\pi [(\bar{s}_m)_e - 1]^2} \tag{12.6.52}$$

The right-hand side of (12.6.52) contains as a multiplier the interference factor K_w (12.2.60) for the body-empennage combination. With this in view, after introducing (12.6.52) into (12.6.35), we find

$$i_e = -\frac{4\bar{z}_v [(\bar{s}_m)_e - 1] (K_w)_e}{(\bar{y}_v^2 + \bar{z}_v^2)(\bar{s}_m)_e} \tag{12.6.53}$$

where $\bar{z}_v = z_v/(s_m)_e$, $\bar{y}_v = y_v/(s_m)_e$, and $(\bar{s}_m)_e = (s_m)_e/r_e$. In approximate calculations, we may assume that $a \approx 2.7\text{-}2.8$ instead of $a = 4(K_w)_e$.

Let us now determine the effectiveness of the empennage from the value of i_e. Adopting the area of the separate wing as the characteristic area, we can write Eq. (12.6.14) as

$$\eta_e = 1 + (\Delta c_y)_{(b,e)v}/[c_{y,e}(K_w + K_b)_e] \tag{12.6.54}$$

Introducing the value of $(\Delta c_y)_{(b,e)v}/c_{y,e} = \Delta Y_{(b,e)v}/Y_e$ found from (12.6.35), we obtain

$$\eta_e = 1 + i_e \Gamma_0 / \{2 (K_w + K_b)_e \pi \alpha V_\infty [(s_m)_e - r_e]\} \quad (12.6.55)$$

Inserting the value of Γ_0 from (12.6.21), we find

$$\eta_e = 1 + i_e K_w (\partial c_y/\partial \alpha)_w S_w / \{8 (K_w + K_b)_e \pi [(s_m)_e - r_e] \times (z_v - r_w)\} \quad (12.6.56)$$

By using η_e and Eq. (12.6.54), we can find the reduction of the normal force coefficient due to a vortex:

$$(\Delta c_y)_{(b,e)v} = c_{y,e} (K_w + K_b)_e (\eta_e - 1) \quad (12.6.57)$$

This reduction is due to the appearance of downwash of the flow ahead of the empennage determined by the mean angle $\varepsilon_m = (d\varepsilon/d\alpha)_e \alpha$. Consequently,

$$(\Delta c_y)_{(b,e)v} = c_{y,e} (K_w + K_b)_e (-d\varepsilon/d\alpha)_e \alpha \quad (12.6.58)$$

Comparing the above relations, we find

$$(d\varepsilon/d\alpha_e) = 1 - \eta_e \quad (12.6.59)$$

Relation (12.6.59) corresponds to the aerodynamic theory of a slender body according to which the influence of a vortex extends to the entire area of the empennage. This occurs in practice at subsonic and low supersonic velocities. With an increase in the number M_∞ ($M_\infty > 1$), the zone of influence of a vortex confined by the Mach cone (issuing from the point where the vortex is cast off, see Fig. 12.6.12 below) narrows, and this leads to a reduction of the downwash angle. This reduction can be taken into account by the factor $\Delta_\varepsilon = S_e'/S_e$, where S_e' is the panel area inside the Mach cone. This allows us to refine derivative (12.6.59):

$$(d\varepsilon/d\alpha)_e = (1 - \eta_e)] \Delta_e \quad (12.6.60)$$

Taking Eq. (12.6.60) into account, we can write (12.6.57) as follows:

$$(\Delta c_y)_{(b,e)v} = c_{y,e} (K_w + K_b)_e (\eta_e - 1) \Delta_\varepsilon \quad (12.6.61)$$

In practice, it is convenient to find Δ_ε graphically (see Fig. 12.6.12 below). At increased numbers M_∞, the Mach cone becomes so narrow that the empennage panels emerge from the zone of vortex influence. In this case, $S_e' \approx 0$, the factor $\Delta_\varepsilon = 0$, and, consequently, no downwash occurs. The coordinate of the centre of pressure of the empennage, like the normal force, changes under the influence of the wing vortices. We can consider approximately here that the point of application of the normal force due to the wing vortices coincides with the centre of pressure of the empennage for a body-empennage (wing) combination, i.e. $(x_p)_{\alpha, e(v)} = (x_p)_{\alpha, w(b)}$.

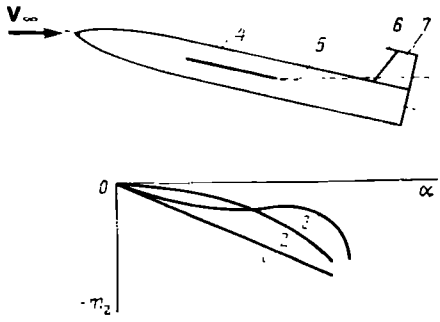

Fig. 12.6.10
Influence of a horizontal tail surface (empennage) on the moment characteristics of a body-wing-empennage combination:
1 – without interference; *2* – with account of interference for a conventional tail unit; *3* – with account of interference for a non-tandem cruciform tail unit; *4* – wing; *5* – vortex; *6* – horizontal tail surface; *7* – vertical tail surface

Influence of the Angle of Attack and Shocks on the Empennage Effectiveness

An increase in the angle of attack may lead to diminishing of the unfavourable action of interference. The explanation is that a vortex continues to move in the direction of the flow, while the empennage with an increase in α lowers. This leads to a growth in the coordinates z_v and y_v and, consequently, to a lower value of $|i_\varepsilon|$. If the position of the vortex with respect to the empennage did not change, the unfavourable influence of the interference would be of a linear nature because the strength of a vortex is proportional to the angle of attack. In a real case, with an increase in the angles of attack, the moment characteristic of the empennage is non-linear, and the static stability may grow.

At small angles of attack, the unfavourable influence of interference on stability may be reduced by using what is called a **non-tandem empennage (tail unit)** arranged higher than the wing (Fig. 12.6.10). In this case, the characteristics of the empennage are improved because the vortices cast off the wing will pass below the tail unit (empennage) at a considerable distance from it. But with an increase in the angles of attack, its upper surfaces become closer to the vortices, and the unfavourable influence of interference grows. When after a further increase in the angle of attack the tail unit passes through the vortices and moves away from them, the unfavourable influence diminishes.

At high supersonic velocities, there is an additional interference effect caused by interaction with shocks (Fig. 12.6.11). Examination of the figure reveals that at a certain angle of attack α_1 the horizontal tail surface is in the zone between the tail shock and the expansion fan. Consequently, this tail surface is at a zero angle of attack for the flow that has passed through the expansion fan and produces no normal force. The effectiveness of this tail surface is practically close to zero ($\eta_e \approx 0$). At a larger angle of attack ($\alpha_2 > \alpha_1$), the shock angle grows and the plane of the shock may be

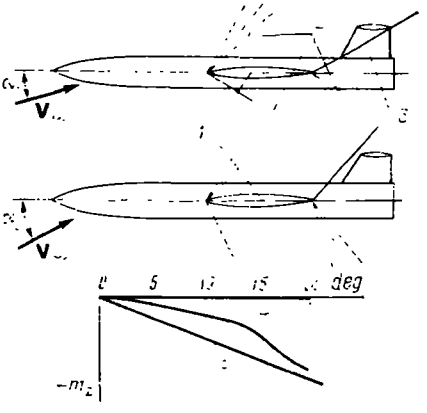

Fig. 12.6.11
Tail unit-wing interference when a shock is produced:
1–wing; *2*–expansion fan; *3*–tail shock; *4*–tail unit effectiveness $\eta_e=0$; *5*–real curve; *6*–tail unit effectiveness $\eta_e=1$

ahead of the tail surface. Since a streamline behind the shock almost coincides with the direction of the free stream, the tail surface regains its effectiveness to a considerable extent. A certain decrease in the normal force is due to the reduction of the number M and of the velocity head behind the shock. Curve *5* in Fig. 12.6.11 shows how the moment of the tail surface changes because of the influence of the shock, and also of expansion of the flow. The curve passes between lines corresponding, on the one hand, to a complete loss of effectiveness ($\eta_e = 0$), and on the other, to its complete recovery ($\eta_e = 1$)

Influence of Flow Stagnation

The effectiveness of a tail unit (empennage) depends on the stagnation of the flow due to the action of not only the nose, but also of the wings arranged ahead of the tail unit. The degree of stagnation can be characterized by the coefficient $q_2 = q/q_\infty$ that is a function of the number M_∞, the relative dimensions of the nose part, the ratio of the tail unit and wing areas ($\bar{S}_e = S_e/S_w$), and also of the relative distance between them [$\bar{x}_c = x_c/(b_A)_w$].

For a craft with a conical nose (see [13]), we have

$$k_2 = \frac{q}{q_\infty} = k_1 \frac{k' + \bar{S}_e}{1 + \bar{S}_e} \qquad (12.6.62)$$

where k_1 is the stagnation coefficient for a wing determined by (12.4.44), and k' is a variable depending on the number M_∞ and the distance between the wing and tail unit (it can be found from the graph in Fig. 12.6.12 plotted according to experimental data).

For a craft with its empennage behind the wing (the normal arrangement), we usually have $S_e/S_w \ll 1$. We can therefore assume that $k_2 \approx k_1 k'$. When the empennage is ahead of the wing (a canard), we

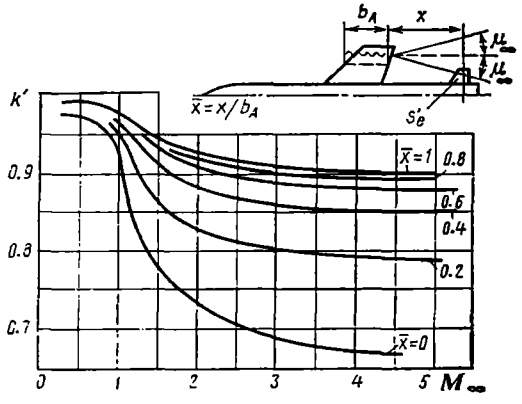

Fig. 12.6.12
Graphs for determining the coefficient k' in Eq. (12.6.62)

have $S_e/S_w] \gg 1$, therefore the stagnation coefficient ahead of the wing arranged in the tail part is $k_2 \approx k_1$. The corresponding Mach number used to determine the normal force coefficient for the tail unit is

$$M_1 = M_\infty \sqrt{k_2} \tag{12.6.63}$$

Aerodynamic Characteristics

The results of calculating wing-empennage interference can be used to find the aerodynamic characteristics for body-empennage or body-wing-empennage combinations. For a winged craft provided with an empennage, the interaction of the latter with the wing must be taken into consideration.

Let us consider a combination with an identical arrangement of the wing and tail unit panels (Fig. 12.6.13). By analogy with (12.4.47), the normal force coefficient for the combination is

$$c_y = Y/(q_\infty S_w) = c_{y,b} + c^\alpha_{y,w}\,(K_w + K_b)_w\, k_1\alpha + c^\alpha_{y,e}\,(K_w + K_b)_e\,[1 - (d\varepsilon/d\alpha)_e]\, k_2\alpha S_e/S_w \tag{12.6.64}$$

In accordance with this value of c_y, let us find a relation for the coefficient of the pitching moment about the nose of the body:

$$m_z = m_{z,b} - \{K_{b,w}\,[(c_p)_{\alpha,\,b(w)}\,(\bar{b}_0)_w + \bar{x}_w] + K_w\,[(c_p)_{\alpha,w(b)}\,(\bar{b}_0)_w + \bar{x}_w]\}\, c^\alpha_{y,w}\,\alpha k_1 - \{K_{b,e}\,[(c_p)_{\alpha,b(e)}\,(\bar{b}_0)_e + \bar{x}_e] + K_e\,[(c_p)_{\alpha,e(b)}\,(\bar{b}_0)_e + \bar{x}_e]\}\, c^\alpha_{y,e}\,[1 - (d\varepsilon/d\alpha)_e]\, k_2\alpha S_e/S_w \tag{12.6.65}$$

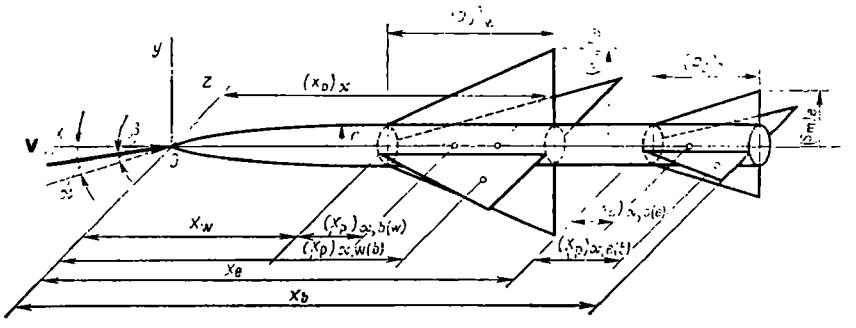

Fig. 12.6.13
General view of a craft with a tandem wing-tail unit arrangement

In these relations, we find the interference factors with the subscripts "w" and "e" from Table 12.2.1 for the values of $r_w/(s_m)_w$ and $r_e/(s_m)_e$, respectively. We use the table to find the values of $(c_p)_\alpha = (x_p)_\alpha/(b_0)_w$ [for example, $(c_p)_{\alpha,b(w)} = (x_p)_{\alpha,b(w)}/(b_0)_w$]. All the geometric parameters in (12.6.65) are dimensionless and have been related to the length of the craft body x_b, namely, $\bar{x}_w = x_w/x_b$, $(\bar{b}_0)_w = (b_0)_w/x_b$, etc.

By differentiating with respect to $\alpha = \alpha_v \cos\varphi$ [see (12.6.64) and (12.6.65)], we can find the derivatives of the normal force and pitching moment coefficients c_y^α and m_z^α. We use these quantities to calculate the derivatives of the lateral force and yawing moment coefficients with respect to the sideslip angle:

$$c_z^\beta = -c_y^\alpha; \quad m_y^\beta = -m_z^\alpha \tag{12.6.66}$$

and also the centre-of-pressure coefficient for the combination:

$$(c_p)_\alpha = (c_p)_\beta = -m_z^\alpha/c_y^\alpha \tag{12.6.67}$$

All the aerodynamic coefficients for the separate elements of a combination (body, wing, empennage) in the above relations are determined according to the linearized theory with account taken of compressibility.

The interference factors for the wing $K_{b,w}$, K_w and the empennage (tail unit) $K_{b,e}$, K_e are found, in addition, depending on the taper ratio of the panels, the boundary layer displacement thickness, and also on the length of the tail part of the body behind the wing and tail unit.

Rolling Moment of a Tail Unit

This moment changes under the influence of the vortices cast off the wings of a craft in sideslip and at an angle of attack.

In a combination with flat wings, a pair of vortex cores is generat-

ed. One forms an angle with the vertical plane of symmetry that is close in value to β, while the other forms an angle close to α with the horizontal plane. With cruciform wings, four such vortices are generated. Usually, the sign of this moment for a flat tail unit is opposite to that of its intrinsic moment. Bearing this in mind, and also that the dimensions of the tail unit are small in comparison with the wings, and therefore the rolling moments it produces are small in magnitude, the additional interference component of the rolling moment is not taken into account when computing its total value for a craft.

With a cruciform wing-tail combination, the interference rolling moments due to the vertical and horizontal panels, as a rule, are opposite in sign and close in magnitude. Hence, the total rolling moment of the combination can be taken equal to zero. This is also true for a body-cruciform tail craft in which the vortices ahead of the tail unit are generated by the body, this being due to the appearance of a relatively small normal force on the body.

12.7. Controls

Basic Kinds of Controls

The trajectory of an unguided craft experiencing only drag and gravity is usually called a **free-flight** or **ballistic** one. Such a craft is characterized by the absence of an artificially produced controlling force normal to the trajectory.

The trajectory of a guided craft executing a manoeuvre differs from a free-flight one because of the additional control force coinciding in direction with a normal to the flight velocity vector. Devices producing the required control force are called **controls.**

The controls are part of the flight-control system, by which is meant the collection of apparatus and devices provided to measure the deviations of a craft from the preset flight conditions, form the corresponding signal, and produce a control force.

Depending on the physical nature of the control force, controls can be divided into three basic kinds, namely, aerodynamic, gasdynamic, and combined.

Aerodynamic controls produce a control force by changing the external flow conditions, consequently, the control force has an aerodynamic origin. Such controls are a means of changing the magnitude and direction of the resultant vector of the aerodynamic forces. Their use is very effective for craft travelling at a high velocity in the dense atmosphere.

Gasdynamic controls are based on the use of the effect produced by a change in the direction of the gas jet flowing out of the nozzle of a jet engine. A control force is produced by deviation of the thrust

vector from the direction of a tangent to the flight trajectory. Some designs of gasdynamic controls use special control jet engines. The latter are employed when the aerodynamic controls become poorly effective, for example, in the rarefied atmosphere or at low speeds of a craft (for example, when a rocket is being launched from the Earth).

Combined controls when producing a control force use effects of aerodynamic and gasdynamic controls simultaneously.

An example of such a control is a jet flap. Its main element is a rotating nozzle usually installed on the trailing edge of a wing or empennage and designed in the form of a narrow slot. The control force is generated as a result of air flowing out of the nozzle inclined at a definite angle to the chord. This force consists of two components, namely, the normal component of the thrust produced by the rotating slot and the component of the aerodynamic force produced because of the redistribution of the pressure on the lifting surface. This redistribution is due to the interaction of the oncoming flow and the jet of air flowing out through the slot.

Each kind of control includes a large number of specific kinds of control devices or units. The choice of the kind of controls and the specific kind of control unit is closely related to the **aerodynamic design**, which is determined, in turn, by the designation of the craft and the requirements and specifications which it must meet. Hence, a definite aerodynamic design, kind of control, and its specific design ensuring compliance with the given requirements and specifications correspond to a given craft.

Controls and how to calculate them are set out in greater detail in [2]. We shall deal with some kinds of aerodynamic controls and the ways of calculating them, particularly with the group of control surfaces widely used in practice.

Control surfaces arranged at various places on a craft can be classified as follows (Fig. 12.7.1): completely movable controls such as a rotating wing or empennage; tip controls; and controls arranged along the trailing edge of a lifting or stabilizing surface.

Completely movable control surfaces in the form of a **rotating wing** or **empennage** ensuring good controllability owing to the sufficiently large area of the controls are used for high-manoeuvre craft, and they are very effective at high altitudes and over a wide range of numbers M_∞. Most often, the axes of rotation of the control surfaces (hinge lines) and those of the body are mutually perpendicular, but from the design standpoint it is sometimes convenient to choose an angle between these axes other than a right one (the position of a hinge line is determined by the sweep angle $\varkappa_c$, Fig. 12.7.1).

Some favour has been found by **tip controls** that are part of a lifting or stabilizing surface and arranged at the tips. Such controls are effective over a large range of speeds. The hinge line, like that of

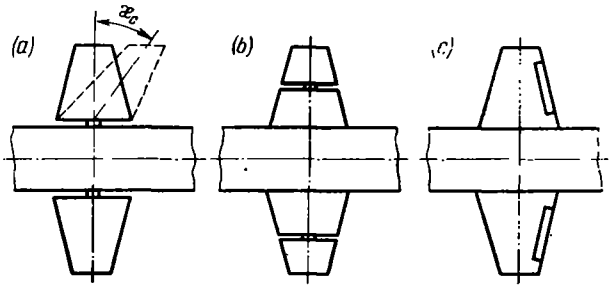

Fig. 12.7.1
Basic kinds of control surfaces:
a–all-movable; *b*–tip; *c*–arranged along the trailing edge

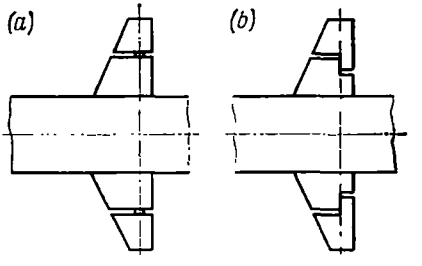

Fig. 12.7.2
Kinds of tip control surfaces:
(a)–ordinary; *(b)*–with compensation

a rotating empennage, may make a right angle with the axis of the body or have a certain sweep angle.

A feature of tip control surfaces is that their effectiveness does not virtually depend on the presence of a body. Their drawback consists in the difficulty of installing the control surface drive and rotating mechanism on a wing or on an empennage with tip control surfaces. The latter can be divided into ordinary tip control surfaces and controls with control surface compensation (Fig. 12.7.2).

At subsonic and low supersonic velocities, the greatest favour is given to **control surfaces arranged along the trailing edge** of a fixed wing or empennage. At low numbers M_∞, deviation of the control surfaces is attended by the appearance of a normal force (a control force) not only on these surfaces themselves, but also on the fixed lifting surface which the disturbances from the control surfaces extend to. This is why such control surfaces can be very effective even with a relatively small area.

At supersonic velocities, there is no reverse action of the control surfaces on the stationary ones, therefore a control force is produced only by the control surface. Notwithstanding the increase in the control force due to the high velocity head, it may be necessary to design control surfaces with a larger area to improve their effective-

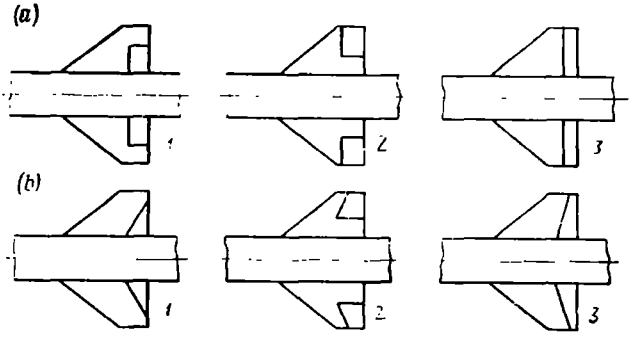

Fig. 12.7.3
Kinds of control surfaces arranged along the trailing edge:
a—with constant chord; *b*—with inverse taper ratio; *1*—internal control surface; *2*—external control surface; *3*—control surface along the entire span

ness. Controls arranged along the trailing edge may be internal and external surfaces occupying part of the edge or installed along the entire span (Fig. 12.7.3).

The **control surfaces** of craft are used as rudders, elevators, ailerons, and elevons.

Rudders in their neutral position are arranged along the longitudinal axis of a craft in the vertical plane of symmetry. Their deviation from this position causes the craft to turn either to the right or to the left. This turning is due to the controlling yawing moment set up by the rudder.

Elevators are arranged at right angles to the plane of the rudders. Their deviation ensures a change in the direction of flight in a vertical plane and, consequently, a change in the altitude. Here rotation of the craft about its lateral axis is due to the controlling pitching moment set up by the elevator.

A combination of rudders and elevators allows a craft to be controlled simultaneously in two mutually perpendicular planes, i.e. virtually any manoeuvre can be performed in space. These control surfaces can also be used to rotate a craft about its longitudinal axis *Ox*.

Designs of aircraft also provide for ailerons in combination with elevators. **Ailerons** are two control surfaces on the tips or trailing edges of the wing panels. They deviate in different directions, which leads to banking of the aircraft. Here a horizontal component of the normal force appears that deviates the craft in the required direction and ensures its turning under the action of the yawing moment. If the elevator is turned simultaneously, the required manoeuvre in space is performed. When ailerons are to be used, one must take into account that owing to their deflection the increments of the

normal force generated on the starboard and port wings with opposite signs produce a corresponding difference of the induced drag. This, in turn, leads to an additional yawing moment causing the craft to turn in the direction of the lowered aileron, and also to sideslip and, consequently, producing a rolling moment opposite in sign to that produced by the ailerons. This lowers the effectiveness of the ailerons, preventing a normal manoeuvre. The rolling moment reaches its maximum value at appreciable angles of attack, as a result of which the effectiveness of ailerons at such angles is very low.

To compensate for this effect, **differential ailerons** are used, in which one aileron deviates upward over a greater distance than its counterpart does downward. The drag of the aileron deflected upward is considerably higher than that of the one deflected downward, which causes the yawing moment to diminish.

Elevons, unlike ailerons, can be deflected to any direction independently of each other, therefore they are used simultaneously as ailerons and elevators. Such devices, simultaneously performing the functions of lateral and longitudinal controls, are installed on tailless aircraft (flying wings).

The aerodynamic properties of controls are determined by their **effectiveness**, by which is meant the increment in the control forces and moments of a craft (or of a separate lifting surface) during the deflection of a control surface. This effectiveness is evaluated by the partial derivatives of the corresponding force or moment coefficients with respect to the control surface angle. For example, for elevators, the longitudinal effectiveness is determined by the derivatives

$$\partial c_y/\partial \delta_{el} = c_y^{\delta_{el}} \text{ or } \partial m_z/\partial \delta_{el} = m_z^{\delta_{el}}.$$

Controllability

The aerodynamic properties of a craft are characterized by its **controllability**—the ability of the craft to react to deflection of the control surfaces by the corresponding changes in the flight parameters (the angle of attack, the pitching, yawing, and flight path angles, etc.). Controllability can be evaluated by the **degree of aircraft sensitivity** to such a deflection of the controls. It is characterized by the intensity of the indicated changes in the flight parameters. When evaluating controllability, we find that the parameters determining the intensity of the change in the path of the centre of mass are of major practical interest. This is associated with the fact that the main task in controlling a flight consists exactly in ensuring a given flight path.

The **manoeuvrability** of a craft, i.e. its ability to change the flight parameters characterizing the altitude, as well as the magnitude and direction of the velocity, depends to a considerable extent on the

controllability. When designing craft and their control systems, one has to take into account the contradictory nature of the requirements of flight stability and controllability. The imparting of stability ensures the elimination of possible violations of the preset flight conditions, whereas controllability is associated with the opposite phenomenon, namely, the possibility of changing these conditions.

The controllability of a craft is related very closely to its static stability. It is more difficult to control a craft with an increased stability (large restoring moments) than one with a lower stability, i.e. the craft requires greater deflections of its control surfaces for changing the flight conditions. If a craft reacts strongly to small control surface deflections, this points to a low stability. Such a low stability is a property of craft intended for rapid manoeuvres. The requirement of greater controllability makes it necessary to use craft that are statically neutral or in some cases that are even statically unstable.

The investigation of controllability based on a knowledge of the aerodynamic characteristics is the cornerstone of the theory of the disturbed motion of craft.

Aerodynamic Calculations of Control Surfaces

The determination of the aerodynamic characteristics of controls is an important and difficult task. The methods of calculating these characteristics are based in the majority of cases on experimental investigations of the control surfaces of various kinds of craft. Theoretical investigations of aerodynamic control surfaces began to be carried out on a broad scale in recent years on the basis of the achievements of mathematics and mechanics. These investigations resulted, particularly, in methods for calculating slender control surfaces on a body of a small thickness. The data of this aerodynamic theory of slender bodies in a number of cases agree well with experimental results and at the same time allow us to understand separate phenomena associated with the mechanism of the appearance of control forces.

We shall consider methods based on this theory and used to calculate aerodynamic control surfaces that are all-movable wing or empennage panels. To do this, we shall use the reverse-flow method that permits us to take into account the influence of the wing and body on the generated normal (control) force. We shall proceed from the relations of the aerodynamic theory of a slender body according to which the planform of a control surface does not affect the magnitude of the force it produces.

Let us assume that the control occupies a portion of length $s_m - s_1$ along the trailing edge of the wing (Fig. 12.7.4). We shall calculate

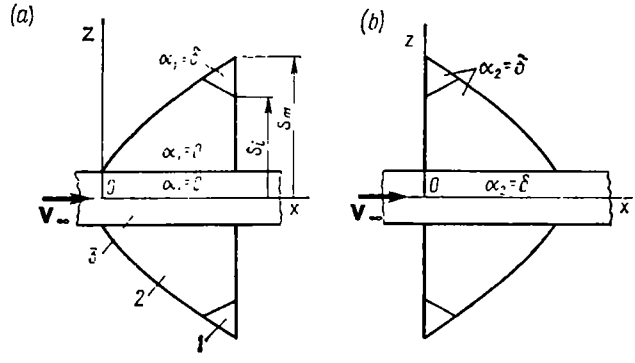

Fig. 12.7.4
To the calculation of the aerodynamic characteristics of an external control surface by the reverse-flow method:
a – forward flow; *b* – inverse flow; *1* – control surface area S_{cs}; *2* – wing area S_w; *3* – area S_b of the body under the wing

the normal force developed by the control surface provided that the body and wing are in a forward flow at a zero angle of attack ($\alpha_1 = 0$), and the control surface is deflected through the angle δ ($\alpha_1 = \delta$). We shall assume that in the inverse flow the body-wing-control surface combination is arranged at the overall angle of attack $\alpha_2 = \delta$. By formula (8.13.8′) of the reverse-flow method, for the case being considered, we have

$$\int\limits_{(S_{cs}+S_w+S_b)}\int \Delta\bar{p}_1\delta\, dS = \int\limits_{(S_{cs})}\int \Delta\bar{p}_2\delta\, dS$$

or, cancelling δ,

$$\int\limits_{(S_{cs}+S_w+S_b)}\int \Delta\bar{p}_1\, dS = \int\limits_{(S_{cs})}\int \Delta\bar{p}_2\, dS \qquad (12.7.1)$$

Here the left-hand side determines the normal force being sought of the body-wing-control surface combination due to deflection of the control related to the velocity head $q_\infty = \rho_\infty V_\infty^2/2$, i.e.

$$Y_{cs} = q_\infty \int\limits_{(S_{cs})}\int \Delta\bar{p}_2\, dS \qquad (12.7.2)$$

Assuming the elementary area of the control surface to be $dS = dx\, dz$, we have

$$Y_{cs} = 2q_\infty \int\limits_{s_i}^{s_m} dz \int\limits_{x_{ld}}^{x_{tr}} \Delta\bar{p}_2\, dx \qquad (12.7.3)$$

(the subscripts "tr" and "ld" stand for "trailing" and "leading", respectively).

The quantity

$$\int_{x_{ld}}^{x_{tr}} \Delta\bar{p}_2\, dx = bc'_y \qquad (12.7.4)$$

i.e. it equals the load in a wing section determined during deflection of the body and panel through the angle δ. By the aerodynamic theory, this flow when the combination is in the inverse flow does not depend on the planform of the wing and is determined as the normal force of the section concentrated at the leading edge.

The pressure-drop coefficient is

$$\Delta\bar{p}_2 = \bar{p}_L - \bar{p}_u = -\frac{2}{V_\infty}\left(\frac{\partial\varphi_L}{\partial x} - \frac{\partial\varphi_u}{\partial x}\right)$$

Hence, the load in a wing section with a view to (12.6.27) is

$$bc'_y = \int_{x_{ld}}^{x_{tr}} \Delta\bar{p}_2\, dx = \frac{-2}{V_\infty}\int_{x_{ld}}^{x_{tr}} \left(\frac{\partial\varphi_L}{\partial x} - \frac{\partial\varphi_u}{\partial x}\right) dx$$

$$= \frac{-2}{V_\infty}(\varphi_L - \varphi_u) = 4\delta\left[\left(s_m + \frac{r^2}{s_m}\right)^2 - \left(z + \frac{r^2}{z}\right)^2\right]^{1/2} \qquad (12.7.5)$$

Inserting this expression into (12.6.39), we find

$$Y_{cs} = 8q_\infty\delta\int_{s_i}^{s_m} [(s_m + r^2/s_m)^2 - (z + r^2/z)^2]^{1/2}\, dz \qquad (12.7.6)$$

Expression (12.7.6) is similar to relation (12.6.41) obtained in the preceding section. By performing integration and relating (12.7.6) to the normal force of the separate wing

$$Y_w = 2\delta\pi q_\infty (s_m - s_1)^2 \qquad (12.7.7)$$

formed by two joined tip controls, we obtain

$$\frac{Y_{cs}}{Y_w} = \frac{2}{\pi(1-\bar{s}_1)^2}\left[\frac{\pi}{4}(1-r_m^2)^2 - (\bar{s}_1^2 - r_m^4)^{1/2}(1-\bar{s}_1^2)^{1/2}\right.$$

$$\left. + \frac{1}{2}(1+r_m^4)\sin^{-1}\frac{1-2\bar{s}_1^2+r_m^4}{1-r_m^4} + r_m^2\sin^{-1}\frac{(1+r_m^4)\bar{s}_1^2 - 2r_m^4}{(1-r_m^4)\bar{s}_1^2}\right] \qquad (12.7.8)$$

where $r_m = r/s_m$ and $\bar{s}_1 = s_1/s_m$.

The ratio Y_{cs}/Y_w depends only on the geometric parameters at the trailing edge. A plot of Y_{cs}/Y_w against r/s_m for various values of s_1/s_m is shown in Fig. 12.7.5. The normal force of the combination as a result of interaction of the body and a wing with a deflected

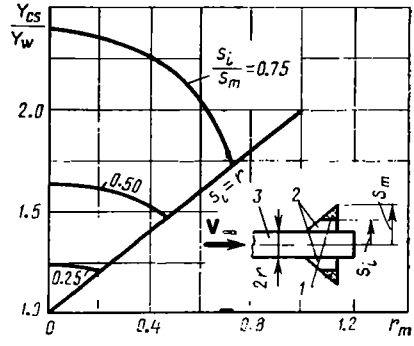

Fig. 12.7.5
Aerodynamic effectiveness of controls:
1 – control surfaces; *2* – wing; *3* – body

tip control surface may substantially exceed the normal force Y_w of a separate wing. At a fixed value of $r_m = r/s_m$ and an increase in the ratio s_1/r, the normal force of the combination grows because of the influence of the control surface. The explanation is that the field of pressures formed upon flow over the control is "captured" by a considerable area of the wing.

Formula (12.7.8) determines the control force of a tip control surface. In a particular case, assuming in this formula that $s_1 = r_m$ ($s_1 = r$), we obtain a relation for Y_{cs} for all-movable controls:

$$\frac{Y_{cs}}{Y_w} = \frac{2}{\pi(1-r_m)^2}\left[\frac{\pi}{4}(1-r_m^2)^2 - r_m(1-r_m^2) + \frac{(1+r_m^2)^2}{2}\sin^{-1}\frac{1-r_m^2}{1+r_m^2}\right] \qquad (12.7.9)$$

Expression (12.7.9) coincides with formula (12.2.60) determining the interference factor K_w for a fixed wing. The nature of the change in the ratio Y_{cs}/Y_w depending on the magnitude of r_m is shown in Fig. 12.7.5.

Hence, we have obtained an interesting result according to which *the effect of interference as a whole for a body-movable wing combination is the same as for a fixed wing interacting with the body when the combination is in a flow at an angle of attack.*

Accordingly, we have

$$Y_{cs}/Y_w = K_w \qquad (12.7.10$$

The normal force can be expressed in terms of the sum

$$Y_{cs} = \Delta Y_{w(b)\delta} + \Delta Y_{b(w)\delta} \qquad (12.7.11)$$

Here the first term is the normal force of the wing deflected through the angle δ and influenced by the body, and the second term is the normal force of the part of the body due to its interaction with

the wing:

$$\Delta Y_{w(b)\delta} = k_w Y_w \tag{12.7.12}$$

$$\Delta Y_{b(w)\delta} = k_b Y_w \tag{12.7.13}$$

where k_w and k_b, by analogy with the factors K_w and K_b introduced above, are **interference factors** due to the deflection of the all-movable control surfaces through the angle δ at $\alpha = 0$.

By (12.7.11), we have

$$Y_{cs} = (k_w + k_b) Y_w \tag{12.7.14}$$

and with a view to (12.7.10),

$$k_w + k_b = K_w \tag{12.7.15}$$

To determine the factors k_w and k_b, we must have another equation establishing the relation between these factors. To obtain such an equation, we shall proceed from the assumption that the wing "transfers" to the body a part of its normal force regardless of whether this force is produced by the angle of attack α of the combination or by the angle of wing setting δ. This part of the normal force due to the influence of the angle of attack α is determined by the ratio

$$\Delta Y_{b(w)\alpha}/\Delta Y_{w(b)\alpha} = K_b/K_w \tag{12.7.16}$$

while the ratio

$$\Delta Y_{b(w)\delta}/\Delta Y_{w(b)\delta} = k_b/k_w \tag{12.7.17}$$

determines the part of the normal force transferred to the body at the angle δ. According to the adopted hypothesis, both these parts are equal, consequently,

$$k_b/k_w = K_b/K_w \tag{12.7.18}$$

This equation can be written as

$$(k_b + k_w)/k_w = (K_b + K_w)/K_w \tag{12.7.18'}$$

Using the values given by (12.7.15) and (12.2.61) for $k_b + k_w$ and $K_b + K_w$, respectively, we obtain the following expression for the interference factor:

$$k_w = K_w^2/(1 + r_m)^2 \tag{12.7.19}$$

By (12.7.15), we have

$$k_b = K_w - k_w \tag{12.7.20}$$

These values of the factors are used when studying the interaction of the movable empennage of non-slender combinations for which the aerodynamic characteristics of the separate panels are chosen in accordance with the data of the linearized theory of flow. We can refine the results of the investigations if we take into consideration

the change in the factors k_w and k_b under the influence of the taper ratio of a panel, the number M_∞, the length of the body nose, the boundary layer, etc. Here we proceed from relations similar to (12.4.29):

$$k_w = (k_w)_{th}\, \nu_\eta \nu_{bl} \nu_l \nu_f; \quad k_b = (k_b)_{th}\, \nu_\eta \nu_{bl} \nu_l \nu_f \qquad (12.7.21)$$

where $(k_w)_{th}$ and $(k_b)_{th}$ are the interference factors evaluated according to the aerodynamic theory of a slender body by (12.7.19) and (12.7.20):

$$(k_w)_{th} = (K_w^2)_{th}/(1 + r_m^2); \quad (k_b)_{th} = (K_w)_{th} - (k_w)_{th} \qquad (12.7.22)$$

The tail part of the body affects the magnitude of the factor k_b (as the value of K_b); the factor k_w remains unchanged (like K_w). Accordingly, when a body has a part after a movable panel, the factor k_b is

$$k_b = (k_b)_{th}\, \nu_\eta \nu_{bl} \nu_l \nu_f F \qquad (12.7.23)$$

where F is determined by (12.4.31).

Let us consider the calculation of the aerodynamic characteristics for a *body-all-movable empennage combination* with the use of the obtained interference factors. By (12.7.14), the coefficient of the normal force due to the deflection of the panels of an all-moving wing is

$$c_{y,\delta} = Y_{cs}/(q_\infty S_w) = c_{y,w}^{\alpha}\, (k_w + k_b)\, \delta_{vt} k_1 \qquad (12.7.24)$$

Here δ_{vt} is the angle of attack of the panel equal to the turning angle measured in the vertical plane of symmetry passing through the body axis. Its value is the same as that of the turning ang e δ'_{vt} when the hinge line makes a right angle with the body axis, i.e. when the sweep angle of this axis is $\varkappa_{cs} = 0$. If $\varkappa_{cs} \neq 0$, the angle of attack of the panel δ_{vt} does not equal the turning angle δ'_{vt} measured in a plane at right angles to the hinge line. The magnitude of this angle is

$$\delta_{vt} = \delta'_{vt} \cos \varkappa_{cs} \qquad (12.7.25)$$

By adding to (12.7.24) the coefficient $c_{y,\alpha} = c_{y,b,w}$ computed from the value of the normal force $Y_\alpha = Y_{b,w}$ of the combination for $\alpha \neq 0$ and $\delta_{vt} = 0$, we obtain the total normal force coefficient related to the area of the wing panels:

$$c_y = c_{y,\alpha} + c_{y,\delta} = c_{y,b}\, \frac{S_{mid}}{S_w} + [(K_b + K_w)\, \alpha + (k_b + k_w)\, \delta_{vt}]\, c_{y,w}^{\alpha} k_1 \qquad (12.7.26)$$

We can find the dimensionless coordinate of the centre of pressure (the coordinate of the aerodynamic centre with respect to the angle δ_{vt}) of the all-moving wing panels at $\alpha = 0$ from the expression

$$(c_p)_{\delta,w(b)} = (x_p/x_b)_{\delta,w(b)} = \bar{x}_w + (c_p)_{\delta,w(b)} \bar{b}_0 \qquad (12.7.27)$$

The values of $(c_p)_{\delta,w(b)}$ calculated according to the aerodynamic theory of a slender body are virtually the same as the values of the coefficients $(c_p)_{\alpha,w(b)}$ found for fixed panels at $\alpha \neq 0$.

The data obtained indicate the relatively weak influence of interference on the displacement of the centre of pressure of an all-moving wing. This gives us grounds to consider that as a first approximation the centre of pressure of such a wing at $\alpha = 0$ and $\delta_{vt} \neq 0$ may be taken the same as for a separate wing.

If the body moves at the angle of attack α and the wing is additionally deflected through the angle δ_{vt}, the relative coordinate of the centre of pressure is

$$(c_p)_{w(b)} = (x_p/x_b)_{w(b)} = \bar{x}_w + (c_p')_{w(b)}\bar{b}_0 \qquad (12.7.28)$$

where the coefficient

$$(c_p)_{w(b)} = (x_p/b_0)_{w(b)}$$
$$= [K_w\alpha\,(c_p)_{\alpha,w(b)} + k_w\delta_{vt}\,(c_p)_{\delta,w(b)}]/(K_w\alpha + k_w\delta_{vt}) \qquad (12.7.29)$$

Upon the turning of a control, in addition to a change in the position of its centre of pressure because of interaction with the body, there is also a change in the coordinate of the point of application of the additional normal force on the body due to the influence of the empennage. If such turning is attended by a change in the angle of attack of the body, the relative coordinate of the centre of pressure is

$$(c_p)_{b(w)} = (x_p/x_b)_{b(w)} = \bar{x}_w + (c_p')_{b(w)}\bar{b}_0 \qquad (12.7.30)$$

where

$$(c_p')_{b(w)} = (x_p/b_0)_{b(w)}$$
$$= [K_b\alpha\,(c_p)_{\alpha,b(w)} + k_b\delta_{vt}\,(c_p)_{\delta,b(w)}]/(K_b\alpha + k_b\delta_{vt}) \qquad (12.7.31)$$

When calculating the position of the centre of pressure on the body with a view to the influence of the empennage, we assume that the centre of pressure is not sensitive to whether the normal force develops due to the angle of attack or the wing turning angle. Accordingly, $(x_p)_{\alpha,b(w)} = (x_p)_{\delta,b(w)}$.

The centre-of-pressure coefficient for a body-all-moving wing combination is

$$c_p = x_p/x_b = -m_z/c_y = \Big[(c_p)_b c_{y,b}\frac{S_{mid}}{S_w}$$
$$+ (c_p)_{w(b)}\Delta c_{y,w(b)} + (c_p)_{b(w)}\Delta c_{y,b(w)}\Big]\Big/c_y \qquad (12.7.32)$$

where c_y is the total normal force coefficient evaluated by (12.7.26). Its components are found from the expressions

$$\Delta c_{y,w(b)} = \Delta c_{y,\alpha,w(b)} + \Delta c_{y,\delta,w(b)} = (K_w\alpha + k_w\delta_{vt})\,c^{\alpha}_{y,w_l}k_1 \qquad (12.7.33)$$

$$\Delta c_{y,b(w)} = \Delta c_{y,\alpha,b(w)} + \Delta c_{y,\delta,b(w)} = (K_b\alpha + k_b\delta_{vt})\,c^{\alpha}_{y,w}\,k_1 \qquad (12.7.34)$$

Let us consider the **longitudinal effectiveness of controls** in the form of an all-moving wing. Its magnitude is determined by the derivative $m_z^{\delta_{vt}}$ for symmetric deflection of the horizontal panels provided that the pitching moment is calculated about the centre of mass. It is not difficult to compute the coefficient of this moment m_z according to the known values of $\Delta c_{y,w(b)}$ from (12.7.33) and $\Delta c_{y,b(w)}$ from (12.7.34), and also according to the given relative coordinates of the centres of pressure $(c_p)_{\delta,w(b)}$ and $(c_p)_{\delta,b(w)}$. Calculation of the derivative of m_z with respect to δ_{vt} yields

$$m_z^{\delta_{vt}} = -\bar{b}_0 \{k_w [(c_p)_{\delta,w(b)} + (\bar{x}_{CM})_w] + k_b [(c_p)_{\delta\ b(w)} + (\bar{x}_{CM})_w]\} c_{y,w}^{\alpha} k_1 \quad (12.7.35)$$

where $(\bar{x}_{CM})_w = (x_{CM}/b_0)_w$ [here $(x_{CM})_w$ is the distance from the centre of mass of the combination to the vertex of the wing on the body].

The derivative (12.7.35) is usually negative for a tail unit and positive for a canard control unit.

When determining the aerodynamic characteristics of a *body-all-moving wing-all-movable empennage combination*, one must take into account the interaction of the empennage and the wing. The aerodynamic calculations of the body-all-movable empennage part of the combination are performed in the same way as for the body-all-moving wing combination for which the normal force coefficients of the wing with account taken of a body (and also of the body with account taken of the wing) are found by formulas (12.7.33) and (12.7.34), respectively. It should be assumed in them that $\delta_{vt} = \delta_{vt,w}$, while the interference factors $K_b = K_{bw}$, $k_b = k_{b,w}$, K_w, and k_w should be calculated from the wing parameter $r_w/(s_m)_w$.

By analogy with (12.7.33), the normal force coefficient of the empennage with regard to a body is

$$c_{y,e(b)} = (K_e\alpha + k_e\delta_{vt.e}) c_{y,e}^{\alpha} k_2 S_e/S_w \quad (12.7.36)$$

where K_e and k_e are the interference factors of the empennage similar to the corresponding factors K_w and k_w of the wing, and $\delta_{vt.e}$ is the turning angle of the empennage panels.

The normal force coefficient for the body with regard to an empennage is

$$c_{y,b(e)} = (K_{b,e}\alpha + k_{b,e}\delta_{vt,e}) c_{y,e}^{\alpha} k_2 S_e/S_w \quad (12.7.37)$$

where $K_{b,e}$ and $k_{b,e}$ are interference factors; they are computed in the same way for the empennage as the values of $K_{b,w}$ and $k_{b,w}$ for a wing.

The more accurate finding of the normal force coefficient for the tail part of a body-wing-empennage combination is associated with determination of the correction to this coefficient due to interaction

with the wing. The magnitude of this correction is

$$c_{y\,(b,e)v} = i_e \frac{c_{y.w}^{\alpha} c_{y.e}^{\alpha} (K_w \alpha + k_w \delta_{vt.w})(s_m - r)_e k_{e2} \lambda_e}{2\pi \lambda_e (r_v - r)_w} \qquad (12.7.38)$$

The interference factor i_e in this expression is determined as a function of $(r_m)_e = r_e/(s_m)_e$, η_e, $z_v/(s_m)_e$, and $y_v/(s_m)_e$ from the graphs depicted in Fig. 12.6.9. The vertical coordinate of a vortex y_v (see Fig. 12.6.8) if a wing panel turns through the angle $\delta_{vt.w}$ is

$$y_v = (x_b)_e \alpha - b_{rot} \delta_{vt.w} \qquad (12.7.39)$$

where b_{rot} is the distance between the axis of rotation of the panel and the point where the vortex is cast off.

By summing the found values of the normal force coefficient components and adding the normal force coefficient for the separate body, we obtain the overall coefficient for the entire combination:

$$c_y = c_{y.b} S_{mid}/S_w + \Delta c_{y.w(b)} + \Delta c_{y.b(w)} + \Delta c_{y.e(b)} + \Delta c_{y.b(e)} + \Delta c_{y.b(e)v} \qquad (12.7.40)$$

With a view to the above values of the normal force coefficients for the parts of the combination and the relevant values of the centre-of-pressure coefficients, by analogy with (12.7.32) we find the following relation for the centre-of-pressure coefficient for the entire combination (relative to the nose of the body):

$$c_p = x_p/x_b = -m_z/c_y = \Big[(c_p)_b c_{y.b} \frac{S_{mid}}{S_w} + (c_p)_{w(b)} \Delta c_{y.w(b)} + (c_p)_{b(w)} \Delta c_{y.b(w)} + (c_p)_{e(b)} \Delta c_{y.e(b)} + (c_p)_{b(e)} \Delta c_{y.b(e)} + (c_p)_{(b,e)v} \Delta c_{y(b,e)v} \Big] \Big/ c_y \qquad (12.7.41)$$

In this expression, the centre-of-pressure coefficient for the body-empennage part (see Fig. 12.6.13) is

$$(c_p)_{e(b)} = (x_p)_{e(b)}/x_b = \bar{x}_e + (c_p')_{e(b)} (\bar{b}_0)_e \qquad (12.7.42)$$

$$(c_p)_{b(e)} = (x_p)_{b(e)}/x_b = \bar{x}_e + (c_p')_{b(e)} (\bar{b}_0)_e \qquad (12.7.43)$$

where $\bar{x}_e = x_e/x_b$, $(\bar{b}_0)_e = (b_0)_e/x_b$ [here x_b is the distance from the nose of the body to the empennage, and $(b_0)_e$ is the root chord of the empennage]:

$$(c_p')_{e(b)} = \left(\frac{x_p}{b_0}\right)_{e(b)} = \frac{K_e \alpha (c_p)_{\alpha.e(b)} + k_e \delta_{vt.e} (c_p)_{\delta.e(b)}}{K_e \alpha + k_e \delta_{vt.e}} \qquad (12.7.44)$$

$$(c_p')_{b(e)} = \left(\frac{x_p}{b_0}\right)_{b(e)} = \frac{K_{b.e} \alpha (c_p)_{\alpha.b(e)} + k_{b.e} \delta_{vt.e} (c_p)_{\delta.b(e)}}{K_{b.e} \alpha + K_{b.e} \delta_{vt.e}} \qquad (12.7.45)$$

For the body-wing part of the combination, we determine the centre-of-pressure coefficients $(c_p)_{w(b)}$ and $(c_p)_{b(w)}$ by formulas (12.7.28) and (12.7.30) with the use of (12.7.29) and (12.7.31), and take the value of $(c_p)_{(b,e)v}$ equal to $(c_p)_{e(b)}$.

To determine the **pitching effectiveness of control surfaces,** we calculate the derivatives of the normal force coefficient with respect to the angles of deflection of the controls $\delta_{vt} = \delta_{vt,w}$ and $\delta_{vf} = \delta_{vt,e}$. By (12.7.40), we have

$$c_y^{\delta_{vt,w}} = \Delta c_{y,\,b(w)}^{\delta_{vt,w}} + \Delta c_{y,\,b(w)}^{\delta_{vt,w}} + \Delta c_{y(b,e)v}^{\delta_{vt,w}} \qquad (12.7.46)$$

where we determine the derivatives on the right-hand side by differentiation of (12.7.33), (12.7.34), and (12.7.38) with respect to $\delta_{vt,w}$:

$$\Delta c_{y,\,w(b)}^{\delta_{vt,w}} = k_w c_{y,w}^{\alpha} k_1; \quad \Delta c_{y,\,b(w)}^{\delta_{vt,w}} = k_{b,w} c_{y,w}^{\alpha} k_1 \qquad (12.7.47)$$

$$\Delta c_{y,\,(b,e)vx}^{\delta_{vt,w}} = i_e \frac{c_{y,w}^{\alpha} c_{y,e}^{\alpha} k_w (s_m - r)_e k_2 \Delta_\varepsilon}{2\pi\lambda_e (z_v - r)_w} \qquad (12.7.48)$$

Expression (12.7.48) takes into consideration the change in the derivative of the normal force coefficient with respect to the angle of turning of the wing caused by downwash of the flow ahead of the empennage. The derivative of this coefficient with respect to the angle of deflection of the empennage panels by (12.7.40) is

$$c_y^{\delta_{vt,e}} = \Delta c_{y,\,e(b)}^{\delta_{vt,e}} + \Delta c_{y,\,b(e)}^{\delta_{vt,e}} \qquad (12.7.49)$$

We find the derivatives on the right-hand side by (12.7.36) and (12.7.37):

$$\Delta c_{y,e(b)}^{\delta_{vt,e}} = k_e c_{y,e}^{\alpha} k_2 S_e/S_w; \quad \Delta c_{y,b(e)}^{\delta_{vt,e}} = k_{b,e} c_{y,e}^{\alpha} S_e/S_w \qquad (12.7.50)$$

To determine the pitching effectiveness from the angle of deflection of the wing, we should use the relation (Fig. 12.7.6);

$$\begin{aligned} m_z^{\delta_{vt,w}} &= \Delta c_{y,w(b)}^{\delta_{vt,w}} [\bar{x}'_w - (c_p)_{\delta,w(b)} (\bar{b}_0)_w] \\ &+ \Delta c_{y,b(w)}^{\delta_{vt,w}} [\bar{x}'_w - (c_p)_{\delta,b(w)} (\bar{b}_0)_w] \\ &- \Delta c_{y,(b,e)v}^{\delta_{vt,w}} [\bar{x}_e + (c_p)_{(b,e)vt} (\bar{b}_0)_e] \end{aligned} \qquad (12.7.51)$$

where $\bar{x}'_w = x'_w/x_b$, $(\bar{b}_0)_w = (b_0)_w/x_b$, $\bar{x}_e = x_e/x_b$, and $(\bar{b}_0)_e = (b_0)_e/x_b$.

The pitching effectiveness with respect to the angle of turning of an empennage panel is

$$\begin{aligned} m_z^{\delta_{vt,e}} &= -\Delta c_{y,e(b)}^{\delta_{vt,e}} [\bar{x}_e + (c_p)_{\delta,e(b)} (\bar{b}_0)_e] \\ &- \Delta c_{y,b(e)}^{\delta_{vt,e}} [\bar{x}_e + (c_p)_{\delta,(e)} (\bar{b}_0)_e] \end{aligned} \qquad (12.7.52)$$

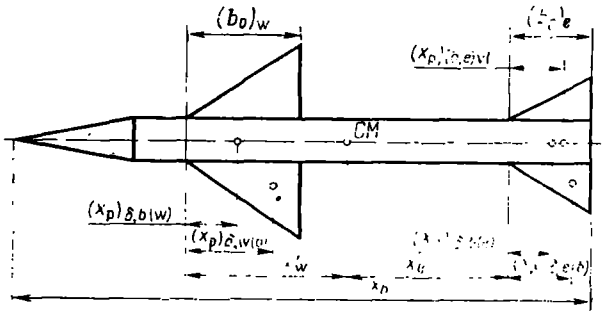

Fig. 12.7.6
To the determination of the pitching effectiveness of control surfaces

In formulas (12.7.51) and (12.7.52), the centre-of-pressure coefficients are calculated as the ratios of the relevant distances to the root chord of the wing or empennage, for example. $(c_p)_{\delta,w(b)} = (x_p)_{\delta,w(b)}/(b_0)_w$, and $(c_p)_{(b,e)v} = (x_p)_{(b,e)v}/(b_0)_e$.

The above values of the pitching effectiveness can be related *to a cruciform configuration* of a craft moving without sideslip ($\alpha \neq 0$, $\beta = 0$). If such a craft is banked ($\alpha \neq 0$, $\beta \neq 0$), it becomes necessary to determine the **yawing effectiveness** $m_y^{\delta_r}$ in addition to the pitching effectiveness $m_z^{\delta_{vt}}$. The latter can be found with the aid of formulas (12.7.51) and (12.7.52) in the plane of the angle $\alpha = \alpha_v \cos\varphi$ without taking into account the interaction between the vertical and horizontal panels. We determine the yawing effectiveness computed with symmetric deflection of the rudders ($\delta_r = \delta_{r,w}$; $\delta_r = \delta_{r,e}$) in the plane of the sideslip angle $\beta = \alpha_v \sin\varphi$. Here

$$m_z^{\delta_{vt}} = -m_y^{\delta_r} \qquad (12.7.53)$$

In rolling motion, the pitching effectiveness in the plane of the angle of attack α_v increases, which is explained by the growth in the lifting capacity of a cruciform empennage upon rotation through the angle φ.

One of the reasons why the effectiveness of the control surfaces diminishes and the linear dependence of their aerodynamic characteristics on the angle of deflection is violated is the formation of **slots** between the controls and the body. This phenomenon appears at sufficiently large slots whose dimensions grow with a greater deflection of the control surfaces. The drop in their lifting capacity and the violation of linearity are due to the sharp decrease in the pressure drop at the root chord caused by the slot.

The effectiveness of the controls can be improved and linearity can be restored by reducing the dimensions of the slots in a craft

and simultaneously decreasing the permissible angles of deflection of the control surfaces. In real conditions of a viscous flow, the boundary layer, as it were, overlaps small slots, which leads to a reduction in their negative influence on the control surfaces.

The influence of slots formed in production and service conditions on the change in the effectiveness of control surfaces can be taken into consideration by introducing the correction factor k_{s1} into the values of the aerodynamic characteristics obtained above for the controls. For subsonic velocities ($M_\infty < M_{\infty,w}$), we can assume approximately that $k_{s1} = 0.8\text{-}0.85$, while at increased Mach numbers ($M_\infty > 1.4$), the factor $k_{s1} = 0.9\text{-}0.95$.

12.8. Aerodynamic Drag

The relations for determining the aerodynamic drag of a craft including a body, wings, and an empennage must take into account the influence on the drag of the interaction between the separate elements of the craft. The total drag X_a in the presence of a lift force ($c_{y_a} \neq 0$) can be represented as the sum of the drag X_0 when there is no lift force, the induced drag X_i produced by the body, wings, and empennage, and of the induced component ΔX_α that includes some aerodynamic forces arising together with the lift force and not taken into consideration otherwise, i.e. $X_a = X_0 + X_i + \Delta X_\alpha$. The corresponding coefficient of the total drag related to a characteristic area S is

$$c_{x_a} = X/(q_\infty S) = c_{x,0} + c_{x,i} + \Delta c_{x,\alpha_i^2} \qquad (12.8.1)$$

Drag in the Absence of a Lift Force ($c_{y_a}=0$)

The value of the coefficient of this drag is

$$c_{x,0} = \Delta c_{x,b} + \Delta c_{x,w} + \Delta c_{x,e} \qquad (12.8.2)$$

where

$$\left.\begin{aligned} &\Delta c_{x,b} = c_{x,b} + \Delta c_{x,b(w)} + \Delta c_{x,b(e)};\\ &\Delta c_{x,w} = c_{x,w} + \Delta c_{x,w(b)}; \quad \Delta c_{x,e} = c_{x,e} + \Delta c_{x,e(b)} \end{aligned}\right\} \qquad (12.8.2')$$

Here $c_{x,b}$, $c_{x,w}$, and $c_{x,e}$ are the drag coefficients for the separate body, wings, and empennage, respectively; the remaining components in the sum give the correction for interference. The subscript in parentheses on each component indicates the element of the craft as a result of interaction with which the additional drag of the body, wing, and empennage is created.

The main part of the drag of the entire combination is the drag of its separate elements:

$$\Delta c_{x,0} = c_{x,b} + c_{x,w} + c_{x,e} \qquad (12.8.3)$$

Separating from each component the drag caused by the rarefaction behind the bottom section (the wake or base drag), we obtain

$$\Delta c_{x,0} = c'_{x,b} + c'_{x,w} + c'_{x,e} + c_{x,b,bot} + c_{x,w,bot} + c_{x,e,bot} \qquad (12.8.3')$$

where the first three components are the drag coefficients due to the pressure and friction on the body, wing, and empennage, and the other three components are the corresponding components of the base drag coefficient.

Body Drag. The total drag of a body is determined with a view to its shape, which in the general case may differ from a body of revolution. If this difference is not great, the body is considered as a body of revolution with the radii distributed along the longitudinal axis x according to the law $r(x) = \sqrt{S(x)/\pi}$, where $S(x)$ is the cross-sectional area of a body of a given shape. Investigations show that the lift force and moment characteristics of such a body of revolution remain the same as those of a body of the given shape. The difference in the drag is more appreciable, therefore it is expedient to take it into account. The shape of a body may deviate from that of a body of revolution because of various "superstructures" such as fairing and aerials.

The aerodynamic drag of a body depends on the arrangement of the superstructures. Investigations show that the drag is the smallest when these superstructures are arranged in the middle. When they are brought forward, the drag grows because of the increased pressure on the nose, while when they are arranged near the tail it grows because of flow separation and an increase in the bottom rarefaction. The drag due to such rarefaction behind the bottom section with an area of S_{bot} is determined by the magnitude of the base pressure coefficient $\bar{p}_{bot} = (p_{bot} - p_\infty)/q_\infty$, hence the coefficient $c_{x,b,bot}$ in (12.8.3') related to the characteristic area S (Fig. 12.8.1) is

$$c_{x,b,bot} = \frac{X_{b,bot}}{q_\infty S} = \frac{-(p_{bot} - p_\infty) S_{bot}}{q_\infty S} = -\bar{p}_{bot} \frac{S_{bot}}{S} \qquad (12.8.4)$$

In practical cases when calculating the drag, we can assume that its component due to friction does not depend on the interference. Hence we must only take into consideration the change in the drag due to the pressure of the body because of interaction with the lifting surfaces. If the wings and empennage are on the cylindrical part of the body, its drag does not change. If, on the other hand, the wings or empennage are on narrowing or broadening parts of the body, the influence of interference may be quite noticeable. The quantities

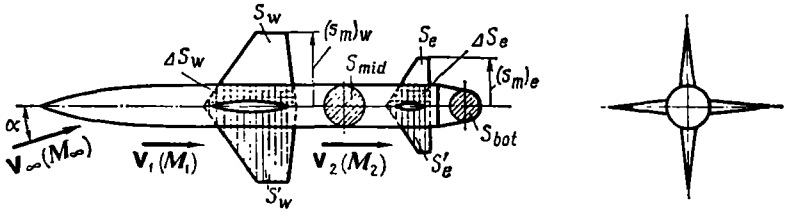

Fig. 12.8.1
To the calculation of the aerodynamic drag of a craft

$\Delta c_{x,b(w)}$ or $\Delta c_{x,b(e)}$ can be determined by assuming the body to be in the pressure field of a separate panel of a lifting or stabilizing surface. This field can be computed according to the supersonic theory of a wing (see Sec. 8.3).

Wing and Empennage Drag. When calculating the drag of separate wings and empennage, it is good practice to consider them as panels protruding above the body and fictitious parts of the lifting surface inside the body. The previous span of such a wing (or empennage) is retained, but its area S'_w is larger. The value of $c_{x,w}$ (X_w) [or $c_{x,e}$ (X_e)] taken into consideration by formula (12.8.2) is determined by the drag of this wing without its fictitious part with an area of ΔS_w under the body,

$$c_{x,w} = (c_{x,w})_{sep}\ (1 - \Delta S_w/S'_w)$$

where $(c_{x,w})_{sep}$ is the drag coefficient for a pair of separate panels computed for the value of S'_w with account taken of the area under the body.

The influence of interference on the drag can be taken into account by introducing a correction to the expression for $c_{x,w}$ in the form

$$c_{x,w} = (c_{x,w})_{sep}\ (1 - k_{1,w}\Delta S_w/S_w) \qquad (12.8.5)$$

where $k_{1,w}$ is an interference factor varying greatly depending on the arrangement of the wing on the body and how they are joined, and also on the shape and aspect ratio of the wing. At a small sweep and aspect ratio ($\lambda_w > 2$) of wings smoothly joined to the body, the value of $k_{1,w}$ differs only slightly from unity. With positive interference diminishing the drag, the value of $k_{1,w}$ is larger than unity.

We calculate the drag of empennage panels in the same way as for a wing. According to the results obtained, the sum of the terms $\Delta c_{x,w} + \Delta c_{x,e}$ in (12.8.2) can be written as

$$\Delta c_{x,w} + \Delta c_{x,e} = (c_{x,w})_{sep}\left(1 - k_{1,w}\frac{\Delta S_w}{S'_w}\right)\frac{\sum S'_w}{S}k_1$$

$$+ (c_{x,e})_{sep}\left(1 - k_{1,e}\frac{\Delta S_e}{S'_e}\right)\frac{\sum S'_e}{S}k_2 \qquad (12.8.6)$$

where $\sum S'_w$ and $\sum S'_e$ are the total areas of the panels with account taken of the parts occupied by the body, k_1 and k_2 are stagnation coefficients, $(c_{x,w})_{sep}$ and $(c_{x,e})_{sep}$ are the drag coefficients for the separate wings and empennage calculated for the numbers M_1 and M_2 of the flows ahead of the wings and the empennage, respectively.

Total Drag at $c_{y_a} = 0$. The sum of the components of the coefficient $\Delta c_{x,b}$ (12.8.2′) relating to the body is

$$\Delta c_{x,b} = [c'_{x,b} + \Delta c'_{x,b(w)} + \Delta c'_{x,b(e)}] S_{mid}/S \qquad (12.8.7)$$

where we find the primed coefficients for the middle section of the body, while the quantity $\Delta c_{x,b}$ is related to the characteristic area S of the combination being considered. With a view to (12.8.6), we shall find a general relation for the total drag coefficient:

$$c_{x_a} = [c'_{x,b} + \Delta c'_{x,b(w)} + \Delta c'_{x,b(e)}] \frac{S_{mid}}{S}$$
$$+ (c_{x,w})_{sep} \left(1 - k_{1,w} \frac{\Delta S_w}{S'_w}\right) \frac{\sum S_w}{S} k_1$$
$$+ (c_{x,e})_{sep} \left(1 - k_{1,e} \frac{\Delta S_e}{S'_e}\right) \frac{\sum S_e}{S} k_2 \qquad (12.8.8)$$

According to experimental investigations, in the major part of designs, interference affects the drag only slightly, and it can be taken into consideration by introducing a correction factor to the drag coefficient Δc_{x0} (12.8.3), i.e. the summary interference factor k_{sum}. Accordingly, the total drag coefficient is $c_{x_a} = \Delta c_{x0} k_{sum}$. The factor k_{sum} depends, among others, on the speed and altitude of flight, the design of the craft and of its separate elements. The value of this factor usually differs only slightly from unity and may be taken approximately equal to $k_{sum} \approx 1.05\text{-}1.06$.

Area Rule. Of practical interest is an estimate of the drag of a body-wing combination based on the use of the area rule. According to this rule, the drag of the combination equals the corresponding value for a separate body with the same distribution of the cross-sectional areas as the body-wing combination. Such a separate body is called an **equivalent body.**

When constructing an equivalent body, a body-wing combination is dissected by parallel planes perpendicular to the longitudinal axis, and its area in the chosen section is measured. This area is considered to belong to an equivalent body differing from the given one in that it becomes convex after the place containing the leading edges (Fig. 12.8.2). If the shape of the equivalent body has been determined, the coefficient of its wave drag can be found, for example, with the aid of integral relation (11.3.28). We evaluate the second derivative $S''(\xi)$ in it for the equivalent body.

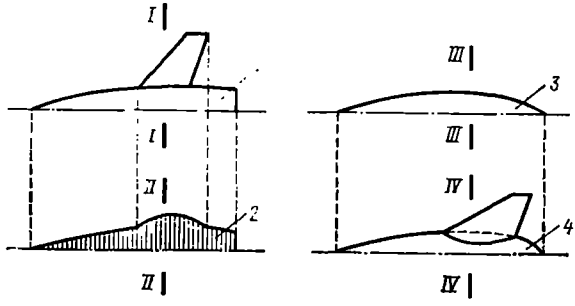

Fig. 12.8.2
The use of the area rule for calculating the aerodynamic drag:
1 – given configuration of a craft; *2* – equivalent body of revolution with bulging (in sections *I-I* and *II-II* the cross-sectional areas are identical); *3* – body of revolution with a minimum drag; *4* – configuration of an equivalent body (with inward bulging) having a reduced drag (the areas in sections *III-III* and *IV-IV* are identical)

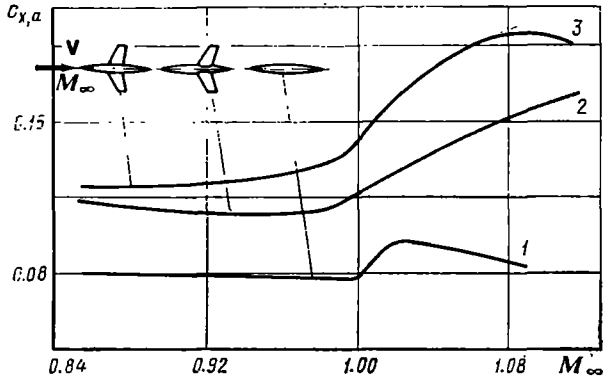

Fig. 12.8.3
Dependence of the drag coefficient of a craft designed according to the area rule on the number M_∞:
1 – minimum-drag body; *2* – body-wing combination designed according to the area rule; *3* – body-wing combination designed without account taken of the area rule

In the supersonic range, the above method may be employed only for very slender configurations with swept low-aspect-ratio wings. This method can also be used for unswept wings provided that $M_\infty \leqslant 1$.

Experimental investigations show that the area rule can be used to obtain such a design of a craft that would ensure the lowest drag in the transonic region. By this rule, a craft should be designed so that the areas of its cross sections would change along its longitudinal axis according to the same law as for a body of revolution with the minimum drag (Fig. 12.8.2).

Figure 12.8.3 shows the experimental dependence of the drag coefficient $c_{x,\alpha}$ at $c_{y_a} = 0$ on the number M_∞. A glance at this figure reveals that a body-wing combination designed according to the area rule has a lower drag in comparison with a combination designed without account taken of this rule.

The use of the area rule gives satisfactory results for the nearsonic range $0.8 \leqslant M_\infty \leqslant 1.4$.

Induced Drag

When $c_{y_a} \neq 0$, the additional (induced) drag is determined by the sum of the corresponding aerodynamic coefficients $c_{x,1} + \Delta c_{x,\alpha}$ [see (12.8.1)]. The induced drag coefficient $c_{x,1}$ for subsonic velocities, in turn, can be considered as the sum of the induced drag coefficients for the horizontal panels of the wing $(c_{x,1})_w$ and empennage $(c_{x,1})_e$ (in the absence of sideslip):

$$c_{x,1} = (c_{x,1})_w + (c_{x,1})_e = (\bar{c}_{x,1})_w (S'_w/S) k_1 + (\bar{c}_{x,1})_e (S'_e/S) k_2 \qquad (12.8.9)$$

where

$$(\bar{c}_{x,1})_w = (c^2_{y_a})_w/[\pi (\lambda_{ef})_w]; \quad (\bar{c}_{x,1})_e = (c^2_{y_a})_e/[\pi (\lambda_{ef})_e] \qquad (12.8.10)$$

In these expressions, the lift force coefficients are found for the separate panels with account taken of the area under the body, i.e. according to their actual span. To take interference into consideration, we have introduced empirical coefficients that are the effective aspect ratios:

$$(\lambda_{ef})_w = \lambda_w (1 + \Delta S_w/S'_w); \quad (\lambda_{ef})_e = \lambda_e (1 + \Delta S_e/S'_w) \qquad (12.8.11)$$

where $\lambda_w = 4 (s^2_m)_w/S'_w$; $\lambda_e = 4 (s^2_m)_e/S'_e$ are the aspect ratios of the separate wings and empennage, respectively.

At supersonic velocities, the induced drag coefficient $c_{x,1} = X_1/(q_\infty S) = c_{y_a}\alpha$. By (12.6.64), (12.7.26), (12.7.36), and (12.7.37), we have

$$c_{x,1} = c_{y,1}\alpha \frac{S_{mid}}{S} + \left\{\left[(K_w + K_b)_w + (k_w + k_b)_w \frac{\delta_{vt,w}}{\alpha}\right] \times k_1 c^\alpha_{y,w} \frac{S_w}{S} + \left[(K_w + K_b)_e + (k_w + k_b)_e \frac{\delta_{vt,e}}{\alpha}\right] \times k_2 [1 - (d\varepsilon/d\alpha)_e] c^\alpha_{y,e}\right\} \alpha^2 \qquad (12.8.12)$$

Let us consider the component of the total drag coefficient $c_{x,\alpha} = \Delta X_\alpha/(q_\infty S)$ depending on the angle of attack [see (12.8.1)]. The value of this coefficient is determined to a considerable extent by the suction ("reactive" or "pushing") force of the wings and empennage. When computing it account must be taken of the change in the lift force of the wings and empennage because of their interaction with

the body. By (8.11.5), and also having in view (12.6.64), (12.7.36), and (12.7.37) (with account taken of the minus sign), we have

$$(\Delta c_{x,\alpha})_w + (\Delta c_{x,\alpha})_e = (c_{x,b})_w + (c_{x,b})_e$$

$$= -\left[(\bar{c}_b\Delta_b)_w \left\{\left[(K_w + K_b)_w + (k_w + k_b)_w \frac{\delta_{vt,w}}{\alpha}\right] k_1 c^{\alpha}_{y,w}\right\}^2 \frac{S_w}{S}\right.$$

$$+ (\bar{c}_b\Delta_b)_e \left\{\left[(K_w + K_b)_e + (k_w + k_b)_e \frac{\delta_{vt,e}}{\alpha}\right]\right.$$

$$\left.\left. \times k_2 [1 - (d\varepsilon/d\alpha)_e] c^{\alpha}_{y,e}\right\}^2 \frac{S_e}{S}\right] \alpha^2 \qquad (12.8.13)$$

In the particular case when the controls are not deflected ($\delta_{vt,w} = \delta_{vt,e} = 0$), we have

$$(\Delta c_{x,\alpha})_w + (\Delta c_{x,\alpha})_e$$

$$= -\left\{(\bar{c}_b\Delta_b)_w \left[(K_w + K_b)^2_w k_1^2 (c^{\alpha}_{y,w})^2 \frac{S_w}{S}\right]\right.$$

$$\left. + (\bar{c}_b\Delta_b)_e \left[(K_w + K_b)^2_e k_2^2 [1 - (d\varepsilon/d\alpha)_e]^2 (c^{\alpha}_{y,e})^2 \frac{S_e}{S}\right]\right\} \alpha^2 \qquad (12.8.13')$$

When determining the suction force of the wings and empennage at subsonic velocities ($M_\infty < 1$), we can use formulas (8.11.5) and (8.11.6), taking interference factors for the interaction of slender configurations with the body such as in (12.8.13). We determine the suction force coefficient for the body calculated according to the characteristic area S in accordance with (11.5.43) in the form

$$(\Delta c_{x,\alpha})_b = c_{x,b} = \xi\alpha^2 S_{mid}/S \qquad (12.8.14)$$

Hence, the additional drag coefficient is

$$\Delta c_{x,\alpha} = (\Delta c_{x,\alpha})_b + (\Delta c_{x,\alpha})_w + (\Delta c_{x,\alpha})_e \qquad (12.8.15)$$

Many high-speed craft have wings and empennage with sharp leading edges, therefore the sum $(\Delta c_{x,\alpha})_w + (\Delta c_{x,\alpha})_e = 0$.

If we take into consideration that the suction force of the body forms an insignificant part of the total drag, we may consider that $(\Delta c_{x,\alpha})_b \approx 0$. Accordingly, the drag coefficient due to the angle of attack is determined by the formula $c_{x,i} = c_{y_a}\alpha$, i.e. by relation (12.8.12). In this relation, we may assume that $\delta_{vt,w} = \delta_{vt,e} \approx 0$ for craft in which the lift force changes insignificantly upon deflection of the controls, and, consequently, the induced drag produced by this deflection is negligibly small.

12.9. Non-Stationary Characteristics of a Craft

Numerical Method of Determining the Stability Derivatives at Subsonic Velocities

The main elements of modern flying craft, especially high-speed ones, are comparatively slender and only slightly bent. Hence, for the major part of the surface, the cosine of the angle between a normal to the surface at a given point and the longitudinal axis Ox is small, i.e. $\cos(\widehat{n, x}) \ll 1$. Using this inequality and considering the aerodynamic problems in a linear approximation, we can show (see [17, 18]) that when calculating the loads causing a normal force to be produced, a real craft can be replaced with a schematized basic plane parallel to the axis Ox. The corresponding boundary conditions are projected onto this plane. Consequently, it is assumed that the aerodynamic loads do not depend on the thickness of the craft. Accordingly, we solve the problem on determining the stability derivatives of a wing (see Sec. 9.8). By the adopted scheme, a craft of the given configuration for which we are evaluating the stability derivatives will be represented as one basic plane. We replace this plane, in turn, with a system of non-stationary vortices. Figure 12.9.1 shows such a system relating to circulatory flow over the given craft.

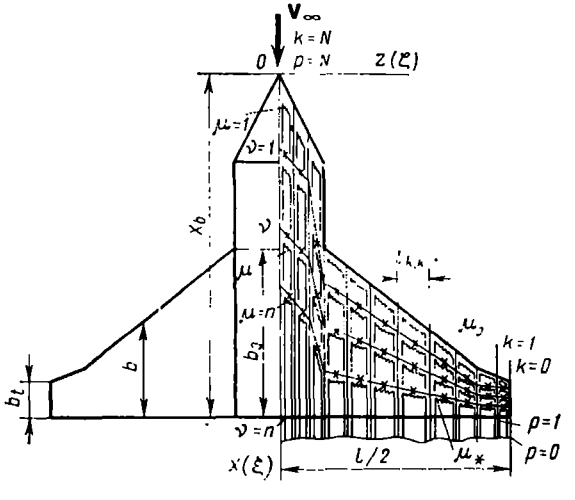

Fig. 12.9.1
Vortex model of a flat configuration of a craft

We shall perform all our further numerical calculations in the same way as for a wing. We choose the length of the craft x_b as the characteristic length when calculating the pitching moment coefficient m_z and the dimensionless kinematic parameter:

$$m_z = M_z/(q_\infty S_w x_b), \quad \omega_z = \Omega_z x_b/V_\infty$$

The wing span with account taken of the part under the fuselage is the characteristic length when calculating the rolling moment m_x, and the wing semi-span is the characteristic length when calculating the kinematic parameter ω_x:

$$m_x = M_x/(q_\infty, S_w, l), \quad \omega_x = \Omega_x l/(2V_\infty)$$

The obtained aerodynamic coefficients are converted to the number $M_\infty < 1$ (a compressible fluid) with the aid of formulas (9.8.95)-(9.8.98).

Pitch Damping

Let us consider the calculation of the pitch damping coefficient assuming that the craft in question is moving in a longitudinal plane without rolling. The characteristics of damping obtained as a result of such calculations are helpful for appraising the dynamic properties of a craft. Assume that the craft is in curvilinear motion at a zero angle of attack (Fig. 12.9.2) in a longitudinal plane. The damping can be investigated by assuming that this motion from the aerodynamic viewpoint is equivalent to the rotation of the craft about its centre of mass at a certain angular velocity.

Owing to such rotation, the empennage and part of the body under it are at a certain local angle of attack $\Delta\alpha = \Omega_z(x_{CM})_e/V$, where $(x_{CM})_e$ is the distance from the centre of mass of the craft to the centre of mass of the area of the part with an empennage, $\Omega_z(x_{CM})_e$ is the velocity of the additional vertical flow, and V is the velocity of the disturbed flow coming onto the empennage.

The angle of attack leads to the arising of a normal force of the tail part. Given the direction of rotation as shown in Fig. 12.9.2, this force acts upward, and when the direction of this rotation is reversed, downward. Hence, in both cases, the directions of rotation and of the additional damping moment are opposite.

The magnitude of the normal force is determined with account taken of interaction with the body. In addition, a correction may be introduced into the total value of the tail normal force due to the additional force of the body arising because of its interaction with the empennage. With this in view, we have

$$c_{y,e} = (K_e + K_b)\, c^{\alpha}_{y,e} \sqrt{k_1}\, \Omega_z\, (x_{CM})_e/V_\infty \qquad (12.9.1)$$

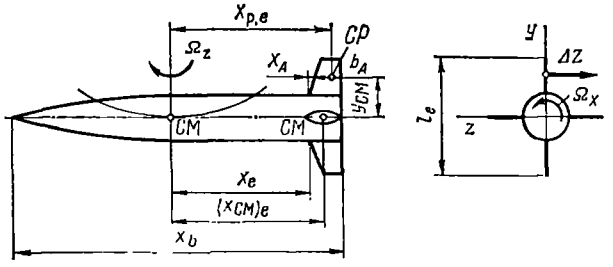

Fig. 12.9.2
Curvilinear motion of a body-empennage combination

where $(x_{CM})_e$ is a coordinate determined as the distance from the centre of mass of the craft to the middle of the mean aerodynamic chord of an empennage panel (Fig. 12.9.2), $(x_{CM})_e = x_e + x_A + b_A/2$.

The value of the coefficient $c_{y,e}$ is relatively small and is usually disregarded in calculations of the total normal force coefficient; here the additional pitching moment may substantially affect the dynamic properties of a craft. We calculate the coefficient of this moment using the quantity $c_{y,e}$ and the distance $(x_p)_e$ from the centre of mass to the centre of pressure:

$$m_{z,e} = -(K_e + K_b)\, c^{\alpha}_{y,e} \sqrt{\bar{k}_1}\, \Omega_z\, (x_{CM})_e\, (x_p)_e / (x_b V_\infty) \qquad (12.9.2)$$

The corresponding rotary derivatives with respect to the parameter $\omega_z = \Omega_z x_b / V_\infty$ have the following form:

$$c^{\omega_z}_{y,e} = (K_e + K_b)\, c^{\alpha}_{y,e} \sqrt{\bar{k}_1}\, (\bar{x}_{CM})_e \qquad (12.9.3)$$

$$m^{\omega_z}_{z,e} = -(K_e + K_b)\, c^{\alpha}_{y,e} \sqrt{\bar{k}_1}\, (\bar{x}_{CM})_e\, (\bar{x}_p)_e \qquad (12.9.4)$$

where $(\bar{x}_{CM})_e = (x_{CM})_e / x_b$ and $(\bar{x}_p)_e = (x_p)_e / x_b$; for approximate calculations, we can assume that $(x_p)_e = (x_{CM})_e$.

Derivative (12.9.4) always has a minus sign because the directions of the damping moment and of rotation are opposite. Formula (12.9.4) may be used for cases when the empennage is at a sufficient distance from the centre of mass of the body.

To determine the total stability derivatives for a body-empennage combination, we shall use the general relations for the normal force and the pitch damping moment:

$$c^{\Omega_z}_{y} q_\infty S_{mid} \Omega_z = c^{\Omega_z}_{y,b} q_\infty S_{mid} \Omega_z + c^{\Omega_z}_{y,e} q_\infty S_e \Omega_z$$

$$m^{\Omega_z}_{z} q_\infty S_{mid} x_b = m^{\Omega_z}_{z,b} q_\infty S_{mid} \Omega_z x_b + m^{\Omega_z}_{z,e} q_\infty S_e x_b \Omega_z$$

Going over in these relations to the derivatives with respect to the dimensionless variable $\omega_z = \Omega_z x_b / V_\infty$, we obtain

$$c_y^{\omega_z} = c_{y,b}^{\omega_z} + c_{y,e}^{\omega_z} S_e / S_{mid}; \quad m_z^{\omega_z} = m_{z,b}^{\omega_z} + m_{z,e}^{\omega_z} S_e / S_{mid} \qquad (12.9.5)$$

where $c_{y,b}^{\omega_z}$ and $m_{z,b}^{\omega_z}$ are derivatives determined from the relations for a separate body, and $c_{y,e}^{\omega_z}$ and $m_{z,e}^{\omega_z}$ are determined by relations (12.9.3) and (12.9.4), respectively.

If when finding the normal force and pitch moment coefficients for the part with the empennage we choose the mean aerodynamic chord as the characteristic length ($x_b = b_{A,e}$), then the derivatives are calculated by the formulas

$$\left.\begin{aligned} c_y^{\omega_z} &= c_{y,b}^{\omega_z} + c_{y,e}^{\omega_{z,A}} S_e b_{A,e} / (S_{mid} x_b) \\ m_z^{\omega_z} &= m_{z,b}^{\omega_z} + m_{z,e}^{\omega_{z,A}} S_e b_{A,e}^2 / (S_{mid} x_b^2) \end{aligned}\right\} \qquad (12.9.6)$$

where $\omega_{z,A} = \Omega_z b_{A,e} / V_\infty$. The derivatives with respect to $\omega_{z,A}$ can be found with a view to (12.9.3) and (12.9.4):

$$c_{y,e}^{\omega_{z,A}} = c_{y,e}^{\omega_z} x_b / b_{A,e}; \quad m_{z,e}^{\omega_{z,A}} = m_{z,e}^{\omega_z} x_b^2 / b_{A,e}^2 \qquad (12.9.7)$$

Yawing Moment

The above method of calculating pitch damping can be employed for evaluating the stability derivatives of the part of the body with the empennage in yawing and provided that all other kinds of motion are absent. In accordance with this method, the stability derivatives for yawing are determined for a cruciform (plus-shaped) empennage by the relations

$$c_{z,e+}^{\omega_y} = -c_{y,e+}^{\omega_z}; \quad m_{y,e+}^{\omega_y} = -m_{z,e+}^{\omega_z} \qquad (12.9.8)$$

where $\omega_y = \Omega_y x_b / V_\infty$.

The rotation of a craft about its longitudinal axis may set up an additional yawing moment known as a **spiral moment**. This is due to longitudinal suction forces on the leading edges of the horizontal empennage. If the rotation occurs in the direction of the starboard empennage panel, the force on this panel is greater than that on the port one because of the increase in the local angle of attack. As a result, a positive yawing moment ΔM_y is produced that for relatively slow rotation is proportional to the angular velocity Ω_x. Such a moment is produced only at subsonic velocities (or at numbers $M_\infty > 1$ for empennage panels with subsonic leading edges). For empennage panels with supersonic edges, the spiral moment equals zero because no suction force appears.

Investigations show that when a spiral moment appears (in the presence of a horizontal empennage or wings), its magnitude is so insignificant that in practical calculations of the total yawing moment it is usually disregarded.

When a craft provided with empennage having vertical panels symmetric about the body performs rotation, no spiral yawing moment occurs. The explanation is that the lateral forces arising on the panels because of such rotation are opposite in sign.

If there is one panel (upper or lower), the spiral moment does not equal zero. We evaluate this moment as follows. An additional sideslip angle β appears as a result of the rotation at the velocity Ω_x. The mean value of this angle is $\beta = \Omega_x y_{CM}/V$ (where y_{CM} is the distance from the axis to the centre of mass of the empennage area, approximately equal to the distance to the mean chord b_A, Fig. 12.9.2). The lateral force corresponding to this angle is

$$\Delta Z = -(K_e + K_b)\, c^{\alpha}_{y,e} \beta q S_e$$

The moment of this force about the centre of mass of the craft is

$$\Delta M_y = -(K_e + K_b)\, c^{\alpha}_{y,e} \Omega_x y_{CM} (x_p)_e\, q S_e / V$$

Upon calculating the spiral moment coefficient and the corresponding derivative with respect to $\omega_x = \Omega_x l_e/(2V_\infty)$ related to the velocity head q_∞ and body length x_b, we find

$$m_y^{\omega_x} = -2(K_e + K_b)\, c^{\alpha}_{y,e} \bar{y}_{CM} (\bar{x}_p)_e \sqrt{k_1} \qquad (12.9.9)$$

where $\bar{y}_{CM} = y_{CM}/l_e$ and $(\bar{x}_p)_e = (x_p)_e/x_b$ (here l_e is the span of the empennage with account taken of the body thickness).

Roll Damping

Method of Reduced Angle of Attack. When a craft rotates at an angular velocity Ω_x, each section of a horizontal panel has an additional velocity $\Delta V_y = -\Omega_x z$ that is variable along its span (Fig. 12.9.3). We can calculate the average value of this velocity as $V_{y,av} = -\Omega_x (z_{CM})_e$, where $(z_{CM})_e$ is a coordinate of the centre of mass of the panel area. Such an additional crossflow corresponds to an increase in the angle of attack of the starboard panel by the magnitude $\Delta\alpha = -V_{y,av}/V = \Omega_x (z_{CM})_e/V_\infty$ and a decrease in its value for the port panel by the same amount (these values of the angles of attack are called **reduced**). Consequently, normal forces ΔY equal in magnitude, but opposite in sign, arise on both panels:

$$\Delta Y = \pm\, c^{\alpha}_{y,e} K_e q\, (S_{e(b)}/2)\, \Omega_x (z_{CM})_e / V$$

where $S_{e(b)}$ is the area of the empennage panels with account taken of the part under the body (fuselage).

The corresponding normal force coefficient is

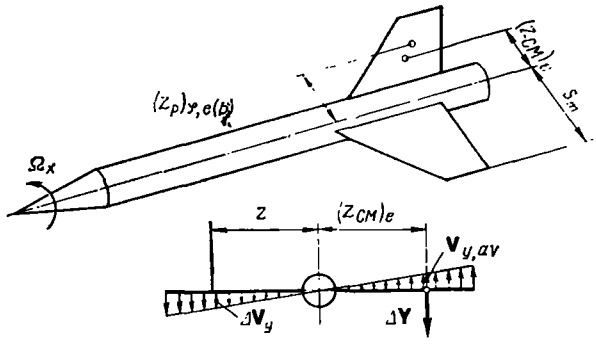

Fig. 12.9.3
To the definition of the reduced angle of attack method

$$\Delta c_y = \Delta Y/(q_\infty S_{e(b)}/2) = \pm 2c^{\alpha}_{y,e} K_e \sqrt{\bar{k}_1}\, \omega_x (\bar{z}_{CM})_e \qquad (12.9.10)$$

where $\omega_z = \Omega_x l_e/(2V_\infty)$, $(\bar{z}_{CM})_e = (z_{CM})_e/l_e$, and $c^{\alpha}_{y,e}$ is a coefficient determined for the separate empennage panels.

By (12.9.10), the rotary derivative of the rolling moment coefficient (the roll-damping derivative) is determined by the expression

$$m_x^{\omega_x} = \Delta M_x/(q_\infty S_{e(b)} l_e \omega_x) = \Delta Y (z_p)_{\Gamma,e(b)}/(q_\infty S_{e(b)} l_e \omega_x)$$
$$= -c^{\alpha}_{y,e} K_e \sqrt{\bar{k}_1}\, (\bar{z}_{CM})_e [r_m + (1-r_m)(\bar{z}_p)_{\Phi,e(b)}] \qquad (12.9.11)$$

where $r_m = 2r/l_e$, $(\bar{z}_p)_{\Phi,e(b)} = [(z_p)_{\Phi,e(b)} - r]/(0.5l_e - r)$.

By halving the magnitude of the damping derivative found with the aid of (12.9.11), to a first approximation we can determine the corresponding value of the damping moment coefficient derivative produced by a vertical panel of an asymmetric empennage of an aircraft. Here, evidently, all the calculations must be performed with a view to the configuration and geometry of the panel.

With a cruciform ("+" or "×") arrangement of a craft, the value given by (12.9.11) must be doubled, and, in addition, a correction factor must be introduced into it that takes the interaction between the panels into consideration.

Let us consider the nature of interference. Let us assume that a pressure difference producing a normal force has appeared on the upper and lower sides of a horizontal panel. The increased pressure on the upper side of the horizontal panel extends partly to the inner side of the upper vertical panel, and the rarefaction on its lower side, to the inner side of the lower vertical panel. As a result, an additonal rolling moment due to the vertical panels is produced that is opposite in sign to the moment due to the horizontal control surfaces. Hence, the total rolling moment diminishes. Investigations show that the decrease can be taken into account by introduc-

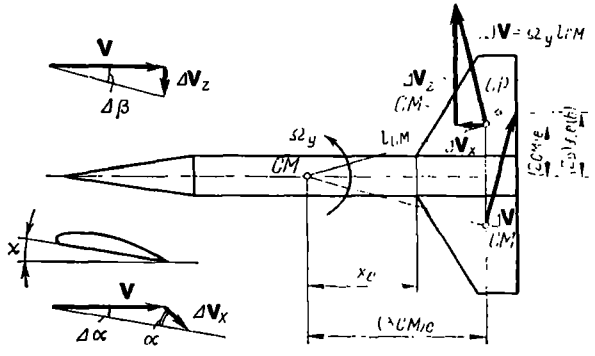

Fig. 12.9.4
To the determination of the rolling moment rotary derivatives

ing a correction factor $\varkappa$ to the magnitude of the rolling moment due to the deflection of the cruciform controls and calculated without considering interference. The factor $\varkappa$ can be found as a function of $r_m = r/s_m = r/(0.5l_e)$ by the approximate formula

$$\varkappa = 1 - \exp(-4.5r_m) \qquad (12.9.12)$$

applicable for the values of r_m from 0.4 to 1. When $r_m \leqslant 0.4$, we may assume $\varkappa = 0.75$. Accordingly, for a cruciform empennage configuration, the rotary derivative is

$$m_{x+}^{\omega_x} = m_{x\times}^{\omega_x} = 2\varkappa m_x^{\omega_x} \qquad (12.9.13)$$

Rotary Derivatives $m_x^{\omega_y}$ and $m_x^{\omega_z}$. The rolling moments arising because of rotation of a craft about its centre of mass at the angular velocities Ω_y and Ω_z are called **spiral moments**. Let us consider the calculation of the rotary derivatives of the coefficients of these moments determined by the values of $m_x^{\omega_y}$ and $m_x^{\omega_z}$ (where $w_y = \Omega_y x_b/V_\infty$, and $\omega_z = \Omega_z x_b/V_\infty$).

When a craft rotates about its centre of mass at the angular velocity Ω_y (Fig. 12.9.4), a wing panel acquires the additional linear velocity $\Delta V = \Omega_y l_{CM}$ (where l_{CM} is the distance from the centre of mass of the craft to that of the panel area). With a positive value of Ω_y, this velocity is directed forward at the starboard panel and backward at the port one. The longitudinal components of the additional velocity ΔV_x have the same direction. Accordingly, the velocity of the flow over the starboard panel grows, and over the port one diminishes. Simultaneously, the angles of attack change. This change for a panel can be evaluated by the mean increment of the angle of attack $\Delta\alpha$ for a section passing through the centre of mass of the

cross-sectional area. Inspection of Fig. 12.9.4 reveals that

$$\Delta\alpha = \pm [\Omega_y (z_{CM})_e / V] \alpha$$

(this angle is positive for the starboard panel and negative for the port one).

The change in the angles of attack causes the arising of additional normal forces of the opposite sign on the starboard and port panels:

$$\Delta Y_\alpha = \pm c^\alpha_{y,e} K_e q (S_{e(b)}/2) \Omega_y (z_{CM})_e \alpha / V \qquad (12.9.14)$$

The coefficients of these forces are

$$\Delta c_{y,\alpha} = \Delta Y_\alpha / (q_\infty S_{e(b)}/2) = \pm c^\alpha_{y,e} \alpha K_e \sqrt{\bar{k}_1}\, \omega_y (\bar{z}_{CM})_e \bar{l}_e \qquad (12.9.15)$$

where $(\bar{z}_{CM})_e = (z_{CM})_e / l_e$ and $\bar{l}_e = l_e / x_b$.

We can use the quantity ΔY_α computed by (12.9.14) to determine the rolling moment coefficient:

$$m_{x,\alpha} = \Delta Y_\alpha (z_p)_{\varphi,e(b)} / [q_\infty (S_{e(b)}/2)_e l_e]$$
$$= -c^\alpha_{y,e} \alpha K_e \sqrt{\bar{k}_1}\, \omega_y (\bar{z}_{CM})_e \bar{l}_e (z_p)_{\varphi,e(b)} / l_e \qquad (12.9.16)$$

The corresponding mixed derivative is

$$m^{\alpha\omega_y}_{x,\alpha} = -0.5 c^\alpha_{y,e} K_e \sqrt{\bar{k}_1}\, (\bar{z}_{CM})_e \bar{l}_e [r_m + (1 - r_m)(\bar{z}_p)_{\varphi,e(b)}] \qquad (12.9.17)$$

This derivative at a positive angular velocity Ω_y is always negative.

In addition to longitudinal flow, the rotation of a craft at the angular velocity Ω_y also produces an additional crossflow at the velocity $\Delta V_z = \Omega_y (x_{CM})_e$ at the sideslip angle $\Delta\beta = \Delta V_z / V = \Omega_y (x_{CM})_e / V$ (Fig. 12.9.4). Sideslip is attended by the rolling moment $\Delta M_{x,\beta}$ whose coefficient is

$$m_{x,\beta} = \Delta M_{x,\beta} / (q_\infty S_{e(b)} l_e) = m^\beta_x \Omega_y (x_{CM})_e / V = m^\beta_x \omega_y (\bar{x}_{CM})_e \qquad (12.9.18)$$

where $(\bar{x}_{CM})_e = (x_{CM})_e / x_b$ is the dimensionless coordinate of the empennage centre of mass.

The corresponding rotary derivative is

$$m^{\omega_y}_{x,\beta} = m^\beta_x (\bar{x}_{CM})_e \qquad (12.9.19)$$

We can find the derivative m^β_x with the aid of expression (12.5.11) determining the rolling moment coefficient m_x depending on the sweep and dihedral angle, the body-wing interference, and also the shape of the panels.

Hence, the total rotary derivative is

$$m^{\omega_y}_x = m^{\omega_y}_{x,\alpha} + m^{\omega_y}_{x,\beta} = m^{\omega_y}_{x,\alpha} + m^\beta_x (\bar{x}_{CM})_e \qquad (12.9.20)$$

If the horizontal panels producing a spiral moment belong to a cruciform empennage, then when computing the rotary derivative $m_x^{\omega_y}$ one should take into consideration all four panels by introducing the correction factor $\varkappa$ (12.9.12) into (12.9.20):

$$m_{x+}^{\omega_y} = \varkappa m_x^{\omega_y} \tag{12.9.21}$$

The vertical panels of an empennage produce a spiral moment when they rotate about the lateral axis Oz at the angular velocity Ω_z. For a craft with a cruciform empennage, the rotary derivative of the coefficient of this moment is determined in accordance with aerodynamic symmetry by the expression

$$m_{x+}^{\omega_z} = m_{x+}^{\omega_y} \tag{12.9.22}$$

The vertical empennage can also produce a spiral moment upon rotation about the vertical axis Oy at the velocity Ω_y if it is not symmetric. This moment is caused by the additional lateral force ΔZ_β arising on the lower or upper panels in sideslip at the angle $\Delta\beta = \Omega_y (x_{CM})_e/V$:

$$\Delta Z_\beta = c_{y,e}^{\alpha} K_e q (S_{e(b)}/2) \Omega_y (x_{CM})_e/V \tag{12.9.23}$$

Multiplying this quantity by the coordinate of the centre of pressure $(y_p)_{\varphi, e(b)} = (z_p)_{q, e(b)}$, we obtain the spiral rolling moment $\Delta M_{x,\beta}$.

The corresponding coefficient of this moment is

$$m_{x,\beta} = \Delta M_{x,\beta}/[q_\infty (S_{e(b)}/2) s_m]$$

$$= -c_{y,e}^{\alpha} K_e q \Omega_y (x_{CM})_e (z_p)_{q,e(b)}/(q_\infty s_m V) \tag{12.9.24}$$

Bearing in mind that the dimensionless kinematic parameter $\omega_y = \Omega_y x_b/V_\infty$, we obtain the derivative

$$m_{x,\beta}^{\omega_y} = -c_{y,e}^{\alpha} K_e \sqrt{k_1} (\bar{x}_{CM})_e [r_m + (1 - r_m)(\bar{z}_p)_{\varphi,e(b)}] \tag{12.9.25}$$

Application of the Results of Calculating the Wing and Body Derivatives

The stability derivative of a craft consisting of a combination of a body of revolution and a wing (empennage) can be calculated as the sum of the relevant derivatives found for the separate bodies of revolution and wings by using the interference factors.

We shall proceed in our calculations from the assumption that the interference factors K_w and K_b obtained for a steady flow are the same as for unsteady flow. Accordingly, any aerodynamic characteristic (c_y, m_x, m_z) for such motion of a body-wing (empennage) combi-

nation can be written in the form of a series:

$$c_{\mathrm{b,w}} = \sum_{i=1}^{3} (c_{\mathrm{b,w}}^{q_i} q_i + c_{\mathrm{b,w}}^{\dot{q}_i} \dot{q}_i) = \sum_{i=1}^{3} (c_{\mathrm{b}}^{q_i} q_i + c_{\mathrm{b}}^{\dot{q}_i} \dot{q}_i)$$

$$+ (K_{\mathrm{w}} + K_{\mathrm{b}}) \sum_{i=1}^{3} (c_{\mathrm{w}}^{q_i} q_i + c_{\mathrm{w}}^{\dot{q}_i} \dot{q}_i) \qquad (12.9.26)$$

$(i = 1,\ 2,\ 3;\ q_1 = \alpha,\ q_2 = \omega_x,\ q_3 = \omega_z;\ \dot{q}_1 = \dot{\alpha},\ \dot{q}_2 = \dot{\omega}_x,\ \dot{q}_3 = \dot{\omega}_z)$,

The subscript "b, w" signifies the aerodynamic coefficient of the entire combination, while the separate subscripts "b" and "w" stand for the corresponding coefficients of the separate body or wing. In accordance with (12.9.26), the part of the body under the wing (empennage) producing an additional normal force because of interaction with a lifting surface is considered as the part of the wing (empennage) under the fuselage (body). Such a wing with a part under the body whose span is $l = 2s_m$ has a normal force, the coefficient of which by (12.9.26) is

$$\Delta c_{y,\mathrm{w(b)}} + \Delta c_{y,\mathrm{b(w)}} = \sum_{i=1}^{3} (c_{y,\mathrm{w}}^{q_i} q_i + c_{y,\mathrm{w}}^{\dot{q}_i} \dot{q}_i) \qquad (12.9.27)$$

where $c_{y,\mathrm{w}}^{q_i}$ and $c_{y,\mathrm{w}}^{\dot{q}_i}$ are the stability derivatives for a separate wing whose span is $l = 2s_m$.

When using relation (12.9.26), we shall assume that sideslip of the craft is absent, and the rolling moment coefficient and its derivatives for a body (of revolution) are zero. Accordingly, (12.9.26) yields the following relations for the stability derivatives of a craft consisting of a body and a wing (empennage):

$$\left.\begin{aligned} c_{y,\mathrm{b,w}}^{\alpha} &= c_{y,\mathrm{b}}^{\alpha} + (K_{\mathrm{w}} + K_{\mathrm{b}})\, c_{y,\mathrm{w}}^{\alpha} \\ c_{y,\mathrm{b,w}}^{\dot{\alpha}} &= c_{y,\mathrm{b}}^{\dot{\alpha}} + (K_{\mathrm{w}} + K_{\mathrm{b}})\, c_{y,\mathrm{w}}^{\dot{\alpha}} \end{aligned}\right\} \qquad (12.9.28)$$

$$\left.\begin{aligned} c_{y,\mathrm{b,w}}^{\omega_z} &= c_{y,\mathrm{b}}^{\omega_z} + (K_{\mathrm{w}} + K_{\mathrm{b}})\, c_{y,\mathrm{w}}^{\omega_z} \\ c_{y,\mathrm{b,w}}^{\dot{\omega}_z} &= c_{y,\mathrm{b}}^{\dot{\omega}_z} + (K_{\mathrm{w}} + K_{\mathrm{b}})\, c_{y,\mathrm{w}}^{\dot{\omega}_z} \end{aligned}\right\} \qquad (12.9.29)$$

$$\left.\begin{aligned} m_{x,\mathrm{b,w}}^{\omega_x} &= (K_{\mathrm{w}} + K_{\mathrm{b}})\, m_{x,\mathrm{w}}^{\omega_x} \\ m_{x,\mathrm{b,w}}^{\dot{\omega}_x} &= (K_{\mathrm{w}} + K_{\mathrm{b}})\, m_{x,\mathrm{w}}^{\dot{\omega}_x} \end{aligned}\right\} \qquad (12.9.30)$$

$$\left.\begin{aligned} m^{\alpha}_{z,\mathrm{b,w}} &= m^{\alpha}_{z,\mathrm{b}} + (K_{\mathrm{w}} + K_{\mathrm{b}})\, m^{\alpha}_{z,\mathrm{w}} \\ m^{\dot{\alpha}}_{z,\mathrm{b,w}} &= m^{\dot{\alpha}}_{z,\mathrm{b}} + (K_{\mathrm{w}} + K_{\mathrm{b}})\, m^{\dot{\alpha}}_{z,\mathrm{w}} \end{aligned}\right\} \qquad (12.9.31)$$

$$\left.\begin{aligned} m^{\omega_z}_{z,\mathrm{b,w}} &= m^{\omega_z}_{z,\mathrm{b}} + (K_{\mathrm{w}} + K_{\mathrm{b}})\, m^{\omega_z}_{z,\mathrm{w}} \\ m^{\dot{\omega}_z}_{y,\mathrm{b,w}} &= m^{\dot{\omega}_z}_{z,\mathrm{b}} + (K_{\mathrm{w}} + K_{\mathrm{b}})\, m^{\dot{\omega}_z}_{z,\mathrm{w}} \end{aligned}\right\} \qquad (12.9.32)$$

The calculation of the stability derivatives for the unsteady motion of separate wings (empennage) is treated in Chap. 9, and for slender bodies, in Chap. 11. It is shown in these calculations what reduction centre the derivatives are related to. We already know that for a wing we can choose its vertex or the beginning of the mean aerodynamic chord as its reduction centre, and for a body, its centre of mass or the front point of its nose.

Therefore, when using expressions (12.9.28), (12.9.29), (12.9.31), and (12.9.32), the stability derivatives for separate wings (empennage) and a body are recalculated in accordance with the new point of reference for the entire craft. Such conversion is obviously not needed for the stability derivatives with respect to ω_x and $\dot{\omega}_x$ (for rolling) because of coincidence of the longitudinal axes about which the rolling moment M_x is evaluated for a separate wing and for the craft as a whole.

When converting the derivatives to a new reduction centre, one should use formulas (9.3.7) and (9.3.8). Figure 12.9.5 shows points O, O_1, and O_2, which are the reduction centres for the craft as a whole, for the separate body, and separate wing, respectively. Points O and O_1 are usually the centres of mass of the craft and body. Let $\bar{x}_1 = x_1/x_{\mathrm{b}}$ and $\bar{x}_2 = x_2/x_{\mathrm{b}}$ be the dimensionless distances from centres O_1 and O_2 to reduction centre O. In accordance with Fig. 12.9.5 and formulas (9.3.7) and (9.3.8), in which the sign of $\bar{x} = \bar{x}_1$ has to be reversed, we have the following relations for a body:

$$\left.\begin{aligned} c^{\alpha}_{y,1,\mathrm{b}} &= c^{\alpha}_{y,\mathrm{b}}, \quad c^{\dot{\alpha}}_{y,1} = c^{\dot{\alpha}}_{y,\mathrm{b}} \\ c^{\omega_z}_{y,1,\mathrm{b}} &= c^{\omega_z}_{y,\mathrm{b}} - c^{\alpha}_{y,\mathrm{b}}\bar{x}_1, \quad c^{\dot{\omega}_z}_{y,1,\mathrm{b}} = c^{\dot{\omega}_z}_{y,\mathrm{b}} - c^{\dot{\alpha}}_{y}\bar{x}_1 \end{aligned}\right\} \qquad (12.9.33)$$

$$\left.\begin{aligned} m^{\alpha}_{z,1,\mathrm{b}} &= m^{\alpha}_{z,\mathrm{b}} + c^{\alpha}_{y,\mathrm{b}}\bar{x}_1, \quad m^{\dot{\alpha}}_{z,1,\mathrm{b}} = m^{\dot{\alpha}}_{z,\mathrm{b}} + c^{\dot{\alpha}}_{y,\mathrm{b}}\bar{x}_1 \\ m^{\omega_z}_{z,1,\mathrm{b}} &= m^{\omega_z}_{z,\mathrm{b}} - (m^{\alpha}_{z,\mathrm{b}} - c^{\omega_z}_{y,\mathrm{b}})\,\bar{x}_1 - c^{\alpha}_{y,\mathrm{b}}\bar{x}_1^2 \\ m^{\dot{\omega}_z}_{z,1,\mathrm{b}} &= m^{\dot{\omega}_z}_{z,\mathrm{b}} - (m^{\dot{\alpha}}_{z,\mathrm{b}} - c^{\dot{\omega}_z}_{y,\mathrm{b}})\,\bar{x}_1 - c^{\dot{\alpha}}_{y,\mathrm{b}}\bar{x}_1^2 \end{aligned}\right\} \qquad (12.9.34)$$

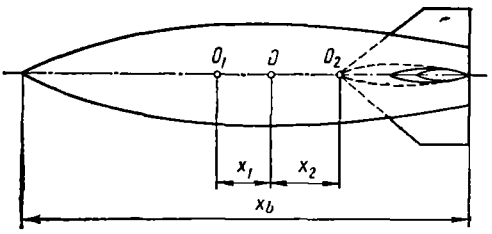

Fig. 12.9.5
To the conversion of the stability derivatives for a body and wing (empennage) to the reduction centre O of a craft

The corresponding formulas for a wing are:

$$\left.\begin{aligned} c^{\alpha}_{y,1,w} &= c^{\alpha}_{y,w}, \quad \dot{c}^{\dot\alpha}_{y,1,w} = \dot{c}^{\dot\alpha}_{y,w} \\ c^{\omega_z}_{y,1,w} &= c^{\omega_z}_{y,w} + c^{\alpha}_{y,w}\bar{x}_2, \quad \dot{c}^{\dot\omega_z}_{y,1,w} = \dot{c}^{\dot\omega_z}_{y,w} + \dot{c}^{\dot\alpha}_{y,w}\bar{x}_2 \end{aligned}\right\} \quad (12.9.35)$$

$$\left.\begin{aligned} m^{\alpha}_{z,1,w} &= m^{\alpha}_{z,w} - c^{\alpha}_{y,w}\bar{x}_2, \quad \dot{m}^{\dot\alpha}_{z,1,w} = \dot{m}^{\dot\alpha}_{z,w} - \dot{c}^{\dot\alpha}_{y,w}\bar{x}_2 \\ m^{\omega_z}_{z,1,w} &= m^{\omega_z}_{z,w} + (m^{\alpha}_{z,w} - c^{\omega_z}_{y,w})\,\bar{x}_2 - c^{\alpha}_{y,w}\bar{x}_2^2 \\ \dot{m}^{\dot\omega_z}_{z,1,w} &= \dot{m}^{\dot\omega_z}_{z,w} + (\dot{m}^{\dot\alpha}_{z,w} - \dot{c}^{\dot\omega_z}_{y,w})\,\bar{x}_2 - \dot{c}^{\dot\alpha}_{y,w}\bar{x}_2^2 \end{aligned}\right\} \quad (12.9.36)$$

When computing the total derivatives of a craft from their corresponding values for the separate body and wings, one must take into account that all these derivatives have to be related to the same geometric characteristics. We usually take the length x_b of a craft and the wing planform area as the characteristic for the pitching moment coefficient m_z of a craft; when evaluating the kinematic parameters $\dot{\alpha}$, ω_z and $\dot{\omega}_z$, we usually take the same length x_b as this characteristic, i.e.

$$\left.\begin{aligned} m_{z,b,w} &= M_{z,b,w}/(q_\infty S_w x_b), \quad \dot{\bar{\alpha}} = (d\alpha/dt)\,x_b/V_\infty \\ \omega_z &= \Omega_z x_b/V_\infty, \qquad\qquad \dot{\omega}_z = (d\Omega_z/dt)\,x_b^2/V_\infty^2 \end{aligned}\right\} \quad (12.9.37)$$

Let us assume that the length x_b and the area of the middle section S_{mid} are the characteristics for the body, while the mean aerodynamic chord b_A and the area S_w are those for the wing. Accordingly,

$$\left.\begin{aligned} m_{z,b} &= M_{z,b}/(q_\infty S_{mid} x_b), \quad \dot{\bar{\alpha}}_b = (d\alpha/dt)\,x_b/V_\infty \\ \omega_{z,b} &= \Omega_z x_b/V_\infty, \qquad\qquad \dot{\omega}_{z,b} = (d\Omega_z/dt)\,x_b^2/V_\infty \end{aligned}\right\} \quad (12.9.37')$$

$$\left.\begin{aligned} m_{z,w} &= M_{z,w}/(q_\infty S_w b_A), \quad \dot{\bar{\alpha}}_w = (d\alpha/dt)\,b_A/V_\infty \\ \omega_{z,w} &= \Omega_z b_A/V_\infty, \qquad\qquad \dot{\omega}_{z,w} = (d\Omega_z/dt)\,b_A^2/V_\infty^2 \end{aligned}\right\} \quad (12.9.38)$$

Assuming that the aerodynamic coefficients and the corresponding stability derivatives of the body and wing are related to the same reduction centre, we obtain the following equation for the sum of the moments $M_{z,b,w} = M_{z,b} + M_{z,w}$:

$$m_{z,b,w} q_\infty S_w x_b = m_{z,1b} q_\infty S_{mid} x_b + m_{z,1w} q_\infty S_w b_A$$

whence the total pitching moment coefficient is

$$m_{z,b,w} = m_{z,1b} S_{mid}/S_w + m_{z,1w} b_A/x_b \qquad (12.9.39)$$

The corresponding relation for the derivative with respect to the angle α has the form

$$m^{\alpha}_{z,b,w} = m^{\alpha}_{z,1b} S_{mid}/S_w + m^{\alpha}_{z,1w} b_A/x_b \qquad (12.9.39')$$

Let us consider the expression for the component of the pitching moment due to longitudinal rotation at the angular velocity Ω_z:

$$M_{z,b,w} = m^{\Omega_z}_{z,b,w} q_\infty S_w x_b \Omega_z$$

$$M_{z,1b} = m^{\Omega_z}_{z,1b} q_\infty S_{mid} x_b \Omega_z, \quad M_{z,1w} = m^{\Omega_z}_{z,1w} q_\infty S_w b_A \Omega_z$$

Summation yields

$$m^{\omega_z}_{z,b,w} q_\infty S_w x_b (\Omega_z x_b/V_\infty) = m^{\omega_{z,b}}_{z,1b} q_\infty S_{mid} x_b (\Omega_z x_b/V_\infty)$$

$$+ m^{\omega_{z,w}}_{z,1w} q_\infty S_w b_A (\Omega_z b_A/V_\infty)$$

Hence it follows that the derivative of the craft is

$$m^{\omega_z}_{z,b,w} = m^{\omega_{z,b}}_{z,1b} S_{mid}/S_w + m^{\omega_{z,w}}_{z,1w} b_A^2/x_b^2 \qquad (12.9.40)$$

We shall write the expressions for the other aerodynamic coefficients and their derivatives in a similar way. Here we obtain the derivatives $m^{\alpha}_{z,1b}$, $m^{\alpha}_{z,1w}$, $m^{\omega_{z,b}}_{z,1b}$, and $m^{\omega_{z,w}}_{z,1w}$ for the body and wing in formulas (12.9.39') and (12.9.40) by conversion to the corresponding reduction centre with the aid of relations (12.9.33)-(12.9.36).

Rotary Derivatives of a Craft

The rotary derivatives of craft of the body-wing-empennage type (see Fig. 12.6.3) in pitching are determined from the parameters obtained for pitch damping of the empennage. By analogy with (12.9.3) and (12.9.4), with account taken of stagnation, we find the rotary derivatives of the wing and part of the body under it ($c^{\omega_z}_{y,w}$, $m^{\omega_z}_{z,w}$, with substitution of the subscript "w" for "e"). In the calculations, the quantities $(x_{CM})_w$ and $(x_p)_w$ may be assumed to be identical.

When determining the stability derivatives for the section with an empennage, one must take into account the wash of the flow behind the wing. The wash angle is

$$\varepsilon = -(d\varepsilon/d\alpha)_e \, \Omega_z \, (x_p)_w / V'$$

With a view to the wash angle, the lift force coefficient for this section is

$$c_{y,e} = (K_w + K_b)_e \, c^{\alpha}_{y,e} \left[\frac{\Omega_z (x_p)_e}{V''} - \frac{\Omega_z (x_p)_w}{V'} \left(\frac{d\varepsilon}{d\alpha} \right)_e \right] \frac{q}{q_\infty} \frac{S_e}{S_w}$$

where V' and V'' are the velocities ahead of the wing and empennage, respectively, and $q = \rho_\infty V''^2/2$.

Taking into consideration the values of $k_1 = (V'/V_\infty)^2$, $k_2 = (V''/V_\infty)^2$ and calculating the derivative with respect to $\omega_z = \Omega_z x_b / V_\infty$, we obtain

$$c^{\omega_z}_{y,e} = (K_w + K_b)_e \, c^{\alpha}_{y,e} \left[(\bar{x}_p)_e \sqrt{k_2} - (\bar{x}_p)_w \left(k_2 / \sqrt{k_1} \right) (d\varepsilon/d\alpha)_e \right] S_e / S_w \tag{12.9.41}$$

The corresponding derivative of the damping moment coefficient calculated from the wing area S_w and the body length x_b is

$$m^{\omega_z}_{z,e} = -(K_w + K_b)_e \, c^{\alpha}_{y,e}$$

$$\left[(\bar{x}_p)_e \sqrt{k_2} - (\bar{x}_p)_w \left(k_2 / \sqrt{k_1} \right) (d\varepsilon/d\alpha)_e \right] S_e \, (\bar{x}_p)_e / S_w \tag{12.9.42}$$

The total rotary derivatives of a body-wing empennage combination are

$$\left.\begin{aligned} c^{\omega_z}_y &= c^{\omega_z}_{y,b} S_{mid}/S_w + c^{\omega_z}_{y,w} + c^{\omega_z}_{y,e} \\ m^{\omega_z}_z &= m^{\omega_z}_{z,b} S_{mid}/S_w + m^{\omega_z}_{z,w} + m^{\omega_z}_{z,e} \end{aligned}\right\} \tag{12.9.43}$$

The rotary derivatives for the separate body in this formula are found using the linearized theory (see Sec. 11.6).

When performing calculations according to the above procedure, one should take into account that the expressions for the derivatives of the coefficient c_y are suitable for arbitrary distances between the centre of mass and the panels. If the centre of pressure of one of them coincides with the centre of mass, the corresponding lift force vanishes. As regards the damping moment, its action manifests itself in this case too. At the same time, formula (12.9.42) yields a zero value of the derivative, but this does not correspond to reality. To obtain more accurate values of the damping coefficient for the wing (empennage), one should use the data in [13].

13

Friction

13.1. Boundary Layer Equation

Let us consider the steady plane flow of a viscous compressible fluid over a curved surface. **The Navier-Stokes differential equations** employed for studying this motion have the form of the first two equations in system (3.3.10). Performing the substitutions $\operatorname{div} \mathbf{V} = \partial V_x/\partial x + \partial V_y/\partial y$ and $\varepsilon_z = 0.5\,(\partial V_x/\partial y + \partial V_y/\partial x)$ in them and assuming that the partial derivatives $\partial V_x/\partial t$ and $\partial V_y/\partial t$ equal zero, we obtain

$$\left.\begin{aligned} V_x \frac{\partial V_x}{\partial x} + V_y \frac{\partial V_x}{\partial y} &= -\frac{1}{\rho}\cdot\frac{\partial p}{\partial x} + \frac{1}{\rho}\cdot\frac{\partial}{\partial x}\left\{\mu\left[2\frac{\partial V_x}{\partial x} - \frac{2}{3}\left(\frac{\partial V_x}{\partial x} + \frac{\partial V_y}{\partial y}\right)\right]\right\} + \frac{1}{\rho}\cdot\frac{\partial}{\partial y}\left[\mu\left(\frac{\partial V_x}{\partial x} + \frac{\partial V_y}{\partial y}\right)\right] \\ V_x \frac{\partial V_y}{\partial x} + V_y \frac{\partial V_y}{\partial y} &= -\frac{1}{\rho}\cdot\frac{\partial p}{\partial y} + \frac{1}{\rho}\cdot\frac{\partial}{\partial y}\left\{\mu\left[2\frac{\partial V_y}{\partial y} - \frac{2}{3}\left(\frac{\partial V_x}{\partial x} + \frac{\partial V_y}{\partial y}\right)\right]\right\} + \frac{1}{\rho}\cdot\frac{\partial}{\partial x}\left[\mu\left(\frac{\partial V_x}{\partial y} + \frac{\partial V_y}{\partial x}\right)\right] \end{aligned}\right\} \quad (13.1.1)$$

Let us consider the flow of a fluid with a low viscosity, i.e. with low values of the coefficient $\nu = \mu/\rho$. A glance at (13.1.1) reveals that if the viscosity is a significant feature of a flow, then the multipliers of ν should be large enough to compensate the low values of ν. In a free flow, the influence of stagnation due to the friction forces is not great, hence the changes in the velocity in the directions determined by the derivatives $\partial V_x/\partial x$, $\partial V_x/\partial y$, etc. are small. Consequently, the multipliers of ν are small, and we may disregard the terms taking into consideration the influence of the friction forces in the equations. This leads us to the conclusion that *a free flow can be investigated on the basis of Euler's equation for an ideal (inviscid) fluid.* As the flow approaches a surface, the action of the viscosity on the change in the velocity manifests itself to a greater and greater extent. For this reason, the terms containing ν may not be disregard-

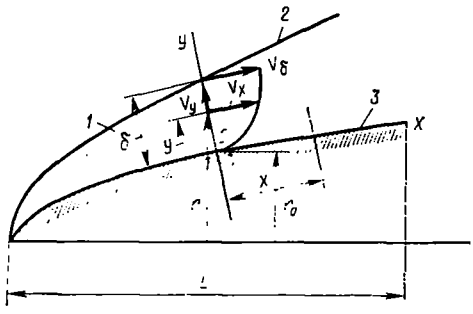

Fig. 13.1.1
Diagram of a boundary layer:
1 – boundary layer; *2* – edge of the boundary layer; *3* – surface in the flow

ed, and the Navier-Stoke equation (13.1.1) must be used to study such a viscous flow. This is the *first statement* of the boundary layer theory.

The *second statement* consists in the possibility of simplifying the Navier-Stokes equations when studying the flow of a fluid in a boundary layer characterized by the small thickness δ. Let us consider the derivation of these simplified equations of a boundary layer based on determination of the order of the terms in (13.1.1) and their comparison.

In accordance with our assumption on the small thickness of the boundary layer, we shall presume that $\delta \ll L$, where L is a characteristic length, for example, the length of the body in the flow (Fig. 13.1.1). Since for the coordinate y of a point in the boundary layer we have the inequality $0 \leqslant y \leqslant \delta$, then y and δ are of one order of magnitude. The second coordinate x determining the distance along the boundary layer has the order L ($x \sim L$). If we introduce the symbol V_δ for the velocity at the edge of the boundary layer, then the order of the velocity V_x at an arbitrary point of the boundary layer with the coordinate y will be $V_x \sim V_\delta$.

To determine the order of magnitude of the second velocity component, we shall use continuity equation (2.4.50′), from which it follows that

$$V_y \sim \frac{1}{\rho} \int_0^\delta \frac{\partial (\rho V_x)}{\partial x}\, dy$$

We shall assume the order of the density ρ to be equal to the density ρ_δ at the edge of the boundary layer. To find the order of the derivative $\partial (\rho V_x)/\partial x$, we shall take advantage of the following condition: along the surface over a distance of the order of the characteristic length L, the quantity ρV_x can vary by a value of the order of $\rho_\delta V_\delta$ (for example, from 0 to $\rho_\delta V_\delta$), i.e. in the given case $\Delta (\rho V_x) \sim \rho_\delta V_\delta$. Since we have assumed that $\Delta x \sim L$, we have

$$\partial (\rho V_x)/\partial x \sim \rho_\delta V_\delta / L \qquad (13.1.2)$$

Consequently,

$$V_y \sim (1/\rho_\delta L)\,\rho_\delta V_\delta \delta = V_\delta \delta / L \qquad (13.1.3)$$

We determine the order of the derivatives in (13.1.1) by analogy with (13.1.2). For example,

$$\partial V_x/\partial x \sim V_\delta/L, \quad \partial V_y/\partial x \sim (V_\delta \delta/L)\,(1/L) = V_\delta \delta/L^2, \quad \text{etc.} \qquad (13.1.4)$$

With a view to these results, let us consider the first equation (13.1.1). The order of the terms on the left-hand side of this equation is as follows:

$$\left.\begin{aligned} V_x \partial V_x/\partial x &\sim V_\delta\,(V_\delta/L) = V_\delta^2/L \\ V_y \partial V_x/\partial y &\sim (V_\delta \delta/L)\,(V_\delta/\delta) = V_\delta^2/L \end{aligned}\right\} \qquad (13.1.5)$$

Examination of (13.1.5) reveals that both terms have the same order.

For the terms on the right-hand side of the equation that take into consideration the friction forces, we find

$$\left.\begin{aligned} &\frac{1}{\rho}\cdot\underbrace{\frac{\partial}{\partial x}\left(\mu\frac{\partial V_x}{\partial x}\right)}_{1} \sim \frac{\mu}{\rho}\cdot\frac{V_\delta}{L^2}, \quad \frac{1}{\rho}\cdot\underbrace{\frac{\partial}{\partial x}\left(\mu\frac{\partial V_y}{\partial y}\right)}_{2} \sim \frac{\mu}{\rho}\cdot\frac{V_\delta}{L^2}, \\ &\frac{1}{\rho}\cdot\underbrace{\frac{\partial}{\partial y}\left(\mu\frac{\partial V_x}{\partial y}\right)}_{3} \sim \frac{\mu}{\rho}\cdot\frac{V_\delta}{\delta^2}, \quad \frac{1}{\rho}\cdot\underbrace{\frac{\partial}{\partial y}\left(\mu\frac{\partial V_y}{\partial x}\right)}_{4} \sim \frac{\mu}{\rho}\cdot\frac{V_\delta}{L^2} \end{aligned}\right\} \qquad (13.1.6)$$

It can be seen from (13.1.6) that since $\delta \ll L$, the first, second, and fourth terms have higher orders of smallness and they may be disregarded in comparison with the third term.

The order of the term $(1/\rho)\,\partial p/\partial x$ is determined from the Bernoulli equation (3.4.11). Excluding the potential function U (thus assuming that the force of gravity, i.e. the weight of the gas, does not affect motion) and performing differentiation, we find the equation $V\,dV = -dp/\rho$. This equation, evidently relating to the boundary layer edge where friction is negligibly small, can also be written as $(1/\rho)\,\partial p/\partial x = -V\,\partial V/\partial x$. Hence it follows that the quantity $(1/\rho)\,\partial p/\partial x$ has the order of V_δ^2/L.

If we consider a flow appreciably affected by viscosity, we must presume that the term taking viscosity into account, i.e. $(1/\rho)\,\partial\,(\mu\,\partial V_x/\partial y)/\partial y$, has the same order as all the other terms, i.e.

$$\frac{1}{\rho}\cdot\frac{\partial}{\partial y}\left(\mu\frac{\partial V_x}{\partial y}\right) \sim \frac{V_\delta^2}{L} \qquad (13.1.7)$$

Hence, instead of the first equation (13.1.1), we have

$$V_x\frac{\partial V_x}{\partial x} + V_y\frac{\partial V_x}{\partial y} = -\frac{1}{\rho}\cdot\frac{\partial p_\delta}{\partial x} + \frac{1}{\rho}\cdot\frac{\partial}{\partial y}\left(\mu\frac{\partial V_x}{\partial y}\right) \qquad (13.1.8)$$

Let us consider the second equation (13.1.1). We determine the order of the terms similarly to the first equation:

$$\underbrace{V_x \frac{\partial V_y}{\partial x} + V_y \frac{\partial V_y}{\partial y}}_{V_\delta^2 \delta / L^2} = -\frac{1}{\rho} \cdot \frac{\partial p}{\partial y} + \underbrace{\frac{4}{3\rho} \cdot \frac{\partial}{\partial y}\left(\mu \frac{\partial V_y}{\partial y}\right)}_{(\mu/\rho) V_\delta/(L\delta)}$$

$$- \underbrace{\frac{2}{3\rho} \cdot \frac{\partial}{\partial y}\left(\mu \frac{\partial V_x}{\partial x}\right)}_{(\mu/\rho) V_\delta/(L\delta)} + \underbrace{\frac{1}{\rho} \cdot \frac{\partial}{\partial x}\left(\mu \frac{\partial V_x}{\partial y}\right)}_{(\mu/\rho) V_\delta/(L\delta)} + \underbrace{\frac{1}{\rho} \frac{\partial}{\partial x}\left(\mu \frac{\partial V_y}{\partial x}\right)}_{(\mu/\rho) V_\delta \delta/L^3} \quad (13.1.9)$$

The last term on the right-hand side of (13.1.9) may be disregarded because it has a higher order of smallness than the other terms that take viscosity into consideration. To determine more accurately the order of the other terms that take viscosity into account, let us determine the order of the quantity $\mu/\rho = \nu$. To do this, we shall use the found relation (13.1.7). The order of the quantity on the left-hand side of this relation is determined by the third expression in (13.1.6), hence $(\mu/\rho)\, V_\delta/\delta^2 \sim V_\delta^2 L$, whence we find the order of the kinematic viscosity

$$\mu/\rho = \nu \sim V_\delta \delta^2 / L \quad (13.1.10)$$

As a result, we obtain the order of the remaining terms on the right-hand side of (13.1.9), that take the viscosity into consideration:

$$(\mu/\rho)\, V_\delta/(L\delta) \sim (V_\delta \delta^2/L)\, V_\delta/(L\delta) = V_\delta^2 \delta / L^2 \quad (13.1.11)$$

The quantity $(1/\rho)\, \partial p/\partial y$ evidently has the same order. Accordingly, the order of the ratio of the gradients $\partial p/\partial y$ and $\partial p/\partial x$ is determined by the value of δ/L, i.e. the gradient $\partial p/\partial y \ll \partial p/\partial x$. Therefore, to a reasonable accuracy, the second equation of the system (13.1.1) may be replaced with the equation

$$\partial p/\partial y = 0 \quad (13.1.12)$$

According to this expression, *the pressure in a boundary layer in the direction of a normal to the wall does not change and equals the pressure p_δ on the edge of the boundary layer.* It follows from the above that a thin boundary layer does not affect the pressure distribution. The result obtained is the content of one of the important hypotheses of the boundary layer theory, namely, of the *hypothesis on the absence of the influence of a boundary layer on the free stream.* According to this hypothesis, the pressure distribution over the surface of a body in a flow when a boundary layer is present can be computed on the basis of the Euler equations for an ideal (inviscid) fluid, while the shear stresses can be found proceeding from the simplified equation (13.1.8). This equation, which is the fundamental one in the boundary layer theory, is known as the **Prandtl equation.**

Such calculations with the aid of the Euler and Prandtl equations may be performed as long as the thickness of the boundary layer is small in comparison with the dimensions of the body in the flow and, consequently, as long as the hypothesis on the absence of the influence of the boundary layer on the free stream holds. On remote parts of a surface where the thickness of the boundary layer is large, this hypothesis may not be applied, and viscous flow must be calculated on the basis of the general Navier-Stokes equations.

The Prandtl equation (13.1.8) includes the dynamic viscosity μ, which in the general case is a function of the pressure and temperature. For a given cross section of the boundary layer, characterized by a constant pressure p_δ, the quantity μ varies along the thickness of the layer as a function of the temperature T. This also relates to the density ρ. Hence, to find solutions for μ and ρ, we have to know the function $T(y)$. To determine this function, we must use an energy equation in the form of the last equation of system (3.3.10).

Like the Navier-Stokes equation. the energy equation for a boundary layer can be simplified. The relevant transformations for deriving a simplified energy equation are given in Chap. 14. We shall use the equation obtained in the form of (14.2.5′) corresponding to the absence of any other kind of heat transfer except for heat conductance in the boundary layer. If we assume in this equation that the Prandtl number equals unity ($Pr = 1$). it acquires the form of (14.2.6). Evidently, one of the possible integrals of Eq. (14.2.6) will be the equality $i_0 = \text{const}$ reflecting the condition of constancy of the total enthalpy of a gas particle, i.e. the condition (14.2.2)

$$i_0 = i + V_x^2/2 = \text{const} \qquad (13.1.13)$$

We can show that this equation corresponds to the condition of the absence of heat transfer at the wall, i.e. to the case of a thermally insulated surface. Indeed, assuming that $i = c_p T$ and differentiating (13.1.13) with respect to y, we find

$$c_p\, \partial T/\partial y + V_x\, \partial V_x/\partial y = 0$$

Since when $y \to 0$ the velocity $V_x \to 0$, it is obvious that the derivative $\partial T/\partial y \to 0$ too (there is no temperature difference), which proves the absence of heat transfer at the wall. Consequently, instead of the intricate energy equation in the form of (14.2.5′) we shall use the simple equation (13.1.13). Naturally, such a form of the energy equation does not correspond completely to the real nature of motion of a viscous gas in a boundary layer and yields approximate values for the parameters determining this motion, particularly for the shear stress. The results obtained, however, are acceptable for practical calculations of skin friction.

The Prandtl equation, and also the equations of continuity, state, and energy form a system of equations of a compressible boundary

layer:

$$\left.\begin{aligned} &V_x\frac{\partial V_x}{\partial x}+V_y\frac{\partial V_x}{\partial y}=-\frac{1}{\rho}\cdot\frac{dp_\delta}{dx}+\frac{1}{\rho}\cdot\frac{\partial}{\partial y}\left(\mu\frac{\partial V_x}{\partial y}\right)\\ &\partial(V_x\rho)/\partial x+\partial(V_y\rho)/\partial y=0;\quad p_\delta=R\rho T;\quad i+V_x^2/2=i_0\end{aligned}\right\} \qquad (13.1.14)$$

Here in the equations of flow and state, the pressure p has been replaced in accordance with (13.1.12) with the quantity p_δ. In the energy equation, the instantaneous value of the enthalpy is $i = c_pT$, and the stagnation enthalpy $i_0 = c_pT_0$.

The obtained system of equations is suitable for studying a **laminar boundary layer**. When solving it, one must satisfy the boundary conditions on the surface of the body in the flow and the conditions of the continuous transition of the parameters in the boundary layer to the corresponding values on the edge. Here the solution makes it necessary to *asymptotically* fulfil the conditions on the edge. Therefore, the boundary conditions for the velocity are

$$V_x = V_y = 0 \text{ at } y = 0;\ V_x = V_\delta(x) \text{ at } y \to \infty \qquad (13.1.15)$$

The density and temperature in (13.1.14) can be expressed in terms of the velocity in the boundary layer.

It follows from (13.1.13) that

$$c_pT + V_x^2/2 = c_pT_0 \qquad (13.1.16)$$

consequently

$$T = T_0(1 - V_x^2/V_{max}^2) \qquad (13.1.17)$$

Using the equation of state $p = \rho RT$ in which the pressure p for the boundary layer is taken equal to its value p_δ at the edge of the layer, we obtain an expression for the density:

$$\rho = p_\delta/(RT) = (p_\delta/RT_0)(1 - V_x^2/V_{max}^2)^{-1} \qquad (13.1.18)$$

Since the stagnation temperature is

$$T_0 = T_\delta(1 - V_\delta^2/V_{max}^2)^{-1} \qquad (13.1.19)$$

and the density at the edge of the boundary layer is

$$\rho_\delta = p_\delta/(RT_\delta) = \rho_0(1 - V_\delta^2/V_{max}^2)^{1/(k-1)} \qquad (13.1.20)$$

we have

$$\begin{aligned}\rho &= \rho_\delta(1 - V_\delta^2/V_{max}^2)(1 - V_x^2/V_{max}^2)^{-1}\\ &= \rho_0(1 - V_\delta^2/V_{max}^2)^{k/(k-1)}(1 - V_x^2/V_{max}^2)^{-1}\end{aligned} \qquad (13.1.21)$$

The obtained equations allow us to calculate the parameters of a boundary layer without account taken of the physicochemical transformations occurring at very high flow velocities when the gas in the boundary layer is heated to very high temperatures. Conse-

quently, these equations hold for comparatively moderate velocities when the temperature in the boundary layer does not reach high values. Diminishing of the flow velocities reduces the influence of compressibility and heating of the gas in the boundary layer.

For an incompressible two-dimensional plane boundary layer, the system of equations has the form

$$\left.\begin{aligned} &V_x \frac{\partial V_x}{\partial x} + V_y \frac{\partial V_x}{\partial y} = -\frac{1}{\rho} \cdot \frac{dp_\delta}{dx} + \nu \frac{\partial^2 V_x}{\partial y^2} \\ &\partial V_x/\partial x + \partial V_y/\partial y = 0; \quad V_\delta^2/2 + p_\delta/\rho_\delta = \text{const} \end{aligned}\right\} \qquad (13.1.22)$$

These equations are integrated for the boundary conditions given by (13.1.15).

13.2. Generalized Boundary Layer Equation

Differential Form of the Equation

Let us derive an equation of a steady boundary layer in the generalized form suitable for studying both a laminar and a turbulent three-dimensional axisymmetric flow with a view to the physicochemical transformations occurring at high temperatures.

We shall consider in the boundary layer an elementary thoroid-shaped particle with an inner radius of r, a width of dx, and a thickness of dy (Fig. 13.2.1). We shall replace the action of the surrounding flow with forces of the pressure and shear stress. Since we are considering a thin boundary layer, we can assume that at each point of the cross section passing through the given point A, the pressure is the same and equals its value p_δ at the edge of the layer. Therefore the force due to the pressure on the left face of the ring in the direction of the x-axis is

$$P = p_\delta \, dS = 2\pi r p_\delta \, dy \qquad (13.2.1)$$

Let P_x be the force acting on the right face with the same area $dS = 2\pi r \, dy$. Since the pressure p_δ is a function of the coordinate x, i.e. $p_\delta = p_\delta(x)$, then the force $P = P(x)$ Accordingly, the right side experiences the force $P_x = P(x + dx)$ or, because we have chosen the coordinate $x = 0$ for the cross section being considered, $P_x = P(dx)$. Expanding this function into a Taylor series and disregarding infinitesimals of the second and higher orders, we obtain

$$P_x = P(0) + (\partial P/\partial x)\, dx = 2\pi r p_\delta \, dy$$
$$+ [\partial (2\pi r p_\delta \, dy)/\partial x]\, dx = 2\pi r [p_\delta + (dp_\delta/dx)\, dx]\, dy \qquad (13.2.2)$$

The excess force acting in the direction of the x-axis is

$$P - P_x = -2\pi r (dp_\delta/dx)\, dx\, dy \qquad (13.2.3)$$

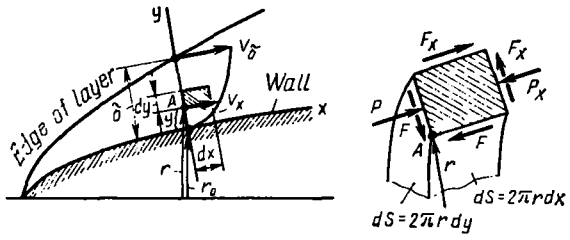

Fig. 13.2.1
To the derivation of the generalized equation of a boundary layer

The friction forces applied to a particle are computed in accordance with the reciprocity principle of shear stresses (Fig. 13.2.1). The friction forces acting on the front and rear areas produce no component onto the x-axis. Such a component is due to the shear stresses on the inner and outer surfaces of the ring and equals $F_x - F$, where

$$F_x = F(y + dy) = F(y) + (\partial F/\partial y)\, dy$$
$$= 2\pi r\tau\, dx + [\partial (2\pi r\tau\, dx)/\partial y]\, dy;$$
$$F = F(y) = \tau\, dS = 2\pi r\tau\, dx$$

here τ is the friction stress on the inner surface of the ring.

Hence, the excess friction force acting in the direction of the x-axis is

$$F_x - F = 2\pi\, [\partial (r\tau)/\partial y]\, dx\, dy \qquad (13.2.4)$$

For the particle being considered, the product of its mass (density $\times$ volume) and acceleration is

$$-2\pi r\rho\, (dV_x/dt)\, dx\, dy \qquad (13.2.5)$$

The sum of this quantity and of the forces acting on the particle in the direction of the x-axis is zero, i.e.

$$-2\pi r\rho\, (dV_x/dt)\, dx\, dy - 2\pi r\, (dp_\delta/dx)\, dx\, dy$$
$$+ 2\pi\, [\partial (r\tau)/\partial y]\, dx\, dy = 0$$

Assuming that the total acceleration $dV_x/dt = V_x\, \partial V_x/\partial x + V_y\, \partial V_x/\partial y$, we find

$$\rho r\, (V_x\, \partial V_x/\partial x + V_y\, \partial V_x/\partial y) = -r\, dp_\delta/dx + \partial\, (r\tau)/\partial y \qquad (13.2.6)$$

Equation (13.2.6) is called the **generalized boundary layer equation in the differential form.**

When studying a turbulent boundary layer, the averaged values of V_x, V_y, ρ, and p_δ have to be taken, while the shear stress is determined from the expression

$$\tau = (\mu + \mu_t)\, \partial V_x/\partial y \qquad (13.2.7)$$

in which μ_t is the **turbulent viscosity.**

The quantity μ_t can be considered as an analogue of the dynamic viscosity μ of a laminar viscous flow. Evidently, for such a flow $\mu_t = 0$, the shear stress $\tau = \mu \partial V_x/\partial y$, and Eq. (13.2.6) becomes

$$\rho r \left(V_x \frac{\partial V_x}{\partial x} + V_y \frac{\partial V_x}{\partial y}\right) = -r \frac{dp_\delta}{dx} + \frac{\partial}{\partial y}\left(r\mu \frac{\partial V_x}{\partial y}\right) \quad (13.2.8)$$

In the general case, when a gas experiences physicochemical transformations under high temperatures, the value of the coefficient μ varies along the thickness of the boundary layer. When these transformations are absent, the quantity μ is assumed to be constant. When investigating a boundary layer near a flat contour, the quantity r has to be eliminated from Eq. (13.2.8).

Integral Relation for a Boundary Layer

We shall transform generalized equation (13.2.6) into a relation of a different form that is widely used in practical calculations of a boundary layer. For this end, we shall write the left-hand side of (13.2.6) in the form

$$\rho r \left(V_x \frac{\partial V_x}{\partial x} + V_y \frac{\partial V_x}{\partial y}\right) = \rho r \left[\frac{\partial V_x^2}{\partial x} + \frac{\partial (V_x V_y)}{\partial y} - V_x \frac{\partial V_x}{\partial x} - V_x \frac{\partial V_y}{\partial y}\right]$$

We calculate the derivatives in the continuity equation (2.4.48)

$$V_x \frac{\partial (\rho r)}{\partial x} + \rho r \frac{\partial V_x}{\partial x} + V_y \frac{\partial (\rho r)}{\partial y} + \rho r \frac{\partial V_y}{\partial y} = 0$$

Hence

$$-\rho r V_x \frac{\partial V_x}{\partial x} - \rho r V_x \frac{\partial V_y}{\partial y} = V_x^2 \frac{\partial (\rho r)}{\partial x} + V_x V_y \frac{\partial (\rho r)}{\partial y}$$

Accordingly,

$$\rho r \left(V_x \frac{\partial V_x}{\partial x} + V_y \frac{\partial V_x}{\partial y}\right) = \rho r \frac{\partial V_x^2}{\partial x} + \rho r \frac{\partial (V_x V_y)}{\partial y}$$

$$+ V_x^2 \frac{\partial (\rho r)}{\partial x} + V_x V_y \frac{\partial (\rho r)}{\partial y} = \frac{\partial (\rho r V_x^2)}{\partial x} + \frac{\partial (\rho r V_x V_y)}{\partial y} \quad (13.2.9)$$

We introduce this expression into (13.2.6):

$$\frac{\partial (\rho r V_x^2)}{\partial x} + \frac{\partial (\rho r V_x V_y)}{\partial y} = -r \frac{dp_\delta}{dx} + \frac{\partial (r\tau)}{\partial y}$$

By combining this expression with the continuity equation in the form of

$$V_\delta \frac{\partial (\rho r V_x)}{\partial x} + V_\delta \frac{\partial (\rho r V_y)}{\partial y} = 0$$

we find

$$V_\delta \frac{\partial (\rho r V_x)}{\partial x} + V_\delta \frac{\partial (\rho r V_y)}{\partial y} - \frac{\partial (\rho r V_x^2)}{\partial x} - \frac{\partial (\rho r V_x V_y)}{\partial y} = r \frac{dp_\delta}{dx} - \frac{\partial (r\tau)}{\partial y}$$

or

$$\frac{\partial}{\partial x}[\rho r V_x (V_\delta - V_x)] - \rho r V_x \frac{\partial V_\delta}{\partial x} + \frac{\partial}{\partial y}[\rho r V_y (V_\delta - V_x)] = r \frac{dp_\delta}{dx} - \frac{\partial (r\tau)}{\partial y}$$

Integration with respect to y between 0 and δ (within the limits of the boundary layer thickness) yields

$$\underbrace{\int_0^\delta \frac{\partial}{\partial x}[\rho r V_x (V_\delta - V_x)]\, dy}_{1} - \underbrace{\int_0^\delta \rho r V_x \frac{dV_\delta}{dx} dy}_{2} + \underbrace{\int_0^\delta \frac{\partial}{\partial y}[\rho r V_y (V_\delta - V_x)]\, dy}_{3} = \underbrace{\int_0^\delta r \frac{dp_\delta}{dx} dy}_{4} - \underbrace{\int_0^\delta \frac{\partial (r\tau)}{\partial y} dy}_{5} \quad (13.2.10)$$

We transform the terms in (13.2.10):

$$1.\ \int_0^\delta \frac{\partial}{\partial x}[\rho r V_x (V_\delta - V_x)]\, dy = \frac{d}{dx}\int_0^\delta \rho r V_x (V_\delta - V_x)\, dy$$

$$\underbrace{-[\rho r V_x (V_\delta - V_x)]_{y=\delta} \frac{d\delta}{dx}} = \frac{d}{dx}\int_0^\delta \rho r V_x (V_\delta - V_x)\, dy \quad (13.2.11)$$

The expression over the brace equals zero because at $y = \delta$ the quantity $V_x = V_\delta$.

$$2.\ \int_0^\delta \rho r V_x \frac{dV_\delta}{dx} dy = \frac{dV_\delta}{dx}\int_0^\delta \rho r V_x\, dy$$

$$= \frac{d}{dx}\left(V_\delta \int_0^\delta \rho r V_x\, dy\right) - V_\delta \frac{d}{dx}\int_0^\delta \rho r V_x\, dy \quad (13.2.12)$$

$$3.\ \int_0^\delta \frac{\partial}{\partial y}[\rho r V_y (V_\delta - V_x)]\, dy = [\rho r V_y (V_\delta - V_x)]_{y=0}^{y=\delta} = 0 \quad (13.2.13)$$

because at $y = \delta$ the value of $V_x = V_\delta$, while at $y = 0$ the velocity $V_y = 0$.

$$4.\ \int_0^\delta r \frac{dp_\delta}{dx} dy = \frac{dp_\delta}{dx}\int_0^\delta r\, dy \quad (13.2.14)$$

$$5.\ \int_0^\delta \frac{\partial (r\tau)}{\partial y} dy = [r\tau]_{y=0}^{y=\delta} = -r_0 \tau_w \quad (13.2.15)$$

By taking these results into consideration, we can write Eq. (13.2.10) as

$$\frac{d}{dx}\int_0^\delta \rho r V_x (V_\delta - V_x)\, dy - \frac{d}{dx}\left(V_\delta \int_0^\delta \rho r V_x\, dy\right)$$

$$+ V_\delta \frac{d}{dx}\int_0^\delta \rho r V_x\, dy = \frac{dp_\delta}{dx}\int_0^\delta r\, dy + r_0\tau_w \qquad (13.2.16)$$

After cancelling and assuming that for a small thickness of the boundary layer the coordinate r may be approximated by the coordinate r_0 of the corresponding point on the surface in the flow (see Fig. 13.2.1), we obtain

$$-\frac{d}{dx}\int_0^\delta \rho r_0 V_x^2\, dy + V_\delta \frac{d}{dx}\int_0^\delta \rho r_0 V_x\, dy - r_0\delta\frac{dp_\delta}{dx} = r_0\tau_w \qquad (13.2.16')$$

This generalized equation, obtained by von Kármán, is known as the **integral relation of a boundary layer.** It allows one to determine directly the shear stress τ_w on a wall, which is associated with the practical problem of determining the friction drag. The use of the integral relation for this purpose presumes that the nature of the velocity distribution over the thickness of the boundary layer, i.e. the form of the function $V_x = V_x(y)$, is known.

The solution of Eq. (13.2.16′) must fulfil the condition on the edge of the boundary layer where at $y = \delta$ the velocity $V_x = V_\delta$. This velocity and the pressure p_δ, which are known parameters, are calculated by solving the Euler equations for an ideal (inviscid) flow over the body. The quantities V_x, δ, and τ are unknown. Hence, relation (13.2.16′) must be supplemented with two more unknown equations relating the indicated unknown parameters. The integral nature of Eq. (13.2.16′) makes it possible to use these equations in the approximate form. Particularly, it is sufficient to set a quite approximate relation for the velocity V_x to obtain a result acceptable in practice because the velocity V_x is inside the integral, and when the latter is evaluated, the error diminishes.

Conditional Thickness of the Boundary Layer

Let us write integral relation (13.2.16) in a different form. To do this, we shall replace the last two terms on the left-hand side with a view to relation (13.2.12), and by using (3.6.3) we shall write dp_δ/dx in the form

$$dp_\delta/dx = -\rho_\delta V_\delta\, dV_\delta/dx \qquad (13.2.17)$$

The result is

$$\frac{d}{dx}\int_0^\delta \rho r V_x (V_\delta - V_x)\, dy - \frac{dV_\delta}{dx}\int_0^\delta \rho r V_x\, dy$$

$$= -\int_0^\delta \rho_\delta r V_\delta \frac{dV_\delta}{dx}\, dy + r_0\tau_w$$

or

$$\frac{d}{dx}\int_0^\delta \rho r V_x (V_\delta - V_x)\, dy + \frac{dV_\delta}{dx}\int_0^\delta r(\rho_\delta V_\delta - \rho V_x)\, dy = r_0\tau_w \quad (13.2.18)$$

We shall write this equation in the form

$$\frac{d}{dx}\int_0^\delta 2\pi r\rho V_x (V_\delta - V_x)\, dy$$

$$+\frac{dV_\delta}{dx}\int_0^\delta 2\pi r(\rho_\delta V_\delta - \rho V_x)\, dy = 2\pi r_0\tau_w \quad (13.2.18')$$

The first integral in (13.2.18′) determines the decrease in the momentum transferred through the area $2\pi r\delta$ due to stagnation of the flow in the boundary layer. Let us introduce the concept of the **momentum thickness** δ^{**}—the conditional thickness of a layer confining the area $2\pi r_0\delta^{**}$ through which the momentum $2\pi r_0\delta^{**}\rho_\delta V_\delta^2$ is transferred in unit time at the constant velocity V_δ. This quantity equals the indicated decrease in the momentum, i.e.

$$2\pi r_0\delta^{**}\rho_\delta V_\delta^2 = \int_0^\delta 2\pi r\rho V_x (V_\delta - V_x)\, dy$$

Assuming inside the integral that $r \approx r_0$, we find

$$\delta^{**} = \int_0^\delta \frac{\rho}{\rho_\delta}\cdot\frac{V_x}{V_\delta}\left(1 - \frac{V_x}{V_\delta}\right) dy \quad (13.2.19)$$

The second integral in (13.2.18′) determines the difference between the flow rate through the area $2\pi r\delta$ for a flow of an inviscid gas $\int_0^\delta 2\pi r\rho_\delta V_\delta\, dy$ and for a flow of a viscid fluid $\int_0^\delta 2\pi r\rho V_x\, dy$.

This decrease in the flow rate is due to stagnation of the flow in the boundary layer. Let us introduce the concept of the **displacement thickness** δ^*, which in an inviscid flow is the conditional thick-

ness of the layer confining the area $2\pi r_0\delta^*$ through which an amount of fluid equal to the above-mentioned decrease in the flow rate flows in unit time and at a constant velocity V_δ at all points on the surface, i.e.

$$2\pi r_0\delta^*\rho_\delta V_\delta = \int_0^\delta 2\pi r\,(\rho_\delta V_\delta - \rho V_x)\,dy$$

Assuming that $r = r_0$, we find

$$\delta^* = \int_0^\delta \left(1 - \frac{\rho}{\rho_\delta}\cdot\frac{V_x}{V_\delta}\right) dy \qquad (13.2.20)$$

It can be seen that expressions (13.2.19) for δ^{**} and (13.2.20) for δ^* do not contain the quantity r; consequently, the conditional thicknesses for a three-dimensional boundary layer to a first approximation are determined in the same way as for a two-dimensional layer. For an incompressible flow, it is necessary to assume that $\rho = \rho_\delta = \text{const}$ in the above expressions. The introduction of parameters such as the displacement thickness δ^* and the momentum thickness δ^{**} reflecting definite physical properties of the boundary layer allows us to obtain more effective methods of solving the problem on the flow of a viscid fluid in a number of cases. With the aid of these parameters, particularly, we can obtain a differential equation in a form that is more convenient for calculating the boundary layer near curved surfaces (see [19, 20]).

Let us consider an application of the concept of the displacement thickness δ^* to aerodynamic investigations. It is clear from physical notions that a boundary layer, as it were, displaces an external inviscid flow, moving its streamlines away from the surface. The thickness δ^* may be considered as a quantity determining the **mean displacement of these streamlines.** Hence, the external flow, as it were, passes over a surface obtained from the actual surface of a body by adding to it a hypothetic layer with a thickness of δ^*. The distribution of the velocities and pressures in the external flow should be evaluated as if it flows over a new surface belonging to the fictitious thicker body. Accordingly, the use of the concept of the displacement thickness allows us to take into account the *influence of the boundary layer* on the parameters of the external flow.

13.3. Laminar Boundary Layer on a Flat Plate

Let us consider the calculation of the boundary layer on a flat plate in a compressible flow. The solution of this problem is of major significance in the theory of a viscous flow. The boundary layer para-

meters obtained as a result of such calculations are used in practical cases for an approximate estimate of the parameters of a viscid flow near surfaces not only close in shape to a plate, but also differing appreciably from one, for example, near bodies of revolution. At the same time, as shown below, the found formulas for calculating the parameters of an incompressible and compressible boundary layers on a flat plate are similar in appearance.

We shall use an integral relation for a flat plate. It is obtained from Eq. (13.2.18) provided that r is deleted from it and the derivative dV_δ/dx is taken equal to zero because the velocity of the free stream along the plate does not change. Hence

$$\frac{d}{dx}\int_0^\delta \rho V_x (V_\delta - V_x)\, dy = \tau_w \qquad (13.3.1)$$

Let us transform (13.3.1) to the new variables ξ and η introduced by academician A. Dorodnitsyn [21]:

$$\xi = \int_0^x f(x)\, dx; \quad \eta = \int_0^y g(x, y)\, dy \qquad (13.3.2)$$

where $f(x)$ and $g(x, y)$ are functions selected with a view to the condition that the transformed integral relation for a compressible boundary layer must be close in form to the relevant relation for an incompressible fluid. The integration of such a relation is a simpler task.

Applying (13.3.2), we shall write Eq. (13.3.1) in the form

$$\frac{\partial}{\partial \xi}\cdot\frac{\partial \xi}{\partial x} + \frac{\partial}{\partial \eta}\cdot\frac{\partial \eta}{\partial x} = f\frac{\partial}{\partial \xi}\int_0^{\eta_\delta} \rho V_x (V_\delta - V_x)\frac{d\eta}{g}$$

$$+ \frac{\partial \eta}{\partial x}\cdot\frac{\partial}{\partial \eta}\int_0^{\eta_\delta} \rho V_x (V_\delta - V_x)\frac{d\eta}{g} = \tau_w$$

where η_δ is the value of η corresponding to the edge of the boundary layer.

In this equation

$$\frac{\partial}{\partial \eta}\int_0^{\eta_\delta} \rho V_x (V_\delta - V_x)\frac{d\eta}{g} = \frac{1}{g}\rho V_x (V_\delta - V_x)\Big|_0^{\eta_\delta} = 0$$

because at the wall when $\eta = 0$, the component $V_x = 0$, while at the edge of the layer when $\eta = \eta_\delta$, its value is $V_x = V_\delta$. For this

reason, (13.3.1) can be written as

$$f\frac{d}{d\xi}\int_0^{\eta_\delta}\rho V_x(V_\delta - V_x)\frac{d\eta}{g} = \tau_w \tag{13.3.3}$$

For the integral (13.3.3) to coincide with the corresponding expression for an incompressible medium, we must assume that $\rho/g = \text{const}$. Since according to (13.3.2), the function g is dimensionless, this constant can be taken equal to the stagnation density, i.e. $\rho/g = \rho_0$. Consequently,

$$\eta = \int_0^y \frac{\rho}{\rho_0}\,dy \tag{13.3.4}$$

Hence, for (13.3.3), we have

$$\frac{d}{d\xi}\int_0^{\eta} V_x(V_\delta - V_x)\,d\eta = \tau_w\frac{g_w}{f_w\rho_w}$$

In this equation, the right-hand side is

$$\frac{\tau_w}{\rho_w}\cdot\frac{g_w}{f_w} = \frac{\tau_w}{\rho_w}\cdot\frac{\rho_w}{\rho_0}\cdot\frac{1}{f_w}$$

It follows from (13.1.21) that the density at the wall is

$$\rho_w = \rho_\delta\,(1 - V_\delta^2/V_{max}^2) = \rho_\delta T_\delta/T_0 = p_\delta\rho_0/p_0 \tag{13.3.5}$$

whence

$$\rho_w/\rho_0 = p_\delta/p_0 \tag{13.3.5'}$$

Consequently,

$$\frac{\tau_w}{\rho_w}\cdot\frac{g_w}{f_w} = \frac{\tau_w}{\rho_w}\cdot\frac{p_\delta}{p_0}\cdot\frac{1}{f_w}$$

With this expression in view, we have

$$\frac{d}{d\xi}\int_0^{\eta_\delta} V_x(V_\delta - V_x)\,d\eta = \frac{\tau_w}{\rho_w}\cdot\frac{p_\delta}{p_0}\cdot\frac{1}{f_w}$$

Let us assume here that $p_\delta/p_0 = f_w$, i.e.

$$\xi = \int_0^x \frac{p_\delta}{p_0}\,dx = \frac{p_\delta}{p_0}\,x \tag{13.3.6}$$

Accordingly,

$$\frac{d}{d\xi}\int_0^{\eta_\delta} V_x(V_\delta - V_x)\,d\eta = \frac{\tau_w}{\rho_w} \tag{13.3.7}$$

Equation (13.3.7) coincides in form with the relevant boundary layer relation for an incompressible medium in the coordinate system ξ, η. Consequently, to solve the integral relation in such a form, we can use the *method employed in the theory of the boundary layer of an incompressible fluid.* This method provides for presetting the distribution of the velocity V_x over the cross section of the boundary layer, which has to be known when using the integral relation.

Let us consider a laminar boundary layer for which the integral relation has the form

$$\frac{d}{d\xi}\int_0^{\eta_\delta} V_x (V_\delta - V_x)\, d\eta = \frac{\mu_w}{\rho_w}\left(\frac{\partial V_x}{\partial y}\right)_{y=0}$$

$$= \frac{\mu_w}{\rho_w}\left(\frac{\partial V_x}{\partial \eta}\right)_{\eta=0}\left(\frac{\partial \eta}{\partial y}\right)_{y=0} \qquad (13.3.8)$$

In the theory of a laminar boundary layer for an incompressible fluid on an arbitrary surface, Paulhausen proposed the third-degree polynomial function $V_x(\eta, \xi)$:

$$V_x = a(\xi) + b(\xi)\,\eta + c(\xi)\,\eta^2 + d(\xi)\,\eta^3 \qquad (13.3.9)$$

The coefficients $a(\xi)$, $b(\xi)$, $c(\xi)$, and $d(\xi)$ of this polynomial are determined from the boundary conditions, which must be satisfied by the velocity. According to the boundary conditions at a wall, i.e. at $\eta = 0$, the velocity $V_x = 0$. Hence, the coefficient $a = 0$. Examination of the first equation of system (13.1.14) transformed to the variables ξ, η and related to the conditions on a flat plate ($dp_\delta/dx = 0$) reveals that at the wall where $V_x = V_y = 0$, the derivative

$$(\partial^2 V_x/\partial\eta^2)_{\eta=0} = 0 \qquad (13.3.10)$$

From (13.3.9), we have

$$\partial^2 V_x/\partial\eta^2 = 2c + 6d\eta \qquad (13.3.11)$$

whence upon fulfillment of condition (13.3.10), the coefficient $c = 0$. Hence,

$$V_x = b\eta + d\eta^3 \qquad (13.3.12)$$

To determine the coefficients b and d, we shall use the boundary conditions at the edge of the boundary layer. At $\eta = \eta_\delta$, the velocity component $V_x = V_\delta$, therefore

$$V_\delta = b\eta_\delta + d\eta_\delta^3 \qquad (13.3.13)$$

At the edge, the shear stress is $(\tau_w)_{\eta=\eta_\delta} = 0$.

By Newton's formula $\tau = \mu\, \partial V_x/\partial y$, the derivative $(\partial V_x/\partial\eta)_{\eta=\eta_\delta} = 0$. With this in view, we obtain from (13.3.12)

$$(\partial V_x/\partial\eta)_{\eta=\eta_\delta} = b + 3d\eta_\delta^2 = 0 \qquad (13.3.14)$$

This simultaneous solution of (13.3.13) and (13.3.14) relative to the coefficients b and d yields

$$b=\frac{3}{2}\cdot\frac{V_\delta}{\eta_\delta},\qquad d=-\frac{1}{2}\cdot\frac{V_\delta}{\eta_\delta^3}$$

Consequently, for the velocity distribution, we have

$$V_x=\left[\frac{3}{2}\cdot\frac{\eta}{\eta_\delta}-\frac{1}{2}\left(\frac{\eta}{\eta_\delta}\right)^3\right]V_\delta \tag{13.3.15}$$

We introduce this expression into (13.3.8):

$$\frac{d}{d\xi}\int_0^{\eta_\delta}\left(\frac{3}{2}V_\delta\frac{\eta}{\eta_\delta}-\frac{1}{2}V_\delta\frac{\eta^3}{\eta_\delta^3}\right)$$
$$\times\left(V_\delta-\frac{3}{2}V_\delta\frac{\eta}{\eta_\delta}+\frac{1}{2}V_\delta\frac{\eta^3}{\eta_\delta^3}\right)d\eta=\frac{3}{2}\cdot\frac{\nu_w V_\delta}{\eta_\delta}\cdot\frac{\rho_w}{\rho_0}$$

By evaluating the integral and performing differentiation, we obtain the equation

$$\frac{d\eta_\delta^2}{d\xi}=\frac{280}{13}\cdot\frac{\nu_w\rho_w}{V_\delta\rho_0}$$

Upon integrating with the assumption that along the plate $\nu_w = \text{const}$ and $\rho_w = \text{const}$, we obtain

$$\eta_\delta^2=\frac{280}{13}\cdot\frac{\nu_w\rho_w}{V_\delta\rho_0}\xi+C$$

Assuming for the initial point of the plate that the thickness $\eta_\delta = 0$ at $\xi = 0$, we find $C = 0$. Therefore

$$\eta_\delta=4.64\sqrt{\frac{\nu_w\rho_w}{\nu_\delta\rho_0}\xi} \tag{13.3.16}$$

Taking into consideration formula (13.3.5) for ρ_w/ρ_δ and expression (13.3.6) for ξ, we obtain

$$\eta_\delta=4.64\sqrt{\frac{\nu_w x}{V_\delta}\cdot\frac{p_\delta}{p_0}\cdot\frac{\rho_w}{\rho_0}}=4.64\frac{p_\delta}{p_0}\sqrt{\frac{\nu_w x}{V_\delta}} \tag{13.3.16'}$$

We find the thickness of the layer from the expression

$$\delta=\int_0^\delta dy=\int_0^{\eta_\delta}\frac{\rho_0}{\rho}d\eta$$

Taking into account (13.1.21) and that $V_x = V_\delta \eta/\eta_\delta$, we shall write ρ_0/ρ in the form

$$\frac{\rho_0}{\rho} = \frac{\rho_0 (1 - V_x^2/V_{max}^2)}{\rho_\delta (1 - V_\delta^2/V_{max}^2)} = \frac{(1 - V_\delta^2/V_{max}^2)^{-1/(k-1)} (1 - V_x^2/V_{max}^2)}{1 - V_\delta^2/V_{max}^2}$$

$$= \frac{p_0}{p_\delta} \left(1 - \frac{V_x^2}{V_{max}^2}\right) = \frac{p_0}{p_\delta} \left(1 - \frac{V_\delta^2}{V_{max}^2} \cdot \frac{\eta^2}{\eta_\delta^2}\right)$$

To replace V_x, we used a simpler relation in which the velocity depends linearly on the function η instead of (13.3.15). When determining the thickness of a boundary layer, this does not produce appreciable errors, but does facilitate the simplification of the calculations. Accordingly,

$$\delta = \frac{p_0}{p_\delta} \int_0^{\eta_\delta} \left(1 - \frac{V_\delta^2}{V_{max}^2} \cdot \frac{\eta^2}{\eta_\delta^2}\right) d\eta = \frac{p_0}{p_\delta} \left(1 - \frac{V_\delta^2}{3V_{max}^2}\right) \eta_\delta$$

$$= \frac{p_0}{p_\delta} \left[1 - \frac{1}{3} + \left(1 - \frac{V_\delta^2}{V_{max}^2}\right) \frac{1}{3}\right] \eta_\delta = \frac{p_0}{p_\delta} \left(\frac{2}{3} + \frac{T_\delta}{3T_0}\right) \eta_\delta$$

Introducing into this expression the value of η_δ from (13.3.16'), we find

$$\delta = 4.64 \, [2/3 + T_\delta/(3T_0)] \sqrt{\nu_w x/V_\delta}$$

We shall write the coefficient ν_w in the form

$$\nu_w = \frac{\mu_w}{\rho_w} = \frac{\mu_\delta}{\rho_\delta} \cdot \frac{\mu_w}{\mu_\delta} \cdot \frac{p_\delta}{\rho_w} = \nu_\delta \left(\frac{T_w}{T_\delta}\right)^n \frac{\rho_\delta}{\rho_0} \cdot \frac{\rho_0}{\rho_w}$$

$$= \nu_\delta \left(\frac{T_w}{T_\delta}\right)^n \frac{\rho_\delta}{\rho_0} \cdot \frac{p_0}{p_\delta} = \nu_\delta \left(\frac{T_w}{T_\delta}\right)^n \frac{T_0}{T_\delta} \qquad (13.3.17)$$

Since we are dealing with a thermally insulated wall on which for the adopted value of $Pr = 1$ the gas temperature is

$$T_w = T_0 = T_\delta \left(1 - \frac{V_\delta^2}{V_{max}^2}\right)^{-1} = T_\delta \left(1 + \frac{k-1}{2} M_\delta^2\right) \qquad (13.3.18)$$

then, consequently,

$$\nu_w = \nu_\delta \left(\frac{T_0}{T_\delta}\right)^{1+n} = \nu_\delta \left(1 + \frac{k-1}{2} M_\delta^2\right)^{1+n} \qquad (13.3.17')$$

Accordingly,

$$\delta = \delta_{com} = 4.64 \left(1 + \frac{k-1}{3} M_\delta^2\right) \left(1 + \frac{k-1}{2} M_\delta^2\right)^{(n-1)/2} \sqrt{\frac{\nu_\delta x}{V_\delta}} \qquad (13.3.19)$$

Assuming here that $M_\delta = 0$, we obtain a relation for the thickness of the boundary layer in an incompressible fluid:

$$\delta_{ic} = 4.64 \sqrt{\nu_\delta x/V_\delta} \qquad (13.3.19')$$

or in the dimensionless form

$$\bar{\delta}_{1c} = \delta_{1c}/L = 4.64\,(\bar{x}/Re_L)^{1/2} \qquad (13.3.19'')$$

where $\bar{x} = x/L$, and $Re_L = V_\delta L/\nu_\delta$.

The ratio of the thicknesses is

$$\frac{\delta_{com}}{\delta_{1c}} = \left(1 + \frac{k-1}{3} M_\delta^2\right)\left(1 + \frac{k-1}{2} M_\delta^2\right)^{(n+1)/2} \qquad (13.3.20)$$

Compressibility can be seen to increase the thickness of the boundary layer. The explanation is that the gas being compressed becomes heated upon stagnation, as a result of which its viscosity grows, and a greater thickness of the gas is affected by it.

We determine the shear stress at the wall by Newton's formula with a view to (13.3.15) and (13.3.4):

$$\tau_w = \mu_w \left(\frac{\partial V_x}{\partial y}\right)_{y=0} = \mu_w \left(\frac{\partial V_x}{\partial \eta}\right)_{\eta=0} \left(\frac{\partial \eta}{\partial y}\right)_{y=0}$$

$$= \mu_w \frac{3V_\delta}{2\eta_\delta} \cdot \frac{\rho_w}{\rho_0} = \nu_w \frac{3V_\delta}{2\eta_\delta} \cdot \frac{\rho_w^2}{\rho_0}$$

Let us insert into this expression the value of η_δ from (13.3.16') and substitute p_δ/p_0 for ρ_w/ρ_0:

$$\tau_w = \frac{3}{2} \cdot \frac{V_\delta \rho_w}{4.64} \sqrt{\frac{\nu_w V_\delta}{x}} \qquad (13.3.21)$$

Inserting into (13.3.21) the value of ν_w from (13.3.17') and taking into account that

$$\rho_w = \rho_\delta \frac{\rho_w}{\rho_0} \cdot \frac{\rho_0}{\rho_\delta} = \rho_\delta \frac{p_\delta}{p_0} \cdot \frac{\rho_0}{\rho_\delta} = \rho_\delta \frac{T_\delta}{T_0} \qquad (13.3.21')$$

we obtain

$$\tau_w = 0.323 \rho_\delta V_\delta^2 \sqrt{\frac{\nu_\delta}{V_\delta x}} \left(\frac{T_0}{T_\delta}\right)^{(n-1)/2} \qquad (13.3.22)$$

or with a view to Eq. (13.3.18) and the symbol for the local Reynolds number $Re_x = V_\delta x/\nu_\delta$, we have

$$\tau_w = (\tau_w)_{com} = 0.323 \rho_\delta V_\delta^2 \sqrt{\frac{1}{Re_x}} \left(1 + \frac{k-1}{2} M_\delta^2\right)^{(n-1)/2} \qquad (13.3.22')$$

For an incompressible fluid ($M_\delta = 0$)

$$(\tau_w)_{1c} = 0.323 \rho_\delta V_\delta^2 \sqrt{1/Re_x} \qquad (13.3.23)$$

The ratio of the shear stresses is

$$\frac{(\tau_w)_{com}}{(\tau_w)_{1c}} = \left(\frac{T_0}{T_\delta}\right)^{(n-1)/2} = \left(1 + \frac{k-1}{2} M_\delta^2\right)^{(n-1)/2} \qquad (13.3.24)$$

It follows from relation (13.3.24) that with an increase in the number M_δ or with elevation of the temperature in the boundary

layer *the shear stress, notwithstanding the increase in the viscosity, diminishes* ($n < 1$). This is due to the dominating influence of the density ρ_w on the friction. The density, as can be seen from (13.3.21'), decreases with elevation of the temperature $T_w = T_0$, and, consequently, the ability of the gas to withstand shear diminishes.

Let us determine the local friction factor:

$$(c_{f,x})_{com} = \frac{2(\tau_w)_{com}}{\rho_\delta V_\delta^2} = 0.646 \sqrt{\frac{1}{Re_x}} \left(1 + \frac{k-1}{2} M_\delta^2\right)^{(n-1)/2} \qquad (13.3.25)$$

For an incompressible fluid ($M_\delta = 0$), we have

$$(c_{f,x})_{ic} = 2(\tau_w)_{ic}/(\rho_\delta V_\delta^2) = 0.646 \sqrt{1/Re_x} \qquad (13.3.26)$$

The ratio of the local friction factors is the same as that of the shear stresses (13.3.24):

$$\frac{(c_{f,x})_{com}}{(c_{f,x})_{ic}} = \frac{(\tau_w)_{com}}{(\tau_w)_{ic}} = \left(\frac{T_0}{T_\delta}\right)^{(n-1)/2} = \left(1 + \frac{k-1}{2} M_\delta^2\right)^{(n-1)/2} \qquad (13.3.27)$$

Let us calculate the friction drag of a plate. The elementary value of this force acting on an area of $dx \cdot 1$ is

$$dX_{f,com} = (\tau_w)_{com}\, dx \cdot 1$$

The total friction drag on one side of a plate with an area of $L \cdot 1$ (L is the length of the plate) is

$$X_{f,com} = \int_0^L (\tau_w)_{com}\, dx \qquad (13.3.28)$$

The coefficient of this force is

$$(c_{x,f})_{com} = \frac{X_{f,com}}{(\rho_\delta V_\delta^2/2)\, L \cdot 1} = \frac{1}{L} \int_0^L \frac{(\tau_w)_{com}}{\rho_\delta V_\delta^2/2}\, dx = \frac{1}{L} \int_0^L (c_{f,x})_{com}\, dx \qquad (13.3.28')$$

Introducing into (13.3.28') the value of $(c_{f,x})_{com}$ from (13.3.25), we obtain

$$(c_{x,f})_{com} = 0.646 \left(1 + \frac{k-1}{2} M_\delta^2\right)^{(n-1)/2} \frac{1}{L} \int_0^L \sqrt{\frac{\nu_\delta}{V_\delta x}}\, dx$$

Integration of this expression yields

$$(c_{x,f})_{com} = \frac{1.292}{\sqrt{Re_L}} \left(1 + \frac{k-1}{2} M_\delta^2\right)^{(n-1)/2} \qquad (13.3.29)$$

where the Reynolds number based on the length L of the plate is

$$Re_L = V_\delta L/\nu_\delta$$

For an incompressible fluid

$$(c_{x,f})_{ic} = 1.292/\sqrt{Re_L} \qquad (13.3.30)$$

Let us see how the conditional thicknesses of the boundary layer are determined. We find their values for an incompressible flow from the expressions

$$\delta^{**} = \int_0^{\delta} \frac{V_x}{V_\delta}\left(1 - \frac{V_x}{V_\delta}\right) dy; \quad \delta^{*} = \int_0^{\delta} \left(1 - \frac{V_x}{V_\delta}\right) dy \qquad (13.3.31)$$

We introduce into these expressions the ratio V_x/V_δ proceeding from velocity distribution law (13.3.15):

$$\frac{V_x}{V_\delta} = \frac{3}{2}\frac{y}{\delta} - \frac{1}{2}\left(\frac{y}{\delta}\right)^2 \qquad (13.3.32)$$

Integration yields

$$\delta_{ic}^{**} = 0.146\delta_{ic}; \quad \delta_{ic}^{**} = 0.376\delta_{ic} \qquad (13.3.33)$$

where δ_{ic} is determined from (13.3.19').

To take into account the influence of compressibility on δ^{**}, let us consider Eq. (13.3.1), from which for ρ = const we find

$$d\delta_{ic}^{**}/dx = 0.5c_{f,x} \qquad (13.3.34)$$

whence $\delta_{ic}^{**} = 0.5\int_0^x c_{f,x}\,dx$, or $\delta_{ic}^{**} = 0.5c_{x,f}x$ ($c_{x,f}$ is the mean friction factor on the part of the plate from 0 to x). In accordance with this result, the ratio $\delta_{com}^{**}/\delta_{ic}^{**}$ is the same as (13.3.27):

$$\frac{\delta_{com}^{**}}{\delta_{ic}^{**}} = \frac{(c_{x,f})_{com}}{(c_{x,f})_{ic}} = \left(1 + \frac{k-1}{2}M_\delta^2\right)^{(n-1)/2} \qquad (13.3.35)$$

The ratio of the conditional displacement thicknesses is determined by analogy with (13.3.20):

$$\frac{\delta_{com}^{*}}{\delta_{ic}^{*}} = \frac{\delta_{com}}{\delta_{ic}} = \left(1 \quad \frac{k-1}{2}M_\delta^2\right)\left(1 + \frac{k-1}{2}M_\delta^2\right)^{(n-1)/2} \qquad (13.3.36)$$

13.4. Turbulent Boundary Layer on a Flat Plate

Use of a Logarithmic Velocity Distribution Law

To solve the problem on determining the parameters of a turbulent boundary layer on a flat plate in a compressible fluid, we shall use integral relation (13.3.7) in the variables ξ, η, in which it is the same in form as for an incompressible fluid.

When determining the law of distribution of the velocity V_x in the boundary layer, which we have to know for computing the integral in relation (13.3.7), we proceed from formula (1.1.10). Taking the averaged value of the velocity component $\overline{V}_x = V_x$, we shall write this formula as

$$\tau = \rho l^2 (\partial V_x/\partial y)^2 \qquad (13.4.1)$$

whence $\partial V_x/\partial y = (1/l) \sqrt{\tau/\rho}$.

According to Prandtl, the mixing length is

$$l = ky \qquad (13.4.2)$$

where k is a proportionality constant, and y is the distance from the wall.

Accordingly, $\partial V_x/\partial y = (1/ky) \sqrt{\tau/\rho}$, whence

$$V_x = \int \frac{1}{ky} \sqrt{\frac{\tau}{\rho}}\, dy + C_1 \qquad (13.4.3)$$

where C_1 is a constant determined from the flow boundary conditions in the boundary layer.

Let us transform (13.4.3), using the variables η (13.3.4) and ξ (13.3.6). To facilitate transformations, we shall introduce the function

$$\theta = (\tau/\rho_0)(1 - \overline{V}_\delta^2)^{-k/(k-1)} \qquad (13.4.4)$$

where $\overline{V}_\delta = V_\delta/V_{max}$.

We replace the density ρ in (13.4.3) with its value from (13.1.21):

$$\rho = \rho_0 (1 - \overline{V}_\delta^2)^{k/(k-1)} (1 - V_x^2)^{-1} \qquad (13.4.5)$$

where $\overline{V}_x = V_x/V_{max}$.

We use (13.3.4) and (13.4.5) to write the differential dy in (13.4.3) in the form

$$dy = (\rho_0/\rho)\, d\eta = (1 - \overline{V}_\delta^2)^{-k/(k-1)} (1 - \overline{V}_x^2)\, d\eta \qquad (13.4.6)$$

Let us now consider the transformation for the mixing length (13.4.2). Academician A. Dorodnitsyn [21] adopts $k = 0.3914$, i.e. equal to the value of this constant near the wall for a boundary layer in an incompressible fluid. But near a wall we can assume that $\overline{V}_x \approx 0$, and by (13.4.6), we have

$$y \approx (1 - V_\delta^2)^{-k/(k-1)} \eta \qquad (13.4.7)$$

Introduction of relations (13.4.4)-(13.4.7) into (13.4.3) yields

$$V_x = \int \frac{1}{k\eta (1 - \overline{V}_\delta^2)^{-k/(k-1)}} \sqrt{\frac{\theta (1 - \overline{V}_\delta^2)^{k/(k-1)} (1 - \overline{V}_x^2)}{(1 - \overline{V}_\delta^2)^{k/(k-1)}}}$$

$$\times (1 - \overline{V}_\delta^2)^{-k/(k-1)} (1 - \overline{V}_x^2)\, d\eta + C_2 = \int \frac{(1 - \overline{V}_x^2)^{3/2}}{k\eta} \sqrt{\theta}\, d\eta + C_2 \qquad (13.4.8)$$

where C_2 is a constant determined in accordance with the boundary conditions for the variable η.

The quantity $k\eta/(1-\overline{V}_x^2)^{3/2}$, which we shall designate by $\overline{l}$, corresponds to the mixing length l in (13.4.1). Since it is customary practice to find this length according to the constant k for the conditions near the wall, where $\overline{V}_x \ll 1$, we have

$$\overline{l} \approx k\eta \tag{13.4.9}$$

which exactly coincides with the adopted law for the mixing length in an incompressible flow. Hence,

$$V_x = \int \frac{\sqrt{\bar{\theta}}}{k\eta}\, d\eta + C_2$$

The derivation of the velocity distribution law being considered is based on the *hypothesis that the shear stress is constant over the cross section of the boundary layer*, in accordance with which $\tau = \tau_w = $ $= \text{const}$ and, consequently, $\theta = \theta_w = \text{const}$. Therefore,

$$V_x = \frac{\sqrt{\theta_w}}{k} \int \frac{d\eta}{\eta} + C_2$$

or

$$V_x = (\sqrt{\theta_w}/k) \ln \eta + C_2 \tag{13.4.10}$$

Relating this equation to the conditions at the edge of the boundary layer, where at $\eta = \eta_\delta$ we have $V_x = V_\delta$, we obtain

$$V_\delta = (\sqrt{\theta_w}/k) \ln \eta_\delta + C_2 \tag{13.4.11}$$

Combining (13.4.11) with (13.4.10), we find

$$V_x - V_\delta = (\sqrt{\theta_w}/k) \ln (\eta/\eta_\delta) \tag{13.4.12}$$

In the above form, the equations for V_x express the *logarithmic distribution of velocity over a cross section of a boundary layer*. Equations (13.4.10) and (13.4.12) according to their derivation hold only near a surface, i.e. in the vicinity of the laminar sublayer. Such a layer forms directly at a wall, which prevents mixing (turbulization). This phenomenon of the decrease in turbulization near a wall is described by formula (13.4.2), by which at a wall (when $y = 0$) mixing stops. An assumption was introduced in [21] according to which the velocity distribution inside the turbulent core of a boundary layer can be represented on the basis of logarithmic law (13.4.10) with the aid of the equation

$$V_x = (\sqrt{\theta_w}/k) [\ln \eta + C_2 + f(\eta/\eta_\delta)] \tag{13.4.10'}$$

where the quantity $f(\eta/\eta_\delta)$ is Dorodnitsyn's correction to the logarithmic law.

The correction $f(\eta/\eta_\delta)$ is a universal function not depending on the Mach number or the velocity V_δ. In other words, as for a laminar boundary layer, we assume that the velocity distribution does not depend on the compressibility in the coordinates η, ξ.

Assuming in (13.4.10′) that the variable $\eta = \eta_\delta$, we find the velocity at the edge of the boundary layer:

$$V_\delta = (\sqrt{\theta_w}/k)\,[\ln \eta_\delta + C_2 + f(1)] \qquad (13.4.11')$$

By (13.4.10′) and (13.4.11′), we have

$$V_x - V_\delta = (\sqrt{\theta_w}/k)\,F(\eta/\eta_\delta) \qquad (13.4.12')$$

where

$$F(\eta/\eta_\delta) = \ln(\eta/\eta_\delta) - f(1) - f(\eta/\eta_\delta) \qquad (13.4.12'')$$

A calculation of the parameters of a turbulent boundary layer based on Eq. (13.4.12′) containing Dorodnitsyn's correction is also given in [21]. Without altering in principle the scheme of solving the problem on the determination of these parameters, to simplify this solution we can consider the possibility of using a *conventional logarithmic law* without introducing the above correction, i.e. assuming that the function $F(\eta/\eta_\delta) = \ln(\eta/\eta_\delta)$. Calculations show that the numerical coefficients in the obtained expression for the boundary layer parameters differ somewhat from the data in [21]. This difference is quite permissible if we take into consideration the general nature of the approximate calculations.

The equation for the velocity corresponding to the adopted logarithmic law in its conventional form (13.4.12) can be transformed by expressing the thickness η_δ in terms of θ_w. For this purpose, let us consider Eq. (13.4.12) as applied to the conditions at the edge of the laminar sublayer, where at $\eta = \eta_{lam}$ the velocity at this edge is $V_x = V_{lam}$:

$$V_{lam} - V_\delta = (\sqrt{\theta_w}/k)\ln(\eta_{lam}/\eta_\delta) \qquad (13.4.13)$$

To determine the thickness of the laminar sublayer η_{lam} and the velocity V_{lam} at its edge, we shall use von Kármán's equation, which we shall write as follows for a variable y:

$$\delta_{lam} = \alpha\mu_w/\sqrt{\rho_w\tau_w} \qquad (13.4.14)$$

where we take the coefficient α the same as for an incompressible fluid, and equal to 11.5 (according to experimental data).

Let us transform Eq. (13.4.14) to the new variable η. The quantity $\delta_{lam} = \int_0^{\delta_{lam}} dy$, or with a view to (13.3.4) and (13.1.21)

$$\delta_{lam} = (1-\bar{V}_0^2)^{-k/(k-1)} \int_0^{\eta_{lam}} (1-\bar{V}_x^2)\,d\eta \qquad (13.4.15)$$

Near a wall, $\bar{V}_x \ll 1$, therefore

$$\delta_{\text{lam}} \approx (1-\bar{V}_\delta^2)^{-k/(k-1)}\,\eta_{\text{lam}} \tag{13.4.16}$$

We obtain an expression for τ_w in (13.4.14) from (13.4.4):

$$\tau_w = \theta_w \rho_0 (1-\bar{V}_\delta^2)^{k/(k-1)} \tag{13.4.17}$$

We find the density at the wall from (13.4.5), assuming that $V_x = 0$:

$$\rho_w = \rho_0 (1-\bar{V}_\delta^2)^{k/(k-1)} \tag{13.4.5'}$$

We introduce (13.4.16), (13.4.17), and (13.4.5') into (13.4.14):

$$\eta_{\text{lam}} = \alpha\mu_w/(\rho_0\sqrt{\theta_w}) \tag{13.4.18}$$

We can determine the quantity θ_w in this expression by Newton's formula $\tau_w = \mu_w (\partial V_x/\partial y)_{y=0}$. Having in view the small thickness of the laminar sublayer, we can assume for it a linear velocity distribution $V_x = V_{\text{lam}} y/\delta_{\text{lam}}$, according to which $\tau_w = \mu_w V_{\text{lam}}/\delta_{\text{lam}}$, whence $V_{\text{lam}} = (\tau_w/\mu_w)\,\delta_{\text{lam}}$, or with account taken of (13.4.16) for δ_{lam} and (13.4.17) for τ_w,

$$V_{\text{lam}} = (\rho_0\theta_w/\mu_w)\,\eta_{\text{lam}} \tag{13.4.19}$$

Substitution for η_{lam} of its value from (13.4.18) yields

$$V_{\text{lam}} = \alpha\sqrt{\theta_w} \tag{13.4.19'}$$

We introduce the value of η_{lam} from (13.4.18) and V_{lam} from (13.4.19') into (13.4.13):

$$\alpha\sqrt{\theta_w} - V_\delta = \frac{\sqrt{\theta_w}}{k}\ln\left(\frac{\alpha\mu_w}{\rho_0\sqrt{\theta_w}}\cdot\frac{1}{\eta_\delta}\right)$$

whence

$$\eta_\delta = \frac{\alpha\mu_w}{\rho_0\sqrt{\theta_w}}\exp(kV_\delta/\sqrt{\theta_w})\exp(-k\alpha) \tag{13.4.20}$$

Let us introduce the parameter

$$z = kV_\delta/\sqrt{\theta_w} \tag{13.4.21}$$

and designate the constant quantity $\alpha\exp(-k\alpha)$ by A. Hence,

$$\eta_\delta\sqrt{\theta_w} = e^z A\mu_w/\rho_0 \tag{13.4.22}$$

We use integral relation (13.3.7), into which we introduce the value

$$\tau_w/\rho_w = \theta_w \tag{13.4.23}$$

that is obtained from (13.4.17) and (13.4.5'). Simultaneously in accordance with (13.4.12), we perform the substitution:

$$V_x = V_\delta + (\sqrt{\theta_w}/k)\ln(\eta/\eta_\delta) \tag{13.4.24}$$

The result is

$$-\frac{d}{d\xi}\int_0^{\eta_\delta}\left(V_\delta+\frac{\sqrt{\theta_w}}{k}\ln\frac{\eta}{\eta_\delta}\right)\frac{\sqrt{\theta_w}}{k}\ln\frac{\eta}{\eta_\delta}=\theta_w$$

or

$$\frac{d}{d\xi}\left(\frac{V_\delta\sqrt{\theta_w}}{k}\int_0^{\eta_\delta}\ln\frac{\eta}{\eta_\delta}\,d\eta\right)+\frac{d}{d\xi}\left(\frac{\theta_w}{k^2}\int_0^{\eta_\delta}\ln^2\frac{\eta}{\eta_\delta}\,d\eta\right)=\theta_w \qquad (13.4.25)$$

Here we evaluate the integrals in the explicit form:

$$\left.\begin{aligned}\int_0^{\eta_\delta}\ln\frac{\eta}{\eta_\delta}\,d\eta&=\eta_\delta\int_0^1\ln\frac{\eta}{\eta_\delta}\,d\left(\frac{\eta}{\eta_\delta}\right)=-\eta_\delta\\ \int_0^{\eta_\delta}\ln^2\frac{\eta}{\eta_\delta}\,d\eta&=\eta_\delta\int_0^1\ln^2\frac{\eta}{\eta_\delta}\,d\left(\frac{\eta}{\eta_\delta}\right)=2\eta_\delta\end{aligned}\right\} \qquad (13.4.26)$$

Accordingly,

$$-\frac{d}{d\xi}\left[\eta_\delta\frac{\sqrt{\theta_w}}{k}\left(-V_\delta+\frac{2\sqrt{\theta_w}}{k}\right)\right]=\theta_w$$

We introduce the value of $\eta_\delta\sqrt{\theta_w}$ from (13.4.22) and θ_w from (13.4.21):

$$-\frac{d}{d\xi}\left[e^z\frac{A\mu_w}{k\rho_0}\left(-V_\delta+2\frac{V_\delta}{z}\right)\right]=\frac{k^2V_\delta^2}{z^2}$$

We divide both sides of the equation by $A\mu_w/(\rho_0 k)$:

$$\frac{d}{d\xi}\left[e^z\left(1-\frac{2}{z}\right)\right]=\frac{\rho_0k^3}{A\mu_w}\cdot\frac{V_\delta}{z^2} \qquad (13.4.27)$$

Differentiation yields

$$e^z\left(1-\frac{2}{z}\right)\frac{dz}{d\xi}+e^z\frac{2}{z^2}\cdot\frac{dz}{d\xi}=\frac{k^3\rho_0V_\delta}{A\mu_wz^2}$$

Dividing both sides of the equation by

$$e^z\,(1-2/z)+e^z2/z^2=e^z\,(1-2/z+2/z^2)$$

we obtain

$$\frac{dz}{d\xi}=\frac{k^3\rho_0V_\delta}{A\mu_w}\cdot\frac{e^{-z}}{z^2\,(1-2/z+2/z^2)}$$

or

$$\frac{d\,(z^2e^z)}{d\xi}=\frac{\rho_0V_\delta k^3}{A\mu_w}\cdot\frac{1+2/z}{1-2/z+2/z^2} \qquad (13.4.28)$$

Investigations show that at large Reynolds numbers the quantity $(1 + 2/z)/(1 - 2/z + 2/z^2) \approx \text{const} = 1.38$, consequently,

$$d(z^2e^z) = 1.38\rho_0 V_\delta k^3/(A\mu_w) \tag{13.4.29}$$

Assuming that $k = 0.3914$ and $\alpha = 11.5$, we find the constant quantity

$$1.38k^3/A = 1.38k^3e^{k\alpha}/\alpha = 0.656 \tag{13.4.30}$$

Consequently,

$$d(z^2e^z) = (0.656\rho_0 V_\delta/\mu_w)\, d\xi \tag{13.4.31}$$

Assuming that $z = 0$ at $\xi = 0$, after integration we find

$$z^2e^z = (0.656\rho_0 V_\delta/\mu_w)\, \xi \tag{13.4.32}$$

By (13.3.6), we have

$$\xi = (p_\delta/p_0)\, x = (1 - \bar{V}_\delta^2)^{k/(k-1)}x \tag{13.4.33}$$

By also taking (13.4.5′) into consideration, we obtain

$$z^2e^z = 0.656\rho_w V_\delta x/\mu_w \tag{13.4.34}$$

We can express the ratio ρ_w/μ_w by (13.3.17) as follows:

$$\frac{\rho_w}{\mu_w} = \frac{1}{\nu_\delta}\left(\frac{T_\delta}{T_w}\right)^n \frac{T_\delta}{T_0} = \frac{1}{\nu_\delta}\left(\frac{T_\delta}{T_0}\right)^{n+1} = \frac{(1-\bar{V}_\delta^2)^{n+1}}{\nu_\delta} \tag{13.4.35}$$

Substituting (13.4.35) into (13.4.34) and also introducing the notation $\boldsymbol{Re}_x = V_\delta x/\nu_\delta$, we have

$$z^2e^z = 0.656\,(1 - \bar{V}_\delta^2)^{n+1}\boldsymbol{Re}_x \tag{13.4.36}$$

The value of z found from (13.4.36) allows us to determine the shear stress. To find how τ_w depends on z, let us use relations (13.4.5′) and (13.4.21):

$$\tau_w = \frac{k^2V_\delta^2}{z^2}\rho_0(1-\bar{V}_\delta^2)^{k/(k-1)} = \frac{k^2V_\delta^2\rho_\delta}{z^2}(1-\bar{V}_\delta^2) = \frac{k^2\rho_\delta V_\delta^2}{z^2}\cdot\frac{T_\delta}{T_0} \tag{13.4.37}$$

The local friction factor is

$$c_{f,x} = \frac{2\tau_w}{\rho_\delta V_\delta^2} = \frac{2k^2}{z^2}(1-\bar{V}_\delta^2) = \frac{2k^2}{z^2}\cdot\frac{T_\delta}{T_0} \tag{13.4.38}$$

whence

$$z = k\sqrt{2(1-\bar{V}_\delta^2)/c_{f,x}} \tag{13.4.39}$$

Taking the logarithm of expression (13.4.36), we obtain

$$\ln z + z = (n+1)\ln(1-\bar{V}_\delta^2) + \ln \boldsymbol{Re}_x + \ln 0.656$$

Introduction into this equation of the value of z from (13.4.39) yields

$$2\ln\left|k\sqrt{2(1-\bar{V}_\delta^2)/c_{f,x}}\right|+k\sqrt{2(1-\bar{V}_\delta^2)/c_{f,x}}$$
$$=(n+1)\ln(1-\bar{V}_\delta^2)+\ln Re_x+\ln 0.656$$

or

$$k\sqrt{2(1-\bar{V}_\delta^2)/c_{f,x}}=\ln(Re_x c_{f,x})+n\ln(1-\bar{V}_\delta^2)+C_3$$

where $C_3=\ln 0.656-2\ln(k\sqrt{2})$.

Assuming that $k=0.3914$ and going over to common logarithms, we obtain

$$0.242\sqrt{1-\bar{V}_\delta^2}\Big/\sqrt{c_{f,x}}=\log(Re_x c_{f,x})+n\log(1-\bar{V}_\delta^2)+0.33 \tag{13.4.40}$$

Taking into account the expression $1-\bar{V}_\delta^2=\left(1+\frac{k-1}{2}M_\delta^2\right)^{-1}$ and designating $c_{f,x}$ by $(c_{f,x})_{com}$, we find

$$\frac{0.242}{\sqrt{(c_{f,x})_{com}}}=\sqrt{1+\frac{k-1}{2}M_\delta^2}$$
$$\times\left\{\log[Re_x(c_{f,x})_{com}-n\log\left(1+\frac{k-1}{2}M_\delta^2\right)+0.33\right\} \tag{13.4.41}$$

Formula (13.4.41) corresponds to the expression obtained in [21] on the basis of a logarithmic law with account taken of Dorodnitsyn's correction; on the right-hand side of this expression the numerical coefficient is 0.15 instead of 0.33. This difference, however, does not appreciably affect the value of $(c_{f,x})_{com}$.

A glance at (13.4.41) reveals that *the local friction factor of a plate decreases with an increasing number* M_δ. This result, suitable for a plate, may not be obtained when considering the boundary layer near a curved surface owing to the influence of the longitudinal pressure gradient on the flow in this case.

The friction factor in formula (13.4.41) is computed by successive approximations. In a first approximation, the factor $c_{f,x}=(c_{f,x})_{com}^{(1)}$ can be found for a given ratio T_δ/T_0 by (13.4.38) assuming that z ranges from 10 to 12. Introducing this value of $(c_{f,x})_{com}$ into the right-hand side of (13.4.41), we find the value of $c_{f,x}=(c_{f,x})_{com}^{(2)}$ as a second approximation. This result can be refined by introducing the value of $c_{f,x}=(c_{f,x})_{com}^{(2)}$ into the right-hand side of (13.4.41) and again calculating the value of $c_{f,x}=(c_{f,x})_{com}^{(3)}$.

The total friction factor for a plate with account taken of compressibility is determined by formula (13.3.28') by numerical integration with the use of expression (13.4.41) for $(c_{f,x})_{com}$.

For an incompressible fluid, we find the local friction factor from (13.4.41), assuming that $M_\delta = 0$:

$$0.242/\sqrt{(c_{f.x})_{1c}} = \log [Re_x (c_{f.x})_{1c}] + 0.33 \qquad (13.4.42)$$

To determine the thickness of the boundary layer, one should use formula (13.4.6) by which

$$\delta = (1 - \bar{V}_\delta^2)^{-k/(k-1)} \int_0^{\eta_\delta} (1 - \bar{V}_x^2)\, d\eta \qquad (13.4.43)$$

Power Law of Velocity Distribution

To establish the law of velocity distribution over the section of a turbulent boundary layer and determine the relation for the shear stress on the surface of a flat plate, we shall take advantage of the analogy with a viscous incompressible flow in a circular pipe (Figure 13.4.1). Let us consider this flow. We shall separate the part of fluid contained between sections 1 and 2 with a spacing of l. We shall assume that these sections are sufficiently remote from the pipe entrance, and therefore the flow through them is identical, i.e., for example, the shear stresses and velocity distribution are identical. The identical value of the velocities in the sections signifies that the fluid particles are moving without acceleration. Therefore the forces acting on the separated volume of fluid between sections 1 and 2 are in equilibrium, i.e.

$$F = (p_1 - p_2)\, \pi d^2/4 = \tau_w \pi l d \qquad (13.4.44)$$

where $d = 2r_0$ is the pipe diameter, and τ_w is the shear stress on the wall.

Hence,

$$p_1 - p_2 = 4\tau_w l/d \qquad (13.4.45)$$

In addition, the force F in (13.4.44) can be expressed with the aid of formula (1.3.5) for the hydrodynamic drag. Let us insert into this formula the symbols for the drag force $X = F$ and for the hydrodynamic drag coefficient $c_x = \lambda$ and determine the velocity head $q = \rho V_{av}^2/2$ according to the average velocity V_{av} in the pipe (Fig. 13.4.1). Adopting the side surface area $S = \pi l d$ as the characteristic area, we obtain $(p_1 - p_2)\, \pi d^2/4 = \lambda\, (\rho V_{av}^2/2)\, \pi l d$. Hence we find a formula for determining the friction losses:

$$p_1 - p_2 = 4\lambda\, (\rho V_{av}^2/2)\, l/d \qquad (13.4.46)$$

where the average velocity is determined from the given flow rate Q in the pipe:

$$V_{av} = 4Q/(\pi d^2) \qquad (13.4.47)$$

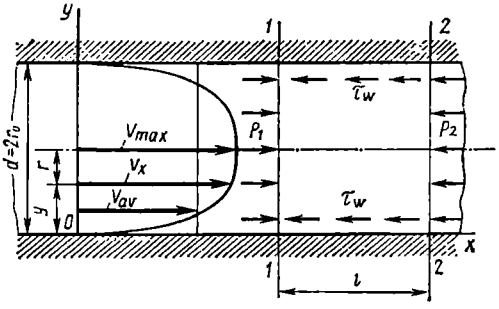

Fig. 13.4.1

Viscous flow in a circular pipe

The drag coefficient λ can be determined experimentally. Such investigations were performed by H. Blasius, who established that for smooth pipes the drag coefficient for turbulent conditions and pipe Reynolds numbers (based on the pipe diameter) within the range of

$$2.3 \times 10^3 \leqslant Re_d = \rho V_{av} d/\mu \leqslant 10^5 \qquad (13.4.48)$$

equals

$$\lambda = 0.3164/Re_d^{1/4} \qquad (13.4.49)$$

Let us introduce this value into (13.4.46) and replace $p_1 - p_2$ with its value from (13.4.45). The result is

$$\tau_w = 0.3164\rho V_{av}^2/(8\,Re_d^{1/4}) = 0.03955 V_{av}^{7/4}\rho^{3/4}\mu^{1/4}d^{-1/4} \qquad (13.4.50)$$

To determine the average velocity V_{av}, we shall use the results of studying the flow of a fluid in a circular pipe, according to which the velocity over its cross section varies according to a **seventh root law:**

$$V_x = V_{max}\,(y/r_0)^{1/7} \qquad (13.4.51)$$

This law reflects a hypothesis according to which in the flow of a fluid kinematic similarity is retained, i.e. regardless of the absolute dimensions of a pipe, at points with the same value of y/r_0 the ratio of the local velocity V_x to that at the pipe axis V_{max} is also the same.

The average velocity over the cross section of a pipe by (13.4.47) is

$$V_{av} = \frac{Q}{\pi r_0^2} = V_{max}\int_0^{r_0} 2\pi r \left(\frac{r_0 - r}{r_0}\right)^{1/7} dr/(\pi r_0^2) = 0.816 V_{max} \qquad (13.4.52)$$

Let us insert (13.4.52) into (13.4.50):

$$\tau_w = 0.03955\,(0.816 V_{max})^{7/4}\rho^{3/4}\mu^{1/4}\,(2r_0)^{-1/4}$$
$$= 0.0233\rho V_{max}^2\,(\nu/V_{max}r_0)^{1/4} \qquad (13.4.53)$$

When considering a viscous turbulent flow through a circular pipe and in the boundary layer, we can note a similarity in the velocity profiles over their cross sections. The velocity V_δ at the edge of the boundary layer corresponds to the maximum velocity at the pipe axis, and the layer thickness δ, to the pipe radius r_0. Investigations reveal that this analogy can be used to obtain relations determining the flow in a turbulent boundary layer. By substituting δ for r_0 and V_δ for V_{max} in (13.4.51), we find for the boundary layer a power law (a seventh root law) of velocity distribution over its cross section:

$$V_x = V_\delta (y/\delta)^{1/7} \tag{13.4.54}$$

A similar substitution in (13.4.53) allows us to obtain a formula for the shear stress on the wall:

$$\tau_w = 0.0233 \rho V_\delta^2 [\nu/(V_\delta \delta)]^{1/4} \tag{13.4.55}$$

To evaluate the shear stress by (13.4.55), we must first determine the boundary layer thickness δ. To do this, we shall use integral relation (13.3.1). Introducing into it relation (13.4.54) instead of V_x and (13.4.55) instead of τ_w, we find

$$\rho V_\delta^2 \frac{d}{dx} \int_0^\delta \left(\frac{y}{\delta}\right)^{1/7} \left[1 - \left(\frac{y}{\delta}\right)^{1/7}\right] dy = 0.0233 \rho V_\delta^2 \left(\frac{\nu}{V_\delta \delta}\right)^{1/4} \tag{13.4.56}$$

We calculate the integral:

$$d\delta/dx = 0.2395 \ [\nu/(V_\delta \delta)]^{1/4}$$

Separation of the variables in this differential equation yields

$$\delta^{1/4} \, d\delta = 0.2395 \ (\nu/V_\delta)^{1/4} \, dx$$

As a result of solving this equation, we obtain

$$(4/5) \ \delta^{5/4} = 0.2395 \ (\nu/V_\delta)^{1/4} x + C \tag{13.4.57}$$

The integration constant C is determined for the point of transition of a laminar boundary layer into a turbulent one from the condition that at this point, at a distance of $x = x_{cr}$ from the leading edge, the layer thickness is $\delta = \delta_{cr}$. The distance x_{cr} is determined according to the given critical Reynolds number $Re_{cr} = V_\delta x_{cr}/\nu$, while the thickness δ_{cr} is found for this number Re_{cr} by the corresponding formula for a laminar boundary layer. At large Reynolds numbers, the length of the laminar portion is not large, and in practical calculations its influence on the thickness of the turbulent boundary layer may be negligibly small. We may consider in these cases that the turbulent boundary layer originates at the leading edge, where at $x = 0$ the layer thickness is $\delta = 0$. Accordingly, in (13.4.57)

the constant $C = 0$, and, therefore, the layer thickness is

$$\delta = \delta_{1c} = (0.37/\boldsymbol{Re}_x^{1/5})\, x \qquad (13.4.58)$$

where $\boldsymbol{Re}_x = V_\delta x/\nu_\delta$ and $\nu_\delta = \nu$.

Introducing the dimensionless quantities $\bar{\delta}_{1c} = \delta_{1c}/L$, $\bar{x} = x/L$, and the Reynolds number $\boldsymbol{Re}_L = V_\delta L/\nu_\delta$, we can write Eq. (13.4.58) as

$$\bar{\delta} = \bar{\delta}_{1c} = \delta_{1c}/L = 0.37\,(\bar{x}^{4/5}/\boldsymbol{Re}_L^{1/5}) \qquad (13.4.58')$$

A comparison of (13.3.19") and (13.4.58') allows us to conclude that the thickness of a turbulent boundary layer grows more intensely than that of a laminar one. This is explained by mixing of the macroscopic particles that features the turbulent nature of a fluid flow and facilitates the intensive growth of the layer.

We shall compute the stress τ_w by formula (13.4.55). Assuming that $\rho = \rho_\delta$, $\nu = \nu_\delta$, and inserting the value of δ from (13.4.58), we obtain

$$\tau_w = (\tau_w)_{1c} = 0.0299\rho_\delta V_\delta^2/\boldsymbol{Re}_x^{1/5} \qquad (13.4.59)$$

By introducing the quantities $\boldsymbol{Re}_L = V_\delta L/\nu_\delta$ and $\bar{x} = x/L$, we shall write (13.4.59) in the form

$$(\tau_w)_{1c} = 0.0299\rho_\delta V_\delta^2/(\boldsymbol{Re}_L x)^{1/5} \qquad (13.4.59')$$

A comparison of (13.3.23) and (13.4.59) reveals that the shear stress in turbulent flow is considerably greater than in laminar flow at the same values of the number $\boldsymbol{Re}_x$. Hence, turbulization of the boundary layer is attended by a sharp increase in the shear stresses. At the same time, in turbulent flow the shear stress and other parameters of the boundary layer depend more slightly on the Reynolds number than in laminar flow. This number is known to be due to molecular forces of viscosity that manifest themselves most significantly in a laminar boundary sublayer. At a higher velocity and, consequently, a larger Reynolds number, this sublayer is thinner, the viscosity has a smaller influence, and the Reynolds number thus affects the friction parameters less.

The magnitude of the shear stress can be used to determine the local friction factor:

$$(c_{f,x})_{1c} = 2\,(\tau_w)_{1c}/(\rho_\delta V_\delta^2) = 0.0598/\boldsymbol{Re}_x^{1/5} \qquad (13.4.60)$$

or

$$(c_{f,x})_{1c} = 0.0598/(\boldsymbol{Re}_L\bar{x})^{1/5} \qquad (13.4.60')$$

The friction drag for one side of a plate is determined by formula (13.3.28):

$$X_{f,1c} = \int_0^L (\tau_w)_{1c}\, dx \qquad (13.4.61)$$

By this formula and with a view to (13.4.60'), the friction factor is

$$(c_{x,f})_{lc} = \frac{2X_{f,lc}}{\rho_\delta V_\delta^2 L \cdot 1} = \frac{1}{L}\int_0^L \frac{2(\tau_w)_{lc}}{\rho_\delta V_\delta^2}\,dx = \frac{0.0598}{Re_L^{1/5}}\int_0^1 \frac{d\bar{x}}{\bar{x}^{1/5}}$$

whence

$$(c_{x,f})_{lc} = 0.075/Re_L^{1/5} \qquad (13.4.62)$$

This formula yields reliable results if the number Re_L does not exceed 10^6. For larger values of Re_L, better results are obtained by other relations. For example, at $2 \times 10^6 < Re_L < 10^{10}$, the friction factor is

$$(c_{x,f})_{lc} = 0.032Re^{-0.145} \qquad (13.4.63)$$

In this case, we may also use the Prandtl-Schlichting universal formula to calculate the factor $(c_{x,f})_{lc}$, namely,

$$(c_{x,f})_{lc} = 0.455\,(\log Re_L)^{-2.58} \qquad (13.4.64)$$

We shall use formulas (13.3.31) to determine the conditional thicknesses of the boundary layer. By introducing into them the velocity ratio V_x/V_δ in accordance with power law (13.4.54), integrating, and employing relations (13.4.58) and (13.4.60), we obtain

$$\delta_{lc}^{**} = 0.097\delta_{lc} \text{ and } \delta_{lc}^{*} = 0.125\delta_{lc} \qquad (13.4.65)$$

where δ_{lc} is determined from (13.4.58).

13.5. Temperature and Enthalpy in a Boundary Layer with Heat Transfer

Distribution of the Temperature and Enthalpy

At a low flow velocity, heating of the gas due to stagnation in the boundary layer is almost absent, and its temperature may be considered virtually equal to its free-stream value. Indeed, it follows from (13.3.18) that in the absence of heat transfer for $M_\delta = 0.5$, the gas temperature at the wall T_w, equal to the stagnation temperature, is $T_w = T_0 = T_\delta(1 + 0.2 \times 0.25) = 1.05T_\delta$, i.e. it differs from the free-stream temperature by only 5%.

At high velocities, stagnation of the gas leads to a substantial increase in the temperature and enthalpy in the boundary layer, which corresponds in its nature to the change in the velocity over the cross section of the boundary layer.

If the only kind of heat transfer is conduction, the number $Pr = 1$, and the heat transfer at the wall is zero, then by (13.1.16) the tem-

perature in the boundary layer is

$$T = T_0 - V_x^2/[2\,(c_p)_{av}] \qquad (13.5.1)$$

where $(c_p)_{av}$ is the average specific heat for the temperature interval from T_0 to T. The temperature T_0, which is a measure of the total energy, does not change over the thickness of the layer and is determined by the parameters $T = T_\delta$ and $V_x = V_\delta$ at the edge of the boundary layer in accordance with the expression

$$T_0 = T_\delta + V_\delta^2/[2\,(c_p)_{av}] \qquad (13.5.2)$$

Let us perform the following substitutions here:

$$V_\delta^2 = M_\delta^2 a_\delta^2 = M_\delta^2 \bar{k} R T_\delta; \quad (c_p)_{av} = R\,\frac{(c_p)_{av}}{(c_p)_{av} - (c_v)_{av}} = \frac{R\bar{k}}{\bar{k}-1} \qquad (13.5.3)$$

where $\bar{k} = (c_p)_{av}/(c_v)_{av}$ is the average value of the specific heat ratio for the temperature interval from T_0 to T_δ. Hence,

$$T_0 = T_\delta\left(1 + \frac{\bar{k}-1}{2} M_\delta^2\right) \qquad (13.5.4)$$

At constant specific heats, we should assume that $(c_p)_{av} = c_p = $ $= \text{const}$, and $\bar{k} = k = \text{const}$. When the specific heat varies greatly with the temperature because of dissociation and ionization, and it may not be replaced with its average value, it is good to use the enthalpies i and i_0, respectively, instead of T and T_0. By (3.4.14) and by analogy with (13.5.1), the enthalpy at a point of the boundary layer cross section is

$$i = i_0 - V_x^2/2 \qquad (13.5.5)$$

Introducing the values of $i = i_\delta$ and $V_x = V_\delta$, we find the following expression for the stagnation enthalpy:

$$i_0 = i_\delta + V_\delta^2/2 \qquad (13.5.6)$$

For constant specific heats

$$i_\delta = c_p T_\delta = kRT_\delta/(k-1) = a_\delta^2/(k-1) \qquad (13.5.7)$$

therefore, bearing in mind that $V_\delta^2 = M_\delta^2 a_\delta^2$, the stagnation enthalpy is

$$i_0 = i_\delta\left(1 + \frac{k-1}{2} M_\delta^2\right) \qquad (13.5.8)$$

The assumption that there is no heat transfer at the wall and that the number $Pr = 1$ does not correspond to what actually occurs, therefore in real conditions the temperature and enthalpy at the wall differ from the above values T_0 and i_0.

Let us consider the known case of an adiabatic (thermally insulated) wall. The heat supplied to such a wall from the boundary layer

is not used for heating the wall, and the latter, in turn, gives up no heat to the boundary layer. Energy is transferred in the boundary layer as follows. Owing to stagnation of the flow because of viscosity forces, the temperature grows from its value at the edge of the layer to a certain value at the wall, and this gives rise to a temperature gradient $\partial T/\partial y \neq 0$. In this case in accordance with Fourier's law (3.2.7), heat transfer occurs by conduction to the outer layers of the gas with a lower temperature. The heating grows until equilibrium is established between this heat transfer and the opposite flow of heat from the outer layers to the inner ones because of the work done by the viscous forces. Owing to the removal of heat from the boundary layer near the wall, the temperature on the surface $T_w = T_r$ is lower than the stagnation temperature T_0. The temperature T_r and the enthalpy i_r corresponding to it are known as the **recovery temperature** and **enthalpy**, respectively. The lowering of the temperature at the wall can be characterized by the parameter

$$r = (T_r - T_\delta)/(T_0 - T_\delta) \tag{13.5.9}$$

called the **temperature recovery factor.** It shows how close the recovery temperature is to the stagnation one. This factor characterizes the fraction of the kinetic energy of the external flow that is converted into enthalpy upon stagnation.

Equation (13.5.9) yields the following expression for the recovery temperature:

$$T_r = T_\delta + r(T_0 - T_\delta) = T_\delta[1 + r(T_0/T_\delta - 1)] \tag{13.5.10}$$

Introducing the values of the difference $T_0 - T_\delta$ from (13.5.2) and of the ratio T_0/T_δ from (13.5.4), we obtain

$$T_r = T_\delta + r\frac{V_\delta^2}{2(c_p)_{av}} \tag{13.5.11}$$

$$T_r = T_\delta\left(1 + r\frac{\bar{k}-1}{2}M_\delta^2\right) \tag{13.5.12}$$

When studying the flow of viscous dissociating gases, it is good to go over to other relations. Such gases are characterized by a substantial increase in the specific heat because the dissociation energy should be added to the thermal energy of the gas. In such cases, it is no longer expedient to use the temperature as a measure of the energy. The enthalpy is more suitable for these purposes.

To estimate the influence of the heat conductance on the boundary layer in a dissociating gas in the case being considered, one should use the concept of the recovery enthalpy i_r and the corresponding enthalpy recovery factor

$$r = (i_r - i_\delta)/(i_0 - i_\delta) \tag{13.5.13}$$

When studying high-velocity heat transfer in the absence of dissociation for $Pr \neq 1$, we introduced the concept of the temperature recovery factor r. Similarly, when chemical reactions occur, we are justified in introducing a similar **enthalpy recovery factor** that takes into account the degree of conversion of chemical energy into thermal energy.

It follows from (13.5.10) that

$$i_r = i_\delta + r(i_0 - i_\delta) = i_\delta [1 + r(i_0/i_\delta - 1)] \tag{13.5.14}$$

Using formulas (13.5.6) for $i_0 - i_\delta$ and (13.5.8) for i_0/i_δ, we obtain

$$i_r = i_\delta + rV_\delta^2/2 \tag{13.5.15}$$

$$i_r = i_\delta \left(1 + r \frac{k-1}{2} M_\delta^2\right) \tag{13.5.16}$$

We can use the recovery factor r to characterize the change in the temperature T and enthalpy i over the cross section of the boundary layer. By analogy with (13.5.11) and (13.5.15), we have

$$T_r = T + rV_x^2/[2(c_p)_{av}]; \quad i_r = i + rV_x^2/2$$

whence

$$T = T_r - rV_x^2/[2(c_p)_{av}] \tag{13.5.17}$$

$$i = i_r - rV_x^2/2 \tag{13.5.18}$$

whence $(c_p)_{av}$ is the average specific heat for the temperature interval from T_r to T.

We noted in Sec. 3.5 that the relation between the heat flow due to friction and the amount of heat removed by the molecules when they are mixed is determined by the Prandtl number [see (3.5.11)]. It is therefore natural to assume that the recovery factor r depends on the Prandtl number. The latter is as follows for the conditions at the wall, by analogy with (3.5.11):

$$Pr = \mu_w (c_p)_w/\lambda_w \tag{13.5.19}$$

Theoretical and experimental investigations have established that the recovery factors for a laminar and turbulent boundary layers can be taken as follows, respectively:

$$r_{lam} = \sqrt{Pr} \tag{13.5.20}$$

$$r_{trb} = \sqrt[3]{Pr} \tag{13.5.21}$$

The Prandtl number for air varies from 0.75 at low temperatures to 0.65 at high ones. In practical calculations, one may use the mean value of the number $Pr = 0.7$, and the corresponding values

$$r_{lam} \approx 0.84 \text{ and } r_{trb} \approx 0.89 \tag{13.5.22}$$

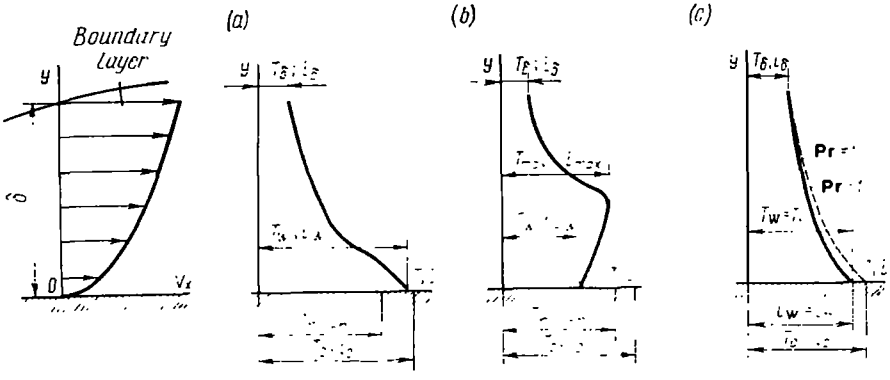

Fig. 13.5.1
Change in the temperature and enthalpy over the cross section of a boundary layer:
a—adiabatic wall (thermally insulated); *b*—cooled wall; *c*—heated wall

For $Pr = 1$, the recovery factor $r = 1$. In this case, the recovery temperature and enthalpy coincide respectively with the stagnation temperature and enthalpy.

The change in the temperature and enthalpy over the boundary layer cross section for various flow conditions is shown in Fig. 13.5.1. The curves in Fig. 13.5.1*a* show the change in the temperature and enthalpy for a thermally insulated wall in two cases, when $Pr = 1$ and $Pr \neq 1$. The distribution of the temperature and enthalpy naturally differs for a wall without thermal insulation, i.e. when heat is removed or supplied (Fig. 13.5.1*b*, *c*). When heat is taken away (a cooled wall), the boundary layer without thermal insulation gives up its heat to the wall and cools, therefore the temperature of the gas T_w at such a wall is lower than the recovery temperature T_r, and, correspondingly, the gas enthalpy i_w is lower than the recovery enthalpy i_r. The temperature of the gas T_w may be treated as the temperature of the surface, which we shall conditionally call the **wall temperature.** If heat is supplied from an external source and the temperature of the wall exceeds the maximum temperature of the boundary layer (a heated wall), the boundary layer is also heated; hence, for the gas at the surface $T_w > T_r$ and $i_w > i_r$.

At very high craft velocities, the wall usually cools ($i_w < i_r$, $T_w < T_r$). This is explained by the thermal radiation from the surface that cannot be compensated by the comparatively small inflow of heat because of conduction along the wall from heat sources inside the craft. We shall denote the temperature of such a wall by T_w, i.e. like the temperature of the gas at the wall. In a most general case, however, the gas temperature does not coincide with that of the wall and, in addition, differs from the value T_r. The quantity i_w

indicated above should be treated as the enthalpy of a conditional gas whose temperature equals that of the wall T_w.

A craft may be heated ($i_w > i_r$, $T_w > T_r$) if the flight occurs with deceleration and is attended by a drop in the recovery temperature, whereas the overheated wall does not have time to cool.

In wind tunnels where there is no special heating of the air, while the stagnation temperature is close to the ambient one, the wall of an experimental model may be heated. The explanation is that heat may flow to the surface of the model through the sting, while the radiation flux from the cold wall of the model is negligibly small.

Reference Temperature

The presence of the Mach number in the relations given above for determining the flow parameters of a viscous fluid reflects the fact that the density changes because of stagnation of the flow in the boundary layer and the associated elevation of the temperature. This is a manifestation of the compressibility affecting the flow of the gas in the boundary layer. The growth of the velocities is attended by an increase in the temperature, which in addition to the change in the density also leads to a change in the thermodynamic parameters and the kinetic coefficients of the gas in the boundary layer. At high temperatures, chemical reactions may occur in it.

These phenomena are of major significance in the formation of the skin friction and heat transfer processes in a boundary layer. But great difficulties are involved when taking these phenomena into consideration in calculating the parameters of a boundary layer and, particularly, the temperature distribution over its thickness. We shall therefore consider the comparatively simple approximate methods of computing the boundary layer parameters for very high flow velocities. One of these methods is based on the use of relations similar in their appearance to the relations we obtained when investigating the boundary layer in an incompressible fluid. This possibility follows from the fact that near the surface, in the region of the boundary layer near the wall, the flow experiences great stagnation, and, consequently, the gas is close in its properties to an incompressible medium. If we consider that the flow in this region has the main influence on skin friction and heat transfer, then, consequently, we may use relations whose structure is the same as for an incompressible fluid to calculate the parameters of a boundary layer. The difference is that these relations include parameters as functions of the temperature.

Let us establish the boundary layer temperature which we should use to evaluate these parameters. Theoretical and experimental investigations show that satisfactory results are obtained when the effective, or **reference temperature** T^* is used in the calculations.

This temperature is an average value over the cross section of the boundary layer. The gas parameters calculated according to the temperature T^* are also called **effective, or reference** (the enthalpy i^*, density ρ^*, dynamic viscosity μ^*, etc.).

At high flow velocities, when physicochemical transformations in the boundary layer are important, the calculation of the layer parameters should be based on the reference enthalpy i^*. The latter is used to compute the other reference parameters including the temperature T^*.

By solving the heat transfer equation for a laminar boundary layer, E. Eckert obtained the following formula for the reference enthalpy:

$$i^* = 0.5\,(i_w + i_\delta) + 0.22\,(i_r - i_\delta) \qquad (13.5.23)$$

The reference enthalpy depends on the boundary layer structure and the number M_∞. Quite a few relations are available for calculating the value of i^* separately for laminar and turbulent boundary layers, and also for various intervals of the numbers M_∞. Formula (13.5.23) differs advantageously from these relations because of its universal nature, and it may be used in a first approximation for both laminar and turbulent flows within a quite wide range of numbers M_∞.

A close look at (13.5.23) reveals that to calculate i^* we should know the enthalpy of the gas i_w at the wall temperature. In a particular case, when the temperature of the surface is maintained with the aid of special cooling means at the required level, this enthalpy is known. On the other hand, if heating occurs spontaneously, the determination of i_w is associated with solution of the problem on the heat transfer between the wall and the gas. For the case of a thermally insulated wall ($i_w = i_r$), the reference enthalpy is

$$i^* = 0.72 i_r + 0.28 i_\delta \qquad (13.5.24)$$

Without account taken of heat transfer in the boundary layer at $Pr = 1$, the enthalpy i_r equals the stagnation enthalpy i_0 that is evaluated by (13.5.6). Accordingly,

$$i^* = 0.72\,(i_\delta + V_\delta^2/2) + 0.28 i_\delta = i_\delta + 0.36 V_\delta^2 \qquad (13.5.24')$$

The enthalpy i_δ at the upper edge of the boundary layer can be found by solving the problem on the inviscid flow over a given surface. The recovery enthalpy i_r in (13.5.23) and (13.5.24) is determined from the expression

$$i_r = i_\delta + r^* V_\delta^2/2 \qquad (13.5.25)$$

in which the recovery factor is calculated as the reference parameter by (13.5.20) and (13.5.21):

$$r^*_{lam} = \sqrt{Pr^*} \qquad (13.5.26)$$

$$r^*_{turb} = \sqrt[3]{Pr^*} \qquad (13.5.27)$$

Here the Prandtl number

$$Pr^* = c_p^* \mu^* / \lambda^* \tag{13.5.28}$$

is based on the reference values of the specific heat, dynamic viscosity, and thermal conductivity.

Relation (13.5.23) is used for a dissociating gas, and also when the gas in a boundary layer is heated to a temperature at which no dissociation sets in, but the specific heats change. In the first case, we find the reference temperature T^* as a function of p and i^*. Tables or phase diagrams of air for very high temperatures can be used for the calculations. In the second case, we can find the reference temperature by relation (13.5.23) in which the enthalpy is replaced with the temperature in accordance with the expressions

$$\begin{aligned} i^* - i_\delta &= (c_p)^*_{av} (T^* - T_\delta) \\ i_w - i_\delta &= (c_p)^w_{av} (T_w - T_\delta) \\ i_r - i_\delta &= (c_p)^r_{av} (T_r - T_\delta) \end{aligned} \tag{13.5.29}$$

where $(c_p)^*_{av}$, $(c_p)^w_{av}$, and $(c_p)^r_{av}$ are the average values of the specific heats found for the temperature intervals $T^* - T_\delta$, $T_w - T_\delta$, and $T_r - T_\delta$, respectively.

By inserting into (13.5.23) the values of the enthalpies from (13.5.29), we obtain a relation for the reference temperature T^*. Here we find the recovery temperature with the aid of formulas (13.5.11) and (13.5.12) written in the form

$$T_r = T_\delta + r^* V_\delta^2 / [2 (c_p)^*_{av}] \tag{13.5.30}$$

$$T_r = T_\delta \left(1 + r^* \frac{\bar{k}^* - 1}{2} M_\delta^2\right) \tag{13.5.31}$$

When the specific heats do not virtually depend on the temperature (at $T \approx 700$-800 K and below), the reference temperature is

$$T^* = 0.5 (T_w + T_\delta) + 0.22 (T_r - T_\delta) \tag{13.5.32}$$

For a thermally insulated wall, we assume that $T_w = T_r$,

$$T^* = 0.72 T_r + 0.28 T_\delta \tag{13.5.33}$$

We calculate the thermodynamic functions and the kinetic parameters in terms of the reference temperature by formulas (1.5.1), (1.5.2), and (1.5.4) written as follows:

$$c_p^*/c_{p\infty} = (T^*/T_\infty)^\varphi; \quad \mu^*/\mu_\infty = (T^*/T_\infty)^n; \quad \lambda^*/\lambda_\infty = (T^*/T_\infty)^\chi \tag{13.5.34}$$

13.6. Use of the Reference Parameters for Calculating the Boundary Layer on a Flat Plate at High Flow Velocities

Laminar Boundary Layer

By using the reference parameters, let us find the relation between the basic characteristics of an incompressible laminar boundary layer and a compressible core such as occurs at high flow velocities. For this purpose, we shall introduce the corresponding parameters into the relations obtained above (see Secs. 13.3 and 13.4) for an incompressible boundary layer.

Let us consider the thickness of the boundary layer. Its value for an incompressible fluid is determined by formula (13.3.19'):

$$\delta_{ic} = 4.64 \sqrt{\mu_\delta x / (V_\delta \rho_\delta)}$$

where the subscript δ signifies the parameters of the boundary layer in an incompressible fluid.

We obtain a similar formula for a compressible gas if we substitute the corresponding effective parameters μ^* and ρ^* for the quantities μ_δ and ρ_δ:

$$\delta_{com} = 4.64 \sqrt{\mu^* x / (V_\delta \rho^*)} \tag{13.6.1}$$

The thickness ratio is

$$\delta_{com}/\delta_{ic} = \sqrt{(\mu^*/\mu_\delta)\, \rho_\delta/\rho^*} \tag{13.6.2}$$

A similar expression can be obtained for the shear stress. For an incompressible fluid by (13.3.23), we have

$$(\tau_w)_{ic} = 0.323 \rho_\delta V_\delta^2 \sqrt{\mu_\delta / (V_\delta \rho_\delta x)}$$

and for a compressible gas

$$(\tau_w)_{com} = 0.323 \rho^* V_\delta^2 \sqrt{\mu^* / (V_\delta \rho^* x)} \tag{13.6.3}$$

The ratio of the shear stresses is

$$(\tau_w)_{com} / (\tau_w)_{ic} = \sqrt{(\rho^*/\rho_\delta)\, \mu^*/\mu_\delta} \tag{13.6.4}$$

For the local friction factors related to the velocity head $q_\delta = \rho_\delta V_\delta^2/2$ of the free stream, we have

$$(c_{f,x})_{ic} = 2 (\tau_w)_{ic} / (\rho_\delta V_\delta^2) = 0.646 \sqrt{\mu_\delta / (V_\delta \rho_\delta x)}$$

$$(c_{f,x})_{com} = 2 (\tau_w)_{com} / (\rho_\delta V_\delta^2) = 0.646 \sqrt{\mu^* / (V_\delta \rho^* x)} \cdot \rho^*/\rho_\delta \tag{13.6.5}$$

The ratio of these factors is

$$(c_{f,x})_{com} / (c_{f,x})_{ic} = (\tau_w)_{com} / (\tau_w)_{ic} = \sqrt{(\rho^*/\rho_\delta)\, \mu^*/\mu_\delta} \tag{13.6.6}$$

The friction factor (or the average friction factor over the length of a plate) in an incompressible fluid, by (13.3.30), is

$$(c_{x,f})_{1c} = 1.292 \sqrt{\mu_\delta / (V_\delta \rho_\delta L)}$$

For a compressible gas in accordance with (13.3.28′) and (13.6.5)

$$(c_{x,f})_{com} = \frac{1}{L} \int_0^L (c_{f,x})_{com}\, dx$$

$$= \frac{0.646}{L} \int_0^L \sqrt{\frac{\mu^*}{V_\delta \rho^*}} \cdot \frac{\rho^*}{\rho_\delta} \cdot \frac{dx}{\sqrt{x}} \qquad (13.6.7)$$

At a constant wall temperature, the parameters μ^* and ρ^* do not depend on the coordinate x, therefore

$$(c_{x,f})_{com} = 1.292 \sqrt{\mu^* / (V_\delta \rho^* L)} \cdot \rho^* / \rho_\delta \qquad (13.6.8)$$

Consequently, the ratio of the friction factors is

$$(c_{x,f})_{com} / (c_{x,f})_{1c} = (c_{f,x})_{com} / (c_{f,x})_{1c}$$

$$= (\tau_w)_{com} / (\tau_w)_{1c} = \sqrt{(\mu^*/\mu_\delta)\, \rho^*/\rho_\delta} \qquad (13.6.9)$$

Let us consider the case when dissociation occurs in the boundary layer as a result of a high temperature, whereas the free-stream flow occurs at constant specific heats. Assuming here that the pressure does not change over the thickness of the layer, for the density ratio we obtain the following formula based on an equation of state

$$\rho^*/\rho_\delta = (m^*/m_\delta)\, T_\delta / T^* \qquad (13.6.10)$$

where m^* is the reference average molar mass of the gas.

Using power law (1.5.2) for the dynamic viscosity, we find

$$\mu^*/\mu_\delta = (T^*/T_\delta)^n \qquad (13.6.11)$$

Let us introduce (13.6.10) and (13.6.11) into (13.6.2) and (13.6.9):

$$\delta_{com}/\delta_{1c} = (T^*/T_\delta)^{(n+1)/2}\, (m_\delta/m^*)^{1/2} \qquad (13.6.12)$$

$$(c_{x,f})_{com} / (c_{x,f})_{1c} = (c_{f,x})_{com} / (c_{f,x})_{1c}$$

$$= (\tau_w)_{com} / (\tau_w)_{1c} = (T^*/T_\delta)^{(n-1)/2}\, (m^*/m_\delta)^{1/2} \qquad (13.6.13)$$

Formula (13.6.12) shows that the thickness of a laminar boundary layer depends greatly on the quantity T^*/T_δ and, consequently, on the number M_δ (the velocity V_δ) and ratio T_w/T_δ and it grows when these parameters increase. The dependence of the friction factor on the effective temperature and, therefore, on M_δ and T_w/T_δ is weaker and is of the opposite nature: elevation of the temperature is attended by lowering of the friction factor.

The use of formulas (13.6.12) and (13.6.13) is associated with the calculation of T^* and m^* for a dissociating gas in a boundary layer. Here one first finds the reference enthalpy i^*, and then uses it to evaluate T^* and m^* for the given pressure p_δ with the aid of tables or graphs of the thermodynamic functions. If dissociation is not taken into consideration, then T^* is determined directly by (13.5.32), while the ratio m^*/m_δ in (13.6.12) and (13.6.13) is taken equal to unity, i.e.

$$\delta_{\text{com}}/\delta_{\text{ic}} = (T^*/T_\delta)^{(n+1)/2} \tag{13.6.14}$$

$$(c_{x,\text{f}})_{\text{com}}/(c_{x,\text{f}})_{\text{ic}} = (c_{\text{f},x})_{\text{com}}/(c_{\text{f},x})_{\text{ic}} = (\tau_{\text{w}})_{\text{com}}/(\tau_{\text{w}})_{\text{ic}} = (T^*/T_\delta)^{(n-1)/2} \tag{13.6.15}$$

By comparing the values obtained respectively by formulas (13.6.12) and (13.6.14), and also by (13.6.13) and (13.6.15), we can see how dissociation affects the thickness of the boundary layer and the friction force. It follows directly from a comparison of relations (13.6.12) and (13.6.14), in which the ratios T^*/T_δ are assumed to be identical, that *dissociation leads to a decrease in the layer thickness* (because $m_\delta/m^* < 1$). Actually, however, the ratios T^*/T_δ are not the same, and the decrease in the thickness is still larger because the temperature T^* in a dissociating boundary layer (13.6.12) is lower than in an undissociated one (13.6.14).

The shear stress is greater in a dissociating gas because of lowering of the temperature, which has a stronger effect than a certain growth in the average molar mass [see (13.6.13)]. From the physical viewpoint, such a change in the shear stress is due to the fact that an increase in the dissociation and the related lowering of the temperature are attended by an increase in the density and a decrease in the viscosity. The influence of density on the friction force is opposite: this force grows when the density increases, and becomes smaller when it decreases. But the increase in the density is more intensive than the decrease in the viscosity, and, consequently, the friction force grows. It should be noted that the growth in the friction forces is somewhat greater owing to the formation of additional gas molecules upon dissociation (i.e. to an increase in the average molar mass) and to the increase in the viscosity.

The simple method of calculating a boundary layer according to the reference parameters is very efficient because it allows us to take account of the influence on the boundary layer thickness and the friction force of factors such as the compressibility, variation of the specific heats, dissociation, and heat transfer. The latter factor is taken into account in the dependence of the effective temperature T^* on the recovery temperature T_{r} and the temperature $T_{\text{w}} \neq T_{\text{r}}$ (when heat is supplied to or rejected from the wall).

Turbulent Boundary Layer

Following the procedure used for a laminar boundary layer, we shall employ reference parameters to obtain relations for the boundary layer thickness, stress, and friction factor for turbulent flow. We shall proceed from the relations for the parameters of a turbulent boundary layer in an incompressible fluid found with the aid of the power law of velocity distribution over the cross section of the boundary layer (the seventh root law).

The boundary layer thickness in an incompressible fluid is determined by formula (13.4.58), which we shall write as

$$\delta_{1c} = 0.37\,(\mu_\delta/V_\delta\rho_\delta)^{1/5}x^{4/5}$$

Replacing μ_δ and ρ_δ with their effective values μ^* and ρ^*, we obtain a relation for the boundary layer thickness in a compressible gas

$$\delta_{com} = 0.37\,(\mu^*/V_\delta\rho^*)^{1/5}x^{4/5} \tag{13.6.16}$$

The thickness ratio is

$$\delta_{com}/\delta_{1c} = (\mu^*/\mu_\delta)^{1/5}\,(\rho_\delta/\rho^*)^{1/5} \tag{13.6.17}$$

Let us see how we can find the shear stress in a turbulent compressible boundary layer. For this purpose, using (13.4.59), we shall write the expression for τ_w in a turbulent incompressible boundary layer as follows:

$$(\tau_w)_{1c} = 0.0299\rho_\delta V_\delta^2\,(\mu_\delta/V_\delta\rho_\delta)^{1/5}x^{-1/5}$$

By introducing the reference parameters, we find the corresponding relation for a compressible gas:

$$(\tau_w)_{com} = 0.0299\rho^* V_\delta^2\,(\mu^*/V_\delta\rho^*)^{1/5}x^{-1/5} \tag{13.6.18}$$

The ratio of the shear stresses is

$$(\tau_w)_{com}/(\tau_w)_{1c} = (\mu^*/\mu_\delta)^{1/5}\,(\rho^*/\rho_\delta)^{4/5} \tag{13.6.19}$$

The ratios of the local $c_{f,x}$ and average $c_{x,f}$ friction factors have the same values, namely,

$$(c_{x,f})_{com}/(c_{x,f})_{1c} = (c_{f,x})_{com}/(c_{f,x})_{1c} = (\tau_w)_{com}/(\tau_w)_{1c} = (\mu^*/\mu_\delta)^{1/5}(\rho^*/\rho_\delta)^{4/5} \tag{13.6.20}$$

where $(c_{f,x})_{1c}$ and $(c_{x,f})_{1c}$ are determined by formulas (13.4.60) and (13.4.62), respectively.

Considering the general case of a dissociating gas, we calculate the ratios ρ^*/ρ_δ and μ^*/μ_δ by (13.6.10) and (13.6.11), respectively. Hence,

$$\delta_{com}/\delta_{1c} = (T^*/T_\delta)^{(n+1)/5}(m_\delta/m^*)^{1/5} \tag{13.6.21}$$

$$(c_{x,f})_{com}/(c_{x,f})_{1c} = (c_{f,x})_{com}/(c_{f,x})_{1c} = (\tau_w)_{com}/(\tau_w)_{1c} = (T^*/T_\delta)^{(n-4)/5}(m^*/m_\delta)^{4/5} \tag{13.6.22}$$

A glance at these formulas reveals that the qualitative nature of the change in the boundary layer thickness and the friction force in turbulent flow is the same as in laminar flow, namely, with an increase in the reference temperature, the layer thickness grows, while the friction force lowers. But a quantitative estimate of such a change reveals that in accordance with (13.6.21), *the layer thickness with elevation of the reference temperature grows considerably more slowly and the friction factor drops more intensely* [see (13.6.22)] for a turbulent boundary layer than for a laminar one.

As in a laminar boundary layer, dissociation manifests itself in a certain decrease in the boundary layer thickness and a growth in the shear stress. The boundary layer thickness and friction factors with dissociation are determined by (13.6.21) and (13.6.22) by successive approximations. First we use the given wall temperature T_w and the undisturbed flow parameters M_δ, p_δ, ρ_δ, i_δ, and others to find the reference enthalpy i^* by formula (13.5.23), assuming in a first approximation that $r^*_{lam} = 0.84$ or $r^*_{trb} = 0.89$. Next we find T^*, taking i^* and p_δ with the aid of graphs or tables of the thermodynamic and kinetic functions of air. The same tables or graphs allow us to find $(c_p)^*$, μ^*, λ^* from the temperature T^* and pressure p_δ, to refine the number Pr^* by formula (13.5.28), and to find the recovery factor r^* by formula (13.5.26) or (13.5.27). We use this value of r^* to calculate in a second approximation the enthalpy i^*, and then determine the temperature T^* and the corresponding molar mass m^*. We insert their values into (13.6.21) and (13.6.22).

In the absence of dissociation, the ratio of the molar masses is $m^*/m_\delta = 1$. Hence

$$\delta_{com}/\delta_{ic} = (T^*/T_\delta)^{(n+1)/5} \tag{13.6.23}$$

$$(c_{x,f})_{com}/(c_{x,f})_{ic} = (c_{f,x})_{com}/(c_{f,x})_{i\cdot} = (\tau_w)_{com}/(\tau_w)_{ic} = (T^*/T_\delta)^{(n-4)/5} \tag{13.6.24}$$

Relation (13.6.24) can be written for constant specific heats in the approximate form

$$(c_{x,f})_{com}/(c_{x,f})_{ic} = (1 + 0.12M^2_\delta)^{-0.65} \tag{13.6.24'}$$

It is not difficult to obtain these formulas from (13.5.31), (13.5.33), and (13.6.24), assuming that $n = 0.75$, $\bar{k}^* = 1.4$, and $r^* = 0.85$. For the same values, we find an approximating relation determining the ratio of the boundary layer thicknesses (13.6.23), and also of the conditional thicknesses:

$$\delta_{com}/\delta_{ic} = \delta^*_{com}/\delta^*_{ic} = (1 + 0.12M^2_\delta)^{0.35} \tag{13.6.23'}$$

The values of δ_{ic} and δ^*_{ic} are found from (13.4.58) and (13.4.63), respectively. It is not difficult to obtain formula (13.6.23') from

(13.5.31), (13.5.33), and (13.6.23), assuming that $n = 0.75$, $\bar{k}^* = 1.4$, and $r^* = 0.85$.

The ratio of the conditional thicknesses $\delta^{**}_{com}/\delta^{**}_{inc}$ is determined by analogy with a laminar boundary layer, like the ratio of the corresponding friction factors with the use of (13.6.24).

Skin Friction on a Cone in Supersonic Flow

Laminar Boundary Layer. A supersonic flow about a sharp-nosed cone has the property that along the conical surface generatrix the velocity $V_\delta = V_c$ is constant, and, consequently, the longitudinal pressure gradient is zero. An "inviscid" flow about a flat plate along which the parameters on the boundary layer edge are constant has the same property. This flow similarity allows us to use the results of calculating the boundary layer for a flat plate in determining the relevant parameters of a viscous flow about a conical surface.

For this purpose, we shall use integral relation (13.2.16). Taking into account that the gas parameters at the edge of the boundary layer are identical everywhere on the cone ($V_\delta = V_c = \text{const}$, $p_\delta = p_c = \text{const}$, etc.) and, therefore, that the longitudinal pressure gradient is zero ($dp_\delta/dx = 0$), we can write this relation as

$$\frac{d}{dx}\int_0^\delta \rho r_0 V_x (V_x - V_c)\, dy = -r_0\tau_w \qquad (13.6.25)$$

where r_0 is the distance from the axis to a point on the cone surface with the coordinate x (Fig. 13.6.1), and τ_w is the shear stress at this point.

Let us use relation (13.6.25) to calculate a laminar boundary layer. At an arbitrary point of its cross section at a distance x from the point, we find the shear stress by the formula $\tau = \mu\, \partial V_x/\partial y$. In accordance with this formula, we can substitute $dy = (\mu/\tau)\, dV_x$ in Eq. (13.6.25). Dividing both sides of this equation by $\rho_c V_c^3 \mu_c$, where ρ_c and μ_c are the density ($\rho_c = \rho_\delta$) and dynamic viscosity ($\mu_c = \mu_\delta$), respectively, at the boundary layer edge of the cone, we obtain the integral relation

$$\frac{d}{dx}\int_0^1 \frac{\rho V_x}{\rho_c V_c}\cdot\frac{\mu}{\mu_c}\cdot\frac{r_0}{\tau}\left(1-\frac{V_x}{V_c}\right) d\left(\frac{V_x}{V_c}\right) = \frac{r_0\tau_w}{\rho_c V_c^3 \mu_c} \qquad (13.6.26)$$

For the case of a "gradientless" boundary layer being considered, the velocity ratio $V_x/V_c = f_1(y/\delta)$ is a function of only the relative coordinate y/δ and does not depend on x. Therefore, with a view to the formulas $\tau = \mu\, \partial V_x/\partial y$ and $\tau_w = \mu_c\, (dV_x/dy)_c$, the ratio of the shear stresses in the layer also depends on the same relative

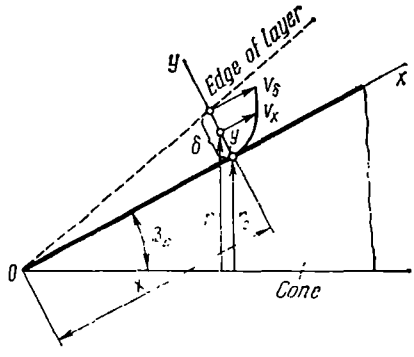

Fig. 13.6.1
Boundary layer on a cone

coordinate, i.e. $\tau/\tau_w = f_2(y/\delta)$. Let us insert the functions f_1 and f_2 into (13.6.26) and introduce the symbol

$$J = \int_0^1 \frac{\rho V_x}{\rho_c V_c} \cdot \frac{\mu}{\mu_c} \cdot \frac{1-f_1}{f_2}\, df_1 \tag{13.6.27}$$

Taking into consideration here that with a constant temperature over the entire surface of the cone the ratio μ/μ_c does not depend on the coordinate x and that the density ratio ρ/ρ_c, which is a function of V_x/V_c, also does not depend on this coordinate, we find the relation

$$J \frac{r_0}{\tau_w} \cdot \frac{d}{dx}\left(\frac{r_0}{\tau_w}\right) = \frac{r_0^2}{\rho_c V_c^3 \mu_c} \tag{13.6.28}$$

Substituting $x \sin \beta_c$ for r_0 on the right-hand side of the formula and separating variables, we obtain

$$\frac{J}{2} d\left(\frac{r_0}{\tau_w}\right)^2 = \frac{\sin^2 \beta_c}{\rho_c V_c^3 \mu_c} x^2\, dx \tag{13.6.29}$$

Integration yields

$$\frac{J}{2} \cdot \frac{r_0^2}{\tau_w^2} = \frac{1}{3} \cdot \frac{x^3 \sin^2 \beta_c}{\rho_c V_c^3 \mu_c} + \text{const} \tag{13.6.30}$$

Assuming at the initial point (at $x = 0$) that the ratio $r_0/\tau_w = 0$ and, therefore, that the constant on the right-hand side of (13.6.30) equals zero, and also performing the reverse substitution of r_0 for $x \sin \beta_c$ and designating the shear stress on the cone by $\tau_w = \tau_{w,c}$, we have

$$\tau_{w,c} = \sqrt{3}\left(\frac{J}{2} \cdot \frac{\rho_c V_c^3 \mu_c}{x}\right)^{1/2} \tag{13.6.31}$$

A similar expression can be obtained for the shear stress $\tau_w = \tau_{w,pl}$ on a flat plate. We shall proceed here from the assumption

that the plate is in a hypothetic supersonic flow with parameters that will be the same as on a cone. Now as a result of integrating Eq. (13.6.28), in which we shall take no account of r_0, we obtain the relation

$$\tau_{w,pl} = \left(\frac{J}{2} \cdot \frac{\rho_c V_c^3 \mu_c}{x}\right)^{1/2} \tag{13.6.32}$$

Formulas (13.6.31) and (13.6.32) yield an important relation:

$$\tau_{w,c} = \sqrt{3}\,\tau_{w,pl} \tag{13.6.33}$$

according to which *the shear stress on a cone is* $\sqrt{3}$ *times larger than the shear stress on a plate calculated from the parameters on a cone.* We use a formula similar to (13.6.33) to determine the local and average values of the friction factors:

$$c_{f,x,c} = \sqrt{3}\,c_{f,x,pl} \tag{13.6.34}$$

$$c_{x,f,c} = (2/\sqrt{3})\,c_{x,f,pl} \tag{13.6.35}$$

These values are related to the velocity head of the disturbed flow $q_c = \rho_c V_c^2/2$. The following relations have to be used to calculate the friction factors according to the velocity head of an undisturbed flow:

$$c_{f,x,\infty,c} = c_{f,x,c} q_c/q_\infty = \sqrt{3}\,c_{f,x,pl}\,(\rho_c V_c^2/\rho_\infty V_\infty^2) \tag{13.6.36}$$

$$c_{x,f,\infty,c} = c_{x,f,c} q_c/q_\infty = 2/\sqrt{3}\,[c_{x,f,pl}\,(\rho_c V_c^2/\rho_\infty V_\infty^2)] \tag{13.6.37}$$

We calculate the friction drag according to the average friction factor $c_{x,f,\infty,c}$ and the side surface area S_c of the cone:

$$X_f = c_{x,f,\infty,c} q_c S_c = 2/\sqrt{3}\,[c_{f,x,pl}\,(\rho_c V_c^2/2)\,S_c] \tag{13.6.38}$$

We find the shear stress $\tau_{w,pl} = (\tau_w)_{com}$ and the friction factors $c_{x,f,pl} = (c_{x,f})_{com}$ and $c_{f,x,pl} = (c_{f,x})_{com}$ from relation (13.6.13) according to the reference parameters in the general case for dissociating air.

We can also establish an approximate relation between the thicknesses of the boundary layer on a cone and plate. For this purpose, we shall use the Paulhausen method to calculate the velocity distribution over a cross section of the boundary layer in an incompressible fluid. By this method, we calculate the velocity using Eq. (13.3.15). Substitution of y for η, δ for η_δ, and V_c for V_δ yields

$$V_x = V_c\left(\frac{3}{2} \cdot \frac{y}{\delta} - \frac{1}{2} \cdot \frac{y^2}{\delta^2}\right) \tag{13.6.39}$$

By Newton's formula, the shear stress on the surface of a cone is

$$\tau_{w,c} = \mu_c V_c \left[\frac{\partial}{\partial y}\left(\frac{3}{2} \cdot \frac{y}{\delta} - \frac{1}{2} \cdot \frac{y^2}{\delta^2}\right)\right]_{y=0} = \mu_c V_c \frac{3}{2\delta_c} \tag{13.6.40}$$

where δ_c is the thickness of the boundary layer on a cone.

We can compile a similar expression for a plate:

$$\tau_{w,pl} = \mu_c V_c (3/2\delta_{pl}) \tag{13.6.41}$$

where δ_{pl} is the thickness of the boundary layer on a plate.

It follows from (13.6.40) and (13.6.41) that

$$\delta_{pl}/\delta_c = \tau_{w,c}/\tau_{w,pl} \tag{13.6.42}$$

whence, by (13.6.33)

$$\delta_c = (\tau_{w,pl}/\tau_{w,c})\,\delta_{pl} = \delta_{pl}/\sqrt{3} \tag{13.6.43}$$

Hence, in accordance with formula (13.6.43), *the thickness of a laminar boundary layer on a cone is* $1/\sqrt{3}$ *of that on a plate.* The thickness $\delta_{pl} = \delta_{com}$ for a plate can be calculated in the general case of a dissociating gas according to the reference parameters for a conical surface with the use of formula (13.6.12).

Turbulent Boundary Layer. By using integral relation (13.2.16), we obtain similar approximate relations for a turbulent boundary layer. Let us go over in (13.6.25) to reference parameters and introduce instead of τ_w expression (13.4.55), in which we use the notation $V_\delta = V_c$ and $\delta = \delta_c$:

$$\frac{d}{dx}\int_0^\delta \rho^* r_0 V_x (V_c - V_x)\,dy = 0.0233\rho^* V_c^2 \left(\frac{\mu^*}{V_c\rho^*}\right)^{1/4} \frac{r_0}{(\delta^*)^{1/4}}$$

Taking into consideration that the temperature of the surface is the same everywhere and, therefore, the reference parameters are constant (the density ρ^* on the left-hand and right-hand sides cancels out), we obtain the following equation after simple transformations:

$$\frac{d}{dx}\left[r_0\delta_c \int_0^1 \frac{V_x}{V_c}\left(1 - \frac{V_x}{V_c}\right) d\left(\frac{y}{\delta_c}\right)\right]$$

$$= 0.0233 \left(\frac{\mu^*}{V_c\rho^*}\right)^{1/4} \frac{r_0^{5/4}}{(r_0\delta_c)^{1/4}} \tag{13.6.44}$$

If we proceed from the seventh root power law, the dimensionless velocity $V_x/V_c = (y/\delta_c)^{1/7}$, therefore

$$J_1 = \int_0^1 \frac{V_x}{V_c}\left(1 - \frac{V_x}{V_c}\right) d\left(\frac{y}{\delta_c}\right) = \text{const}$$

Accordingly, we shall write (13.6.44) as

$$J_1 (r_0\delta_c)^{1/4} d(r_0\delta_c) = 0.0233\ (\mu^*/V_c\rho^*)^{1/4} r_0^{5/4}\,dx \tag{13.6.45}$$

Substituting $x \sin \beta_c$ for r_0 on the right-hand side and integrating provided that for $x = 0$ the quantity $r_0\delta_c = 0$, we obtain

$$(4J_1/5)\,(r_0\delta_c)^{5/4} = 0.0233\,(\mu^*/V_c\rho^*)^{1/4} \sin^{5/4}\beta_c\,(4x^{9/4}/9)$$

Performing the reverse substitution here $(x \sin \beta_c)^{5/4} = r_0^{5/4}$ and cancelling this quantity on both sides, we have

$$\delta_c^{5/4} = (4/9)\,J_2 x$$

whence

$$\delta_c = (4/9)^{4/5}\,(J_2 x)^{4/5} \tag{13.6.46}$$

where

$$J_2 = (0.0292/J_1)\,(\mu^*/V_c\rho^*)^{1/4} \tag{13.6.47}$$

Introducing δ_{pl} instead of δ_c in (13.6.45) and excluding r_0, we obtain a similar expression for the thickness of the boundary layer on a flat plate. Integration yields

$$(4J_1/5)\,(\delta_{pl})^{5/4} = 0.0233\,(\mu^*/V_c\rho^*)^{1/4} x$$

whence

$$\delta_{pl} = (J_2 x)^{4/5} \tag{13.6.48}$$

From expressions (13.6.46) and (13.6.48), we find the relation between the thicknesses of the boundary layer on a cone and plate:

$$\delta_c = (4/9)^{4/5}\delta_{pl} = 0.523\delta_{pl} \tag{13.6.49}$$

We establish the relation for the shear stress from (13.4.55) by introducing the reference parameters and writing this expression separately for a cone and plate:

$$\tau_{w,c} = 0.0233\rho^* V_c^2\,(\nu^*/V_c)^{1/4}\,(1/\delta_c^{1/4})$$

$$\tau_{w,pl} = 0.0233\rho^* V_c^2\,(\nu^*/V_c)^{1/4}\,(1/\delta_{pl}^{1/4})$$

Assuming that the reference parameters are the same on a cone and a plate, we find the following relation from the last two formulas

$$\tau_{w,c}/\tau_{w,pl} = (\delta_{pl}/\delta_c)^{1/4} \tag{13.6.50}$$

Let us introduce into (13.6.50) the value of δ_c from (13.6.49):

$$\tau_{w,c} = (9/4)^{1/5}\tau_{w,pl} = 1.176\tau_{w,pl} \tag{13.6.51}$$

Comparing formulas (13.6.33) and (13.6.51), we can conclude that *the difference between the shear stresses on a cone and those on a plate is smaller for a turbulent boundary layer than for a laminar boundary layer*. The explanation is that the friction force in a turbulent boundary layer is affected more by flow mixing than by the action of the surface shape. The values of the layer thicknesses [see (13.6.43) and (13.6.49)] on a cone for a turbulent and laminar boundary layers differ by about 10%. Such a small difference points

to the stronger influence of the shape of surfaces in a flow on the boundary layer thickness than of mixing.

The known shear stress can be used to determine the local and average friction factor:

$$c_{f,x,c} = 1.176 c_{f,x,pl} \tag{13.6.52}$$

$$c_{x,f,c} = 1.045 c_{x,f,pl} \tag{13.6.53}$$

These factors were calculated from the velocity head $q_c = \rho_c V_c^2/2$. To convert them to the velocity head of the undisturbed flow, formulas similar to (13.6.36) and (13.6.37) should be used.

We determine the friction drag in a turbulent boundary layer by an expression similar to (13.6.38):

$$X_f = 1.045 c_{x\,f,pl} (\rho_c V_c^2/2) S_c \tag{13.6.54}$$

The shear stress $\tau_{w,pl} = (\tau_w)_{com}$, and the friction factors $c_{x,f,pl} = (c_{x,f})_{com}$ and $c_{f,x,pl} = (c_{f,x})_{com}$ for a flat plate can be found from relation (13.6.22), and the boundary layer thickness $\delta_{pl} = \delta_{com}$, from (13.6.17) according to the reference parameters with a view to dissociation.

13.7. Influence of the Longitudinal Pressure Gradient on Friction

Boundary Layer on a Curved Surface

A supersonic boundary layer on a flat plate and a conical surface is characterized by the same pressure in all its cross sections ($p_\delta = \text{const}$). Hence, the longitudinal pressure gradient $dp_\delta/dx = 0$. But for a flow over a curved surface (for example, an airfoil or a body of revolution with a curved generatrix) this gradient is other than zero because the pressure at the edge of the boundary layer is a variable quantity depending on the coordinate x. As can be seen from integral relation (13.2.16), where $dp_\delta/dx \neq 0$, this causes a change in the shear stress and, consequently, in the distribution of the velocity and in the boundary layer thickness in comparison with flow over a flat plate or a cone.

If we consider an airfoil with a curved contour in a subsonic flow (Fig. 13.7.1*a*), then on its front part (from stagnation point 0 to point B) the pressure gradient will be negative ($dp_\delta/dx < 0$), while from point B to point C on the trailing edge it will be positive ($dp_\delta/dx > 0$). Such a nature of the change in the pressure gradient is due to the features of the flow over the airfoil. On the front part, the velocity in a direction from point 0 to point B increases, and, consequently, the pressure according to the Bernoulli equation

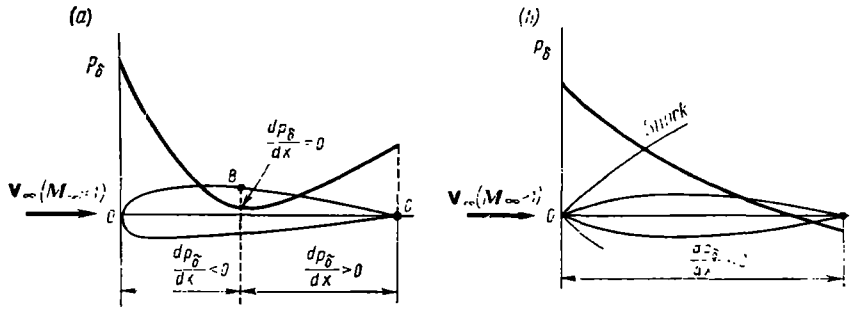

Fig. 13.7.1
Airfoil pressure distribution:
a—subsonic flow; *b*—supersonic flow

lowers; on the part adjoining the trailing edge, the velocity, conversely, decreases, and the pressure grows.

With supersonic flow (Fig. 13.7.1*b*), the velocity V_δ in a direction toward the trailing edge of the airfoil continuously grows, therefore the pressure p_δ and the derivative dp_δ/dx diminish, i.e. the flow in the boundary layer over the entire surface experiences the effect of a negative pressure gradient.

Let us use integral relation (13.2.16) for a qualitative appraisal of the change in the shear stresses with the above distribution of the longitudinal pressure gradient. If the derivative $dp_\delta/dx < 0$, the first term on the left-hand side is positive, while when $dp_\delta/dx > 0$, it is negative. This signifies that when the other conditions are equal, *the shear stresses in the zone of a negative pressure gradient where the flow is accelerated are larger than in uniform flow.* Conversely, on the part of the surface where the pressure grows and the flow is retarded, the shear stress diminishes. On this part, we can indicate a point on the surface where the shear stress is zero, and behind this point it becomes negative.

Such a nature of the change in the shear stress is closely associated with the distribution of the velocity V_x over the boundary layer cross section. If we consider a laminar boundary layer for which $\tau_w = \mu_w (\partial V_x/\partial y)_w$, in the zone with a negative pressure gradient, where $\tau_w > 0$, the derivative $(\partial V_x/\partial y)_w > 0$. The corresponding velocity distribution is shown in Fig. 13.7.2*a*, where the velocity V_x near the wall coincides in direction with the free-stream velocity V_δ.

At the point of the airfoil where $\tau_w = 0$ and, consequently, $(\partial V_x/\partial y)_w = 0$, a tangent to the curve of velocity distribution in the boundary layer (Fig. 13.7.2*b*) coincides with a normal to the wall. After this point, the stress τ_w is negative, and the derivative $(\partial V_x/\partial y)_w < 0$. Such a nature of the flow in the boundary layer, as

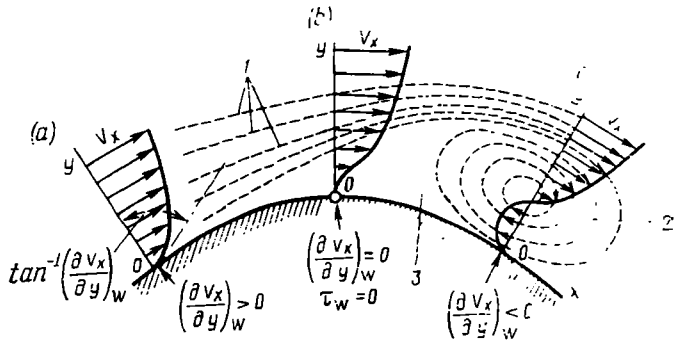

Fig. 13.7.2
Change in the velocity profile over a boundary layer cross section and the formation of a vortex in its separation zone:
1—streamline; *2*—vortex; *3*—separation zone

is shown in Fig. 13.7.2*c*, is due to the fact that the velocities of the particles near the wall are directed oppositely to the free stream.

The shear stress should not be determined in this zone because its influence on the flow is small in comparison with the normal stress (pressure). This stress may be taken equal to zero. The shear stresses on the parts of a curved surface with non-separated flow can be investigated with the use of the boundary layer integral relation together with relations establishing the velocity distribution over a layer cross section and the law of the change in the shear stresses.

Calculation of Laminar Boundary Layer

Let us consider a method of calculating a laminar boundary layer on a curved surface of an airfoil in a compressible gas flow (see [21]).

According to this method, the local friction factor is

$$c_{f,x} = \frac{2\tau_w}{\rho_\delta V_\delta^2} = \frac{2}{V_\delta}\sqrt{\frac{\mu_\delta V_\delta'}{\rho_\delta}}\,(1-\bar{V}_\delta^2)^{-\frac{1}{2}\left(n+\frac{1}{k-1}\right)}\left(2+\frac{\lambda}{6}\right)\frac{1}{\sqrt{\bar{\lambda}}} \qquad (13.7.1)$$

and the boundary layer thickness is

$$\delta = (1-\bar{V}_\delta^2)^{-k/(k-1)}\,\eta_\delta\,[1-\bar{V}_\delta^2\Phi(\lambda)] \qquad (13.7.2)$$

where the function

$$\Phi(\lambda) = 367/630 + (71/7560)\,\lambda + (1{\cdot}9072)\,\lambda^2 \qquad (13.7.3)$$

The reduced layer thickness is

$$\eta_\delta = \sqrt{\lambda \nu_0 V'_\delta / (1 - \overline{V}_\delta^2)} \qquad (13.7.4)$$

where the derivative $V'_\delta = dV_\delta/d\xi$, and $\overline{V}_\delta = V_\delta/V_{max}$.

A significant element of the calculations is the determination of the parameter

$$\lambda = \eta_\delta^2 V'_\delta [\nu_0 (1 - \overline{V}_\delta^2)]^{-1} \qquad (13.7.5)$$

taking account of the influence of a curved surface on viscous flow that is observed with a longitudinal velocity gradient ($V'_\delta \neq 0$). This parameter is found by solving the differential equation

$$d\lambda/d\overline{\xi} = M_1(\lambda) N_1(\overline{\xi}) + M_2(\lambda) N_2(\overline{\xi}) \qquad (13.7.6)$$

in which

$$M_1(\lambda) = \frac{\lambda(213 - 1.92\lambda - 0.2\lambda^2)}{213 - 5.76\lambda - \lambda^2}; \qquad M_2(\lambda) = \frac{7258 - 1336\lambda + 37.92\lambda^2 + 0.8\lambda^3}{213 - 5.76\lambda - \lambda^2} \qquad (13.7.7)$$

$$N_1(\overline{\xi}) = \frac{4\overline{V}_\delta \overline{V}'_\delta}{1 - \overline{V}_\delta^2} + \frac{\overline{V}''_\delta}{\overline{V}'_\delta}; \qquad N_2(\overline{\xi}) = \frac{\overline{V}_\delta \overline{V}'_\delta}{1 - \overline{V}_\delta^2} + \frac{\overline{V}'_\delta}{\overline{V}_\delta} \qquad (13.7.8)$$

In these expressions, we have introduced symbols for the relative coordinate $\overline{\xi} = \xi/L$ and also for the first and second derivatives of the velocity in the form of $\overline{V}'_\delta = d\overline{V}_\delta/d\xi$ and $\overline{V}''_\delta = d^2\overline{V}_\delta/d\overline{\xi}^2$.

A boundary layer on a curved wall is computed as follows. First we find the theoretical or experimental velocity distribution at the edge of the boundary layer $V_\delta(x)$, and then calculate the derivatives V'_δ, V''_δ, and the corresponding functions N_1 and N_2 [see (13.7.8)]. Next we determine the quantity λ by numerical integration of Eq. (13.7.6). This quantity must satisfy the boundary condition according to which at the branching point of the flow that coincides with the stagnation point, i.e. at $\xi = 0$ ($x = 0$), the function λ equals a finite value λ_0. According to A. Dorodnitsyn, $\lambda_0 = 7.052$.

We shall apply the considered calculation procedure to both subsonic and supersonic flow over airfoils with a blunted leading edge. For a supersonic flow, we must replace the stagnation pressure and density p_0 and ρ_0 in formulas (13.3.4) and (13.3.6) with the corresponding values p'_0 and ρ'_0 calculated for conditions of flow behind the straight part of a curved shock wave detached from the airfoil.

For supersonic flow over a sharp-nosed airfoil, we calculate the values of p'_0 and ρ'_0 for the number $M_\infty > 1$ and the shock angle θ_s at the leading edge. We determine the initial value $\lambda = \lambda_0$ (at $\xi = 0$)

from the condition that at the sharp edge of an airfoil, like on a plate, the thickness of the boundary layer is zero. According to this value, λ_0 also equals zero.

The corresponding values for the parameters of a boundary layer in an incompressible fluid can be found by assuming in the obtained relations that $1 - \overline{V}_\delta^2 = 1 - V_\delta^2/V_{\max}^2 = 1$ [this follows from the formula $1 - \overline{V}_\delta^2 = \{1 + [(k-1)/2]\, M_\delta^2\}^{-1}$, in which one must assume that for an incompressible fluid the Mach number $M_\delta = 0$].

By (13.7.1), the friction factor is

$$c_{f,x} = \frac{2\tau_w}{\rho_\delta V_\delta^2} = \frac{2}{V_\delta} \sqrt{\frac{\mu_\delta V_\delta'}{\rho_\delta}} \left(2 + \frac{\lambda}{6}\right) \frac{1}{\sqrt{\lambda}} \qquad (13.7.9)$$

The thickness of the boundary layer by formula (13.7.2), in which $\overline{V}_\delta = 0$, equals the value $\delta = \eta_\delta$. We find this value from (13.7.5) in the form

$$\delta = \sqrt{\lambda \mu_\delta / (\rho_\delta V_\delta')} \qquad (13.7.10)$$

The quantity λ in formulas (13.7.9) and (13.7.10) is determined by solving differential equation (13.7.6) in which instead of (13.7.8) one should assume that

$$N_1(\bar{\xi}) = V_\delta''/V_\delta', \quad N_2(\bar{\xi}) = V_\delta'/V_\delta \qquad (13.7.11)$$

The **method of reference parameters** can be used for airfoils with a small curvature of their contours. The characteristics of an incompressible boundary layer are converted by this method to the relevant values with account of compressibility and high temperatures.

As a particular case, the above relations for the boundary layer on a curved surface can yield the corresponding relations for a flat plate in either a compressible or an incompressible flow if we assume in these relations that the longitudinal velocity gradient is zero.

Influence of Boundary Layer Separation on the Aerodynamic Characteristics

Separation of the boundary layer is a typical phenomenon attending flow. In separation, the pressure on the surface of a craft is redistributed, which leads to a change in the aerodynamic drag and lift force. In the range of transonic velocities, separation hinders controllability because the non-stationary aerodynamic loads grow. At high supersonic velocities, it leads to large heat fluxes on individual parts of a surface in the flow.

At the same time, separation of the flow may be useful when employing some kinds of craft or their elements. For example, a thin airfoil suitable for high-speed flight can be adapted for low velocities by artificially causing separation at a certain place on its upper

side and ensuring subsequent attachment. As a result, we obtain the effect of a thickened airfoil that is better for low-speed flight.

Owing to flow separation, various aerodynamic characteristics of spacecraft descending to the Earth can be improved. Some parts of such craft are in conditions of high temperatures. By using separation, one can sometimes reduce the heating and thereby ensure allowable conditions of heat transfer.

Flow separation is the subject of intensive aerodynamic investigations. The classical concept of such separation is associated with viscosity, therefore it is often considered as a problem of boundary layer separation.

An essential condition for flow separation is a positive pressure gradient. No separation occurs if such a gradient is absent. For example, a flow does not separate from a flat plate characterized by a constant pressure in all the cross sections of the boundary layer and, consequently, by the equality to zero of the longitudinal pressure gradient. *In a flow over a smooth curved surface* (for example, a wing airfoil or a body of revolution with a curved generatrix), however, this gradient is other than zero. This results in a change in the local shear stress, boundary layer thickness, and in the velocity distribution over its cross section in comparison with flow over a flat plate.

We have already indicated (Fig. 13.7.2) that in the tail part of a body the velocities of the particles near the wall are directed oppositely to the free stream. This phenomenon is explained by the action of viscosity leading to a decrease in the kinetic energy of the fluid particles. In the tail part of the airfoil, the store of this energy may be insufficient for overcoming the positive pressure gradient. Consequently, the fluid near the surface first experiences stagnation, and then changes the direction of its flow. The formation of this counterflow results in forcing away of the streamlines and, therefore, in separation of the boundary layer from the surface. The value of $\tau_w = 0$ corresponds to the separation point.

Separation of the boundary layer from a surface leads to a substantial change in the nature of the flow and appreciably affects the aerodynamic characteristics of craft.

A boundary layer after a separation point is characterized by the presence of two opposite flows, namely, an external one in the direction of the free flow, and an internal one in the opposite direction. The boundary layer, as it were, rolls up, forming a vortex (Fig. 13.7.2). The formation and carrying off of vortices are attended by the accumulation of the stagnated fluid and the formation of a stagnation zone.

Owing to the vortices, the velocity of the particles is higher in the afterbody in this zone than in flow without separation, while the pressure is lower (Fig. 13.7.3). Therefore, *an additional drag*

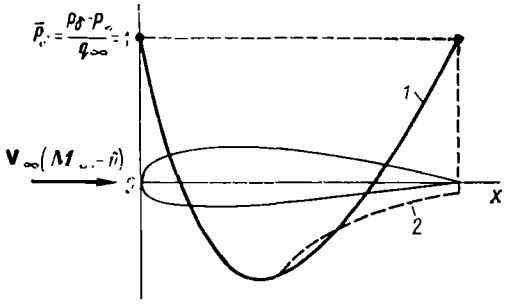

Fig. 13.7.3
Airfoil pressure distribution in an incompressible flow ($M_\infty = 0$):
1—without separation; *2*—with separation

due to pressure redistribution develops. It is called the **suction** or **vortex drag.** The increase in the drag can be explained by the fact that an additional part of the kinetic energy of the flow over the body is spent on the formation of vortices and separation of the flow.

The position of the separation point and, consequently, the size of the region determining the magnitude of the additional drag depend on the pressure gradient. For surfaces in the form of airfoils or elongated bodies of revolution with a small curvature and at small angles of attack, the positive pressure gradient is not large, separation does not virtually occur, and the vortex drag is negligibly small. With an increase in the angle of attack and in the surface curvature, the pressure gradient dp_δ/dx grows, and separation occurs. The larger the derivative dp_δ/dx, the closer is the separation point to the vertex of the surface in the flow.

All these phenomena are observed both with laminar and with turbulent boundary layers. For turbulent flow, however, we can note some features of the separating flow. A section of such a turbulent flow forms, as is known, when the Reynolds number becomes larger than its critical value. The velocities are distributed more uniformly over the cross section of a turbulent boundary layer, hence the particles near the surface have a higher velocity and, consequently, an increased kinetic energy. This is why they resist more strongly the retarding action of the pressure increasing along the flow, thus facilitating a less intense lowering of the shear stress, and move farther than in a laminar layer along the surface to the separation point, where $\tau_w = 0$.

Hence, a transition through the critical Reynolds number is attended by a *downstream displacement of the separation point.* As a result, the width and strength of the vortex region behind the body diminish, and the drag due to the pressure (the vortex drag)

sharply drops. Notwithstanding a certain increase in the drag due to turbulent friction, the total drag is lower than in a laminar boundary layer. This phenomenon of drag reduction in **bluff bodies** (bodies, the flow over which is attended by intensive separation, while their drag is mainly due to pressure forces and to a lesser extent to friction) upon the development of a turbulent boundary layer occurs in the critical region of the Reynolds numbers. Upon a further (supercritical) increase in the Reynolds numbers, the drag grows somewhat because the separation point is displaced upstream.

We must note that the indicated effect is observed only for bluff bodies such as, particularly, a cylinder and a sphere. For **streamlined bodies**, for example, wing airfoils, and aircraft fuselages, narrowing of the separation zone in the afterbody and a certain reduction in the pressure drag are overbalanced by an increase in the friction drag because of the formation of a turbulent boundary layer in this part of the body.

Let us see how compressibility affects the position of the separation point and the drag. It was found that for a flat plate the boundary layer thickness increases and the shear stress diminishes with an increase in the Mach number. This also holds for curved surfaces [see (13.7.1) and (13.7.2)]. It thus follows that *with an increase in the number* M_∞ *the separation point is displaced counter to the flow*, i.e. toward the nose of the body in the flow. As a result, the separation zone broadens, while the pressure drag and total drag increase.

It follows that the calculation of a flow and the determination of the aerodynamic drag are associated with finding the separation point of the boundary layer from the surface. An approximate value of the coordinate of a laminar boundary layer separation point in a subsonic flow can be determined using **Dorodnitsyn's method** described above. For this purpose, Eq. (13.7.1) should be used. Assuming that $c_{f,x} = 0$ in it, we find the value of the parameter $\lambda = -12$, according to which we find the position of the separation point for the given body shape by solving Eq. (13.7.5).

Dorodnitsyn's method, and also the other methods described above, are based on the solution of differential equations for a boundary layer at whose lower edge the fluid parameters are determined from the equations of an inviscid flow over the given surface without separation. In other words, these methods take no account of how the separated boundary layer affects the free flow. The data on separation obtained by these methods are satisfactory for streamlined bodies in which the free stream separated together with the boundary layer moves away from the surface insignificantly and therefore differs only slightly from an inviscid flow without separation. But with sufficiently intensive separation in bluff bodies when the external flow moves away from the wall considerably, this difference is

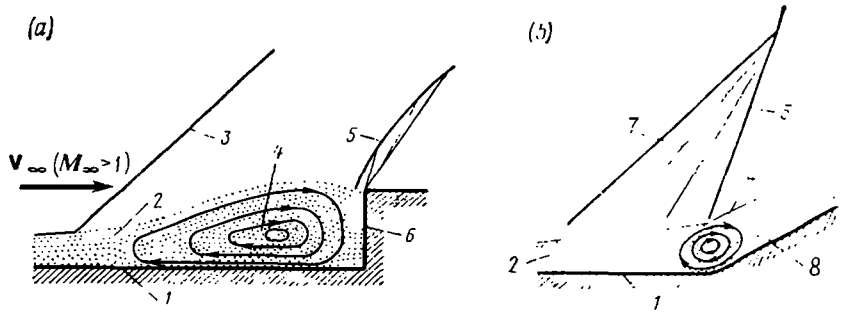

Fig. 13.7.4
Models of separated flows:
a—separation due to a step; *b*—separation due to a wedge; *1*—plate; *2*—boundary layer; *3*—main shock; *4*—zone of separation and inverse flow; *5*—shock; *6*—step; *7*—compression waves; *8*—inclined plane (wedge)

quite significant, and such a flow has a large influence on the boundary layer and the place of its separation.

The separation of the boundary layer caused by the positive pressure gradient that forms in the tail part of a curved surface and is not associated with protrusions or roughness can be observed in both a compressible and incompressible flows. In a compressible flow, specific processes may occur that give rise to the same separation effect that we have considered. We know that in a compressible flow at numbers M_∞ larger than the critical ones, local shocks are formed in the disturbed flow. The increased pressure behind such shocks propagates not only downstream, but also upstream through the subsonic part of the boundary layer adjoining the wall. In addition, thickening of the boundary layer ahead of a shock leads to forcing of the streamlines away from the surface of the body in the supersonic part of the boundary layer and in the external flow. This leads to the fact that a supersonic flow over this part experiences additional turning, which causes the formation of an oblique shock (a λ-shaped shock).

The *action of a shock on the boundary layer* causes the pressure to grow, which results in separation of the layer. The increase in the drag at above-critical Mach numbers is due not only to the losses in the local shocks, but also to separation of the boundary layer caused by the shocks. The separation effect increases at supersonic flow velocities if the boundary layer experiences a shock. Such a shock produces a considerable increase in the pressure in the boundary layer, as a result of which the layer becomes thicker and then detaches.

The separation of a flow with the formation of a shock may occur if a plate has discontinuities. Figure 13.7.4 shows schematically such separation caused by a step and an inclined plane. The shock

is due to the deflection of the flow near the place of separation through a certain angle because of the formation of a stagnation zone ahead of the step or inclined plane. The additional pressure gradient developing at the wall facilitates the forward displacement of the separation point.

Investigations show that all these phenomena occur the most intensely when in laminar flow. Turbulence weakens the interaction between the shocks and the boundary layer because thickening of the layer, and also the role of the pressure gradient in its formation, are much less noticeable in a turbulent flow than in a laminar one. Owing to the smaller forcing away of the streamlines in a turbulent flow, as shown by experiments, no additional oblique shock is formed ahead of a normal shock. The separation of a three-dimensional flow also occurs without a reverse flow, and in shear flows. It occurs at the point where the three-dimensional streamlines tangent to the wall meet.

Boundary Layer Control (BLC)

The favoured ways of flow control include boundary-layer bleed and blowing. This prevents flow separation that may occur when the angle of attack of a lifting or stabilizing surface grows to above-critical values. As a result, the lift force grows. This is attended by an increase in the critical angles of attack and in the maximum values of the lift coefficients.

The physical effect produced by bleed and blowing is the same and consists in an increase in the kinetic energy of the particles in the boundary layer, owing to which their stagnation diminishes. In bleed, this effect is mainly achieved because of an increase in the velocity, and in blowing, because of the increase in the mass of the air flowing through the boundary layer.

Bleed is performed by vacuum pumps, and blowing, by pressure pumps through a profiled slot, a system of openings, or permeable surfaces (**discrete** and **distributed bleed** or **blowing**, respectively).

The location of the openings or slots when bleed is used coincides with the assumed location of separation, while with blowing, the slots or openings are upstream.

Boundary-layer bleed and blowing can be used to reduce the aerodynamic drag. For this purpose, the slots or openings should be located in the tail part of the body where prevention of separation is achieved that lowers the suction effect behind the tail and, consequently, reduces the pressure drag.

Experimental investigations show that boundary-layer blowing is the best for improving the aerodynamic characteristics of a wing (increasing $c_{y_a, \max}$). Blowing is usually performed at the leading

edge of the wing, and also near controls (ailerons, elevons, flaps, etc.).

Bleed is an important means for stabilizing a laminar boundary layer (laminarization) that *lowers the friction drag, and also heat transfer.* From a physical viewpoint, the stabilization effect is explained by the fact that bleed eliminates the sources of fluctuation characteristic of a turbulent boundary layer, and thus ensures a higher stability of a laminar boundary layer.

One must remember that bleed may never be used for stabilizing a laminar boundary layer. Moreover, it leads to the opposite effect, i.e. to the diminishing of its stability because it promotes the development of the velocity pulsations forming in the boundary layer.

The slots or openings through which bleed is performed must be located at the point of loss of stability, the distance to which from the leading edge can be calculated according to the value of the critical Reynolds number. One must bear in mind that laminarization presumes the elimination of the disturbing factors (roughness, local separations of the boundary layer, wall vibrations) that help to retain a turbulent flow.

Measurements show that the friction drag is lower on a cooled surface than on a hot wall. This indicates that upon cooling, the transition of a laminar boundary layer to a turbulent one occurs at a greater distance from the leading edge of the wall.

Hence, cooling increases the stability of the boundary layer.

The physical effect of *stabilization of the boundary layer by cooling* is explained by the action of the lowered temperatures on the viscosity and density of the gas flowing over the body. When a gas is cooled, its dynamic viscosity diminishes and density grows. This eliminates the causes of the instability of a laminar boundary layer in a gas, and as a result it withstands the action of disturbances causing turbulent fluctuations more successfully.

The removal of heat, due to which the temperature at the edge of the layer becomes lower than at the wall, is performed by a variety of technical means depending on the design of the craft and its application.

The aerodynamic efficiency of a craft and characteristics of its stability and controllability are improved by the use of *auxiliary surfaces* on individual elements. They include **aerodynamic fences** that are small steps on the upper surface of the wing parallel to the longitudinal axis of the craft. Their purpose is to prevent the flow of the boundary layer along the wing span and reduce the separation of the flow from its tips. This purpose is served by **wing-tip plates** installed, as their name implies, at these tips. Like fences, they improve the slip, and it manifests itself in the smaller action of the tip vortices on the wing. The result is lowering of the induced drag and an increase in the aerodynamic efficiency.

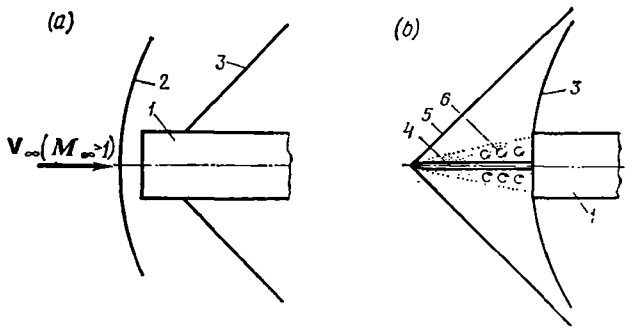

Fig. 13.7.5
Shock ahead of a blunt body:
a—curved detached shock; *b*—attached shock ahead of a centerbody; *1*—wedge or cylinder; *2*—nose shock; *3*—shock; *4*—centerbody; *5*—main attached shock; *6*—separation zone

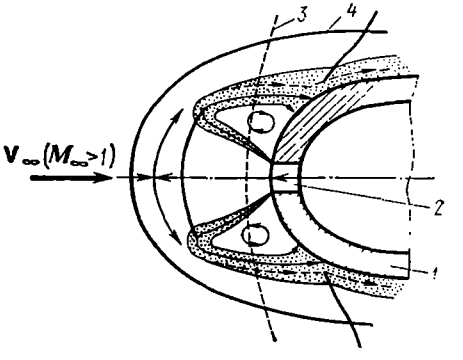

Fig. 13.7.6
Flow over a blunt body with gas injection:
1—body; *2*—orifice for injection; *3*—position of shock without injection; *4*—shock with injection

The drag and heat transfer at high supersonic velocities are lowered by a centerbody ahead of a blunt body.

Let us consider this phenomenon. A detached, almost normal shock ahead of a blunt body (Fig. 13.7.5*a*) can change its shape if we install a centerbody ahead of the body (Fig. 13.7.5*b*). The flow can separate at the centerbody and form a wedge-shaped or cone-shaped flow region depending on whether the body is flat or cylindrical. Such a separating flow causes the shape of the nose shock to change from an almost normal to an oblique one, and this leads to a reduction in the drag and heat transfer at the stagnation point of the blunt surface. But high local heat fluxes may arise in the region between the shock and the end piece, which lowers the effectiveness of the centerbody somewhat.

Experimental investigations reveal that an effect similar to the use of a centerbody can be achieved by a gas jet blown out through a small orifice on the nose wall toward the oncoming flow, or by

using a system of minute orifices (a porous wall) through which the gas is injected into the flow. In both cases, the introduction of an additional mass of gas causes the flow to separate from the blunt body and form, as it were, a new immersed body (pseudobody) with a smaller blunting and a larger length. As a result, the nose shock, while retaining its curved shape, moves away from the nose and reduces its strength. This leads to a more favourable redistribution of the pressures and velocities on the blunt nose and, therefore, to lowering of the drag and heat transfer. Such a flow model is shown in Fig. 13.7.6, which depicts a blunt wall with one orifice.

13.8. Mixed Boundary Layer. Critical Reynolds Number

To calculate a boundary layer, we have to analyse its nature on a surface in a flow. Observations show that the nature of a boundary layer depends appreciably on the flow conditions determined by the Reynolds number. Consider a surface in the form of a flat plate (Fig. 13.8.1). On its front part at comparatively low Reynolds numbers $Re = V_\delta x \rho_\delta / \mu_\delta$ a laminar boundary layer forms. Next comes a zone of transition of the laminar layer into a turbulent one, followed on the tail parts by a fully developed turbulent flow which large numbers Re correspond to. Such a boundary layer on a surface in a flow is called **mixed** (or **laminar-turbulent**).

It should be noted that both a laminar and turbulent boundary layers are possible at any Reynolds numbers. Actually, a flow that is stable in the given conditions sets in in the boundary layer. At small numbers Re, the laminar flow is stable. At large numbers, a laminar boundary layer is not stable. By using artificial procedures, for example by ensuring the even supply of a fluid to a smooth plate, one can also create a laminar boundary layer at large Reynolds numbers.

Such a flow is not stable, however, and upon any, even small, disturbance, it transforms into a stable turbulent one. This also relates to the instability of a turbulent boundary layer that may appear on the nose of a plate (where the Reynolds numbers are low) if initial disturbances are present. But no matter how great these disturbances are, at the leading edge they attenuate if the local number $Re = V_\delta x \rho_\delta / \mu_\delta$ does not exceed a certain limiting value of the Reynolds number. The number Re separating the zone of a stable laminar flow from the other parts of a surface on which there are zones of transition and a stable turbulent flow is called the **critical Reynolds number** $Re'_{cr} = V_\delta x'_{cr} \rho_\delta / \mu_\delta$. Sometimes this number, based on the distance x'_{cr} to the origin of the transition zone, is called the first or minimum critical number. The second critical

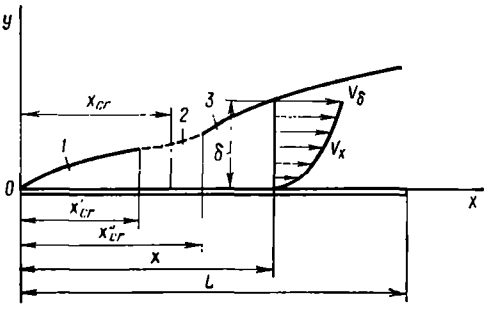

Fig. 13.8.1
Mixed boundary layer on a flat plate:
1—laminar boundary layer; *2*—transition zone; *3*—turbulent boundary layer

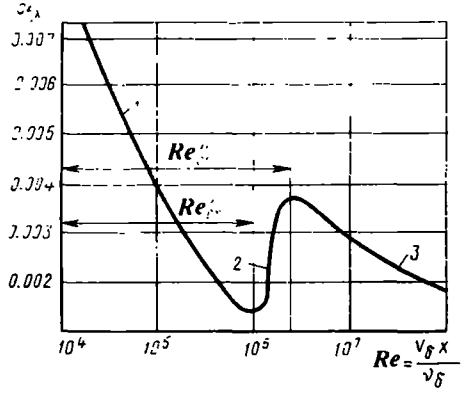

Fig. 13.8.2
Distribution of the local friction factor on a plate and the values of the critical Reynolds numbers:
1—laminar boundary layer; *2*—transition zone; *3*—turbulent boundary layer

Reynolds number $Re''_{cr} = V_\delta x''_{cr} \rho_\delta / \mu_\delta$ separates the transition zone from that of developed turbulence and is based on the coordinate x''_{cr} of the end of the transition zone. In the transition zone, the flow is of an intermittent nature: the laminar and turbulent flows replace each other irregularly. The physical properties of such a flow are characterized by the **intermittence factor**. The latter takes into account the fraction of the time interval during which turbulence exists in a definite flow cross section.

Investigations usually yield the range of Reynolds numbers limited by their first and second critical values and thus determining the transition zone length. Approximate values of these numbers can be found from the graph in Fig. 13.8.2 obtained according to experimental results for a plate in an incompressible flow with a low initial turbulence.

The first critical Reynolds number is determined from the minimum value of the friction factor corresponding to the end of the zone with a laminar boundary layer and equals $Re'_{cr} \approx 3 \times 10^6$. The point of minimum $c_{f,x}$ is followed by a sharp, almost stepwise growth in the local friction factor that reaches a peak value corre-

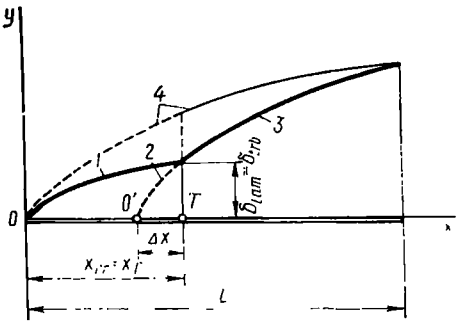

Fig. 13.8.3
Transition of a laminar boundary layer to a turbulent one:
1—laminar boundary layer; *2*—fictitious part of turbulent boundary layer; *3*—turbulent boundary layer behind the transition point; *4*—turbulent boundary layer originating at point 0

sponding to the limit of the transition zone and the second critical Reynolds number of $Re''_{cr} \approx 4 \times 10^9$. To the right of this edge, the turbulent boundary layer is stable.

In approximate practical calculations, we may proceed from the fact that the laminar boundary layer is separated from the turbulent one by an infinitely small transition zone, i.e. by a point. The coordinate x_{cr} of this transition point T (Fig. 13.8.3) is determined from the critical Reynolds number found as the arithmetic mean of the first and second critical numbers.

Experimental data should be used when finding the value of the number Re_{cr}. Such an **experimental critical Reynolds number** allows us to make quantitative estimates, and also to analyse qualitatively the phenomenon of stabilization of the laminar boundary layer, the process of its transition to a turbulent layer, and the mechanism of flow formation in this layer. Particularly, it has been established that a laminar and transition zones do not affect the mechanism of development of the turbulent boundary layer behind the transition point. Therefore, to calculate the boundary layer behind the transition point, we may use the conventional relations obtained by assuming that the flow in this layer is fully turbulent.

The location of the transition point (or zone) on a surface in a flow depends on many factors, mainly on the intensity of turbulence of the external flow, the surface state, the wall temperature, the number M_δ at the boundary layer edge, the configuration of the surface, and on the longitudinal pressure gradient.

How the intensity of turbulence of an external incompressible flow affects the number Re_{cr} is shown in Fig. 13.8.4. An increase in the intensity of turbulence results in additional disturbances in the boundary layer leading to early turbulization and, consequently, to diminishing of the critical Reynolds number.

The highest value of this number found for a sphere in free flight when the initial turbulence is taken equal to zero is determined by the number $Re_{cr} = 4 \times 10^5$. Wind tunnel tests with an initial

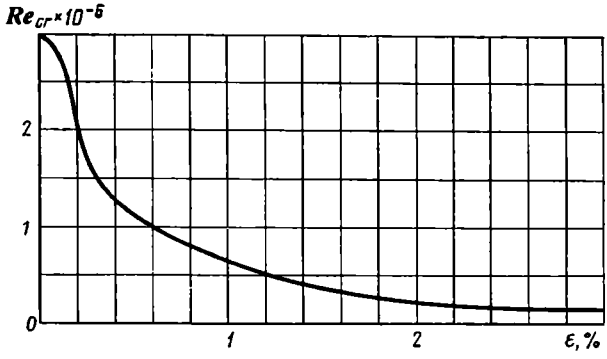

Fig. 13.8.4
Influence of the intensity of turbulence in an incompressible fluid on the critical Reynolds number for flow over a plate

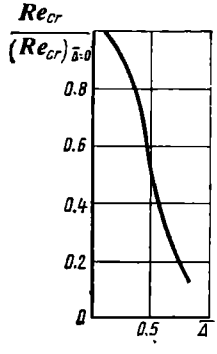

Fig. 13.8.5
Influence of plate surface roughness on the critical Reynolds number

flow turbulence of 6% yielded a Reynolds number only one-fourth of this value ($Re_{cr} \approx 10^5$). Similar measurements for a plate yield a six-fold to eight-fold reduction of this number (from 2.8×10^6 to 5×10^5).

Qualitatively, the same effect of lowering the stability of a laminar boundary layer is provided by roughness on the surface, which should also be considered as a source of disturbances. If the state of a surface is characterized by a relative roughness of $\bar{\Delta} = \Delta/\delta^*$ (where Δ is the height of the roughness asperities, and δ^* is the displacement thickness), then the influence of this state on the critical Reynolds number for an incompressible fluid can be depicted by the curve shown in Fig. 13.8.5. A glance at this figure reveals that a small roughness does not virtually affect the transition of the laminar boundary layer to a turbulent one. According to experimental data, at low velocities with a *single cylindrical* or *two-dimensional roughness* (for example, in the form of a round thin wire fixed

across the flow), the height of an element of this roughness at which it still fails to affect the transition can be determined from the relation $V^*\Delta_1/\nu_\delta = 7$, where Δ_1 is the height of a roughness element, and $V^* = \sqrt{\tau_w/\rho_\delta}$ is the **friction velocity** determined from the shear stress on the wall at the location of this element.

The height of a roughness element at which the transition of the laminar boundary layer to a turbulent one occurs directly near this element is determined from the relation $V^*\Delta_2/\nu_\delta = 15$ or 20. The heights Δ_1 and Δ_2, known as **critical** ones, correspond to roughnesses with virtually any flat dome-shaped elements or cavities, these values being smaller for pointed elements. A further increase in the height Δ_2 causes upstream displacement of the transition point until the distance from it to the leading edge reaches a minimum value (a minimum critical Reynolds number $Re_{cr} = V_\delta x_{cr}/\nu_\delta$ corresponds to this distance). Such a height is effective. Its value is determined for supersonic velocities from the condition

$$\frac{\Delta}{x_\Delta} = a\left(1 + \frac{k-1}{2} M_\delta^2\right) Re_{x\Delta}^{-3/4} \qquad (13.8.1)$$

in which $Re_{x\Delta} = V_\delta x_\Delta/\nu_\delta$, where x_Δ is the distance to a roughness element, and $a = 32.8$ and 43.2 for a cone and plate, respectively.

A minimum critical Reynolds number Re_{cr} corresponds to the effective roughness height. It is determined by the empirical relation

$$Re_{cr} - Re_{x\Delta} = 5.5 \times 10^4 M_\delta^2 \qquad (13.8.1')$$

Given the value of Re_{cr}, we can use this relation to evaluate the quantity $Re_{x\Delta}$ determining the distance from the leading edge to a roughness element (vortex generator), and formula (13.8.1) to find the corresponding value of the height of this element. Estimates show that the intensity of roughness action lowers with increasing M_δ (i.e. with increasing compressibility).

A boundary layer in a compressible fluid is thus less sensitive to roughness than in an incompressible flow. In accordance with experimental data, a turbulent boundary layer is insensitive to roughness if the height of a roughness element is smaller than the thickness of the laminar sublayer. The thickness for a flat surface can be approximated by the relation $\Delta = 100\nu_\delta/V_\delta$.

Let us see how the wall temperature affects the stability of a laminar boundary layer. It has been established that *surface cooling stabilizes a boundary layer and increases the critical Reynolds numbers.* The explanation is that cooling lowers the temperature and increases the density of the gas at the wall, as a result of which the kinetic energy of the flow grows. Particles with a high energy are influenced to a smaller extent by disturbances. It was noted that at very high flow velocities the Reynolds number has a substantial significance as a stability criterion in comparison with parameters such as the

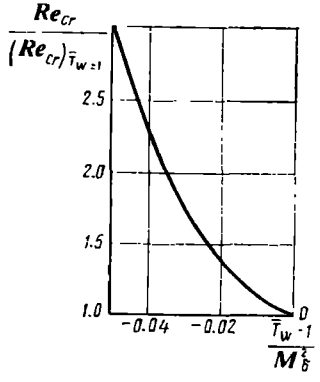

Fig. 13.8.6
Experimental curve of the number Re_{cr} versus the dimensionless temperature and the number M_∞

dimensionless wall temperature T_w/T_δ (T_w/T_∞ or T_w/T_r) and the number M_δ. Experimental dependences of the critical Reynolds number on the temperature of a plate surface are shown in Fig. 13.8.6. These results can be used to find the dependence of the quantity $Re_{cr}/(Re_{cr})_{\bar{T}w=1}$ [where $(Re_{cr})_{\bar{T}w=1}$ is the critical Reynolds number at $\bar{T}_w = T_w/T_r = 1$] on the parameter $(\bar{T}_w - 1)/M_\delta^2$ containing the dimensionless temperature $\bar{T}_w$ and the number M_δ.

Hence, the above data also allow us to see how the number M_δ at the edge of a laminar boundary layer affects its stability. It is not difficult to see that *when M_δ increases, the critical Reynolds number decreases* because an increase in M_δ is attended by elevation of the recovery temperature, and this leads to lowering of the density and kinetic energy of the gas at the wall.

Gas particles with a lower kinetic energy are naturally affected substantially by disturbances, which causes earlier turbulization of the boundary layer.

Let us see how the stability of a laminar boundary layer is affected by the intensity of turbulence of the external flow and by the wall roughness at various numbers M_δ. Observations reveal that this influence diminishes with a growth in M_δ, and at M_δ exceeding four the critical Reynolds number does not virtually depend on the intensity of turbulence and roughness.

As for the physical mechanism of this phenomenon, we know that a growth in the number M_δ is attended by an increase in the boundary layer thickness, and, therefore, a larger mass of the gas is involved in the viscous flow. This is exactly why such a thickened laminar boundary layer experiences a smaller disturbance on the part of the external flow turbulence and of roughness. This must not make us conclude that the number M_δ has a stabilizing influence. In the given case, we observe a smaller role of factors such as turbu-

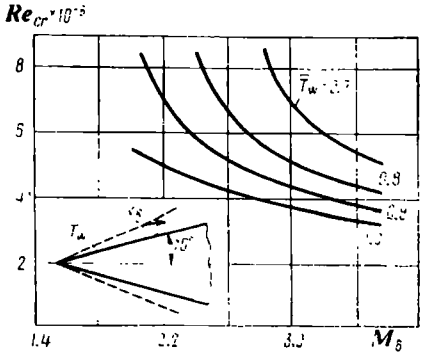

Fig. 13.8.7
Critical Reynolds number for a cone

lence and roughness in the changing of the critical Reynolds number. But at the same time, the influence of this number diminishes with a growth in M_δ.

The critical Reynolds number based on the local parameters at the edge of a layer depends on the shape of the surface in the flow. Let us consider, for example, the flow over a cone. At the same value of the number M_δ and the wall temperature, the thickness of the boundary layer on a cone is smaller than that on a plate at the corresponding point. In such a thinner layer of a viscous fluid, the tendency of lateral movements of the particles weakens, and the critical value of the Reynolds number grows. Experimental data on the change in this number depending on the number M_δ and the dimensionless temperature $\bar{T}_w = T_w/T_r$ are given in Fig. 13.8.7. An analysis of these data reveals that the qualitative nature of the influence of the number M_δ and the surface temperature on the boundary layer stability is the same as for a plate. At the same time, we can note a feature of the flow according to which at M_δ exceeding four the critical Reynolds numbers for a conical surface virtually remain constant and correspond to the given value of the dimensionless temperature $\bar{T}_w$. Calculations show that the values of the critical Reynolds number are approximately inversely proportional to the dimensionless wall temperatures $\bar{T}_w = T_w/T_r$ determined with the aid of expression (13.5.12) for T_r.

When investigating the stability of a laminar boundary layer on a curved surface, one must also take into consideration the longitudinal pressure gradient in addition to the above factors. If the gradient is positive, the gas particles move with deceleration, therefore their kinetic energy diminishes. This gives rise to a lower resistance to disturbance, which leads to more intensive lateral mixing and, consequently, to lowering of the critical Reynolds number.

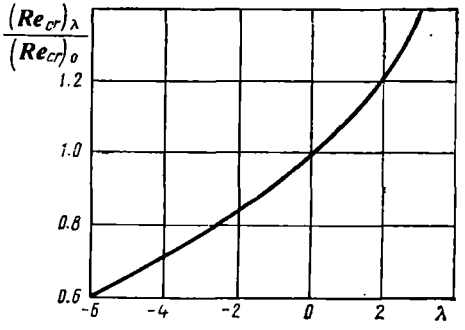

Fig. 13.8.8
Influence of the longitudinal pressure gradient on the critical Reynolds number for a flow over an airfoil

The acceleration of particles produced by a negative pressure gradient facilitates the "spreading" of the laminar motion, characterized by a larger Reynolds number. Figure 13.8.8 shows a curve plotted as a result of the experimental investigation of subsonic flow over an airfoil and allowing us to determine the influence of the longitudinal pressure gradient on the critical Reynolds number. The following empirical formula corresponds to this curve:

$$(Re_{cr})_\lambda/(Re_{cr})_0 = (1 - 0.048\lambda)^{-2} \qquad (13.8.2)$$

where $\lambda = -18x\, d\tilde{p}_\delta/dx$, $\tilde{p}_\delta = 2p_\delta/(\rho_\delta V_\delta^2)$ is the dimensionless value of the pressure in the boundary layer, and $(Re_{cr})_\lambda$ and $(Re_{cr})_0$ are the critical Reynolds numbers corresponding to $\lambda \neq 0$ (the pressure gradient is other than zero) and $\lambda = 0$ (the pressure gradient equals zero), respectively.

Experiments show that the transition point for wing airfoils coincides approximately with the coordinate of the point of minimum pressure. This coordinate, in turn, is very close to the place of the maximum airfoil thickness. This is why laminar-flow airfoils (with a great length of the laminar boundary layer) have the parts of the maximum thickness displaced toward the trailing edge. Experimental data reveal that the point of the minimum pressure may be removed from the leading edge over a distance from 60 to 65% of the airfoil chord. The drag of such an airfoil due to laminar friction can be lowered from one-and-a-half to two times in comparison with that of a conventional airfoil.

After determining the critical Reynolds number with account taken of the above factors, we can compute the parameters of a mixed boundary layer, evaluating them separately for the parts with a laminar and turbulent flows. Let us consider, for example, how such a boundary layer is calculated on a flat plate (see Fig. 13.8.3). On the part of the plate from the leading edge to point T (the length

of this part is $x_{cr} = x_T$), the viscous flow parameters (the layer thickness and friction factor) are calculated according to the usual relations for a laminar boundary layer. But for calculating the turbulent flow that arises after point T, we cannot use the relation given above for a turbulent boundary layer because this layer originates not from a zero thickness, but from a finite one. Experiments verified that these relations may be used with an adequate approximation if the coordinate x is measured from the conditional onset of the turbulent boundary layer shown by point O' in Fig. 13.8.3.

To find this point, we can use one of the following schemes. In accordance with the **first scheme**, it is assumed that the distance $O'T = \Delta x$ equal to the length of a conditional plate with a turbulent boundary layer must be such as to ensure a thickness of the turbulent boundary layer δ_{trb} at the transition point equal to the thickness of a laminar boundary layer δ_{lam} on the length $x_{cr} = x_T$. For an incompressible fluid, this leads to the condition

$$A_1 x_T (Re_{cr})_{x_T}^{-1/2} = A_2 \Delta x (Re_{\Delta x})^{-1/5} \qquad (13.8.3)$$

where by (13.3.19′) and (13.4.58) $A_1 = 4.64$ and $A_2 = 0.37$;

$$(Re_{cr})_{x_T} = V_\delta x_T/\nu_\delta, \quad Re_{\Delta x} = V_\delta \Delta x/\nu_\delta \qquad (13.8.4)$$

the critical number $(Re_{cr})_{x_T}$ being considered as a known quantity ranging from 1×10^6 to 5×10^6. Knowing this quantity, we can find Δx from (13.8.3).

To take account of the influence of compressibility and high temperatures, we shall use the reference parameters. For this purpose, we shall write the expressions for the Reynolds numbers as follows:

$$(Re_{cr})_{x_T} = V_\delta x_T/\nu^*, \quad Re_{\Delta x} = V_\delta \Delta x/\nu^* \qquad (13.8.5)$$

In the case being considered, the critical number $(Re_{cr})_{x_T}$ should be found with account taken of the wall temperature and the number M_δ. By inserting the values (13.8.5) into (13.8.3), we can calculate the length Δx, which is already determined with a view to high flow velocities.

In accordance with the **second scheme**, it is assumed that not the layer thicknesses, but the momentum thicknesses δ^{**} at the transition point are the same for the laminar and turbulent boundary layers, i.e.

$$(\delta^{**}_{lam})_{x_T} = (\delta^{**}_{trb})_{\Delta x} \qquad (13.8.6)$$

For an incompressible fluid, we find the momentum thickness by Eq. (13.2.19) in which we assume that $\rho = \rho_\delta$:

$$\delta^{**} = \int_0^\delta \frac{V_x}{V_\delta}\left(1 - \frac{V_x}{V_\delta}\right) dy$$

By introducing for the integral the designation

$$B=\int_0^1 \frac{V_x}{V_\delta}\left(1-\frac{V_x}{V_\delta}\right)d\left(\frac{y}{\delta}\right)=\text{const} \qquad (13.8.7)$$

we obtain

$$\delta^{**}=\delta B \qquad (13.8.8)$$

Introducing this value into (13.8.6) and taking into consideration expression (13.8.3) for the thicknesses, we find

$$A_1B_1x_T\,(Re_{cr})_{x_T}^{-1/2}=A_2B_2\,\Delta x\,(Re_{\Delta x})^{-1/5} \qquad (13.8.9)$$

where B_1 is evaluated from (13.8.7) with the substitution of V_x/V_δ by Eq. (13.3.15) in which we assume that $\eta/\eta_\delta = y/\delta$, while B_2 is found from the same equation (13.8.7) with the substitution of V_x/V_δ in accordance with (13.4.54). The value of Δx found from (13.8.9) is larger than that obtained from (13.8.3). The mean value of Δx found by these formulas is expected to be closer to the actual one.

The results of calculating the coordinate of point O' can be used for finding the thicknesses, the distribution of the local friction factors and also of the average values of these factors for a mixed boundary layer.

The average friction factor for a plate of length L is

$$(c_{x,f})_{lc}=(c_{x,f,lam})_{lc}\frac{x_T}{L}+(c'_{x,f,trb})_{lc}\frac{x'}{L}-(c''_{x,f,trb})_{lc}\frac{\Delta x}{L} \qquad (13.8.10)$$

where $(c_{x,f,lam})_{lc}$ is the average factor of laminar friction on part OT (see Fig. 13.8.3) calculated from the critical Reynolds number: $(c'_{x,f,trb})_{lc}$ and $(c''_{x,f,\,trb})_{lc}$ are the average factors of turbulent friction on parts $x'=L-x_T+\Delta x$ and Δx, respectively. The factor $(c'_{x,f,trb})_{lc}$ has been found for a Reynolds number based on the length x', and the factor $(c''_{x,f,\,trb})_{lc}$, for the number Re based on the length Δx.

The friction factor can be approximated proceeding from the assumption that the turbulent layer originates directly at a point on the leading edge (see Fig. 13.8.3). In this case, the quantity Δx should be taken equal to the length of the laminar part, i.e. $\Delta x = x_T$. With this condition, formula (13.8.10) can be written in the form

$$c_{x,f}=c_{x,f,lam}x_T/L+c'_{x,f,trb}-c''_{x,f,trb}x_T/L \qquad (13.8.11)$$

Here the length of the transition part x_T is considered to be a preset quantity determined from the known critical Reynolds number.

Formula (13.8.11) can be used when calculating the friction factor for bodies of revolution. Here x_T should be replaced with the part S_{lam} of the side surface area, and L with the side surface

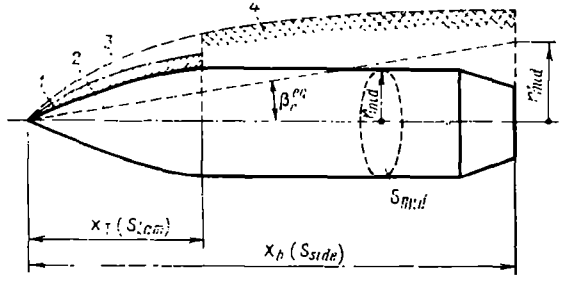

Fig. 13.8.9
Shape of an equivalent cone:
1—given body of revolution; *2*—equivalent cone; *3*—laminar boundary layer; *4*—turbulent boundary layer

area S_{side}. If we relate the factor $c_{x,f}$ to the characteristic area S_{mid}, we have

$$c_{x,f} = c_{x,f,lam} S_{lam}/S_{mid} + c'_{x,f,trb}\, S_{side}/S_{mid} - c''_{x,f,trb}\, S_{lam}/S_{mid} \qquad (13.8.12)$$

For subsonic flow, the critical Reynolds number Re_{cr} used to calculate the length x_T can be found for a body of revolution in the same way as for a plate. Here we must have in view that for a body the actual values of this number are larger.

For supersonic flow, the number Re_{cr}, like the component friction factors in (13.8.12), can be found by replacing the given curved body of revolution with an equivalent cone whose semiapex angle β_c^{eq} is calculated from the condition that $\pi r'_{mid} x_b = S_{side}$. This yields $\beta_c^{eq} = r'_{mid}/x_b = S_{side}/(\pi x_b^2)$ (Fig. 13.8.9). Therefore

$$c_{x,f} = \sqrt{3}\,(c_{x,f,lam})_{pl}\,\frac{S_{lam}}{S_{mid}} + 1.17\left[(c'_{x,f,trb})_{pl}\,\frac{S_{side}}{S_{mid}} - (c''_{x,f,trb})_{pl}\,\frac{S_{lam}}{S_{mid}}\right] \qquad (13.8.13)$$

The friction factors on the right-hand side are determined for a flat plate according to the relevant gas parameters on the equivalent cone.

14

Heat Transfer

14.1. Aerodynamic Heating

Heat Balance Equation

In a flight in the atmosphere, the heat from the surroundings transfers to a craft when the temperature of the gas in close proximity to its surface becomes higher than that of the body. Regions with a high temperature form because of stagnation of the flow in shock waves and in the boundary layer that causes the static enthalpy of the air to grow.

The calculation of heat transfer consists in determining *the specific heat flow* (*the heat flux per unit area or the heat transfer rate*) *equal to the amount of heat transferred to a unit surface area in unit time*, and also *the heat flux to the entire surface*. Such calculations allow us to properly choose the cooling system or other means ensuring protection of the surface against overheating, and also to determine the spots where excessive thermal stresses develop and destruction of the surface is possible.

Let us consider the **heat balance equation**, which in the general form determines the resultant specific heat flow to a wall. The magnitude of the specific heat flow q_w equals the difference between the heat fluxes supplied to a wall q_{sup} and rejected from it q_{rej}, i.e.

$$q_w = q_{sup} - q_{rej} \tag{14.1.1}$$

The heat flux supplied to a wall is due to heat transfer by conduction and diffusion in the gas (the **aerodynamic heat flux**) $q_c = q_h + q_d$, by radiation by the gas q_{rad}, and also solar q_s and terrestrial q_{ter} radiation, and to the heat transfer from the equipment $q_{eq.tr}$:

$$q_{sup} = q_c + q_{rad} + q_s + q_{ter} + q_{eq.tr} \tag{14.1.2}$$

The rejected flow consists of the heat q_{em} emitted by the heated surface, the heat q_{ab} absorbed by the wall material and dissipated into the surroundings upon ablation, the heat q_{cl} removed by various cooling means, and the heat $q_{eq.h}$ spent on heating the equipment.

Consequently,

$$q_{rej} = q_{em} + q_{ab} + q_{cl} + q_{eq.h} \tag{14.1.3}$$

The components $q_{eq.tr}$, $q_{eq.h}$, and q_{cl} may play a major role in the heat balance. The problems associated with the permissible values of $q_{eq.tr}$ and $q_{eq.h}$ and with the required values of q_{cl} are primarily of a design and technological nature and are solved in each specific case with a view to the features of the craft. We shall consider here only the processes of the natural heat supply and rejection of heat associated with heating of the gas, emission from the wall, and also with solar and terrestrial radiation.

Heat Transfer from a Heated Gas

Molecular Heat Conduction. When studying phenomena associated with the high-speed flow over bodies, the non-uniform heating of the gas that causes three-dimensional distribution of both the temperatures and the composition of the gas should be considered. The temperature gradients produce a heat flux due to molecular heat conduction. This flux is determined by Fourier's law

$$q_h = -\lambda_w (\partial T/\partial y)_w \tag{14.1.4}$$

where λ_w and $(\partial T/\partial y)_w$ are the heat conductivity and the temperature gradient, respectively, for the heated gas at the wall. The minus sign on the right-hand side has been taken with a view to the fact that the quantity q_h is positive, while the temperature gradient $(\partial T/\partial y)_w$ is negative because the temperature lowers in the direction of heat propagation.

Heat Flux by Diffusion. A feature of heat transfer in a boundary layer at very high flow velocities is that the atoms and ions produced by dissociation and ionization participate in the transfer of heat, diffusing into regions with a lower concentration of atoms and ions. Diffusion attended by the recombination of atoms and ions leads to the liberation of additional heat

$$q_d = \sum Q_{i,d} i_i \tag{14.1.5}$$

where $Q_{i,d}$ is the diffusion mass flux [see (3.2.1)], and i_i is the enthalpy of the i-th component of the mixture determined by the formula

$$i_i = \left(\int_0^T c_p \, dT \right)_i + (i_{chem})_i \tag{14.1.6}$$

in which $\left(\int_0^T c_p \, dT \right)_i$ is the enthalpy of the i-th component of the gas, and $(i_{chem})_i$ is the chemical energy of its formation.

For a model of the air, which is a reacting atomic-molecular mixture (the subscript "A" is used on the atomic component, and "M" on the molecular one), we have

$$q_d = Q_{A,d} i_A + Q_{M,d} i_M \qquad (14.1.5')$$

$$i_A = \int_0^T c_{p,A}\, dT + i_{chem},\quad i_M = \int_0^T c_{p,M}\, dT \qquad (14.1.6')$$

In addition, we can consider that the mass transfer in the given direction y is

$$Q_{A,d} = -Q_{M,d} = -\rho D_{A,M}\, \partial c_A/\partial y;\ D_{A,M} = D_{M,A} = \bar{D} \qquad (14.1.7)$$

where $D_{A,M} = D_{M,A} = \bar{D}$ is the diffusivity of the atomic (molecular) component into the molecular (atomic) one, and c_A is the mass concentration of the atoms.

To a first approximation, we can evidently proceed from the indicated binary structure of dissociated air because the transport coefficients characterizing the viscosity, heat conduction, and diffusion, and also the relative atomic masses of oxygen and nitrogen are close to each other. We also assume that the nitrogen oxide concentration is low, and its influence on the transfer of energy may be disregarded. Ionization may also be left out of consideration because it only begins to be significant at M_∞ exceeding 20 or 25.

Inserting (14.1.7) into (14.1.5') and considering the conditions at the wall, we obtain

$$q_d = -\rho_w \bar{D}\, (\partial c_A/\partial y)_w\, (i_A - i_M) \qquad (14.1.8)$$

The enthalpies of the atomic i_A and molecular i_M components determine the enthalpy i of the mixture:

$$i = i_A c_A + i_M (1 - c_A) \qquad (14.1.9)$$

By (14.1.6), the difference

$$i_A - i_M = \int_0^T (c_{p,A} - c_{p,M})\, dT + i_{chem} \qquad (14.1.10)$$

In real cases, the second term on the right-hand side of Eq. (14.1.10) is considerably larger than the first one, and, therefore, we can assume that $i_A - i_M \approx i_{chem}$.

In addition to mass transfer due to a non-uniform concentration, diffusion mass fluxes form that are produced by gradients of the temperature (thermal diffusion) and pressure (pressure diffusion). These two components of the diffusion flux do not have a significant value, and for this reason they are left out of account when studying

heat conduction in a gas flow. The gas components diffusing because of the concentration gradient when transferring enthalpy are sources of an energy flow that in some conditions can exceed the heat flux due to conduction.

Resultant Specific Heat Flow. The magnitude of the resultant specific heat flow is determined by heat transfer due to conventional molecular heat conduction and the release of heat as a result of the recombination of the atoms participating in diffusion. Hence the resultant specific heat flow to a wall by (14.1.4) and (14.1.8) is

$$q_c = q_h + q_d = -\lambda_w (\partial T/\partial y)_w - \rho_w \overline{D} (i_A - i_M)_w (\partial c_A/\partial y)_w \quad (14.1.11)$$

The derivative $(\partial T/\partial y)_w$ can be determined as follows. We differentiate (14.1.9) with respect to y:

$$\frac{\partial i}{\partial y} = \frac{\partial c_A}{\partial y}(i_A - i_M) + \frac{\partial i_A}{\partial y} c_A - \frac{\partial i_M}{\partial y}(1 - c_A) \quad (14.1.9')$$

We use formula (14.1.6), transforming it to the differential form $di_i = c_{p,i}\, dT$ and taking into account that $d(i_{chem})_i = 0$ because for each component the enthalpy of its formation $(i_{chem})_i = \text{const}$. From the obtained expression for di_i, we find that $di_A = c_{p,A}\, dT$ and $di_M = c_{p,M}\, dT$. Hence (14.1.9′) can be transformed as follows:

$$\frac{\partial i}{\partial y} = \frac{\partial c_A}{\partial y}(i_A - i_M) + \frac{\partial T}{\partial y}[c_{p,A} c_A - c_{p,M}(1 - c_A)]$$

where $c_{p,A} c_A + c_{p,M}(1 - c_A) = (c_p)_{av}$ is the average specific heat of the mixture.

From the expression for $\partial i/\partial y$, we find the derivative

$$\left(\frac{\partial T}{\partial y}\right)_w = \frac{1}{(c_p)_w}\left(\frac{\partial i}{\partial y}\right)_w - \frac{1}{(c_p)_w}\left(\frac{\partial c_A}{\partial y}\right)_w (i_A - i_M)_w$$

where $[(c_p)_{av}]_w$ has been designated by $(c_p)_w$.

Let us introduce the expression obtained for $(\partial T/\partial y)_w$ into (14.1.11):

$$q_c = -\frac{\lambda_w}{(c_p)_w}\left[\left(\frac{\partial i}{\partial y}\right)_w - \left(\frac{\partial c_A}{\partial y}\right)_w (i_A - i_M)_w + \frac{\rho_w (c_p)_w \overline{D}}{\lambda_w}\left(\frac{\partial c_A}{\partial y}\right)_w (i_A - i_M)_w\right] \quad (14.1.12)$$

or

$$q_c = -\frac{\lambda_w}{(c_p)_w}\left(\frac{\partial i}{\partial y}\right)_w \left\{\underbrace{\left[1 - \frac{(\partial c_A/\partial y)_w (i_A - i_M)_w}{(\partial i/\partial y)_w}\right]}_{\text{Heat conduction (1)}} + \underbrace{Le \frac{(\partial c_A/\partial y)_w (i_A - i_M)_w}{(\partial i/\partial y)_w}}_{\text{Diffusion (2)}}\right\} \quad (14.1.12')$$

In Eq. (14.1.12'), we used the dimensionless number

$$Le = \rho_w (c_p)_w \overline{D}/\lambda_w \qquad (14.1.13)$$

called the **Lewis number**, which is one of the important criteria of heat transfer by diffusion. The physical meaning of this criterion consists in that it determines the ratio of the intensity of heat transfer in mass transfer by diffusion to that of heat transfer by conduction. In the general case, $Le > 1$, hence heat conduction is less intensive than the transfer of heat by diffusion. Let us write the number Le (14.1.13) in the form

$$Le = \frac{\mu_w (c_p)_w}{\lambda_w} \frac{\rho_w \overline{D}}{\mu_w}$$

The first multiplier on the right-hand side of this expression is the Prandtl number $Pr = \mu_w (c_p)_w/\lambda_w$, while the second one is a dimensionless number that can be considered as a characteristic of the heat transfer by diffusion. A number that is the reciprocal of this quantity is introduced in the theory of heat transfer. It is known as the **Schmidt number**:

$$Sc = \mu_w/(\rho_w \overline{D}) \qquad (14.1.14)$$

The physical meaning of the number Sc consists in that it determines the relation between the kinetic energy due to molecular transport and the energy transferred by diffusion. Like the Prandtl number, the Schmidt number for gases $Sc < 1$, and $Sc < Pr$. The Schmidt and Lewis numbers are related as follows:

$$Le = Pr/Sc \qquad (14.1.13')$$

Of practical importance are investigations of the numerical values of the above numbers. It was established theoretically that for a two-component atomic-molecular mixture the Schmidt number varies very slightly over a wider range of temperatures. For example, if at $T = 252$ K the value of $Sc = 0.495$, then at $T = 3360$ K the number $Sc = 0.482$. This is also characteristic of the change in the Prandtl number whose value is about 0.71. If we assume that the Schmidt number equals a certain average value $Sc = 0.49$, then the Lewis number is

$$Le = Pr/Sc = \rho \overline{D} c_p/\lambda = 0.71/0.49 = 1.45$$

According to available data, this number depends only slightly on the temperature up to values of $T \approx 9000$ K.

Analysis of Heat Transfer Cases. Let us consider Eq. (14.1.12') and analyse various cases of heat transfer in a boundary layer. Inspection of (14.1.12') reveals that if the temperature at the wall is below the dissociation limit, the concentration of atoms is zero,

hence, $(\partial c_A/\partial y)_w = 0$, and the heat flux is

$$q_c = q_h = -[\lambda_w/(c_p)_w](\partial i/\partial y)_w \qquad (14.1.15)$$

In the limiting case of thermodynamic equilibrium being considered, heat transfer is characterized by molecular heat conduction. It consists in the transfer of the kinetic energy of the translational motion of the molecules, and also in their vibrational and rotational energy.

The real flow in a dissociated boundary layer is characterized by a concentration gradient of the atoms and molecules and by a non-equilibrium nature of the chemical reactions. In this case, the heat transfer mechanism in the boundary layer may differ appreciably from the process of purely molecular heat conduction. In addition to molecular heat transfer, heat is transferred owing to the chemical energy released upon recombination. This process is characterized by the following limiting cases.

In the *first limiting case*, when $Le = 1$, the heat flux, as can be seen from (14.1.12'), exactly equals (14.1.15). Here a feature of the heat transfer consists in that the amount of heat absorbed in dissociation [the first term in (14.1.12')] exactly equals the heat flux due to diffusion [the second term in (14.1.12')]. Evidently, the case being considered is characterized by an infinitely high rate of recombination. Therefore thermodynamic equilibrium is established at every point of the boundary layer. Accordingly, the diffusion heat transfer in the layer is due to a profile of equilibrium concentrations.

In practice, flow conditions close to such a hypothetic "equilibrium" boundary layer are formed when the rate of diffusion is negligibly small in comparison with the rate of dissociation and recombination (and for ionization, also of the electron reactions).

In the *second limiting case* that occurs at very high flight speeds when the gas in the boundary is strongly dissociated, the parameter $(\partial c_A/\partial y)_w (i_A - i_M)_w/(\partial i/\partial y)_w \approx 1$. This can be proved by using (14.1.9'). According to our assumption, at very high speeds $c_A \to 1$, consequently

$$\frac{\partial i}{\partial y} \to \frac{\partial c_A}{\partial y}(i_A - i_M) + \frac{\partial i_A}{\partial y}$$

Here the derivative

$$\frac{\partial i_A}{\partial y} = \frac{\partial}{\partial y}\left[\int_0^T c_{p,A}\,dT + i_{chem}\right]$$

Bearing in mind that in real cases the heat of formation $i_{chem} \gg \int_0^T c_{p,A}\,dT$ and is a constant quantity, we can assume that

$\partial i_A/\partial y \approx 0$. Hence, for the conditions at the wall, $(\partial i/\partial y)_w \to$ $\to (\partial c_A/\partial y)_w \cdot (i_A - i_M)_w$. Accordingly,

$$q_c = q_d = -\frac{\lambda_w}{(c_p)_w} Le \left(\frac{\partial i}{\partial y}\right)_w \qquad (14.1.15')$$

In the limiting case being considered, all the heat is thus transferred owing to diffusion. This heat transfer is characterized by very low rates of recombinations. As a result, although diffusion of the atoms does occur, no energy is released in the boundary layer. In practice, this may occur in a flow if the reaction time is large in comparison with the characteristic time of particle motion. Such flows are called **frozen**. In a frozen flow, the atoms formed upon dissociation diffuse toward the cold wall, where they then combine. The released energy depends on the catalytic properties of the wall, which manifest themselves in different values of the rate of the recombination catalytic reaction.

All the actual heat transfer processes are assumed to be between the two limiting cases indicated above.

Newton's Formula. The total heat flux from a heated gas to a wall $q_c = q_h + q_d$ determined by Eq. (14.1.11) can be represented as **heat transfer by convection**, i.e. heat transfer between a solid wall and a gas flowing over it. The magnitude of such a heat flux in practical calculation is usually expressed with the aid of Newton's formula

$$q_c = \alpha_w (T - T_w) \qquad (14.1.16)$$

where T is the representative temperature of the flow over the surface, T_w is the wall temperature, and α_w [W/(m²K)] is the **heat-transfer coefficient** numerically equal to the amount of heat transferred to (or rejected by) a unit surface area in unit time at a temperature difference between the wall and the gas of one kelvin.

When choosing the temperature T in (14.1.16), we proceed from the following. It is general knowledge that if a wall is thermally insulated, the temperature of the gas reaches its maximum value at the surface and equals the recovery temperature T_r. It is justifiable from a physical viewpoint to consider this temperature to be the most important factor for heat transfer from a heated gas to a surface depending on what the temperature of this surface is. It is important to note here that for the given conditions, the quantity T_r is a weak function of the flow parameters. The temperature T in (14.1.16) is taken as just this temperature, which makes it possible to avoid ambiguity in the concept of the temperature of the flow over a body. Accordingly, we shall write Newton's formula as

$$q_c = \alpha_w (T_r - T_w) \qquad (14.1.16')$$

Such a notion of the specific heat flow has an important feature consisting in that the heat-transfer coefficient α_w is a weak function

of the temperature difference, and in practical calculations the influence of this difference may be disregarded. But it is had in view here that the heat-transfer coefficient depends on a number of factors such as the gas velocity, the shape, dimensions, position (angle of attack) of the body in the flow, the structure of the boundary layer (laminar or turbulent), and on the physical properties of the fluid (heat conductivity, viscosity, specific heat, etc.).

Heat-transfer equation (14.1.16′) may be used for flow velocities when chemical reactions are absent in the boundary layer. At very high velocities, chemical processes are of a major importance, therefore when calculating heat transfer one must take into consideration the change in the enthalpy in accordance with the formula

$$q_c = [\alpha_w/(c_p)_w]\ (i_r - i_w) \qquad (14.1.17)$$

where $(c_p)_w$ is the average specific heat for the conditions in the gas at the wall, while i_r and i_w are the recovery enthalpy and enthalpy of the gas at the wall surface, respectively.

Calculations reveal that the ratio $\alpha_w/(c_p)_w$ in (14.1.17) varies slightly upon dissociation (up to 10 or 15%), and in a first approximation it is chosen from the solutions for the boundary layer without chemical reactions. The enthalpies i_r and i_w are calculated with account taken of dissociation. It follows from calculations by formula (14.1.17) that notwithstanding the small change in $\alpha_w/(c_p)_w$, the heat fluxes may differ appreciably from the values calculated by (14.1.16′) without considering dissociation.

It is convenient to use dimensionless criteria instead of the dimensional heat-transfer coefficient. These criteria include the **Stanton number**

$$St = q_c/[\rho_\delta V_\delta\ (i_r - i_w)] = \alpha_w/[\rho_\delta V_\delta\ (c_p)_w] \qquad (14.1.18)$$

and the **Nusselt number**

$$Nu = \alpha_w l/\lambda_w \qquad (14.1.19)$$

where l is an arbitrary linear dimension, and λ_w is the thermal conductivity of the gas at the wall.

The relation between these two numbers is established by the obvious expression

$$Nu = St\ Re\ Pr \qquad (14.1.20)$$

where $Re = V_\delta \rho_\delta l/\mu_\delta$ and $Pr = (c_p)_w \mu_\delta/\lambda_w$.

The determination of the heat-transfer coefficient α_w or the dimensionless criteria of heat transfer is the *basic task of the theory of aerodynamic heat transfer*. We shall note that since additional terms affecting the heat flux have been separated in formulas (14.1.18) and (14.1.19), the numbers St and Nu depend on the flow conditions to a smaller extent than $\alpha_w = \rho_\delta V_\delta (c_p)_w\ St$ and $\alpha_w = (\lambda_m/l)\ Nu$. In a general case, the values of St and Nu, in turn, are functions of

the dimensionless criteria Re, Pr, $Sc = \mu_\delta/(\rho_\delta \bar{D})$, and $M_\delta = V_\delta/a_\delta$ determining the flow conditions and depend on the nature of the boundary layer and the wall temperature.

Radiant Heat Flux. The high elevation of the temperature behind a shock wave or in a boundary layer increases the degree of dissociation, and, consequently, the amount of atomic oxygen and nitrogen in the air grows. The result is more intensive proceeding of reactions with the formation of nitrogen oxide and an increase in its concentration.

A growth in the pressure leads to a higher rate of recombination by the reaction $A + A \rightleftarrows A_2$ and to an increase in the concentration of the nitrogen oxide NO forming by the equation $O_2 + N_2 \rightleftarrows 2NO$. Unlike nitrogen and oxygen, nitrogen oxide is optically opaque, i.e. it can absorb and emit radiant energy. Air containing even a small fraction of nitrogen oxide has this property of opaqueness. This is why air heated to very high temperatures becomes a source of a radiant heat flux.

The optical properties of air are characterized by the parameter ε that is the radiation capacity of unit length of the emitting layer and has the dimension $1/l$. For an emitting layer of thickness s_0, a dimensionless characteristic of radiation capacity is the quantity εs_0 called the **effective emissivity of a gas.**

According to the Stefan-Boltzmann law, the heat emitted by a blackbody $q_{rad} = \sigma T^4$, where σ is the Stefan-Boltzmann constant, or the radiation coefficient of a blackbody [$\sigma = 5.6 \times 10^{-8}$ W/(m^2·K^4)], and T is the temperature of the radiating gas. A function $f(\varepsilon s_0)$ depending on the effective emissivity is introduced into this formula to take transparency into consideration. It is called the **emittance** of a gas. Hence, the relation for determining the radiant heat flux to a wall has the form

$$q_{rad} = f(\varepsilon s_0)/\sigma T^4 \qquad (14.1.21)$$

Formula (14.1.21) relates to the case when the wall emits no heat and its temperature $T = T_w < 3000$ K.

Figure 14.1.1 presents a curve characterizing the change in the function $f(\varepsilon s_0)$ depending on the effective emissivity of air. This curve can be approximated by the equation

$$f = 1 - \exp(-\varepsilon s_0) \qquad (14.1.22)$$

by which the error is not over 20%.

A glance at Fig. 14.1.2 giving the results of experimental investigations reveals that the parameter ε (cm^{-1}) depends on the temperature and density of the air. Within the temperature range of $8000 \text{ K} \leqslant T \leqslant 16\,000$ K, the family of curves is well approximated by the formula

$$\varepsilon = 0.138\,(\rho/\rho_{\infty,E})^{1.28}\,(T/10^4)^{6.54} \qquad (14.1.23)$$

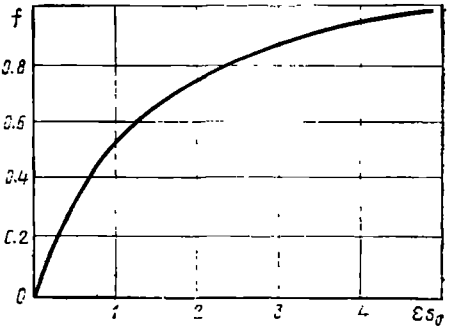

Fig. 14.1.1
Function characterizing the emittance (absorptance) of a radiating gas

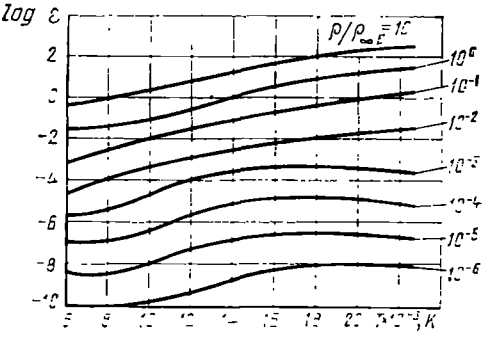

Fig. 14.1.2
Experimental data on the emissivity of a gas (ε, cm^{-1})

where $\rho_{\infty,E}$ is the density of the atmospheric air at the Earth's surface.

The maximum radiant heat fluxes form at the stagnation point and in its vicinity. Their values can be calculated by (14.1.21) provided that the separation of the wave s_0 is determined with a view to the spatial configuration of the nose, while the density and temperature equal their corresponding values at the stagnation point ($\rho = \rho_0'$ and $T = T_0'$). We can also use the following experimental relation for a spherical nose (see [1]):

$$q_{rad} = 8.9 \times 10^7 R_n \, (V_\infty/10^4)^{8.5} \, (\rho_{\infty,H}/\rho_{\infty,E})^{1.6} \qquad (14.1.21')$$

where q_{rad} is the heat flux, W/(m²·s); R_n is the radius of the nose, m; V_∞ is the velocity, m/s; $\rho_{\infty,H}$ and $\rho_{\infty,ter}$ are the density of the atmosphere at the altitude H and at the Earth's surface, respectively.

By substituting for the radius R_n its equivalent value (see Sec. 10.4), we can calculate the value of q_{rad} at the centre of a flat nose to a first approximation.

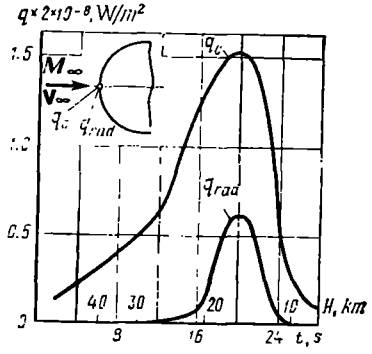

Fig. 14.1.3
Aerodynamic and radiant heat fluxes at a stagnation point:
t — flight time; H — altitude

Figure 14.1.3 shows how the radiant heat flux changes along a flight path in certain flight conditions. It can be noted that the heat flux q_{rad} takes on large values at low altitudes. Its value corresponds to the maximum of the aerodynamic heat flow q_c and is about one-third of this maximum value.

Solar and Terrestrial Radiations. Radiant Flux from a Wall Surface

The radiant heat flux from the Sun is

$$q_s = \bar{q}\beta_s \cos\psi \qquad (14.1.24)$$

where ψ is the angle between the direction of the Sun's rays and a normal to the surface of the body, and $\bar{q}$ is the irradiance power of the Sun, depending mainly on the flight altitude and the meteorological conditions. For temperate geographical conditions, the values of $\bar{q}$ for the Sun at its zenith and without account taken of the absorption of its rays by the atmosphere are given in Fig. 14.1.4. Data on the coefficient β_s taking account of the absorptivity of a material are given in Table 14.1.1.

In flights at low altitudes (H is about 10 to 15 km), the irradiance $\bar{q}$ diminishes because of cloudiness. For example, at an average cloudiness, the actual value of $\bar{q}$ is 0.5 to 0.7 of the values corresponding to the data in Fig. 14.1.4 and 0.1 to 0.2 for an overcast sky. In night conditions, the irradiance is nil.

Formula (14.1.24) may be applied to the part of a craft's surface facing the Sun. But the parts of this surface in the shade also absorb heat because of diffuse solar radiation. The magnitude of this heat flux is about one-third to one-fourth of that on the bright side.

The specific heat flow due to terrestrial radiation is very small. It can be considered in the form of the sum $q_{ter} = q_{ter,\,p} + q_{ter,\,r}$,

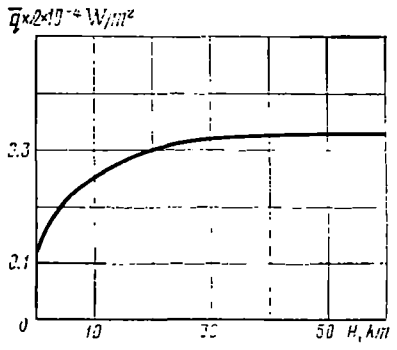

Fig. 14.1.4
Irradiance of the Sun depending on the altitude H

where $q_{ter,\,p}$ is the radiant flux from the Earth, and $q_{ter,\,r}$ is the energy of the solar rays reflected from the Earth's surface and clouds. Investigations show that for conditions of flight at an altitude of 500 km,

$$q_{ter,p} = 0.007\ (1 + 2\cos\varphi)\ \beta_{ter} \qquad (14.1.25)$$

where φ is the angle between a normal to the surface and the "body-Earth" line.

Table 14.1.1

Materials	Kind of radiation	
	terrestrial β_{ter}	solar β_s
Al	0.04-0.10	0.10-0.49
Fe	0.06-0.74	0.45
Ni	0.04-0.39	0.40
Alloys:		
of duralumin type	0.04-0.55	0.53
alloyed steels	0.12-0.62	0.60
Insulating materials:		
plexiglass (a transparent thermoplastic)	0.89	—
glass	0.85	—
Painted surfaces:		
dark	0.80-0.99	0.97
light	0.80-0.90	0.14-0.18

Note. The data on the coefficients β_{ter} and β_s are given for a wall temperature ranging from 200 to 600 °C.

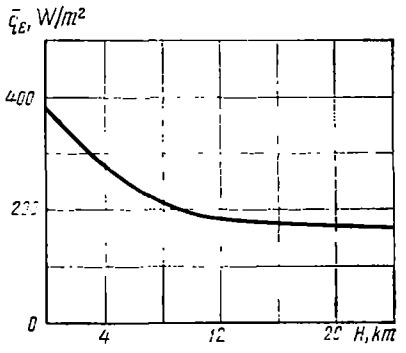

Fig. 14.1.5
Irradiance of the Earth depending on the altitude

According to experimental data, the maximum value of the terrestrial radiant flux is

$$q_{\text{ter,p max}} = \bar{q}_{\text{ter}}\beta_{\text{ter}} \tag{14.1.26}$$

where $\bar{q}_{\text{ter}}$ is the Earth's irradiance power.

The values of $\bar{q}_{\text{ter}}$ and β_{ter} are given in Fig. 14.1.5 and Table 14.1.1, respectively.

Data on the specific heat flow $q_{\text{ter, r}}$ are also experimental and have been obtained for a body at an altitude of 500 km on the "Earth-Sun" line. According to these data,

$$q_{\text{ter, r}} = 0.016\ (1 + 2\cos\varphi)\ \beta_{\text{ter}} \tag{14.1.27}$$

By the Stefan-Boltzmann law, the heat flux emitted from a unit of wall surface is

$$q_{\text{em}} = \varepsilon\sigma T_{\text{w}}^4 \tag{14.1.28}$$

where ε is the emittance of the surface depending on the material, roughness of the surface, and its temperature.

The emittance shows how many times the radiation coefficient of a surface is less than that of a blackbody. The value of ε grows with an increase in the surface roughness. If the height of the asperities is several times larger than the wavelength λ of the radiation with the maximum intensity, the value of ε_{r} for a rough surface can be expressed in terms of the emittance of a smooth surface ε as follows:

$$\varepsilon_{\text{r}} = \varepsilon\ [1 + 2.8\ (1 - \varepsilon)^2] \tag{14.1.29}$$

The wavelength λ (μm) depends on the temperature and is

$$\lambda = 2898/T \tag{14.1.30}$$

14.2. Relation Between Skin Friction and Heat Transfer

The problem of aerodynamic heat transfer consists in determining the heat-transfer coefficient α_w in (14.1.16) and (14.1.16'), or the corresponding dimensionless criteria St or Nu. These calculations in the general case are associated with the solution of a system of differential equations of the boundary layer including the equations of motion, energy, continuity, and diffusion. As a result of this solution, we find a *relation between the heat-transfer and skin friction parameters.* With certain simplifying assumptions, such a relation has the form of elementary expressions allowing us to directly determine α_w, St or Nu from the friction factor at the relevant point on the surface.

To obtain these expressions, we shall use Eq. (14.1.8) for the laminar flow of a gas, and also the equation of energy in the form it is used in the boundary layer theory. First, using the general form of energy equation (3.2.14), we shall write it in a form such that contains the numbers Le, Sc, and Pr introduced above. It is convenient to use the obtained energy equation for analysing various heat-transfer phenomena and processes. Next this equation is transformed with respect to the conditions of a viscous flow in a thin boundary layer, and we thus find an **energy equation for the boundary layer** in a simplified form. Bearing in mind the expression $i = \sum_i i_i c_i$ for the enthalpy of a mixture, we can find the differential

$$di = \sum_i i_i \, dc_i + \sum_i c_i \, di_i$$

where $di_i = c_{p,i} \, dT$. Taking into account the formula $(c_p)_{av} = \sum_i c_{p,i} c_i$ for the average specific heat of a mixture, we find

$$di = \sum_i i_i \, dc_i + (c_p)_{av} \, dT$$

Going over to the temperature gradient, we have

$$\operatorname{grad} T = \frac{1}{(c_p)_{av}} \operatorname{grad} i - \frac{1}{(c_p)_{av}} \sum_i i_i \operatorname{grad} c_i$$

Inserting this value into (3.2.14) and introducing for the local values of the Prandtl number $Pr = \mu (c_p)_{av}/\lambda$ and Schmidt number

$Sc = \mu/(\rho\bar{D})$, we obtain the energy equation

$$\frac{di}{dt} = \frac{1}{\rho}\cdot\frac{dp}{dt} + \nu\left[\left(\frac{\partial V_x}{\partial x}\right)^2 + \left(\frac{\partial V_y}{\partial y}\right)^2 + \frac{2}{3}(\operatorname{div} V)^2 + 4\varepsilon_z^2\right] + \frac{1}{\rho}\operatorname{div}\left[\frac{\lambda}{(c_p)_{av}}\operatorname{grad} i\right] + \sum_i i_i \operatorname{div}\left[\bar{D}\left(1 - \frac{Sc}{Pr}\right)\operatorname{grad} c_i\right] + \frac{\varepsilon}{\rho} \qquad (14.2.1)$$

where instead of the ratio Sc/Pr we can introduce $1/Le$, i.e. the reciprocal of the Lewis number.

The energy equation in the form of (14.2.1) expressed in terms of the enthalpy is the *fundamental one in the dynamics of dissociating gases.* In the most general case, the number $Sc < Pr$ ($Le > 1$). The physical meaning of this consists in that diffusion proceeds more intensely than heat conduction, and, consequently, the chemical energy does not transform entirely into heat. In a particular case, when $Pr = Sc$, Eq. (14.2.1) becomes

$$\frac{di}{dt} = \frac{1}{\rho}\cdot\frac{dp}{dt} + \nu\left[\left(\frac{\partial V_x}{\partial x}\right)^2 + \left(\frac{\partial V_y}{\partial y}\right)^2 + \frac{2}{3}(\operatorname{div} V)^2 + 4\varepsilon_z^2\right] + \frac{1}{\rho}\operatorname{div}\left[\frac{\lambda}{(c_p)_{av}}\operatorname{grad} i\right] + \frac{\varepsilon}{\rho} \qquad (14.2.1')$$

Equation (14.2.1′) in form is an equation of energy for flows in which chemical reactions are absent. At $Sc = Pr$, the intensity of heat transfer by heat conduction and diffusion is the same. This corresponds to the fact that part of the chemical energy at the edge of the boundary layer exceeding the chemical energy at the wall temperature completely transforms into heat.

We shall assume for our further investigation that radiation is not taken into consideration, i.e. that $\varepsilon = 0$ in Eq. (14.2.1′). To transform this equation for the flow conditions in the boundary layer, we shall determine the order of magnitude of its terms [see (13.1.3), (13.1.4), etc.].

Unlike the equation of motion, the energy equation includes terms containing the enthalpy i. It is therefore good to additionally consider the estimation of the order of these terms. For this end, we shall use the formula for the stagnation enthalpy in the form

$$i_0 = i + V_x^2/2 \qquad (14.2.2)$$

In a particular case, when $Pr = 1$, the quantity $i_0 = \text{const}$. But for real flow conditions, this enthalpy is a variable quantity because of the thermodynamically irreversible processes caused by chemical reactions and the dissociation of the gas in the boundary layer, i.e. $i_0 \neq I_0$ (where I_0 is the enthalpy of stagnation in isentropic flow).

The order of these quantities is the same ($i_0 \sim I_0 = \text{const}$), however. With this in view, we find that $\partial i/\partial x \sim \partial V_x^2/\partial x$ and $\partial i/\partial y \sim \partial V_x^2/\partial y$, whence the order of the derivatives is $\partial i/\partial x \sim V_\delta^2/L$ and $\partial i/\partial y \sim V_\delta^2/\delta$. These data are used when determining the order of the summand on the right-hand side of Eq. (14.2.1′) containing the enthalpy i. Upon estimating the order of magnitude of all the terms on the right-hand side of (14.2.1′) [except for the first term $(1/\rho)\, dp/dt$] and taking into account that the order of the number $Pr = \mu\,(c_p)_{av}/\lambda \sim 1$, we shall give the results of this estimation directly under each summand of the equation written in the expanded form

$$\frac{di}{dt} = \frac{1}{\rho}\cdot\frac{dp}{dt} + \underbrace{\frac{\mu}{\rho}\left\{\left(\frac{\partial V_x}{\partial x}\right)^2 + \left(\frac{\partial V_y}{\partial y}\right)^2\right.}_{(\mu/\rho)V_\delta^2/L^2}$$

$$+ \underbrace{\frac{2}{3}\left[\left(\frac{\partial V_x}{\partial x}\right)^2 + 2\,\frac{\partial V_x}{\partial x}\cdot\frac{\partial V_y}{\partial y} + \left(\frac{\partial V_y}{\partial y}\right)^2\right]}_{(\mu/\rho)V_\delta^2/L^2}$$

$$\underbrace{+\left(\frac{\partial V_x}{\partial y}\right)^2}_{(\mu/\rho)V_\delta^2/\delta^2} + \underbrace{2\,\frac{\partial V_x}{\partial y}\cdot\frac{\partial V_y}{\partial x}}_{(\mu/\rho)V_\delta^2/L^2} + \underbrace{\left.\left(\frac{\partial V_y}{\partial x}\right)^2\right\}}_{(\mu/\rho)V_\delta^2\delta^2/L^4}$$

$$\underbrace{+\frac{1}{\rho}\left[\frac{\partial}{\partial x}\left(\frac{\mu}{Pr}\cdot\frac{di}{dx}\right)\right.}_{(\mu/\rho)V_\delta^2/L^2} + \underbrace{\left.\frac{\partial}{\partial y}\left(\frac{\mu}{Pr}\,\frac{\partial i}{\partial y}\right)\right]}_{(\mu/\rho)V_\delta^2/\delta^2} \qquad (14.2.3)$$

Considering the right-hand side of Eq. (14.2.3), we can conclude that the terms $\frac{\mu}{\rho}\left(\frac{\partial V_x}{\partial y}\right)^2$ and $\frac{1}{\rho}\cdot\frac{\partial}{\partial y}\left(\frac{\mu}{Pr}\cdot\frac{\partial i}{\partial y}\right)$ have a larger order than the remaining ones. By retaining the terms with a larger order, we obtain the energy equation

$$\frac{di}{dt} = \frac{1}{\rho}\cdot\frac{dp}{dt} + \frac{\mu}{\rho}\left(\frac{\partial V_x}{\partial y}\right)^2 + \frac{1}{\rho}\cdot\frac{\partial}{\partial y}\left(\frac{\mu}{Pr}\cdot\frac{\partial i}{\partial y}\right) \qquad (14.2.4)$$

Let us perform a substitution in (14.2.4) in accordance with (13.1.8):

$$\frac{dp}{dt} = \frac{dp_\delta}{dt} = V_x\frac{dp_\delta}{dx} = -\rho V_x\left[V_x\frac{\partial V_x}{\partial x} + V_y\frac{\partial V_x}{\partial y} - \frac{1}{\rho}\cdot\frac{\partial}{\partial y}\left(\mu\,\frac{\partial V_x}{\partial y}\right)\right]$$

we obtain

$$\frac{di}{dt} = -\frac{V_x}{2}\cdot\frac{\partial V_x^2}{\partial x} - \frac{V_y}{2}\cdot\frac{\partial V_x^2}{\partial y} + \frac{V_x}{\rho}\cdot\frac{\partial}{\partial y}\left(\mu\,\frac{\partial V_x}{\partial y}\right)$$
$$+ \frac{\mu}{\rho}\left(\frac{\partial V_x}{\partial y}\right)^2 + \frac{1}{\rho}\cdot\frac{\partial}{\partial y}\left(\frac{\mu}{Pr}\cdot\frac{\partial i}{\partial y}\right)$$

The first two terms on the right-hand side of the equation can be written as $-\frac{1}{2}\frac{dV_x^2}{dt}$, and the third and fourth ones, as $\frac{1}{\rho}\cdot\frac{\partial}{\partial y}\left(\frac{\mu}{2}\cdot\frac{\partial V_x^2}{\partial y}\right)$. With this in view, we have

$$\rho\frac{d}{dt}\left(i+\frac{V_x^2}{2}\right)=\frac{\partial}{\partial y}\left[\frac{\mu}{Pr}\frac{\partial}{\partial y}\left(i+\frac{V_x^2}{2}\right)\right]+\frac{\partial}{\partial y}\left[\frac{\mu}{2}\left(1-\frac{1}{Pr}\right)\frac{\partial V_x^2}{\partial y}\right] \qquad (14.2.5)$$

Taking into account expression (14.2.2) for the enthalpy i_0 and expanding the total derivative of the left-hand side of (14.2.5), we obtain

$$\rho V_x\frac{\partial i_0}{\partial x}+\rho V_y\frac{\partial i_0}{\partial y}=\frac{\partial}{\partial y}\left(\frac{\mu}{Pr}\cdot\frac{\partial i_0}{\partial y}\right)+\frac{\partial}{\partial y}\left[\frac{\mu}{2}\left(1-\frac{1}{Pr}\right)\frac{\partial V_x^2}{\partial y}\right] \qquad (14.2.5')$$

Let us consider a flow characterized by the quantity with $Pr = 1$. For such a flow, the energy equation has the form

$$\rho V_x\frac{\partial i_0}{\partial x}+\rho V_y\frac{\partial i_0}{\partial y}=\frac{\partial}{\partial y}\left(\mu\frac{\partial i_0}{\partial y}\right) \qquad (14.2.6)$$

If the flow being considered passes over a flat plate for which $dp_\delta/dx = 0$, the equation of motion for the boundary layer by (13.1.8) is

$$\rho V_x\frac{\partial V_x}{\partial x}+\rho V_y\frac{\partial V_x}{\partial y}=\frac{\partial}{\partial y}\left(\mu\frac{\partial V_x}{\partial y}\right) \qquad (14.2.7)$$

We can see that the equations of energy (14.2.6) and motion (14.2.7) are similar. If we go over to the variables

$$\theta=(i_0-i_w)/(i_{0,\delta}-i_w),\quad \overline{V}_x=V_x/V_\delta \qquad (14.2.8)$$

where

$$i_{0,\delta}=i_\delta+V_\delta^2/2 \qquad (14.2.9)$$

then Eqs. (14.2.6) and (14.2.7) become identical because θ and $\overline{V}_x$ satisfy the same boundary conditions: at the wall θ and $\overline{V}_x$ equal zero because $V_x = 0$ and $i_0 = i_w$, while at the edge of the boundary layer, where $V_x = V_\delta$ and $i_0 = i_{0,\delta}$, they equal unity. Therefore, according to the theorem of the uniqueness of a solution, the functions $\overline{V}_x$ and θ should coincide, i.e.

$$(i_0-i_w)/(i_{0,\delta}-i_w)=V_x/V_\delta \qquad (14.2.10)$$

Hence, the condition adopted above ($Pr = 1$) and other assumptions determine the *similarity of the velocity and enthalpy profiles*

in a boundary layer. If the velocity profile is known, the shear stress is

$$\tau_w = \mu_w \left(\frac{\partial V_x}{\partial y}\right)_w = \frac{\mu_w V_\delta}{i_{0,\delta} - i_w}\left(\frac{\partial i_0}{\partial y}\right)_w = \frac{\mu_w V_\delta (c_p)_w}{i_{0,\delta} - i_w}\left(\frac{\partial T}{\partial y}\right)_w$$

Multiplying the numerator and denominator of the right-hand side of the equation by λ_w and assuming that $q_w - q_c = \lambda_w (\partial T/\partial y)_w$, we find

$$\tau_w = \frac{\mu_w V_\delta (c_p)_w}{\lambda_w (i_{0,\delta} - i_w)} q_c$$

Introducing the value of q_c from (14.1.17) and replacing τ_w with $c_{f,x} \rho_\delta V_\delta^2/2$, we obtain

$$c_{f,x} \frac{\rho_\delta V_\delta^2}{2} = \alpha_w \frac{\mu_w V_\delta}{\lambda_w} \cdot \frac{i_r - i_w}{i_{0,\delta} - i_w}$$

Since $\boldsymbol{Pr} = 1$, the recovery coefficient $r = 1$ and

$$i_r = i_\delta + rV_\delta^2/2 = i_\delta + V_\delta^2/2 = i_{0,\delta};$$

$$(i_r - i_w)/(i_{0,\delta} - i_w) = 1$$

Hence, we obtain a relation between the heat-transfer coefficient and friction factor in the following form:

$$\alpha_w = \alpha_x = (c_{f,x}/2)\, \rho_\delta V_\delta \lambda_w/\mu_w \qquad (14.2.11)$$

Expression (14.2.11) yields a formula for the local Nusselt number

$$\boldsymbol{Nu}_w = \boldsymbol{Nu}_x = \alpha_x x/\lambda_w = (c_{f,x}/2)\, \boldsymbol{Re}_x \qquad (14.2.12)$$

where $\boldsymbol{Re}_x = \rho_\delta V_\delta x/\mu_w$.

From (3.1.20) for $\boldsymbol{Pr} = 1$, we find

$$\boldsymbol{St}_w = \boldsymbol{St}_x = \boldsymbol{Nu}_x/\boldsymbol{Re}_x = c_{f,x}/2 \qquad (14.2.13)$$

The relation between the friction and heat-transfer parameters is approximate because actually the numbers $\boldsymbol{Pr}$ and $\boldsymbol{Sc}$ differ from unity. The influence of these parameters can be taken into consideration if we write the expressions for the Nusselt and Stanton numbers as

$$\boldsymbol{Nu}_x = (c_{f,x}/2)\, \boldsymbol{Re}_x f_1(\boldsymbol{Pr}, \boldsymbol{Sc}) \qquad (14.2.14)$$

$$\boldsymbol{St}_x = (c_{f,x}/2)\, f_2(\boldsymbol{Pr}, \boldsymbol{Sc}) \qquad (14.2.15)$$

where f_1 and f_2 are functions of the numbers $\boldsymbol{Pr}$ and $\boldsymbol{Sc}$. From a physical viewpoint, when we take into account the influence of these numbers differing from unity we consider that part of the chemical and kinetic energy transforms into heat. The specific form of the functions f_1 and f_2 is determined by solving the boundary layer equations provided that $\boldsymbol{Pr} \neq 1$ and $\boldsymbol{Sc} \neq 1$ ($\boldsymbol{Le} \neq 1$).

Investigations show that if we adopt the condition $Le = 1$, then $f_1 = Pr^{1/3}$, while by (14.1.20) we also have $f_2 = Pr^{-2/3}$. Accordingly, the local Stanton number is

$$St_x = (c_{f,x}/2)\, Pr^{-2/3} \tag{14.2.16}$$

We find the expression for the Nusselt number from (14.1.20). We can go over from the local Nusselt or Stanton number to the corresponding average values over the length of the plate by excluding the subscript x. We can assume here that the local and average Prandtl numbers are identical.

Formula (14.2.16) is of a major practical significance and reflects the Reynolds analogy, according to which the criterion of heat transfer depends mainly on the same parameter the friction factor depends on, namely, Re_x. The quantity $f_2 = Pr^{-2/3}$ in (14.2.16) is accordingly called the **Reynolds analogy factor.**

Investigations reveal that formula (14.2.15) is also suitable for a turbulent boundary layer, but provided that the friction factor $c_{f,x}$ and the parameter f_2 are evaluated by the corresponding relations for a turbulent boundary layer. Particularly,

$$f_2 = [1 + 2.135 Re_x^{-0.1}\, (Pr - 1)]^{-1} \tag{14.2.17}$$

When calculating the average value of the Stanton number over the length of a plate, the parameter

$$f_2 = [1 + 2.2 Re\, (Pr - 1)]^{-1} \tag{14.2.18}$$

where $Re = V_\delta \rho_\delta L/\mu_w$. Calculations show here that as for a laminar boundary layer, the quantity f_2 in the absence of diffusion in a turbulent boundary layer can be taken equal to $Pr^{-2/3}$ in a first approximation.

The influence of physicochemical transformations on the heat transfer in a boundary layer at high temperatures can be taken into account by using the reference parameters. Particularly, by using the Reynolds analogy, in accordance with (14.2.16) we obtain the following expression for the reference value of the Stanton number:

$$St_x^* = (c_{f,x}^*/2)\, (Pr^*)^{-2/3}, \tag{14.2.19}$$

where $c_{f,x}^* = (c_{f,x}^*)_{com}$ is the friction factor. For a laminar boundary layer, we find this factor from formula (13.6.15), and for a turbulent one, from relation (13.6.22). The reference Prandtl number is calculated from the reference parameters: $Pr^* = c_p^* \mu^*/\lambda^*$.

Hence, the heat flux to a wall is

$$q_x^* = (\alpha_x^*/c_p^*)\, (i_r - i_w) = St_x^* \rho_\delta V_\delta\, (i_r - i_w) \tag{14.2.20}$$

where the reference heat-transfer coefficient is

$$\alpha_x^* = c_p^* q_x^*/(i_r - i_w) = St_x^* c_p^* \rho_\delta V_\delta \tag{14.2.21}$$

It follows from formula (14.2.16) or (14.2.19) that the dimensionless heat-transfer variable changes along a plate in the same way as the local friction factor. Formula (14.2.20) reveals that the specific heat flow varies similarly. Its average value along the length of a plate q_{av} is evidently determined as the average integral value of the local heat fluxes. Calculating according to the reference parameters [see (1.42.20)], we obtain

$$q^*_{av} = \frac{1}{L}\int_0^L q^*_x\,dx = \rho_\delta V_\delta \int_0^1 St^*_x\,(i_r - i_w)\,d\bar{x} \qquad (14.2.22)$$

where $\bar{x} = x/L$.

Assuming that i_w is constant along the plate and replacing St^*_x by formula (14.2.19), we find

$$q^*_{av} = 0.5\rho_\delta V_\delta\,(Pr^*)^{-2/3}\,(i_r - i_w)\int_0^1 c^*_{f,x}\,d\bar{x}$$

The integral on the right-hand side of the equation determines the average friction factor $c^*_{x,f} = (c_{x,f})_{com}$ along the length of the plate computed by formula (13.6.15) for a laminar and by (13.6.22) for a turbulent boundary layer. Consequently, the average heat flux is

$$q^*_{av} = (c^*_{x,f}/2)\;(Pr^*)^{-2/3}\rho_\delta V_\delta\,(i_r - i_w) \qquad (14.2.23)$$

Introducing the concept of the average value of the Stanton number

$$St^*_{av} = (c^*_{x,f}/2)\;(Pr^*)^{-2/3} \qquad (14.2.24)$$

we obtain

$$q^*_{av} = St_{av}\rho_\delta V_\delta\,(i_r - i_w) \qquad (14.2.25)$$

The parameters of heat transfer for a plate can be used to calculate the relevant parameters for a cone in a supersonic flow. They are found by formulas (13.6.34), (13.6.35), (13.6.52), and (13.6.53) relating the friction coefficients (local and average) on a plate and a cone. By multiplying the left-hand and right-hand sides of these formulas by $(Pr^*)^{-2/3}$, we have:

for the local friction factor

$$(c^*_{f,x,c}/2)\;(Pr^*)^{-2/3} = A\;(c^*_{f,x,pl}/2)\;(Pr^*)^{-2/3}$$

for the average value of this factor

$$(c^*_{x,f,c}/2)\;(Pr^*)^{-2/3} = B\;(c^*_{x,f,pl}/2)\;(Pr^*)^{-2/3}$$

where for a laminar boundary layer the coefficients $A = \sqrt{3}$, $B = 2/\sqrt{3}$ and for a turbulent one they are $A = 1.176$, $B = 1.045$.

According to (14.2.19) and (14.2.24), the left-hand sides of these equations determine, respectively, the local and average Stanton

numbers on a cone, and the right-hand ones, on a plate. Hence,

$$St^*_{x,c} = ASt^*_{x,pl} \tag{14.2.26}$$

$$St^*_{av,c} = BSt^*_{al,pl} \tag{14.2.27}$$

By formulas (14.2.26) and (14.2.27), the Stanton number on a cone is calculated according to its value found for a plate from the parameters of the boundary layer on a conical surface. Introducing into the right-hand sides of these formulas the values $St^*_{x,pl} = St^*_x$ and $St^*_{av,pl} = St^*_{av}$ calculated by (14.2.19) and (14.2.24), respectively, we obtain

$$St^*_{x,c} = (Ac^*_{f,x,pl}/2)\ (Pr^*)^{-2/3} \tag{14.2.28}$$

$$St^*_{av,c} = (Bc^*_{x,f,pl}/2)\ (Pr^*)^{-2/3} \tag{14.2.29}$$

The total amount of heat transferred by a gas to a wall in unit time for a cone with a side surface area of $S_{side} = \pi r_{mid} x_c$ (where r_{mid} and x_c are the radius of the base and the length of the generatrix of the cone, respectively) by (14.2.25) and (14.2.28) is

$$Q_c = q^*_{av}\pi r_{mid}x_c = (B/2)\ c^*_{x,f,pl}\ (Pr^*)^{-2/3}\rho_\delta V_\delta\ (i_r - i_m)\ \pi r_{mid}x_c \tag{14.2.30}$$

The formulas for the heat-transfer parameters point to the direct dependence of heating on the skin friction on the surface in the flow. *The shear stress and, therefore, heat transfer are considerably higher for a turbulent boundary layer.* Consequently, to reduce the transfer of heat from a heated gas to the surface in the flow, one must ensure laminarization of the boundary layer, which reduces the friction losses.

14.3. Heat Transfer in a Laminar Boundary Layer on a Curved Surface

Arbitrary Surface Shape

Let us consider the calculation of heat transfer on a curved surface with a laminar boundary layer in which equilibrium dissociation may occur. If we accordingly assume that the number $Le = 1$, which in a first approximation is justified for hypersonic flows, then this calculation, based on the use of formula (14.1.15), reduces to solving a system of equations for a laminar boundary layer including the

equations of continuity (2.4.48'), motion (13.1.8), and energy (14.2.5'):

$$\left.\begin{aligned}
&\frac{\partial(\rho V_x r_0^{\varepsilon})}{\partial x}+\frac{\partial(\rho V_y r_0^{\varepsilon})}{\partial y}=0\\
&\rho\left(V_x\frac{\partial V_x}{\partial x}+V_y\frac{\partial V_x}{\partial y}\right)=-\frac{dp_\delta}{dx}+\frac{\partial}{\partial y}\left(\mu\frac{\partial V_x}{\partial y}\right)\\
&\left(V_x\frac{\partial i_0}{\partial x}+V_y\frac{\partial i_0}{\partial y}\right)=\frac{\partial}{\partial y}\left(\frac{\mu}{Pr}\cdot\frac{\partial i_0}{\partial y}\right)\\
&\qquad+\frac{\partial}{\partial y}\left[\frac{\mu}{2}\left(1-\frac{1}{Pr}\right)\frac{\partial V_x^2}{\partial y}\right]
\end{aligned}\right\}\qquad(14.3.1)$$

Here the continuity equation differs from (2.4.48') in that the radial coordinate r of a point of the boundary layer has been replaced with the coordinate r_0 of a point of the contour in the corresponding boundary layer cross section. In this equation, the value $\varepsilon = 0$ corresponds to a wing airfoil, and $\varepsilon = 1$, to a body of revolution. In the energy equation, as previously, the number $Pr = (c_p)_{av}\mu/\lambda$.

The energy equation in system (14.3.1) was obtained from the general equation (3.2.14) under the assumption that $Sc = Pr$ ($Le = 1$). But there the condition may be fulfilled in accordance with which grad $c_i \neq 1$. It would therefore seem necessary to add to system (14.3.1) diffusion equation (3.2.4) relating the concentration c_i and the rate of formation of each component of the gas mixture. But upon thermodynamic equilibrium, the concentration of each component is uniquely determined by the local values of the pressure and temperature, while the rate of formation of the components $W_{\text{chem},i}$ is sufficiently high to compensate their entrainment because of convection and diffusion. This is why diffusion equation (3.2.4) in the case of equilibrium heat transfer being considered will be superfluous.

The system of equations (14.3.1) is solved with the following boundary conditions:

at the wall (at $y = 0$)

$$V_x = V_y = 0,\ i_0 = i_w,\ \rho = \rho_w,\ i = i_w,\ T = T_w \qquad (14.3.2)$$

at the edge of the layer (at $y \to \infty$)

$$V_x = V_\delta,\ V_y = 0,\ i_0 = i_{0,\delta},\ \rho = \rho_\delta,\ i = i_\delta,\ T = T_\delta \qquad (14.3.3)$$

The following relations also exist for the coefficients μ and λ:

$$\mu = \mu(p, T),\quad \lambda = \lambda(p, T) \qquad (14.3.4)$$

Let us transform Eqs. (14.3.1) by introducing new independent variables and the functions being sought. According to data in [22], we shall introduce variables whose form is close to that of the Do-

rodnitsyn variables [see (13.3.2)]:

$$\eta(x,\ y)=\frac{V_\delta r_0^\varepsilon}{(\tilde{2x})^{1/2}}\int_0^y \rho\,dy,\quad \tilde{x}(x)=\int_0^x \rho_\delta V_\delta \mu_\delta r_0^{2\varepsilon}\,dx \qquad (14.3.5)$$

Using these expressions for the variables, we find the derivatives:

$$\partial\eta/\partial y=\rho V_\delta r_0^\varepsilon/(2\tilde{x})^{1/2},\ d\tilde{x}/dx=\rho_\delta V_\delta \mu_\delta r_0^{2\varepsilon} \qquad (14.3.6)$$

To go over from the coordinates x and y to the coordinates $\tilde{x}$ and η, we must use differentiation operators:

$$\frac{\partial}{\partial y}=\frac{\partial}{\partial\eta}\cdot\frac{\partial\eta}{\partial y}=\frac{\rho V_\delta r_0^\varepsilon}{(\tilde{2x})^{1/2}}\cdot\frac{\partial}{\partial\eta} \qquad (14.3.7)$$

$$\frac{\partial}{\partial x}=\frac{\partial}{\partial\eta}\cdot\frac{\partial\eta}{\partial x}+\frac{\partial}{\partial\tilde{x}}\cdot\frac{\partial\tilde{x}}{\partial x}=\frac{\partial}{\partial\eta}\cdot\frac{\partial\eta}{\partial x}+\rho_\delta V_\delta \mu_\delta r_0^{2\varepsilon}\frac{\partial}{\partial\tilde{x}} \qquad (14.3.8)$$

We shall further introduce the stream function ψ which is determined by relations (2.5.1). Substituting r_0 for r in them, we obtain

$$\partial\psi/\partial y=\rho V_x r_0^\varepsilon,\ \partial\psi/\partial x=-\rho V_y r_0^\varepsilon \qquad (14.3.9)$$

If we introduce the values (14.3.9) into the continuity equation of the system (14.3.1), this equation transforms into an identity: $\partial^2\psi/\partial x\,\partial y-\partial^2\psi/\partial y\,\partial x\equiv 0$. Hence, the introduced stream function ψ satisfies the continuity equation.

Let us see how the other two equations in the system (14.3.1) are transformed with the aid of the stream function. Using (14.3.7), we have

$$\frac{\partial\psi}{\partial y}=\frac{\partial\psi}{\partial\eta}\cdot\frac{\partial\eta}{\partial y}=\frac{\partial\psi}{\partial\eta}\cdot\frac{\rho V_\delta r_0^\varepsilon}{(\tilde{2x})^{1/2}}$$

whence with a view to the first of relations (14.3.9), the derivative

$$\frac{\partial\psi}{\partial\eta}=(2\tilde{x})^{1/2}\frac{V_x}{V_\delta} \qquad (14.3.10)$$

Integrating yields the stream function:

$$\psi=\int_0^\eta (2\tilde{x})^{1/2}\frac{V_x}{V_\delta}\,d\eta$$

By (14.3.5), the expression $(2\tilde{x})^{1/2}$ does not depend on η. Therefore, excluding the constant quantity, we obtain

$$\psi=(2\tilde{x})^{1/2}f(\eta) \qquad (14.3.11)$$

where

$$f(\eta)=\int_0^\eta \frac{V_x}{V_\delta}\,d\eta \qquad (14.3.12)$$

In accordance with this expression,

$$V_x/V_\delta = \partial f/\partial\eta = f' \qquad (14.3.13)$$

Let us use relations (14.3.7) and (14.3.8), expressions (14.3.9) and (14.3.11) for the stream function, and also Eqs. (14.3.12) and (14.3.13) to find the operator that will help us transform the left-hand side of the motion and energy equations of the system (14.3.1):

$$\rho V_x \frac{\partial}{\partial x} + \rho V_y \frac{\partial}{\partial y} = r_0^{-\varepsilon}\left(\frac{\partial\psi}{\partial y}\cdot\frac{\partial}{\partial x} - \frac{\partial\psi}{\partial x}\cdot\frac{\partial}{\partial y}\right)$$

$$= r_0^{-\varepsilon}\left(\frac{\partial\psi}{\partial\eta}\cdot\frac{\partial}{\partial\tilde{x}} - \frac{\partial\psi}{\partial\tilde{x}}\cdot\frac{\partial}{\partial\eta}\right)\frac{\partial\eta}{\partial y}\cdot\frac{\partial\tilde{x}}{\partial x}$$

Here we determine the derivatives $\partial\psi/\partial\eta$ and $\partial\psi/\partial\tilde{x}$ by differentiating (14.3.11):

$$\frac{\partial\psi}{\partial\eta} = (2\tilde{x})^{1/2}\frac{\partial f}{\partial\eta}; \quad \frac{\partial\psi}{\partial\tilde{x}} = (2\tilde{x})^{-1/2}f + (2\tilde{x})^{1/2}\frac{\partial f}{\partial\tilde{x}} \qquad (14.3.14)$$

After inserting these quantities into the expression for the operator, and also replacing the derivatives $\partial\eta/\partial y$ and $\partial\tilde{x}/\partial x$ with their values from (14.3.6), we obtain

$$\rho V_x \frac{\partial}{\partial x} + \rho V_y \frac{\partial}{\partial y}$$

$$= \rho\rho_\delta V_\delta^2 \mu_\delta r_0^{2\varepsilon}\left(\frac{\partial f}{\partial\eta}\cdot\frac{\partial}{\partial\tilde{x}} - \frac{f}{2\tilde{x}}\cdot\frac{\partial}{\partial\eta} - \frac{\partial f}{\partial\tilde{x}}\cdot\frac{\partial}{\partial\eta}\right) \qquad (14.3.15)$$

The right-hand sides of the motion and energy equations (14.3.1) include expressions of the form

$$\frac{\partial}{\partial y}\left(h\frac{\partial}{\partial y}\right) \qquad (14.3.16)$$

where $h(x, y)$ is a function of the coordinates x and y. In the new variables η and $\tilde{x}$, operator (14.3.16) acquires the form

$$\frac{\partial}{\partial y}\left(h\frac{\partial}{\partial y}\right) = \frac{\partial}{\partial\eta}\left(h\frac{\partial}{\partial\eta}\cdot\frac{\partial\eta}{\partial y}\right)\frac{\partial\eta}{\partial y}$$

or with a view to the value (14.3.6) for the derivative $\partial\eta/\partial y$,

$$\frac{\partial}{\partial y}\left(h\frac{\partial}{\partial y}\right)\frac{\rho V_\delta^2 r_0^{2\varepsilon}}{2\tilde{x}}\cdot\frac{\partial}{\partial\eta}\left(\rho h\frac{\partial}{\partial\eta}\right) \qquad (14.3.17)$$

Let us use operators (14.3.15) and (14.3.17) to transform the equation of motion:

$$\rho\rho_\delta V_\delta^2 \mu_\delta r_0^{2\varepsilon} \left(\frac{\partial f}{\partial \eta} \cdot \frac{\partial V_x}{\partial \tilde{x}} - \frac{f}{2\tilde{x}} \cdot \frac{\partial V_x}{\partial \eta} - \frac{\partial f}{\partial \tilde{x}} \cdot \frac{\partial V_x}{\partial \eta} \right)$$

$$= -\frac{dp_\delta}{dx} + \frac{\rho V_\delta^2 r_0^{2\varepsilon}}{2\tilde{x}} \cdot \frac{\partial}{\partial \eta} \left(\rho\mu \frac{\partial V_x}{\partial \eta} \right)$$

Here the derivative dp_δ/dx can be found by the equation

$$\frac{dp_\delta}{dx} = -\rho_\delta V_\delta \cdot \frac{dV_\delta}{d\tilde{x}} \frac{d\tilde{x}}{dx}$$

or with a view to the value (14.3.6), for $d\tilde{x}/dx$,

$$\frac{dp_\delta}{dx} = -\rho_\delta^2 V_\delta^2 \mu_\delta r_0^{2\varepsilon} \frac{dV_\delta}{d\tilde{x}} \tag{14.3.18}$$

Taking this into account and substituting in accordance with (14.3.13), we have

$$V_x = V_\delta \, \partial f/\partial \eta \tag{14.3.13'}$$

we obtain

$$\frac{\partial f}{\partial \eta} \cdot \frac{\partial}{\partial \tilde{x}} \left(V_\delta \frac{\partial f}{\partial \eta} \right) - \frac{V_\delta f}{2\tilde{x}} \cdot \frac{\partial^2 f}{\partial \eta^2} - V_\delta \frac{\partial f}{\partial \tilde{x}} \cdot \frac{\partial^2 f}{\partial \eta^2}$$

$$= \frac{\rho_\delta}{\rho} \cdot \frac{dV_\delta}{d\tilde{x}} + \frac{V_\delta}{2\tilde{x}\rho_\delta \mu_\delta} \cdot \frac{\partial}{\partial \eta} \left(\rho\mu \frac{\partial^2 f}{\partial \eta^2} \right)$$

Since the derivative

$$\frac{\partial}{\partial \tilde{x}} \left(V_\delta \frac{\partial f}{\partial \eta} \right) = \frac{dV_\delta}{d\tilde{x}} \cdot \frac{\partial f}{\partial \eta} + V_\delta \frac{\partial^2 f}{\partial \tilde{x} \, \partial \eta}$$

we obtain a transformed equation of motion:

$$2\tilde{x} \left(\frac{\partial f}{\partial \eta} \cdot \frac{\partial^2 f}{\partial \tilde{x} \, \partial \eta} - \frac{\partial f}{\partial \tilde{x}} \cdot \frac{\partial^2 f}{\partial \eta^2} \right) = f \frac{\partial^2 f}{\partial \eta^2}$$

$$+ \frac{2\tilde{x}}{V_\delta} \cdot \frac{dV_\delta}{d\tilde{x}} \left[\frac{\rho_\delta}{\rho} - \left(\frac{\partial f}{\partial \eta} \right)^2 \right] + \frac{\partial}{\partial \eta} \left(\overline{\rho\mu} \frac{\partial^2 f}{\partial \eta^2} \right) \tag{14.3.19}$$

where

$$\overline{\rho\mu} = \rho\mu/(\rho_\delta \mu_\delta) \tag{14.3.20}$$

Now with the aid of the same operators (14.3.15) and (14.3.17), and also of expression (14.3.13'), we can write the energy equation

as follows:

$$\rho\rho_\delta V_\delta^2 \mu_\delta r_0^{2\varepsilon}\left(\frac{\partial f}{\partial \eta}\cdot\frac{\partial i_0}{\partial \tilde{x}}-\frac{f}{2\tilde{x}}\cdot\frac{\partial i_0}{\partial \eta}-\frac{\partial f}{\partial \tilde{x}}\cdot\frac{\partial i_0}{\partial \eta}\right)$$

$$=\frac{\rho V_\delta^2 r_0^{2\varepsilon}}{2\tilde{x}}\cdot\frac{\partial}{\partial \eta}\left(\frac{\rho\mu}{Pr}\cdot\frac{\partial i_0}{\partial y}\right)$$

$$+\frac{\rho V_\delta^4 r_0^{2\varepsilon}}{2\tilde{x}}\frac{\partial}{\partial \eta}\left[\rho\mu\left(1-\frac{1}{Pr}\right)\frac{\partial f}{\partial \eta}\cdot\frac{\partial^2 f}{\partial \eta^2}\right]$$

For further transformations, let us introduce the dimensionless variable

$$g(\eta) = i_0/i_{0,\delta} \tag{14.3.21}$$

that determines the ratio of the stagnation enthalpy at a point of a boundary layer cross section $i_0 = i + V_x^2/2$ to its value $i_{0,\delta} = i_\delta + V_\delta^2/2$ at the border of the layer. Hence, having in view that

$$\frac{\partial i_0}{\partial \eta} = i_{0,\delta}\frac{\partial g}{\partial \eta},\quad \frac{\partial i_0}{\partial \tilde{x}} = \frac{\partial (g i_{0,\delta})}{\partial \tilde{x}} = i_{0,\delta}\frac{\partial g}{\partial \tilde{x}} + g\frac{\partial i_{0,\delta}}{\partial \tilde{x}}$$

we have

$$2\tilde{x}\left(\frac{\partial f}{\partial \eta}\cdot\frac{\partial g}{\partial \tilde{x}}-\frac{\partial f}{\partial \tilde{x}}\cdot\frac{\partial g}{\partial \eta}\right) = f\frac{\partial g}{\partial \eta}+\frac{\partial}{\partial \eta}\left(\frac{\overline{\rho\mu}}{Pr}\cdot\frac{\partial g}{\partial \eta}\right)$$

$$+\frac{V_\delta^2}{i_{0,\delta}}\frac{\partial}{\partial \eta}\left[\overline{\rho\mu}\left(1-\frac{1}{Pr}\right)\frac{\partial f}{\partial \eta}\cdot\frac{\partial^2 f}{\partial \eta^2}\right]-\frac{2\tilde{x}g}{i_{0,\delta}}\cdot\frac{\partial i_{0,\delta}}{\partial \tilde{x}}\cdot\frac{\partial f}{\partial \eta}, \tag{14.3.22}$$

The functions $f(\eta)$ and $g(\eta)$, which are solutions of the system of equations (14.3.19) and (14.3.22), must satisfy the following boundary conditions:

at the wall when $\eta = 0$ ($y = 0$)

$$f(0) = (\partial f/\partial \eta)_{\eta=0} = 0,\ g(0) = g_w \tag{14.3.23}$$

at the edge of the layer at $\eta \to \infty$ ($y \to \infty$)

$$f(\infty) = 0,\ (\partial f/\partial \eta)_{\eta\to\infty} = 1,\ g(\infty) = 1,\ (\partial g/\partial \eta)_{\eta\to\infty} = 0 \tag{14.3.24}$$

The above system of equations (14.3.19) and (14.3.22) can be seen to include complicated non-linear partial differential equations. Although in this form they are simpler than the initial equations (14.3.1), their solution nevertheless involves great difficulties. But in the above form, the system of equations is very convenient because it allows one to find a large class of problems that are of a considerable practical interest, for which under certain assumptions this system can be reduced to a system of "similar" ordinary differential equations.

The solutions of such a system, called **similar**, have the property that the required functions f and g will depend only on the single variable η. This property allows us to simplify Eqs. (14.3.19) and (14.3.22) because their left-hand sides equal zero since $dg/d\tilde{x} = df/d\tilde{x} = 0$. As a result of simplification, the equations acquire the form

$$ff'' + \frac{2\tilde{x}}{V_\delta} \cdot \frac{dV_\delta}{d\tilde{x}} \left(\frac{\rho_\delta}{\rho} - f'^2 \right) + (\overline{\rho\mu} f'')' = 0 \qquad (14.3.25)$$

$$fg' + \left(\frac{\overline{\rho\mu}}{Pr} g' \right)' + \frac{V_\delta^2}{i_{0,\delta}} \left[\overline{\rho\mu} \left(1 - \frac{1}{Pr} f' f'' \right) \right]' - \frac{2\tilde{x}_g}{i_{0,\delta}} \cdot \frac{di_{0,\delta}}{d\tilde{x}} f' = 0 \qquad (14.3.26)$$

where the primes signify differentiation with respect to the variable η. This system has similar solutions if the following conditions are fulfilled:

(a) $\frac{\tilde{x}}{V_\delta} \cdot \frac{dV_\delta}{d\tilde{x}} = \text{const}$, $\frac{\tilde{x}}{i_{0,\delta}} \cdot \frac{di_{0,\delta}}{d\tilde{x}} = \text{const}$, $\frac{V_\delta^2}{i_{0,\delta}} = \text{const}$;

(b) the ratio ρ_δ/ρ, the number Pr, and the quantity $\overline{\rho\mu}$ are functions of η or are constants;

(c) the function g is uniform everywhere at the wall, i.e. $g(0) = g_w = \text{const}$, which corresponds to a constant surface temperature.

Except for particular cases (a uniform external flow over a plate, wedge or cone attended by an attached shock wave), all these conditions of similarity are never fulfilled simultaneously even if a constant surface temperature is retained. The density ratio ρ_δ/ρ, the Prandtl number, and the quantity $\overline{\rho\mu} = \rho\mu/(\rho_\delta\mu_\delta)$ are functions not only of the enthalpy ratio i/i_δ, but also of the enthalpy i_δ and pressure p_δ because they affect the dissociation of the gas. We can note another particular case of flow for which the solution will be a similar one, namely, the flow over a small part of a blunted surface near the stagnation point where the enthalpy i_δ and pressure p_δ remain almost unchanged.

Is it possible to obtain a similar solution that would relate to the major part of a curved surface? Such a solution can be obtained in the following two cases that are of a practical interest: (1) upon a slight change in the external flow parameters; and (2) upon strong cooling of the surface in the flow, i.e. when $g_w = i_w/i_{0,\delta} \ll 1$.

In the first case, the velocity gradient

$$\beta = \frac{2\tilde{x}}{V_\delta} \cdot \frac{dV_\delta}{dx} = \frac{2d \ln V_\delta}{d \ln \tilde{x}} \qquad (14.3.27)$$

and the quantity $V_\delta^2/i_{0,\delta}$ are assumed to be constant along the entire surface. We simultaneously assume that $di_{0,\delta}/d\tilde{x} = 0$, which cor-

responds to the condition of total energy conservation in the external flow ($i_{0,\delta} = i_\delta + V_\delta^2/2 = \text{const}$). In addition, $\overline{\rho\mu}$ and the number Pr are considered to be constant, while the density ratio $\rho_\delta/\rho = T/T_\delta = i/i_\delta$ is considered only as a function of η.

The second case is characterized by the fact that the wall temperature is very low, i.e. $T_w/T_\delta \ll 1$, and, consequently, $\rho_w/\rho_\delta \gg 1$. The density at the wall increases with a diminishing wall temperature not only because of the removal of heat (with the use of special cooling means for this purpose), but also because of the increase in the degree of dissociation upon hypersonic flow.

Since the longitudinal pressure gradient depends on the density ρ_δ on the edge ($dp_\delta/dx = -\rho_\delta V_\delta\, dV_\delta/dx$) and is constant for a given layer cross section, then at $\rho_w \gg \rho_\delta$, the velocity profile at the wall is much less sensitive to the pressure gradient than with a low temperature difference across the boundary layer. The explanation is that a greatly compressed gas is not so liable to a change in the nature of the flow upon a pressure drop. Therefore, in Eq. (14.3.25), we can disregard the term including the pressure gradient β (14.3.27), and write this equation as

$$ff'' + (\overline{\rho\mu}f'')' = 0 \qquad (14.3.28)$$

A comparison of Eqs. (14.3.25) and (14.3.26) reveals that the velocity gradient affects the distribution of the stagnation enthalpies to a still lesser extent. Indeed, examining (14.3.25), we can establish that the function f determined from this equation depends (even though only slightly) on the gradient β that is present in the equation in the explicit form. At the same time, the function $g = i_0/i_{0,\delta}$ is found from Eq. (14.3.26), where the quantity β is absent in the explicit form. The dependence of g on the gradient manifests itself in terms of a slight dependence of the function f on β. Hence, the system of equations (14.3.25) and (14.3.26), simplified in accordance with the condition $\rho_w/\rho_\delta \gg 1$, is more preferable for calculating the heat-transfer parameters determined by the derivative g' than for calculating the friction parameters (the function f').

Equation (14.3.26) can be simplified bearing in mind that the total enthalpy of the free flow is constant ($di_{0,\delta}/dx = 0$). The value of $V_\delta^2/i_{0,\delta}$ on blunted bodies varies from zero at the stagnation point where $V_\delta = 0$ to the value $V_\delta^2/(i_\delta + V_\delta^2/2) \approx 2$ (on flow sections where the velocities V_δ are such that $i_\delta \ll V_\delta^2/2$). Taking this into account and noting that $Pr \approx 0.7$-1, we conclude that the third term in (14.3.26) is numerically small.

Discarding the third and fourth terms in this equation, we obtain

$$fg' + \left(\frac{\overline{\rho\mu}}{Pr}\, g'\right)' = 0 \qquad (14.3.29)$$

The function $\overline{\rho\mu}$ can be estimated with the aid of the equations of state $p = R_0\rho T/m$ and $p = p_\delta = R_0\rho_\delta T_\delta/m_\delta$ (where R_0 is the universal gas constant):

$$\overline{\rho\mu} = \frac{\rho\mu}{\rho_\delta\mu_\delta} = \frac{T_\delta}{T}\cdot\frac{m}{m_\delta}\cdot\left(\frac{T}{T_\delta}\right)^n = \left(\frac{T_\delta}{T}\right)^{1-n}\frac{m}{m_\delta} \qquad (14.3.30)$$

Replacing T and m here with their reference values T^* and m^*, we have

$$\overline{\rho\mu} = \left(\frac{T_\delta}{T^*}\right)^{1-n}\frac{m^*}{m_\delta} \qquad (14.3.31)$$

Let us see how the heat flux depends on the quantity $\overline{\rho\mu}$. Using the Fourier law, and also expression (14.3.6) for the derivative $\partial\eta/\partial y$, we find

$$q_x = \frac{\lambda_w}{(c_p)_w}\left(\frac{\partial i}{\partial y}\right)_w = \frac{\lambda_w}{(c_p)_w}\left(\frac{\partial i_0}{\partial\eta}\right)_w\left(\frac{\partial\eta}{\partial y}\right)_w$$
$$= \frac{\lambda_w g'(0)\,\rho_w V_\delta r_0^\varepsilon i_{0,\delta}}{(c_p)_w\,(2\tilde{x})^{1/2}} \qquad (14.3.32)$$

where by (14.3.5)

$$(2\tilde{x})^{1/2} = \left[2\int_0^x \rho_\delta\mu_\delta V_\delta r_0^{2\varepsilon}dx\right]^{1/2} = \left[2\int_0^x \frac{\rho_w\mu_w}{(\overline{\rho\mu})_w}V_\delta r_0^{2\varepsilon}dx\right]^{1/2} \qquad (14.3.33)$$

We can see that in expression (14.3.33) determining the specific heat flow, the quantity $\overline{\rho\mu} = (\overline{\rho\mu})_w$ has the power 1/2. This diminishes the total error introduced by an approximate choice of this quantity.

Investigations show that at $T_w/T_\delta \ll 1$ and $n = 0.75$ or 0.8, the quantity $\overline{\rho\mu}$ is close to unity. Therefore, we can assume in our calculations that $\overline{\rho\mu} \approx 1$, i.e. consider that

$$\rho\mu \approx \rho_\delta\mu_\delta \approx \rho_w\mu_w \qquad (14.3.34)$$

Hence, we obtain a system of equations of the boundary layer:

$$ff'' + f''' = 0 \qquad (14.3.35)$$
$$Pr\,fg' + g'' = 0 \qquad (14.3.36)$$

These equations reflect local similarity, when if Pr = const, the dimensionless velocity V_x/V_δ and the enthalpy $i_0/i_{0,\delta}$ are the same at points of different flows where the parameter η is the same, it being a **similarity criterion.**

By integrating the system of ordinary differential equations (14.3.35) and (14.3.36) at the above boundary conditions, we can find similar solutions for the functions $f(\eta)$ and $g(\eta)$, and also, particularly, for the derivative $g'(\eta)$. Double integration of (14.3.36) yields

$$g(\eta) - g(0) = g'(0) \int_0^{\eta} \exp\left(-\int_0^{\eta} \boldsymbol{Pr} f d\eta\right) d\eta \qquad (14.3.37)$$

Numerical calculations show that for $\eta \to \infty$ the value of the integral is approximated by $(0.5\boldsymbol{Pr}^{1/3})^{-1}$. Therefore, noting that $g(\eta) = i_0/i_{0,\delta} \to q_w$ at $\eta \to 0$, we find

$$g'(0) = \frac{1}{i_{0,\delta}}\left(\frac{\partial i_0}{\partial \eta}\right)_w = \frac{1}{i_{0,\delta}}\left(\frac{\partial i}{\partial \eta}\right)_w = 0.5\boldsymbol{Pr}^{1/3}[1 - g(0)] \qquad (14.3.38)$$

where $g(0) = g_w = i_w/i_{0,\delta}$ and $\boldsymbol{Pr} = (c_p)_w \mu_w/\lambda_w$.

Introducing the value obtained for $g'(0)$ into (14.3.32), and also taking into account that $g(0) = g_w = i_w/i_{0,\delta}$, we obtain

$$q_x = 0.5 \frac{\lambda_w \rho_w V_\delta r_0^\varepsilon \boldsymbol{Pr}^{1/3}}{(c_p)_w (2\tilde{x})^{1/2}} (i_{0,\delta} - i_w)$$

We insert into this equation the value of $\lambda_w/(c_p)_w = \mu_w/\boldsymbol{Pr}$, then replace $\rho_w \mu_w$ with $\rho_\delta \mu_\delta$ and $i_{0,\delta}$ with the recovery enthalpy i_r [bearing in mind the use of this enthalpy in Eq. (14.1.15) for the heat flux]:

$$q_x = 0.5\boldsymbol{Pr}^{-2/3} \frac{\rho_\delta V_\delta r_0^\varepsilon}{(2\tilde{x})^{1/2}} (i_r - i_w) \qquad (14.3.39)$$

Investigations reveal that in such a form this equation allows us to determine the heat transfer in a first approximation when cooling does not ensure a sufficiently low wall temperature.

By using an equation of state, in (14.3.39) it is convenient to go over to the dimensionless parameter

$$\frac{\rho_\delta \mu_\delta}{\rho_0' \mu_0'} = \frac{p_\delta}{p_0'} \cdot \frac{\mu_\delta}{\mu_0'} \cdot \frac{m_\delta}{m_0} \cdot \frac{T_0'}{T_\delta} \qquad (14.3.40)$$

Introducing the notation

$$\omega_\delta = \mu_\delta m_\delta / T_\delta, \quad \omega_0' = \mu_0' m_0 / T_0' \qquad (14.3.41)$$

we can write this dimensionless parameter in the form

$$\frac{\rho_\delta \mu_\delta}{\rho_0' \mu_0'} = \frac{p_\delta}{p_0'} \cdot \frac{\omega_\delta}{\omega_0'} \qquad (14.3.42)$$

Here the parameters p_0', ρ_0', μ_0', and m_0 [see (14.3.40)] relate to the edge of the boundary layer at the stagnation point of the blunted surface. Inserting the value of ρ_δ from (14.3.42) into (14.3.39) and

taking relation (14.3.5) into account, we find

$$q_x = 0.5Pr^{-2/3}\sqrt{\rho_0'\mu_0' V_\infty}F(x)(i_r - i_w) \qquad (14.3.43)$$

where the function

$$F(x) = \frac{\sqrt{2}}{2}\cdot\frac{p_\delta}{p_0'}\cdot\frac{\omega_\delta}{\omega_0'}\frac{V_\delta}{V_\infty}r_0^\varepsilon\left(\int_0^x \frac{p_\delta}{p_0'}\frac{V_\delta}{V_\infty}\frac{\omega_\delta}{\omega_0'}r_0^{2\varepsilon}dx\right)^{-1/2} \qquad (14.3.44)$$

The quantity ω_δ/ω_0' at $n = 0.75$ to 0.8 is only slightly greater than unity.

If we take into consideration that the ratio ω_δ/ω_0' enters expression (14.3.44) for the heat transfer to the power 1/2, then the error as a result of the substitution $\omega_\delta/\omega_0' = 1$ will be only several per cent. Accordingly, we shall write function (14.3.44) in the form

$$F(x) = \frac{\sqrt{2}}{2}\cdot\frac{p_\delta}{p_0'}\frac{V_\delta}{V_\infty}r_0^\varepsilon\left(\int_0^x \frac{p_\delta}{p_0'}\frac{V_\delta}{V_\infty}r_0^{2\varepsilon}dx\right)^{-1/2} \qquad (14.3.44')$$

Hence, to determine the specific heat flow at a point on a surface of a given shape, we must know the distribution of the velocity and pressure over its entire part between the stagnation point and the point being considered. Particularly, to calculate heat transfer on the surface near the stagnation point, we can assume that

$$p_\delta/p_0' \approx 1 \text{ and } r_0 \approx x \qquad (14.3.45)$$

and also consider in accordance with Eq. (10.4.74) with V_δ substituted for V_x, that

$$V_\delta = \tilde{\lambda}x \qquad (14.3.46)$$

where the velocity gradient $\tilde{\lambda}$ is found with the aid of one of the expressions (10.4.72) or (10.4.78). With a view to (14.3.45) and (14.3.46), the function

$$F = \frac{\sqrt{2}}{2}\cdot\frac{\tilde{\lambda}x}{V_\infty}x^\varepsilon\left(\int_0^x \frac{\tilde{\lambda}x}{V_\infty}x^{2\varepsilon}dx\right)^{-1/2}$$

Integration yields

$$F = F_0 = \sqrt{(\tilde{\lambda}/V_\infty)(\varepsilon+1)} \qquad (14.3.47)$$

Inserting this value into (14.3.43) and introducing the symbol $q_x = q_0$ for the heat flux at the stagnation point, we find

$$q_0 = 0.5Pr^{-2/3}\sqrt{\rho_0'\mu_0'\tilde{\lambda}(\varepsilon+1)}(i_r - i_w) \qquad (14.3.48)$$

It is convenient to evaluate the heat transfer q_x at an arbitrary point of the surface with the aid of a dimensionless variable determined

from (14.3.43) and (14.3.48) in the form

$$q_x/q_0 = \sqrt{V_\infty/[\tilde{\lambda}(\varepsilon+1)]}\,F(x) \qquad (14.3.49)$$

Hence, the heat flux at an arbitrary point of a curved surface depends directly on its value at the stagnation point. It is very important to determine the value of q_0 because it corresponds to the point on the surface in the flow with the highest thermal factor. The nature of the change in the specific heat flow along the trajectory is shown in Fig. 14.1.3 ($q_0 = q_c$). We can note that its maximum value is reached at a relatively low altitude ($H \approx 15$ km).

Processing of the results of numerical calculations and also of experimental data for hypersonic velocities allows us to obtain an approximate formula for the heat-transfer rate (W/m^2) at the stagnation point (see [1]):

$$q_0 = q_{0,\,\mathrm{sph}} = (1.3 \times 10^8/\sqrt{R_n})\sqrt{\rho_{\infty,\,H}/\rho_{\infty,\,\mathrm{ter}}}\,(V_\infty/V_0)^{3.25}(1 - i_w/i_r) \qquad (14.3.48')$$

where $V_0 = 7.93 \times 10^3$ m/s is the orbital velocity.

The recovery enthalpy can be taken equal to the stagnation enthalpy. A glance at the above relation reveals that heat transfer varies inversely proportional to the radius of the spherical surface ($q_{0,\mathrm{sph}} \sim \sim 1/\sqrt{R_n}$, where R_n is expressed in metres). Accordingly, the inflow of heat to the stagnation point can be reduced by increasing this radius. The smallest value of q_0 is achieved at the centre of a flat nose. At this point, the local velocity gradient whose value determines the specific heat flow is not large. By experimental data, for a flat nose

$$q_{0,n} = (0.55 \pm 0.05)\,q_{0,\,\mathrm{sph}} \qquad (14.3.48'')$$

The value of $q_{0,n}$ can also be found approximately from (14.3.48') according to the value of the equivalent radius R_n^{eq} (see Sec. 10.4.).

Hemisphere

Let us consider the use of Eq. (14.3.49) for calculating the heat flux on a hemispherical surface. Assuming in formula (14.3.44) that

$$\varepsilon_\lambda = 1,\ dx = R_n\,d\varphi,\quad r_0 = R_n \sin\varphi \qquad (14.3.50)$$

and also taking into account that by (10.4.74') and (10.4.76) on the major part of a spherical nose

$$V_\delta = \tilde{\lambda} R_n \varphi \qquad (14.3.51)$$

$$\frac{p_\lambda}{p_0'} = \cos^2\varphi + \frac{p_\infty}{p_0'}\sin^2\varphi \qquad (14.3.52)$$

we find

$$F(\varphi)=\frac{\sqrt{2}}{2}\cdot\frac{\left(\cos^2\varphi+\frac{p_\infty}{p_0'}\sin^2\varphi\right)\widetilde{\lambda}R_n^2\,\varphi\sin\varphi}{\left[\int\limits_0^\varphi\left(\cos^2\varphi+\frac{p_\infty}{p_0'}\sin^2\varphi\right)\widetilde{\lambda}R_n^4V_\infty\varphi\sin^2\varphi\,d\varphi\right]^{1/2}}$$

Let us introduce this expression into formula (14.3.49) in which we assume that $\varepsilon=1$:

$$\frac{q_x}{q_0}=\frac{1}{2}\cdot\frac{\varphi\sin\varphi\left(\cos^2\varphi+\frac{p_\infty}{p_0'}\sin^2\varphi\right)}{\left[\int\limits_0^\varphi\left(\cos^2\varphi+\frac{p_\infty}{p_0'}\sin^2\varphi\right)\varphi\sin^2\varphi\,d\varphi\right]^{1/2}}$$

Introducing the notation

$$D(\varphi)=4\int\limits_0^\varphi\left(\cos^2\varphi+\frac{p_\infty}{p_0'}\sin^2\varphi\right)\varphi\sin^2\varphi d\varphi \qquad (14.3.53)$$

we obtain

$$\frac{q_x}{q_0}=\varphi\sin\varphi\left(\cos^2\varphi+\frac{p_\infty}{p_0'}\sin^2\varphi\right)[D(\varphi)]^{-1/2} \qquad (14.3.54)$$

By formula (14.3.54), as by other similar relations, the distribution of the heat fluxes should be calculated for flow conditions at high supersonic velocities. In these conditions, the inequality $p_\infty/p_0'<$ <0.03 or 0.04 must be satisfied. Approximately the same results are obtained if we use the empirical relation

$$q_x/q_0=0.2\,(1+4\cos^2\varphi) \qquad (14.3.54')$$

The change in the quantity q_x/q_0 is shown in Fig. 14.3.1. The data in this figure were obtained for the condition that at every point of the spherical surface the wall temperature is constant and sufficiently low ($T_w/T_\delta\ll 1$). These data correspond to theoretical and experimental results according to which heat transfer reaches a maximum at the stagnation point and monotonically decreases on the remote parts of a hemisphere because of lowering of the pressure and density.

We can use the known distribution of the specific heat flows to find their total value for a part or the total surface of a hemisphere (Fig. 14.3.1):

$$Q=\int\limits_{(S)}q_x dS=2\pi R_n^2 q_0\int\limits_0^\varphi(q_x/q_0)\sin\varphi\,d\varphi$$

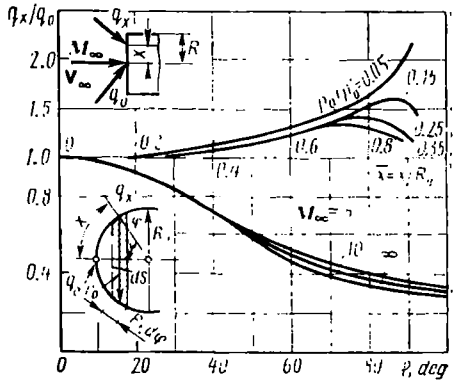

Fig. 14.3.1
Change in the ratio of the specific heat flows for a sphere and a flat nose (a laminar boundary layer)

For a part of the surface, the angle $\varphi < \pi/2$, while for the entire hemisphere we must assume that $\varphi = \pi/2$. Introducing the value of q_x/q_0 from (14.3.54′), we can obtain a simple relation for calculating the total heat transfer on a spherical surface. For $\varphi \neq \pi/2$, its magnitude $Q = Q_0\bar{q}$, where $Q_0 = 2\pi R_n^2 q_0$ is the heat flux calculated for a hemisphere from the specific heat flow at the stagnation point; the coefficient $\bar{q} = 0.2 \int_0^{\varphi} (1 + 4\cos^2\varphi)\sin\varphi\, d\varphi$. This coefficient varies within the limits from 0 to 1.

Blunt-Nosed Cone

Let us consider the calculation of the heat flux on the surface of a cone-sphere (Fig. 14.3.2). We shall assume that on the conical surface the inviscid parameters of the gas are constant and equal the corresponding values at the tip of a spherical nose. Particularly, the velocity

$$V_\delta = \tilde{\lambda} R_n \varphi_c = \tilde{\lambda} R_n (\pi/2 - \beta_c) \qquad (14.3.55)$$

where β_c is the semiapex angle.

The pressure ratio is

$$\frac{p_\delta}{p_0'} = \cos^2\varphi_c + \frac{p_\infty}{p_0'}\sin^2\varphi_c = \sin^2\beta_c + \frac{p_\infty}{p_0'}\cos^2\beta_c \qquad (14.3.56)$$

For one of the geometric parameters, namely, the polar coordinate of arbitrary point A on the surface of the cone (Fig. 14.3.2), we have

$$r_0 = x_c\cos\varphi_c = x_c\sin\beta_c \qquad (14.3.57)$$

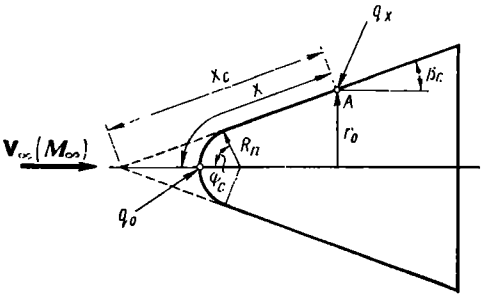

Fig. 14.3.2
Cone-sphere

where x_c is the distance along the surface measured from the imaginary apex of a sharp-nosed cone to the point being considered:

$$x_c = x - R_n\varphi_c + R_n \tan \varphi_c \qquad (14.3.58)$$

or, taking into account that $\varphi_c = \pi/2 - \beta_c$,

$$x_c = x - R_n (\pi/2 - \beta_c) + R_n \cot \beta_c \qquad (14.3.58')$$

Let us find the values of the function $F(x)$. Evidently, the integral in (14.3.44') between the limits 0 and x (where x is the curvilinear coordinate of point A) is found as the sum of two integrals: one between the limits 0 and $x = R_n\varphi_c = R_n(\pi/2 - \beta_c)$ (or 0 and φ_c for angles), and the other between the limits $\varphi_c R_n$ and x. One integral obviously corresponds to the value of the heat flux at the end of the spherical part (or, which is the same, at the origin of the conical surface). The distribution of the heat flux on this part is the same as the distribution obtained above for a hemisphere. With this in view, we find the function $F(x)$ (14.3.44') in the following form:

$$F(x) = \frac{\sqrt{2}}{2}\left(\cos^2\varphi_c + \frac{p_\infty}{p_0'}\sin^2\varphi_c\right)\tilde{\lambda} R_n\varphi_c$$

$$\times \cos\varphi_c x_c V_\infty^{-1/2} \Big/ \Big[\int_0^{\varphi_c}\left(\cos^2\varphi + \frac{p_\infty}{p_0'}\sin^2\varphi\right)\tilde{\lambda} R_n^4 \varphi \sin^2\varphi\, d\varphi$$

$$+ \int_{R_n\varphi_c}^{x}\left(\cos^2\varphi_c + \frac{p_\infty}{p_0'}\sin^2\varphi_c\right)\tilde{\lambda} R_n\varphi_c r_0^2 dx\Big]^{1/2} \qquad (14.3.59)$$

The integral calculated for the straight generatrix of the cone with a view to (14.3.58), can be written as

$$\int_{R_n\varphi_c}^{x}\left(\cos^2\varphi_c + \frac{p_\infty}{p_0'}\sin^2\varphi_c\right)\tilde{\lambda} R_n\varphi_c r_0^2 dx$$

$$= \left(\cos^2 \varphi_c + \frac{p_\infty}{p_0'} \sin^2 \varphi_c\right) \tilde{\lambda} R_n \varphi_c \cos^2 \varphi_c \int_{R_n \tan \varphi_c}^{x_c} x_c^2 dx_c$$

$$= \frac{1}{3} \left(\cos^2 \varphi_c + \frac{p_\infty}{p_0'} \sin^2 \varphi_c\right) \tilde{\lambda} R_n \varphi_c \cos^2 \varphi_c (x_c^3 - R_n^3 \tan^3 \varphi_c) \quad (14.3.60)$$

Let us introduce the notation

$$G(\bar{x}_c) = \frac{4}{3} \left(\cos^2 \varphi_c + \frac{p_\infty}{p_0'} \sin^2 \varphi_c\right) (\bar{x}_c^3 - \tan^3 \varphi_c) \varphi_c \cos^2 \varphi_c \quad (14.3.61)$$

where $\bar{x}_c = x_c/R_n$, with account of which, introducing (14.3.59) into (14.3.49) at $\varepsilon = 1$, we obtain the relation

$$\frac{q_x}{q_0} = \left(\cos^2 \varphi_c + \frac{p_\infty}{p_0'} \sin^2 \varphi_c\right) \bar{x}_c \varphi_c \cos \varphi_c / \sqrt{D(\varphi_c) + G(\bar{x}_c)} \quad (14.3.62)$$

Here the function $D(\varphi_c)$ is determined by (14.3.53) for $\varphi = \varphi_c$.

Equation (14.3.62) is suitable only for a conical surface, i.e. for values of $\bar{x}_c = x_c/R_n \geqslant \tan \varphi_c$.

At the point where the spherical nose joins the cone, i.e. at $\bar{x}_c = \tan \varphi_c$, expression (14.3.62) conforms with Eq. (14.3.54). For the parts of the conical surface far from this point ($\bar{x}_c \gg 1$), we have

$$\frac{q_x}{q_0} \to \bar{x}_c \varphi_c \cos \varphi_c \Big/ \sqrt{\frac{4}{3} \bar{x}_c^3 \varphi_c \cos^2 \varphi_c} = \frac{\sqrt{3}}{2} \sqrt{\frac{\varphi_c}{\bar{x}_c}} \quad (14.3.63)$$

In deriving formula (14.3.63), it was assumed that the influence of blunting is small for a very long cone, and the latter may be considered conditionally as a sharp-nosed one for which the pressure on the nose $p_0' = p_\delta$ and, therefore, $p_\delta/p_0' = \cos^2 \varphi_c + (p_\infty/p_0') \sin^2 \varphi_c \approx \approx 1$. Replacing in accordance with this condition ρ_0' with $\rho_\delta = \rho_c$ and μ_0' with $\mu_\delta = \mu_c$ and assuming that $\varepsilon = 1$, we obtain from (14.3.48) that

$$q_0 = (\sqrt{2}/2) Pr^{-2/3} \sqrt{\rho_c \mu_c \tilde{\lambda}} (i_r - i_w)$$

Consequently, at remote parts of such an "equivalent" sharp-nosed conical surface, the heat flux is

$$q_c = 0.61 Pr^{-2/3} \sqrt{\rho_c \mu_c \tilde{\lambda} \varphi_c / \bar{x}_c} (i_r - i_w) \quad (14.3.64)$$

where ρ_c and μ_c are the density and dynamic viscosity on the sharp-nosed cone.

The distribution of the heat fluxes calculated by (14.3.54), (14.3.62), and (14.3.63) is shown in Fig. 14.3.3. Inspection of the figure reveals

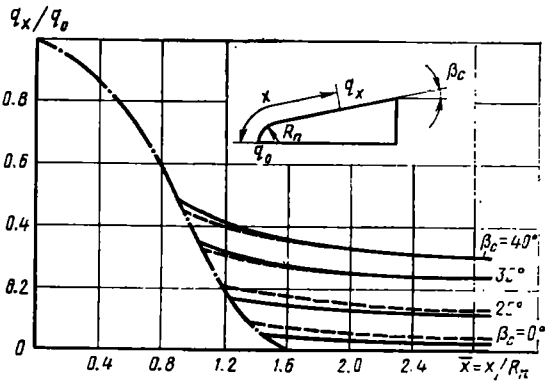

Fig. 14.3.3
Distribution of the heat flux along the surface of a blunt-nosed cone in a supersonic flow (for a laminar boundary layer):
dash-and-dot line—by (14.3.54); solid line—by (14.3.62); dash line—by (14.3.63)

that at angles β_c equal to 30 and 40°, the heat flux is distributed on a blunted and equivalent cones virtually identically, while on the surface of slender blunted bodies, the heat fluxes are smaller than on the surface of the corresponding "equivalent" cones.

We can go over from an equivalent cone to an ordinary sharp-nosed one if in formula (14.3.64), in which $\bar{x}_c = x_c/R_n$, we substitute the velocity V_c on the conical surface for $\tilde{\lambda}\varphi_c R_n = (\partial V_\delta/\partial x)_{x\to 0} x = V_\delta$. Accordingly, for an ordinary sharp-nosed cone, we have

$$q_x = q_c = 0.61 Pr^{-2/3} \sqrt{\rho_c \mu_c V_c / x_c}\,(i_r - i_w) \qquad (14.3.65)$$

The total heat flux on a cone is $Q_c = 2\pi \int_0^{x_c} q_c r\,dx$. After introducing q_c from (14.3.65), assuming that $x_0 = x$, we obtain

$$Q_c = 0.81 Pr^{-2/3} S_c \sqrt{\rho_c \mu_c V_c / x_c}\,(i_r - i_w) \qquad (14.3.66)$$

where $S_c = \pi x_c^2 \sin \beta_c$ is the side surface area of a cone with a generatrix length of x_c and a semiapex angle of β_c.

Flat Nose

Investigations reveal that the heat fluxes to a flat surface are smaller than to a spherical one. This is explained not only by the smaller surface area of the nose, but also by the more intensive stagnation of the flow on it, which, particularly, results in an appreciable drop in the velocity and its gradient $\tilde{\lambda}$ on the edge of the boundary layer.

If the distribution of the flow parameters is known, the change in the ratio q_x/q_0 can be determined approximately with the aid of formula (14.3.49) in which we must assume that $r_0 = x$. Figure 14.3.1 shows the results of calculating this change for several values of the quantity ρ_∞/ρ_0' which different free-stream velocities correspond to. At very large M_∞ (the density ratio for the stagnation point is $\rho_\infty/\rho_0' = 0.05$), the specific heat flows grow in value nearer to the sharp edge of the nose. This is explained by the influence of the pressure and density, which at this spot decrease slightly, while still remaining quite large in magnitude.

A drop in the flow velocity is attended by a change in the nature of specific heat flow distribution (the curves corresponding to the values of $\rho_\infty/\rho_0' = 0.15$, 0.25 and 0.35). Up to a value of $\bar{x} = x/R_n < 1$, the ratio q_x/q_0 increases, reaches its maximum value at a definite value of $\bar{x}$ depending on the number M_∞, and then decreases. The explanation of the decrease is that near a sharp edge at comparatively slow flow velocities the drop in the pressure may have a decisive influence, and, notwithstanding the growth in the velocity, the heat flux after reaching a maximum value begins to diminish.

Calculation of Heat Transfer in a Turbulent Boundary Layer

We have treated a number of problems associated with the determination of heat transfer in a laminar boundary layer on a curved surface.

The solution of these problems is very important for practical purposes because in real conditions the front part of a surface is always surrounded by a laminar boundary layer. In addition, heat transfer is the most intensive near the nose. At the peripheral parts of a blunt-nosed body, the boundary layer is turbulent, therefore it becomes necessary to estimate the corresponding magnitude of heat transfer. To do this, we can use a system of equations similar to what we used when studying a laminar boundary layer and that takes into consideration the features of a turbulent flow.

The magnitude of heat transfer can be estimated by formula (14.2.16) in which for a cooled surface we take the friction factor the same as for an incompressible fluid. If a wall is cooled only slightly, we find this coefficient from the reference parameters.

Figure 14.3.4 shows experimental results obtained on a hemisphere-cylinder (see [23]). It can be seen that within the interval of values of Re_x from 4×10^5 to 6×10^5, the laminar flow (region I) transforms into a turbulent one (region II). Heat transfer increases here almost five times.

Modern rocket and aeronautical engineering places heavy demands on the accuracy of calculating skin friction and heat transfer. This

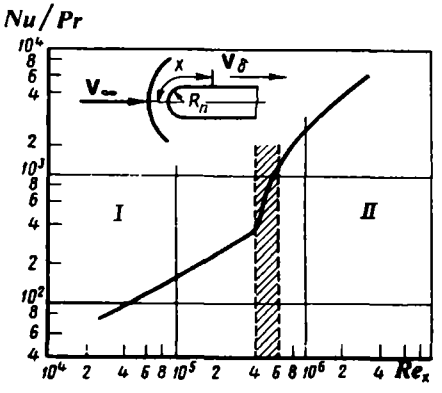

Fig. 14.3.4
Curves characterizing heat transfer on a hemisphere cylinder: $Re_x=\rho_\delta V_\delta x/\mu_\delta$; $Nu/Pr=q_w x/[\mu_\delta(i_r-i_w)]$; $Pr=0.72$

can be achieved by improving the methods of solving boundary layer equations. Lately, the **method of direct solution of these equations** for a specific problem has come into favour. This relates especially to a turbulent boundary layer in which the flow is quite intricate and has therefore been studied to a smaller extent. The method of direct solution of boundary layer equations is attracting greater and greater attention of investigators because of the increasing possibilities of using high-speed computers. This is why the technique of complicated calculations of the boundary layer parameters for both a laminar and especially a turbulent layer is finding constantly growing use in engineering.

14.4. Diffusion Heat Transfer

To estimate diffusion heat transfer quantitatively, it is necessary in the general case to solve a system of boundary layer equations including motion and energy ones (14.3.1) and diffusion equation (3.2.4). Under the assumptions made in Sec. 14.3, the motion and energy equations in the variables η and $\tilde{x}$ (14.3.5) have the form of (14.3.35) and (14.3.36). Let us consider the diffusion equation for the flow conditions in a "frozen" boundary layer. We noted that such a flow is characterized by low rates of recombination which may be disregarded in comparison with the rate of diffusion across the streamlines. The concentration of atoms in such a frozen boundary layer is determined by the diffusion of the substance to a wall, which is just where recombination occurs. In this case, the concentration is not an equilibrium one determined by the local temperature and pressure values. The concentration and temperature distributions do not virtually depend on each other.

Assuming in Eq. (3.2.4) that $(W_{\text{chem}})_i = 0$ and relating this equation to the conditions of flow in the boundary layer by substituting the derivative $\partial/\partial y$ for $\partial/\partial r$, and also assuming that $r = r_0$ and $V_r = V_y$, we obtain

$$\frac{\partial (\rho V_x r_0 c_i)}{\partial x} + \frac{\partial (\rho V_y r_0 c_i)}{\partial y} = -\frac{\partial (Q_i r_0)}{\partial y}$$

Expanding the derivative on the left-hand side and replacing Q_i in accordance with (14.1.7), we have

$$\left[\frac{\partial (\rho V_x r_0)}{\partial x} + \frac{\partial (\rho V_y r_0)}{\partial y}\right] c_i + \rho r_0 \left(V_x \frac{\partial c_i}{\partial x} + V_y \frac{\partial c_i}{\partial y}\right) = \frac{\partial}{\partial y}\left(\rho \overline{Dr}_0 \frac{\partial c_i}{\partial y}\right)$$

In accordance with continuity equation (2.4.48), the binomial in brackets equals zero. Also bearing in mind that r_0 for a given boundary layer cross section is constant, we find

$$\rho \left(V_x \frac{\partial c_i}{\partial x} + V_y \frac{\partial c_i}{\partial y}\right) = \frac{\partial}{\partial y}\left(\rho \overline{D} \frac{\partial c_i}{\partial y}\right) \qquad (14.4.1)$$

For an atomic component, Eq. (14.4.1) becomes

$$\rho \left(V_x \frac{\partial c_A}{\partial x} + V_y \frac{\partial c_A}{\partial y}\right) = \frac{\partial}{\partial y}\left(\rho \overline{D} \frac{\partial c_A}{\partial y}\right) \qquad (14.4.2)$$

For a molecular component, the diffusion equation has the same form as (14.4.2) with c_M substituted for c_A, which follows from the condition that $c_A = 1 - c_M$.

We transform Eq. (14.4.2) to the variables η and $\tilde{x}$ with a view to the values of the operators (14.3.15) and (14.3.17):

$$\rho\rho_\delta V_\delta^2 \mu_\delta r_0^{2\varepsilon} \left(\frac{\partial f}{\partial \eta} \cdot \frac{\partial c_A}{\partial x} - \frac{f}{2\tilde{x}} \cdot \frac{\partial c_A}{\partial \eta} - \frac{\partial f}{\partial \tilde{x}} \cdot \frac{\partial c_A}{\partial \eta}\right)$$

$$= \frac{\rho V_\delta^2 r_0^{2\varepsilon}}{2\tilde{x}} \cdot \frac{\partial}{\partial \eta}\left(\rho^2 \overline{D} \frac{\partial c_A}{\partial \eta}\right)$$

Assuming that the concentration and velocity profile are only a function of η (we are considering a similar solution), we obtain

$$\rho_\delta \mu_\delta f \frac{\partial c_A}{\partial \eta} + \frac{\partial}{\partial \eta}\left(\rho^2 \overline{D} \frac{\partial c_A}{\partial \eta}\right) = 0$$

Let us introduce the dimensionless dependent variable

$$z(\eta) = c_A/c_{A,\delta} \qquad (14.4.3)$$

Transforming the diffusion equation to this variable with the assumption that $\rho\mu = \rho_\delta \mu_\delta$, and that the Schmidt number $Sc = \mu/(\rho\overline{D})$ is constant and equal to its value at the wall, we have

$$Sc\, fz' + z'' = 0 \qquad (14.4.4)$$

where a prime signifies differentiation with respect to η.

Equation (14.4.4) is the same in form as (14.3.36) provided that Sc is substituted for Pr. The boundary conditions for the function z for which Eq. (14.4.4) is solved are similar to those for the function g [see (14.3.23) and (14.3.24)], i.e. at $\eta = 0$ ($y = 0$) the quantity $z(0) = z_w = c_{A,w}/c_{A,\delta}$, at $\eta \to \infty$ ($y \to \infty$) the function $z(\infty) \to 1$, while the derivative $\partial z/\partial\eta \to 0$.

Double integration of (14.4.4) leads to an equation similar to (14.3.37):

$$z(\eta) - z(0) = z'(0) \int_0^\eta \exp\left(-\int_0^\eta Scf\, d\eta\right) d\eta \qquad (14.4.5)$$

Taking into account this analogy, we determine the integral for $\eta \to \infty$

$$\int_0^\eta \exp\left(-\int_0^\eta Scf\, d\eta\right) d\eta = (0.5Sc^{1/3})^{-1}$$

Since at $\eta \to \infty$ the function $z(\eta) \to 1$, we find

$$z'(0) = 0.5Sc^{1/3}[1 - z(0)] \qquad (14.4.6)$$

We can simultaneously find the derivative $z'(0) = (\partial z/\partial\eta)_w$ using the relation from chemical kinetics for determining the amount of a substance evolved at a wall as a result of a catalytic reaction,

$$Q_w = k_w c_{A,w} \rho_w \qquad (14.4.7)$$

where k_w is the rate constant of the catalytic reaction.

This amount of substance equals the diffusion mass flux (in magnitude):

$$Q_w = \rho_w \overline{D} \left(\frac{\partial c_A}{\partial y}\right)_w = \rho_w \overline{D} \left(\frac{\partial z}{\partial y}\right)_w c_{A,\delta}$$

Consequently,

$$\left(\frac{\partial z}{\partial y}\right)_w = \frac{k_w}{\overline{D}} \cdot \frac{c_{A,w}}{c_{A,\delta}} = \frac{k_w}{\overline{D}} z(0)$$

or in the variables η and $\tilde{x}$, *by* (14.3.5)

$$z'(0) = \left(\frac{\partial z}{\partial \eta}\right)_w = \left(\frac{\partial z}{\partial y}\right)_w \left(\frac{\partial y}{\partial \eta}\right)_w = \frac{(2\tilde{x})^{1/2}}{V_\delta r_0^\varepsilon} \cdot \frac{k_w}{\rho_w \overline{D}} z(0) \qquad (14.4.8)$$

We solve the system of equations (14.4.6) and (14.4.8) for $z(0)$ and $z'(0)$:

$$z(0) = z_w = \left[\frac{(2\tilde{x})^{1/2}}{V_\delta r_0^\varepsilon} \cdot \frac{k_w}{0.5Sc^{1/3}\rho_w \overline{D}} + 1\right]^{-1} \qquad (14.4.9)$$

$$z'(0) = 0.5Sc^{1/3}\left[1 + \frac{V_\delta r_0^\varepsilon}{(2\tilde{x})^{1/2}} \cdot \frac{0.5Sc^{1/3}\rho_w \overline{D}}{k_w}\right]^{-1} \qquad (14.4.10)$$

The magnitude of the specific heat flow released upon recombination at a wall can be obtained from (14.1.8). Determining the magnitude of the heat flux, we find its local value:

$$q_{d,x} = \rho_w \overline{D} \, (\partial c_A/\partial \eta)_w \, (\partial \eta/\partial y)_w (i_A - i_M)$$

or, having in view that $(\partial c_A/\partial \eta)_w = c_{A,\delta} z' \, (0)$ and taking into account the value given in (14.3.6) for $(\partial \eta/\partial y)_w$, we obtain the relation

$$q_{d,x} = 0.5 Sc^{1/3} \overline{D} \rho_w^2 V_\delta r_0^\varepsilon (2\tilde{x})^{-1/2} \times \left[1 + \frac{V_\delta r_0^\varepsilon}{(2\tilde{x})^{1/2}} \cdot \frac{0.5 Sc^{1/3} \rho_w \overline{D}}{k_w} \right]^{-1} c_{A,\delta} (i_A - i_M) \qquad (14.4.11)$$

Examination of the obtained expressions reveals that in the limiting case corresponding to an infinitely high rate of recombination (the wall is catalytic, the rate constant of the catalytic reaction $k_w \to \infty$) the quantity $z \, (0) = 0$ and, consequently, the concentration at the wall is zero. By (14.4.11), at such an infinitely rapid catalysis, the heat flux is

$$q_{d,x} = 0.5 Sc^{1/3} \rho_w^2 V_\delta \overline{D} r_0^\varepsilon (2\tilde{x})^{-1/2} c_{A,\delta} (i_A - i_M) \qquad (14.4.12)$$

Hence, in the limiting case being considered, the atoms reach the wall even at a zero concentration at the surface. Here the maximum heat is released due to the recombination of these atoms into molecules. In the other limiting case of an infinitely slow catalytic reaction (a non-catalytic wall, $k_w \to 0$), the concentration at the wall remains the same as at the outer edge, i.e. $z \, (0) = 1$. Now the flow of atoms because of diffusion is zero, and, consequently, no additional heat is released, i.e. $q_{d,x} = 0$. The same result follows from (14.4.11) if we assume that the catalytic reaction rate constant $k_w \to 0$.

Let us perform some transformations in Eq. (14.4.11).

Assuming that $\rho_w \mu_w = \rho_\delta \mu_\delta$ and introducing the ratio $\rho_\delta \mu_\delta / (\rho_0' \mu_0')$ according to formula (14.3.42), in which we set $\omega_\delta / \omega_0' = 1$, we have

$$\frac{0.5 Sc^{1/3} \rho_w^2 \overline{D} V_\delta r_0^\varepsilon}{(2\tilde{x})^{1/2}} = \frac{0.5 Sc^{-2/3} (p_\delta / p_0') V_\delta r_0^\varepsilon \sqrt{\rho_0' \mu_0'}}{\left[2 \int_0^x (p_\delta / p_0') V_\delta r_0^{2\varepsilon} \, dx \right]^{1/2}} \qquad (14.4.13)$$

or by formula (14.3.44) for the function $F \, (x)$, the expression

$$A = 0.5 Sc^{-2/3} \sqrt{\rho_0' \mu_0' V_\infty} \, F \, (x) \qquad (14.4.13')$$

in which $Sc = \mu_w / (\rho_w \overline{D})$.

With a view to (14.4.13') and taking into account that

$$c_{A,\delta} (i_A - i_M) \approx c_{A,\delta} i_{chem} \qquad (14.4.14)$$

and also introducing the dissociation enthalpy

$$i_d = c_{A,\delta} i_{chem} \tag{14.4.15}$$

we obtain the following expression instead of (14.4.11):

$$q_{d,x} = 0.5 Sc^{-2/3} \sqrt{\rho_0' \mu_0' V_\infty}\, F(x)\, i_d \varphi \tag{14.4.16}$$

where the **catalytic coefficient**

$$\varphi = [1 + A/(\rho_w k_w)]^{-1} \tag{14.4.17}$$

This coefficient takes into consideration the influence of the finite rate of recombination because its expression contains the parameter k_w. It is evident that at $k_w \to \infty$ the value of $\varphi \to 1$ (infinitely rapid catalysis), while at $k_w \to 0$, the value of $\varphi \to 0$ (a non-catalytic wall).

For the flow conditions near the stagnation point, we obtain from (14.4.13') with a view to (14.3.47) that

$$A = A_0 = 0.5 Sc^{-2/3} \sqrt{\rho_0' \mu_0' \tilde{\lambda} (\varepsilon + 1)} \tag{14.4.18}$$

and from (14.4.17)

$$\varphi = \varphi_0 = [1 + 0.5 Sc^{-2/3} \sqrt{\rho_0' \mu_0' \tilde{\lambda} (\varepsilon + 1)}/(\rho_w k_w)]^{-1} \tag{14.4.19}$$

Accordingly, the heat flux at the stagnation point is

$$q_{d,0} = 0.5 Sc^{-2/3} \sqrt{\rho_0' \mu_0' \tilde{\lambda} (\varepsilon + 1)}\, \varphi_0 i_d \tag{14.4.20}$$

Hete $\varepsilon = 1$ for bodies of revolution, and $\varepsilon = 0$ for an airfoil.

We find the resultant specific heat flow to the wall by adding the heat flux due to diffusion $q_{d,x}$ to that due to molecular heat conduction $q_{h,x}$. The magnitude of this heat flux in a general form is determined by Eq. (14.1.12), which we shall write as

$$q_c = q_{h,x} + q_{d,x} = \underbrace{-\frac{\lambda_w}{(c_p)_w}\left(\frac{\partial i}{\partial y}\right)_w \left[1 - \frac{(\partial c_A/\partial y)_w (i_A - i_M)_w}{(\partial i/\partial y)_w}\right]}_{(q_c)_{Le=1}}$$

$$\underbrace{-\rho_w \bar{D}\left(\frac{\partial c_A}{\partial y}\right)_w (i_A - i_M)_w}_{q_c = q_{d,x}}$$

Using (14.1.8) and (14.1.13), we obtain

$$q_c = (q_c)_{Le=1}\left[1 - \frac{(\partial c_A/\partial y)_w (i_A - i_M)_w}{(\partial i/\partial y)_w} + \frac{q_{d,x}}{(q_c)_{Le=1}}\right] \tag{14.4.21}$$

where $(q_c)_{Le=1}$ is the specific heat flow corresponding to the value

$$Le = \rho_w \bar{D} (c_p)_w / \lambda_w = 1$$

With a view to (14.3.43) and (14.4.16), we have

$$q_c = (q_c)_{Le=1}\left[1 - \frac{(\partial c_A/\partial y)_w (i_A - i_M)_w}{(\partial i/\partial y)_w} + \left(\frac{Sc}{Pr}\right)^{-2/3} \frac{\varphi^{i_d}}{i_r - i_w}\right]$$

Let us estimate the values of the derivatives $(\partial c_A/\partial y)_w$ and $(\partial i/\partial y)_w$, assuming that at the cold wall the concentration $c_{A,w} = 0$:

$$\left(\frac{\partial c_A}{\partial y}\right)_w \sim \frac{c_{A,\delta}}{\delta}, \quad \left(\frac{\partial i}{\partial y}\right)_w = \left(\frac{\partial i_0}{\partial y}\right)_w \sim \frac{i_{0,\delta} - i_w}{\delta} = \frac{i_r - i_w}{\delta}$$

where δ is the boundary layer thickness, and $i_{0,\delta} = i + V_x^2/2$.

With a view to this estimate of the derivatives and to the expressions $Le = Pr/Sc$ and $c_{A,\delta}(i_A - i_M) = i_d$, we find

$$q_c = (q_c)_{Le=1}\left[1 + (\varphi Le^{2/3} - 1)\frac{i_d}{i_r - i_w}\right] \qquad (14.4.22)$$

We find the heat flux $(q_c)_{Le=1}$ for an arbitrary point on a surface from (14.3.43), and for the stagnation point from (14.3.48). We determine the coefficients φ from (14.4.17) and (14.4.19), respectively. The value of i_d can be computed by the formula

$$i_d = i_\alpha - i_{\alpha=0} \qquad (14.4.23)$$

in which the enthalpy i_α is determined with account taken of dissociation at the corresponding temperature T, while the enthalpy $i_{\alpha=0}$ is determined for the same temperature T, with no account taken of dissociation. It can be found by the formula $i_{\alpha=0} = c_{p,\infty}(T/T_\infty)^\varphi T$. The number Le is determined for the conditions at the stagnation point and is assumed to be constant for the entire surface. From (14.4.22), we obtain relations corresponding to the two limiting cases of heat transfer. In the first of them, when the wall in the flow is non-catalytic ($k_w \to 0$, $\varphi \to 0$), diffusion heat transfer is absent, and the heat flux to the surface occurring only as a result of heat conduction is

$$q_{c(k_w \to 0)} = (q_c)_{Le=1}\left(1 - \frac{i_d}{i_r - i_w}\right) \qquad (14.4.24)$$

In the second case, when the wall is catalytic and recombination at it proceeds at an infinite rate ($k_w \to \infty$, $\varphi \to 1$), the total heat flux is

$$q_{c(k_w \to \infty)} = (q_c)_{Le=1}\left[1 + (Le^{2/3} - 1)\frac{i_d}{i_r - i_d}\right] \qquad (14.4.25)$$

The ratio of the heat flux q_c (14.4.22) released at a finite rate of recombination to the heat flux $q_{c(k_w \to \infty)}$ with infinitely rapid catalysis is

$$\bar{q} = \frac{q_c}{q_{c(k_w \to \infty)}} = \frac{1 + (\varphi Le^{2/3} - 1)\tilde{i}_d}{1 + (Le^{2/3} - 1)\tilde{i}_d} \qquad (14.4.26)$$

where $\tilde{i}_d = i_d/(i_r - i_w)$.

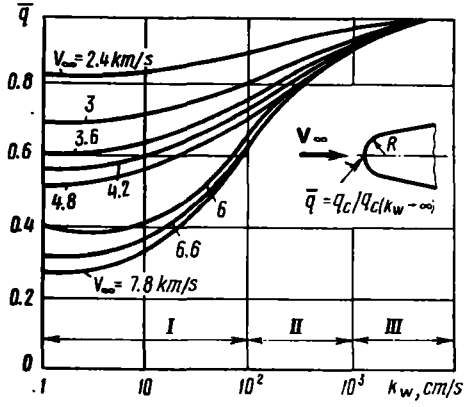

Fig. 14.4.1
Heat transfer vs. flight speed V_∞ and rate constant k_w of the catalytic reaction:
I – non-catalytic wall (glass); *II* – intermediate surface (oxides); *III* – catalysts (metals)

The results of calculating the quantity $\bar{q}$ for the stagnation point depending on the free-stream velocity V_∞ and the rate constant of the catalytic reaction k_w are shown in Fig. 14.4.1. These results indicate the need of taking into consideration the finite rate of recombination and the possibility of lowering heat transfer by using an outer skin made from a non-catalytic material. With such a skin, the low rates of recombination featuring the air change insignificantly. This results in greater heat absorption because of dissociation and, consequently, in diminishing of the heat flux to the wall.

The limiting value of the non-equilibrium heat flux corresponds to a zero catalytic coefficient.

With this in view and by (14.4.26), we have

$$\bar{q} = (1 - \tilde{i}_d)/[1 + (Le^{2/3} - 1)\tilde{i}_d] \qquad (14.4.26')$$

The change in heat transfer because of diffusion is taken into consideration to a certain extent by formula (14.3.48′). It gives the resultant specific heat flow determined not only by the heat conduction, but also by the diffusion transfer of heat due to recombination of the atoms at the catalytic wall. If a surface in a flow is not catalytic (for example, the surface of a non-metallic outer skin) the heat flux obtained by formula (14.3.48′) is somewhat understated. The inaccuracy of the formula grows with increasing altitude, when the deviation of the gas state from equilibrium becomes greater.

The present section deals with heat transfer in the two limiting cases of equilibrium and frozen flows in the boundary layer. But a heat transfer mechanism characterized in that the concentration of each chemical component in the boundary layer is determined from Eq. (3.2.4) by a finite rate of chemical reactions $W_{chem.i}$ is the most general one. After acquaintance with the above information on heat transfer in the limiting cases, one can study by oneself its mechanism

in the more general case when $W_{\text{chem.i}} \neq 0$. One should use the system (3.2.4), (3.2.14) and (13.1.8) for this purpose. Some ways and results of solving this system are treated in [22. 24. 25].

14.5. Determination of Wall Temperature

Equilibrium Emission Temperature

In steady motion of a craft, the heat conditions on its surface are characterized by equality of the heat fluxes directed toward the surface and away from it. Here the equation of the heat balance (14.1.1) has the form $q_{\text{sup}} - q_{\text{rem}} = 0$, or with a view to expressions (14.1.2) for the supplied q_{sup} and (14.1.3) for the removed q_{rem} heat fluxes,

$$q_{\text{c}} + q_{\text{rad}} + q_{\text{s}} + q_{\text{ter}} + q_{\text{eq.tr}} = q_{\text{em}} + q_{\text{ab}} + q_{\text{cl}} + q_{\text{eq.h}} \tag{14.5.1}$$

The wall temperature determined from the condition of equality of the heat fluxes (14.5.1) and corresponding to steady flow is called the **equilibrium temperature.**

Let us assume that heat transfer is characterized only by the supply of a convective heat flux to a wall ($q_{\text{sup}} = q_{\text{c}}$) and the removal of heat energy from it by emission ($q_{\text{rem}} = q_{\text{em}}$). Now (14.5.1) with a view to (14.1.17) for q_{c} and (14.1.28) for q_{em} becomes

$$[\alpha_{\text{w}}/(c_p)_{\text{w}}]\,(i_{\text{r}} - i_{\text{w}}) = \varepsilon\sigma T_{\text{w}}^4 \tag{14.5.2}$$

The wall temperature determined by Eq. (14.5.2) is called the **equilibrium emission temperature** and is designated $T_{\text{w}} = T_{\text{e}}$. It differs from the recovery temperature T_{r} which, as is known, is the temperature of the gas at a wall in the absence of heat transfer, i.e. on a thermally insulated surface.

The temperature T_{e} is an upper limit for an emitting surface that is reached when a heated wall completely emits the energy it has received. This temperature with very high heat fluxes is not real because it is so high that it cannot be reached before the skin material is destroyed (by melting, sublimation, burning). Sometimes, however, the equilibrium emission temperature may be real, for example, on the surface of a gliding craft. In gliding, the kinetic energy transforms into heat energy gradually, and the intensity of the heat flow by convection may be comparatively small. Therefore, the possibility of emission of all the absorbed energy at the equilibrium temperature allowable for a craft is quite real.

In Eq. (14.5.2), we may assume that the Stefan-Boltzmann constant σ and the emittance ε are known and constant quantities. The heat-transfer coefficient α_{w}, the average specific heat at the wall $(c_p)_{\text{w}}$,

and also the enthalpies i_r and i_w for a dissociating gas are functions of the required temperature $T_w = T_e$, and also of the given pressure p_δ. Hence, the total number of required variables will be five. Consequently, Eq. (14.5.2) must be supplemented with four independent equations for determining α_w, $(c_p)_w$, i_r, and i_w.

For a laminar boundary layer, by (14.1.17) and (14.4.22) we can write the equation for α_w as

$$\alpha_w = \frac{(c_p)_w q_c}{i_r - i_w} = \frac{(c_p)_w}{i_r - i_w} (q_c)_{Le=1} \left[1 + (\varphi Le^{2/3} - 1) \frac{i_d}{i_r - i_w}\right] \quad (14.5.3)$$

We shall write the equations for $(c_p)_w$ and i_w in a general form:

$$(c_p)_w = f_1 (p_\delta, T_w) \quad (14.5.4)$$

$$i_w = f_2 (p_\delta, T_w) \quad (14.5.5)$$

where f_1 and f_2 are calculated with the aid of tables or graphs of the thermodynamic functions for air at high temperatures.

The recovery enthalpy is

$$i_r = i_\delta + rV_\delta^2/2 \quad (14.5.6)$$

where the recovery factor $r = f_3 (p_\delta, T_w)$ is found as a function f_3 of the pressure p_δ and of T_w by formulas (13.5.20) and (13.5.21).

Solution of the system (14.5.2)-(14.5.6) allows us to find the equilibrium emission temperature of a wall in a flow with a laminar boundary layer in a dissociating gas. By using the equation for turbulent heat transfer instead of (14.5.3), we can find the temperature $T_w = T_e$ for a turbulent boundary layer. Such an equation was obtained on a previous page for flow over a flat plate.

The system of equations (14.5.2)-(14.5.6) is solved by the method of successive approximations. The flight speed V_∞ (or number M_∞) and the altitude H are given; they are used to calculate the parameters of "inviscid" flow over the surface (the pressure p_δ, density ρ_δ, temperature T_δ, etc.).

To find the temperature $T_w = T_e$ for a point on this surface, we determine the enthalpy i_r (14.5.6) for it as a first approximation, using $r = r_{lam} = 0.84$ (a laminar boundary layer) or $r = r_{trb} = 0.89$ (a turbulent layer) by (13.5.22) and then find the corresponding value of T_r as a function of i_r and p_δ. Next several values of the temperature $T_w < T_r$ and the corresponding values of $i_w < i_r$ are preset. For each of these values of T_w (i_w), we calculate α_x and $(c_p)_w$ in a first approximation and determine the difference of the heat fluxes:

$$[\alpha_x/(c_p)_w] (i_r - i_w) - \varepsilon\sigma T_w^4 = q_w \quad (14.5.7)$$

The data obtained are used to compile a table or plot a curve of q_w versus T_w. By setting $q_w = 0$ and interpolating the tabulated data or using a graph, we determine the temperature $T_w = T_e$.

We use this value of the wall temperature to refine the factor r and the enthalpy i_r, determine in the next approximation the heat-transfer coefficient α_x and the specific heat $(c_p)_w$, and then repeat the calculations using Eq. (14.5.7) until a value of $T_w = T_e$ is obtained with the given degree of approximation. When solving this problem, we find the enthalpy i_d in (14.5.3) by formula (14.4.23).

The temperature $T_w = T_e$ can be estimated in this way with the assumption that the numbers Pr, Sc, and Le are chosen equal to certain fixed values, particularly $Pr = 0.64$, $Sc = 0.49$, and $Le = 1.45$.

The temperature $T_w = T_e$ is calculated in a simpler way for a *plate and a cone*, the flow over which is characterized by constant values of the inviscid gas parameters on their surface. The equilibrium emission temperature can be computed by the method of reference enthalpy (temperature). These calculations can also be performed with account taken of a mixed boundary layer on the surface in the flow, using the appropriate relations for the skin friction and heat-transfer parameters.

The equilibrium emission temperature in the vicinity of the *stagnation point of a sphere* is calculated with the assumption that the boundary layer is laminar. This can be done by solving a system of equations found for the conditions where the local velocity $V_\delta = 0$. Such a system has the form

$$\left.\begin{aligned}
T_w^4 &= [A_1/(\varepsilon\sigma)]\,(i_r - i_w)\,[1 + (\varphi Le^{2/3} - 1)\,\tilde{i}_d] \\
\tilde{i}_d &= (i_r - i_w)^{-1}\,(i_\alpha - i_{\alpha=0}) \\
\varphi &= (1 + A_2/\rho_w)^{-1} \\
\rho_w &= p_0' m_w/(gR_0 T_w) \\
m_w &= f_1(p_0',\ T_w) \\
i_w &= f_2(p_0',\ T_w) \\
i_\alpha &= f_3(p_0',\ T_w) \\
i_{\alpha=0} &= c_{p,\infty}(T_w/T_\infty)^\varphi\, T_w
\end{aligned}\right\} \qquad (14.5.8)$$

where the coefficients $A_1 = 0.5 Pr^{-2/3}\sqrt{2\rho_0'\mu_0'\tilde{\lambda}}$ and $A_2 = 0.5 Sc^{-2/3} k_w^{-1}\sqrt{2\rho_0'\mu_0'\tilde{\lambda}}$.

The values of p_0', ρ_0', μ_0', $i_r = i_0$, and $\tilde{\lambda}$ are calculated by solving the problem on the free flow in the vicinity of the stagnation point.

When solving the system of equations (14.5.8), we take a temperature $T_w < T_0'$ as a first approximation. We use this temperature and the pressure p_0' to find the initial values of i_w and m_w, next we determine $\tilde{i}_d$, ρ_w, φ and the corresponding temperature T_w. We per-

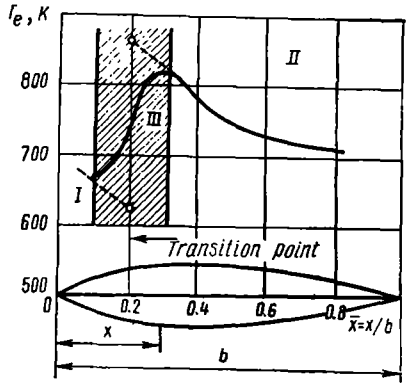

Fig. 14.5.1
Distribution of the equilibrium emission temperature over the surface of an airfoil in a supersonic flow:
I — laminar layer; *II* — turbulent layer; *III* — transition region

form the subsequent approximations in a similar way and terminate them when we reach the preset accuracy of temperature calculations.

For moderate flow velocities, when we may take no account of dissociation and consider that the thermodynamic and kinetic characteristics of the air are constant, the calculation of the temperature $T_w = T_e$ is simplified. In this case, the corresponding system of equations becomes

$$\alpha_x^i (T_r - T_w) = \varepsilon\sigma T_w^4, \quad \alpha_x = h(T_w) \qquad (14.5.9)$$

where h is the heat-transfer coefficient that is a function of the temperature T_w.

The results of calculating the equilibrium emission temperature with the aid of system (14.5.9) for a parabolic airfoil in a supersonic flow are shown in Fig. 14.5.1. The calculations were performed employing relations for α_x found for a flat plate. Local parameters of inviscid flow over the airfoil were used in these relations: the influence of the longitudinal pressure gradient was not taken into consideration, and the fixed values of $r_{lam} = 0.84$ and $r_{trb} = 0.89$ corresponding to the number $Pr = 0.71$ were adopted.

When plotting a graph similar to that shown in Fig. 14.5.1 one should take into account the **transition region** in which the heat fluxes change smoothly along a curve. The latter should have no discontinuities because in real conditions longitudinal heat fluxes form that equalize the temperature.

Equations (14.5.9) to a first approximation can be used for calculating the equilibrium emission temperature at high velocities. Here attention must be given to the influence of compressibility, dissociation, or variation of the specific heats by introducing the reference parameters in the equations, namely,

$$\alpha_x^* (T_r - T_w) = \varepsilon\sigma T_w^4, \quad \alpha_x^* = h^*(T_w) \qquad (14.5.10)$$

where T_r is determined with a view to dissociation from the reference enthalpy (13.5.23), and α_x^* from expression (14.2.21).

When calculating heat transfer on a plate and cone, we find the Stanton number St_x^* in the expression for α_x^* from expressions (14.2.19) or (14.2.26) relating the skin friction and heat-transfer parameters.

An analysis of the equations for the equilibrium emission temperature and the results of calculations allow us to conclude that the main way of lowering the temperature is to reduce the ratio α_x/ε. We can do this, first, by reducing the heat-transfer coefficient α_x thereby ensuring laminarization of the boundary layer. The value of α_x also diminishes when a craft rises to a high altitude because here heating decreases owing to the drop in the air density. Second, we can increase the emittance of the surface in the flow. For this purpose, a special coating is applied that can increase the value of ε to 0.7 or 0.8 and thus increase cooling by emission. A growth of the emittance to a value close to unity is also observed when a metal wall is thin and becomes heated to high temperatures.

Equilibrium Temperature When Additional Heat Sources or Sinks are Present

The equilibrium temperature when other kinds of heat transfer are present in addition to convective and radiation heat flows is calculated similarly to the determination of the equilibrium emission temperature. Equation (14.5.1) should be used for these calculations. With a view to the values for $q_c = \alpha_x (T_r - T_w)$ and $q_{em} = \varepsilon\sigma T_w^4$, we shall write it in the form

$$\alpha_x (T_r' - T_w) = \varepsilon\sigma T_w^4 \qquad (14.5.11)$$

where the **reduced recovery temperature** is

$$T_r' = T_r [1 + \Sigma q_l/(\alpha_x T_r)] \qquad (14.5.12)$$

The sum of the specific heat flows is

$$\sum_i q_l = q_{rad} + q_s + q_{ter} + q_{eq.tr} - q_{ab} - q_{cl} - q_{eq.h} \qquad (14.5.13)$$

The components in (14.5.13) include the radiation flux q_{rad} to the wall from the overheated gas and the heat flux q_{ab} dissipated upon the ablation of the skin material, which are found as a function of the wall temperature. The remaining components may be considered as preset quantities.

Examination of (14.5.11) reveals that the task of determining $T_w = T_e$ is solved in principle in the same way as when heat is removed only by emission. The only difference is that instead of

the recovery temperature T_r we determine its reduced value T'_r.

An analysis of relations (14.5.11)-(14.5.13) shows that by using artificial cooling q_{cl} and ablation of the skin when the heat q_{ab} is carried off together with the particles of the destroyed skin, we can lower the wall temperature $T_w = T_e$.

At moderate supersonic flow velocities, the radiation heat flux q_{rad} and the heat q_{ab} absorbed in ablation may be disregarded. In this case, we have

$$\sum_i q_i = q_s + q_{ter} + q_{eq.tr} - q_{cl} - q_{eq.h} \qquad (14.5.14)$$

and the calculation of the temperature $T_w = T_e$ is simplified because the components of heat transfer in (14.5.14) do not depend on the wall temperature and are preset.

At high altitudes (from 100 to 500 km, and sometimes more), the aerodynamic heat flux is insignificant in comparison with radiant energy. Disregarding the dissipation of heat along the surface, we may consider that the heat balance equation for a stationary process is

$$q_s + q_{ter} + q_{ref} = q_{em} \qquad (14.5.15)$$

where q_{ref} is the solar energy reflected from the Earth.

For high altitudes, the heat q_{ter} radiated by the Earth and also the energy q_{ref} may be ignored, and, consequently, $q_s = q_{em}$. Introducing the values of q_s from (14.1.24) and q_{em} from (14.1.28), we obtain

$$\bar{q}\beta_s \cos\psi = \varepsilon\sigma T_w^4$$

whence

$$T_w = \left(\frac{\beta_s}{\varepsilon}\frac{\bar{q}}{\sigma}\cos\psi\right)^{1/4} \qquad (14.5.16)$$

The maximum temperature is reached at $\psi = 0$. For practical purposes, in formula (14.5.16) we can use a constant value of $\bar{q} = 1.39 \times 10^3$ W/m^2. Assuming also that $\sigma = 5.67 \times 10^{-8}$ W/(m^{2}K^4), we obtain the following relations for the temperature:

$$T_w = 395\,(\beta_s/\varepsilon)^{1/4} \qquad (14.5.17)$$

By this formula, the highest equilibrium temperature at a point on a body in a flow is determined only by the properties of the wall material characterizing its absorptivity β_s and the emittance of the surface ε.

15

Aerodynamics of Rarefied Gases

15.1. Limits of Validity of the Continuum Flow Theory

The experimental data on the flow over bodies in a rarefied gas differ considerably from the values of the force and moment characteristics, and also of the skin-friction and heat-transfer parameters calculated by the gasdynamic relations for a continuum. This difference is explained by the structure of these relations corresponding to the hypothesis of a continuum. This hypothesis is not valid for a rarefied atmosphere, and the kinetic theory must be used, which studies gas dynamics with the aid of **molecular mechanics.** The most important conclusions of this theory are based on the assumption of a discrete structure according to which a fluid consists of colliding molecules travelling a large free path. We shall not treat the kinetic theory of gases in detail, and shall consider only the information needed to understand physical phenomena, and also for aerodynamic calculations associated with flights in a rarefied gas.

Mean Free Path of Molecules

Let us consider the limits of the validity of the theoretical relations based on the assumption of a continuum. It should be noted here that the limits of validity are of a conditional nature because, for example, it is impossible to indicate exactly the altitude above which only the molecular theory has to be used. To establish these limits, we must determine the **free path of the molecules.** It is clear from physical considerations that when the free path is smaller, the gas is closer to a hypothetic continuum. The flow of such a gas is characterized by a large number of collisions between the molecules. The collisions determine the short relaxation time when in the disturbed flow, i.e. the time needed for equilibrium of the energy levels of the colliding molecules to set in.

Statistical physics distinguishes a certain mean distance travelled by a molecule between collisions known as the **mean free path.** This

length is

$$l = \bar{c}t \qquad (15.1.1)$$

where $\bar{c}$ is the average velocity of the chaotic motion of the molecules [see (15.2.4)], t is the time between two collisions of a molecule determined from the expression $t = 1/n$ in which $n = NA\bar{c}$ is the number of collisions per unit time (here N is the number of molecules in unit volume, and A is the cross-sectional area of a molecule).

Hence,

$$l = 1/(NA) \qquad (15.1.1')$$

For example, for air in standard conditions, $N = 2.69 \times 10^{19}$ cm^{-3} and $A = 10^{-15}$ cm^2; therefore, the free path is $l = 4 \times 10^{-5}$ cm. It follows from (15.1.1') that the mean free path grows with a decreasing density. Hence, this path grows with the altitude and may appreciably exceed the length of a craft.

Formula (15.1.1') is not convenient for practical use because the cross-sectional area of a moleclue cannot be determined by direct measurement. One should use the relation for l that can be obtained from formula (1.1.8) of the kinetic theory of gases determining the dynamic viscosity. By inserting into (1.1.8) instead of $\bar{c}$ relation (15.2.8') for the mean velocity in terms of the speed of sound a, we find

$$l = 1.255\, \nu\sqrt{k}/a \qquad (15.1.2)$$

where k is the adiabatic exponent and ν is the kinematic viscosity.

Conditions of Gas Flow

The conditions of a gas flow depend on its rarefaction, by which is meant the ratio of the mean free path of the molecules to a characteristic length of the region of the flow being considered.

A notion on these conditions and the parameters used to determine them can be obtained if we consider the flow between two plates at a small distance δ apart. The space between the plates is filled with a gas, and one of the plates moves parallel to the other one at the speed V. When evaluating the gas rarefaction and the corresponding flow conditions, it is expedient to proceed from a comparison of the mean free path l of the molecules and the spacing δ of the plates, i.e. from the relation

$$\frac{l}{\delta} = 1.255\frac{\nu\sqrt{k}}{V\delta}\cdot\frac{V}{a} = 1.255\sqrt{k}\frac{M}{Re} \qquad (15.1.3)$$

where $Re = V\delta/\nu$ is the Reynolds number.

The parameter l/δ is called the **Knudsen number** (Kn). If $Kn = l/\delta \leqslant 0.01$, the gas is considered to be a **continuum.** The disturb-

ances caused by collisions with the wall in such a gas are transmitted almost instantaneously to all the molecules because of the smallness of the mean free path, hence the continuum hypothesis may be used in studying flows. If the mean free path is larger than the distance between the walls and the number $Kn \geqslant 10$, the gas must be considered **highly rarefied**, and the continuum hypothesis may not be applied.

In such a gas, our conventional concept of the number ***Re*** as of the ratio of the inertial to viscous forces has no meaning because the collisions between the particles are rare and, consequently, viscosity does not practically manifest itself. This is why we must determine the impact action of the particles on a body instead of a continuous flow over it when defining the forces acting on it and the heat fluxes. The above two cases reflect two characteristic flow conditions. The first of them is **continuum flow**, and the second is **free-molecule flow**.

It is customarily assumed that notwithstanding the high rarefaction and the negligibly small number of collisions, the number of molecules in an elementary volume of a free-molecule flow is still high enough to consider the properties of the gas to be macroscopic. For example, at an altitude exceeding 150 km, the free path of the molecules is 3 m, which points to the high rarefaction of the air. But the number of molecules per cubic centimetre remains quite large and is about 1.5×10^{12}. For such a rarefied gas, the pressure and mass density may be calculated as the mean quantities in the given volume. The flow properties of such a gas are determined on the basis of the Maxwellian distribution of molecular velocities. Hence, by using this law, we can investigate the forces of interaction of the molecules with the surface of a moving body.

Between the continuum flow and free-molecule flow, there are an **intermediate flow** ($1 \leqslant Kn \leqslant 10$) and a **slip flow** ($0.01 \leqslant Kn \leqslant 1$). The intermediate flow is characterized by the same significance of collisions of molecules with the wall and with one another. Such a flow appears in a flight at altitudes of about 100 km. In slip flow, which appears at altitudes under 100 km, collisions between the molecules are more important. But although the mean free path is small in comparison with the linear dimension δ, it cannot be disregarded.

The difference in the flow conditions manifests itself in *different velocity profiles* between the parallel plates. In a continuum flow, the gas particles after colliding with the moving plate acquire the velocity V of the latter and the corresponding momentum (Fig. 15.1.1*a*). The momentum transferred to neighbouring particles because of skin friction diminishes. As a result, their velocity also drops, reaching zero at the surface of the plate at rest.

In a free-molecule flow (Fig. 15.1.1*b*), the particles after colliding with the wall do not change their momentum over the thick-

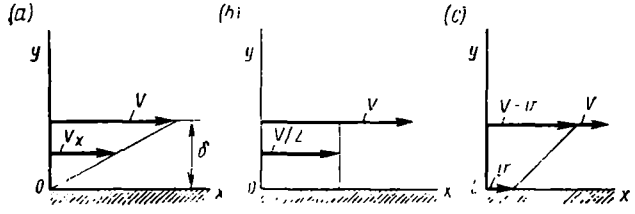

Fig. 15.1.1
Influence of flow conditions on the change in the velocity of a gas near a wall: *a*—continuum flow; *b*—free-molecule flow; *c*—slip flow

ness of the layer because upon rebounding they do not collide with other molecules. As a result, the transverse velocity gradient remains "zero". With diffusion interaction, the velocity of a molecule at the upper moving plate has the finite value V, while at the lower plate at rest it is zero. Hence, the average velocity of the molecules between the plates is $V/2$.

This is why the concept of a boundary layer loses its meaning in a free-molecule flow over a body because the flow near the surface has the same velocity as at a certain distance from it (as we usually consider—at the edge of the boundary layer).

The velocity profile with slip flow (Fig. 15.1.1*c*) occupies an intermediate position. The moving plate, as in a continuum flow, transmits to the particles a momentum corresponding to the velocity V. The particles rebounding from the plate, before reaching the opposite wall, collide with other particles and change their velocity. The explanation is that the mean path of the molecules is comparable with the distance δ. This velocity changes continuously between the plates, while the shape of the velocity profile is the mean one between the profiles for a continuum and a free-molecule flows. On the lower plate, the molecules, as it were, slip relative to the surface at a certain velocity v; their velocity on the upper plate evidently equals the difference $V - v$. This explains the name "slip flow". In an external slip flow over a body, the gas at the surface does not adhere to it, but acquires a certain non-zero velocity that is lower than at the edge of the boundary layer.

Hence, when slip is present, there is a velocity jump at the gas-solid interface. Near the wall, the transverse, velocity gradient is other than zero. This indicates that a boundary layer still exists in a slightly rarefied gas in a slip flow. Consequently, the motion near the surface does not obey the Maxwellian velocity distribution, and the general equations for a viscous heat-conducting compressible gas should be used to determine this motion. They have to be used, however, with a view to the more general boundary conditions reflecting a possible velocity, temperature, and pressure jump at

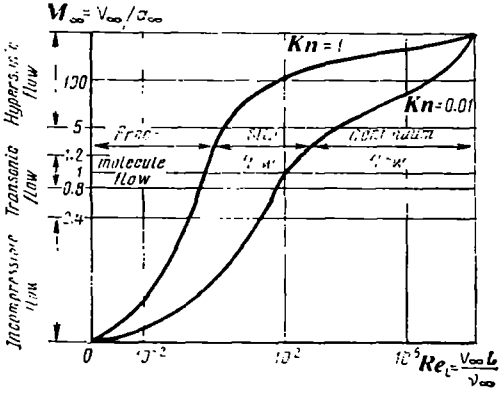

Fig. 15.1.2
Curves characterizing various flow conditions of a gas

the surface. The kind of flow is determined in accordance with formula (15.1.3) by the relation between the local numbers M and Re. If the distance between the plates is taken the same as the layer thickness in laminar flow, we can go over from the number $Re = V\delta/\nu$ to $Re_L = Re\,(L/\delta)$. Replacing the ratio δ/L by formula (13.3.19″) in which we assume that $\bar{x} = 1$ (we are considering the trailing edge of the plate) and inserting it into (15.1.3), we obtain a relation for the Knudsen number:

$$Kn = l/\delta = 0.264\sqrt{\bar{k}}\,(M/\sqrt{Re_L}) \qquad (15.1.4)$$

This relation for various flows is shown graphically in Fig. 15.1.2, where the curves have been plotted without account taken of the effect of possible physicochemical transformations of the air on the mean free path of the molecules. One must bear in mind here that dissociation is attended, as is known, by an increase in the number of particles, the result being a smaller mean free path.

The curves shown in Fig. 15.1.2 relate to an undisturbed flow. Investigations show, however, that they can be used to estimate the flow over a body if the local values of the numbers M and Re are used. It was found that far from the nose of a body of revolution where the influence of the nose shock is negligible, slip flow or free-molecule flow may arise even at low altitudes owing to overexpansion. At the same time, near the nose, the compression behind the shock wave may lead to the formation of a continuum even in high-altitude flights. This can be seen by using formula (15.1.4) and calculating the Knudsen number from the local gas parameters. When determining this number, we must choose the characteristic length δ. Since the expected flow conditions are determined approximately, the boundary layer thickness evaluated by the formula for a continuum is conditionally taken as δ.

15.2. Pressure and Skin Friction in a Free-Molecule Flow

Molecule-Wall Interaction

The investigation of the flow of a gas near a surface is associated with the solution of equations of motion for the boundary conditions imposed on this motion. Particularly, when studying a continuous flow over a surface, the condition of flow without separation as a form of interaction of this surface and the gas is the boundary condition. In free-molecule flow, the interaction is more involved.

A number of hypothetic schemes of molecule-wall interaction have been advanced in the theory of free-molecule flow. Let us consider schemes of the limiting kind of interaction—specular and diffuse reflection. We shall also treat an intermediate scheme, assuming that interaction which is a combination of the two indicated limiting kinds of reflection is closer to reality.

Specular Reflection. Specular molecular reflection is realized if the surface is very smooth and is inclined at a small angle of attack. The particles approaching the wall, after a collision with it, are reflected at an angle equal to the angle of attack (Fig. 15.2.1*a*). Hence, in the given scheme, the molecules behave like perfectly elastic spheres. In specular reflection, the magnitudes of the velocity components do not change; the tangential component to the surface retains its sign, while the normal component reverses it. With such perfect interaction of the particles with the wall, friction forces are absent. Investigations reveal that even thoroughly polished surfaces are not smooth enough to completely realize specular reflection. In practice, only an insignificant part of the molecules—a few per cent—are reflected in this way.

Diffuse Reflection. In diffuse reflection (Fig. 15.2.1*b*), it is assumed that the surface is rough. The height of the asperities and the

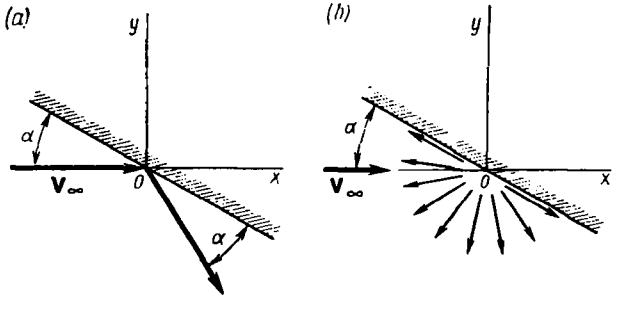

Fig. 15.2.1
Interaction of molecules with a wall:
a—specular reflection; *b*—diffuse reflection

width of the valleys should be comparable with the size of the molecules. As a result of collisions, the molecules get into a valley or between asperities and are almost completely absorbed by the wall, transmitting their momentum and energy to it. Next, after a short time, they are reflected from it in any arbitrary direction at a certain velocity, all directions being equally probable. The absence of a predominating direction of motion of diffuse reflected molecules leads to their producing no shear stress. Since a real surface always differs from a perfectly smooth one, the major part of the molecules interact by diffuse reflection.

Mass Transfer

Let us consider some features of a free-molecule flow over a body [26]. We shall assume that diffuse reflection of the molecules occurs, the temperature of the reflected particles being equal to the value T_r differing in the general case from the wall temperature T_w and the initial gas temperature T_1.

Let us consider the expression for mass transfer. The components of the velocity of a molecule are

$$u = u' + U, \quad v = v' + V, \quad w = w' + W$$

The first terms in these expressions are the components of the velocity V_∞ of the bulk (or ordered) motion of the gas relative to the wall determined from the expression

$$V_\infty^2 = u'^2 + v'^2 + w'^2$$

The second terms are the components of the velocity c of the thermal motion (the velocity of a molecule relative to the bulk motion of the gas). The square of this velocity is

$$c^2 = U^2 + V^2 + W^2 \qquad (15.2.1)$$

We shall assume that the y-axis, which the component v corresponds to, is normal to the surface at the given point.

Let us determine the transfer of molecules to the surface of a body that depends on the number of incident molecules contained in a unit volume. If the molecules travel at a velocity whose components in magnitude are within the intervals $u, u + du$; $v, v + dv$, and $w, w + dw$, the number of these molecules equals the product $n_1 f\, du\, dv\, dw$ in which n_1 is the number of incident molecules in unit volume (here and below the subscript "i" relates to the particles of the undisturbed flow whose parameters are T_∞, p_∞, ρ_∞, etc.), and f is a function of the velocity distribution of the molecules called the **Maxwellian distribution.**

In the kinetic theory, the distribution function is determined by the exponential relation

$$f = (\pi c_m^2)^{-3/2} \exp(-c^2/c_m^2) \tag{15.2.2}$$

in which the quantity c_m is related to the mean velocity of random motion $\bar{c}$ by the expression

$$c_m = \bar{c}\sqrt{\pi/4} \tag{15.2.3}$$

and is called the **most probable velocity of a molecule**. According to the kinetic theory of gases, the **mean velocity of the random motion** of molecules is

$$\bar{c} = 2\sqrt{2RT/\pi} \tag{15.2.4}$$

The function f relates only to the disordered part of motion of the molecules. It depends on the velocity of thermal motion c and, as can be seen from (15.2.3), on the mean velocity $\bar{c}$ determining the internal energy of a unit mass of the gas equal to $\bar{c}^2/2$. In the general case, the values of $\bar{c}$ and c depend on the coordinates and time. But if we consider the equilibrium velocity distribution (which is of major practical importance) when as a result of collisions in each given volume element $\tau = dx\,dy\,dz$ the number of molecules whose velocities belong to the velocity space element $du\,dv\,dw$ corresponding to this volume τ does not change, then the distribution function f will not depend on the time t. Such a gas state is defined as **local Maxwellian equilibrium.**

Let us consider the concept of the mean square velocity $\overline{c^2}$ of random motion determined from the condition

$$\overline{c^2}/3 = \overline{U^2} = \overline{V^2} = \overline{W^2} \tag{15.2.5}$$

where $\overline{U}$, $\overline{V}$, and $\overline{W}$ are the mean values of the velocity components in random motion. By the kinetic theory of gases,

$$\overline{c^2} = 3RT \tag{15.2.6}$$

Hence with a view to formulas (15.2.3) and (15.2.4) for $\bar{c}$, we find

$$\sqrt{\overline{c^2}} = 0.5\bar{c}\sqrt{3\pi/2} = c_m\sqrt{3/2} \tag{15.2.7}$$

i.e.

$$\sqrt{\overline{c^2}} = 1.086\bar{c} = 1.225c_m \tag{15.2.8}$$

We shall also note the relation existing between $\bar{c}$, $\sqrt{\overline{c^2}}$, and the speed of sound a:

$$a = \sqrt{kRT} = \bar{c}\sqrt{\pi k/8} = \sqrt{\overline{c^2}}\sqrt{k/3} \tag{15.2.8'}$$

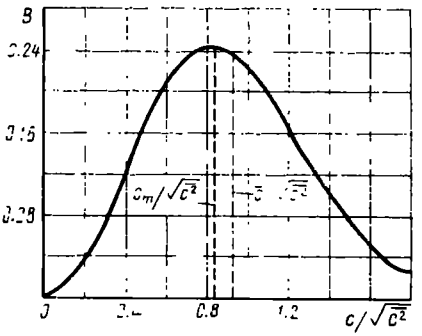

Fig. 15.2.2
Dependence of the distribution function on the parameter $c/\sqrt{\overline{c^2}}$

Hence it follows that the mean molecular velocities have the same order as the speed of sound.

The distribution function f can be determined with the aid of the graph shown in Fig. 15.2.2 and giving the dependence of the quantity $B = (\pi c_m^2)^{3/2}\,(c^2/\overline{c^2})\,f$ on the parameter $c/\sqrt{\overline{c^2}}$. Also shown in the figure are the relative quantities $c_m/\sqrt{\overline{c^2}}$ and $\bar{c}/\sqrt{\overline{c^2}}$.

Of the number of incident molecules contained in unit volume, the fraction that collides with a unit surface area per second is $n_1 v f\, du\, dv\, dw$. Consequently, in this case we consider the molecules that intersect the surface and occupy the separated volume with a unit base area and a height equal to the vertical velocity component v. This velocity is within the limits of $\infty > v > 0$. Particles with a velocity component $v < 0$ do not reach the separated area. We can find the total number of molecules N_1 colliding with a unit surface area per second by integration over all the possible velocities $-\infty < u < \infty$, $0 < v < \infty$, and $-\infty < w < \infty$, i.e.

$$N_1 = \int_{-\infty}^{\infty} du \int_{0}^{\infty} v\, dv \int_{-\infty}^{\infty} n_1 f\, dw \qquad (15.2.9)$$

or with a view to expressions (15.2.2) for f and (15.2.1) for c^2,

$$N_1 = n_1 (\pi c_{m,i}^2)^{-3/2} \int_{-\infty}^{\infty} \exp\left(-\frac{1}{2} H_1^2\right) du \int_{0}^{\infty} v \exp$$

$$\times \left(-\frac{1}{2} H_2^2\right) dv \int_{-\infty}^{\infty} \exp\left(-\frac{1}{2} H_3^2\right) dw \qquad (15.2.9')$$

where

$$\left.\begin{aligned} u = u' + \frac{c_{m,i}}{\sqrt{2}} H_1, \quad v = v' + \frac{c_{m,i}}{\sqrt{2}} H_2, \quad w = w' + \frac{c_{m,i}}{\sqrt{2}} H_3 \\ H_1/\sqrt{2} = U/c_{m,i}, \quad H_2/\sqrt{2} = V/c_{m,i}, \quad H_3/\sqrt{2} = W/c_{m,i} \end{aligned}\right\} \qquad (15.2.10)$$

With a view to (15.2.10), we can write the first integral in (15.2.9′) (the third integral will be similar to it) as follows:

$$\int_{-\infty}^{\infty} \exp\left(-\frac{1}{2}H_1^2\right) du = c_{m,1} \int_{-\infty}^{\infty} \exp\left(-\frac{1}{2}H_1^2\right) d\left(H_1/\sqrt{2}\right)$$

The integral on the right-hand side of this expression is the well known **Euler-Poisson integral**

$$\int_{-\infty}^{\infty} \exp\left(-\frac{1}{2}H_1^2\right) d\left(H_1/\sqrt{2}\right) = 2\int_{-\infty}^{\infty} \exp\left(-\frac{1}{2}H_1^2\right) \times d\left(H_1/\sqrt{2}\right) = \sqrt{\pi} \qquad (15.2.11)$$

Consequently,

$$\int_{-\infty}^{\infty} \exp\left(-\frac{1}{2}H_1^2\right) du = \int_{-\infty}^{\infty} \exp\left(-\frac{1}{2}H_3^2\right) dw = c_{m,i}\sqrt{\pi} \qquad (15.2.11')$$

The second integral in (15.2.9′) can be written as

$$\int_{0}^{\infty} v \exp\left(-\frac{1}{2}H_2^2\right) dv = c_{m,i} \int_{-v'/c_{m,i}}^{\infty} \left(v' + \frac{H_2}{\sqrt{2}} c_{m,i}\right) \times \exp\left(-\frac{1}{2}H_2^2\right) d\left(\frac{H_2}{\sqrt{2}}\right) = c_{m,i}^2 \int_{-\bar{x}}^{\infty} (\bar{x}+y)\, e^{-y^2}\, dy \qquad (15.2.12)$$

where we have introduced the notation

$$\bar{x} = v'/c_{m,i}, \quad y = H_2/\sqrt{2} \qquad (15.2.13)$$

Integration of (15.2.12) yields

$$\int_{0}^{\infty} v \exp\left(-\frac{1}{2}H_2^2\right) dv = \frac{c_{m,i}^2}{2} e^{-\bar{x}^2} + c_{m,i}^2 \bar{x} \int_{-\bar{x}}^{\infty} e^{-y^2}\, dy \qquad (15.2.12')$$

We shall write the integral on the right-hand side of (15.2.12′) in the form

$$\int_{-\bar{x}}^{\infty} e^{-y^2}\, dy = -\int_{0}^{-\bar{x}} e^{-y^2}\, dy + \int_{0}^{\infty} e^{-y^2}\, dy$$

The second integral of the last expression by (15.2.11) is

$$\int_{0}^{\infty} e^{-y^2}\, dy = \sqrt{\pi}/2 \qquad (15.2.14)$$

To determine the first integral of the same expression, we shall introduce a new variable $y = -z$ with account of which

$$-\int_0^{-\bar{x}} e^{-y^2}\,dy = \int_0^{\bar{x}} e^{-z^2}\,dz$$

The integral on the right-hand side of this expression can be calculated with the aid of the special function

$$\operatorname{erf}\bar{x} = \frac{2}{\sqrt{\pi}}\int_0^{\bar{x}} e^{-z^2}\,dz \qquad (15.2.15)$$

that is the probability integral. Its values are tabulated.

With account taken of (15.2.14) and (15.2.15), relation (15.2.12′) becomes

$$\int_0^{\infty} v\exp\left(-\frac{1}{2}H_2^2\right)dv = \frac{c_{m,i}^2}{2}\left[e^{-\bar{x}^2} + \bar{x}\sqrt{\pi}\,(1+\operatorname{erf}\bar{x})\right] \qquad (15.2.16)$$

With a view to (15.2.11′) and (15.2.16), we obtain the following relation for the total number of molecules N_1 instead of (15.2.9):

$$N_1 = \frac{n_1 c_{m.1}}{2\sqrt{\pi}}\left[e^{-\bar{x}^2} + \bar{x}\sqrt{\pi}\,(1+\operatorname{erf}\bar{x})\right] \qquad (15.2.17)$$

Since by (15.2.7) we have

$$c_{m,1} = \sqrt{2RT_1} \qquad (15.2.18)$$

then

$$N_1 = n_1\sqrt{\frac{RT_1}{2\pi}}\left[e^{-\bar{x}^2} + \bar{x}\sqrt{\pi}\,(1+\operatorname{erf}\bar{x})\right] \qquad (15.2.17')$$

The product RT_1 in formula (15.2.18) is related to the speed of sound by the expression

$$a_1 = \sqrt{kRT_1} \qquad (15.2.19)$$

A glance at (15.2.17′) reveals that the number of incident molecules is determined by the parameter $\bar{x}$ corresponding to the point of the surface being considered. If we express $c_{m.1}$ in terms of the speed of sound, then $\bar{x} = (v'/a_1)\sqrt{k/2}$. In addition, taking into consideration that β is the angle between the direction of the vector $\mathbf{V}_\infty$ and a tangent to the surface at the given point (Fig. 15.2.3), we find

$$\bar{x} = \sin\beta\frac{V_\infty}{a_1}\sqrt{\frac{k}{2}} = \bar{x}_\infty\sin\beta; \quad \bar{x}_\infty = \frac{V_\infty}{a_1}\sqrt{\frac{k}{2}} = M_\infty\sqrt{\frac{k}{2}} \qquad (15.2.20)$$

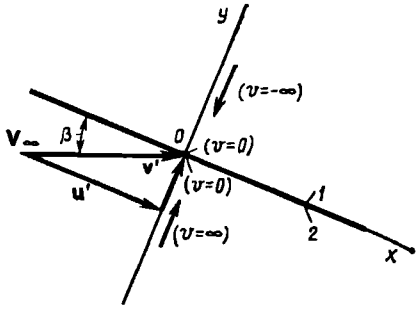

Fig. 15.2.3
Free-molecule flow over a flat surface:
1—upper surface; *2*—lower surface

Formula (15.2.17′) was obtained for the conditions on a surface which the limits $0 < v < \infty$ in the second definite integral of (15.2.9′) correspond to. The equation of mass transfer is different for the upper side of a surface, because in the integral in accordance with Fig. 15.2.3 the limits are $-\infty < v < 0$. Hence, for the upper surface, we have

$$N_1 = -n_1 (\pi c_{m,i}^2)^{-\frac{3}{2}} \int_{-\infty}^{\infty} \exp\left(-\frac{1}{2} H_1^2\right) \times du \int_{-\infty}^{0} v \exp\left(-\frac{1}{2} H_2^2\right) dv \int_{-\infty}^{\infty} \exp\left(-\frac{1}{2} H_3^2\right) dw \quad (15.2.21)$$

Here the first and third integrals are determined by the value of (15.2.11′). By analogy with (15.2.12), we shall write the second integral in the form

$$\int_{-\infty}^{0} v \exp\left(-\frac{1}{2} H_2^2\right) dv = c_{m,1}^2 \int_{-\infty}^{-\bar{x}} (\bar{x} + y) e^{-y^2} dy$$

$$= -0.5 c_{m,1}^2 e^{-\bar{x}^2} + c_{m,1}^2 \bar{x} \int_{-\infty}^{-\bar{x}} e^{-y^2} dy$$

The integral on the right-hand side of this expression is

$$\int_{-\infty}^{-\bar{x}} e^{-y^2} dy = \int_{0}^{-\bar{x}} e^{-y^2} dy + \int_{-\infty}^{0} e^{-y^2} dy = \frac{\sqrt{\pi}}{2} (1 - \operatorname{erf} \bar{x})$$

Conseguently,

$$\int_{-\infty}^{0} v \exp\left(-\frac{1}{2} H_2^2\right) dv = 0.5 c_{m,1}^2 [e^{-\bar{x}^2} - \bar{x} \sqrt{\pi} (1 - \operatorname{erf} \bar{x})]$$

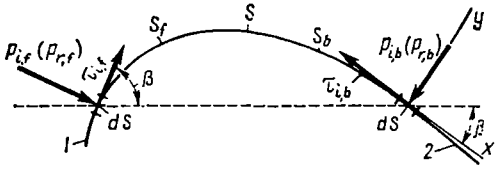

Fig. 15.2.4
Free-molecule flow over a curved surface:
1–front side; *2*–back side

Taking into account the obtained values of the integrals in (15.2.21), by analogy with (15.2.17′) we find a relation for the number of incident molecules on the upper area:

$$N_1 = n_1 \sqrt{\frac{RT_1}{2\pi}} [e^{-\bar{x}^2} - \bar{x}\sqrt{\pi}\,(1 - \operatorname{erf}\bar{x})] \qquad (15.2.22)$$

When considering a free-molecule flow over a curved surface (Fig. 15.2.4), we may use formula (15.2.17′) to calculate the number of molecules incident on the front side of this surface, and formula (15.2.22), on the back side. Formulas (15.2.17′) and (15.2.22) can be simplified for high velocities, taking advantage of the fact that already for $\bar{x} \geqslant 2$ the quantity $\exp(-\bar{x}^2)$ is at least by a factor of 10^2 smaller than unity, while the probability integral $\operatorname{erf} x$ differs only slightly from unity. For example, at $\bar{x} = 2$, the quantity $\exp(-\bar{x}^2) = 0.018$, and $\operatorname{erf}\bar{x} = 0.995$. The value

$$M_\infty = (\bar{x}/\sin\beta)\sqrt{2/k}$$

corresponds to each value of x. Particularly, for $\bar{x} = 2$, $\sin\beta = 0.2$, and $k = 1.4$, the number $M_\infty = 12$. At $\beta = 90°$, the smallest of the possible numbers M_∞ for $\bar{x} = 2$ drops to 2.4. Consequently, formula (15.2.17′) can be simplified as follows:

$$N_{1,f} = \bar{x} n_1 \sqrt{2RT_1} = n_1 V_\infty \sin\beta \qquad (15.2.23)$$

Here the subscript "f" indicates that we are dealing with the front side of the curved surface. If we are dealing with the back side (subscript "b"), it is not difficult to see that formula (15.2.22) with a view to our assumptions transforms into the equality

$$N_{1,b} = 0 \qquad (15.2.24)$$

because at a high flight speed of a body the molecules do not reach the back side of its surface.

Let us consider the transfer of the reflected molecules. Diffuse reflection occurs according to the Maxwellian distribution, hence we may use relations (15.2.17′) and (15.2.22), assuming that $\bar{x} = 0$ because after a collision the particles lose their bulk velocity. Since

the reflected particles have a different temperature T_r, then

$$N_r = n_r \sqrt{RT_r/(2\pi)} \qquad (15.2.25)$$

where n_r is the number of reflected molecules in unit volume.

If we assume that the total number of incident particles equals the number of reflected ones, i.e. $N_1 = N_r$, by equating the right-hand sides of expressions (15.2.17′) and (15.2.25), we can find a relation between the concentrations n_r and n_1 for the front side of the surface in the flow:

$$n_{r,f} = n_1 \sqrt{T_1/T_r}\,[e^{-\bar{x}^2} + \bar{x}\sqrt{\pi}\,(1 + \operatorname{erf}\bar{x})] \qquad (15.2.26)$$

We obtain a similar expression for the back side by equating the right-hand sides of (15.2.22) and (15.2.25):

$$n_{r,b} = n_1 \sqrt{T_1/T_r}\,[e^{-\bar{x}^2} - \bar{x}\sqrt{\pi}\,(1 - \operatorname{erf}\bar{x})] \qquad (15.2.27)$$

Pressure

The pressure on an area is determined by the total loss of momentum by a group of molecules in a direction normal to the surface as a result of their collisions with the wall, i.e. the pressure equals the sum of the momenta per unit time of these molecules before colliding. A general expression for the pressure is obtained as follows. The pressure produced by a molecule numerically equals its momentum mv. That produced by a group of molecules colliding in unit time with unit surface area is $mn_1v^2f\,du\,dv\,dw$. Consequently, the pressure exerted by the molecules incident on the front area is

$$p_{1,f} = \rho_1 (\pi c_{m,1}^2)^{-\frac{3}{2}} \int_{-\infty}^{\infty} \exp\left(-\tfrac{1}{2} H_1^2\right)$$

$$\times\, du \int_0^{\infty} v^2 \exp\left(-\tfrac{1}{2} H_2^2\right) dv \int_{-\infty}^{\infty} \exp\left(-\tfrac{1}{2} H_3^2\right) dw \qquad (15.2.28)$$

where $\rho_1 = mn_1$ is the density of the gas.

The values of the first and third integrals have been determined by (15.2.11′).

The second integral by analogy with (15.2.12) has the form

$$\int_0^{\infty} v^2 \exp\left(-\tfrac{1}{2} H_2^2\right) dv = c_{m,1}^3 \int_{-\bar{x}}^{\infty} (\bar{x} + y)^2 e^{-y^2}\, dy$$

$$= c_{m,1}^3 \bar{x}^2 \int_{-\bar{x}}^{\infty} e^{-y^2}\, dy + 2c_{m,1}^3 \bar{x} \int_{-\bar{x}}^{\infty} y e^{-y^2}\, dy + c_{m,1}^3 \int_{-\bar{x}}^{\infty} y^2 e^{-y^2}\, dy$$

Here the first and second integrals on the right-hand side were calculated previously. Let us determine the third integral, taking it by parts:

$$\int_{-\bar{x}}^{\infty} y^2 e^{-y^2}\, dy = \frac{1}{2}\left(-\bar{x}\, e^{-\bar{x}^2} + \frac{\sqrt{\pi}}{2}\operatorname{erf}\bar{x} + \frac{\sqrt{\pi}}{2}\right)$$

Hence,

$$\int_{0}^{\infty} v^2 e^{-\frac{1}{2}H_2^2}\, dv = \frac{\sqrt{\pi}}{2}\, c_{\mathrm{m,i}}^3 (1+\operatorname{erf}\bar{x})\left(\bar{x}^2+\frac{1}{2}\right) + \frac{c_{\mathrm{m,i}}^2}{2}\,\bar{x}\, e^{-\bar{x}^2}$$

Taking into account this relation and the values of the first and third integrals in (15.2.28), each of which equals $c_{\mathrm{m,i}}\sqrt{\pi}$, and also the expression $\bar{x}^2 = \sin^2\beta\,\frac{V_\infty^2}{a_1^2}\cdot\frac{k}{2} = \sin^2\beta\,\frac{V_\infty^2}{c_{\mathrm{m,i}}^2}$, after the corresponding substitutions in (15.2.28) we find a formula for the dimensionless pressure on the front side of the surface:

$$\bar{p}_{1,\mathrm{f}} = \frac{2p_{1,\mathrm{f}}}{\rho_1 V_\infty^2} = \sin^2\beta\left[\frac{1}{\bar{x}\sqrt{\pi}}\, e^{-\bar{x}^2} + \left(1+\frac{1}{2\bar{x}^2}\right)(1+\operatorname{erf}\bar{x})\right] \qquad (15.2.29)$$

To find the pressure on the back side of the surface, we must use the same expression (15.2.28) after replacing the integration limits with $-\infty < v < 0$. Accordingly

$$p_{1,\mathrm{b}} = \rho_1 (\pi c_{\mathrm{m,i}}^2)^{-3/2} \int_{-\infty}^{\infty} \exp\left(-\frac{1}{2}H_1^2\right)$$

$$\times\, du \int_{-\infty}^{0} v^2 \exp\left(-\frac{1}{2}H_2^2\right) dv \int_{-\infty}^{\infty} \exp\left(-\frac{1}{2}H_3^2\right) dw$$

where

$$\int_{-\infty}^{0} v^2 \exp\left(-\frac{1}{2}H_2^2\right) dv = c_{\mathrm{m,i}}^3 \int_{-\infty}^{-\bar{x}} (\bar{x}+y)^2 e^{-y^2}\, dy$$

$$= \frac{\sqrt{\pi}}{2}\, c_{\mathrm{m,i}}^2 (1-\operatorname{erf}\bar{x})\left(\bar{x}^2+\frac{1}{2}\right) - \frac{c_{\mathrm{m,i}}^3}{2}\,\bar{x}\, e^{-\bar{x}^2} \qquad (15.2.30)$$

With a view to (15.2.30), we shall find the dimensionless pressure on the back area:

$$p_{1,\mathrm{b}} = \frac{2p_{1,\mathrm{b}}}{\rho_1 V_\infty^2} = \sin^2\beta\left[\frac{-1}{\bar{x}\sqrt{\pi}}\, e^{-\bar{x}^2} + \left(1+\frac{1}{2\bar{x}^2}\right)(1-\operatorname{erf}\bar{x})\right] \qquad (15.2.31)$$

It is easy to see that the relations for the flow of a gas over the back side of a surface can be obtained from the corresponding expressions for the front side, substituting $-\bar{x}$ for $\bar{x}$.

In addition to the incident particles, the diffuse reflected ones also produce a pressure whose magnitude equals the sum of the moments of the molecules leaving the wall normally to it. Since the process of reflection of a particle occurs according to the Maxwellian velocity distribution corresponding to the temperature T_r and the zero velocity of bulk ordered motion (reflection occurs from a surface at rest), we use expression (15.2.28), assuming that $u' = v' = w' = 0$, and go over to parameters with the subscript r. Accordingly, for the front area

$$p_{r,f} = \rho_r (\pi c_{m,r}^2)^{-\frac{3}{2}} \int_{-\infty}^{\infty} \exp\left(-\frac{1}{2} H_1^2\right) \times dU \int_0^{\infty} V^2 \exp\left(-\frac{1}{2} H_2^2\right) dV \int_{-\infty}^{\infty} \exp\left(-\frac{1}{2} H_3^2\right) dW$$

After calculating the integrals, we have

$$p_{r,f} = R\rho_r T_r/2 \qquad (15.2.32)$$

Since the density of the reflected particles is $\rho_r = mn_r$, while their number in unit volume n_r is determined from the condition of steady flow $N_r = N_1$ by formula (15.2.26), then for the pressure due to diffuse reflection we obtain

$$\bar{p}_{r,f} = \frac{2p_{r,f}}{\rho_1 V_\infty^2} = \frac{\sin^2\beta}{2\bar{x}^2} \sqrt{\frac{\overline{T_r}}{T_1}} \left[e^{-\bar{x}^2} + \bar{x}\sqrt{\pi}\,(1 + \operatorname{erf}\bar{x})\right] \qquad (15.2.33)$$

A similar formula for an area on the back surface is

$$\bar{p}_{r,b} = \frac{2p_{r,b}}{\rho_1 V_\infty^2} = \frac{\sin^2\beta}{2\bar{x}^2} \sqrt{\frac{\overline{T_r}}{T_1}} \left[e^{-\bar{x}^2} - \bar{x}\sqrt{\pi}\,(1 - \operatorname{erf}\bar{x})\right] \qquad (15.2.34)$$

The total value of the dimensionless pressure equals the sum of the corresponding values of p_1 and p_r. For an area on the front surface

$$\bar{p}_f = 2\,(p_{1,f} + p_{r,f})/(\rho_1 V_\infty^2) = \bar{p}_{1,f} + \bar{p}_{r,f} \qquad (15.2.35)$$

and on the back one

$$\bar{p}_b = 2\,(p_{1,b} + p_{r,b})/(\rho_1 V_\infty^2) = \bar{p}_{1,b} + \bar{p}_{r,b} \qquad (15.2.36)$$

where the values of the dimensionless pressure $\bar{p}_{1,f}$ and $\bar{p}_{r,f}$ are found from expressions (15.2.29) and (15.2.33), and of $\bar{p}_{1,b}$ and $\bar{p}_{r,b}$, from (15.2.31) and (15.2.34).

Instead of relations (15.2.35) and (15.2.36), we can use a generalized expression for the dimensionless pressure obtained after the corresponding summation:

$$\bar{p} = \frac{2(p_1 + p_r)}{\rho_1 V_\infty^2} = \sin^2\beta \left[\frac{\pm 1}{\bar{x}} \left(\frac{1}{\sqrt{\pi}} \pm \frac{1}{2\bar{x}} \sqrt{\frac{T_r}{T_1}} \right) e^{-\bar{x}^2} \right.$$
$$\left. + \left(1 + \frac{1}{2\bar{x}^2} \pm \frac{\sqrt{\pi}}{2\bar{x}} \sqrt{\frac{T_r}{T_1}} \right) (1 \pm \operatorname{erf} \bar{x}) \right] \qquad (15.2.37)$$

where the plus sign relates to an area on the front surface, and the minus sign on the back one.

Examination of (15.2.37) reveals that the pressure depends on the orientation of the area being considered relative to the velocity vector $\mathbf{V}_\infty$ (i.e. on the angle β), the number M_∞, and the temperature ratio T_r/T_1.

At high velocities, which values of $\bar{x} \geqslant 2$ correspond to, the formulas for the dimensionless pressure can be simplified. We obtain the following approximate relations from (15.2.29) and (15.2.31):

$$\bar{p}_{1,f} = 2 \sin^2 \beta \, [1 + 1/(2\bar{x}^2)] \qquad (15.2.38)$$

$$\bar{p}_{1,b} = 0 \qquad (15.2.39)$$

By (15.2.33) and (15.2.34), we can write the corresponding formulas relating to the reflection process in the form

$$\bar{p}_{r,f} = \frac{\sin^2 \beta}{\bar{x}} \sqrt{\pi \frac{T_r}{T_1}} \qquad (15.2.40)$$

$$\bar{p}_{r,b} = 0 \qquad (15.2.41)$$

With a view to these expressions, we obtain simplified relations or the total value of the dimensionless pressure:

$$\bar{p}_f = \bar{p}_{1,f} + \bar{p}_{r,f} = 2 \sin^2 \beta \left(1 + \frac{1}{2\bar{x}^2} + \frac{\sqrt{\pi}}{2\bar{x}} \sqrt{\frac{T_r}{T_1}} \right) \qquad (15.2.42)$$

$$\bar{p}_b = 0 \qquad (15.2.43)$$

Shear Stress

The shear stress is a result of the momentum of the molecules completely losing their tangential component in a collision. This loss of momentum for one molecule is mu, and for those colliding with unit surface area in unit time is $n_1 mfuv \, du \, dv \, dw$. Consequently, the shear stress due to the incidence of all the molecules on a front

surface area is

$$\tau_1 = \rho_1 (\pi c_{m,i}^2)^{-\frac{3}{2}} \int_{-\infty}^{\infty} u \exp\left(-\frac{1}{2} H_1^2\right) \times du \int_0^{\infty} v \exp\left(-\frac{1}{2} H_2^2\right) dv \int_{-\infty}^{\infty} \exp\left(-\frac{1}{2} H_3^2\right) dw \quad (15.2.44)$$

Using (15.2.10), we transform (15.2.44) as follows:

$$\tau_1 = \rho_1 (\pi c_{m,i}^2)^{-\frac{3}{2}} c_{m,i}^3 \underbrace{\int_{-\infty}^{\infty} \left(u' + \frac{H_1}{\sqrt{2}} c_{m,1}\right) \exp\left(-\frac{1}{2} H_1^2\right) d\left(\frac{H_1}{\sqrt{2}}\right)}_{1} \times \underbrace{\int_{-v'/c_{m,i}}^{\infty} \left(v' + \frac{H_2}{\sqrt{2}} c_{m,1}\right) \exp\left(-\frac{1}{2} H_2^2\right) d\left(\frac{H_2}{\sqrt{2}}\right)}_{2} \times \underbrace{\int_{-\infty}^{\infty} \exp\left(-\frac{1}{2} H_3^2\right) d\left(\frac{H_3}{\sqrt{2}}\right)}_{3} \quad (15.2.44')$$

The integrals on the right-hand side of the equation have the following values:

$$\left.\begin{array}{l} (1)\ u'\sqrt{\pi} \\ (2)\ 0.5 c_{m,1} \left[e^{-\bar{x}^2} + \bar{x}\sqrt{\pi}(1 - \operatorname{erf} \bar{x})\right] \\ (3)\ \sqrt{\pi} \end{array}\right\} \quad (15.2.45)$$

Friction on an area of the back surface is determined by the same expression (15.2.44') with substitution of $-\infty < v < 0$ for the limits of the second integral. Accordingly, for the second integral, we have

$$0.5 c_{m,1} \left[e^{-\bar{x}^2} - \bar{x}\sqrt{\pi}(1 - \operatorname{erf} \bar{x})\right] \quad (15.2.46)$$

Bearing in mind these values of the integrals, and also taking into consideration that

$$u' = V_\infty \cos\beta, \quad \bar{x} = (V_\infty / c_{m,1}) \sin\beta \quad (15.2.47)$$

we obtain the following relation for the friction factor from (15.2.44'):

$$c_{f,1} = 2\tau_1/(\rho_1 V_\infty^2) = \sin\beta \cos\beta \left[\pm e^{-\bar{x}^2}/(\bar{x}\sqrt{\pi}) + (1 \pm \operatorname{erf} \bar{x})\right] \quad (15.2.48)$$

where the plus sign relates to an area on the front surface, and the minus sign, to an area on the back one.

Since all directions of motion of the reflected molecules are equally probable, their overall action produces no shear stress, i.e. $\tau_r = 0$ and, therefore,

$$c_{f,r} = 0 \tag{15.2.49}$$

We shall note that for a surface without inclination ($\beta = 0$), the friction factor is

$$c_{f,1} = 1/(\bar{x}_\infty \sqrt{\pi}) = (1/M_\infty)\sqrt{2/(k\pi)} \tag{15.2.50}$$

The relations are also simplified when $\bar{x} \geqslant 2$. For the conditions on a front and back areas, they are, respectively,

$$c_{(f,1)_f} = \sin 2\beta \tag{15.2.51}$$

$$(c_{f,1})_b = 0 \tag{15.2.52}$$

Transfer of Kinetic Energy

To determine the pressure, we must know the temperature ratio T_r/T_1. Calculation of this ratio is associated with finding of the energy of translational motion of the molecules that is transferred to the surface when the molecules collide with it and that is rejected from it as a result of their reflection. Each molecule upon colliding with the surface gives up to it the energy

$$0.5\, mc^2 = 0.5\, m\,(U^2 + V^2 + W^2) \tag{15.2.53}$$

The energy supplied by the number of molecules incident on unit surface area per unit time is $0.5mn_1c^2fv\ du\ dv\ dw$. Integrating this expression with respect to u and w between the limits from $-\infty$ to ∞, and with respect to v from 0 to ∞ for an area on the front surface (or from $-\infty$ to 0 for an area on the back one), we obtain the total amount of transferred energy E_1 upon a collision. With a view to the value of f given by (15.2.2), we have

$$E_1 = 0.5mn_1(\pi c_{m,i}^2)^{-3/2} \int_{-\infty}^{\infty} \int_{t_L}^{t_u} \int_{-\infty}^{\infty} c^2 \exp\left(-\frac{c^2}{c_{m,i}^2}\right) v\, du\, dv\, dw \tag{15.2.54}$$

where for a front area $t_L = 0$, $t_u = \infty$, and for a back one $t_L = -\infty$, $t_u = 0$.

Taking into consideration expression (15.2.53) for $0.5\, mc^2$, and also relation (15.2.10) and performing integration, we find

$$E_1 = 0.5mN_1\{V_\infty^2 + RT_1[4 + 1/(\varphi + 1)]\} \tag{15.2.55}$$

where N_1 is determined by formulas (15.2.17′) for a front area and by (15.2.22) for a back one, while the function

$$\varphi = e^{-\bar{x}^2}[\pm \bar{x}\sqrt{\pi}(1 \pm \operatorname{erf}\bar{x})]^{-1} \tag{15.2.56}$$

The reflected particles carry away the elementary energy $0.5mn_r c^2 f U\,dU\,dV\,dW$ from a unit of surface area. Integrating with respect to U and W between the limits from $-\infty$ to ∞ and with respect to V from $-\infty$ to zero, we obtain the total carried off energy:

$$E_r = 0.5mn_r (\pi c_{m,r}^2)^{-3/2} \int_{-\infty}^{\infty} \int_{-\infty}^{0} \int_{-\infty}^{\infty} c^2 \exp\left(-\frac{c^2}{c_{m,r}^2}\right) V\,dU\,dV\,dW \tag{15.2.57}$$

Evaluation of the triple integral yields

$$E_r = \rho_r (RT_r)^{3/2} (2/\pi)^{1/2} \tag{15.2.58}$$

Let us substitute mn_r for the density ρ_r and then substitute for n_r its value from (15.2.25):

$$E_r = 2mN_r RT_r \tag{15.2.59}$$

Inserting the value of $N_r = N_i$ with a view to (15.2.17′) and (15.2.22) and taking into consideration that $m = \rho_i/n_i$, we obtain

$$E_r = 2mN_i RT_r = \sqrt{2/\pi}\,\rho_i RT_r \sqrt{RT_i}\,[e^{-\bar{x}^2} \pm \bar{x}\sqrt{\pi}\,(1 \pm \operatorname{erf}\bar{x})] \tag{15.2.60}$$

where $mR = 1.38 \times 10^{-23}$ J/K is the **Boltzmann constant.**

The total kinetic energy of the molecules equals the difference between the supplied and carried off energies:

$$E = E_i - E_r$$

At high velocities ($\bar{x} \gg 2$), we can assume that $\varphi_f \approx \varphi_b \approx 0$ both for the front and back surfaces. With a view to formulas (15.2.17′), (15.2.22), (15.2.55), and (15.2.56), and also simplifying, we obtain

$$E_{i,f} = 0.5\bar{x}\rho_i \sqrt{2RT_i}\,(V_\infty^2 + 5RT_i) \tag{15.2.61}$$

$$E_{i,b} = 0 \tag{15.2.62}$$

For the energy of the reflected particles, the corresponding relations using (15.2.60) become

$$E_{r,f} = 2\sqrt{2}\,\rho_i RT_r \bar{x} \sqrt{RT_i} \tag{15.2.63}$$

$$E_{r,b} = 0 \tag{15.2.64}$$

15.3. Accommodation

Momentum Exchange

We already know that in transfer processes, on the basis of the hypothesis of diffuse reflection, the molecules have time to completely adapt themselves to the conditions on a wall, and the contact be-

tween the wall and the molecules is sufficient to transfer the momentum of all the molecules to the wall.

Experimental research reveals that the real processes of interaction of molecules with a surface differ from diffuse reflection and are characterized by reflection of a more general kind.

The concept of reflection being considered is founded on the idea that the normal and tangential components of the force produced by the reflected flow are determined, respectively, by the **accommodation coefficient of the normal momentum component**

$$f_n = (p_1 - p_r)/(p_1 - p_w) \tag{15.3.1}$$

and the **accommodation coefficient of the tangential momentum component**

$$f_\tau = (\tau_1 - \tau_r)/\tau_1 \tag{15.3.2}$$

In accordance with this concept, only a fraction of the incident molecules f_n transfer the normal momentum component to the wall. The fraction of all the molecules transmitting a tangential momentum component is determined by the coefficient f_τ. It is evident that for completely specular reflection $f_n = f_\tau = 0$ (with $p_1 = p_r$ and $\tau_1 = \tau_r$), while for completely diffuse reflection $f_n = f_\tau = 1$ (with $p_r = p_w$ and $\tau_r = 0$).

The pressure p_w in (15.3.1) can be considered as the normal component of the momentum of the molecules that are reflected in accordance with the Maxwell distribution of the velocity corresponding to thermodynamic equilibrium at a surface temperature of T_w when the surface is at rest ($V_\infty = 0$). By (15.2.32)

$$p_w = 0.5\, R\rho_w T_w$$

or, taking into consideration that $\rho_w = mn_w$, we have

$$p_w = 0.5 mRn_w T_w$$

To go over to the free-stream density, we shall use the relation $\rho_1 = mn_1$, by means of which we obtain

$$p_w = 0.5\, R\rho_1 T_w n_w/n_1$$

To find the ratio n_w/n_1, we shall use the relationship determining the equality of the number of reflected N_w and incident N_1 molecules:

$$n_w \sqrt{RT_w/(2\pi)} = N_1 = (N_1/n_1)\, n_1$$

where N_1 is determined by (15.2.17') and (15.2.22). Having calculated the ratio n_w/n_1, we find the following formula for the pressure:

$$\bar{p}_w = \frac{2p_w}{\rho_1 V_\infty^2} = \frac{\sin^2\beta}{2\bar{x}^2} \sqrt{\frac{T_w}{T_1}} \left[e^{-\bar{x}^2} \pm \bar{x}\sqrt{\pi}\,(1 \pm \operatorname{erf}\bar{x})\right] \tag{15.3.3}$$

where the plus sign corresponds to an area on the front surface, and the minus sign to an area on the back one.

The coefficients f_n and f_τ are not identical because they characterize different processes of momentum transfer upon reflection. But in approximate calculations, we can proceed from the Maxwell hypothesis according to which the reflection process is characterized by the same momentum accommodation coefficient $f = f_n = f_\tau$ indicating that the fraction f of all the molecules undergo diffuse reflection, and the fraction $(1 - f)$, specular reflection.

Consequently, by (15.3.1), the pressure p_r upon reflection is

$$p_r = p_1 (1 - f) + f p_w$$

The total pressure is

$$p = p_1 + p_r = (2 - f)\, p_1 + f p_w \qquad (15.3.4)$$

Inserting into (15.3.4) instead of p_1 either the value of $p_{1,f}$ from (15.2.29) or of $p_{1,b}$ from (15.2.31), and also the value of p_w from (15.3.3), we obtain

$$\bar{p} = \frac{2(p_1 + p_r)}{\rho_1 V_\infty^2} = \sin^2\beta \left\{ (2-f) \left[\frac{\pm e^{-\bar{x}^2}}{\bar{x}\sqrt{\pi}} + \left(1 + \frac{1}{2\bar{x}^2}\right)(1 \pm \operatorname{erf}\bar{x}) \right] \right.$$
$$\left. + \frac{f}{2\bar{x}^2} \sqrt{\frac{T_w}{T_1}} \left(e^{-\bar{x}^2} \pm \bar{x}\sqrt{\pi}\,(1 \pm \operatorname{erf}\bar{x})\right) \right\} \qquad (15.3.5)$$

The total shear stress due to the incident and reflected molecules is $\tau = \tau_1 - \tau_r$. Introducing the value of $\tau_r = (1 - f)\,\tau_1$ obtained from (15.3.2), we find

$$\tau = \tau_1 - \tau_r = \tau_1 f \qquad (15.3.6)$$

The corresponding friction factor by (15.2.48) is

$$c_f = \frac{2\tau}{\rho_1 V_\infty^2} = \frac{2\tau_1 f}{\rho_1 V_\infty^2} = f \sin\beta \cos\beta \left[\frac{\pm e^{-\bar{x}^2}}{\bar{x}\sqrt{\pi}} + (1 \pm \operatorname{erf}\bar{x}) \right] \qquad (15.3.6')$$

For very high velocities ($\bar{x} \geqslant 2$) and a greatly cooled wall ($T_w < T_1$), relation (15.3.5) can be simplified. Adopting the plus sign (we are considering an area on the front surface), we find

$$\bar{p}_f = 2\,(2 - f) \sin^2\beta \qquad (15.3.7)$$

For the same high velocities, the friction factor on a front area is

$$(c_f)_f = f \sin 2\beta \qquad (15.3.8)$$

and on a back area for the indicated conditions

$$\bar{p}_b = 0, \quad (c_f)_b = 0 \qquad (15.3.9)$$

Equations (15.3.7) and (15.3.8) reveal the influence of accommodation on the pressure and skin friction. With an increase in f, the

pressure coefficient $\bar{p}_f$ lowers, while the friction factor $(c_f)_f$ grows. Such an effect is explained physically by the reduction in the number of specularly reflected molecules. This causes a reduction in the additional momentum ("reactive force"), which lowers the pressure. At the same time, the number of the molecules that do not transfer their momentum to the tangential component diminishes, which leads to an increase in the friction factor.

The coefficient f in the above expressions is close to unity and may be taken equal to it in calculations. In the limiting case of completely specular reflection, which is not real, the coefficient $f = 0$. In the other limiting case of completely diffuse reflection, which is more probable, the coefficient $f = 1$.

Experimental investigations of the interaction of hydrogen, helium, and oxygen with the polished surface of silver oxide, and also of the contact of air with brass show that $f \approx 0.99$; this confirms the presence of virtually complete diffuse reflection. At the same time, similar investigations allow us to establish that for some combinations of a gas and a surface, the coefficient f may be appreciably lower than unity.

Energy Exchange

The absence of complete accommodation features not only the process of momentum transfer, but also to a greater extent, as shown by experimental studies, the process of energy exchange between the incident molecules and a wall. It is therefore assumed in formula (15.2.60) for the energy of the reflected molecules that their temperature T_r differs from that of the wall T_w. In this case, the contact of the incident molecules with the wall is not long enough to transfer to them upon reflection the average energy corresponding to the temperature T_w and equal, by (15.2.60), to

$$E_w = 2mN_1RT_w = \sqrt{2/\pi}\,\rho_1 RT_w \sqrt{RT_1}\,[e^{-\bar{x}^2} \pm \bar{x}\sqrt{\pi}\,(1 \pm \operatorname{erf}\bar{x})] \tag{15.3.10}$$

The case of reflection being considered is the most general one and is characterized by the absence of complete accommodation between the solid boundary and the molecules upon the exchange of energy. Therefore, in this general case, the relation

$$\eta = (E_1 - E_r)/(E_1 - E_w) \tag{15.3.11}$$

known as the **thermal accommodation coefficient** is other than unity. The arising discontinuity in the energy affects the temperature jump, i.e. the difference between T_r and T_w.

The accommodation coefficient η is of major importance in calculating heat transfer. This is why we must be able to appraise its

value, which at present is possible only experimentally. Observations reveal that the nature of the change in the thermal accommodation coefficient is very complicated. It was established, particularly, that the value of η grows with an increase in the molar mass and the temperature of the surface. We can assume that the accommodation coefficient depends on the flight speed of a body, the angle of incidence of the molecules, the properties of the material, and the state of the surface. Investigations show that the values of the accommodation coefficient for air interacting with aluminium and steel having various surface processing are close to unity and range from 0.7 to 0.97. For machined surfaces and light molecules, particularly of gases such as hydrogen and helium, the value of η may reach about 0.01.

A comparison of the thermal η and "force" f accommodation coefficients shows that $f \gg \eta$. It follows that although the incident molecules experience multifold collisions with the wall and the reflection process is close to a diffuse one, the duration of contact of these molecules with the wall is insufficient for the reflected molecules to acquire the wall temperature.

We can consider the limiting case when $\eta = 1$. This corresponds to the instant when the temperature T_r of the reflected molecules approaches the wall temperature T_w. In this case, the molecules, as it were, completely adapt themselves to the conditions at the wall.

15.4. Aerodynamic Forces

General Expression for the Drag Force

To use the relations obtained in Secs. 15.2 and 15.3, let us consider the determination of the aerodynamic drag force. We shall find a general expression for the force acting on a local unit area without taking the effect of accommodation into account, i.e. assuming that the coefficient $f = 1$. As a result of collision with such an area on the front side of a body (see Fig. 15.2.4), the pressure and skin friction cause a longitudinal force to arise that by (15.2.29) and (15.2.48) is

$$F_{1,f} = p_{1,f} \sin\beta + \tau_{1,f} \cos\beta = \frac{\rho_1 V_\infty^2}{2} \sin\beta \left[\frac{e^{-\bar{x}^2}}{\bar{x}\sqrt{\pi}} + \left(1 + \frac{\sin^2\beta}{2\bar{x}^2}\right)(1 + \operatorname{erf}\bar{x}) \right] \tag{15.4.1}$$

The force acting on an elementary area dS on the front side is

$$dX_{1,f} = F_{1,f}\, dS \tag{15.4.2}$$

while the total longitudinal force is

$$X_{1,f} = \int\limits_{(S_f)} F_{1,f}\, dS \qquad (15.4.3)$$

where S_f is the surface area of the front side.

The corresponding drag coefficient is

$$c_{x.1,f} = \frac{2X_{1.f}}{\rho_1 V_\infty^2 S_{mid}}$$

$$= \int\limits_{(\bar{S}_f)} \sin\beta \left[\frac{e^{-\bar{x}^2}}{\bar{x}\sqrt{\pi}} + \left(1 + \frac{\sin^2\beta}{2\bar{x}^2}\right)(1 + \operatorname{erf}\bar{x}) \right] d\bar{S} \qquad (15.4.4)$$

where $\bar{S} = S/S_{mid}$, $\bar{x} = (V_\infty/c_{m,1}) \sin\beta = \bar{x}_\infty \sin\beta$, and $\bar{S}_f = S_f/S_{mid}$.

We integrate through the front part of the surface with an area of S_f. We obtain similar relations for the force and coefficient corresponding to the back side of the surface.

Examination of Fig. 15.2.4 reveals that

$$F_{1,b} = p_{1,b} \sin\beta + \tau_{1,b} \cos\beta$$

Here we take the magnitude of the angle β. Using formula (15.2.31) for $p_{1,b}$ and computing $\tau_{1,b}$ by expression (15.2.48) with the minus sign, we obtain the following expression after the corresponding substitutions:

$$F_{1,b} = \frac{\rho_1 V_\infty^2}{2} \sin\beta \left[\frac{-e^{-\bar{x}^2}}{\bar{x}\sqrt{\pi}} + \left(1 + \frac{\sin^2\beta}{2\bar{x}^2}\right)(1 - \operatorname{erf}\bar{x}) \right] \qquad (15.4.5)$$

The drag force coefficient is

$$c_{x.1,b} = \frac{2X_{1.b}}{\rho_1 V_\infty^2 S_{mid}} = \int\limits_{(\bar{S}_b)} \sin\beta \left[\frac{-e^{-\bar{x}^2}}{\bar{x}\sqrt{\pi}} + \left(1 + \frac{\sin^2\beta}{2\bar{x}^2}\right)(1 - \operatorname{erf}\bar{x}) \right] d\bar{S} \qquad (15.4.6)$$

We take the integral through the back part of the surface with an area of S_b. We can obtain the same result from expression (15.4.4) by substituting $-\bar{x}$ for $\bar{x}$.

We determine the drag coefficient of a body in a flow as the difference between the coefficients of the forces arising at the expense of the molecules incident on the front and back surface areas and acting in opposite directions:

$$c_{x,1} = c_{x,1,f} - c_{x,1,d} = 2\,(X_{1,f} - X_{1,b})/(\rho_1 V_\infty^2 S_{mid}) \qquad (15.4.7)$$

The reflected particles produce an additional force. Upon reflection from the front area, they act on it with a force whose magnitude

by (15.2.33) is

$$F_{r,f} = p_{r,f} \sin\beta = \frac{\rho_1 V_\infty^2}{2} \cdot \frac{\sin^3\beta}{2\bar{x}^2} \sqrt{\frac{T_r}{T_1}} \left[e^{-\bar{x}^2} + \bar{x}\sqrt{\pi}\,(1+\operatorname{erf}\bar{x})\right] \tag{15.4.8}$$

The coefficient of the force acting on the front area S_f is

$$c_{x,r,f} = \frac{2X_{r,f}}{\rho_1 V_\infty^2 S_{mid}} = \frac{1}{2} \int\limits_{(\bar{S}_f)} \frac{\sin^3\beta}{\bar{x}^2} \sqrt{\frac{T_r}{T_1}} \times \left[e^{-\bar{x}^2} + \bar{x}\sqrt{\pi}\,(1+\operatorname{erf}\bar{x})\right] d\bar{S} \tag{15.4.9}$$

The force related to unit area and due to the action of the reflected molecules on the back surface area is determined by relation (15.2.34) for $p_{r,b}$ in the following form:

$$F_{r,b} = p_{r,b} \sin\beta = \frac{\rho_1 V_\infty^2}{2} \cdot \frac{\sin^3\beta}{2\bar{x}^2} \sqrt{\frac{T_r}{T_1}} \left[e^{-\bar{x}^2} - \bar{x}\sqrt{\pi}\,(1-\operatorname{erf}\bar{x})\right] \tag{15.4.10}$$

The corresponding coefficient of the force $X_{r,b}$ acting on a back area is

$$c_{x,r,b} = \frac{2X_{r,b}}{\rho_1 V_\infty^2 S_{mid}} = \frac{1}{2} \int\limits_{(\bar{S}_b)} \frac{\sin^3\beta}{\bar{x}^2} \sqrt{\frac{T_r}{T_1}} \left[e^{-\bar{x}^2} - \bar{x}\sqrt{\pi}\,(1-\operatorname{erf}\bar{x})\right] d\bar{S} \tag{15.4.11}$$

The total drag coefficient at the expense of reflected molecules is

$$c_{x,r} = c_{x,r,f} - c_{x,r,b} = 2\,(X_{r,f} - X_{r,b})/(\rho_1 V_\infty^2 S_{mid}) \tag{15.4.12}$$

We determine this drag coefficient as the difference between the corresponding values for the front and back areas. This is due to the nature of interaction of the reflected molecules with the wall when a lifting force arises on the back surface area instead of a drag. This force in its nature is the reactive force produced when the particles rebound from the surface.

The total drag coefficient for a body in a flow is obtained by summing (15.4.7) and (15.4.12):

$$c_{x_a} = c_{x,1} + c_{x,r} \tag{15.4.13}$$

If $\bar{x} \geqslant 2$, the above formulas are simplified. Instead of (15.4.1) and (15.4.4), we have the following relations, respectively:

$$F_{1,f} = \rho_1 V_\infty^2 \sin\beta\,[1 + 1/(2\bar{x}_\infty^2)] \tag{15.4.14}$$

$$c_{x,1,f} = 2\,[1 + 1/(2\bar{x}_\infty^2)] \int\limits_{(\bar{S}_f)} \sin\beta\, d\bar{S} \tag{15.4.15}$$

and instead of (15.4.5) and (15.4.6), the values

$$F_{1,b} = 0, \quad c_{x,1,b} = 0 \tag{15.4.16}$$

Relations (15.4.8) and (15.4.9) are also simplified:

$$F_{r,f} = \frac{\rho_1 V_\infty^2}{2} \cdot \frac{\sin^2\beta}{\bar{x}_\infty} \sqrt{\pi \frac{T_r}{T_1}} \tag{15.4.17}$$

$$c_{x,r,f} = \frac{\sqrt{\pi}}{\bar{x}_\infty} \int\limits_{(\bar{S}_f)} \sin^2\beta \sqrt{\frac{T_r}{T_1}}\, d\bar{S} \tag{15.4.18}$$

while instead of (15.4.10) and (15.4.11), we have

$$F_{r,b} = 0, \quad c_{x,r,b} = 0 \tag{15.4.19}$$

For simultaneous diffuse and specular reflection (the momentum accommodation coefficient $f < 1$), the forces are computed by the following formulas:

$$F_{1,f} = p_{1,f} \sin\beta + f\tau_{1,f} \cos\beta \tag{15.4.20}$$

$$F_{1,b} = F_{1,f}(-\bar{x}) \tag{15.4.21}$$

$$F_{r,f} = [p_{1,f}(1-f) + f p_{w,f}] \sin\beta \tag{15.4.22}$$

$$F_{r,b} = F_{r,f}(-\bar{x}) \tag{15.4.23}$$

where p_w is determined by formula (15.3.3) in which the plus sign is taken. The notation in (15.4.21) and (15.4.23) indicates that $F_{1,b}$ and $F_{r,b}$ are obtained from the expressions for $F_{1,f}$ and $F_{r,f}$ by substituting $-\bar{x}$ for $\bar{x}$.

Cone

To apply the obtained relations, let us calculate the aerodynamic drag of a body that is a combination of two cones (Fig. 15.4.1*a*) in an axisymmetric flow. The relative quantity $d\bar{S}$ in the formulas for the drag coefficients is

$$d\bar{S} = 2\pi r\, dl/(\pi r_{mid}^2) = 2\pi r\, dr/(\pi r_{mid}^2 \sin\beta_c) = dr^2/\sin\beta_c \tag{15.4.24}$$

Inserting the values of $d\bar{S}$ into (15.4.4) and (15.4.6) and taking into account that for a cone

$$\bar{x}_c = \bar{x}_\infty \sin\beta_c = M_\infty \sqrt{k/2} \sin\beta_c = \text{const} \tag{15.4.25}$$

we obtain the drag coefficient in the following form:

$$c_{x,1,f} = \frac{1}{\bar{x}_c \sqrt{\pi}} e^{-\bar{x}_c^2} + \left(1 + \frac{1}{2\bar{x}_\infty^2}\right)(1 + \operatorname{erf}\bar{x}_c) \tag{15.4.26}$$

$$c_{x,1,b} = \frac{-1}{\bar{x}_c \sqrt{\pi}} e^{-\bar{x}_c^2} + \left(1 + \frac{1}{2\bar{x}_\infty^2}\right)(1 - \operatorname{erf}\bar{x}_c) \tag{15.4.27}$$

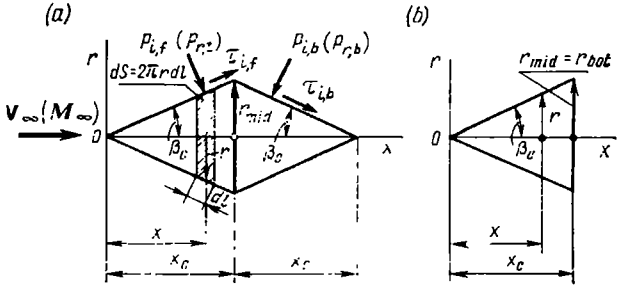

Fig. 15.4.1
To the calculation of the free-molecule flow over a conical body:
a — combination of two conical surfaces; *b* — cone with a cut bottom

The total drag coefficient for the incident molecules is

$$c_{x,i}=c_{x,i,f}-c_{x,i,b}=\frac{2}{\bar{x}_c\sqrt{\pi}}e^{-\bar{x}_c^2}+2\left(1+\frac{1}{2\bar{x}_\infty^2}\right)\operatorname{erf}\bar{x}_c \qquad (15.4.28)$$

Let us consider the action of the reflected molecules, assuming for the conditions of flow over a cone that the ratio $T_r/T_1 = \text{const}$. For these conditions from (15.4.9), we find

$$c_{x,r,f}=\frac{1}{2\bar{x}_\infty^2}\sqrt{\frac{T_r}{T_1}}\left[e^{-\bar{x}_c^2}+\bar{x}_c\sqrt{\pi}\,(1+\operatorname{erf}\bar{x}_c)\right] \qquad (15.4.29)$$

and from (15.4.11), we find

$$c_{x,r,b}=\frac{1}{2\bar{x}_\infty^2}\sqrt{\frac{T_r}{T_1}}\left[e^{-\bar{x}_c^2}-\bar{x}_c\sqrt{\pi}\,(1-\operatorname{erf}\bar{x}_c)\right] \qquad (15.4.30)$$

Bearing in mind that this coefficient characterizes the lifting force on a back surface area, by (15.4.12) we determine the total drag coefficient due to the reflected molecules:

$$c_{x,r}=c_{x,r,f}-c_{x,r,b}=\frac{\sin\beta_c}{\bar{x}_\infty}\sqrt{\pi\frac{T_r}{T_1}} \qquad (15.4.31)$$

Summing (15.4.28) and (15.4.31), we find the total drag coefficient for a cone:

$$c_{x_a}=c_{x,i}+c_{x,r}=\frac{2}{\bar{x}_c\sqrt{\pi}}e^{-\bar{x}_c^2}+2\left(1+\frac{1}{2\bar{x}_\infty^2}\right)\operatorname{erf}\bar{x}_c + \frac{\sin\beta_c}{\bar{x}_\infty}\sqrt{\pi\frac{T_r}{T_1}} \qquad (15.4.32)$$

Axisymmetric Flow over a Flat-Bottom Cone. For this case (Fig. 15.4.1*b*), formulas (15.4.26) for $c_{x,i,f}$ and (15.4.29) for $c_{x,r,}$

do not change. Expressions (15.4.27) for $c_{x,l,b}$ and (15.4.30) for $c_{x,r,b}$ are different because $\bar{x}_c = \bar{x}_\infty \sin \beta_c$ should be replaced in them with $\bar{x}_c = \bar{x}_\infty$ since the bottom surface is inclined at the angle $\beta_c = \pi/2$. Bearing this in mind, for the coefficient acting on the front surface, we obtain

$$c_{x,f} = c_{x,l,f} + c_{x,r,f} = \frac{e^{-\bar{x}_c^2}}{\bar{x}_c}\left(\frac{1}{\sqrt{\pi}} + \frac{\sin\beta_c}{2\bar{x}_\infty}\sqrt{\frac{T_r}{T_l}}\right)$$
$$+ (1 + \operatorname{erf}\bar{x}_c)\left(1 + \frac{1}{2\bar{x}_\infty^2} + \frac{\sin\beta_c}{2\bar{x}_\infty}\sqrt{\pi\frac{T_r}{T_l}}\right) \quad (15.4.33)$$

The coefficient of the force acting on the bottom surface is

$$c_{x,b} = c_{x,l,b} + c_{x,r,b} = \frac{e^{-\bar{x}_\infty^2}}{\bar{x}_\infty}\left(\frac{-1}{\sqrt{\pi}} + \frac{1}{2\bar{x}_\infty}\sqrt{\frac{T_r}{T_l}}\right)$$
$$+ (1 - \operatorname{erf}\bar{x}_\infty)\left(1 + \frac{1}{2\bar{x}_\infty^2} - \frac{1}{2\bar{x}_\infty}\sqrt{\pi\frac{T_r}{T_l}}\right) \quad (15.4.34)$$

The force determined by this coefficient acts on the bottom section in a direction opposite to the free stream and, consequently, is a propelling force. Accordingly, the total drag coefficient for a cone is

$$c_{x_a} = c_{x,f} - c_{x,b} \quad (15.4.35)$$

At very high flight speeds ($\bar{x} \gg 1$), formulas (15.4.32) and (15.4.35) become

$$c_{x_a} = 2 \quad (15.4.36)$$

and this result does not depend on the shape of the body.

At flight speeds which small values of $\bar{x}$ correspond to, the values of c_{x_a} grow because of the substantial influence of the reflected molecules. This can be seen from the graph in Fig. 15.4.2 where the values of c_{x_a} are given for a cone and a spherical surface.

We shall note that the value of $c_{x_a} = 2$ exactly corresponds to the conclusions of Newton's collision theory. Indeed, by this theory, the force of resistance is determined by the complete loss of momentum of the particles on the area of the maximum cross section of a body. On this basis, we find that for any body with a mid-section area of $\pi r_{m\,1d}^2$ (for example, for a cone) in a free-molecule flow at the velocity V_∞, the drag force at a zero angle of attack is

$$X_a = \rho_\infty V_\infty \pi r_{m\,1d}^2 V_\infty - \rho_\infty V_\infty \pi r_{m\,1d}^2 \times 0 = \rho_\infty V_\infty^2 \pi r_{m\,1d}^2$$

where the first term of the difference is the momentum of the free stream before a collision, and the second term is the momentum after the collision.

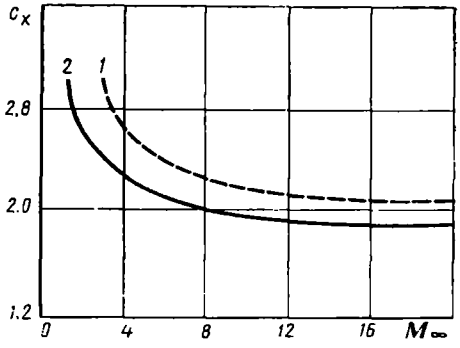

Fig. 15.4.2
Drag coefficient for a sphere (*1*) and cone (*2*) in a free-molecule flow
(the angle of attack $\alpha=0$, the semi-apex cone angle is $\beta_c=60°$)

The coefficient of this force is $c_{x_a} = 2X/(\rho_\infty V_\infty^2 \pi r_{m\,id}^2) = 2$. We also obtain this formula for an arbitrary angle of attack. Here the force should be calculated as the product of the coefficient $c_{x_a} = 2$, the velocity head, and the projection of the surface onto a plane normal to the direction of the velocity vector V_∞.

It can be seen from the above that the collision theory differs from the Newtonian scheme of elastic reflection treated in Sec. 9.4. According to the Newtonian scheme, the particles after colliding with a surface continue to move along the wall, i.e. deviate by the angle of incidence of the molecules. The normal velocity component is cancelled, while the tangential component remains unchanged. In accordance with the collision theory, both components are cancelled and, consequently, a shear appears in addition to the normal stress (pressure).

A glance at Fig. 15.4.2 reveals that notwithstanding a certain difference, the results of accurate calculations for numbers $M_\infty > 4$ do not virtually differ from the value of $c_{x_a} = 2$ found by Newton's collision theory. Therefore, for relatively small numbers M_∞, the aerodynamic forces may be calculated by the diffuse reflection scheme, and for large numbers M_∞, by the collision theory.

Non-Axisymmetric Flow. The calculations of the axial and normal force coefficients, and also of the moment coefficient should be based on the expressions for the local pressure coefficient and friction factor. The angle β in these expressions must be replaced by the angle θ_c between the direction of the molecule flow velocity and the local area.

Knowing how the local pressure coefficient and friction factor are distributed and using the general expressions for calculating the aerodynamic coefficients (see Sec. 1.3), we can compute their specific values for a given body shape. Figure 15.4.3 shows the results of such a calculation for a combination of a truncated cone

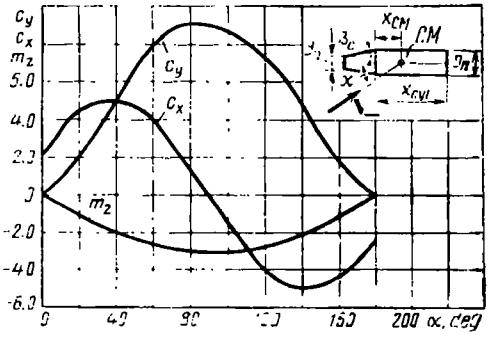

Fig. 15.4.3
Results of calculating the aerodynamic coefficients for free-molecule flow over a body of revolution
($\beta_c=15°$; $d_n/D_n=0.834$; $x_{CM}/D_n=1$; $x_{cyl}/D_n=3$)

with a cylinder obtained provided that the ratio of the flight speed to the molecular velocity is $\bar{x}_\infty = 7$, and the temperature ratio is $T_r / T_1 = 0.18$. The moment coefficient (Fig. 15.4.3) was calculated about the centre of mass at a distance of one cylinder diameter from the major base of the cone.

Cylinder

Let us consider the drag of a cylinder with a cross free-molecule flow according to the scheme of diffuse reflection assuming that the accommodation coefficient $f = 1$ (Fig. 15.4.4). To do this, we shall use formulas (15.4.1)-(15.4.13). Seeing that in (15.4.4)

$$d\bar{S} = dS/S_{mid} = lR_n d\beta/(R_n l) = d\beta \qquad (15.4.37)$$

and the quantity $\bar{x} = \bar{x}_\infty \sin\beta$, we find

$$c_{x,1.f} = \frac{2X_{1.f}}{\rho_1 V_\infty^2 S_{mid}}$$

$$= \int_0^{\pi/2} \left[\frac{e^{-\bar{x}^2}}{\bar{x}_\infty \sqrt{\pi}} + \sin\beta \left(1 + \frac{1}{2\bar{x}_\infty^2}\right)(1 + \operatorname{erf}\bar{x}) \right] d\beta \quad (15.4.38)$$

For the coefficient $c_{x,1.b}$ with account taken of (15.4.6), we have

$$c_{x,1.b} = \frac{2X_{1.b}}{\rho_1 V_\infty^2 S_{mid}}$$

$$= \int_0^{\pi/2} \left[\frac{-e^{-\bar{x}^2}}{\bar{x}_\infty \sqrt{\pi}} + \sin\beta \left(1 + \frac{1}{2\bar{x}_\infty^2}\right)(1 - \operatorname{erf}\bar{x}) \right] d\beta \quad (15.4.39)$$

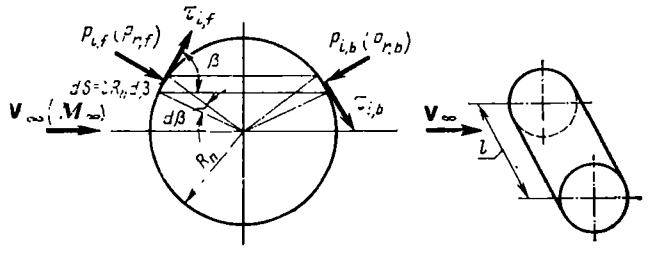

Fig. 15.4.4
Free-molecule flow over a cylinder

The drag due to the reflection of molecules from the front surface area is determined from (15.4.9) by the coefficient

$$c_{x,r,f}=\frac{2X_{r,f}}{\rho_1 V_\infty^2 S_{mid}}$$

$$=\frac{1}{2}\int_0^{\pi/2}\left[\frac{e^{-\bar{x}^2}}{\bar{x}\sqrt{\pi}}+(1+\operatorname{erf}\bar{x})\right]\bar{x}\sqrt{\pi}\,\frac{\sin\beta}{\bar{x}_\infty^2}\sqrt{\frac{T_r}{T_1}}\,d\beta \quad (15.4.40)$$

Reflection from a back surface area produces a force whose coefficient by (15.4.11) is

$$c_{x,\,r,\,b}=\frac{2X_{r,\,b}}{\rho_1 V_\infty^2 S_{mid}}$$

$$=\frac{1}{2}\int_0^{\pi/2}\left[\frac{e^{-\bar{x}^2}}{\bar{x}\sqrt{\pi}}-(1-\operatorname{erf}\bar{x})\right]\bar{x}\sqrt{\pi}\,\frac{\sin\beta}{\bar{x}_\infty^2}\sqrt{\frac{T_r}{T_1}}\,d\beta \quad (15.4.41)$$

The difference between the values determined by (15.4.38) and (15.4.39) allows us to compute the coefficient of the total force due to the incident molecules:

$$c_{x,1}=c_{x,1,f}-c_{x,1,b}=2\int_0^{\pi/2}\left[\frac{e^{-\bar{x}^2}}{\bar{x}_\infty\sqrt{\pi}}+\sin\beta\left(1+\frac{1}{2\bar{x}_\infty^2}\right)\operatorname{erf}\bar{x}\right]d\beta$$

$$=\frac{\sqrt{\pi}\exp\left(-\frac{1}{2}\bar{x}_\infty^2\right)}{\bar{x}_\infty}\cdot\left\{I_0\left(\frac{\bar{x}_\infty^2}{2}\right)+\left(\bar{x}_\infty^2+\frac{1}{2}\right)\right.$$

$$\left.\times\left[I_0\left(\frac{\bar{x}_\infty^2}{2}\right)+I_1\left(\frac{\bar{x}_\infty^2}{2}\right)\right]\right\} \quad (15.4.42)$$

where $I_0\left(\bar{x}_\infty^2/2\right)$ and $I_1\left(\bar{x}_\infty^2/2\right)$ are the modified Bessel functions of orders 0 and 1, respectively:

$$I_0\left(\frac{\bar{x}_\infty^2}{2}\right)=\frac{1}{\pi}\int_0^\pi \exp\left(\frac{\bar{x}_\infty^2}{2}\cos\varphi\right)d\varphi;$$

$$I_1\left(\frac{\bar{x}_\infty^2}{2}\right)=\frac{1}{\pi}\int_0^\pi \cos\varphi\exp\left(\frac{\bar{x}_\infty^2}{2}\cos\varphi\right)d\varphi \qquad (15.4.43)$$

We find the coefficient of the total force due to the reflected molecules by subtracting (15.4.41) from (15.4.40). Assuming that for the entire surface $T_r/T_1 = \text{const}$, we obtain

$$c_{x,r}=c_{x,r,f}-c_{x,r,b}=\frac{1}{\bar{x}_\infty^2}\sqrt{\pi\frac{T_r}{T_1}}\int_0^{\pi/2}\bar{x}\sin\beta\,d\beta$$

$$=\frac{\pi^{3/2}}{4\bar{x}_\infty}\sqrt{\frac{T_r}{T_1}} \qquad (15.4.44)$$

The total drag coefficient of a cylinder is

$$c_{x_a}=c_{x,1}+c_{x,r}=\frac{\sqrt{\pi}\exp\left(-\frac{1}{2}\bar{x}_\infty^2\right)}{\bar{x}_\infty}\left\{I_0\left(\frac{\bar{x}_\infty^2}{2}\right)\right.$$

$$\left.+\left(\bar{x}_\infty^2+\frac{1}{2}\right)\left[I_0\left(\frac{\bar{x}_\infty^2}{2}\right)+I_1\left(\frac{\bar{x}_\infty^2}{2}\right)\right]\right\}+\frac{\pi^{3/2}}{4\bar{x}_\infty}\sqrt{\frac{T_r}{T_1}} \qquad (15.4.45)$$

Plate

In the simplest case, when the flow is calculated according to Newton's collision theory, the drag force on a plate of area S_{pl} is determined by the change in the momentum before and after a collision:

$$X_a=(\rho_\infty V_\infty S_{pl}\sin\alpha)\,V_\infty-(\rho_\infty V_\infty S_{pl}\sin\alpha)\times 0=\rho_\infty V_\infty^2 S_{pl}\sin\alpha$$

where α is the angle of attack (Fig. 15.4.5).

Therefore, the drag coefficient is

$$c_{x_a}=2X/(\rho_\infty V_\infty^2 S_{pl})=2\sin\alpha \qquad (15.4.46)$$

Since a lift force is absent, the lift-drag ratio is zero. These conclusions are close to what actually occurs at very high velocities of free-molecule flows. For low velocities, the reflection effects must be taken into consideration, and the relevant relations used for the pressure coefficient and friction factor.

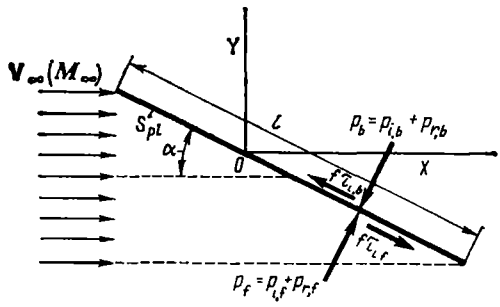

Fig. 15.4.5
Free-molecule flow over a plate

Let us consider reflection with an accommodation coefficient of $f < 1$. The force on the lower surface of the plate due to the incident molecules, by formula (15.4.20) with α substituted for β is

$$X_{i,f} = F_{i,f} S_{pl} = (p_{i,f} \sin\alpha + f\tau_{i,f} \cos\alpha) S_{pl} \qquad (15.4.47)$$

and the coefficient of this force is

$$c_{x,i,f} = \frac{2X_{i,f}}{\rho_1 V_\infty^2 S_{pl}} = \frac{2}{\rho_1 V_\infty^2} (p_{i,f}\sin\alpha + f\tau_{i,f}\cos\alpha) \qquad (15.4.47')$$

Let us replace $\tau_{i,f}$ using (15.2.48) and retaining the plus sign in it. We shall simultaneously insert (15.2.29) instead of $p_{i,f}$. Since the angle α is taken instead of β in (15.2.48) and (15.2.29), we obtain after these transformations

$$c_{x,i,f} = \sin^3\alpha \left[\frac{e^{-\bar{x}^2}}{\bar{x}\sqrt{\pi}} + \left(1 + \frac{1}{2\bar{x}^2}\right)(1 + \operatorname{erf}\bar{x})\right]$$

$$+ f \sin\alpha \cos^2\alpha \left(\frac{e^{-\bar{x}^2}}{\bar{x}\sqrt{\pi}} + 1 + \operatorname{erf}\bar{x}\right) \qquad (15.4.47'')$$

where $\bar{x} = \bar{x}_\infty \sin\alpha$.

Similarly, for the upper surface [see (15.4.21)], we have

$$c_{x,i,b} = \frac{2X_{i,b}}{\rho_1 V_\infty^2 S_{pl}} = \frac{2F_{i,b}}{\rho_1 V_\infty^2} = \frac{2}{\rho_1 V_\infty^2} F_{i,f}(-\bar{x}) = c_{x,i,f}(-\bar{x})$$

$$= \sin^3\alpha \left[\frac{-e^{-\bar{x}^2}}{\bar{x}\sqrt{\pi}} + \left(1 + \frac{1}{2\bar{x}^2}\right)(1 - \operatorname{erf}\bar{x})\right]$$

$$+ f \sin\alpha \cos^2\alpha \left(\frac{-e^{-\bar{x}^2}}{\bar{x}\sqrt{\pi}} + 1 - \operatorname{erf}\bar{x}\right) \qquad (15.4.48)$$

Let us consider the forces due to reflection of the molecules. Inspection of Fig. 15.4.5 reveals that the lower surface experiences the force $X_{r,f}$, which can be represented with the aid of (15.4.22)

in the form

$$X_{r,f} = p_{r,f} S_{pl} \sin \alpha = F_{r,f} S_{pl} \tag{15.4.49}$$

The coefficient of this force with a view to (15.4.22) is

$$c_{x,r,f} = \frac{2X_{r,f}}{\rho_1 V_\infty^2 S_{pl}} = \frac{2F_{r,f}}{\rho_1 V_\infty^2} = \frac{2 \sin \alpha}{\rho_1 V_\infty^2} [p_{1,f}(1-f) + f p_{w,f}] \tag{15.4.50}$$

Substituting for $p_{1,f}$ and $p_{w,f}$ the corresponding values from (15.2.29) and (15.3.3) (with the plus sign), we obtain

$$c_{x,r,f} = (1-f) \sin^3 \alpha \left[\frac{e^{-\bar{x}^2}}{\bar{x}\sqrt{\pi}} + \left(1 + \frac{1}{2\bar{x}^2}\right)(1 + \operatorname{erf} \bar{x}) \right.$$
$$\left. + \frac{f \sin^3 \alpha}{2\bar{x}^2} \sqrt{\frac{T_w}{T_1}} [e^{-\bar{x}^2} + \bar{x}\sqrt{\pi}(1 + \operatorname{erf} \bar{x})] \right] \tag{15.4.50'}$$

The molecules reflected from the upper surface produce a propelling force [see (15.4.23)]:

$$X_{r,b} = F_{r,b} S_{pl} = p_{r,b} S_{pl} \sin \alpha \tag{15.4.51}$$

The coefficient of this force, by (15.4.23), is

$$c_{x,r,b} = \frac{2X_{r,b}}{\rho_1 V_\infty^2 S} = \frac{2F_{r,b}}{\rho_1 V_\infty^2} = \frac{2}{\rho_1 V_\infty^2} F_{r,f}(-\bar{x}) = c_{x,r,f}(-\bar{x}) \tag{15.4.52}$$

By (15.4.50'), we have

$$c_{x,r,b} = (1-f) \sin^3 \alpha \left[-\frac{e^{-\bar{x}^2}}{\bar{x}\sqrt{\pi}} + \left(1 + \frac{1}{2\bar{x}^2}\right)(1 - \operatorname{erf} \bar{x}) \right]$$
$$+ \frac{f \sin^3 \alpha}{2\bar{x}^2} \sqrt{\frac{T_w}{T_1}} [e^{-\bar{x}^2} - \bar{x}\sqrt{\pi}(1 - \operatorname{erf} \bar{x})] \tag{15.4.53}$$

From the difference of the coefficients calculated by formulas (15.4.47″) and (15.4.48), we have

$$c_{x,1} = c_{x,1,f} - c_{x,1,b} = 2 \sin^3 \alpha \left[\frac{1}{\bar{x}\sqrt{\pi}} e^{-\bar{x}^2} + \left(1 + \frac{1}{2\bar{x}^2}\right) \operatorname{erf} \bar{x} \right]$$
$$+ 2f \sin \alpha \cos^2 \alpha \left(\frac{1}{\bar{x}\sqrt{\pi}} e^{-\bar{x}^2} + \operatorname{erf} \bar{x} \right) \tag{15.4.54}$$

Using (15.4.50') and (15.4.53), we obtain a similar expression corresponding to the reflection process:

$$c_{x,r} = c_{x,r,f} - c_{x,r,b} = 2(1-f) \sin^3 \alpha$$
$$\times \left[\frac{1}{\bar{x}\sqrt{\pi}} e^{-\bar{x}^2} + \left(1 + \frac{2}{2\bar{x}^2}\right) \operatorname{erf} \bar{x} \right] + \frac{f \sin^3 \alpha}{\bar{x}} \sqrt{\pi \frac{T_w}{T_1}} \tag{15.4.55}$$

The resultant drag coefficient is

$$c_{x_a} = c_{x,1} + c_{x,r} = 2\,(2-f)\,\sin^3\alpha\left[\frac{1}{\bar{x}\sqrt{\pi}}\,e^{-\bar{x}^2} + \left(1+\frac{1}{2\bar{x}^2}\right)\operatorname{erf}\bar{x}\right]$$

$$+ f\sin\alpha\left[2\cos^2\alpha\left(\frac{e^{-\bar{x}^2}}{\bar{x}\sqrt{\pi}} + \operatorname{erf}\bar{x}\right) + \frac{\sin^2\alpha}{\bar{x}}\sqrt{\pi\frac{T_w}{T_1}}\right] \quad (15.4.56)$$

In a similar way, we can determine the lift force Y_a and the coefficient of this force:

$$c_{y_a} = \frac{2Y_a}{\rho_1 V_\infty^2 S_{pl}} = \frac{2\,(Y_l + Y_r)}{\rho_1 V_\infty^2 S_{pl}} = c_{y,l} + c_{y,r}$$

$$= \frac{2}{\rho_1 V_\infty^2}\,[G_{l,f} - G_{l,f}\,(-\bar{x}) + G_{r,f} - G_{r,f}\,(-\bar{x})] \quad (15.4.57)$$

where

$$G_{l,f} = p_{l,f}\cos\alpha - f\tau_{l,f}\sin\alpha;\quad G_{r,f} = [p_{l,f}\,(1-f) + fp_{w,f}]\cos\alpha \quad (15.4.58)$$

The drag and lift coefficients can be obtained for completely diffuse reflection if in the corresponding expressions we assume that $f = 1$, and for specular reflection if we assume that $f = 0$.

15.5. Heat Transfer

Temperature of Reflected Molecules

We already know that the pressure on a wall due to the reflection of the molecules depends on their temperature T_r. To determine this temperature, we must use the equation of the energy balance between the body and the fluid. Let us derive this equation for a unit area at an arbitrary location on the surface. The energy E_i of the translational motion of the molecules is supplied to this area. The corresponding energy of the reflected molecules can be determined by (15.3.11) and (15.3.10) as follows:

$$E_r = (1-\eta)\,E_i + \eta E_w = (1-\eta)\,E_i + 2\eta\,mN_1RT_w \quad (15.5.1)$$

If we take into account the supply of the heat q_{rad} by external radiation (for example, by solar radiation), the supplied energy will be $E_i + q_{rad}$.

Let us assume that the removal of energy in addition to its transfer by the reflected molecules is also due to radiation by the external surface, and to its additional cooling or heating from inside (correspondingly, a plus or minus sign before q_{cl}). Hence, the equation

of the energy balance for a unit area in stationary heat transfer will be

$$E_1 + q_{rad} = E_r + \varepsilon\sigma T_w^4 + q_{cl} \qquad (15.5.2)$$

or with a view to expression (15.5.1) for E_r

$$\eta E_1 + q_{rad} = \eta E_w + \varepsilon\sigma T_w^4 + q_{cl} \qquad (15.5.2')$$

Relation (15.5.2') and the expressions for E_1 (15.2.55) and E_w (15.3.10) entering it correspond to the motion of a monatomic gas. If a gas consists of polyatomic molecules (particularly, air can be considered as a diatomic model), each particle, in addition to the energy of translational motion, will also have an internal energy due to its rotation and vibration and depending on the properties of the gas. Such particles, when falling on a unit surface area, transfer in unit time an internal energy which by the kinetic theory of gases is

$$E_{1,in} = \frac{5-3k}{k-1} \cdot \frac{mRT_1}{2} N_1 \qquad (15.5.3)$$

The molecules leaving the surface at the temperature T_w carry away the internal energy

$$E_{w,in} = \frac{5-3k}{k-1} \cdot \frac{mRT_w}{2} N_w \qquad (15.5.4)$$

where $N_w = N_1$.

Accordingly, for a diatomic gas, the energy balance equation (15.5.2') has the following form:

$$\eta \bar{E}_1 + q_{rad} = \eta \bar{E}_w + \varepsilon\sigma T_w^4 + q_{cl} \qquad (15.5.5)$$

where

$$\bar{E}_1 = E_1 + E_{1,in}; \quad \bar{E}_w = E_w + E_{w,in} \qquad (15.5.6)$$

Introducing into (15.5.5) the values of E_1 from (15.2.55) and E_w from (15.3.10) (provided that in these expressions the plus sign is chosen for the front surface area, and the minus sign for the back one), we determine the wall temperature T_w at given values of the emittance ε, heat flows q_{rad}, q_{cl}, and the air temperature T_1.

Calculations of T_w by Eq. (15.5.5) for a plate depending on the angle of attack α show that the influence of solar radiation on the wall temperature is more appreciable at small angles α. This influence also grows with an increasing altitude. Beginning from an altitude of 240 km and higher, solar radiation is the main factor determining the wall temperature. The temperature T_w can be lowered by using surfaces with a low accommodation coefficient η. For this purpose, the wall inclination should be as small as possible, which is achieved when flying at small angles of attack. The found temperature T_w can be used to compute the temperature T_r of the reflected molecules. The corresponding relation is obtained as follows.

By analogy with (15.5.1), let us write a formula for the energy of reflected diatomic molecules:

$$\bar{E}_r = (1 - \eta)\,\bar{E}_1 + \eta \bar{E}_w \tag{15.5.7}$$

The value of this energy can also be expressed as

$$\bar{E}_r = E_r + E_{r,\,in} = 2mN_1RT_r + \frac{5-3k}{k-1} \cdot \frac{mRT_r}{2} N_1 = 2mN_1RT_rk_1 \tag{15.5.8}$$

The value of the energy on the right-hand side of (15.5.7) is

$$\bar{E}_w = E_w + E_{w,\,in} = 2mN_1RT_wk_1 \tag{15.5.9}$$

where

$$k_1 = (k + 1)/[4\,(k - 1)] \tag{15.5.10}$$

The value of the second energy component in (15.5.7) is

$$\bar{E}_1 = E_1 + E_{1,\,in} = E_1k_2 \tag{15.5.11}$$

It depends on the coefficient

$$k_2 = 1 + \frac{E_{1,\,in}}{E_1} = 1 + \frac{1}{E_1} \cdot \frac{5-3k}{k-1} \cdot \frac{mRT_1}{2} N_1 \tag{15.5.12}$$

Inserting (15.5.8), (15.5.9), and (15.5.11) into (15.5.7), we find a relation for the temperature of the reflected molecules:

$$\frac{T_r}{T_1} = \frac{T_w}{T_1}\left[\frac{(1-\eta)\,E_1k_2}{2mN_1RT_wk_1} + \eta\right] \tag{15.5.13}$$

We calculate the temperature T_r separately for the front and back surface areas which definite values of N_1 and E_1, and, consequently, of T_w correspond to. If the accommodation coefficient $\eta = 1$, then $T_r = T_w$. We also obtain the same result for what is called an **adiabatic wall**, for which the thermal process is characterized by the absence of any external supply or rejection of heat except for the inflow of energy due to the incident molecules. In this case, the wall is heated only as a result of the translational motion of the molecules. Accordingly, Eq. (15.5.5) becomes $\bar{E}_1 = \bar{E}_w$, or with a view to (15.5.11) and (15.5.9), it becomes

$$E_1k_2 = 2mN_1RT_w\,k_1 = E_wk_1 \tag{15.5.14}$$

If we introduce this relation into (15.5.13), we can see that the temperature of the reflected molecules equals that of the wall. This temperature is determined from (15.5.14) after inserting the value (15.2.55) for E_1 as follows:

$$\frac{T_w}{T_1} = \frac{T_r}{T_1} = \frac{k_2}{4RT_1k_1}\left[V_\infty^2 + RT_1\left(4 + \frac{1}{\varphi+1}\right)\right] \tag{15.5.15}$$

The product RT_1 in this formula can be replaced with the aid of (15.2.19):

$$\frac{T_w}{T_1} = \frac{T_r}{T_1} = \left[1 + \frac{kM_\infty^2}{4} + \frac{1}{4(\varphi+1)}\right]\frac{k_2}{k_1} \qquad (15.5.16)$$

A glance at this formula reveals that the temperature of an adiabatic wall is a distinctive analogue of the stagnation temperature for a continuous flow.

The conditions of flight at high altitudes make it necessary to ensure a certain constant wall temperature. In this case, the wall temperature is preset, and the calculations consist in determining the temperature of the reflected particles by formula (15.5.3). This temperature is then used to calulate the pressure.

Calculation of Heat Transfer and Wall Temperature

The total specific heat flow to a wall can be determined as the difference between the energies of the incident and reflected molecules:

$$q = \bar{E}_1 - \bar{E}_r \qquad (15.5.17)$$

Combining this equation with (15.5.7), we find

$$q = \eta\,(\bar{E}_1 - \bar{E}_w) \qquad (15.5.17')$$

or with a view to expressions (15.5.11) and (15.5.9) for $\bar{E}_1$ and $\bar{E}_w$,

$$q = \eta\,(E_1 k_2 - 2mN_1 R_w k_1) \qquad (15.5.17'')$$

Substituting for E_1 its value from (15.2.55) yields

$$q = \frac{\eta m N_1}{2}\left\{k_2\left[V_\infty^2 + RT_1\left(4 + \frac{1}{\varphi+1}\right)\right] - 4RT_w k_1\right\}$$

Bearing in mind that N_1 is determined by expressions (15.2.17') for the front surface and by (15.2.22) for the back one, while the mass of a molecule $m = \rho_1/n_1$, we obtain

$$q = \frac{\eta\rho_1}{2}\sqrt{\frac{RT_1}{2\pi}}\left\{k_2\left[V_\infty^2 + RT_1\left(4 + \frac{1}{\varphi+1}\right)\right] - 4RT_w k_1\right\} \times \left[e^{-\bar{x}^2} \pm \bar{x}\sqrt{\pi}\,(1 \pm \operatorname{erf}\bar{x})\right] \qquad (15.5.18)$$

where φ is determined by (15.2.56), k_2 by (15.5.12), and k_1 by (15.5.10). With a view to these relations for the front area, we have

$$q = \pi\rho_1\sqrt{\frac{(RT_1)^3}{2\pi}}\left\{\left[e^{-\bar{x}^2} + \bar{x}\sqrt{\pi}\,(1 + \operatorname{erf}\bar{x})\right] \times \left[\bar{x}_\infty^2 - \frac{k+1}{2(k-1)}\cdot\frac{T_w}{T_1} + \frac{k+1}{2(k-1)}\right] + \frac{1}{2}\bar{x}\sqrt{\pi}\,(1 + \operatorname{erf}\bar{x})\right\} \qquad (15.5.18')$$

where

$$RT_1 = p_1/\rho_1 = a_1^2/k; \quad \bar{x} = \bar{x}_\infty \sin\beta; \quad \bar{x}_\infty = (V_\infty/a_1)\sqrt{k/2} \tag{15.5.19}$$

We can also obtain a similar expression for q for the back area of a body in the flow, by substituting $-x$ for $\bar{x}$ in (15.5.18′).

Assuming in the relevant formulas that the heat flux $q = 0$, we can determine the equilibrium temperature of a wall. Particularly, with this assumption, we find from (15.5.18) that

$$T_w = T_e = \frac{k_2}{4Rk_1}\left[V_\infty^2 + RT_1\left(4 + \frac{1}{\varphi+1}\right)\right] \tag{15.5.20}$$

A close look at (15.5.12) and (15.2.55) reveals that at very high velocities ($V_\infty \gg a_1$) the parameter $k_2 \approx 1$. Therefore, using formula (15.5.10) for k_1 and disregarding the second term in brackets in (15.5.20), we obtain

$$T_w = T_e = \frac{k-1}{k+1} \cdot \frac{V_\infty^2}{R} \tag{15.5.21}$$

or

$$T_w = T_e = \frac{2T_1(k-1)}{k+1}\bar{x}_\infty^2 \tag{15.5.21′}$$

Let us consider the expression for the Stanton number, which is a dimensionless number of heat transfer:

$$St = \frac{2k}{k+1} \cdot \frac{q}{\eta\rho_1 V_\infty c_{p,1}(T_e - T_w)} \tag{15.5.22}$$

In such a form, this dimensionless criterion is called the **local modified Stanton number.** When high velocities ($\bar{x}_\infty \gg 1$, $\bar{x} \gg 1$) are involved, the heat flow can be written for a front surface area, as follows from (15.5.18′), in an approximate form:

$$q = \frac{1}{2}\eta R\rho_1 T_1 \sqrt{RT_1}\left(\frac{e^{-\bar{x}^2}}{\bar{x}\sqrt{\pi}} + 1 + \operatorname{erf}\bar{x}\right)\bar{x}\,\bar{x}_\infty^2$$

Using relation (15.5.19) for $\bar{x}$, after introducing the value of q into formula (15.5.22), we obtain

$$St = \frac{2k}{k+1} \cdot \frac{RT_1\sqrt{RT_1}}{V_\infty c_{p,1}(T_e - T_w)\sqrt{2}}\left(\frac{e^{-\bar{x}^2}}{\bar{x}\sqrt{\pi}} + 1 + \operatorname{erf}\bar{x}\right)\bar{x}_\infty^3 \sin\beta$$

Since $T_w \ll T_e$, instead of the difference $T_e - T_w$ we can use T_e determined by (15.5.21′). In addition, performing the substitution $c_{p,1} = kR/(k-1)$ and $\bar{x}_\infty = (V_\infty/\sqrt{kRT_1})\sqrt{k/2}$, we obtain

$$St = \frac{\sin\beta}{2}\left(\frac{e^{-\bar{x}^2}}{\bar{x}\sqrt{\pi}} + 1 + \operatorname{erf}\bar{x}\right) \tag{15.5.23}$$

Now let us consider the friction factor. By (15.2.48) and (15.3.6') for this factor related to the conditions on an area of the front surface, we have the following expression:

$$c_{f,1} = f \sin\beta \cos\beta \left(\frac{e^{-\bar{x}^2}}{\bar{x}\sqrt{\pi}} + 1 + \operatorname{erf} \bar{x} \right) \qquad (15.5.24)$$

By comparing (15.5.23) and (15.5.24), we can establish the relation between the Stanton number and the local friction factor:

$$St = c_{f,1}/(2f \cos\beta) \qquad (15.5.25)$$

Experimental investigations reveal that the specific heat flow (W/m^2) at the stagnation point is

$$q = 3.08 \times 10^{11} \eta \, (\rho_{\infty,H}/\rho_{\infty,\text{ter}})/(V_\infty/V_0)^3 \qquad (15.5.26)$$

where V_0 is the orbital velocity, while the subscripts "H" and "ter" signify the conditions at the altitude H and the Earth ($H = 0$). The corresponding equilibrium temperature at this point is

$$T_w = (q + q_{rad} \pm q_{cl})^{1/4} \, (\varepsilon\sigma)^{-1/4} \qquad (15.5.27)$$

If no heat is supplied to a wall from inside ($q_{cl} = 0$) and external radiation is disregarded ($q_{rad} = 0$), the wall temperature is

$$T_w = 4.83 \times 10^4 \, (\eta/\varepsilon)^{1/4} \, (\rho_{\infty,H}/\rho_{\infty,\text{ter}})^{1/4} (V_\infty/V_0)^{3/4} \qquad (15.5.28)$$

With a greatly cooled surface, the energy of the particles reflected from the wall is very small, i.e. $\bar{E}_w \ll \bar{E}_1$. Therefore, instead of (15.5.17'), we can use the equation

$$q = \eta \bar{E}_1 = \eta E_1 k_2 \qquad (15.5.29)$$

When considering very high velocities at which $k_2 \approx 1$ and E_1 is determined by (15.2.61), we obtain the following expression for the specific heat flow on an area of the front surface:

$$q = (\bar{x}\rho_1\eta/2)/\sqrt{2RT_1} \, (V_\infty^2 + 5RT_1)$$

Expressing RT_1 in terms of the speed of sound a_1 by (15.2.19) and assuming in accordance with (15.2.20) that $\bar{x} = \sin\beta \, (V_\infty/a_1)\sqrt{k/2} = \sin\beta \, M_\infty\sqrt{k/2}$, we find the heat flow [$J/(m^2 s)$]:

$$q = 4.9 \, \eta\rho_1 V_\infty \, [1 + 5/(kM_\infty^2)] \sin\beta \qquad (15.5.30)$$

At the stagnation point, $\beta = \pi/2$, therefore

$$q = 4.9\,\eta\rho_1 V_\infty^3\,[1 + 5/(kM_\infty^2)] \qquad (15.5.31)$$

In these expressions ρ_1 is in kg/m^3, and the velocity V_∞ in m/s.

We have considered skin friction and heat transfer for a continuous and free-molecule gas flows. Slip flow occupies an intermediate position. Most modern methods of calculating skin friction and heat transfer for this flow are based on the use of boundary layer equations whose solution must satisfy special boundary conditions with a velocity jump (slip). These methods are described in [24, 27, 28].

References

1. Krasnov, N.F. *Aerodynamics of Bodies of Revolution*, Trans. by J.B. Gazley. New York, Elsevier (1970).
2. Krasnov, N.F., Koshevoi, V.N., Danilov, A.N., and Zakharchenko, V. F. *Aerodinamika raket* (The Aerodynamics of Rockets). Moscow, Vysshaya shkola (1968).
3. Kibardin, Yu.A., Kuznetsov, S.I., Lyubimov, A.N., and Shumyatsky, B.Ya. *Atlas gasodinamicheskikh funktsii pri bol'shikh skorostyakh i vysokikh temperaturakh vozdushnogo potoka* (Atlas of Gasdynamic Functions for High Velocity and High Temperature Air Flow). Moscow, Gosenergoizdat (1961).
4. Predvoditelev, A.S., Stupachenko, E.V., Ionov, V.P., Pleshanov, A.S., Rozhdestvensky, I.B., and Samuilov, E.V. *Termodinamicheskie funktsii vozdukha dlya temperatur ot 1000 do 12 000 K i davlenii ot 0.001 do 1000 atm (grafiki funktsii)* [The Thermodynamic Functions of Air for Temperatures from 1000 to 12 000 K and Pressures from 0.001 to 1000 Atmospheres (Graphs of Functions)]. Moscow, Izd. AN SSSR (1960).
5. Predvoditelev, A.S., Stupachenko, E.V., Samuilov, E.V. Stakhanov, I.P., Pleshanov, A.S., and Rozhdestvensky, I.B. *Tables of Thermodynamic Functions of Air for the Temperature Range 6000-12 000 K and Pressure Range 0.001-1000 Atm.* London, Infosearch Ltd. (1958).
6. Krasnov, N.F. (Ed.). *Prikladnaya aerodinamika* (Applied Aerodynamics). Moscow, Vysshaya shkola (1974).
7. Belotserkovsky, O.M. (Ed.). *Obtekanie zatuplennykh tel sverkhzvukovym potokom gaza* (Supersonic Gas Flow over Blunt Bodies). Moscow, Izd. Vychisl. tsentra AN SSSR (1967).
8. Irov, Yu.D., Keil, E.V., Pavlukhin, B.N., *et al. Gazodinamicheskie funktsii* (Gasdynamic Functions). Moscow, Mashinostroenie (1965).
9. Cherny G.G. *Introduction to Hypersonic Flow*, 2nd ed., New York-London, Academic Press (1969).
10. *Izvestiya AN SSSR. Mekhanika i mashinostroenie. Mekhanika zhidkostei i gazov* (Bulletin of the USSR Academy of Sciences. Mechanics and Mechanical Engineering. Fluid Mechanics).
11. *Izvestiya AN SSSR. Prikladnaya matematika i mekhanika* (Journal of Applied Mathematics and Mechanics, USSR Academy of Sciences).
12. AIAA Journal.
13. Lebedev, A. A. and Chernobrovkin, L. S. *Dinamika poleta* (Flight Dynamics). Moscow, Mashinostroenie (1973).
14. *Theory of Conical Wings.* National Advisory Committee for Aeronautics (NACA) Tech. Notes No. 1685 (1948).

15. Nielsen, J. *Aerodinamika upravlyaemykh snaryadov* (Missile Aerodynamics). Moscow, Oborongiz (1962).
16. *Lift and Center of Pressure of Wing-Body-Tail Combinations at Subsonic, Transonic and Supersonic Speeds.* NACA, Tech. Reports No. 1307 (1957).
17. Belotserkovsky, S.M., Skripach, B.K., and Tabachnikov, V.G. *Krylo vnestatsionarnom potoke gaza* (A Wing in a Non-Stationary Gas Flow). Moscow, Nauka (1971).
18. Belotserkovsky, S.M. and Skripach, B.K. *Aerodinamicheskie proizvodnye letatel'nogo apparata i kryla pri dozvukovykh skorostyakh* (Aerodynamic Derivatives of an Aircraft and a Wing at Subsonic Velocities). Moscow, Nauka (1975).
19. Loĭtsyansky, L.G. *Mekhanika zhidkosti i gaza* (Fluid Mechanics). Moscow, Nauka (1970).
20. Loĭtsyansky, L.G. *Laminarnyĭ pogranichnyĭ sloĭ* (Laminar Boundary Layer). Moscow, Fizmatgiz (1962).
21. Dorodnitsyn, A.A. *Pogranichnyi sloĭ v szhimaemom gaze* (Boundary Layer in a Compressible Gas), in: Prikladnaya matematika i mekhanika, Vol. VI, vyp. 6 (1942).
22. *Nauchnye problemy iskusstvennykh sputnikov zemli* (Scientific Problems of Artificial Earth Satellites). Moscow, IL (1959).
23. *J. Aeronaut. Sci.*, No. 12 (1968).
24. Rakhmatulin, Kh.A., Sagomonian, A.Ya., Bunimovich, A.I., and Zverev, I.N. *Gazovaya dinamika* (Gas Dynamics). Moscow, Vysshaya shkola (1965).
25. *Problemy dvizheniya golovnoi chasti raket dal'nego deistviya* (Problems of the Motion of the Nose Cone of Long-Range Rockets). Moscow, IL (1959).
26. Patterson, G. N. *Molecular Flow of Gases.* New York, Wiley (1956).
27. *Proceedings of the National Symposium on Hypervelocity Techniques*, Denver, 1960.
28. Hayes, W.D. and Probstein, R.F. *Hypersonic Flow Theory.* New York, Academic Press (1959).

Supplementary Reading

Babenko, K.I., Voskresensky, G.P., Lyubimov, A.N., and Rusakov, V.V. *Prostranstvennoe obtekanie gladkikh tel ideal'nym gazom* (Three-Dimensional Flow of an Ideal Gas over Smooth Bodies). Moscow, Nauka (1964).
Chang, P. *Separation of Flow.* New York (1970).
Chernyi, G.G. *Introduction to Hypersonic Flow* (trans. by R.F. Probstein). New York, Academic Press (1961).
Drakin, I.I. *Aerodinamicheskiĭ i luchistyi nagrev v polete* (Aerodynamic and Radiative Heating in Flight). Moscow, Oborongiz (1961).
Ferri, A. *Elements of Aerodynamics of Supersonic Flows.* New York, Macmillan (1949).
Frankl, F.I. and Karpovich, E.A. *Gas Dynamics of Thin Bodies.* New York, Interscience (1953).
Hilton, *W. High Speed Aerodynamics.* London, Longmans, Green & Co., Ltd. (1951).

Koshkin, V.K. (Ed.). *Osnovy teploperedachi v aviatsionnoi tekhnike* (Fundamentals of Heat Transfer in Aviation Equipment). Moscow, Oborongiz (1960).
Kuznetsov, S.I. *Diagrammy i tablitsy techeniya dissotsiiruyushchego vozdukha okolo klina, konusa i vypukloĭ poverkhnosti* (Graphs and Tables for the Flow of Dissociating Air over Wedges, Cones, and Convex Surfaces). Moscow. Oborongiz (1962).
Landau, L.D. and Lifshits, E.M. *Fluid Mechanics.* London, Pergamon Press (1969).
Liepmann, H.W. and Roshko, A. *Elements of Gasdynamics.* New York, Wiley (1957).
Lin, C.C. *The Theory of Hydrodynamic Stability.* Cambridge (1955).
Lunev, V. V. *Giperzvukovaya aerodinamika* (Hypersonic Aerodynamics). Moscow, Mashinostroenie (1975).
Mkhitaryan, A.M. *Aerodinamika* (Aerodynamics). Moscow, Mashinostroenie (1970).
Schlichting, H. *Boundary Layer Theory*, 6th ed. New York, McGraw-Hill (1968).

Name Index

Babenko, K. I., 412
Belotserkovsky, O. M., 47, 48, 231, 411, 412
Blasius, H., 274
Bunimovich, A. I., 363, 410, 412
Busemann, A., 20

Chang, P., 412
Chernobrovkin, L. S., 110, 151, 179, 205, 244, 411
Cherny, G. G., 411, 412

Danilov, A. N., 24, 209, 411
Dorodnitsyn, A. A., 258, 266, 267, 268, 272, 297, 298, 412
Drakin, I. I., 412

Eckert, E., 283

Ferri, A., 412
Frankl F. I., 412

Hayes, W. D., 410, 412
Hilton, W., 412

Ionov, V. P., 25, 411
Irov, Yu. D., 54, 64, 411

Karpovich, E. A., 412
Keil, E. V., 54, 64, 411
Kibardin, Yu. A., 25, 411
Koshevoi, V. N., 24, 209, 411
Koshkin, V. K., 413
Krasnov, N. F., 24, 27, 75, 90, 109, 209, 327, 349, 411
Kuznetsov, S. I., 25, 411, 413

Landau, L. D., 413
Lebedev, A. A., 110, 151, 179, 205, 244, 411
Liepmann, H. W., 413
Lifshits, E. M., 413
Lin, C. C., 413
Loitsyansky, L. G., 257, 412
Lunev, V. V., 413
Lyubimov, A. N., 25, 411, 412

Mkhitaryan, A. M., 413

Nielsen, J., 190, 412

Patterson, G. N., 375, 412
Paulhausen, 260
Pavlukhin, B. N., 54, 64, 411
Pleshanov, A. S., 25, 26, 411
Prandtl, L., 266
Predvoditelev, A. S., 25, 26, 411
Probstein, R. F., 410, 412

Rakhmatulin, Kh. A., 363, 410, 412
Roshko, A., 413
Rozhdestvensky, I. B., 25, 26, 411
Rusakov, V. V., 412

Sagomonian, A. Ya., 363, 410, 412
Samuilov, E. V., 25, 26, 411
Schlichting, H., 413
Shumyatsky, B. Ya., 25, 411
Skripach, B. K., 231, 412
Stakhanov, I. P., 26, 411
Stupachenko, E. V., 25, 26, 411

Tabachnikov, V. G., 231, 412

Von Kármán, T., 255
Voskresensky, G. P., 412

Zakharchenko, V. F., 24, 209, 411
Zverev, I. N., 363, 410, 412

Subject Index

Accommodation, 388ff
  and pressure, 390f
  and skin friction, 390f
Aerodynamic coefficients,
  analysis of changes in, 123ff
  calculation, 99ff
  flat panels and circular cylinder, 166ff
  in linearized flow, 102ff, 166ff
  in low-frequency oscillations, 118ff
  in nearly uniform supersonic flow, 166ff
  in rotation about lateral axis, 122f
  in wind coordinate system, 105f
Aerodynamic interference, *see* Interference
Aerodynamics,
  blunted bodies, 31, 35
  rarefied gases, 369ff
  steady linearized flows, 78
Ailerons, 211f
  differential, 212
Air, *see also* Gas
  dissociated, 320
  opaqueness, 326
  optical properties, 326
  Prandtl number, 280
Aircraft, *see also* Combination
  banking, 211
  canard, 153, 187, 205f
Aircraft,
  controllability, 212f
    and static stability, 213
  manoeuvrability, 212f
  sensitivity to control deflection, 212
  with tandem wing and tail unit, 207
Airfoil(s),
  laminar-flow, 314
    drag, 314
  pressure distribution on, 295f
    in incompressible flow, 301
  sharp-nosed, in supersonic flow, 298f
  transition point, 314
Angle,
  attack,
    effective, 130
      empennage, 189, 197
      span-averaged, 190
    harmonic oscillations, 116
    local, 130
      tail unit panel, 132
    reduced, 235
  cone, 22
    critical, 21, 23
    and dissociation, 29
  disturbance, 66
  downwash, supersonic flow, 199f, 202
  rolling, and body-wing interference, 155ff
  setting, tail unit, 132

Angle,
shock, 67f
ahead of cone, 29
and cone angle, 22
conical surface, 27
ahead of sharp-nosed cone, 24
sideslip, 155
sweep, 196
wash, 130, 187, 244
wedge, critical, 23

Blackbody, heat emission, 326
Blunting,
degree, 31f
and heat transfer, 34
at hypersonic velocities, 34
landing spacecraft modules, 34f
Boattail, parabolic, 89
Body(ies), *see also* Combination
bluff, 302
and drag reduction, 302
blunt-nosed,
with gas injection, 306f
in supersonic flow, 32
wave drag, 32
conical, in free-molecule flow, 396
equivalent, 227
of revolution, *see* Body(ies) of revolution
slender, aerodynamic theory, 107ff
streamlined, 302
Body(ies) of revolution, 128
affine-similar, 72f, 93
conical, 93
in linearized flow 79
similarily law, 106f
longitudinal moment coefficient, 123
normal force coefficient, 117, 123
parabolic, 86f, 89f
in supersonic flow, 91
with parabolic generatrix, 72f
with parabolic nose and boattail, 89
pitching moment coefficient, 117f, 123, 399
pressure coefficient, 81, 97f, 106
sharp-nosed, 75ff
Body(ies) of revolution,
density, 64
pressure coefficient, 64
in supersonic flow, 61ff
temperature, 64
velocity, 64f
slender, 75ff, 81, 105
in axisymmetric linearized flow, 81ff
centre-of-pressure coefficient, 108f
harmonic oscillations, 119ff
normal force coeffici nt, 107ff
pitching moment coefficient, 108, 117f
pressure on, 85f
wave drag coefficient, 89ff
stability derivatives, 124ff
in supersonic flow, 61ff, 74f
in unsteady flow, 111ff
velocity potential, 79
Boundary condition(s),
flow over cone, 15
on shock, 16
behind shock wave, 39
unsteady flow, 116ff
for velocity, 250
Boundary layer,
bleed, 304f
and aerodynamic drag, 304
blowing, 304
conditional thickness, 256f
control, 304ff
on curved surface, 295ff, 338ff
density, 250
displacement thickness, 256f
incompressible flow, 265, 277
energy equation, 331ff, 339, 343
enthalpy, 278ff
entropy profile, 334f
flow conditions and nose blunting, 33
flow stagnation in, 256
friction force and density, 287
integral relation, 253ff
laminar, *see* Laminar boundary layer
laminar flow, 109

Boundary layer,
laminarization, 305
laminar sublayer, 267, 276
thickness, 268
laminar-turbulent, 307
|transition zone, 308f
mixed, 307
on flat plate, 308, 314ff
momentum thickness, 256
and compressibility, 265
incompressible flow, 265, 277, 315f
motion equation, 334
and Reynolds number, 307ff
separation,
and aerodynamic characteristics, 299ff
in compressible flow, 303
shear stress, 335
ratio at wall, 263f
shock action on, 303f
skin friction, 282, 290ff
stability on curved surface, 313
stabilization, by cooling, 305
temperature, 277ff, 281
thickness, 261f, 297
and compressibility, 263
compressible flow, 261f, 285
incompressible flow, 262f, 285
ratio, 263, 285
reduced, 298
turbulent, *see* Turbulent boundary layer
turbulent flow, 109
turbulization, 312
and shear stress, 276
velocity,
distribution, 261, 296f
at edge, 268
profile over cross section, 275, 334f

Centerbody, 306
Centre of pressure,
body-wing combination, 148ff
position and interference, 150
Characteristics, aerodynamic,
bodies of revolution, slender sharp-nosed, 75ff
body-empennage combination, 206f, 218ff
body-wing-empennage combination, 206f, 220ff
boundary layer separation, 299ff
overall, body, 35
Circulation, distribution, 195
Coefficient(s),
accommodation,
and heat transfer, 391
normal momentum component, 389f
tangential momentum component, 389f
thermal, 391f
aerodynamic, *see* Aerodynamic coefficients
axial force, 100
cone, 103
in linearized flow, 103
catalytic, 360
centre-of-pressure, 105, 221f
body of revolution, 108f
body-wing combination, 147, 150, 163f, 178, 219
linearized flow, 105
slender body of revolution, 105, 108f
slender cone, 105
drag, *see* Drag coefficient
heat transfer, 324f
and friction factor, 335
laminar boundary layer, 364
reference, 336
hinge moment, *see* Coefficient(s), longitudinal moment
lateral force,
body-wing combination, 172
in rolling, 164f
lift (force),
body of revolution, 399
free-molecule flow, 399
and molecule reflection, 404

Coefficient(s),
body-empennage, 198
section with empennage, 244
in wind coordinate system, 106
longitudinal force, 110
longitudinal moment, 123
body of revolution, 123
wing-body combination in rolling, 164
normal force, *see* Normal force coefficient
pitching moment, *see* Pitching moment coefficient
pressure, *see* Pressure coefficient
pressure-drop,
body-wing, 140, 142, 157f, 168f
circular cylinder, 142
control surface, 215
wing-body, 142
wing with subsonic leading edge, 176
wing with supersonic leading edge, 175
radiation, blackbody, 326
rolling moment, 238
additional, 182, 185
body-wing combination, in rolling, 165
in rolling, 184
rotary derivative, 236f
sideslip, 238
total, 182
stagnation, 179f
suction force, 230
wave drag, *see* Wave drag coefficient
yawing moment,
body-wing combination, 172
in rolling, 164
Coincidence, affine, 93
Combination,
body-all-movable empennage, 218ff
body-all moving wing, 219
body-cruciform wing, 166ff, 186
body-empennage, 198, 206f, 218ff, 240f
Combination,
lift (force)
curvilinear motion, 233
stability derivatives, 233f
body-flat empennage, 186
body-flat wing, 132ff, 163, 165, 186
disturbance velocity potential 135
pressure, 157ff
in rolling, 164ff
body-triangular wing, 143ff
body-wing, 132ff, 143ff, 147ff, 153f, 157f, 160f, 163ff, 168f, 172, 178, 193f, 240f
centre of pressure, 148ff
normal force, 153f
rolling moment, 149
with tail part, 177f
without tail part, 177f
body-wing-empennage, 188ff, 206f, 220ff
cylindrical body-flat panel, 166ff
empennage-body, 220
wing-body, 180, 187f, 190ff
wing-empennage, 187ff
Compressibility, and boundary layer thickness, 263
Condition(s), boundary, *see* Boundary condition(s)
Conduction, heat, molecular, 319
Cone,
in axisymmetric supersonic flow, 12f
blunt-nosed, 30ff, 51f
drag, 58f
in supersonic flow, 32ff
wave drag, 55
boundary conditions, 15
density ratio on, 23
with elliptical blunting, 31f
flat-nosed, 31
minimum pressure, 34
pressure coefficient, 34
in flow at constant specific heats, 14ff
laminar boundary layer, 293

Cone,
maximum velocity on, 53
pressure on, 23, 27
sharp-nosed, 12ff, 57
slender,
centre-of-pressure coefficient, 105
normal force coefficient, 104
pitching moment coefficient, 105
at small angle of attack, 97
wave drag coefficient, 88
spherical nose, 35ff, 48f
temperature, 23, 27
turbulent boundary layer, 294
Cone-sphere, 30ff
secant, 31
tangent, 30f
Constant,
Boltzmann, 388
Stefan-Boltzmann, 326
Control surfaces,
aerodynamic calculations, 213ff
all-movable, 209f
pitching effectiveness, 222f
and empennage turning angle, 222
and wing deflection angle, 222
and slot formation, 223f
tip, 210
along trailing edge, 210f
uses, 211
yawing effectiveness, 223
Controllability, craft, 212f
and static stability, 213
Control(s), *see also* Control surfaces
all-movable, normal force, 216f
boundary layer, 304ff
combined, 209
effectiveness, 212
longitudinal, 220
tip, 209f
Correction(s),
Dorodnitsyn's, 267
interference, 133
Craft, *see also* Aircraft
cruciform arrangement, 236
non-stationary characteristics, 231ff
pitch damping, 232ff
Criterion, similarity, 106, 346
Crossflow,
additional velocity potential, 79f, 93f, 102, 111f
velocity, 130
Curve(s),
apple, 19ff
family, 22
gas flow conditions, 373

Degree, stagnation, 205
Density,
boundary layer, 250
on cone, 27
dimensionless, 38
dissociating and ionizing gas, 25f
ratio, on cone, 23
relative, on cone, 27
sharp-nosed body, 64
behind shock, 25f
stagnation, at boundary layer wall, 259
Derivatives,
roll-damping, 236
rotary, 233, 236ff
stability, *see* Stability derivatives
Distribution,
circulation, 195
Maxwellian, 375f
pressure, *see* Pressure distribution
velocity, *see* Velocity, distribution
Disturbance, propagation in supersonic flow, 94f
Dissociation, 319
Doublets, 94
distribution function, 95
Downwash, 131f
Drag, 224ff, 392ff
additional due to pressure redistribution, 300f
body, 225f
and superstructures, 225
conical nose, 110
conical surface, 56
cylinder, 399ff

Drag,
empennage, 226f
in free-molecule flow, 397
friction, 276, 295
cone, 292
plate, 264
induced, 229f
laminar-flow airfoils, 314
plate, 401f
slender blunt cone, 58f
suction, 301
and compressibility, 302
total, 227
two-cone combination, 395f
vortex, 301f
wave, 23
blunt-nosed body, 34, 55
wing, 226f
Drag coefficient,
in absence of lift force, 224
body of revolution, 399
cone, 396ff
conical surface, 56
cylinder, free-molecule flow, 400f
induced, 229f
and angle of attack, 230
and molecule reflection, 402ff
parabolic boattail, 90
plate, 264
free-molecule flow, 401
due to reflected molecules, 396
sharp-nosed cone, 57
slender blunt cone, 59f
sphere, free-molecule flow, 398
total, 56, 224, 227

Edge,
leading,
subsonic, 176
supersonic, 175
sweptback,
subsonic, 176
supersonic, 176
Effect, entropy, 33f
Elevators, 211
Elevons, 212
Emittance,
gas, 326
surface, 330
and roughness, 330
Empennage,
cruciform, 181, 234
effectiveness, 188f, 192, 197, 202f
and flow stagnation, 205f
and shocks, 204f
non-tandem, 204
plus-shaped, 234
rotating, 209
vertical asymmetric, and rolling, 185
Energy,
balance, 405f
exchange, 391f
kinetic, transfer, 387f
Enthalpy,
boundary layer, 278ff, 283
on cone, 26
in dissociating and ionizing gas, 25f
dissociation, 360f
mixture component, 319f
recovery, 279, 364
reference, 283
on shock, 25f
stagnation, 249, 278, 332
total, 249
Entropy,
gradient, 70
profile in boundary layer, 334f
Equation(s),
Bernoulli, 52, 80
Bessel, 114
boundary layer, 245ff, 250f, 346
generalized, 251ff
differential form, 251f
three-dimensional axisymmetric flow, 251f
characteristic element,
first family, 61, 65f, 68
second family, 68ff
continuity, 13, 38, 76, 246, 249f
laminar boundary layer, 339

Equation(s),
differential, disturbance velocity potential, 135
diffusion, flow in frozen boundary layer, 356f
energy, 249f
for boundary layer, 331ff, 339, 343
energy balance,
diatomic gas, 405f
in stationary heat transfer, 405
heat balance, 318f, 363
hodograph, 16
linearized, aerodynamics, 75ff
mass transfer, 375
motion, 36ff, 339, 342
boundary layer, 334
Navier-Stokes differential, 245f
potential function, 76
linearized differential, 77
Prandtl, 248ff
shock polar, 16
state, 249f
system, axisymmetric flow over cone, 12ff
von Kármán's, 268
Equilibrium, local Maxwellian, 376

Factor(s),
correction, 151
for compressibility, 173
for slot influence, 224
enthalpy recovery, 279f
laminar boundary layer, 280
and Prandtl number, 280f
turbulent boundary layer, 280
friction, *see* Friction factor
interference, *see* Interference factor(s)
intermittence, 308
Reynolds analogy, 336
temperature recovery, 279, 283
Fences, aerodynamic, 305
Field, velocity, 19
approximate calculations, 129
Field, velocity,
in disturbed flow over cone, 15
in flow due to interference, 135
isentropic flow, 63
at zero angle of attack, 141
Flap, jet, 209
Flow(s),
axisymmetric, 12f, 24, 101
over flat-bottom cone, 396f
pressure distribution, 102
over slender body of revolution, 81ff
three-dimensional, 251f
unsteady, 112
zero angle of attack, 77, 79
in boundary layer, *see also* Boundary layer
and nose blunting, 33
over circular cylinder, 136
compressible, 257ff, 264, 285f
over cone,
blunt-nosed, 51f
boundary condition, 15
dissociating gas, 14
and equilibrium gas dissociation, 24ff
and gas ionization, 24ff
skin friction, 290ff
with spherical nose, 35ff, 48f
supercritical, 21
supersonic, 20f, 290ff
conical, 12
at constant specific heats, 14ff
continuum, 371f
disturbed,
over cone, 15, 292
incompressible, 135
downward, 199f
external incompressible, and critical Reynolds number, 309f
over flat nose, 57f
free, 245
and viscosity, 245ff
free-molecule, *see* Free-molecule flow
frozen, 324
heat, specific, *see* Specific heat flow

Flow(s),
incompressible, 135, 262ff, 273, 277, 285, 301, 315f
intermediate, 371
isentropic, 63
laminar, boundary layer, 109
linearized, 75f, 79, 81ff, 102ff, 174
disturbed, 77
normal force and angle of attack, 134
three-dimensional, 138
longitudinal, disturbed, 79f
nearly uniform, 77, 79
non-axisymmetric, 77, 93ff, 398
non-isentropic, 63, 67
oblique, 95
over plate, 257ff, 291ff
potential, 71f
separation, 299f
without separation, 79
over sharp-nosed cone, 12ff
over slender body of revolution, 75ff
at angle of attack, 106
slip, 371f, 410
and velocity profile, 372
at small angle of attack, 97
over smooth curved surface, 300
stagnation,
and aerodynamic parameters, 178ff
in boundary layer, 256
and empennage effectiveness, 205f
near stagnation point, 35
steady,
over curved surface, 245ff
inviscid, 76
linearized, 78
at small angles of attack, 75f
viscous compressible fluid, 245ff
subsonic, 189f, 295f, 317
supercritical, over cone, 21
supersonic, *see* Supersonic flow
turbulent boundary layer, 109, 275
undisturbed, 78, 116, 292
Flow(s),
unsteady, 111ff, 118
axisymmetric, 112
over body of revolution, 111ff
boundary conditions, 116ff
viscous,
in circular pipe, 273ff
dissociating gases, 279
in turbulent boundary layer, 275
vortex, 63, 67ff, 72f
vortex-free, 63
over wedge and cone, 22f
at zero angle of attack, 61ff, 77, 79, 141
Force(s),
axial, 99
drag, *see* Drag
friction, 252
excess, 252
lateral, body-wing combination, 160f
lift, and molecule reflection, 404
longitudinal, 99, 392f
normal, *see* Normal force
in rolling, 181
suction, 110f
Formula,
Newton's, 51, 260, 263, 269, 292, 324
modified, 52
Prandtl-Schlichting, universal, 277
Zhukovsky's, 191
Free-molecule flow, 371f, 374ff
aerodynamic coefficients, 396ff
over conical body, 396
over curved surface
drag force, 397
over flat surface, 380f
friction factor, 386f, 390, 409
kinetic energy transfer, 387f
over plate, 401ff
pressure, 382ff
shear stress, 385ff
Friction, *see* Skin friction
Friction factor,
average,

Friction factor,
average
disturbed flow, 292
plate, 316
turbulent boundary layer, 295
undisturbed flow, 292
body of revolution, 316f
compressible flow, 264, 285f
free-molecule flow, 386f, 390, 409
incompressible flow, 264, 273, 276f, 285f
local, 271, 276, 285
disturbed flow, 292
laminar boundary layer, 297
undisturbed flow, 292
supersonic flow, 299
and temperature, 286
Function,
distribution, 377
Maxwellian, 375f
doublet distribution, 95
drag, 92
MacDonald's, 114
potential, 76, *see also* Velocity potential
Laplace-Gauss, 175
stream, 340

Gas, *see also* Air
dissociating, 25f, 28f, 284
effective emissivity, 326
emittance, 326
flow conditions, 370ff
curves, 373
and velocity near wall, 372
highly rarefied, 371
parameters,
on blunt-nosed surface, 54
on conical surface, 27f
on peripheral conical surface, 54
reference, 283
Gradient,
entropy, 70
pressure,
at centre of flat nose, 58
longitudinal, and friction, 295ff
Gradient,
temperature, 319, 331
velocity, 344f
initial, 50, 53
at stagnation point, 50

Heat flux(es),
aerodynamic, 318
at high altitudes, 368
at stagnation point, 328
average over plate, 337
conduction and diffusion, 323f
on cone, 353f
by diffusion, 319ff, 359
distribution on blunt-nosed cone, 353f
to flat nose, 354f
radiant, 326
maximum, 327
spherical nose, 327
from Sun, 328
at stagnation point, 328, 348f, 360
total, to wall, 360f
transition region, 366
Heat transfer,
blunt-nosed bodies, 34
hypersonic velocities, 34
on blunt-nosed cone, 351ff
in boundary layer, 319, 322ff
on curved surface, 338ff
and catalytic reaction rate constant, 362
coefficient, 324f
and friction factor, 335
laminar boundary layer, 364
reference, 336
by convection, 324
by diffusion, 322, 356ff
in boundary layer, 322ff
and dissociation, 325
and flight speed, 362
free-molecule flow, calculation, 407ff
by gas to wall, 338
from heated gas, 319ff
rate, at stagnation point, 349

Heat transfer,
on spherical surface, 351
in turbulent boundary layer, 355f
Heating, aerodynamic, 318ff
Hodograph, 19f
equation, 16
Hypothesis,
absence of boundary layer influence, 248
constant shear stress over boundary layer, 267
continuum, application to flow studying, 371
kinematic similarity in fluid flow, 274

Integral,
Euler-Poisson, 378
probability, 379
Interaction, molecule-wall, 374f
Interference, 128ff, *see also* Combination
aerodynamic, *see* Interference
body-empennage, 183
body-flat wing, 157ff
disturbance velocity potential, 135
rolling angle, 155ff
velocity components, 158
and compressibility, 173
corrections, 133
factors, *see* Interference factor(s)
nature, 128ff
tail unit-wing, and shock, 205
wing-body, 128f, 183
non-slender configuration, 174
normal force, 143
due to sideslip, 160
with sideslip, 160ff
wing-empennage, 130ff
and angle of attack, 204f
subsonic velocities, 189f
supersonic velocities, 190ff
thin combination, 188
wing-tail unit, 132
linearized supersonic flow, 131
Interference factor(s), 133f, 193, 226
body, 173, 217f
non-slender configuration, 174
body-wing, 145ff, 153, 171, 177f
and boundary layer of body, 151f
determination, 143ff, 196ff
empennage, 207
panels, 184
in rolling, 161f, 171
cruciform wing-body combination, 162
flat wing-body combination, 162
triangular empennage, 201f
wing, 173, 207, 217f
wing-body, 145ff, 153
and wing taper ratio, 151
Ionization, 319
Irradiance,
Earth, and altitude, 330
Sun, 328f

Laminar boundary layer, 250, 257ff, 285ff, 290ff
calculation, 297ff
in compressible flow, 257ff
continuity equation, 339
enthalpy recovery factor, 280
on flat plate, 257ff, 285ff
friction factor, 297
heat transfer coefficient, 364
heat transfer on curved surface, 338ff
incompressible, 285
skin friction, 282, 290ff
stability,
and Mach number at edge, 312f
and surface roughness, 310f
and wall temperature, 311, 313
thickness,
on cone, 293
and dissociation, 287
on flat plate, 293
and temperature ratio, 286
Law,
Fourier's, 319

Law,
similarity, 72f, 91f, 106f
body of revolution in linearized flow, 106f
Stefan-Boltzmann, 326, 330
velocity distribution, turbulent boundary layer, 273ff
Layer,
boundary, *see* Boundary layer
high-entropy, 32
flow in, 32f
Length,
characteristic, 242
mixing, 266f
in incompressible flow, 267
Lines, hinge, 209f
Loading, wing, 198f

Manoeuvrability, craft, 212f
Method,
analogy, 94f
characteristics, 61ff
direct solution of equations, 356
Dorodnitsyn's, 302
Newton's, 51
flow over blunt-nosed cone, 51f
reduced angle of attack, 235ff
reference parameters, 299
reverse-flow, 197, 213ff
sources, 82f, 111
Model,
Euler's, 52
Newton's, 52
vortex,
body-wing combination, 193f
flat craft configuration, 231
wing-body combination, 190ff
Modules, landing spacecraft, 34f
Molecules,
reflected, temperature, 404ff
velocity,
mean, random motion, 376
mean square, random motion, 376
most probable, 376

Moment,
damping, 126
pitching, 101
additional due to rolling, 163
body-wing combination, 148
rolling,
additional, 185
in sideslip, 163
body-wing combination, 186f
flat combination, 186f
tail unit, 207f
in rolling, 182
spiral, 234f, 237, 239
yawing, 234f
Momentum, transfer to wall, 389ff
Motion, *see also* Flow(s)
body of revolution, 116f
rolling, 223

Normal force, 100
additional, with V-shaped surface, 183
all-movable controls, 216f
and aspect angle, 217
in linearized flow, 134
body-empennage combination, 198
body-wing combination, 132ff, 143ff, 153f, 160f
in sideslip, 169
supersonic flow, 191
body-wing-empennage combination, 188ff
developed by control urface, 214ff
empennage, 232f
due to rolling, 170f
in rolling, 180ff
wing-body interaction, 143
Normal force coefficient, 101
additional,
due to all-moving wing deflection, 218f
due to interference, 173
with V-shaped surface, 183
axisymmetric flow, 101
body-empennage combination, 220

Normal force coefficient.
body of revolution, 117, 123
slender, 107ff
body-wing combination, 134, 143ff, 153f, 163, 165, 172
body-wing-empennage combination, 206f, 220ff
empennage, 189f
in rolling, 235f
empennage-body combination, 220
in harmonic oscillations, 119
linearized flow, 104
reduction due to vortex, 203
in rotation, 122
slender cone, 104
subsonic sweptback edge, 176
supersonic sweptback edge, 176
tail part, 193
wing-body combination, 180
Noses,
blunt, shape, 30ff
conical, 110
flat, 57f, 354f
velocity gradient at centre, 58
ogive, 93
parabolic, 71ff, 89
spherical, velocity distribution, 50f, 53
Number,
Knudsen, 370, 373
Lewis, 322
Mach,
on conical surface, and velocity, 29
and pressure on cone, 29f
Nusselt, 325f, 335
laminar boundary layer, 335
local, 335
Prandtl, 249, 280, 284, 322
for air, 280
reference, 336
Reynolds, *see* Reynolds number
Schmidt, 322, 357
Stanton, *see* Stanton number
Opaqueness, air, 327
Oscillations, harmonic,
about lateral axis, 119ff
low-frequency, 118ff
normal force coefficient, 120
pitching moment coefficient, 120
pressure coefficient, 119
unsteady flow, 116f

Panel(s),
flat, and circular cylinder, 166ff
horizontal, 181
interference factor, 184
with rounded tips, 182
tail unit, local angle of aspect, 132
triangular, 182, 199
vertical, 181
wing, rectangular, 151
Parameter(s),
gas, 27f, 54, 283
inviscid flow, 74f
kinematic, dimensionless, 122, 232
stagnation pressure, 23
Path, free molecules, 369f
Pitching moment coefficient, 101
additional, 233
body of revolution, 117f, 123, 399
body-wing combination, 149, 172
in rolling, 164
body-wing-empennage combination, 206f
in harmonic oscillations, 120
linearized flow, 104
in rotation, 122
slender body of revolution, 108
slender cone, 105
total, 243
Plates, wing-tip, 305
Point,
separation, 300f
and compressibility, 302
transition,
location, 309
wing airfoils, 314
Polar(s), shock, 22
equation, 16

Potential,
complex, 167
crossflow, 158
disturbance velocities, 158
flow over circular cylinder, 136
horizontal panels, 166
vertical panels, 166
disturbance, 78
velocity, *see* Velocity potential
Pressure, 64
on body, body-flat wing combination, 157ff
in boundary layer, 248
coefficient, *see* Pressure coefficient
on cone, 23, 27
dissociating and ionizing gas, 25
distribution, *see* Pressure distribution
excess, conical body, 51f
on flat-nosed cone, minimum, 34
in free-molecule flow, 382ff
gradient, 295ff
on shock, 25
on slender body of revolution, 85f
stagnation, 67
behind conical shock, 64
ratio, 179
on wing, body-flat wing combination, 159f
Pressure coefficient, 51
body of revolution, 81, 97f, 106
additional, 117
body-wing combination, 139, 157
component,
axisymmetric flow, 81
crossflow, 81
on cone, 23, 27
axisymmetric supersonic flow, 24
flat-nosed, 34
with gas dissociation and ionization, 28
on conical surface, 88
distribution over body with parabolic nose and boattail, 89
in harmonic oscillations, 119
in rotation, 122
Pressure coefficient
sharp-nosed body, 64
wing-body combination, 142, 159
Pressure distribution,
on airfoil,
subsonic flow, 295f
supersonic flow, 296
in axisymmetric flow, 102
near body of revolution, 71f
over flat nose, 57f

Radiation, solar, diffuse, 328
Ratio,
aspect, 196, *see also* Ratio, fineness
effective, 229
base taper, 108
boundary layer thickness, 263, 285, 289
density,
on cone, 23
with dissociation in boundary layer, 286
fineness, 71
nose, 72
friction factor, 285f, 288
lift-drag, plate, in free-molecule flow, 401
pressure,
blunt-nosed cone, 351
three-dimensional linearized flow, 138
shear stress, 285, 294
laminar boundary layer, 285
turbulent boundary layer, 288, 290f
stagnation pressure, 179
taper, 196
thickness, 288
Reflection, molecular,
diffuse, 374f, 381
specular, 374
Region, heat flux transition, 366
Reynolds number,
critical, 275, 307ff
experimental, 309

Reyndols number
longitudinal pressure gradient, 314
subsonic flow, 317
supersonic flow, 317
and surface shape, 313
local, 263
pipe, 274
Rocket, 128
Roll, damping, 235ff
Rotation, about lateral axis, 116f, 121ff
aerodynamic coefficients, 122f
Roughness,
height,
critical, 311
effective, 311
surface, and critical Reynolds number, 310
Rudders, 211
Rule,
area, 227ff
and drag calculation, 228f
conjugate radii, 190

Separation, flow, 299f
Shear stress, 252f
boundary layer, 335
on cone in supersonic flow, 291f
and dissociation, 287
in free-molecule flow, 385ff
laminar flow, 253
on plate in supersonic flow, 291ff
and pressure gradient, 296
turbulent boundary layer, 288, 294
turbulent flow, 252
at wall, 255, 263, 269, 271, 274ff
laminar boundary layer, 285
and temperature, 264
Sheet, vortex, 187, 192, 194
Shock(s), *see also* Shock wave
ahead of blunt body, 306
and empennage effectiveness, 204f
kinetic parameters, 15
motion away from cone tip, 21
velocities ahead and behind, 16
Shock wave, *see also* Shock(s)
detached, 32f
detachment distance, 46ff
and dissociation, 48
from flat nose, 57
and ionization, 48
relative, 47f, 50
deviation from concentric shape, 46
generatrix, 48f
radius of curvature, 49f, 57f
Similarity, aerodynamic, 93
Skin friction,
in boundary layer, 282, 290ff
on cone in supersonic flow, 290ff
and heat transfer, 331ff
Solutions, similar, 344
Specific heat flow, 318
resultant, 321f, 360
due to terrestrial radiation, 328ff
at stagnation point, 409
to wall, 407
Speed, sound, 77
Stability derivatives, 111, 231
body-empennage combination, 240f
body of revolution, 124ff
body-wing combination, 240f
dynamic, 125f
low-frequency oscillations, 120ff
and Mach number, 124f
static, 124ff
total, 242
body-empennage combination, 233f
yawing, 234f
Stanton number, 325f, 335, 408
average value, 337
on cone, 338
on plate, 338
laminar boundary layer, 335
local, 336
modified, 408
and local friction factor, 409
reference value, 336
turbulent boundary layer, 336

Streamline(s),
mean displacement, 257
sonic, 32f
Strength,
vortex, 44
dimensionless, 193
vorticity (vortex sheet), 195
Stress, shear, *see* Shear stress
Sublayer, laminar, 267
thickness, 268
Supersonic flow, 12f, 20f, 24, 29, 32ff, 174, 199f, 290ff, 296, 317, 366
over body of revolution, 74ff, 91
over cone, 20f, 32ff, 54f, 290ff
disturbance propagation, 94f
friction factor, 299
over plate, 291ff
over sharp-nosed airfoil, 298f
over sharp-nosed body of revolution, 61ff
over spherical surface, 36
at zero angle of attack, 61ff
Surface(s),
auxiliary, 305
control, *see* Control surfaces
V-shaped, and rolling moment, 183f

Tail unit,
angle of attack, 132
effectiveness, and flow stagnation, 205f
non-tandem, 204
setting angle, 132
Temperature,
over boundary layer, 281
on cone, 23, 27
and gas dissociation, 28
equilibrium, 363, 408f
with additional heat sources, 367f
equilibrium emission, 363ff
distribution over airfoil surface, 366
at moderate flow velocities, 366
Temperature,
near stagnation point of sphere, 365
in supersonic flow, 366
gradient, 319, 331
recovery, 279, 284
reduced, 367
reference, 282ff
reflected molecules, 404ff
sharp-nosed body, 64
stagnation, 250
wall, 281
and ablation, 368
determination, 363ff
equilibrium, 408f
equilibrium emission, 363ff
and solar radiation
Terms, interaction, 158
Theory,
aerodynamic, slender body, 107ff, 203, 213
boundary layer, 246
conformal transformation, 135
continuum flow, validity limits, 369f
linearized, limits of application, 91f
Newton's,
collision, 397f
corpuscular, 51f
slender body, 109, 122, 126
Thickness, displacement, relative, 152
Transform, Laplace, 112f
Transformation,
affine, 93
conformal, 135f, 166f
Turbulent boundary layer, 252, 268, 275, 288ff, 293ff
enthalpy recovery factor, 280
on flat plate, 265ff
friction factor, 295
heat transfer, 355f
and separating flow, 301f
stability and surface roughness, 311
Stanton number, 336
thickness, 276

Turbulent boundery layer
in compressible gas, 288
thickness,
on cone, 294
and dissociation, 289
on flat plate, 294
in incompressible flow, 288
velocity distribution, 273ff

Upwash, 131f

Velocity(ies),
axial component, 84, 96f, 137, 140f
on body in presence of wing, 139
boundary conditions for, 250
at boundary layer edge, 268
complex, 129
disturbance, 158
components, in body-flat wing interference, 158
on cone, 54
and cone angle, 22
maximum, 53
crossflow, 130
distribution,
on blunt cone in supersonic flow, 54f
in boundary layer, 261, 267, 296f
on spherical nose, 50f, 53
disturbance,
axial component, 137, 140f
complex, 158
lateral component, 138, 140f
vertical component, 138, 140f
disturbed, components, 77
in wind coordinates, 156
field, *see* Field, velocity
free-stream, components in cylindrical coordinates, 78
friction, 311
gradient, 344f
initial, 50, 53
at stagnation point, 50
in high-entropy layer, 33
hypersonic, 34

Velouty(ies),
disturbance,
lateral component, 138, 140f
maximum,
on cone, 53
sharp-nosed body, 64f
molecules, 376
normal component,
behind shock, 17f, 25
undisturbed flow, 116
orbital, 349
over pipe cross section, 274
profile, over boundary layer, 275, 334f
radial component, 25, 84f, 98, 141
sharp-nosed body, 64
near stagnation point, 40ff
total, behind shock, 39
vertical component, 138, 140f
vertical downwash, 200
on wing in presence of body, 140f
Velocity potential,
additional,
crossflow, 79f, 93f, 102, 111f
longitudinal disturbed flow, 79f
axisymmetric unsteady flow, 112
body of revolution, 79
continuously distributed unsteady doublets, 115
determination with interference, 134ff
disturbance, 78, 135
linearized flow, 79
non-axisymmetric flow, 94, 115
undisturbed flow, 78
unsteady flow, 118
unsteady sources, 111, 114f
Viscosity, turbulent, 252f
Vortex(ices),
attached, 190f
bound, *see* Vortex(ices), attached
conjugate, 190f
double component, 40
empennage, 196
formation in separation zone, 297
free, 190f, 193f

Vortex(ices)
influence on rolling, 185ff
on nose surface, 43
rolled-up, 193
sheet, 187, 192, 194
behind shock wave, 43ff
strength, 44
near stagnation point, 45f
strength, 44
dimensionless, 193
wing, 196
zone of influence, 199, 203

Wall, adiabatic, 406f
Wash, 130, 187f
wing, 131f
rectangular, 131
Wave, shock, *see* Shock wave
Wave drag coefficient,
axisymmetric supersonic flow, 24
blunted nose, 56
body of revolution, 74f
parabolic, 74f
slender, 89ff
flat nose, 57
slender cone, 88
spherical nose, 55f
supersonic flow, 74f
in wind coordinate system, 106
Wedge,
critical angle, 23
and flow on oblique shock, 22
Wing(s),
all-moving, 218ff
crossed, 133
cruciform, 166ff
flat, 132f
flying, 212
isolated, 134
loading, 198f
plus-shaped, 133
rectangular, 151
wash, 131
rotating, 209
separate, 134
triangular, 143ff, 161
vertical asymmetric, and rolling, 185
wash, 131f
zone of influence on tail unit, 131

Zone(s),
doubtful similarity, 73
separation, 108f
vortex formation, 297
stagnation, 300
transition, boundary layer, 308f
location, 309
undisturbed flow, 143
vortex influence, 199, 203

Printed in the Union of Soviet Socialist Republics